Schriften des Forschungszentrums Jülich
Energy & Environment Volume 78-2

Forschungszentrum Jülich GmbH
Institute of Energy Research (IEF)
Fuel Cells (IEF-3)

18th World Hydrogen Energy Conference 2010 – WHEC 2010

Parallel Sessions Book 2:
- Hydrogen Production Technologies – Part 1

Editors: Detlef Stolten, Thomas Grube

Schriften des Forschungszentrums Jülich
Energy & Environment Volume 78-2

ISSN 1866-1793 ISBN 978-3-89336-652-1

Bibliographic information published by the Deutsche Nationalbibliothek.
The Deutsche Nationalbibliothek lists this publication in the Deutsche Nationalbibliografie; detailed bibliographic data are available in the Internet at http://dnb.d-nb.de.

Vol. 78 Set (komplett)
ISBN 978-3-89336-657-6
Editors: Detlef Stolten, Thomas Grube, Bernd Emonts

Publisher and Distributor: Forschungszentrum Jülich GmbH
Zentralbibliothek
52425 Jülich
Phone +49 (0) 24 61 61-53 68 · Fax +49 (0) 24 61 61-61 03
e-mail: zb-publikation@fz-juelich.de
Internet: http://www.fz-juelich.de/zb

Cover Design: Grafische Medien, Forschungszentrum Jülich GmbH

Printer: Grafische Medien, Forschungszentrum Jülich GmbH

Schriften des Forschungszentrums Jülich
Reihe Energy & Environment Volume 78-2

ISSN 1866-1793
ISBN 978-3-89336-652-1

The complete volume ist freely available on the Internet on the Jülicher Open Access Server (JUWEL) at http://www.fz-juelich.de/zb/juwel

Book 2: Hydrogen Production Technologies – Part 1

Contents

Posters

Design of a Novel Flat-plate Photobioreactor System for Green Algal Hydrogen Production

B. Tamburic, **F.W. Zemichael**, **G.C. Maitland**, **K. Hellgardt**, Imperial College London, UK

Abstract

Some unicellular green algae have the ability to photosynthetically produce molecular hydrogen using sunlight and water. This renewable, carbon-neutral process has the additional benefit of sequestering carbon dioxide during the algal growth phase. The main costs associated with this process result from building and operating a photobioreactor system. The challenge is to design an innovative and cost effective photobioreactor that meets the requirements of algal growth and sustainable hydrogen production. We document the details of a novel 1 litre vertical flat-plate photobioreactor that has been designed to accommodate green algal hydrogen production at the laboratory scale. Coherent, non-heating illumination is provided by a panel of cool white LEDs. The reactor body consists of two compartments constructed from transparent Perspex sheets. The primary compartment holds the algal culture, which is agitated by means of a recirculating gas flow. A secondary compartment is filled with water and used to control the temperature and wavelength of the system. The reactor is fitted with instruments that monitor the pH, pO_2, temperature and optical density of the culture. A membrane-inlet mass spectrometry system has been developed for hydrogen collection and *in situ* monitoring. The reactor is fully autoclaveable and the possibility of hydrogen leaks has been minimised. The modular nature of the reactor allows efficient cleaning and maintenance.

1 Introduction

1.1 Green algal hydrogen production

Molecular hydrogen (H_2) is a fuel that has the potential to provide the clean energy required for transport, heating and electricity. The aim of our Solar Hydrogen Project is to produce H_2 by a carbon-neutral process that uses unlimited natural resources – sunlight and water. The green alga *C.reinhardtii* has the ability to photosynthetically produce H_2 under anaerobic conditions [1]. Initially, photons are absorbed within the chloroplast of *C.reinhardtii*. This solar energy facilitates the photochemical oxidation of water into protons and molecular oxygen (O_2) by photosystem II (PSII) proteins. Electrons generated in this process are transferred to the iron-hydrogenase enzyme, which catalyses proton-electron recombination to produce H_2. Hydrogenase activity is inhibited in the presence of O_2, which implies that this direct biophotolysis process is self-limiting. In order to maintain continuous H_2 production, it is necessary to remove O_2 as it is being produced. Sulphur deprivation of *C.reinhardtii* diminishes its ability to repair PSII proteins, thus reducing photosynthetic O_2 production below the level of respiratory O_2 consumption so that overall, O_2 is being used up [2]. Algal metabolism is therefore responsible for creating an anaerobic environment that leads to sustained H_2 production. The main barriers to the commercialisation of green algal H_2

production are the low photochemical conversion efficiencies of the process and the prohibitive photobioreactor (PBR) costs [3].

1.2 Photobioreactors

Commercial growth of algal biomass is normally restricted to inexpensive open systems such as natural ponds, circular ponds with a rotating arm for stirring, or raceway ponds [4]. Enclosed PBR systems offer the potential for reproducible cultivation conditions, better biomass and H_2 yield, better product quality and the opportunity for flexible technical design [5]. They can enable algal cultivation in arid regions, hence ensuring that algae do not need to compete for land area with food crops, while also opening new economic possibilities in desert countries [6]. The main drawbacks of enclosed PBR systems are their high capital and operating costs. The productivity of a closed PBR is limited by various factors, but most importantly it needs to operate with optimal light requirements, surface-to-volume ratio, agitation time and mass transfer [7]. The types of PBR commonly considered in the literature are the vertical-column reactor, the stirred-tank reactor (often with internal illumination), the tubular reactor, the flat-plate reactor and various immobilised reactors. Flat-plate reactors consist of a rectangular compartment with a depth of 1-5 cm and a height and width that do not practically exceed 1 metre [8]. Artificially illuminated flat-plate reactors are often vertical, with a light source illuminating the reactor from one side. Outdoor flat-plate reactors are typically tilted at an angle that allows optimal exposure to solar irradiation [4]. All flat-plate reactors are characterised by a high surface-to-volume ratio, which leads to the best photosynthetic efficiencies observed for any PBR [3]. The region immediately adjacent to the illuminated reactor surface is a photic zone where light saturation, and consequently the photoinhibition of algal growth and H_2 production processes, repeatedly occurs [9]. In addition, the light energy available to algal cells decreases exponentially away from this photic zone – it has been estimated that for a fully grown culture of *C.reinhardtii*, effective light penetration is limited to a depth of 0.8 mm [8]. It is therefore important to minimise these light gradients and control the light-dark cycles of the algal cells by means of an effective agitation system [9]. Flat-plate reactors are subject to relatively low mass transfer rates because the space between panels, known as the light path, is restricted and this reduces the clearance efficiency of the dissolved O_2 produced by photosynthesis [10]. Flat-plate reactors provide operational flexibility as they may be run in both batch and continuous modes [5]. Typical limitations are the scaling-up requirements (the need for many compartments and support materials), the difficulty in controlling culture temperature, the possibility of algal wall growth and the incompatibility with certain algal strains [11].

2 Reactor Design

2.1 Design specification

Our motivation for designing the PBR was to create a simple system that would enable quick measurement of the key parameters in the biohydrogen production process under carefully controlled conditions. As part of the design specification, we made a selection of the parameters that should be controlled and/or measured, used these observations to drive the reactor design, and completed the process by developing the ancillary systems and equipment required to service the reactor. The critical control parameters are temperature,

light intensity and wavelength, agitation and mixing, nutrient delivery and dilution, and pH [5]. A continuous, on-line measurement of H_2 production is required. Additionally, it is necessary to determine the algal growth rate, the dissolved oxygen concentration (to determine if the culture is anaerobic), and the uptake rates of key nutrients such as sulphate and acetate [11]. Since the availability of light is normally the limiting factor for algal growth and H_2 production, we selected the reactor geometry that offers the highest surface-to-volume ratio – the vertical flat-plate reactor. When selecting reactor materials, it was important to consider their strength, durability, spectral properties, toxicity for algal cells, and the diffusion coefficient for H_2 [12]. The reactor was designed to be fully autoclaveable to minimise the possibility of contamination, and completely modular to allow easy cleaning and maintenance between experiments [13]. The choice of a minimalistic reactor design and the selection of materials and ancillary systems equipment were made with the intention of keeping the cost of our flat-plate reactor competitive with targets laid out in the literature [2]. The reactor ancillary systems were concerned with illumination, agitation, measurement and datalogging, and user control interface. Illumination was provided by an LED array and the main challenge was to select the correct geometric configuration for optimal light exposure [8]. Diaphragm pumps were used to fulfil the agitation requirements, consisting of turbulent flow, appropriate mixing patterns and low levels of sheer stress on the culture [4]. It was essential to provide instrumentation to measure the pH, pO_2, H_2 production and algal growth rate [13]; commercial probes covered *in situ* pH and pO_2 measurements, H_2 was measured by membrane-inlet mass spectrometry (MIMS) and the algal growth rate was monitored by regularly measuring the optical thickness of the culture using a light meter.

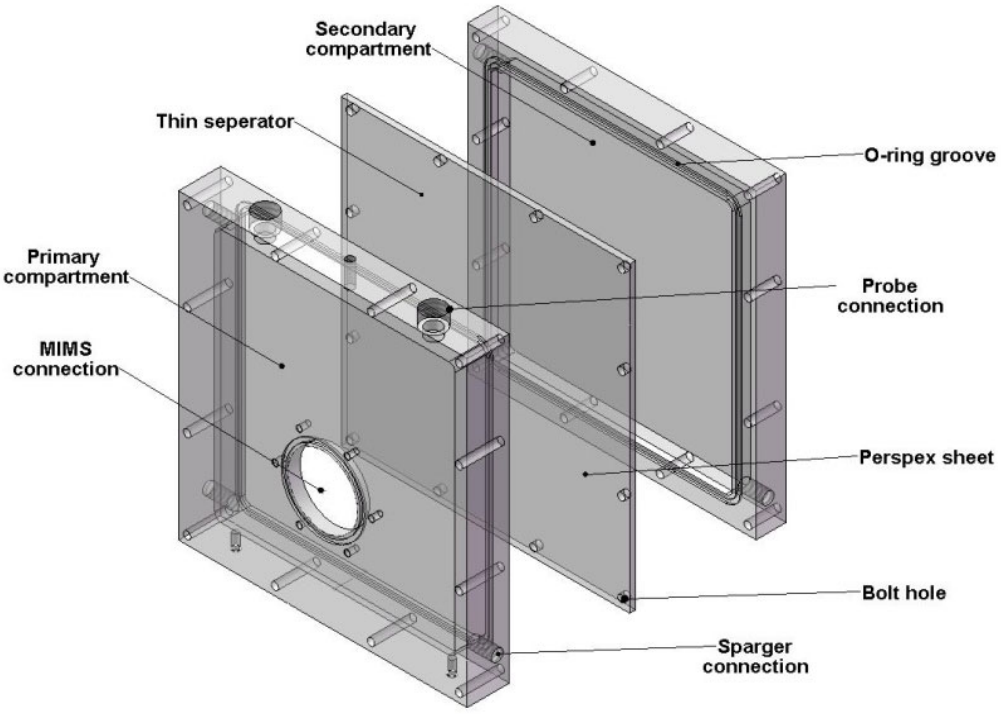

Figure 1: Flat-plate reactor design in Solid Works showing the three-piece Perspex component assembly.

2.2 Dual-compartment design

A novel dual-compartment flat-plate reactor body was designed (Figure 1) and constructed. The primary compartment contains the algal culture, while a secondary compartment is filled with water (or an aqueous solution) and used as a temperature control jacket. Various coloured ions may be dissolved in the secondary compartment to control the intensity and wavelength of illumination reaching the algal culture. The primary compartment also contains a slot for inserting the membrane-inlet mass spectrometry (MIMS) system to be used for H_2 measurement. The critical measuring instruments (thermocouple, pO_2 and pH probe) may be attached via the appropriate slots at the top of the primary compartment. The entire structure may be screw-connected onto a firm, black (matt, to minimise surface reflection) polyoxymethylene base, which also holds the LED array with the aid of a support bracket. The final dual-compartment reactor body dimensions were 250x250x70 mm, and the entire construction could fit into a box with dimensions 350x350x22 mm. The primary compartment has a working volume of approximately one litre. The reactor body is made of Perspex (polymethyl methacrylate), a transparent polymer alternative to glass that is relatively inexpensive, autoclaveable and easy to handle and process. Following a number of design iterations, it was decided to construct the reactor body from a thin (3 mm) Perspex separator sandwiched between two thick (50 mm) slabs of Perspex. The primary and secondary compartments were machined within these two thick Perspex slabs. The machining was carried out by programming the Solid Works design into the computer-aided machining software Feature Cam. Perspex polish was applied to the machined surfaces to improve their optical transparency. A crucial element of the reactor design was that it should be impermeable to H_2. This means that special care had to be taken to ensure a good seal at any location where the culture could potentially be exposed to the surroundings. The Perspex sheets were sealed with an inlaid grooved system of Viton fluoropolymer elastometer o-rings and pressed together using a set of 12 stainless steel bolts, hence also satisfying the requirement for a fully modular design. The agitation system holes were closed by o-ring-sealed stainless steel Swagelok fittings. None of the materials used are known to be toxic to *C.reinhardtii*.

2.3 Illumination

Overall, *C.reinhardtii* cells have modest light intensity requirements – the growth, sulphur deprivation and H_2 production processes need no more than 200 $\mu Es^{-1}m^{-2}$ of photosynthetically active radiation (PAR) – about 10 Wm^{-2} [1]. The main objective is to ensure that as many cells as possible have access to uniform illumination [3]. A light emitting diode (LED) array provides illumination that is uniform, coherent, efficient and non-heating, all desirable properties for the flat-plate PBR. Two cool-white LED array panels, approximately 200x200 mm in size, were purchased from LED Wholesalers. Measurements with a light meter (operating on integrating sphere principles) have shown that the spatial light intensity distribution of our LED array, measured directly from a distance of 30cm away from the array, is relatively consistent across the flat-plate reactor area, with a light intensity of 58±3 Wm^{-2}. When the reactor is placed between the LED array and light meter, the light intensity drops to 43±8 Wm^{-2}, primarily due to limitations in the transparency of machined Perspex. There is also evidence of additional shading effects radially away from the reactor centre; it is therefore important to make certain all algal cells receive sufficient illumination by

providing appropriate agitation to the algal culture. It is possible to use a light meter or photodiode in a similar setup to measure the optical thickness of the culture, which is directly proportional to the algal growth rate. Other advantages of LED illumination are that the intensity is readily controllable and that the wavelength shows a good spectral match with *C.reinhardtii* absorption (Figure 2(a)). *C.reinhardtii* PSII absorbs in the red region of the visible spectrum, with the main absorption peak at 680 nm [3]. PSII absorption is a threshold mechanism, that is to say the algae could use any wavelength lesser-than-or-equal to 680 nm for photosynthesis, but preferentially use 680 nm, as evidenced by the strong absorption peak at this wavelength. There is also additional carotenoid absorption in the 400-500 nm spectral range. It is possible to use the coloured aqueous solutions of various ions to modulate the wavelength of illumination incident on the culture (Figure 2(b)). For example, the purple potassium permanganate (aq) could be used to prevent photoinhibition by unnecessary green light. Orange potassium chromate (aq) could be used to switch-off carotenoid absorption, potentially diverting additional photons to PSII, while red cobalt chloride (aq) could be used to combine the above effects.

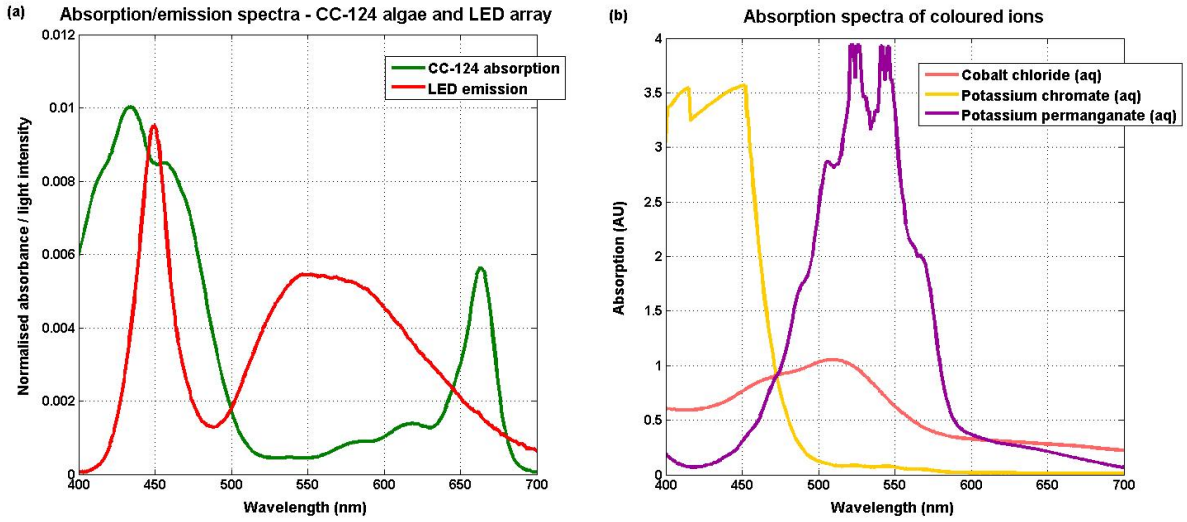

Figure 2: (a) Spectral match between LED emission and *C.reinhardtii* wild-type CC-124 strain absorption;
(b) absorption spectra of some common coloured aqueous solutions that may be used to modulate LED wavelength.

3 Reactor Development

3.1 Agitation system

Primary compartment agitation is provided by a turbulent air-lift system emanating from a dual-entry stainless steel sparger at the bottom of the compartment (Figure 1). The gas flow system is enclosed in stainless steel tubes and circulated around the reactor so that no gaseous hydrogen is lost to the environment. Both dissolved and gaseous H_2 are collected by a specifically designed MIMS system, which is located on the front end of the primary compartment. Gas is circulated by means of a customised gas diaphragm pump from KNF

Neuberger. This pump features a stainless steel pumping head with Swagelok inlet/outlet connections to minimise H_2 diffusion leaks in this critical region, as well as step-voltage control of the pumping speed. A temperature flux and mass flow model is being developed in Comsol to optimise parameters such as the temperature of the secondary compartment and the flow rates through both compartments. During the algal growth phase, the primary compartment could be agitated by sparging a mixture of carbon dioxide and air, thus providing an additional carbon source for photomixotrophic algal growth. An inert gas such as argon would be used during the anaerobic H_2 production phase. Secondary compartment water recirculation is provided by a standard KNF Neuberger liquid diaphragm pump.

3.2 Membrane-inlet mass spectrometry (MIMS) system

Various methods have been used to monitor the gaseous species (O_2, CO_2 and H_2) involved during photobiological H_2 production. The conventional method has been to use *in situ* Clark-type electrode measurements and/or analysis of gas samples by gas chromatography. MIMS is another analytical technique used to measure *in situ* concentrations of dissolved gases or volatile organic compounds in aqueous solutions. The membrane system is the only interface between a liquid sample at atmospheric pressure and the vacuum chamber of a mass spectrometer. The membrane is made from different polymeric materials that allow gases to diffuse simultaneously or selectively depending on the investigation [11]. The technique allows direct comparison of the evolved gases and provides continuous monitoring of process conditions, i.e. light intensity, temperature, pH and system disturbances. Our flat-plate reactor utilises the Aston Analytical Ultra-Trace MIMS System. The mass spectrometer is a compact quadrupole Pfeiffer Vacuum Prisma, running Windows Quadstar 422 software. Gases dissolved in the liquid phase diffuse through a thin polydimethylsiloxane membrane affixed on a perforated disc holder. Inert gas introduced to the disc holder cavity directly carries diffused gaseous products, via a heatable capillary, into the mass spectrometer. To avoid any damage to the vacuum system, a moisture trap is fixed before the inlet of the mass spectrometer. Apart from the direct measurement of gaseous products kinetics, the MIMS system offers the additional benefits of potential H_2 separation and collection, as well as the reduction of possible H_2 induced inhibition of the biophotolytic H_2 production process [14].

4 Conclusion

We have successfully designed and constructed a novel dual-compartment flat-plate vertical 1 litre photobioreactor to facilitate biophotolytic H_2 production. The primary compartment holds the algal culture and contains the key measuring instruments, including the membrane-inlet mass spectrometer system developed for *in situ* H_2 detection and extraction. The secondary compartment is used to control the system temperature and wavelength. The reactor enables quick measurements of the key parameters in the biohydrogen production process under carefully controlled conditions. Preliminary growth and H_2 production experiments are now underway in the reactor.

Acknowledgements

We would like to thank Paul Crudge, whose technical knowledge was instrumental in the flat-plate reactor design and construction process. The Solar Hydrogen project is funded by the UK Engineering and Physical Sciences Research Council (EPSRC).

References

[1] Ghirardi ML, Zhang L, Lee JW, Flynn T, Seibert M, Greenbaum E, Melis A. Microalgae: a green source of renewable H_2. *Trends in Biotechnology* 2000; 18(12):506-511.

[2] Melis A. Green algal hydrogen production: progress, challenges and prospects. *International Journal of Hydrogen Energy* 2002; 27(11-12):1217-1228.

[3] Akkerman I, Janssen M, Rocha J, Wijffels RH. Photobiological hydrogen production: photochemical efficiency and bioreactor design. *International Journal of Hydrogen Energy* 2002; 27(11-12):1195-1208.

[4] Carvalho AP, Meireles LA, Malcata FX. Microalgal reactors: a review of enclosed system design and performances. *Biotechnology Progress* 2006; 22(6):1490-1506.

[5] Ugwu CU, Aoyagi H, Uchiyama H. Photobioreactors for mass cultivation of algae. *Bioresource Technology* 2008; 99(10):4021-4028.

[6] Borowitzka MA. Commercial production of microalgae: ponds, tanks, tubes and fermenters. *Journal of Biotechnology* 1999; 70(1-3):313-321.

[7] Tsygankov AA. Laboratory scale photobioreactors. *Applied Biochemistry and Microbiology* 2001; 37(4):333-341.

[8] Janssen M, Tramper J, Mur LR, Wijffels RH. Enclosed outdoor photobioreactors: light regime, photosynthetic efficiency, scale-up and future prospects. *Biotechnology and Bioengineering* 2003; 81(2):193-210.

[9] Hankamer B, Lehr F, Rupprecht J, Mussgnug JH, Posten C, Kruse O. Photosynthetic biomass and H_2 production by green algae: from bioengineering to bioreactor scale-up. *Physiologia Plantarium* 2007; 131(1):10-21.

[10] Sierra E, Acien FG, Fernandez JM, Garcia JL, Gonzales C, Molina E. Characterization of a flat plate photobioreactor for the production of microalgae. *Chemical Engineering Journal* 2008; 138(1-3):136-147.

[11] Cournac L, Mus F, Bernard L, Guedeney G, Vignais P, Peltier G. Limiting steps of hydrogen production in *Chlamydomonas reinhardtii* and *Synechocystis* PCC 6803 as analysed by light-induced gas exchange transients. *International Journal of Hydrogen Energy* 2002; 27(11-12):1229-1237.

[12] Skjanes K, Knutsen G, Kallqvist T, Lindblad P. H_2 production from marine and freshwater species of green algae during sulphur deprivation and considerations for bioreactor design. *International Journal of Hydrogen Energy* 2008; 33(2):511-521.

[13] Nedbal L, Trtilek M, Cerveny J, Komarek O, Pakrasi HB. A photobioreactor system for precision cultivation of photoautotrophic microorganisms and high-content analysis of suspension dynamics. *Biotechnology and Bioengineering* 2008; 100(5):902-910.

[14] Hemschemeier A, Melis A, Happe T. Analytical approaches to photobiological hydrogen production in green algae. *Photosynthesis Research* 2009; 102(2-3):523-540.

Photobiotechnological Hydrogen Production with Microalgae

Florian Lehr, **Clemens Posten**, Karlsruhe Institute of Technology (KIT), Institute of Engineering in Life Sciences, Department Bioprocess Engineering, Karlsruhe, Germany
Georg Schaub, Karlsruhe Institute of Technology (KIT), Engler-Bunte Institut, Department Chemistry and Technology of Fossil and Renewable Fuels, Karlsruhe, Germany
Olaf Kruse, Bielefeld University, Center for Biotechnology (CeBiTec), Bielefeld, Germany

Abstract
Hydrogen derived from water has been identified as one of the most promising sources of clean fuel for the future. However, the viability of a future hydrogen economy critically depends upon the development of efficient, large-scale and sustainable hydrogen production systems. This has drawn attention to certain green algae like *C. reinhardtii*, which have evolved the ability to use solar energy to produce hydrogen from water.

1 Basics

Towards the end of the 1930s Gaffron and co-workers discovered that under certain conditions unicellular green algae are able to produce hydrogen during illumination [1, 2]. Subsequently the hydrogenase enzymes, which catalyze the recombination of protons and electrons to form molecular hydrogen, were shown to have a high specific activity [3, 4]. However, the algal hydrogenase was found to be highly sensitive to oxygen inhibition. In fact, it was not until the ground breaking work of Melis and co-workers in 2000 that this challenge was overcome through the cyclical depletion and repletion of liquid C. reinhardtii cultures with sulfur [5]. The underlying principle is that solar powered hydrogen production by green algae can be divided into two stages (see figure 1):

During the first aerobic stage, the algae cells are cultivated photoautotrophically in order to produce biomass. Thereby, water is splitted into oxygen, electrons and protons. The energy of the photosynthetic charge separation reactions is used to synthesize carbohydrates from carbon dioxide.

Finally, the initiation of a sulfur deprivation leads to anaerobiosis, which induces the subsequent hydrogen production stage. As sulfur is needed for amino acid synthesis, protein synthesis cannot function properly in sulfur depleted medium and therefore degraded proteins cannot be replaced properly. This particularly affects proteins with high turn-over rates such as the D1 protein, a key component of photosystem II (PSII) [6]. Thus in the absence of sulfur, the water splitting reaction of PSII can not be maintained at high levels. Consequently, oxygen production decreases over time. Simultaneously, oxygen consumption via oxidative respiration results in an overall reduction of cellular oxygen concentration and

ultimately leads to the onset of hydrogenase mediated H_2 production [5]. Thus, hydrogenases serve as terminal acceptors for electrons of the photosynthetic water-splitting reaction and electrons from starch degradation as well during anaerobic conditions.

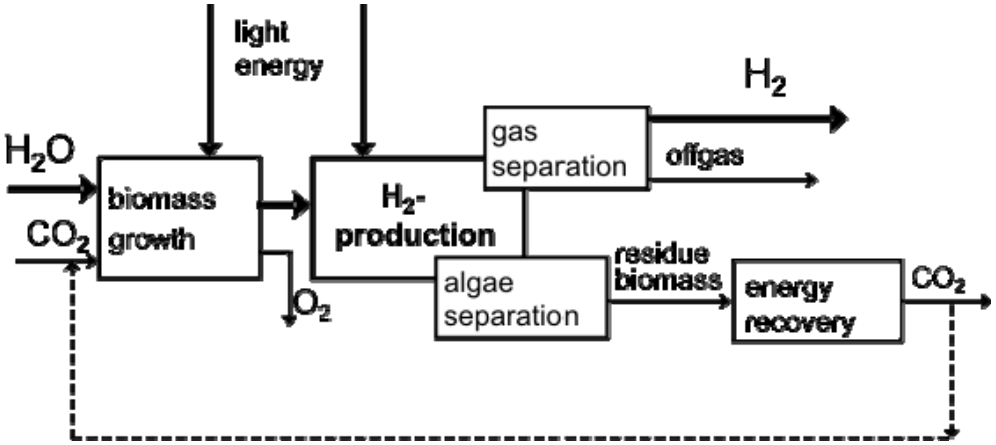

Figure 1: Microalgal hydrogen production – a two-stage process.

2 From Molecular Biology to Bioprocess Engineering

Recently, several micro algae mutant strains related to biohydrogen production have been isolated in different laboratories. One of these is *C. reinhardtii* stm6, which shows increased starch levels and a block in state transitions of the light harvesting complexes resulting in a substantial increase in H_2 production capacity. This strain was calculated to have a photon to hydrogen conversion efficiency of approximately 2% at 20 W/m² in the presence of acetate [7], which is a significant increase compared to wildtype strains. This necessitates the development of appropriate reactor systems and process management strategies to make this process viable also under an economic point of view [8]. In order to generate a data basis for substantiated profitability analyses, precise growth and hydrogen production kinetics are investigated in an ongoing research project [9].

To be able to measure precise phototrophic kinetics, a new reactor system has been developed (see figure 2). This was inevitable due to the fact that light quality and distribution within the photobioreactor is of fundamental importance, as all phototrophic microorganisms need light as an energy source. But due to absorption and shading effects, light intensity drops exponentially from the surface to the centre of the reactor. This results in an uneven light distribution inside the reactor, thus leading to imprecise kinetic data. Due to the special geometry of a new designed LED-lighting system, light is focused to the centre of a 2L-model reactor, which partly compensates the shading effects of the cells and therefore results in an almost homogenous light distribution inside the reactor at moderate cell densities.

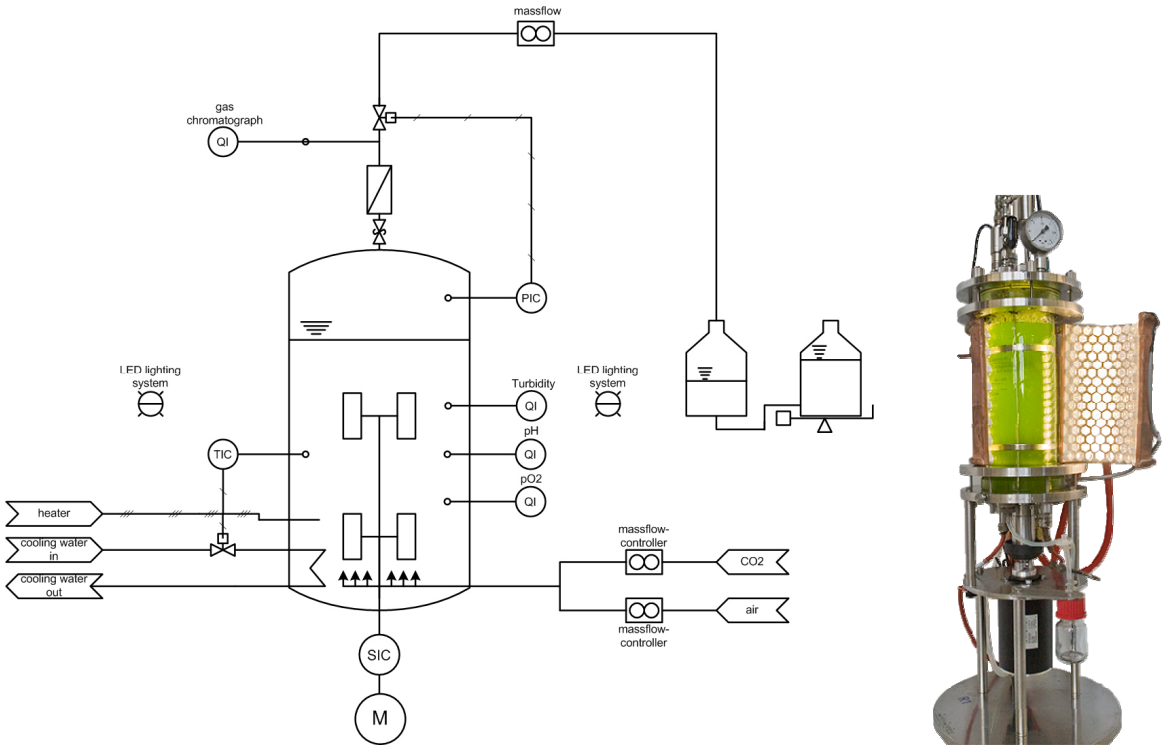

Figure 2: Process flowsheet and photo of the 2L model photobioreactor.

In technical scale, the crucial process step is the establishment of a sulfur deprivation after biomass growth. An exchange of the culture media, as done in laboratory scale, is not economically applicable for large scale. Therefore, two different approaches to initiate hydrogen production in large scale have been developed. The basic underlying principle is to add just as much sulfate as the cells need for biomass growth which leeds to a self-desulfatisation at the end of the first process stage. This can either be realized by a fed-batch or a well balanced batch approach as well. Figure 3 shows exemplarily the transition from biomass growth to the hydrogen production stage via fedbatch approach.

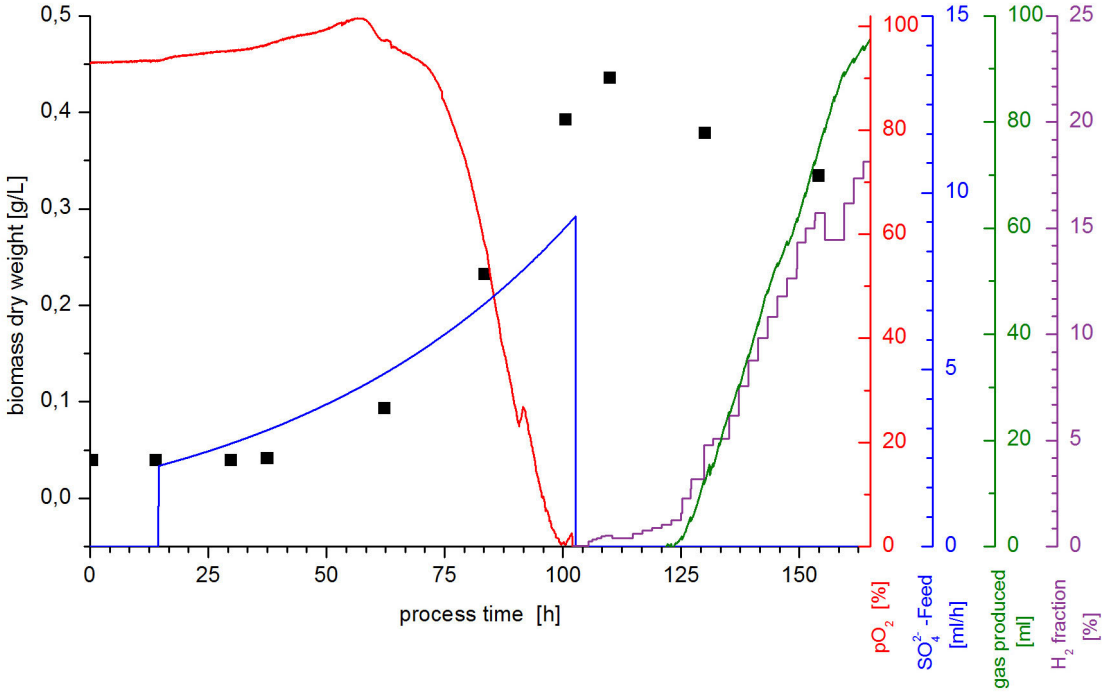

Figure 3: Transition from biomass growth to hydrogen production stage via fed-batch approach.

As can be seen in figure 3, without having sulfate in the basic nutrient solution, biomass growth is clearly controlled by the exponential sulfate-feed. Feeding parameters were adjusted to achieve minimum free sulfate concentration in the culture medium, resulting in an immediate sulfate limitation with stopping the feed flux (see approx. t=100 h, figure 3). Due to this sulfate limiting conditions, the dissolved oxygen concentration (pO_2) of the culture drops continuously and reaches zero with the ending of the sulfate feeding. After a short transition phase, gas production starts with increasing hydrogen fraction of total gas volume (produced gas plus residual gas of the reactor system). These results clearly show that hydrogen production can be induced without expensive exchange of the culture medium.

Similar results were obtained by applying a sulfate-limited batch approach, in which the sulfate amount of the nutrient solution was calculated precisely in order to yield a given biomass concentration. Thus, a self-desulfatisation during biomass growth has been achieved (see figure 4).

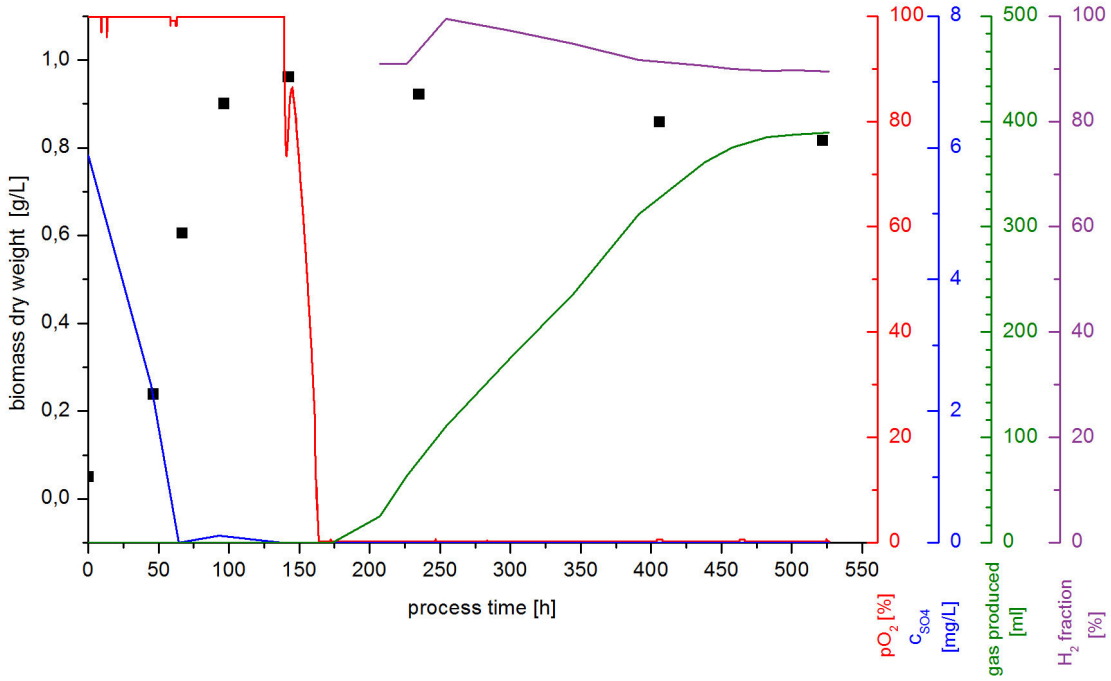

Figure 4: Sulfate-limited batch cultivation of *C. reinhardtii* with subsequent hydrogen production.

With depleting sulfate concentration, biomass growth stops and anoxia is reached. This leads to the transition to the hydrogen production stage, which lasts approximately 300 hours with a hydrogen fraction of the produced gas around 90%.

This new experimental setup is currently used to investigate the hydrogen production kinetics as a function of irradiation. Together with already measured growths kinetics (data not shown), this should lead to precise data sets for an economical assessment of the process. Therefore, these data sets can be fed into mathematical models to evaluate different geographical locations concerning biomass and hydrogen yield on the basis of solar radiation and temperature distribution.

References

[1] Gaffron, H., The reduction of carbon dioxide with molecular hydrogen in green algae. *Nature (London, United Kingdom)* 1939, *143*, 204-205.

[2] Gaffron, H., Rubin, J., Fermentative and photochemical production of hydrogen in algae. *J. Gen. Physiol.* 1942, *26*, 219-240.

[3] Happe, T., Naber, J. D., Isolation, characterization and N-terminal amino acid sequence of hydrogenase from the green alga Chlamydomonas reinhardtii. *European Journal of Biochemistry* 1993, *214*, 475-481.

[4] Florin, L., Tsokoglou, A., Happe, T., A novel type of iron hydrogenase in the green alga Scenedesmus obliquus is linked to the photosynthetic electron transport chain. *Journal of Biological Chemistry* 2001, *276*, 6125-6132.

[5] Melis, A., Zhang, L. P., Forestier, M., Ghirardi, M. L., Seibert, M., Sustained photobiological hydrogen gas production upon reversible inactivation of oxygen evolution in the green alga Chlamydomonas reinhardtii. *Plant Physiology* 2000, *122*, 127-135.

[6] Ohad, I., Kyle, D. J., Arntzen, C. J., Membrane protein damage and repair - removal and replacement of inactivated 32 kilodalton polypeptides in chloroplast membranes. *Journal of Cell Biology* 1984, *99*, 481-485.

[7] Kruse, O., Rupprecht, J., Bader, K. P., Thomas-Hall, S.*, et al.*, Improved photobiological H2 production in engineered green algal cells. *Journal of Biological Chemistry* 2005, *280*, 34170-34177.

[8] Lehr, F., Posten, C., Closed photo-bioreactors as tools for biofuel production. *Curr. Opin. Biotechnol.* 2009, *20*, 280-285.

[9] Hankamer, B., Lehr, F., Rupprecht, J., Mussgnug, J. H.*, et al.*, Photosynthetic biomass and H2 production by green algae: from bioengineering to bioreactor scale-up. *Physiol. Plant.* 2007, *131*, 10-21.

Hydrogen Production by Photosynthetic Bacteria *Rhodobacter capsulatus* Hup$^-$ Strain on Acetate in Continuous Panel Photobioreactors

Dominic Deo Androga, Department of Chemical Engineering, Middle East Technical University, Ankara, Turkey
Ebru Ozgur, **Inci Eroglu**, Department of Chemical Engineering, Middle East Technical University, Ankara, Turkey
Ufuk Gündüz, Department of Biology, Middle East Technical University, Ankara, Turkey

Abstract

Photobiological hydrogen production from organic acids occurs in the presence of light and under anaerobic conditions. Stable and optimized operation of the photobioreactors is the most challenging task in the photofermentation process. The aim of this study was to achieve a stable and high hydrogen production on acetate, using the photosynthetic bacteria *Rhodobacter capsulatus* Hup$^-$ (uptake hydrogenase deleted strain) in continuous panel photobioreactors.

An indoor experiment with continuous illumination (1500-2500 lux, corresponding to 101-169 W/m^2) and controlled temperature was carried out in a 8 L panel photobioreactor. A modified form of basal culture media containing 40 mM of acetate and 2 mM of glutamate with a feeding rate of 0.8 L/day was used. Stable hydrogen productivity of 0.7 mmol H_2/l_c.h was obtained, however, biomass decreased during the continuous operation. Further indoor experiments with a biomass recycle and different feed compositions were carried out to optimise the feed composition for a stable biomass and hydrogen production. The highest hydrogen productivity of 0.8 mmol H_2/l_c.h and yield of 88% was obtained in the 40 mM/ 4 mM acetate/glutamate continuously fed photobioreactor for a period of 21 days.

1 Introduction

Rhodobacter capsulatus is a phototrophic gram-negative purple non sulfur (PNS) bacteria that is able to produce molecular hydrogen under anaerobic and nitrogen-limiting conditions (brought about by having a high C/N ratio). It uses light as the primary energy source and organic compounds such as acetate, lactate and malate as carbon sources [1]. It grows optimally at 25°C – 35°C temperature range and pH 6-9 [2].

Hydrogen production by the PNS bacteria is mediated by nitrogenase metalloenzyme. The membrane bound [Ni-Fe] hydrogenase, also termed as the 'uptake hydrogenase' primarily consumes hydrogen [3]. The removal of the uptake hydrogenase enzyme by genetic modification has been shown to improve hydrogen production [4].

The C/N ratio in the feed media is a significant factor in photofermentative hydrogen production. Glutamate is a suitable nitrogen source for *R. capsulatus* [5, 6]. Eroglu et al. 1999). Different organic acids such as lactate, malate, acetate and butyrate have been used

in photofermentative hydrogen production studies [7]. Being a major product of the dark fermentation process, the use of acetate provides a possibility of integrating dark fermentation with photofermentation to achieve high hydrogen yield. This is the concept employed by the Integrated Project "Non-thermal production of pure hydrogen from biomass" (HYVOLUTION), a Sixth EU Framework supported programme which aims to produce hydrogen from locally obtained biomass using combined thermophillic dark fermentation and photofermentation [8].

The aim of this study is to determine the optimum feed composition for high hydrogen production and stable biomass growth using *Rhodobacter capsulatus* YO3 (Hup^-) in a continuously operated panel photobioreactor (CPBR). Acetate and glutamate were used as carbon and nitrogen sources respectively.

2 Materials and Methods

2.1 Bacteria, growth and hydrogen production media

Rhodobacter capsulatus YO3 (Hup^-), an uptake hydrogenase-deleted strain of the *Rhodobacter capsulatus* MT1131 developed by Öztürk *et al*. [4], was used in this study. The inoculum was prepared by growing cells in modified Biebl and Pfennig (BP) medium [9] that contained 20 mM acetate and 10 mM sodium glutamate. The hydrogen production media comprised the modified BP medium with acetate (40-80 mM) and sodium glutamate (2-4 mM). Sterilization of the media was done by autoclaving.

2.2 Procedure

The experiments were carried out in 8 L panel photobioreactors made of transparent acrylic sheets (plexiglass). The photobioreactors were chemically sterilized using hydrogen peroxide solution (3% w/v) and thoroughly rinsed off with distilled water. Argon gas was flushed to make the system anaerobic [10]. 25% freshly grown bacterial inoculants were used at the start-up.

Continuous feeding with a rate of 0.8 L/day was started when bacterial cell density reached the stationary phase (O.D≥1.5 or 0.7 gdcw/l_c). The indoor experiments were carried out under continuous illumination (1500-2500 lux / 101-169 W/m^2) provided by four 60 W tungsten lamps and controlled room temperature. The photobioreactor temperature was maintained between 30-34 $^{\circ}$C. Hydrogen gas evolved was collected in a water filled graduated glass column.

2.3 Analytical methods

The bacterial cell concentration, pH, temperature, light intensity, gas and organic acid analysis were measured as described previously [11].

3 Results and Discussion

3.1 Hydrogen production experiment

A panel photobioreactor was operated in indoor conditions using feed medium containing 40 mM acetate and 2 mM glutamate. Stable hydrogen productivity of 0.7 mmol H_2/ l_c.h was

obtained but biomass decreased from 0.85 gdw/L_c to 0.42 gdw/L_c within 31 days (Figure 1 - Phase II).

Organic acid analyses showed that acetic acid was well utilized for growth and hydrogen production by the photosynthetic bacteria. Lactic and butyric acids were formed in very low concentrations while formic acid accumulated. pH in the photobioreactors ranged between 6.9-7.2 and gas analysis showed that the total gas produced comprised 95% hydrogen with the rest being carbon dioxide.

3.2 Biomass stabilization in the continuous panel photobioreactors

The biomass decrease trend observed during continuous operation showed that the 40 mM/2 mM Ac/Glu hydrogen production medium was insufficient for maintaining stable biomass and hydrogen production. Hence, further experiments with biomass recycle and changing the C/N ratio by altering glutamate (2-4 mM) and acetate (40-80 mM) concentrations in the feed media were carried out.

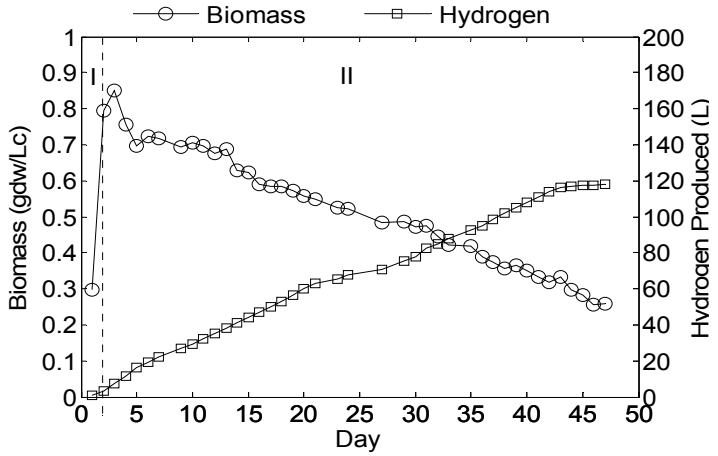

Figure 1: The 40 mM/2 mM Ac/Glu fed indoor CPBR. Phase (I) Startup-Batch, phase (II) Continuous phase.

3.2.1 Biomass recycle

In the biomass recycle experiment, the CPBR effluent was centrifuged, then the pellet was resuspended in hydrogen production medium and fed back into the photobioreactor. Results showed that the biomass recycle was not sufficient to curb the biomass decrease in the CPBR.

3.2.2 Effect of changing C/N ratio

The C/N ratio was decreased by increasing the glutamate concentration in the feed sequentially from 2 mM to 4 mM while maintaining acetate constant at 40 mM. Figure 2 shows the productivities and yields attained. The highest hydrogen productivity (0.8 mmol H_2/ l_c.h) with a stable biomass concentration (0.40 gdw/L_c) was achieved using the 40 mM/4 mM acetate/glutamate containing feed for 21 days. Lactic and butyric acids were formed in very

low concentrations while an increase in formate formation was observed with the increase in glutamate concentration.

In other experiments, The C/N ratio was increased by increasing acetate concentration (40 mM, 60 mM and 80 mM) while keeping the glutamate concentration at 4 mM in the feed. Higher biomass concentrations and lower hydrogen productivities and yields were observed with increasing acetate concentrations (Figure 2). The biomass concentrations obtained were 0.40 gdw/L_c, 0.54 gdw/L_c and 1 gdw/L_c in the 40 mM, 60 mM, and 80 mM acetate fed CPBRs, respectively. Accumulation of acetic acid was observed in the 60 mM and 80 mM acetate fed CPBRs. This shows that continuous systems operating at certain stable biomass concentration have an acetate threshold above which accumulation occurs.

3.2.3 Effect of increasing glutamate and acetate concentration in the feed media keeping C/N ratio constant

The CPBRs fed by the 40 mM /2 mM Ac/Glu, 60 mM /3 mM Ac/Glu and 80 mM /4 mM Ac/Glu (all having C/N= 45) are compared. Higher biomass concentrations were obtained with increasing C and N sources concentration in the feed. However, hydrogen productivity and yield decreased (Figure 2). The highest hydrogen productivity of 0.7 mmol H_2/l_c.h was achieved in the 40 mM /2 mM Ac/Glu CPBR. The other two CPBRs had 0.5 mmol H_2/L_c.h of hydrogen productivity.

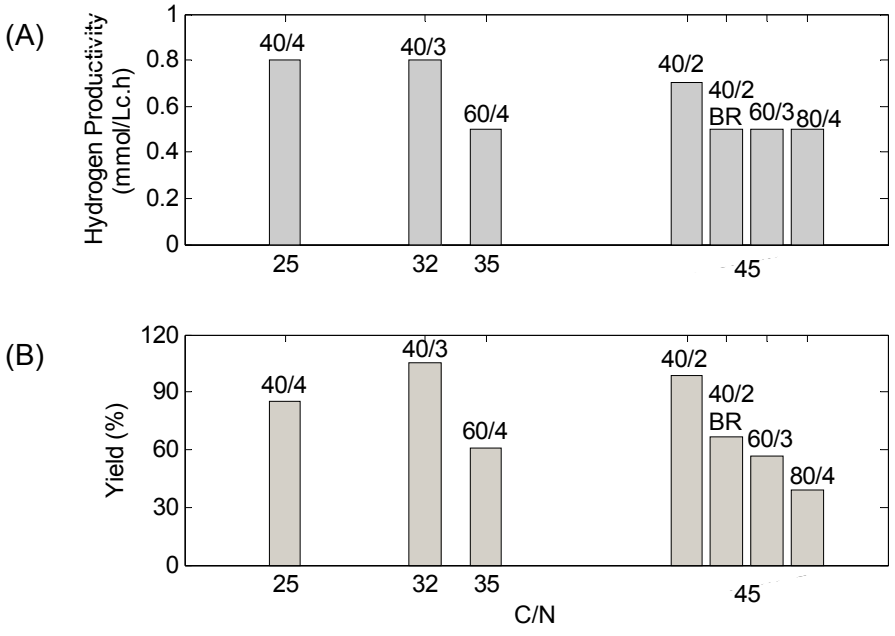

Figure 2: (A) Hydrogen productivity. (B) Yield in the CPBRs operated by different acetate and glutamate containing feeds. (40/4 stands for 40 mM Ac/ 4 mM Glu).

3.3 Light conversion efficiencies in the CPBRs

The light conversion efficiency, which is a percentage measure of the amount of absorbed light energy that is utilized for hydrogen production, was found to range between 0.24-1.21%. Low light conversion efficiency (<10%) has been reported to be the major drawback in photofermentative hydrogen production. Light energy (photons) absorbed is mostly dissipated as heat energy [12].

4 Conclusions

The composition of the feed media is an important factor to be considered in continuous operation. Stable biomass and hydrogen production levels highly depend on the carbon and nitrogen ratio. The optimum C/N ratio of 25 and feed media consisting 40 mM acetate and 4 mM glutamate is recommended in continuously operated photobioreactors with *Rhodobacter capsulatus* YO3 (*Hup*-) strain.

Acknowledgements

This research study was supported by METU (BAP No: 2006-07-020001, BAP No: 07-02-2009-0001) and the EU 6th Framework Integrated Project 019825 (HYVOLUTION).

References

[1] Koku, H., Eroğlu, I., Gunduz, U., Yucel, M., Turker, L., 2002, ‘‘Aspects of the etabolism of Hydrogen Production by *Rhodobacter sphaeroides*’’, Int. J.Hydrogen Energy, 2:1325-1329.

[2] Sasikala, K., Ramana, C.V., Rao, PR.., Kovacs, K.L., 1993, ‘‘Anoygenic Phototropic Bacteria: Physiology and Advances in Hydrogen Production Technology,’’ Advanced Applied Microbiolog., 38:211-295.

[3] Vignais P.M., Jean-Pierre Magnin, John C.Willison, Increasing biohydrogen production by metabolic engineering, International Journal of Hydrogen Energy 31 (2006) 1478 – 1483.

[4] Öztürk Y., Yücel M., Daldal F., Mandacı S., Gündüz U., Türker L., Eroglu I., 2006, ‘‘Hydrogen Production by using *Rhodobacter capsulatus* Mutants with Genetically Modified Electron Transfer Chains’’, Int. J. Hydrogen Energy, 31:1545–52. Biebl, H., Pfennig, N., 1981, “Isolation of Members of the Family *Rhodosprillaceae*.”, In: The prokaryotes. Editors: Starr, M.P., Stolp, H., Trüper, H.G., Balows, A., Schlegel, H.G., New York: Springer-Verlag, 267-273.

[5] Hillmer, P., Gest, H., 1977, “Hydrogen metabolism in the Photosynthetic Bacterium *Rhodopseudomonas capsulata*: Hydrogen Production by Growing Cultures”, J. Bacteriol.,129: 724-731.

[6] Eroglu, I., Aslan, K., Gündüz, U., Yücel, M., Türker, L., 1999, ‘‘Substrate Consumption Rates for Hydrogen Production by *Rhodobacter sphaeroides* in a Column Photobioreactor’’, J. Biotechnol. 70: 103–113.

[7] Li, Ru Ying, Fang, Herberth H.P., 2009, ‘‘Heterotrophic Photo Fermentative Hydrogen Production’’, Critical Reviews in Environmental Science and Technology, 39: 12, 1081 – 1108.

[8] Claassen P.A.M., Vrije T., 2006, ‘‘Non-thermal Production of Pure Hydrogen from Biomass: HYVOLUTION’’, Int. Journal of Hydrogen Energy, 31: 1416 – 1423.

[9] Biebl, H., Pfennig, N., 1981, “Isolation of Members of the Family *Rhodosprillaceae*.”, In: The prokaryotes. Editors: Starr, M.P., Stolp, H., Trüper, H.G., Balows, A., Schlegel, H.G., New York: Springer-Verlag, 267-273.

[10] Eroglu I, Tabanoglu A., Gündüz U., Eroglu E, Yücel M. Hydrogen production by Rhodobacter sphaeroides O.U.001 in a flat plate solar bioreactor. Int J Hydrogen Energy 2008;33:531–41.

[11] Koku H, Eroglu I., Gunduz U., Yucel M., Turker L., Kinetics of biological hydrogen production by *Rhodobacter sphaeroides* OU001. Int J Hydrogen Energy 2003;28(4):381–8.

[12] Akkerman, I., Janssen, M., Rocha, J., Wijffels, R.H., 2002, “Photobiological hydrogen Production: Photochemical Efficiency and Bioreactor Design”, Int. J. Hydrogen Energy, 27: 1195 – 1208.

Hydrogen Production by *Anabaena* sp. CH1 with Two-stage Process

Pei-Chung Chen, Institute of Clinical Nutrition, Hung Kuang University, Taichung, Taiwan
Chang-Ling Chiang, **Chi Mei Lee**, Department of Environmental Engineering, National Chung Hsing University, Taichung, Taiwan

1 Introduction

Hydrogen can be produced by cyanobacteria normally under anoxic conditions without nitrogen [1, 2]. *Anabaena* sp. Ch1 (cyanobacteria) can produce hydrogen with extra addition of fructose as energy source [3]. During hydrogen production process, nitrogen is exhausted gradually and chlorophylls may break down to provide the nitrogen. This phenomenon is unfavorable for a long term operation of bio-hydrogen production by cyanobacteria. In this research, this problem can be solved through a two-stage operation (hydrogen production stage and recovery stage as Fig. 1).

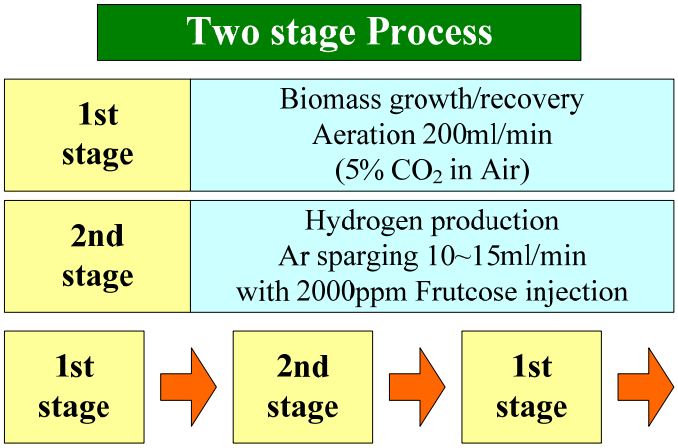

Figure 1: Conditions and sequences of two stage process.

2 Material and Methods

1. Cyanobacteium *Anabaena* sp. CH1 was isolated from Taiwan paddy soils. CH1 cells are cultivated under artificial Arnon medium with 5% CO_2 and 250 μmole/m^2/s light intensity [4]. CH1 will take nitrogen gas in ambient air as nitrogen source and produce nitrate through nitrogenase for cell growth. CH1 will also take CO_2 to produce sugar through photosynthesis [5]. So, in the first stage, we call it biomass growth or recovery stage and in the second stage the hydrogen production stage (Fig. 2).

2. When CH1 cells grow to late log-growth phase, the upper part is flushed with argon gas to create an anaerobic condition in order to change to hydrogen production stage when 2000 ppm fructose is added (Fig. 2).
3. During the two stage process, chlorophyll a, fructose, COD, MLSS and gas carbon dioxide, hydrogen was measured [6, 7, 8, 9].
4. Five liter photo-bioreactor is designed by our laboratory.

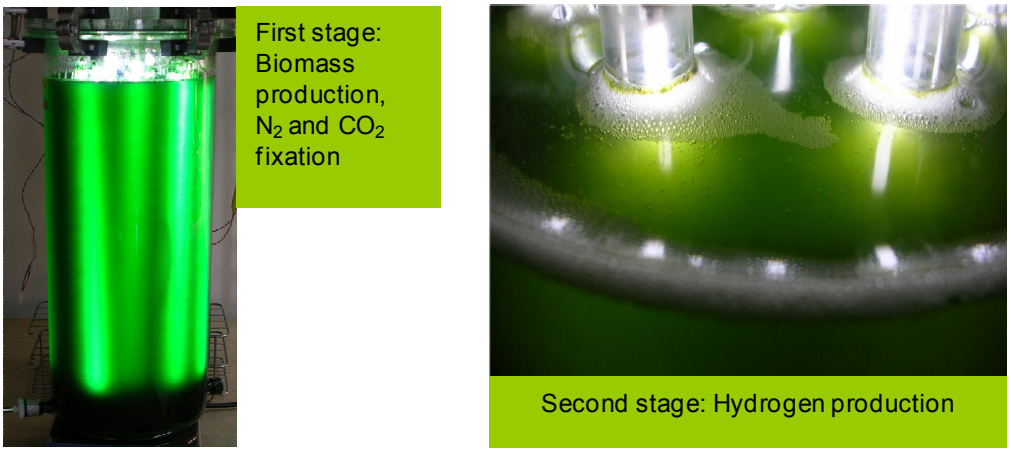

Figure 2: Purpose and image of each stage.

3 Results

During the H_2 production stage, chl-a and specific chl-a (chl-a to MLSS ratio) decreased to 77.2% and 67.5% after aeration with argon for 3 days (Table 1). After operation of hydrogen production for 3-7 days, the cells shifted to normal growth condition (aeration with air+5% CO_2). Within 4 days, cells recovered completely, and then cells shifted again to H_2 production stage. The H_2 production rate was as high as the original rate. This indicated that the effects of nitrogen deprivation on the photosynthetic mechanisms were recoverable and the cells were able to produce H_2 in a cyclic way. The hydrogen production rate is 76.4 μmol/mg chl-a/h. After two cycles, that is twice 2000 ppm fructose is exhausted, the accumulative hydrogen amount is 18.7 liter in a five liter bioreactor, i.e. 1.9 L per day (Fig. 3).

At the recovery stage strain CH1 captured CO_2 and transformed to carbohydrates or cell materials by photosynthetic reaction [10]. The average carbon fixing rate of strain CH1 with 5% CO_2 and illumination was 933.3 mg CO_2/L/day. However, the average carbon release rate at H_2 production stage was 406.4 mg CO_2/L/day. The net carbon sequestration of two-stage process is positive. Therefore, this kind of energy production is useful to eliminate CO_2 emission.

Table 1: **Variation of Chlorophyll a content, MLSS content and specific chl-a ratio at the end of each stage in two operation runs.**

End of each stage	Chl-a (mg/L)	MLSS (mg/L)	Specific chl-a ratio (%)
1st Stage of 1st Run	12.66	738	1.72
2nd Stage of 1st Run	10.27	795	1.29
1st Stage of 2nd Run	18.44	1079	1.71
2nd Stage of 2nd Run	15.36	1244	1.23

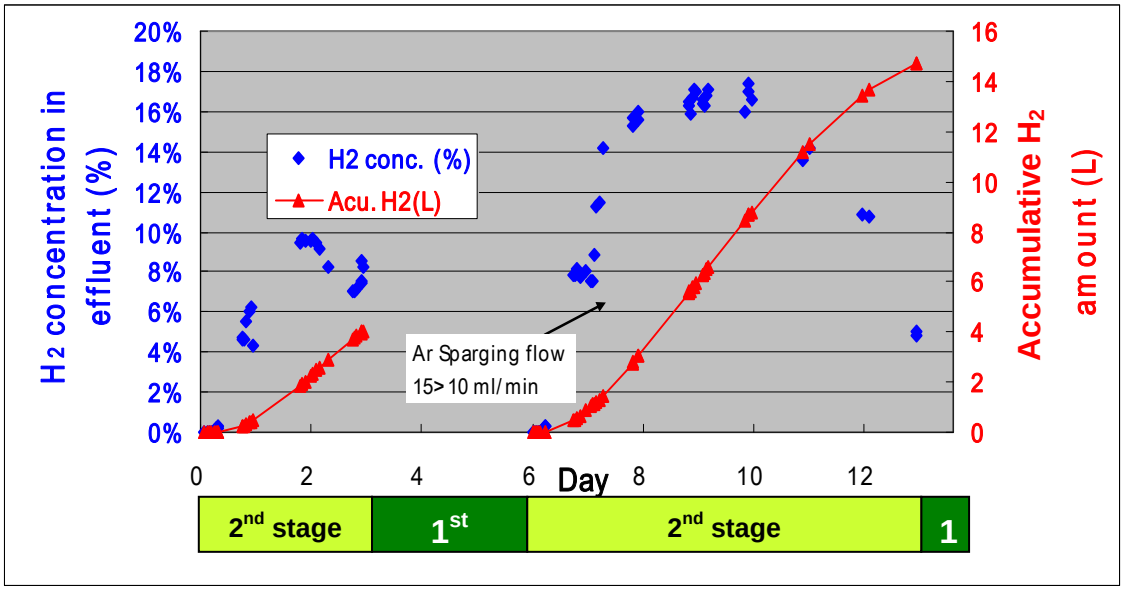

Figure 3: **The H_2 concentration and accumulative H_2 amount during two-run operations.**

References

[1] AA Tsygankov, AS Fedorov, SN Kosourov, KK Rao, (2002), Hydrogen production by cyanobacteria in an automated outdoor photobioreactor under aerobic conditions, Biotechnology and Bioengineering, 80, 777–783.

[2] D Dutta, D De, S Chaudhuri, SK Bhattacharya, (2005), Hydrogen production by Cyanobacteria, Microbial Cell Factories 4, 1 – 11

[3] V Shah, N Garg, D Madamwar, (2001), Ultrastructure of the fresh water cyanobacterium *Anabaena variabilis* SPU 003 and its application for oxygen-free hydrogen production, FEMS Microbiology Letters 194, 71-75.

[4] H Berberoğlu, J Jay, L Pilon, (2008), Effect of nutrient media on photobiological hydrogen production by *Anabaena variabilis* ATCC 29413, International Journal of Hydrogen Energy, 33, 1172-1184.

[5] C Stewart, MA Hessami, (2005), A study of methods of carbon dioxide capture and sequestration—the sustainability of a photosynthetic bioreactor approach, Energy Conversion and Management 46, 403–420.

[6] RJ Porra, WA Thompson, PE Kriedemann, (1989), Determination of accurate extinction coefficients and simultaneous equations for assaying chlorophylls a and b extracted with four different solvents: verification of the concentration of chlorophyll standards by atomic absorption spectroscopy, Biochimica et biophysica acta 975, 384-394.

[7] LY Liu, JF Kaow, MM Lee, (1997), Simple and Rapid Method for the Determination of Fructose in Fructose Syrup. Shih Chien Journal 28, 1-15.

[8] R Schumann, N Häubner, S Klausch, U Karsten, (2005), Chlorophyll extraction methods for the quantification of green microalgae colonizing building facades, International Biodeterioration & Biodegradation 55, 213–222.

[9] RJ Ritchie, (2006), Consistent sets of spectrophotometric chlorophyll equations for acetone, methanol and ethanol solvents, Photosynth Res 89, 27–41.

[10] K Skjånes, P Lindblad, J Muller (2007), BioCO_2 – A multidisciplinary, biological approach using solar energy to capture CO_2 while producing H_2 and high value product, Biomolecular engineering 24, 405-413.

The Effect of Temperature and Light Intensity on Hydrogen Production by *Rhodobacter Capsulatus*

Inci Eroglu, Middle East Technical University Dept. of Chemical Engineering Ankara Turkey
Pelin Sevinç, Middle East Technical University Dept. of Biotechnology Ankara Turkey
Ufuk Gündüz, **Meral Yucel**, Middle East Technical University Dept. of Biological Sciences Ankara Turkey

Abstract

Rhodobacter capsulatus is a purple non-sulfur photosynthetic bacterium which can produce hydrogen by photofermentation on acetate and lactate. Hydrogen productivity depends on several parameters such as medium composition, pH, light intensity and temperature. In the present study, the effects of temperature and light intensity on hydrogen production were investigated. The cell growth curve has been fitted to the logistic model and hydrogen productivity was interpreted by Modified Gompertz Equation. The maximum productivity was obtained at 30°C and light intensity of 4000 lux.

1 Introduction

Hydrogen production by purple non sulphur (PNS) bacteria is mediated by nitrogenase enzyme. There are several factors affecting the activity of nitrogenase enzyme. The required energy for hydrogen production is provided by the conversion of light energy to ATP by photosynthetic membrane apparatus [1]. Nitrogenase enzyme synthesis is strongly stimulated by light. Hence, the light intensity to which the cells are exposed is a very important factor for hydrogen production [2]. Another parameter that strongly affects hydrogen production is temperature. Sasikala et al, [3] have reported the maximum productivity at 5000 lux and 30°C. Özgür et al. [4] have simulated the outdoor conditions and approved that the hydrogen productivity decrease with fluctuating temperatures compared to the productivity obtained at 30°C. Therefore, temperature and light intensity have simultaneous affects on the nitrogenase enzyme synthesis and the activity. The objective of the present study is to obtain phenomenological models to interpret the kinetics of the cell growth and the hydrogen productivity by *Rhodobacter capsulatus* on acetate and lactate, for scale-up purposes in the outdoor applications.

2 Materials & Methods

In this study *Rhodobacter capsulatus* (DSM 1710) was used. Bacteria were inoculated to modified Biebl and Pfennig medium [5] for activation (20 mM acetate, 7.5 mM lactate, 10 mM glutamate). For hydrogen production experiments the activated bacteria were inoculated into hydrogen production medium (40 mM acetate, 7.5 mM lactate, 2 mM glutamate) with 10% inoculation. All experiments were done in 50 ml glass bottles (photobioreactors). In order to

keep the system anaerobic, argon gas was flushed to photobioreactors. All photobioreactors were connected to water filled graduated cylinders by capillary tube and produced hydrogen was measured volumetrically by water replacement method [2].

The photobioreactor (PBR) was placed in an incubator. The incubator temperature was adjusted to 20°C, 30°C and 38°C.The medium temperature of the photobioreactors were determined by a digital thermometer and it was 22±2, 32±2 and 40±2 respectively. The light intensities exposed to the PBR were 1500, 2000, 3000, 4000 and 5000 lux. PBR was illuminated by a tungsten lamp (75-100W). Light intensity was measured by a luxmeter. Liquid and gas samples were taken periodically from the PBR. pH was analysed by using a pH-meter (Testo 830 T-2). Biomass was determined spectrophotometrically at 660nm (Shimadzu UV-1201 Spectrophotometer). Gas composition was analyzed by a Gas Chromotography. (Agilent Technologies 6890N Supelco Carboxen 1010 column). Curves in kinetic analyses were drawn by use of CurveExpert 1.3.

3 Results

3.1 The effect of light intensity and temperature on hydrogen productivity and substrate conversion efficiency

Figure 1 illustrates the hydrogen productivity in terms of mmoles/L.h at different temperatures and at different light intensities. The results indicate that the highest hydrogen productivity is achieved at 30°C, at all light intensities. The substrate conversion efficiency is seen to steadily increase in parallel with increase in light intensity at 20°C. The highest value is obtained at 30°C for 3000 lux light intensity (Figure 2). Substrate conversion efficiency at any light intensity is seen to be the lowest at 38°C.

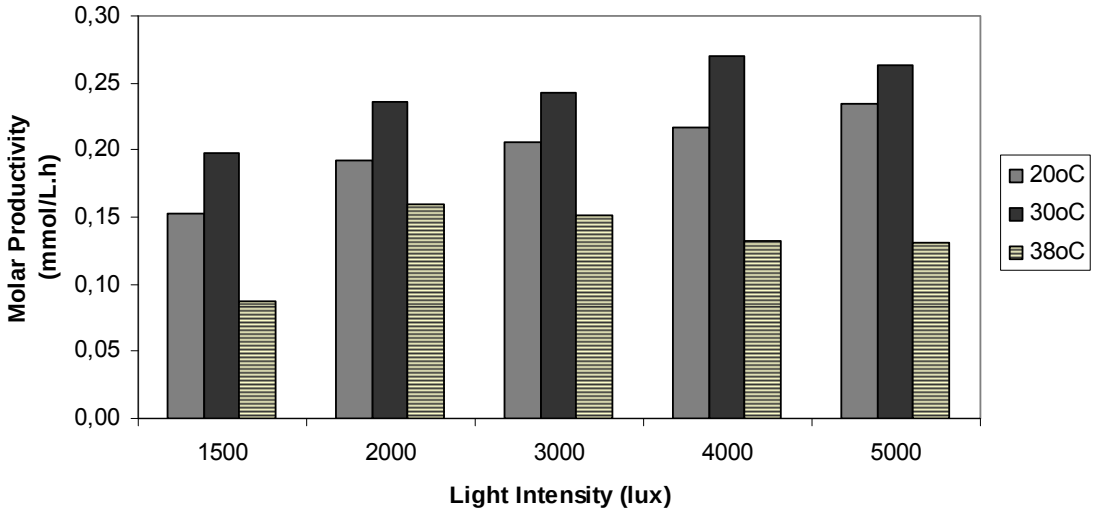

Figure 1: Hydrogen Productivity obtained at different temperatures and light intensities.

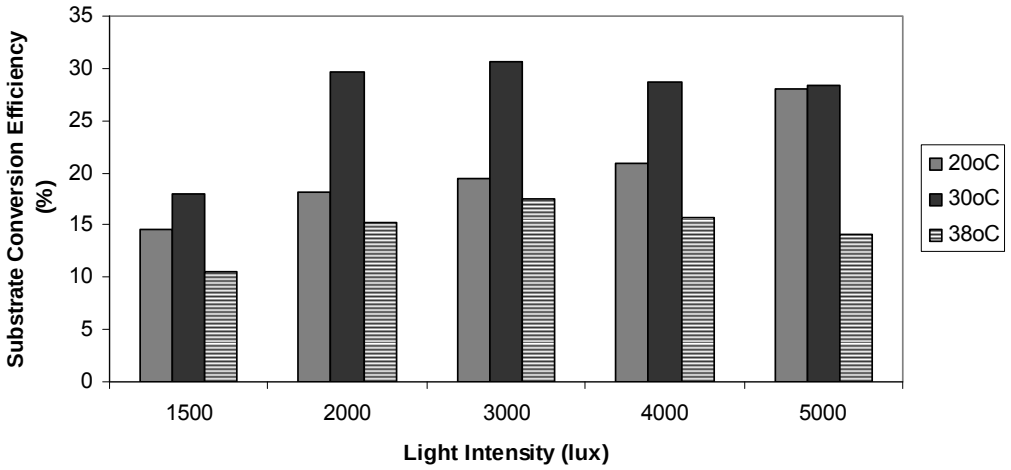

Figure 2: Substrate Conversion Efficiencies for hydrogen production by *R. capsulatus* at different temperatures and light intensities.

3.2 The effect of light intensity and temperature on cell growth

Figure 3 illustrates the maximum biomass values for different light intensities at 20°C, 30°C and 38°C. The maximum biomass concentration decreases with increasing light intensity at 20°C. Whereas, at 38°C biomass concentration increases with increasing light intensity. At 30°C, maximum biomass concentration decreases with increasing light intensity up to 4000 lux, however it increases at 5000 lux. The trends for hydrogen production and maximum cell growth values appear to be in opposite directions.

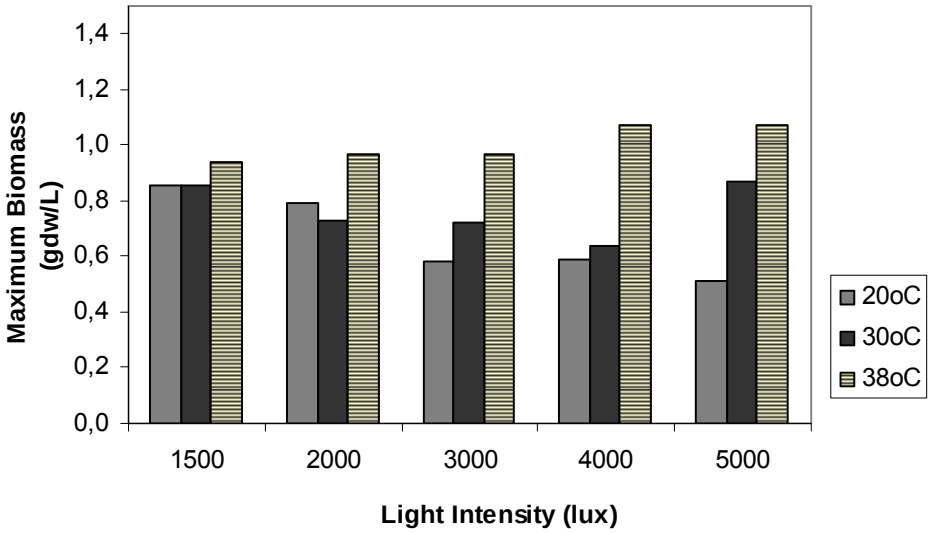

Figure 3: Maximum biomass values of *R. capsulatus* at different temperatures and light intensities.

3.3 Cell growth kinetics

The cell growth of PNS bacteria generally fits to the logistic model [6, 7]. The growth rate for the logistic model is expressed as:

$$dX/dt=k_cX(1-X/X_{max})$$

After integration of this equation the model equation becomes,

$$X=X_{max}/ [1+\exp (-k_c.t) (X_{max}/X_o-1)]$$

where X is the dry cell weight (g/L), X_{max} is the maximum dry cell weight (g/L), X_o is the initial bacterial concentration (g/L), t is time (h) and k_c is the apparent specific growth rate (h^{-1}).

In this study cell growth data were tested whether they would fit to the model equation given above. Correlation of determination (r) values obtained between 0.93 and 0.98 which indicated that the logistic model can be used to express the cell growth in the photobioreactors for all light intensities and all temperatures.

3.4 Hydrogen production kinetics

There are different models to express hydrogen production in literature. Among them Modified Gompertz Equation widely used to describe the changes on hydrogen production [7]. The Modified Gompertz Equation is given below:

$$H= H_{\max} \exp\left[-\exp\left(\frac{R_{\max}.e}{H_{\max}}.(\lambda - t) + 1 \right) \right]$$

Where H is cumulative hydrogen produced (mmole), H_{max} is hydrogen production potential (mmole), R_{max} is the maximum production rate (mmole/h) λ is the lag time (h). e is a constant (2.718282)

In this study Modified Gompertz Equation was used to express the effects of light intensity and temperature on hydrogen production. The extends of correlation values (r) were found to be above 0.98 for all temperatures and light intensities, which indicated a good fit to the model.

4 Discussion

Increasing light intensity resulted in an obvious increase in hydrogen production in comparison to 1500 lux exposure at 30°C. These results are in consistence with previous studies. Uyar et al. [2] demonstrated that the rate of hydrogen production increased with increasing light intensity up to 4000 lux at 30°C for *Rhodobacter sphaeroides* on malate.

Hydrogen production and maximum biomass values appear to be in opposite directions. Maximum biomass is highest for all light intensities at 38°C. This high temperature condition may cause a shift from hydrogen production to cell growth.

There are only a limited number of studies demonstrating the effects of temperature and light intensity on hydrogen production efficiency and kinetics of *R. capsulatus*. The studies of cell growth and hydrogen production kinetics of *R. capsulatus* may provide an insight for further studies and guide for large scale hydrogen production processes.

Acknowledgement

This study is supported by HYVOLUTION (EU 6 th framework Project) and METU BAP

References

[1] Koku H., Eroğlu E., Gündüz U., Yücel M., Türker L., Aspects of the metabolism of hydrogen production by *Rhodobacter sphaeroides.,* International Journal of Hydrogen Energy 2002;27(11-12): 1315-1329

[2] Uyar B., Eroğlu E., Yücel M., Gündüz U., Türker L., Effect of light intensity,wavelength and illumination protocol on hydrogen production in photobioreactors. International Journal of Hydrogen Energy 2007;32: 4670 –7

[3] Sasikala K., Ramana C.V., Rao P.R., Environmental regulation for optimal biomass yield and photoproduction of hydrogen by *Rhodobacter sphaeroides.* International Journal of Hydrogen Energy 1991;16: 597-601

[4] Özgür E., Uyar B., Öztürk Y., Yücel M., Gündüz U., Eroğlu E.,, Biohydrogen production by *Rhodobacter capsulatus* on acetate at flactuating temperatures. Resources, Conservation and Recycling 2010, 54: 310–4

[5] Biebl H., Pfennig N. Isolation of member of the family Rhodosprillaceae. In: Starr MP, Stolp H., Trüper H. G., Balows A., Schlegel H. G., editors. The prokaryotes, vol. 1. New York: Springer; 1981. p. 267–73.

[6] Koku H., Eroglu I., Gunduz U., Yucel M., Turker L., Kinetics of biological hydrogen production by *Rhodobacter sphaeroides* OU001. International Journal of Hydrogen Energy 2003;28(4): 381–8.

[7] Mu Y.,Wang G.,Yu H., Kinetic modeling of batch hydrogen production process by mixed anaerobic cultures. Bioresource Technology 2006;97(11) 1302-7

Photohydrogen Production from Thermophilic Aerobic Digestion Effluent and Distillery Wastewater by Photosynthetic Bacterium *Rhodopseudomonas palustris* WP 3-5

Chi Mei Lee, **Chia-Ling Tsai**, **Chu-Fang Yang**, Department of Environmental Engineering, National Chung Hsing University, Taiwan

1 Introduction

Based on the reserved limitation and environmental consequences of fossil fuel, hydrogen is considered to be one of the most promising clean fuels for the future [1], and can be produced using biological system through exploiting fermentative bacteria, algae, cyanobacteria, and anoxygenic photosynthetic bacteria [2]. Among these hydrogen microproducers, purple nonsulfur photosynthetic bacteria can utilize VFAs as the substrates for growing and producing hydrogen [3]. Thermophilic aerobic digestion (TAD) is a dynamic, new waste-processing technique which uses the heat generated during microbial aerobic metabolism to raise the temperature of waste undergoing treatment in an insulated system to thermophilic levels (45°C). As a relatively new process, it is increasingly being accepted for waste treatment, either in stand-alone processes, or as part of an integrated two-stage process [4]. It was mentioned that when TAD process was modified to be operated under microaerobic condition for sludge digestion, the accumulation of volatile fatty acid (VFAs) was expected [5]. Thus, combining the modified TAD process with photohydrogen production process shall make sludge removal and energy recycle possible. The aim of this research was to investigate the feasibility of biohydrogen production by purple nonsulfur photosynthetic bacterium, strain Rhodopseudomonas palustris WP 3-5, using TAD process effluent.

2 Methods

Before photohydrogen production using TAD process effluent, several strategies were applied to realize optimum operated condition of the TAD process for maximum VFAs accumulation. Moreover, other possible hydrogen production wastewater such as distillery wastewater was also examined. Figure 1 shows the experimental flowchart.

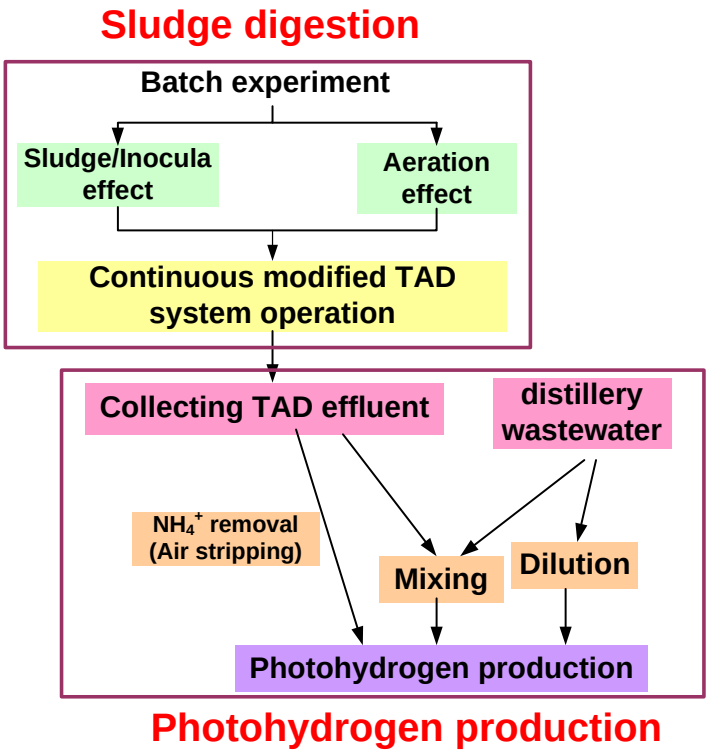

Figure 1: The experimental flowchart.

3 Results

The optimum strategies for maximum VFAs production with TAD process were to inoculate supplementary sludge digestion bacterium *Geobacillus thermocatenulatus* S2 isolated from the sludge produced during the textile industrial wastewater treatment process and control the initial sludge loading concentration: inoculum concentration to 20:1. Moreover, slight aeration (0.25 vvm) caused lower $NH4^+$ accumulation and benefited the followed photohydrogen production. The optimum HRT for better VFAs accumulation was 24 hr, and the continuous TAD process could be maintained at least for 120 hr.

Although the optimum operated conditions of the TAD process were found out, the NH4+-N concentration in the TAD effluent was still too high to inhibit photohydrogen production. In the previous research, photohydrogen production occurred only when the NH4+ concentration was below 17 mg- NH4+/L [6]. Thus, NH4+-N in the TAD effluent was eliminated by pH adjustment and air stripping. When pH value was adjusted to 12.0, NH4+-N concentration could decrease under detection limitation within 17 hr after air stripping. The pretreated TAD effluent was then utilized for photohydrogen production using photosynthetic bacterium R. palustris WP 3-5. The results demonstrated that the highest accumulated hydrogen volume was 25.8 mL (the headspace was 50 mL). Based on high VFAs content but low NH4+-N concentration in the distillery wastewater, we also mixed the distillery wastewater with the TAD effluent for hydrogen production.

The results revealed that the best distillery wastewater:TAD effluent mixed ratio for photohydrogen production was 2:5, and the highest accumulated hydrogen volume and hydrogen production rate (HPR) was 263.9 mL and 12.4 mL H_2/L-culture/hr, respectively.

Moreover, the diluted distillery wastewater was also applied for hydrogen production. When distillery wastewater diluted ratio was 0.4x, the highest accumulated hydrogen volume and HPR were 278.3 mL and 13.06 mL H_2/L-culture/hr, respectively.

4 Conclusion

Comparing the hydrogen producing efficiency of mixed wastewater and diluted distillery wastewater, it was observed that the diluted distillery had better HPR, but the mixed wastewater had higher total accumulated hydrogen volume.

References

[1] Rupprecht, J., B. Hankamer, J.H. Mussgnug, G. Ananyev, C. Dismukes, and O. Kruse, “Perspectives and advances of biological H_2 production in microorganisms,” Applied Microbiology and Biotechnology, Vol. 72, No. 3, pp. 442-449 (2006).

[2] Zabut, B., K. El-Kahlout, M. Yücel, U. Gündüz, L. Türker, and İ. Eroğlu, “Hydrogen gas production by combined systems of *Rhodobacter sphaeroides* O.U.001 and *Halobacterium salinarum* in a photobioreactor,” International Journal of Hydrogen Energy, Vol. 31, No. 11, pp. 1553-1562 (2006).

[3] Lee, C.M., P.C. Chen, C.C. Wang, and Y.C. Tung, “Photohydrogen production using purple nonsulfur bacteria with hydrogen fermentation reactor effluent,” International Journal of Hydrogen Energy, Vol. 27, No. 11-12, pp. 1309-1313 (2002).

[4] Ugwuanyi, J.O., L.M. Harvey, and B. McNeil, (2004) “Protease and xylanase activities and thermophilic populations as potential process monitoring tools during thermophilic aerobic digestion,” Journal of Chemical Technology & Biotechnology Vol. 79, No. 1, pp. 30-38 (2004).

[5] Chu, A., D.S. Mavinic, W.D. Ramey, and H.G. Kelly, “A biochemical model describing volatile fatty acid metabolism in thermophilic aerobic design of wastewater sludge,” Water Research, Vol. 30, pp. 1759-1770 (1996).

[6] Lee, C.M., K.M. Yu, and P.C. Chen, Limiting factors of photo-hydrogen production by *Rhodopseudomonas palustris* WP3-5, In: Antonio Mendez-Vilas (Ed.), Modern Multidisciplinary Applied Microbiology. Wiley-VCH, Weinheim, pp. 236-240 (2006).

Improving the Hydrogen Production Capacity of *Rhodobacter Capsulatus* by Genetically Modifying Redox Balancing Pathways

Yavuz Öztürk, TÜBİTAK Research Institute for Genetic Engineering and Biotechnology, Gebze Kocaeli, Turkey
Abdulmecit Gökçe, Department of Mol. Biology and Genetics, Istanbul Technical University, Turkey
Muazzez Gürgan, **Meral Yücel**, Department of Biology, Middle East Technical University, Turkey

Abstract

In *Rhodobacter capsulatus*, balancing the oxidation-reduction potential (redox-balance) is maintained via a number of inter-dependent regulatory mechanisms that enable these organisms to accommodate divergent growth modes. In order to maintain redox homeostasis, this bacterium possesses regulatory mechanisms functioning as electron sinks affecting the oxidation-reduction state of the ubiquinone pool. Under the photoheterotrophic growth conditions with reduced carbon sources, the excess reducing equivalents are primarily consumed via the reduction of CO_2 through the Calvin–Benson–Bassham (CBB) pathway or by the reduction of protons into hydrogen with the use of dinitrogenase enzyme system. In this study, our aim was to develop strategies to funnel the excess reducing equivalents to nitrogenase-dependent hydrogen production by blocking the carbon-fixation pathway. To realize this purpose, CO_2 fixation was blocked by inactivating the Phosphoribulokinase (PRK) of CBB pathway in wild type (MT1131), uptake-hydrogenase (YO3) and cyt cbb_3 oxidase deficient (YO4) strains. The hydrogen production capacity of newly generated strains deficient in the Calvin-Benson-Bassham pathway were analyzed and compared with wild type strains. The results indicated that, the hydrogen production efficiency and capacity of *R. capsulatus* was further improved by directing the excess reducing equivalents to dinitrogenase-dependent hydrogen production.

1 Introduction

The facultative phototrophic bacterium *Rhodobacter capsulatus* has a number of metabolic pathways to grow under different environmental conditions by performing aerobic respiration, anaerobic respiration, photosynthesis and fermentation [1]. Under photoheterotrophic growth conditions, the oxidation of organic acids (such as malate, acetate and lactate) can result in overreduction of the ubiquinone pool. As cyclic photosynthesis requires oxidized ubiquinone as an electron acceptor, excess reducing equivalents, at the level of the reduced ubiquinone pool are removed by redox-balancing systems [2]. The maintenance of intracellular redox poise was achieved by dissipating reducing equivalents through the CBB cycle, the DMSOR system, or the dinitrogenase system. The CBB pathway, rather than serving as a major means for generating organic carbon under these growth conditions, plays a role in redox

balance of the cell when carbon substrates are oxidized [3]. The dinitrogenase enzyme system, besides its role in nitrogen metabolism, also serves as a redox-balancing system during photoheterotrophic growth under limiting nitrogen sources [4]. Under such conditions, the nitrogenase is activated and the excess reducing equivalents generated by the oxidation of organic acids are consumed by the reduction of protons to molecular hydrogen [5]. Previously, hydrogen production properties of some uptake hydrogenase deleted *R. capsulatus* strains and mutants with genetically modified electron transfer chains were investigated and reported [6, 7]. In this study, we investigate the relationship between the redox balancing system and hydrogen production in various *R. capsulatus* strains deficient in CBB pathway, terminal oxidases and uptake hydrogenase.

2 Materials and Methods

Bacterial Strains and Growth conditions:

The bacterial strains used are described in Table 1. R. *capsulatus* strains were grown on MPYE (magnesium-calcium, peptone, yeast extract) enriched medium [8] and Sistrom's minimal medium A (Med A, containing succinate as carbon and NH_4^+ as nitrogen sources) at 35° C and supplemented with kanamycin, gentamicin and spectinomycin (10, 1, 10 µg per ml, respectively). Ps cultures were incubated under saturating light intensity in anaerobic jars containing H_2 and CO_2 generating gas packs (BBL 270304, Becton Dickenson and Inc). For hydrogen production experiments, the minimal medium of Biebl and Pfennig (BP), supplied with C/N sources (15 mM/2 mM for malate/L-glutamate) without ammonium chloride and yeast extract, was used [9].

Molecular Genetic Techniques

Inactivation of *cbbP* gene*:*

The ∆(*cbbP*::*Spe*) deletion-insertion allele was constructed by replacing the 180 bp *Bam*HI fragment of *cbbP* in plasmid pYO50 with the 2 kb *Bam*HI fragment containing spectinomycin resistance gene, yielding pYO51 (Figure 1). Fragment containing the ∆(*cbbP*::*Spe*) deletion-insertion allele was then cloned in the broad host range plasmid pRK415, yielding pYO52, to transfer the mutant allele to gene transfer agent (GTA) overproducer *R. capsulatus* Y_{262} strain via triparental mating [19]. GTA cross was used to inactivate the chromosomal copy of *cbbP* in *R. capsulatus* MT1131, YO3 (*Hup*$^-$) and YO4 (cyt *cbb*$_3^-$, *Hup*$^-$).

Table 1: *Rhodobacter capsulatus* strains used in this work.

Strain	Genotype	Reference
MT1131	*crtD121*, Wild type, Rif^R	[8]
YO3	*hupSLC*$^-$	[6]
YO4	*hupSLC*$^-$, cyt *cbb*$_3^-$	[6]
YO6	*cbbP*$^-$	This work
YO7	*hupSLC*$^-$, *cbbP*$^-$	This work
YO8	*hupSLC*$^-$, cyt *cbb*$_3^-$, *cbbP*$^-$	This work

3 Results

3.1 Chromosomal inactivation of phosphoribulokinase of *R. capsulatus* strains.

The Phosphoribulokinase deficient (PRK$^-$) derivatives of *R. capsulatus* MT1131 (wild type), YO3 (*hup*$^-$) and YO4 (cyt cbb_3^-, *hup*$^-$) strains were obtained by gene transfer agent (GTA) crosses yielding the strains YO6, YO7 and YO8, respectively (Table 1). Chromosomal inactivation of *cbbP* in these strains was confirmed by PCR amplification of the Δ*cbbP*::Spe allele and by photosynthetic phenotypes in a NH_4^+ containing minimal medium (Figure 1).

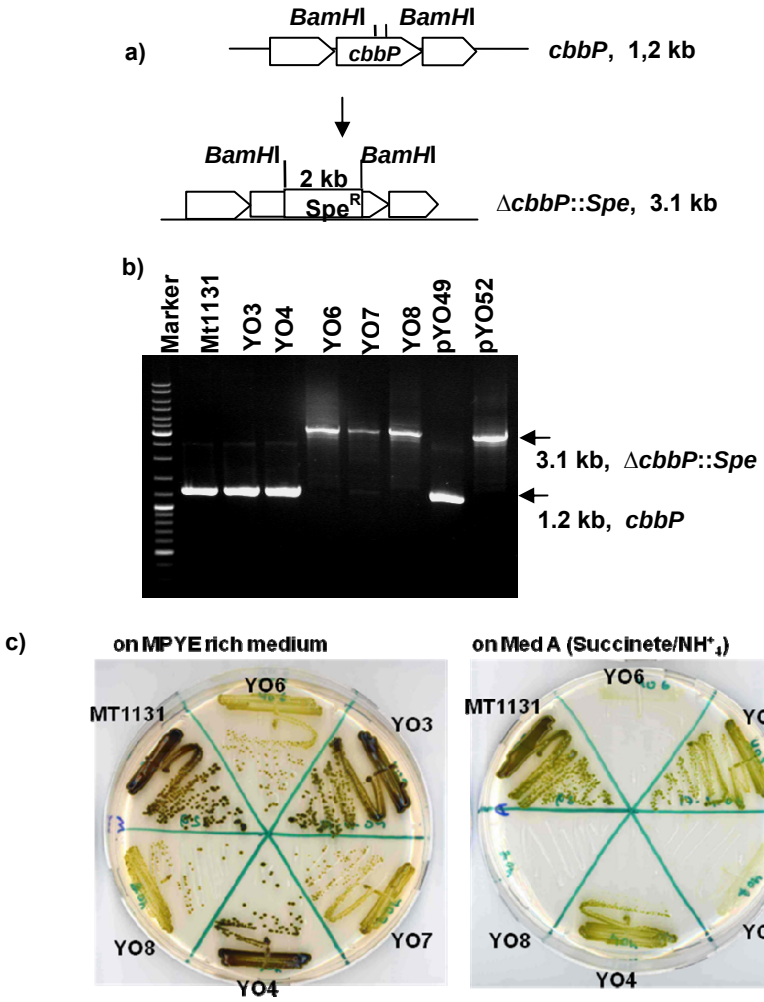

Figure 1: **The Δ*cbbP*::Spe deletion-insertion allele was constructed by replacing the 180 bp *BamH*I fragment of *cbbP* by a 2 kb Spectinomycin cassette (a). *cbbP* deletion was confirmed by PCR amplification of *cbbP* and Δ*cbbP*::Spe insertion-deletion allele from chromosomal DNAs of wild type and mutant *R. capsulatus* strains. pYO49 and pYO52 are the plasmids carrying *cbbP* and Δ*cbbP*::Spe in pBSII respectively (b). Photosynthetic growth properties of various *R. capsulatus* strains on MPYE rich medium (c-left plate) and on minimal medium MedA (succinete/NH^+_4) (c-right plate). The growth of PRK$^-$ derivatives deficient in CBB pathway are very slow on Nitrogenase repressing medium MedA.**

3.2 Hydrogen production by PRK$^-$ strains of R. capsulatus.

Hydrogen production profiles of the newly generated PRK$^-$ strains YO6, YO7 and YO8 were investigated and compared to their respective PRK$^+$ parents. The data obtained demonstrated that the total hydrogen production and substrate conversion efficiency of YO7 and YO8 strains increased as shown in Figure 2, and Table 2. For example, the total hydrogen production and substrate conversation efficiency of YO7 (*Hup*$^-$, PRK$^-$) were 1.15 and 57% respectively. The total hydrogen production was increased 1. 6 fold as compared with the wild type MT1131 and 1.1 fold as compared with the YO3. Likewise, the total hydrogen production and substrate conversation efficiency of YO8 (cyt cbb_3^-, *Hup*$^-$, PRK$^-$) were increased 1.2 fold and 1.1 when comparing the wild type MT1131 and YO4 respectively. The data obtained demonstrated that the inactivating the CBB pathway especially in YO3 and YO4 strains further improved the hydrogen production capacity of the *R. capsulatus* strains. Moreover, under the photoheterotrophic growth condition in minimal medium with ammonium as an nitrogen source, the growth of all PRK$^-$ strains were shown to be impaired in their ability to grow photoheterotrophically due to the lack of a functional CBB cycle and repression of the dinitrogenase system (Figure 1-c). However they gave Ps$^+$ revertants frequently in this medium and several spontaneous revertant variants of PRK$^-$ strains that have become photoheterotrophically competent were isolated. These strains were shown to obviate normal ammonia control and derepress synthesis of the dinitrogenase enzyme complex for the dissipation of excess reducing equivalents and generation of H_2 gas via proton reduction.

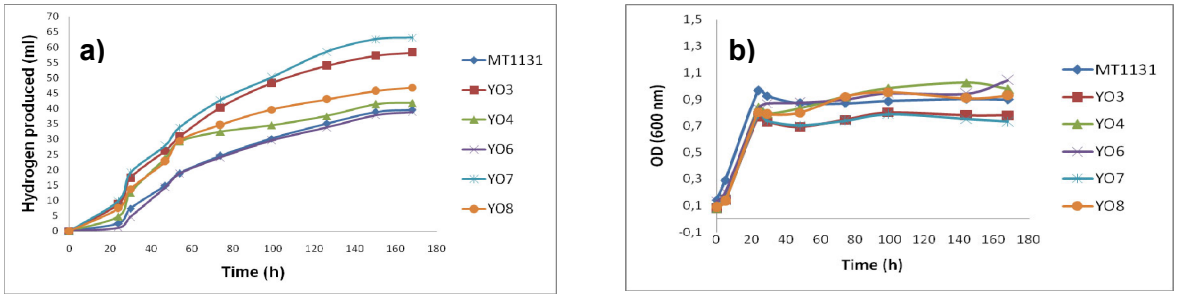

Figure 2: Hydrogen production (a) and phototrophic growth (b) of PRK$^-$ mutants and their respective PRK$^+$ parent strains.

Table 2: Hydrogen production of wild type and different mutants of *R. capsulatus*. The data are means of three different determinations.

strains	Total Hydrogen (ml/ml culture)	Substrate conversion efficiency (%)
Mt1131	0,72	36
YO3 (*Hup*$^-$)	1,06	52
YO4 (cyt *cbb*$_3^-$, *Hup*$^-$)	0,76	38
YO6 (*cbbP*$^-$)	0,71	35
YO7 (*Hup*$^-$, *cbbP*$^-$)	1,15	57
YO8 (cyt *cbb*$_3^-$, *Hup*$^-$, *cbbP*$^-$)	0,85	42

4 Conclusion

Rhodobacter capsulatus produces molecular hydrogen under the photoheterotrophic growth condition with reduced carbon sources (organic acids). Under the this condition, ubiquinol poll is over reduced and excess reducing equivalents are primarily consumed via the reduction of CO_2 through the Calvin–Benson–Bassham (CBB) pathway, the DMSOR system or by the reduction of protons into H_2 gas with the use of dinitrogenase enzyme system to maintain a balanced intracellular oxidation-reduction potential. The relationship between the redox balancing system and the hydrogen metabolism was analyzed by using various mutant strains deficient in terminal oxidases, uptake hydrogenase, Phosphoribulokinase and in their various combinations. The results obtained showed that in the absence of the functional CBB pathway, the excess reducing equivalents were dissipated only through the dinitrogenase system in the form of more hydrogen. Besides, the preliminary data of some isolated revertant of PRK$^-$ strains indicated that hydrogen gas production of these strains were further enhanced by derepression of dinitrogenase system removing the redox poising by H_2 production.

Acknowledgements

This work was supported by TÜBİTAK as Project No. 108T455

Nomenclature:

CBB pathway: Calvin–Benson–Bassham reductive pentose phosphate pathway; PRK: Phosphoribulokinase; Cyt *cbb*$_3$ ox: Cytochrome *cbb*$_3$ oxidase; *Hup*: Uptake hydrogenase

References

[1] Imhoff FJ. Taxonomy and physiology of phototrophic purple bacteria and green sulfur bacteria. Kluwer Academic Publishers 1995. p. 1-15.

[2] Ferguson SJ, Jackson JB, McEwan AG. Anaerobic respiration in the *Rhodospirillaceae*: characterisation of pathways and evaluation of roles in redox balancing during photosynthesis. FEMS Microbiol. 1987; Rev. 46:117–143.

[3] Mary A. Tichi, F. Robert Tabita. Maintenance and control of redox poise in *Rhodobacter capsulatus* strains deficient in the Calvin-Benson-Bassham pathway. Arch Microbiol (2000) 174 :322–333

[4] Joshi HM, Tabita FR. A global two component signal transduction system that integrates the control of photosynthesis, carbon dioxide assimilation, and nitrogen fixation. Proc. Natl. Acad. Sci. USA 1996; 93:14515–14520.

[5] Vignais PM, Colbeau A, Willison JC, Jouanneau Y. Hydrogenase, nitrogenase and hydrogen metabolism in photosynthetic bacteria. Adv. Microbial Phys. 1985; 26: 154-234.

[6] Öztürk Y., Yücel M., Daldal F., Mandacı S., Gündüz U., Türker L., Eroğlu İ.. Hydrogen Production by Using *Rhodobacter capsulatus* mutants with Genetically Modified Electron Transfer Chains. International Journal of Hydrogen Energy 31 (2006) 1545-1552

[7] Özgür E., Uyar B., Öztürk Y., Yücel M., Gündüz U., Eroğlu İ.. Biohydrogen production by *Rhodobacter capsulatus* on acetate at fluctuating temperatures. *Resources, Conservation and Recycling*, Volume 54, Issue 5, Pages 310-314, March 2010

[8] Daldal F, Cheng S, Applebaum J, Davidson E, Prince R. Cytochrome c_2 is not essential for photosynthetic growth of *Rhodopseudomonas capsulata.* Proc .Natl. Acad. Sci. 1986; 83: 2112-2116.

[9] Biebl H, Pfennig N. Isolation of members of the family *Rhodosprillaceae*. In: Starr MP, Stolp H, Trüper HG, Balows A, Schlegel HG, editors. The Prokaryotes. New York: Springer-Verlag 1981; Vol 1. 267-273.

Photosynthetic Hydrogen Production: Computational & Experimental Results are Indicative that Evolutionary Mutants May Allow for Commercial Viability

Scott Plummer, **Richard Chapas**, H_2OPE Biofuels Inc., USA
Mark Plummer, MPr&d LLC, USA

Carbon dioxide and other greenhouse gases are rising to alarming levels in our atmosphere. An economy and a transportation infrastructure based on molecular hydrogen and fuel cells could positively affect global climate change. Generation of molecular hydrogen as a biofuel, i.e. generation of hydrogen via photosynthetic algae (*Chlamydomonas reinhardtii*) would allow for a cheap and renewable energy source. However, the enzyme responsible for hydrogen gas generation (hydrogenase) has a short half-life and is extremely sensitive to oxygen.

One approach toward solving these problems is through directed evolution whereby mutations are introduced into the DNA of the native hydrogenase. Directed evolution is a technique that mimics natural evolution in that multiple mutations are created and tested for enhanced traits. Albeit on a shorter timescale, the proteins with evolved mutations are submitted to repeat cycles of evolutionary pressure.

In this talk, we will present a computational model and the corresponding experimental results, which indicate the near-term feasibility of commercial biohydrogen production. Specifically, we will present a computational model, based on our most promising mutant hydrogenases, that suggests that hydrogenase mutants can produce 40-760X more hydrogen than the wild-type hydrogenase. Ultimately, a mutant with increased hydrogen production will facilitate a practical method of producing hydrogen for use as a commercial fuel source.

The modeling portion of this work had dual objectives. The first was to see if the folding of a hydrogenase protein (575 amino acids) could be more efficiently modeled using electrostatic potential surfaces (EPS) along with molecular dynamics (MD) versus using MD only. The basis of the modeling is that a surface of constant electrostatic potential can be used as a measure of the effort needed to share or transfer an electron from one region of a molecule to another region. And, that electron sharing in hydrogenases should affect their folding mechanisms and kinetics.

It is also proposed that positive and negative EPS regions can be quickly folded and matched by variation of bond angles between regions followed by MD structuring and energy minimization. This approach should minimize computational time for modeling folding kinetics and mechanisms over that required if only MD calculations were used. Lastly, it is proposed that the ratio of water accessible volume to water accessible surface area can be used as a correlation parameter to follow the extent of folding.

MD only calculations showed that folding starts at both ends of the entire hydrogenase mutant and works its way toward the middle. The center point for this folding is the amino

acid 267. Hence to obtain shorter computation times, the rest of the folding work dealt with the 267-575 portion of this mutant. This region shows the greatest diversity of positive (green) and negative (pink) EPS regions in the initial α-helical structure as shown in Figure 1.

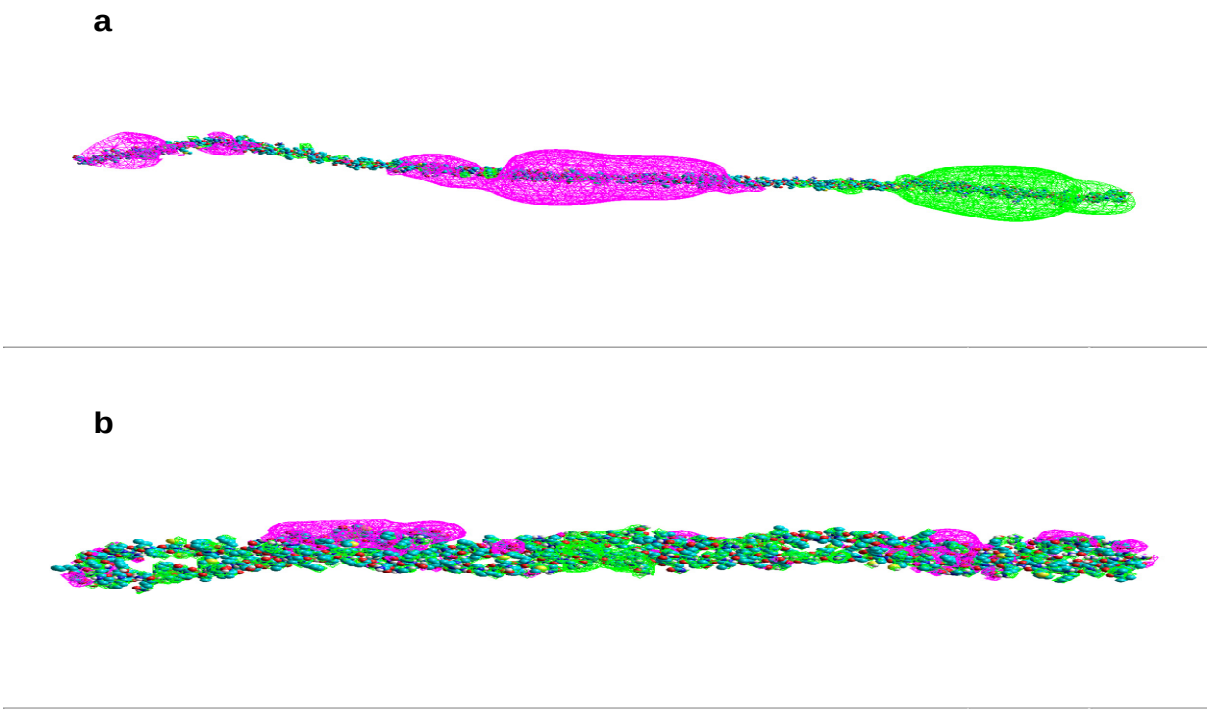

Figure 1: Modeling: Electrostatic potential surfaces.
a) Structure of a typical mutant hydrogenase (green indicates a region of positive electrostatic potential and pink indicates a negative electrostatic potential surface); b) Structure of hydrogenase after one folding iteration.

Protein folding kinetics has been shown to exhibit two folding regions. First, the protein quickly folds from a linear state into a globular structure. Next, the globular structure folds slowly to the final tertiary state. The results from this work support these literature findings. That is, a correlation between RMS error and the water accessible volume to surface area ratio was found to exhibit two straight-line segments of considerable different slopes. It was concluded that these separate straight-line segments represent the fast and slow folding regions. Single correlations of this type were obtained for all folding temperatures and times studied.

Based on the above results, the EPS concept was tested for predicting the hydrogen productions of hydrogenase mutants using their unfolded α-helical structure. The ratio of total positive EPS area to total negative EPS area was evaluated as the correlation parameter. As demonstrated by the above modeling results, folding is affected by long-range electrostatic forces. Those mutants exhibiting a certain EPS ratio would fold correctly to yield the maximum hydrogen production; an EPS of zero indicates no positive EPS regions and an infinite ratio indicates no negative EPS regions. The best fit to this data was obtained with the Log Normal equation yielding a Chi squared error of 1.0, wherein the

maximum hydrogen production would be 758 times that obtained with the control hydrogenase – Figure 2.

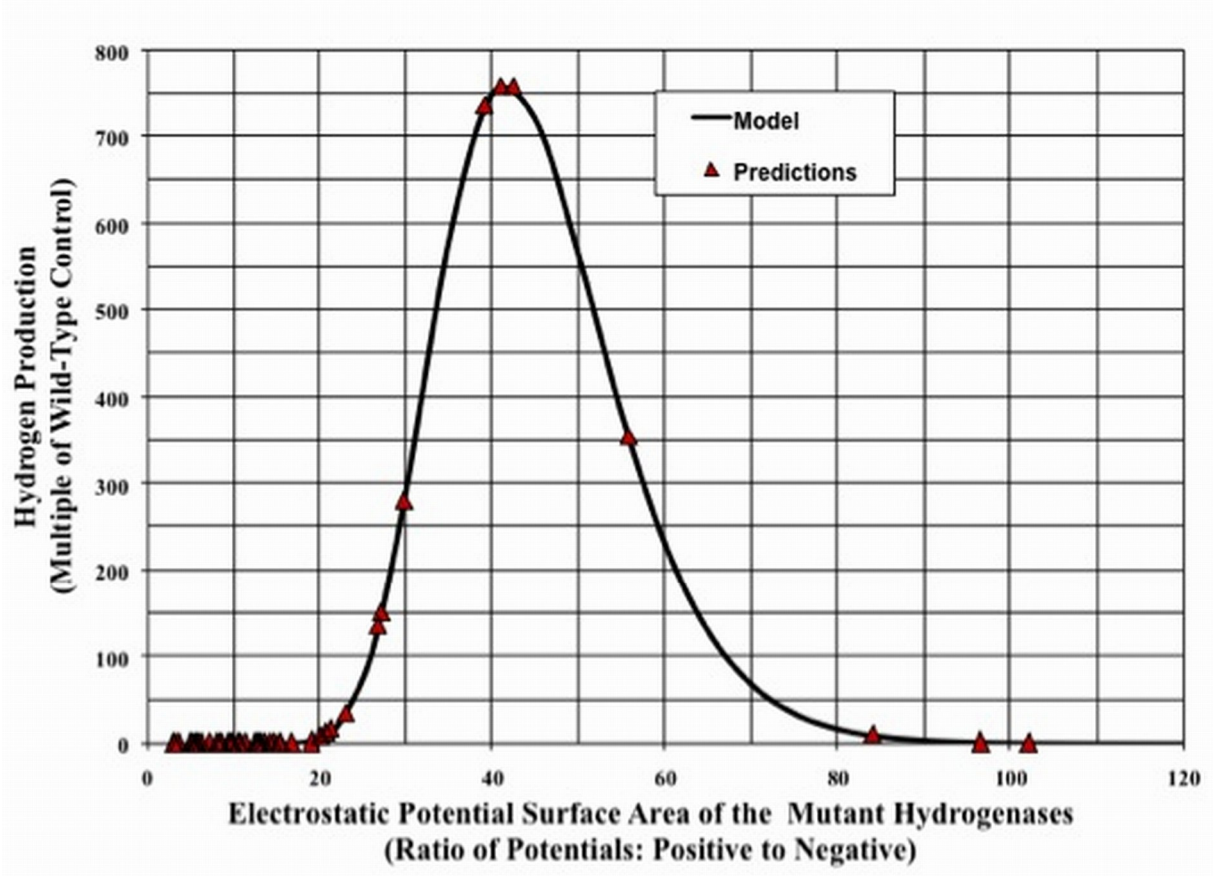

Figure 2: Measured and predicted hydrogen productions versus ratio of positive to negative EPS of unfolded structures.

Based on the above results, 70 of the 256 mutants produced in the experimental work were evaluated using the developed model. Fifteen of these mutants have predicted hydrogen productions in the range of 1.4 to 758 times that for the wild type control.

References

[1] Plummer, M.A., Plummer, S.M., “Modeling the Folding and Hydrogen Production of Clostridium acetobutylicum and Clostridium saccharobutylicum Mutants using Electrostatic Potential Surfaces and Molecular Dynamics”, Computational Biology and Chemistry, 2009, 33, 404-407.

[2] Plummer, S., “Photosynthetic Hydrogen Production from the Green Alga Chlamydomonas reinhardtii”. Doctoral Thesis at the Colorado School of Mines, Department of Chemistry, 2008, 1-134.

An Experimental Study of the Growth and Hydrogen Production of *C. Reinhardtii*

B. Tamburic, **S. Burgess**, **P.J. Nixon**, **K. Hellgardt**, Imperial College London, UK

Abstract

Some unicellular green algae, such as *C. reinhardtii*, have the ability to photosynthetically produce molecular hydrogen under anaerobic conditions. They offer a biological route to renewable, carbon-neutral hydrogen production from two of nature's most plentiful resources – sunlight and water. This process provides the additional benefit of carbon dioxide sequestration and the option of deriving valuable products from algal biomass.

The growth of dense and healthy algal biomass is a prerequisite for efficient hydrogen production. This study investigates the growth of *C. reinhardtii* under different cyclic light regimes and at various continuous light intensities. Algal growth is characterised in terms of the cell count, chlorophyll content and optical density of the culture. The consumption of critical nutrients such as acetate and sulphate is measured by chromatography techniques.

C. reinhardtii wild-type CC-124 strain is analysed in a 3 litre tubular flow photobioreactor featuring a large surface-to-volume ratio and excellent light penetration through the culture. Key parameters of the hydrogen production process are continuously monitored and controlled; these include pH, pO_2, optical density, temperature, agitation and light intensity. Gas phase hydrogen production is determined by mass spectrometry.

1 C. Reinhardtii Growth under Different Light Regimes

1.1 Strains and growth conditions

C.reinhardtii wild-type strain CC-124 (*Chlamydomonas* stock centre) was grown in Tris Acetate Phosphate (TAP) media [1] at 25^{o}C. Cultures were agitated by magnetic stirrer and illuminated with 28 Wm^{-2} (140 $\mu Em^{-2}s^{-1}$) cool fluorescent light or grown in the dark.

1.2 Calculation of cell number and chlorophyll content

Cell samples were stained with iodine and counted using an improved neubauer hemocytometer[1]. Chlorophyll *a* and *b* content was determined spectrophotometrically in 100% Methanol according to Porra *et al* [2].

1.3 Acetate analysis

Cells were pelleted and 100 µl of supernatant analysed on an Aminex HPX-87H anion exchange column according to Mus *et al* [3].

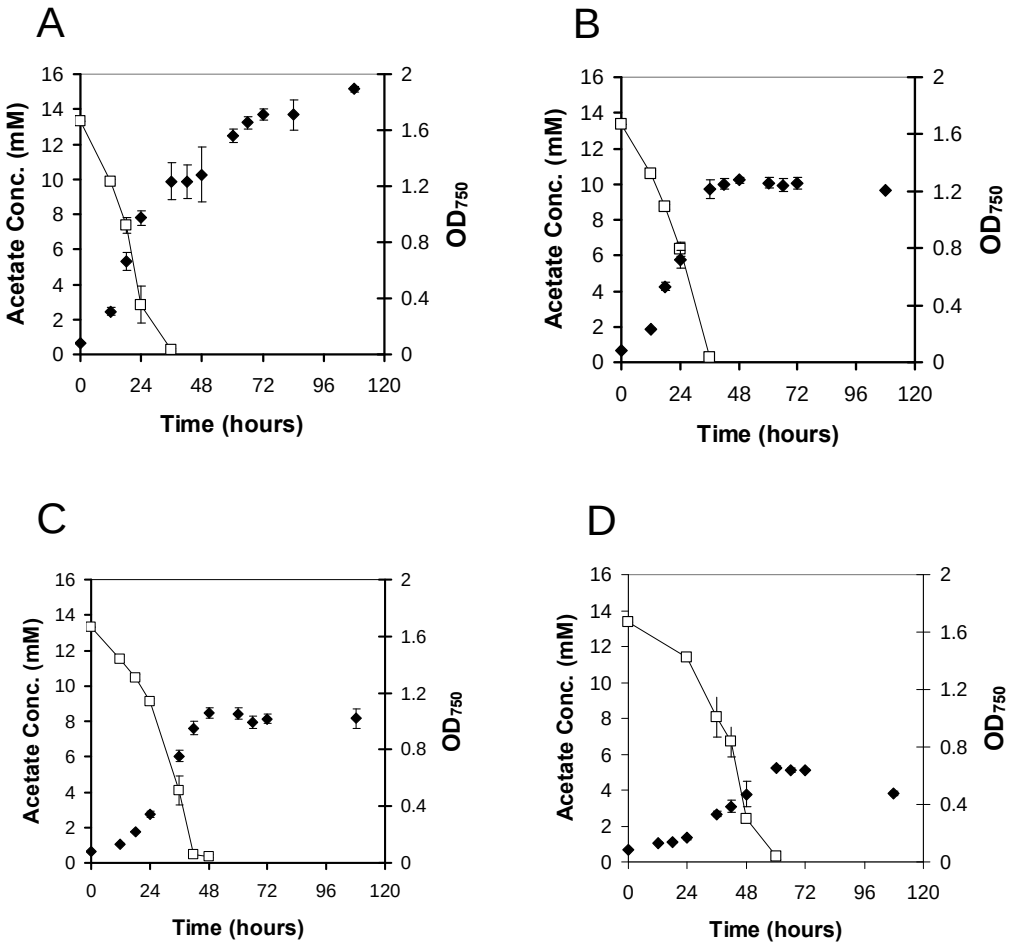

Figure 1: ***C. reinhardtii*** **CC-124 growth under varying environmental conditions; OD_{750} (♦) and acetate (□) concentration, (A) under continuous illumination bubbled with 5% CO_2 air mixture, (B) under continuous illumination, (C) during 12h:12h dark-light cycles, and (D) in the dark.**

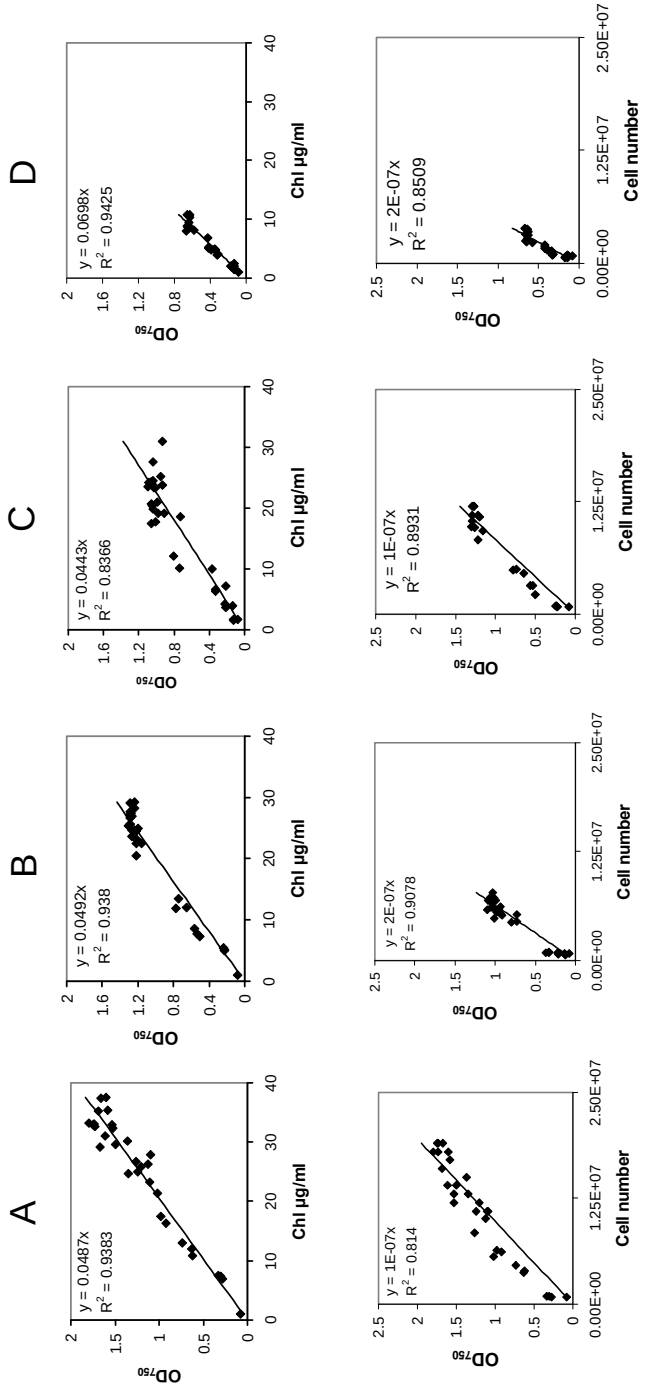

Figure 2: Analysis of the correlation between growth phase optical density (OD_{750}), chlorophyll content and cell number (cell counts were stopped upon reaching stationary phase as clumping of cells was observed) for *C. reinhardtii* CC-124 under varying environmental conditions; (A) under continuous illumination bubbled with 5% CO_2 air mixture, (B) under continuous illumination, (C) during 12h:12h dark-light cycles, and (D) in the dark; there was a good correlation between OD_{750} and Chl content or cell number independent of growth phase.

2 Growth of C. Reinhardtii

Under ambient conditions, the cell density of *C. reinhardtii* increases exponentially with a doubling time of approximately 6 h [1]. Our data (Figure 1) gives doubling times of:

3.6±0.5 h	under continuous illumination
2.8±0.2 h	under continuous illumination bubbled with 5% CO2 air mixture
5.1±0.5 h	during 12h:12h dark-light cycles
15.7±0.8 h	in the dark

In photobioreactors, such as our 3 litre tubular-flow reactor, algal cell density is principally limited by the light penetration through the culture and the availability of key nutrients (carbon, nitrogen, sulphur and phosphate) [4].

We have measured that the *C. reinhardtii* wild-type CC-124 growth rate increases significantly with an increase in light intensity (Figure 3a). Additionally, the maximum attainable optical density at very low light intensities (4 Wm^{-2}) is approximately 15% lower than at 12 Wm^{-2} or 20 Wm^{-2}. Higher light intensities ensure that more algal cells can receive sufficient illumination to facilitate photosynthetic growth, and the culture therefore grows thicker.

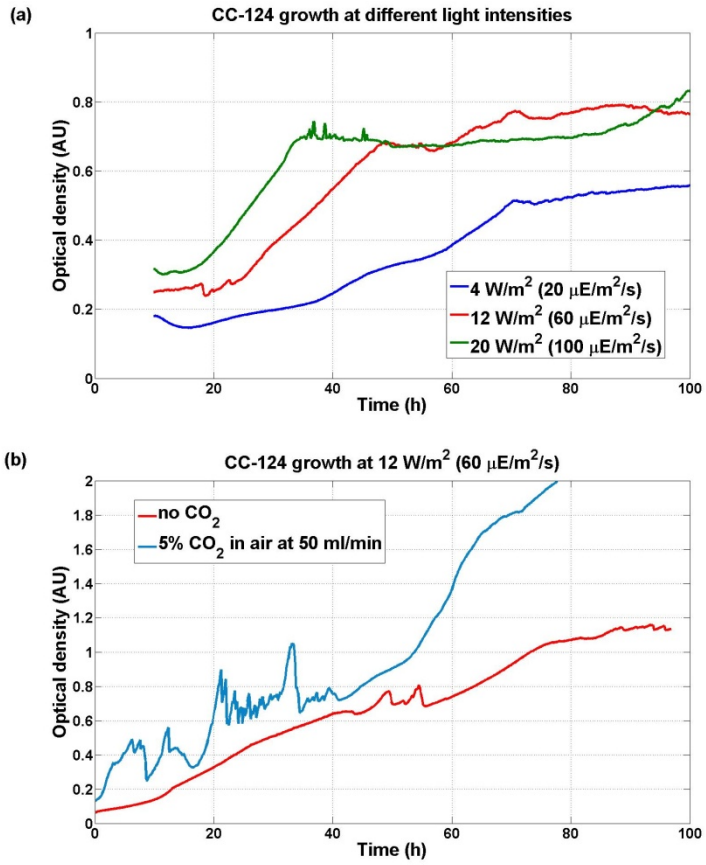

Figure 3: ***C. reinhardtii*** **wild-type strain CC-124 growth, measured in terms of the culture optical density at 875 nm, as a function of (a) light intensity, and (b) the presence of CO_2 sparging.**

C. reinhardtii may be grown using an organic source of carbon such as acetate (photoheterotrophic growth), an inorganic source such as CO_2 (photoautotrophic growth – not studied) or using a combination of acetate and CO_2 (photomixotrophic growth) [5]. Our results show that mixotrophic growth leads to an increase in CC-124 growth rate, and a near-doubling of the maximum attainable OD (Figure 3b).

3 H_2 Production by *C. Reinhardtii*

C. reinhardtii has the ability to photoproduce H_2 under the anaerobic conditions imposed by sulphur deprivation. The dilution method of sulphur deprivation developed by Laurinavichene *et al* is a procedure well suited to laboratory scale H_2 production [6]. A small volume (typically 10% v/v) of growing *C. reinhardtii* culture is diluted in sulphur-deprived TAP medium. The algae continue to photosynthesise and grow as long as they have access to sulphur. Once the sulphur runs out, the algae will use up all oxygen in the system by respiration and eventually enter the phase of anaerobic H_2 production.

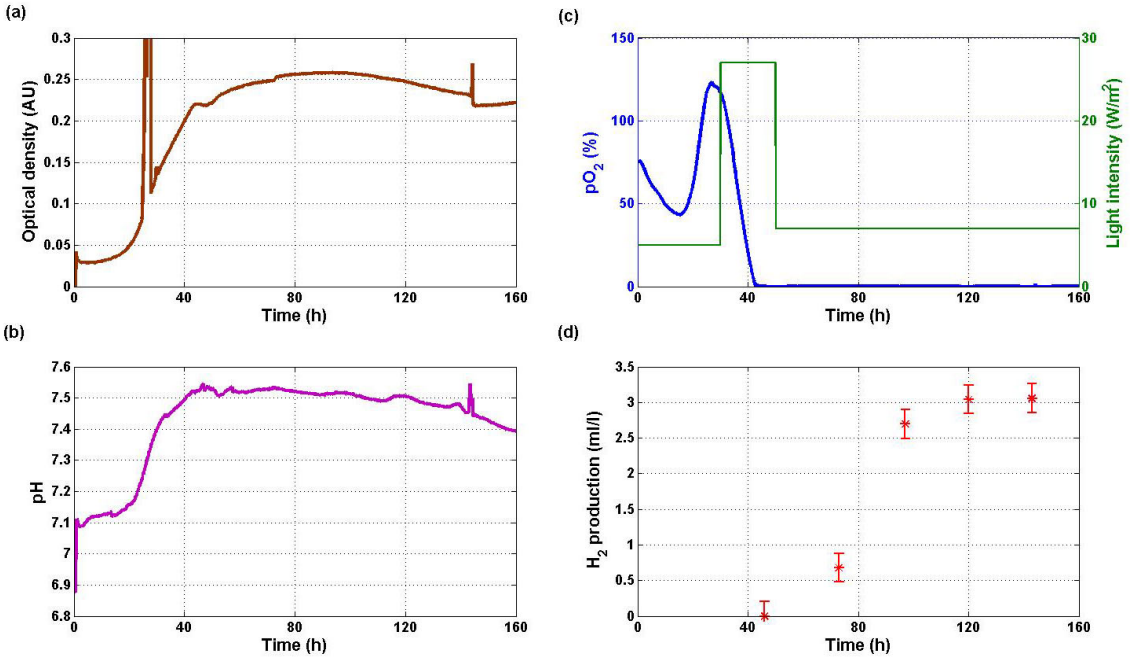

Figure 4: Analysis of the H_2 production process in CC-124, featuring continuous *in situ* measurement of the (a) optical density at 875nm, (b) pH, and (c) dissolved oxygen content (pO_2); light intensity is adjusted to the optimal values required for algal growth, sulphur-deprivation and (d) anaerobic H_2 production phases.

Key parameters of the H_2 production process, such as optical density, pH, light intensity and pO_2 were measured continuously and *in situ* (Figure 4). The optical density initially rose during the algal grow phase, but subsequently fell during the H_2 production phase because some biomass was used up by catabolic processes (Figure 4a). The pH value behaved similarly to optical density (Figure 4b). Light intensity was set at 5 Wm^{-2} during algal growth, 27 Wm^{-2} during sulphur deprivation and 7 Wm^{-2} during H_2 production, as recommended by

Kosourov *et al* [7]. Anaerobic conditions were attained approximately 42h after dilution (Figure 4c). H_2 production was maintained for a period of approximately 5 days (Figure 4d). The total H_2 yield was 3.1±0.2 ml/l of culture. This corresponds to a photochemical efficiency in the order of 0.1%.

Acknowledgements

We would like to thank Geoffrey C. Maitland, Fessehaye W. Zemichael and Marko Boehm for their contributions during this study. The Solar Hydrogen Project is funded by the UK Engineering and Physical Sciences Research Council (EPSRC).

References

[1] Harris EH. The Chlamydomonas Sourcebook. A Comprehensive Guide to Biology and Laboratory Use. San Diego CA: Academic Press; 1989.

[2] Porra RJ, Thompson WA, Kriedemann PE. Determination of accurate extinction coefficients and simultaneous equations for assaying chlorophylls a and b extracted with four different solvents: verification of the concentration of chlorophyll standards by atomic absorption spectroscopy. Biochimica et Biophysica Acta 1989; 975(3):384-394.

[3] Mus F, Dubini A, Seibert M, Posewitz MC, Grossman AR. Anaerobic acclimation in Chlamydomonas reinhardtii: anoxic gene expression, hydrogenase induction, and metabolic pathways. Journal of Biological Chemistry 2007; 282(35):25475-25486.

[4] Melis A. Photosynthetic H_2 metabolism in Chlamydomonas reinhardtii (unicellular green algae). Planta 2007; 226(5):1075-1086.

[5] Tsygankov A, Kosourov S, Tolstygina IV, Ghirardi ML, Seibert M. Hydrogen production by sulphur-deprived Chlamydomonas reinhardtii under photoautotrophic conditions. International Journal of Hydrogen Energy 2006; 31(11):1574-1584.

[6] Laurinavichene T, Kosourov S, Ghirardi ML, Seibert M, Tsygankov A. Prolongation of H2 photoproduction by immobilized sulphur-deprived C.reinhardtii cultures. Journal of Biotechnology 2008; 134(3-4):275-277.

[7] Kosourov S, Patrusheva E, Ghirardi ML, Seibert M, Tsygankov A. A comparison of hydrogen production by sulphur-deprived Chlamydomonas reinhardtii under different growth conditions. Journal of Biotechnology 2007; 128(4):776-787.

Immobilization Techniques of *Rhodobacter Sphaeroides* O.U. 001 in Hydrogen Generation

M. Thiel, **K. Seifert**, **M. Łaniecki**, A. Mickiewicz University, Poland

1 Introduction

Among many alternative routes of hydrogen generation, the microbiological ways belong to the most promising ones. Microbiological methods of hydrogen generation consist of biophotolysis of water, indirect biophotolysis, “dark” fermentation, and photofermentaion [1]. Literature data and our earlier results showed that the application of photoheterotrophic bacteria in hydrogen generation processes can lead towards designing installations on a larger scale and, as a consequence, hydrogen generation on a small industrial scale.

The present paper describes an application of purple non-sulfur *Rhodobacter sphaeroides* O.U. 001 bacteria (PNS), in photofermentative hydrogen generation. These photohetrotrophic bacteria require for growth, not only light, but also simple organic substances [2]. Appropriate growth is assured under anaerobic conditions with a pH close to 7, temperature range of 27-32 ^{o}C and in the absence of ammonium ions. The presence of these ions as well as molecular nitrogen inhibits hydrogen evolution by transformation of ammonium ions and reduction of N_2 to NH_3 by nitrogenase [3]. In contrast, in the absence of nitrogen in this system, nitrogenase catalyzes the reduction of protons to molecular hydrogen [3].

It is important to increase the laboratory scale of the described process into the industrial one. Therefore, a cheap method of separation of liquid medium from bacteria is required. This can be achieved by immobilization of the bacterial culture. The immobilized microorganisms show higher catalytic stability, higher tolerance towards toxic substances or inhibitors and shorter lag phase [4]. Application of the appropriate photobioreactor operating under the continuous and sterile conditions during hydrogen generation is the key point in the efficient generation of hydrogen using the microbiological way. Therefore, the main goal of the presented paper was focused on the design of a new photobioreactor operating with an immobilized culture. Here, different materials were applied for immobilization: Ca-alginate, PVA and large pore silica aerogel. Both systems were deposited onto glass plates or entrapped between polymeric nets. The present paper presents, however, the results obtained for calcium alginate and PVA only. The stability of the system was tested.

2 Materials and Methods

2.1 Inoculum and medium

Photohetrotrophic bacteria *Rhodobacter sphaeroides* O.U.001 (ATCC 4919) were cultivated on Van Niel’s medium containing: K_2HPO_4 (1.0 g/l), $MgSO_4$ (0.5 g/l), yeast extract (10 g/l) and tap water filled up to 1l and then activated according to the procedure already described [5]. For hydrogen generation a modified Biebl and Pfennig medium [6] was applied as reference. Medium was sterilized at 120°C by autoclaving for 20 minutes. In all experiments

temperature was 28 ± 2°C and pH after sterilization varied between 7.0 and 7.2. The mercury-tungsten lamp (300W Ultra-Vitalux from Osram) was applied in all experiments. The intensity of illuminance was 9 klx (116 W/m^2).

2.2 Immobilization techniques

2.2.1 Ca-alginate

The *Rhodobacter sphaeroides* O.U.001 inoculum after centrifugation (12000 rpm for 7 min) was introduced into sterilized solution of sodium alginate. The initial concentration of sodium alginate solution was 5 wt. %, whereas sterilization was performed at 120 ^{o}C for 20 minutes. After introduction of inoculum the final concentration of sodium alginate reached 4 wt. % value. This solution was next introduced into calcium chloride (2 vol. %) solution . After 30 minutes of the crosslinking process, the formation of insoluble gel of calcium alginate was observed [7,8]. Finally the obtained materials were washed with sterile water. Three methods of gel formation were applied:

- injection of bacteria containing alginate solution into dissolved $CaCl_2$ with simultaneous formation of round spheres,
- deposition of bacteria containing alginate solution onto glass plates (sodium glass) followed by immersion of these plates in solution of Ca^{2+} ions,
- similarly, as above but deposition of alginate occurred between two polymeric nets.

2.2.2 PVA crosslinked with boric acid

Medium containing bacteria was centrifuged in similar manner as above and introduced into sterilized polyvinyl alcohol (PVA) solution (13.5 vol.%, av. M_w - 130,000, 99+% hydrolyzed, Aldrich) until concentration of PVA of 9 vol. % was achieved. The obtained suspension was stirred mechanically and transferred into saturated solution of boric acid. The obtained gel [9] after crosslinking and sedimentation (30 minutes) was transferred into 0.5 M solution of NaH_2PO_4. Here the phosphorylation of PVA occurred [10]. This method was applied only for polymeric nets due to difficulties of round spheres formation and lack of adhesion properties on glass plates. Distances between particular fibers in the net were 2mm whereas thickness of these fibers was close to 0.5mm.

2.3 Photobioreactors

2.3.1 Preliminary experiments

The preliminary experiments were performed in small vials made of sodium glass with capacity of 60 cm^3. The working volume was 30 cm^3 whereas remaining volume served for gas collection. The constant concentration of bacterial cells equal 0.576 g biomass/l medium was applied in all experiments but with different volume ratio of alginate to medium (1:14, 1:5, 1:2 and 1:1). Experiments were performed in periodical system: medium was exchanged in each set of experiments whereas bacteria deposited inside calcium alginate spheres represented constant value. In all studied systems the medium was initially degassed with argon after replacement.

2.3.2 Flat plate photobioreactor with immobilized culture (FP PBR with IC)

The main body of modified flat plate photobioreactor was made from stainless steel, (Figure 1) and side walls were made from sodium glass. Seal integrity of the reactor was protected with Viton™ o-rings. Occasionally the system was cooled with water flowing through stainless steel walls. The working capacity of this reactor was 200 ml. The immobilized bacteria were placed on glass plates or between two parallel polymeric nets (dimensions 10 x 10.5 cm). Glass plates were the support for 10 cm^3 of calcium alginate containing different concentrations of bacteria (0.029, 0.087, 0,116 g/l medium). In the case of the polymeric nets the concentration of bacteria cells was constant but the volume of alginate deposited was 10 cm^3 and 20 cm^3 in the case of PVA. System was deoxygenated in stream of argon after each exchange of medium.

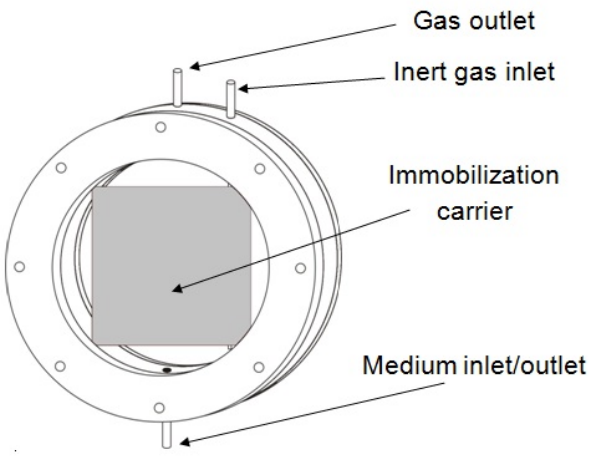

Figure 1: Flat Plate Photobioreactor with Immobilized Culture scheme.

2.4 Analytical methods

Gas metabolites were measured with gas chromatography (Varian GC-3800 equipped with Carboplot P7 capillary column and TCD) [5]. The amount of gaseous products was measured by a volumetric method applying constant detection of the gas volume evolved with a computerized camera. Each cycle of the exchange of liquid medium was completed with pH value measurements. The amount of the evolved cells from immobilizing medium was determined spectrophotometrically, measuring absorption at 660 nm (UV-Vis- Beckman DU 640).

3 Results and Discussion

The experiments performed with immobilized bacteria proved that this technique allows for multiple applications of the same bacterial cells. In all cases the observed, relatively long, lag phase at the beginning of the experiment (directly after immobilization) is significantly shorter in the subsequent replacements of the medium. This indicates a good acclimatization of microorganisms in the porous structure of the immobilizing material. However, in all studied cases the immobilized materials showed decomposition with time, and simultaneous

evolution of cells into the medium (see Figure 2). The preliminary experiments with alginate spheres showed that the best stability of the immobilized bacteria can be reached with samples containing the highest concentration of microorganisms (1:1 – up to seven cycles). Lower concentrations of bacteria in alginate resulted in higher hydrogen productivity due to a better diffusivity of hydrogen but shorter lifetime. Faster hydrogen generation causes faster formation of cracks and finally easier decomposition of the immobilized material.

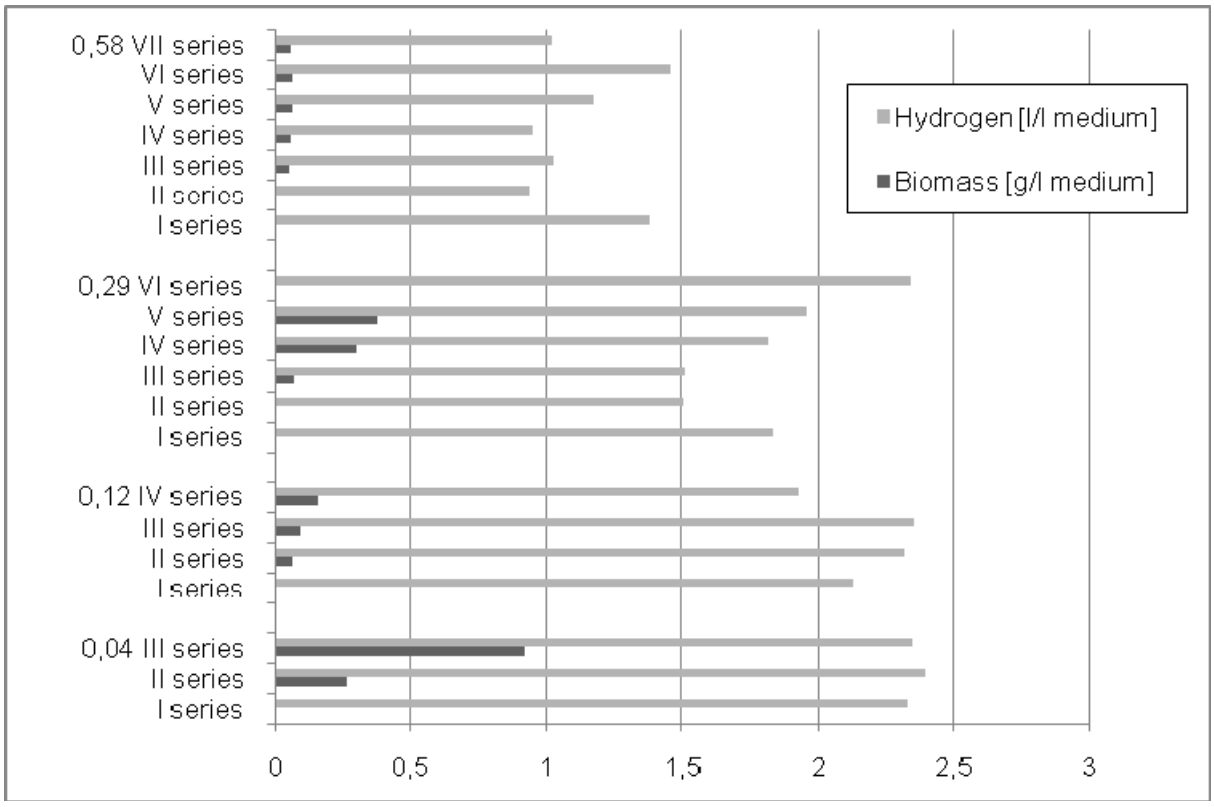

Figure 2: Calcium alginate spheres – maxima of generated hydrogen and concentration of the released cell into the medium. Cell concentrations 0.58, 0.29, 0.12, 0,04 g biomass/l of medium.

Higher activity of the released cells can be explained by better access to substrates and illumination. The access of light for immobilized bacteria is always limited in deeper parts of the alginate spheres. The observed effect leads to the conclusion that the rate of hydrogen evolution in the case of alginate can significantly influence the stability of the immobilized systems. An application of the alginate system deposited on glass plates and FP PBR reactor the best results were obtained with cell concentrations 0.058 and 0.087 g biomass /l of medium (Figure 3).

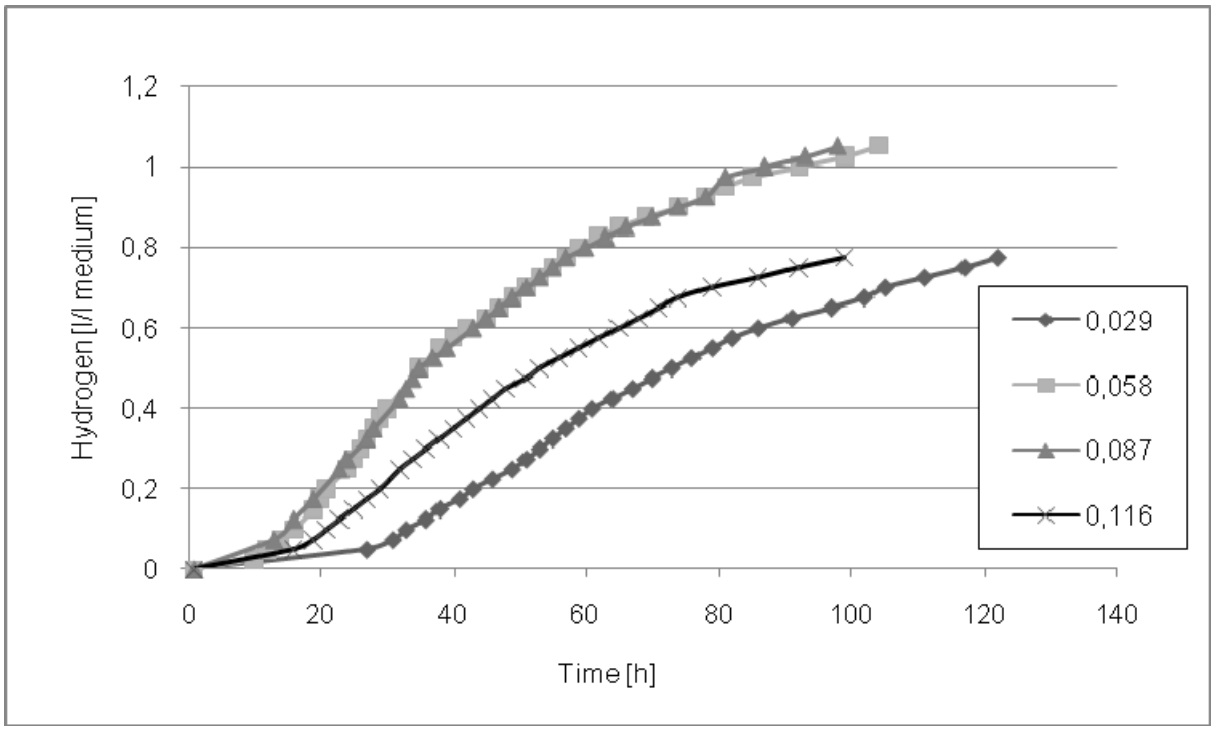

Figure 3: Calcium alginate deposited on glass plate. Different concentrations of immobilized cells.

Low productivity of hydrogen was found at the highest concentration of bacteria in alginate (0.116 g biomass/l medium). This can be related to the autoinhibition process [11]. An application of alginate immobilized on glass plates resulted in much lower stability than with the round spheres. The immobilized material could “survive” only two exchanges of medium. Therefore, new method of alginate method was applied. Here, alginate, with optimized concentration of bacteria (0.058 g biomass/l medium), was located between two parallel polymeric nets. This construction provided much better stability, and relatively high hydrogen generation. After the first run the amount of hydrogen was 0.8 lH_2/l medium and in subsequent runs this amount was close to 1.2 lH_2/l medium (see Figure 4). Much better productivity (about 30 %) can be explained by acclimatization of the bacterial strain as well as partial elution of bacterial cells into the medium. Separation of liquid medium was possible up to 4 runs. After 4 runs the stability of the system was very poor.

The search for new, more stable materials for immobilization showed that PVA is the more stable one. First run with high concentration of entrapped bacteria (0.116g biomass/l medium) indicate low productivity of hydrogen and long lag time phase (see Figure 5).

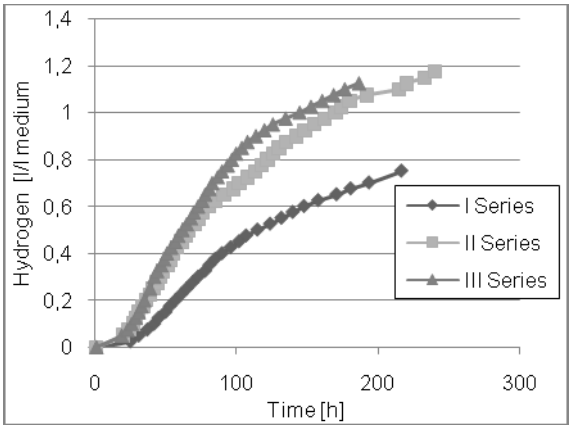

Figure 4: Bacteria immobilized in Ca-alginate located between polymeric nets.

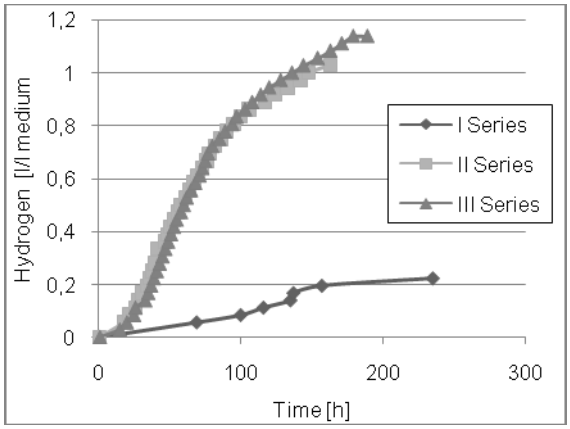

Figure 5: Bacteria immobilized in PVA located between polymeric nets.

This can result from adaptation of bacteria in this new material as well as from transfer of H_3BO_3 into the medium. The amount of photobiogenerated hydrogen was almost the same but stability of the system with PVA appeared to be much better.

The obtained results showed that application of polymeric nets significantly prolong the lifetime of the immobilized bacterial systems. Moreover, it appeared that crosslinked with boric acid and subsequently phosphorylated PVA is much better material for immobilization of bacteria. The amounts of photogenerated hydrogen is identical when alginate gels were applied.

Acknowledgements

This work was supported by grant from MNISW No: N204 031 32/0793.

References

[1] K.L. Kovács et al., International Journal of Hydrogen Energy, 31, 1460 – 1468 (2006)

[2] I. Akkerman et al. *Photobiological*, International Journal of Hydrogen Energy,27,1195–1208 (2002)

[3] A. Melis, M.R. Melnicki, International Journal of Hydrogen Energy, 31, 1563 – 1573 (2006)

[4] M.B. Prieto et al., Journal of Biotechnology, 2002,97,1-11

[5] M. Waligórska, K. Seifert ,K Szymańska, M Łaniecki, Journal of Applied Microbiology, 101, 775-784 (2006)

[6] H. Biebl, N. Pfennig, In: The prokaryotes ed. M. P. Starr, H. Stolp, H.G. Trüper A. Balows, H.G. Schegel, New York Springer 1, 267-273 (1981)

[7] Z.Konsoula, M. Liakopoulou-Kyriakides, Enzyme and Microbial Technology, 39, 690-696 (2006)

[8] J. Ha, C.R. Engler J.R. Wild, Bioresource Technology 100, 1138-1142 (2009)

[9] K-C Chen, S-J Chen and J-Y Houn, Enzyme and Micobial Technology 18, 502-506 (1996)

[10] K-C Chen, J-Y Houng, Methods in Biotechnology Vol.1 Immobilization of Enzymes and Cells Ed. G.F. Bickerstaff Humana Press Inc 207-216 (1996)

[11] W.J. van Niel, P.A.M. Claassen, A.J.M. Stams, Biotechnology and Bioengineering 81, 255-262 (2003)

Continuous Photo-hydrogen Production from Acetate Using *Rhodopseudomonas Palustris* WP 3-5

Kuei-Ling Yeh[1], **Chun-Yen Chen**[1,2], **Yung-Chung Lo**[1] and **Jo-Shu Chang**[1,2,3]
[1] Department of Chemical Engineering, National Cheng Kung University
[2] Sustainable Environment Research Centre, National Cheng Kung University
[3] Microalgae Biotechnology and Bioengineering Laboratory, Center for Biotechnology and Biosciences, National Cheng Kung University, Tainan, Taiwan

Abstract

Phototropic hydrogen production using components of dark fermentation metabolites (i.e. acetate) is an ideal biohydrogen production route since it enables the highest yield possible (i.e., 12 mol H_2/mol hexose) and could also reduce COD content in the dark fermentation effluent to mitigate the environmental burden. In this work, a purple nonsulfur photosynthetic bacterial isolate *Rhodopseudomonas palustris* WP3-5 was utilized to produce H_2. To assess the performance of the photo-H_2 production system, the continuous photobioreactor was operated at a hydraulic retention time (HRT) of 48 h under different acetate concentrations. The optimal H_2 production efficiency occurred when the acetate concentration was 3000 mg COD/l, leading to an overall H_2 production rate and a H_2 yield of 20.4 ml/h/l and 0.98 mol H_2/mol acetate, respectively. In all tests, the acetate conversion was nearly constant at 87.0±3.1%. Next, the preferable HRT leading to the best H_2 production performance was identified. The results show that at an acetate concentration of 3000 mg COD/L, H_2 production rate increased with a decrease in HRT, giving the best performance at HRT=12 h with an overall H_2 production rate of 42.05 ml/h/l and a H_2 yield of 1.39 mol H_2/mol acetate. Operation under the aforementioned optimal substrate concentration and HRT, the overall H_2 production rate could be enhanced two-fold higher when compared with that obtained from preliminary tests. In addition, the HRT setting was found to play a key role in influencing the performance of continuous H_2 production by *R. palustris* WP3-5. The proposed continuous cultures seem to be a favourable choice of bioreactor strategy, possessing the potential to achieve higher H_2 production efficiency with an excellent stability.

1 Introduction

Hydrogen is a clean energy since combustion of H_2 produces only water without greenhouse gases. Hydrogen can also be directly utilized by hydrogen fuel cell to generate electricity at very high efficiency [1], thereby being considered a promising alternative energy carrier of the future. To this end, developing hydrogen production technology leading to a sufficient and sustainable H_2 supply is highly demanded [2]. Biological H_2 production considered as the most environmentally friendly route of producing H2 [3], thereby fulfilling the goals of recycling of renewable resources and clean energy production [4]. Phototrophic H_2 production has the advantage of high theoretical substrate conversion efficiency and

minerialization of organic substrates (e.g., organic acids), thereby being considered a critical step in the integrated fermentative hydrogen production [5-8]. This study was to identify the best carbon substrate (acetate) concentration since the organic loading often plays a critical role in affecting the kinetics of catabolism. Meanwhile, the stability of the continuous H_2 production system using different HRT concentration was also assessed to improve the performance of phototrophic H_2 production by *R. palustris* WP3-5.

2 Materials and Methods

2.1 Bacterial strain and cultivation medium

The *Rhodopseudomonas palustris* WP3-5 isolated from a swine wastewater treatment plant located in central Taiwan [9] was used for phototrophic H_2 production. The culture medium was using 2000 mg COD/l sodium acetate as a sole carbon substrate. The cells were cultivated at 32^{o}C anaerobically for 48 h under a light intensity of approximately 50 W/m^2 (illuminated by tungsten filament lamp). The initial pH value of medium prior to incubation was adjusted to 7.0-7.1. Argon gas was used to create an anaerobic condition.

2.2 Fabrication and operation of photobioreactor

The photobioreactor was a 1.0-liter glass-made vessel illuminated with external light sources (100 W tungsten filament lamp). The total light intensity for each illumination system was adjusted to ca. 95 W/m^2. After the reactor apparatus was sterilized by autoclave, cells of *R. palustris* WP3-5 were inoculated into the reactor with a 10% inoculum. All the fermentation was operated at pH 7.1 with an agitation rate of 200 rpm. A gas meter (Type TG1; Ritter Inc., Germany) was used to measure the amount of gas products generated and the gas volumes were calibrated to 25 ^{o}C and 760 mmHg. Gas samples were taken from sampling port by gas syringe at desired time intervals to measure the gas composition. The liquid sample was also collected from the sealed glass vessel with respect to time to determine cell concentration, pH and residual acetate concentration.

3 Results and Discussion

3.1 Effect of sodium acetate concentration on the photo-hydrogen production performance

Literature shows that the sodium acetate concentration is critical factors affecting the fermentation kinetics of biohydrogen production [10]. Therefore, in this study, acetate was used as the sole carbon source for phototropic H_2 production. The effect of acetate concentration on photo-H_2 production performance was examined in continuous cultures containing different initial acetate concentrations (sodium acetate = 1000–4000 mg COD/l). The results are indicated in Table 1. The volumetric H_2 production rate and specific H_2 production rate appeared to increase with increasing acetate concentration from 1000 to 4000 mg COD/l in all tests. This trend is quite reasonable as higher acetate (carbon substrate) loading usually leads to higher H_2 production. The optimal H_2 production efficiency occurred when the acetate concentration was 3000 mg COD/l, gave the best overall H_2

production rate and H_2 yield of 20.4 ml/h/l and 0.98 mol H_2/mol acetate, respectively. Meanwhile, the acetate conversion was nearly constant at 87.0±3.1%. Therefore, the acetate concentration of 3000 mg COD/l could give the relatively higher overall H_2 production rate and H_2 yield than other sodium acetate concentration used.

3.2 Effect of HRT on the photo-hydrogen production performance

To assess the applicability of the phototrophic H_2 production system, continuous culture by using different HRT was performed for a prolonged period of time under the optimal conditions in the present work (i.e., sodium acetate concentration = 3000 mg COD/l, light source = TL, light intensity = 95 W/m^2). As shown in Table 2, at 48 h HRT, the continuous culture gave a volumetric H_2 production rate of 20.4 ml/l/h. When the HRT was decreased to 12 h, the volumetric H_2 production rate was rapidly increased from 20.4 ml/l/h to 42.05 ml/l/h. Meanwhile, the cell concentration reached a nearly constant value of 3.11 g/l. The acetate conversion efficiency was obviously decreased with a decrease in HRT. These results clearly indicate that HRT was an important effecting factor for the photo-H_2 production of continuous operation by *R. palustris* WP3-5. This suggests that continuous cultures seem to be a more favorable choice of bioreactor strategy, having the potential to achieve higher H_2 production. Meanwhile, the H_2 content in biogas was nearly constant at 81.2±2.9% at 12 h HRT, indicating easier separation in downstream processing to obtain purified H_2 products for fuel cell applications.

Table 1: Photo-H_2 production performance at different sodium acetate concentration (HRT=48 h).

CH_3COOH (mg COD/L)	H_2 yield (mol H_2/mol actate)	Volumetric H_2 production rate (mL/h/L)	Specific H_2 production rate (mL/h/g cell)	Acetate conversion (%)
1000	0.86	6.86	2.65	98
2000	1.15	17.49	5.18	99
3000	0.98	20.40	5.46	87
4000	1.06	22.65	6.51	67

Table 2: Photo-H_2 production performance at different HRT (sodium acetate concentration = 3000 mg COD/L).

HRT (h)	H_2 yield (mol H_2/mol actate)	Volumetric H_2 production rate (mL/h/L)	Specific H_2 production rate (mL/h/g cell)	Acetate conversion (%)
48	0.98	20.40	5.46	87
36	1.46	28.85	7.37	62
24	1.55	35.33	7.90	48
12	1.39	42.05*	9.50	31

Reference

[1] C.Y. Chen, M.H. Yang, K.L. Yeh, C.H. Liu, J.S. Chang, Biohydrogen production using sequential dark and photo fermentation processes, Int. J. Hydrogen Energy, 33 (2008) 4755-4762.

[2] N.Q. Ren, B.F. Liu, J. Ding, W.Q. Guo, G.L. Cao, G.J. Xie, The effect of butyrate concentration on photo-hydrogen production from acetate by *Rhodopseudomonas faecalis* RLD-53, Int. J. Hydrogen Energy, 5981-5985 (2008) 21.

[3] S. Meher Kotay, D. Das, Biohydrogen as a renewable energy resource—Prospects and potentials, Int. J. Hydrogen Energy, 33 (2008) 258-263.

[4] V. Gadhamshetty, A. Sukumaran, N. Nirmalakhandan, M. Thein Myint, Photofermentation of malate for biohydrogen production-- A modeling approach, Int. J. Hydrogen Energy, 33 (2008) 2138-2146.

[5] B. Uyar, I. Eroglu, M. Yücel, U. Gündüz, Photofermentative hydrogen production from volatile fatty acids present in dark fermentation effluents, Int. J. Hydrogen Energy, 34 (2009) 4517-4523.

[6] H. Su, J. Cheng, J. Zhou, W. Song, K. Cen, Improving hydrogen production from cassava starch by combination of dark and photo fermentation, Int. J. Hydrogen Energy, 34 (2009) 1780-1786.

[7] N.Q. Ren, B.F. Liu, G.X. Zheng, D.F. Xing, X. Zhao, W.Q. Guo, J. Ding, Strategy for enhancing photo-hydrogen production yield by repeated fed-batch cultures, Int. J. Hydrogen Energy, 34 (2009) 7579-7584.

[8] N.Q. Ren, B.F. Liu, J. Ding, G.J. Xie, Hydrogen production with *R. faecalis* RLD-53 isolated from freshwater pond sludge, Biores. Technol., 100 (2009) 484-487.

[9] C.Y. Chen, W.B. Lu, J.F. Wu, J.S. Chang, Enhancing phototrophic hydrogen production of *Rhodopseudomonas palustris* via statistical experimental design, Int J Hydrogen Energy, 32 (2007) 940-949.

[10] C.M. Lee, P.C. Chen, C.C. Wang, Y.C. Tung, Photohydrogen production using purple nonsulfur bacteria with hydrogen fermentation reactor effluent, Int. J. Hydrogen Energy, 27 (2002) 1309-1313.

Biological Hydrogen Production from Sucrose and Sugar Beet by *Caldicellulosiruptor Saccharolyticus*

John Panagiotopoulos, National Technical University of Athens, Greece and Wageningen UR Food & Biobased Research, The Netherlands
Robert Bakker, **Truus de Vrije**, **Pieternel Claassen**, Wageningen UR Food & Biobased Research, The Netherlands
Emmanuel Koukios, National Technical University of Athens, Greece

Abstract

Hydrogen production needs to be based on renewable resources in order to be sustainable. Sugar beet is an ideal raw material for fermentative production of hydrogen in the EU and possibly in the USA due to its environmental profile and its potential availability in these areas. In this work, the fermentative production of hydrogen from sucrose of analytical grade and sugar beet extract by pure cultures of *Caldicellulosiruptor saccharolyticus* was investigated, under uncontrolled and controlled conditions. In the first case, growth of pure cultures of *C. saccharolyticus* on sucrose derived from sugar beet was compared to growth of the microorganism on sucrose of analytical grade. The production of hydrogen and organic acids (acetate and lactate) from sugar beet was largely equal to or slightly higher than the production of the control. In the second case, fermentation of sugar beet extract at sucrose concentration 10 g/l was comparable to the fermentation on pure sucrose except that the hydrogen yield was slightly higher on sugar beet extract. In particular, hydrogen yields of 2.9 and 3.0 mol/mol hexose were determined in fermentations of sucrose and sugar beet extract, respectively, corresponding to 73% and 75% of the theoretical value of 4 mol hydrogen/mol hexose. Acetic acid was the main product and very low production of lactic acid was observed.

1 Introduction

The looming energy challenges around the world will probably have to be tackled using a portfolio of different technologies. The production of hydrogen from biomass by biotechnological means is one of the most attractive technological options for efficiently producing clean energy [1,2]. Sugar-rich raw materials are advantageous in comparison to lignocellulosic ones, because they generally have a high content of readily fermentable sugars. Therefore, they are already well established in the literature [3,4,5,6] as substrates for fermentations.

Sugar beet (Table 1) is an ideal raw material for fermentative production of hydrogen in the EU [7] and possibly in the USA due to its environmental profile and its potential availability in these areas. The share of sugar beet in global sugar production is about 30%, with the rest coming mainly from sugar cane. Sugar beet (as well as sugar cane and sweet sorghum) is advantageous over the cereals (wheat, barley) in terms of yield of fresh biomass per hectare, yield of carbohydrates per hectare, and processing. Recently the comparison of the suitability

of several raw materials for fermentative hydrogen production was performed [2], and sugar beet was found one of the most technically attractive raw materials.

The objective of the present study is to assess (a) the fermentability of pure sucrose and sugar beet extract at sucrose concentration of 20 g/l, under fermentation conditions without control of pH and hydrogen pressure, and (b) the fermentative production of hydrogen from sucrose and sugar beet extract in batch fermentations under pH and hydrogen pressure controlled conditions, at an initial sucrose concentration of 10 g/l.

Table 1: Composition of sugar beet root expressed as % of dry matter.

Component	Amount %
Sucrose	67.3
Cellulose	4.2
Hemicellulose	5.2
Lignin	0.8
Protein	1.0
Ash	1.8

2 Materials and Methods

2.1 Raw material

Sugar beet was obtained from commercial farms, either in the south-west of The Netherlands or in Central-North Greece.

2.2 Experimental setup of the production of sugar beet extract

Sucrose extraction from sugar beet was designed to simulate the industrial sugar beet processing; the process included combined extraction of sugar and pressing, and has been previously described in details [2].

2.3 Fermentation

2.3.1 Microorganism, medium, cultivation

C. saccharolyticus DSM 8903 was obtained from the Deutsche Sammlung von Mikroorganismen und Zellkulturen (DSMZ). The culture medium consisted of (per litre) KH_2PO_4 0.3 g, K_2HPO_4 0.3 g, $MgCl_2.6H_2O$ 0.4 g, NH_4Cl 0.9 g, yeast extract 1.0 g, cysteine-HCl 0.75 g, $FeCl_3.6H_2O$ 2.5 mg, SL-10 trace elements 1 ml, and resazurine 0.5 mg. 4-morpholine propanesulfonic acid (MOPS, 10.5 g/l) was used as a buffer under uncontrolled conditions. The pH was adjusted to 7.0 at room temperature. Inoculation was done by adding 5% or 10% (v/v) of a preculture that was grown overnight on sucrose. Medium was made anaerobic by flushing with nitrogen. Experiments were carried out under non-sterile conditions. The culture was grown at 72 °C.

Fermentability was tested under uncontrolled conditions with closed flasks of 118 ml with 20 ml culture medium under a nitrogen atmosphere. The sucrose concentration was 10 g/l coming from sucrose of analytical grade, the sugar beet extract or various combinations of both. The detailed procedure of the fermentability experiments is described by Panagiotopoulos et al. [2].

Batch fermentations under controlled conditions were performed in a jacketed 2 l bioreactor (Applikon, Delft, The Netherlands) at a working volume of 1 l. The pH was controlled at circa 6.8 (measured at room temperature) by automatic addition of 2 N NaOH. Cultures were continuously stirred at 350 rpm and sparged with nitrogen at 7 l/h. The concentration of sucrose was 10 g/l coming from sucrose of analytical grade (hereafter referred to as pure sucrose) or the sugar beet extract. Fermentation was considered to have ended when the hydrogen concentration was less than 0.1% in the off-gas. Samples of 7 ml were regularly taken from the culture medium for measurement of the cell density, and substrate and product analyses.

2.3.2 Hydrogen yield and productivity

Hydrogen production yield was calculated as the molar amount of hydrogen divided by the molar amount of consumed hexose equivalent (mmol hydrogen/mmol hexose). The consumed unknown organic compounds were considered as carbohydrates with the same product yield as for sucrose. COD in mmol O_2/l was converted to mmol hexose/l according to the equation $C_6H_{12}O_6 + 6O_2 \rightarrow 6CO_2 + 6H_2O$. Details of the calculations are described by de Vrije et al. [8].

2.4 Analytical methods

The determination of the chemical composition of sugar beet as well as the analysis of sucrose, organic acids, hydrogen and carbon dioxide were performed as described earlier [2,8].

3 Results

The present study investigated the fermentative production of hydrogen from pure sucrose and sugar beet extract in uncontrolled small-scale fermentations, and in controlled batch fermentations at an initial sucrose concentration of 20 and 10 g/l, respectively. Focus was given on hydrogen and organic acid production from the sugar beet extract-containing medium, compared to the control sample with pure sucrose, in order to evaluate the comparative suitability of sugar beet for hydrogen fermentation. Particularly interesting was the determination of the hydrogen yield (mol hydrogen/mol hexose) obtained when sugar beet is used as substrate.

3.1 Fermentability of sucrose and sugar beet extract on small scale

The fermentability of sugar beet extract was tested in small-scale experiments with closed flasks. The ratio of (pure sucrose)-(sucrose derived from sugar beet extract) ranged from 100-0 (control sample) to 0-100. The total sucrose concentration in all samples was 20 g/l. The production of hydrogen and the main organic acids (acetate and lactate) by *C. saccharolyticus* in fermentations with increasing amounts of sugar beet extract was determined. *C. saccharolyticus* was able to grow and produce hydrogen from sucrose in all experiments performed (Figure 1A). Hydrogen production roughly seemed to increase with increasing sugar beet extract. This is in accordance with the growth of *C. saccharolyticus* which was maximised when 100% sugar beet extract was used. Moreover, increased acetate production and decreased lactate production were observed with increasing sugar beet

contents (results not shown). In total, organic acid production after 16 and 40 h of fermentation was largely equal to the control (Figure 1B).

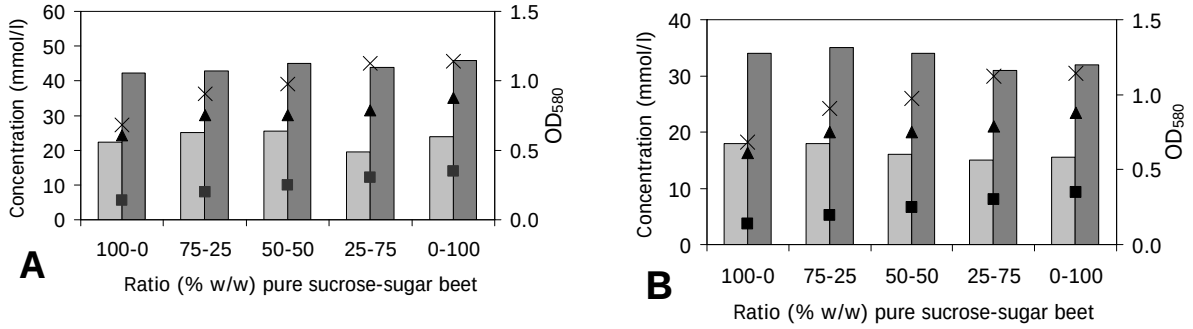

Figure 1: Hydrogen (A) and organic acid (sum of acetate and lactate) (B) production by culture of *C. saccharolyticus* grown on various ratios of pure sucrose and sugar beet extract. Measurements were done after 16 (light grey bars) and 40 (dark grey bars) h after the start of the fermentation. The growth of *C. saccharolyticus* (OD_{580}) after 0 (■), 16 (▲) and 40 (×) h of fermentation is also indicated.

3.2 Batch fermentations under controlled conditions in a bioreactor

Normal growth of *C. saccharolyticus* on pure sucrose and the sugar beet extract was achieved in batch fermentations under pH and hydrogen pressure controlled conditions, at an initial sucrose concentration of 10 g/l. Consumption of sucrose in both fermentations was almost complete after 26 h. The main products of the fermentations were hydrogen, acetate and carbon dioxide (Fig. 2). Production of lactate was minimal in both fermentations.

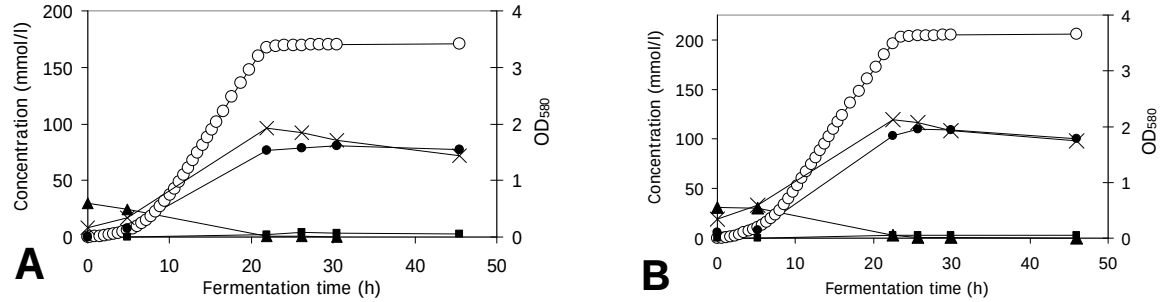

Figure 2: Fermentation profiles of batch cultivations of *C. saccharolyticus* in pH-controlled bioreactors on sucrose (A) and sugar beet extract (B) (10 g/l sucrose). The production of H_2 (○), acetate (●), lactate (■), the consumption of sucrose (▲) and the growth (×) of *C. saccharolyticus* are indicated. Amounts of sucrose and products are expressed in millimole per litre of culture.

For the pure sucrose-containing medium, a maximum hydrogen production rate of approximately 12.1 mmol/(l · h) was determined (Table 2), which was higher than the one of 8.4 mmol/(l · h) previously reported by van Niel et al. [9]. For the sugar beet extract-containing medium, maximum hydrogen production rate was approximately 12.8 mmol/(l · h).

The increased hydrogen production rate from the latter medium is possibly due to some compounds naturally present in sugar beet, such as phosphoric acid and amino acids, which may act as nutrients for cell growth. Hydrogen yields of 2.9 and 3.0 mol/mol hexose were observed in fermentations of sucrose and sugar beet extract, respectively, corresponding to 73% and 75% of the theoretical value of 4 mol/ hydrogen/mol hexose. The hydrogen to acetic acid molar ratio was 2.0-2.1 which is close to the theoretical value of 2.

Table 2: Molar yields and maximal volumetric hydrogen productivity (max. Q_{H2}) of *C. saccharolyticus* batch cultures grown on sucrose and sugar beet extract at 72 °C.

Substrate	Y_{H2} mol/mol C6	Y_{HAc} mol/mol C6	$Y_{HAc+HLac}$ mol/mol C6	max. Q_{H2} mmol/(l·h)
Sucrose	2.9	1.4	1.4	12.1
Sugar beet	3.0	1.5	1.6	12.8

Notable is the build-up of particulate matter, which took place during fermentation of the sugar beet extract, and did not cause any major disturbances in the process, but possibly led to a tendency to short periods of decreased hydrogen production after 4 and 12 h of fermentation (Fig. 3).

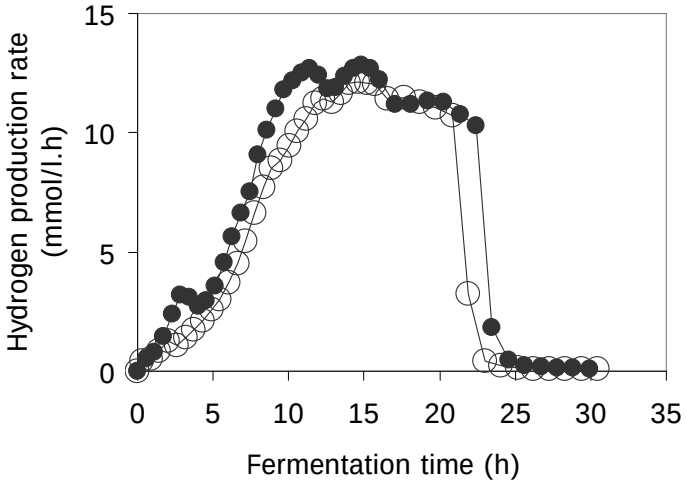

Figure 3: Hydrogen production rate by *C. saccharolyticus* grown on pure sucrose (open circles) and sugar beet extract (filled circles). The initial sucrose concentration was 10 g/l.

4 Conclusions

Sugar beet is a raw material well established in the literature as a substrate for fermentations, and can be instrumental in the middle-term in a sustainable hydrogen economy. The results of the present study suggest that *C. saccharolyticus* is suitable for efficient hydrogen production from sugar beet. In particular, *C. saccharolyticus* appears to

have a preference for sugar beet extract rather than for pure sucrose. Hydrogen yields of 2.9 and 3.0 mol/mol hexose were determined in controlled fermentations of sucrose and sugar beet extract, respectively, corresponding to 73% and 75% of the theoretical value of 4 mol hydrogen/mol hexose. Moreover, the results from the controlled fermentations are consistent with the notion that a fermentability experiment is a useful tool to rapidly determine the suitability of a raw material for hydrogen production.

Future research should address, from a biomass-oriented point of view, the utilization of sugar beet pulp for hydrogen production. The potential suitability of the pulp for hydrogen fermentation might contribute to the utilization of the whole plant as raw material for hydrogen production. From a biotechnological point of view, it might be interesting that future research focuses on the impact of several compounds naturally present in sugar beet on the fermentation of the sugar beet extract.

Acknowledgements

This work was financially supported by the Commission of the European Communities (6th Framework Programme, Sustainable Energy Systems, HYVOLUTION Integrated Project, Contract Nr. 019825) and the Foundation for Education and European Culture (Athens, Greece). The authors wish to thank M.A.W. Budde for her valuable assistance on the performance of the fermentability tests and the 1 litre-scale batch fermentations.

References

[1] http://www.hyvolution.nl

[2] Panagiotopoulos IA, Bakker RR, Budde MAW, de Vrije T, Claassen PAM, Koukios EG. Fermentative hydrogen production from pretreated biomass: A comparative study. Bioresource Technology 2009;100:6331–38.

[3] Hussy I, Hawkes FR, Dinsdale R, Hawkes DL. Continuous fermentative hydrogen production from sucrose and sugar beet. International Journal of Hydrogen Energy 2005;30:471–83.

[4] Chen CC, Lin CY. Using sucrose as a substrate in an anaerobic hydrogen producing reactor. Advances in Environmental Research 2003;7:695–9.

[5] Claassen PAM, de Vrije T, Budde MAW, Koukios EG, Glynos A, Réczey K, 2004. Biological hydrogen production from sweet sorghum by thermophilic bacteria. Proceedings of the Second World Conference on Biomass for Energy, Industry and Climate Protection, Rome, Italy. Vol. II 1522-1525.

[6] Ntaikou I, Gavala HN, Kornaros M, Lyberatos G. Hydrogen production from sugars and sweet sorghum biomass using *Ruminococcus albus*. International Journal of Hydrogen Energy 2008;33:1153–63.

[7] Panagiotopoulos IA, Bakker RR, de Vrije T, Urbaniec K, Koukios EG, Claassen PAM, 2010. Prospects of utilization of sugar beet carbohydrates for biological hydrogen production in the EU. Journal of Cleaner Production, in press, doi:10.1016/j.jclepro.2010.02.025.

[8] de Vrije T, Mars AE, Budde MAW, Lai MH, Dijkema C, de Waard P, Claassen PAM. Glycolytic pathway and hydrogen yield studies of the extreme thermophile

Caldicellulosiruptor saccharolyticus. Applied Microbiology and Biotechnology 2007;74:1358–67.

[9] van Niel EWJ, Budde MAW, de Haas GG, van der Wal FJ, Claassen PAM, Stams AJM. Distinctive properties of high hydrogen producing extreme thermophiles, *Caldicellulosiruptor saccharolyticus* and *Thermotoga elfii*. International Journal of Hydrogen Energy 2002;27:1391–8.

Microbial Electrolysis Cells for High-yield Biohydrogen Production from Fermentable Substrates

Bruce E. Logan, **Priscilla Selembo**, **Elodie Lalaurette**, **Geoffrey Rader**, Penn State University, USA
Pin-Ching Maness, **US Department of Energy**, National Renewable Energy Laboratory, USA

A microbial fuel cell (MFC) can be used to generate electrical current from the breakdown of organic matter by bacteria. Bacteria on the anode oxidize the organic matter, releasing electrons to the anode. Current flows to the cathode, where electrons combine with protons in the water and oxygen to form water. The voltage that is generated is about 0.5 V. The reaction is thermodynamically favourable, and so far a variety of biodegradable substrates have been used to generate electrical power, including pure compounds such as acetate and glucose [1, 2], as well as complex wastewaters from humans, animals and industry [3-5].

A microbial electrolysis cell (MEC) is a modified microbial fuel cell that can produce hydrogen gas at the cathode from the current generated by bacteria during the breakdown of organic matter [6]. Using an MEC it is possible to produce hydrogen gas at much higher yields than that possible by fermentation.

We conducted experiments here using a cube-shaped reactor consisting of a 4-cm long cylindrical chamber formed in a solid block of Lexan, with a liquid volume of 28 mL [7], as shown in Figure 1. The anodes used in these MECs were graphite fiber brush electrodes [8] pre-treated using an ammonia gas process [9]. Cathodes were flat carbon cloth containing a Pt catalyst (10% Pt/C) on the anode-facing side of the electrode. Gas produced in the reactor is collected in a glass anaerobic tube cut at the bottom and sealed to the top of the reactor. The top of the tube contains a thick rubber stopper and an aluminum crimp top. A needle pierces the topper, allowing gas to leave through tubing, flowing through a respirometer for gas measurement.

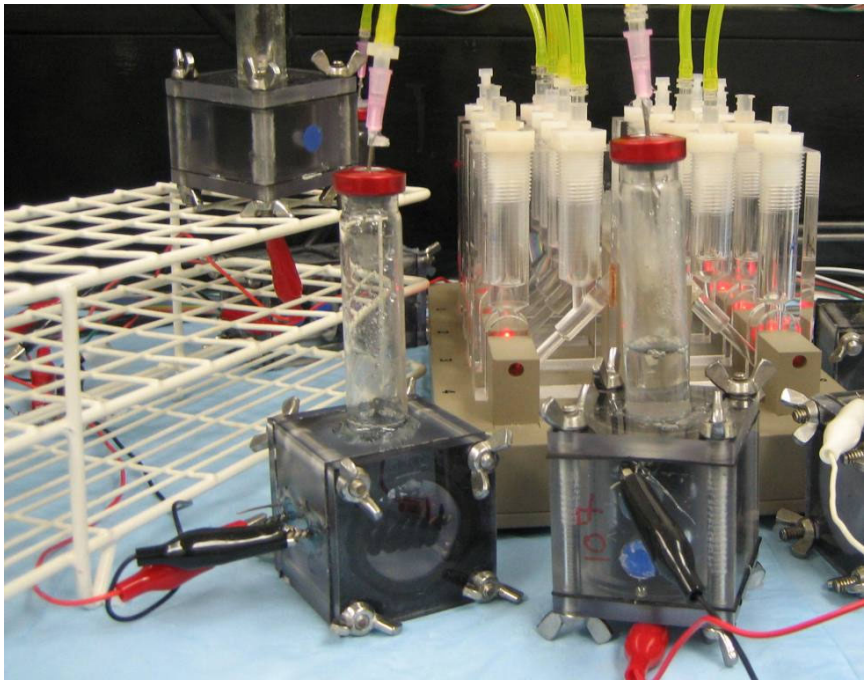

Figure 1: MEC reactor shown with tubing and bubble meters used to measure gas production in the reactor.

MEC tests with glycerol and glucose. Tests were conducted with two different fermentable substrates. In one set of tests we examined the use of glycerol, which is a side product of biodiesel fuel production. The production of 10 liters of biodiesel fuel results in the production of 1 liter of glycerol, and thus the production of useful products from glycerol is needed to make biodiesel production more economically viable as a renewable fuel. Tests were run using glucose as a positive control for hydrogen production from an easily fermentable substrate.

Dark fermentation tests were initially conducted to determine the amount of hydrogen that could be produced without the MEC. In fermentation tests, we achieved from glycerol a total of 0.28 mol-H_2/mol-glycerol, or only 4% of that possible by stoichiometric conversion of glycerol to hydrogen gas (a maximum of 7 mol/mol) [10]. With glucose we obtained 1.06 mol/mol compared to a maximum of 12 mol/mol.

In MEC tests using glycerol, we obtained 3.9 mol-H_2/mol-glycerol (56% of the maximum theoretical yield) [11]. This was comparable to that obtained with glucose, where we obtained 7.2 mol-H_2/mol-glucose (59% of the theoretical maximum). These percentage yields are both lower than those obtained with non-fermentable substrates such as acetate, where we can obtain up to 98% of the theoretical yields using an MEC [12]. To increase hydrogen yields it should be possible to use a two-stage process, where we can have fermentation in the first stage in order to maximize hydrogen production by fermentation, followed by a second stage using the MEC as described below.

Cellobiose and lignocelluose. Tests were conducted using a two stage process with cellobiose and lignocellulose. With cellobiose, we obtained in the first stage 1.64 mol H_2/mol-hexose-equivalent using *Clostridium thermocellum* for cellobiose fermentation [13]. In the

second stage, we achieved the equivalent of 2.9 mol H_2/mol for the mixture of the specific substrates in the feed using an MEC, or the equivalent of 8.31 mol H_2/mol for the MEC based on the starting substrate. Taken together, this is equivalent to 9.95 mol/mol overall for the two-stage process with cellobiose. Hydrogen yields and production rates using an actual fermentation effluents with lignocellulose were 750 ± 180 mL/g-COD and 1.00 ± 0.19 L/L-d (lignocellulose) [13]. These results show a two-stage system is a promising approach for biohydrogen production using fermentable substrates.

Figure 2: Photograph of a 1000-liter MEC being tested for hydrogen production using wastewater from a winery.

Field tests. The next step in development of this process is to examine the performance of larger scale systems. A 1000 liter reactor was recently constructed using graphite fiber brush anodes. The cathodes were made of stainless steel, based on our findings that stainless steel was able to catalyze hydrogen evolution at the cathode, and recent successes in using high surface area cathodes. Results for the field test will be presented at this meeting.

References

[1] Liu H, Grot S, Logan BE. Electrochemically assisted microbial production of hydrogen from acetate. Environ Sci Technol 2005;39(11):4317-20.

[2] Rabaey K, Lissens G, Siciliano SD, Verstraete W. A microbial fuel cell capable of converting glucose to electricity at high rate and efficiency. Biotechnol Lett 2003;25(18):1531-35.

[3] Min B, Kim JR, Oh S, Regan JM, Logan BE. Electricity generation from swine wastewater using microbial fuel cells. Water Res 2005;39(20):4961-68.

[4] Liu H, Ramnarayanan R, Logan BE. Production of electricity during wastewater treatment using a single chamber microbial fuel cell. Environ Sci Technol 2004;38(7):2281-85.

[5] Feng Y, Wang X, Logan BE, Lee H. Brewery wastewater treatment using air-cathode microbial fuel cells. Appl Microbiol Biotechnol 2008;78(5):873-80.

[6] Logan BE, Call D, Cheng S, Hamelers HVM, Sleutels THJA, Jeremiasse AW, Rozendal RA. Microbial electrolysis cells for high yield hydrogen gas production from organic matter. Environ Sci Technol 2008;42(23):8630-40.

[7] Call D, Logan BE. Hydrogen production in a single chamber microbial electrolysis cell (mec) lacking a membrane. Environ Sci Technol 2008;42(9):3401-06.

[8] Logan BE, Cheng S, Watson V, Estadt G. Graphite fiber brush anodes for increased power production in air-cathode microbial fuel cells. Environ Sci Technol 2007;41(9):3341-46.

[9] Cheng S, Logan BE. Ammonia treatment of carbon cloth anodes to enhance power generation of microbial fuel cells. Electrochem Commun 2007;9(3):492-96.

[10] Selembo PA, Perez JM, Lloyd WA, Logan BE. Enhanced hydrogen and 1,3-propanediol production from glycerol by fermentation using mixed cultures. Biotechnol Bioengin 2009;104(6):1098-106.

[11] Selembo PA, Perez JM, Lloyd WA, Logan BE. High hydrogen production from glycerol or glucose by electrohydrogenesis using microbial electrolysis cells. Int J Hydrogen Energy 2009;34(13):5373-81.

[12] Cheng S, Logan BE. Sustainable and efficient biohydrogen production via electrohydrogenesis. Proc Natl Acad Sci USA 2007;104(47):18871-73.

[13] Lalaurette E, Thammannagowda S, Mohagheghi A, Maness P-C, Logan BE. Hydrogen production from cellulose in a two-stage process combining fermentation and electrohydrogenesis. Int J Hydrogen Energy 2009;34(15):6201-10.

Visible-light Operated Biomass-oxygen Biofuel Cell

Yutaka Amao, **Yuka Sakai**, **Yukino Teshima**, Oita University, Japan

The visible light-operated starch-O_2 biofuel cell consisting of chlorophyll derivative, chlorin-e_6 (Chl-e_6) adsorbed on nanocrystalline TiO_2 layer coated onto optical transparent conductive glass electrode (OTE) as an anode, billirubin oxidase (BOD) immobilized OTE as a cathode, and the fuel solution containing starch as a polysaccharide biomass, glucoamylase, glucose dehydrogenase (GDH) and NAD^+ is studied as a new type of biofuel cell. The short-circuit photocurrent (I_{SC}) and the open-circuit photovoltage (V_{OC}) of this cell are 6.0 μA cm^{-2} and 530 mV, respectively. The fill factor of this cell is estimated to be 35 %. The maximum power output is calculated to be 1.6 μWcm^{-2}. Thus, a new type of visible light-operated starch -O_2 biofuel cell with the visible photosensitization of Chl-e_6 molecules on nanocrystalline TiO_2 film electrode and BOD immobilized OTE is accomplished. The advantage of this biofuel cell is to use BOD immobilized OTE instead of the platinum electrode. We opened a new avenue in the development of the biofuel cell that did not depend on platinum.

1 Introduction

Energy utilization of the biomass resources is important in the environmental science and the development of energy source research fields [1]. Biofuel cells using biomass have been attracted much attention in recent years. By developing these photoinduced hydrogen production systems in a photoelectrochemical conversion system, a new type of photo-operated saccharide-O_2 biofuel cell can be developed. We previously reported the photo-operated biofuel cell using chlorophyll derivative adsorbed on nanocrystalline TiO_2 layer coated onto optical transparent conductive glass electrode (OTE) as an anode, platinum-coated OTE as a cathode, and the solution containing glucose, glucose dehydrogenase (GDH) and NAD^+ as a fuel [2-5]. In the view point of biomass utilization, however, the development of photo-operated biofuel cell using oligo- and polysaccaride is desirable.

In this paper, we describe the visible light-operated starch-O_2 biofuel cell consisting of chlorin-e_6 (Chl-e_6) adsorbed on nanocrystalline TiO_2 layer coated onto optical transparent conductive glass electrode (OTE) as an anode, billirubin oxidase (BOD) immobilized OTE as a cathode, and the solution containing polysaccaride starch, glucoamylase, glucose dehydrogenase (GDH) and NAD^+ as a fuel as shown in Figure 1.

2 Experimental Section

The nanocrystalline TiO_2 film is prepared by a similar procedure to that described in the literature [6]. TiO_2 powder is dispersed by grinding water and HNO_3 aqueous solution. The viscous suspension is spread onto optical transparent conductive glass plate (OTE) (1 x 5 cm) at room temperature using scotch tape as a spacer. A thin film is obtained by raking off the excess of suspension with a glass rod. After the tape is removed and the plate is dried using hot plate at 80 °C for 30 min, this plate is annealed at 450 °C for 30 min under ambient

condition to form a nanocrystalline TiO_2 film electrode. The thickness of the film, determined by using a micron-sensitive calliper, is about 10 μm.

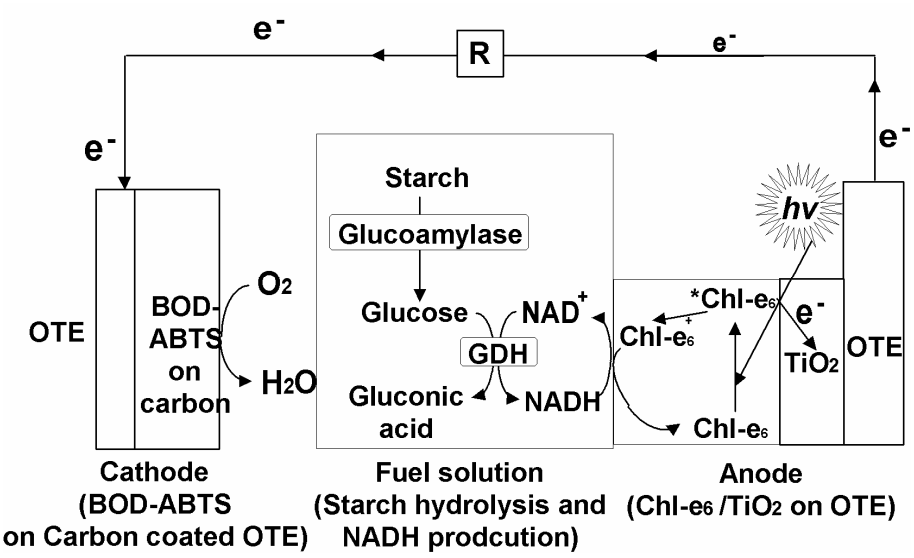

Figure 1: Visible light-operated starch-O_2 biofuel cell based on the combination of NAD^+ reduction with enzymatic starch hydrolysis photosensitization of Chl-e_6 on nanocrystalline TiO_2 layer coated OTE (anode) and the electrochemical reduction to the water of oxygen on to the BOD immobilized OTE (cathode).

Chl-e_6 adsorbed nanocrystalline TiO_2 electrode is prepared as follows. An OTE glass plate with a nanocrystalline TiO_2 film is dipped into 0.2 mmol dm^{-3} Chl-e_6 in methanol solution at room temperature for 6 h. After dipping, the plate is washed with methanol several times and then the plate is dried under vacuum overnight.

The BOD immobilized carbon-coated OTE electrode is prepared as following method. An OTE glass plate is dipped into BOD and 2,2'-Azino-bis((3-ethylbenzo-)thiazoline-6-sulfonic acid (ABTS) in Tris-HCl buffer solution at room temperature for 30 min. After dipping, the plate is dried at room temperature for 30 min under ambient condition. The active area of electrode is 1.0 cm^2.

Photocurrent-photovoltage characteristic of the Chl-e_6 adsorbed on TiO_2 electrode is measured with a sandwich type cell. The working electrode with the Chl-e_6 adsorbed on TiO_2 film is gently squeezed together with a BOD immobilized carbon-coated OTE glass electrode (counter electrode) using spring and irradiated from the substrate side of working electrode. The anodic solution is consisted of 0.1 mol dm^{-3} starch, 5 units glucoamylase, 3.5 mmol dm^{-3} NAD^+, 5 units GDH and 0.1 mol dm^{-3} KCl in 50 mmol dm^{-3} in 50 μl of 10 mmol dm^{-3} potassium phosphate buffer (pH 7.0). The dissolved oxygen in anodic solution is used as cathodic reaction of oxygen to water. A solar simulator (YSS-40, Yamashita Denso) is used as a light source (A.M. 1.5 100 mW cm^{-2}) for the photocurrent and photovoltage characteristics with the two digital multimeter with model 2000-J (Keithley) as a current meter and model 34401A (Agilent) as a voltage meter, respectively.

3 Results and Discussion

The photocurrent responses of photoinduced starch-O_2 biofuel cell were measured under 100 mWcm^{-2} irradiation. Figure 2 shows the photocurrent responses of starch-O_2 biofuel cell with 100 mWcm^{-2} irradiation. From Figure 2, the generated photocurrent increased with irradiation ("ON" in Figure 2). The photocurrent was estimated to be 6.0 μA cm^{-2}. In contrast, no current generation was observed under dark condition ("OFF" in Figure 2). The current changes also were fully reversible and hysterisis was not observed during the measurements.

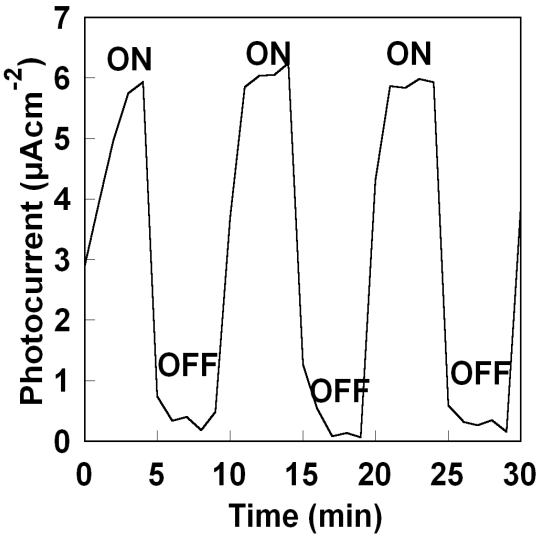

Figure 2: Photocurrent response of photo-operated starch fuel cell with 100 mWcm^{-2} irradiation.

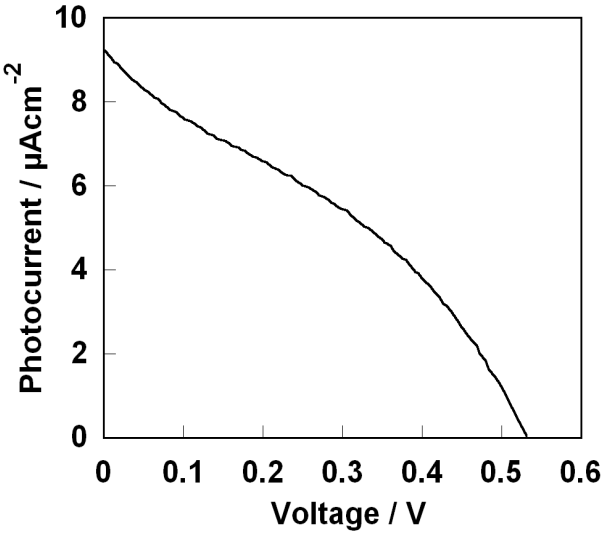

Figure 3: Photocurrent-photovoltage characteristic of photo-operated starch-O_2 biofuel cell under 100 mW cm^{-2} condition.

Figure 3 shows the photocurrent-photovoltage characteristics of photo-operated starch-O_2 biofuel cell irradiated with 100 mWcm^{-2}. The short-circuit photocurrent (I_{SC}) was 9.0 μA cm^{-2}, and the open-circuit photovoltage (V_{OC}) is 530 mV, respectively. The maximum power is estimated to be 1.6 μW cm^{-2}. In contrast, I_{SC} and V_{OC} under the dark condition are *c.a.* zero. Thus, this cell is operated with the visible-light photosensitization of TiO_2 film by Chl-e_6. These results show that photo-operated starch-O_2 biofuel cell based on the visible-light photosensitization of TiO_2 film by Chl-e_6 was developed.

Thus, a new type of visible light-operated starch- O_2 biofuel cell with the visible photosensitization of Chl-e_6 molecules on nanocrystalline TiO_2 film electrode and BOD immobilized carbon-coated OTE was accomplished.

4 Conclusion

In this work, visible light-operated starch-O_2 biofuel cell consisting of Chl-e_6 adsorbed on nanocrystalline TiO_2 layer coated onto optical transparent conductive glass electrode (OTE) as an anode, BOD immobilized carbon-coated OTE as a cathode, and the solution

containing starch, glucoamylase, glucose dehydrogenase (GDH) and NAD^+ as a fuel was studied. The I_{SC} and V_{OC} values of this cell are 9.0 μA cm^{-2} and 530 mV, respectively. As the conversion efficiency of photon-to-current and cell performance are still low, however, new type of starch-O_2 biofuel cell operated with photoenergy was developed by using the visible-light sensitization of Chl-e_6 on nanocrystalline TiO_2 film electrode and BOD immobilized electrode.

Acknowledgement

This work was partially supported by special found from Venture Business Laboratory of Oita University, and TEPCO Research Foundation.

References

[1] Taylor G Energy Policy (2008) 36:4406.

[2] Takeuchi Y, Amao Y (2003) Bioconjugate Chem 14: 268.

[3] Kim MS, Ahn JH, Yoon YS (2004) Biohydrogen III, 45.

[4] Amao Y, Takeuchi Y (2007) Int J Global Issue 28:295.

[5] Amao Y, Takeuchi Y (2008) Int J Hydro Energy 33: 2845.

[6] Nakade S, Kambe S, Kitamura T, Wada Y, Yanagida S (2001) J Phys Chem B 105: 9150.

Development of a Combined Bio-Hydrogen- and Methane-Production Unit Using Dark Fermentation

R. Brunstermann, **R. Widmann**, University of Duisburg-Essen, Faculty of Engineering Sciences (Building Sciences), Department of Urban Water and Waste Management, Germany

Abstract

Hydrogen is regarded as a source of energy of the future. Currently, hydrogen is produced, predominantly, by electrolysis of water by using electricity or by stream reforming of natural gas. So both methods are based on fossil fuels. If the used electricity is recovered from renewable recourses, hydrogen produced by water electrolysis may be a clean solution. At present, the production of hydrogen by biological processes finds more and more attention world far. The biology provides a wide range of approaches to produce hydrogen, including bio-photolysis as well as photo-fermentation and dark-fermentation. Currently these biological technologies are not suitable for solving every day energy problems [1]. But the dark-fermentation is a promising approach to produce hydrogen in a sustainable way and was already examined in some projects. At mesophilic conditions this process provides a high yield of hydrogen by less energy demand, [2]. Short hydraulic retention times (HRT) and high metabolic rates are advantages of the process. The incomplete transformation of the organic components into various organic acids is a disadvantage. Thus a second process step is required. Therefore the well known biogas-technique is used to degrade the organic acids predominantly acetic and butyric acid from the hydrogen-production unit into CH_4 and CO_2.

This paper deals with the development of a combined hydrogen and methane production unit using dark fermentation at mesophilic conditions. The continuous operation of the combined hydrogen and methane production out of DOC loaded sewages and carbohydrate rich bio-waste is necessary for the examination of the technical and economical implementation. The hydrogen step shows as first results hydrogen concentration in the biogas between 40 % and 60 %.The operating efficiency of the combined production of hydrogen and methane shall be checked as a complete system.

1 Introduction

The four steps of anaerobic digestion are shown in Figure 1. Only the last step, the methane production, is completely divided by eliminating methanogenic bacteria in the first process-step.

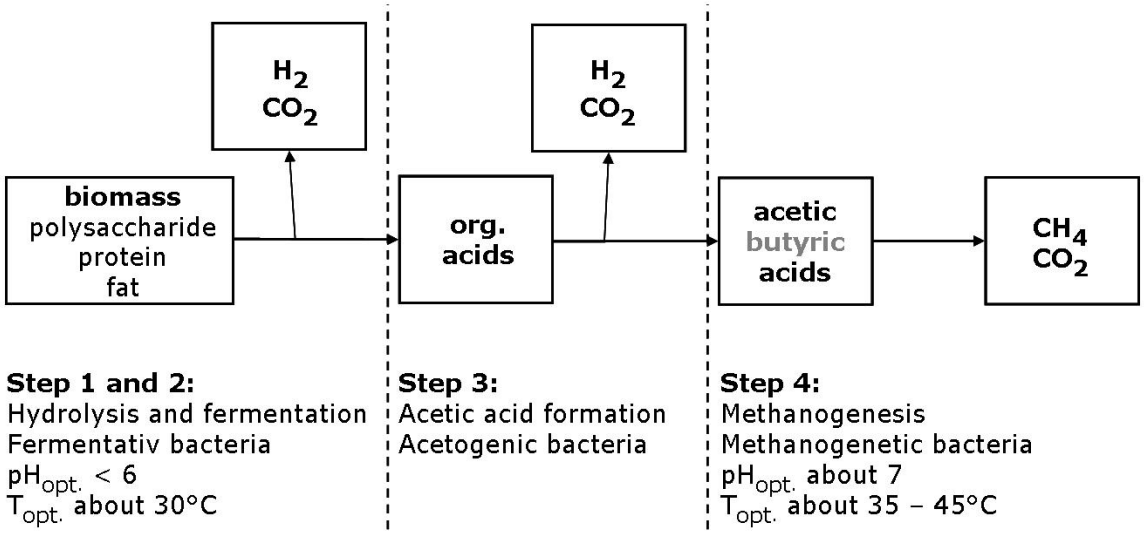

Figure 1: Four steps of anaerobic digestion.

According to [3], [4] hydrogen yields of 4 [mol/mol glucose] (Eq.1) at maximum are possible by dark fermentation with only 2 mol acetates as by-product. If only butyric acid accrue as by-product, the hydrogen yield decreases to 2 [mol/mol glucose] (Eq. 2).Typically, the end product of dark fermentation with mixed culture is a mix of different volatile fatty acids like acetic and butyric acid [2]; [5]. In consequence the stoichiometrical possible hydrogen yield is 2.5 [mol/mol glucose] (Eq.3).

If the liquid effluent of the H_2-reactor is used as carbon source in a methane reactor, the organic acids become degraded to CO_2 and CH_4. The theoretical methane yield that can be generated stoichiometrically depends on the liquid products of the hydrogen stage. The stoichiometric of possible bio-chemical reactions for the combined hydrogen and methane production with glucose as carbon source are given in table 1. The chemical equitation for the degradation of glucose in a conventional fermentation is also given in this table (Eq 4) [6].

Table 1: Bio-chemical reactions of the bio-hydrogen and methane production.

	substrate	1st reactor hydrogen	2nd reactor methane
Eq. 1	$C_6H_{12}O_6 + 2\ H_2O \rightarrow$	$2\ CH_3COOH + \mathbf{2\ CO_2 + 4\ H_2}$ [3], [4] $2\ CH_3COOH \rightarrow$	 **$2\ CH_4 + 2\ CO_2$**
Eq. 2	$2\ C_6H_{12}O_6 \rightarrow$	$2\ C_3H_7COOH + \mathbf{4\ CO_2 + 4\ H_2}$ [3] $2\ C_3H_7COOH + 2\ H_2O \rightarrow$	 **$5\ CH_4 + 3\ CO_2$**
Eq. 3	$8\ C_6H_{12}O_6 + 4\ H_2O \rightarrow$	$4\ CH_3COOH + 6\ C_3H_7COOH +$ **$16\ CO_2 + 20\ H_2$** [2]; [5] $4\ CH_3COOH + 6\ C_3H_7COOH + 6\ H_2O \rightarrow$	 **$19\ CH_4 + 13\ CO_2$**
Eq. 4	$C_6H_{12}O_6 \rightarrow$		**$3\ CH_4 + 3\ CO_2$** [6]

2 Materials and Methods

Continuous stirred-tank reactors (CSTR) were used. The hydrogen reactor had a working volume of 4 litres and the methane stage 30 litres.

For the hydrogen production several test-runs were made to verify optimal condition. In these experiments two seed materials (compost and heat treated digested sludge) at different conditions were tested. The temperature varied from ambient temperature of around 20°C up to 35°C, and the pH-value from 4.0 up to 5.5.

A nutrient solution according [7] was added to all reactors to provide optimal conditions for the mixed culture during the whole time of the test-runs. The hydraulic retention time (HRT) was decreased from 120 h to 24 h. By this, the organic loading rate (ORL) was increased. A survey of test runs discussed in this paper is given in Table 2.

Table 2: Survey of test-runs.

Reactor		Volume [L]	Temp. [°C]	pH [-]	HRT	Carbon source	Inocula	Duration [d]
R1	H2	10	without heating	4.5 - 5.2	15 – 26.5 h	Waste sugar	Heat treated digested sludge	200
R2	H2	3	30	4.5 - 4.8	48 – 30 h	Waste sugar	Heat treated digested sludge	50
R3	CH4	35	35	7.0	20 – 12.5 d	Output of R2	digested sludge	50

The pH-value of the hydrogen and methane reactors was regulated by using one molar NaOH-solution. During the tests the amount of produced gas was detected continuously with a gas meter and collected in a sample bag. The composition of the gas samples was detected once a day by thermal conductivity (H_2) and an infrared (CO_2 and CH_4).

The pH-value of the hydrogen and methane reactors was controlled by using one molar NaOH-solution. During the tests the amount of produced gas was continuous detected with a gas meter and collected in a sample bag. The composition of the gas samples was detected once a day by heat conductivity.

The experimental set-up of each reactor is shown in Figure 2 schematically.

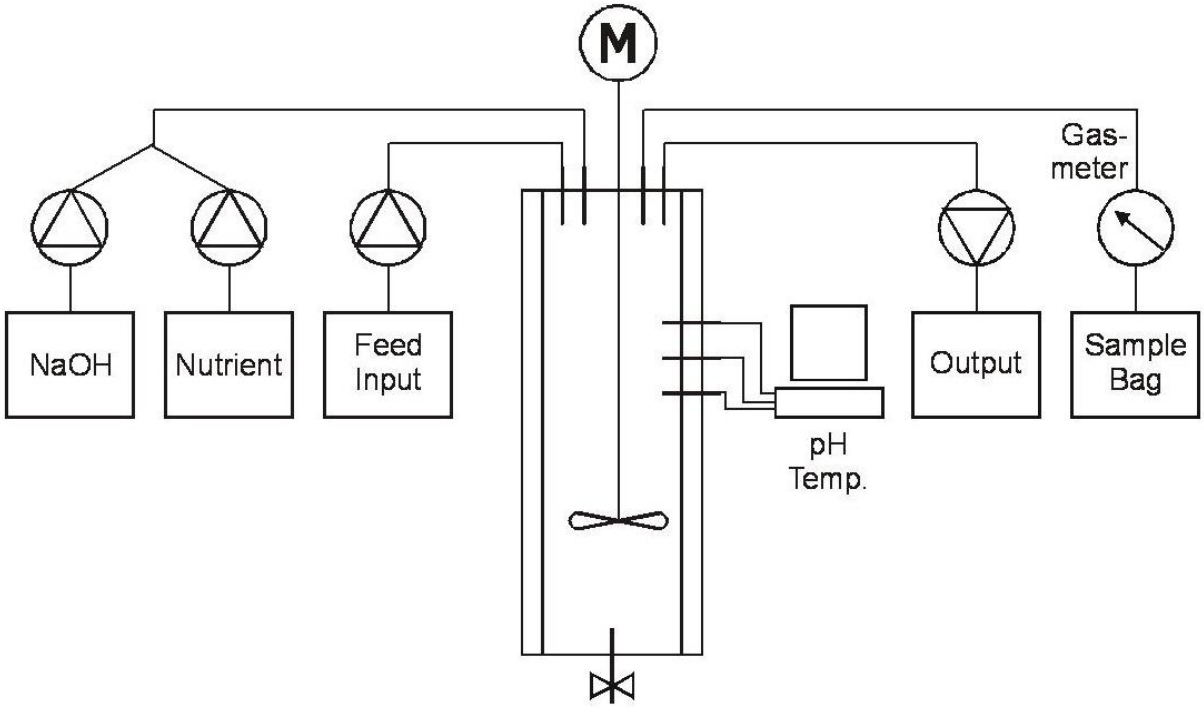

Figure 2: Experimental set-up for continuous hydrogen- and methane-production.

One H_2-reactor (R1) was working without heating at ambient temperature for 200 days. The temperature was only measured. Digested sludge of a wastewater treatment plant, which was boiled at 70°C for one hour, was used as seed material. The sludge was chosen, because of its consistency. The in- and output could be pumped with a peristaltic pump. A solution of a waste sugar with a concentration of 10 g/l and 15 g/l repetitively was used as carbon or rather hydrogen source in all hydrogen reactors.

The reactor R2 with a volume of 3 L was heated at 35 °C. The pH-value varied from 4.5 up to 4.8. Sugar solution was used as substrate. The output of this reactor was used directly as carbon source for the methane stage with a volume of 30 L (R3). So for the combined hydrogen and methane production the reactors R2 and R3 were directly connected with a tube.

Analysis of the sugar solution and the seed materials included the determination of dry matter (DM), volatile solids (VS) and total content of nitrogen and carbon (N, C). Furthermore, the analysis of the liquid end-products as well as the sugar solution included chemical oxygen demand (COD), dissolved organic carbon (DOC) and volatile fatty acids (VFA) measured as acetic acid.

3 Results and Discussion

Interesting findings of the continuous hydrogen production of R1 at ambient temperature are shown in Figure 3.

This figure shows, that gas yields of 2.5 [Nl/l*d] are reachable at hydraulic retention times (HRT) of 20 hours at 25 °C with a hydrogen concentration of approximately 58% (day 39 – 56).

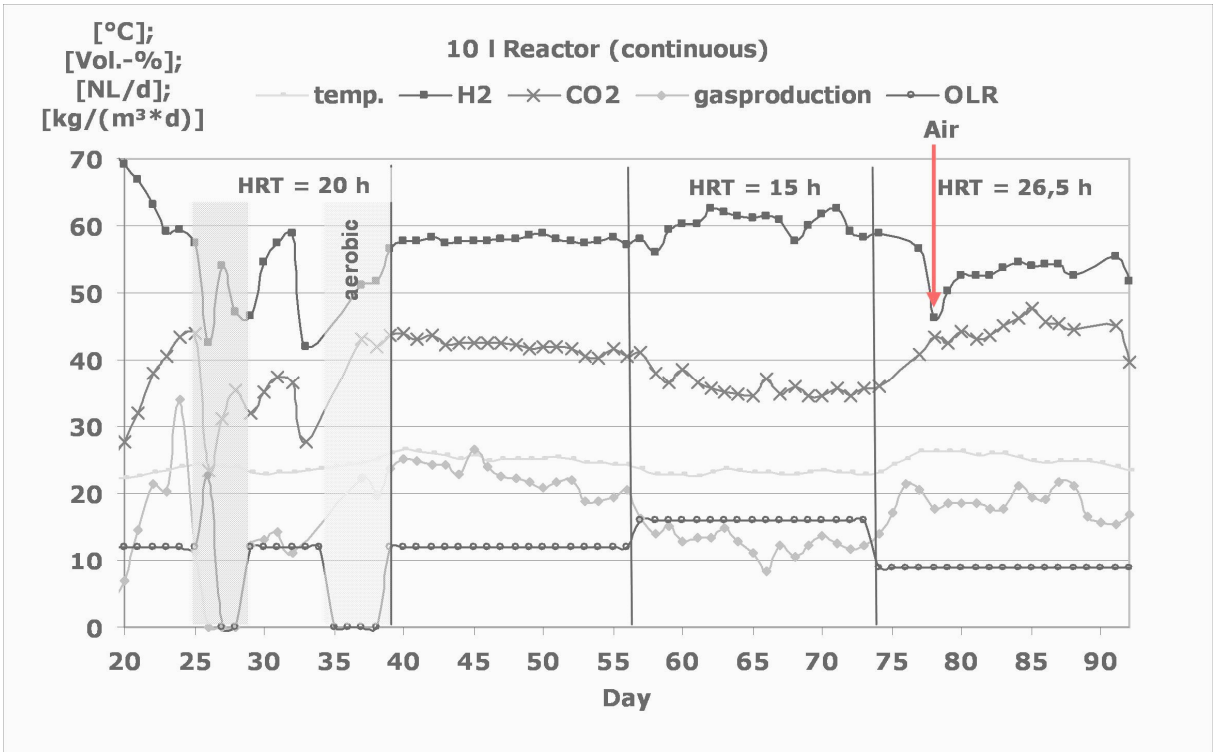

Figure 3: Effect of different HRT on continuous hydrogen production (Input feed: sugar water 10g/l).

Reduction of HRT (day 56 – 74) from 20 hours to 15 hours with according increase of OLR from 12 [g/L*d] to 16 [g/L*d] waste sugar, increased the hydrogen concentration to 63 %, but the gas yield decreased to approximately 1 [Nl/l*d]. So the overall hydrogen yields decreased. Therefore the ORL was reduced to 9 [g/L*d] in accordance with a HRT of 26.5 hours. At these conditions the gas yield increased to 2 [Nl/l*d] and the hydrogen content in the gas decreases to 55% on average (day 74 – 95).

Furthermore, Figure 3 shows the consequences from an overload of the digester caused by a pump fault between the 25th and the 28th day. The organic loading rate (OLR) suddenly became increased from 12 [g/L *d] waste sugar to 22.5 [g/L *d]. Due to this fault the hydraulic retention time (HRT) was reduced from 20 hours to 10.6 hours. As a result of overloading the gas production and hydrogen concentration went down. By switching off the pumps and therefore the temporary rearrangement of the continuous to the batch process the reactor recovered within a few days and the gas production started again.

The decrease of hydrogen concentration caused by continuous penetration of air into the anaerobic reactor at day 34, for several hours, was rearrange by switching to batch operation for a short period (2 days). The short aeration at day 78 caused by maintenance and repair did not affect the hydrogen production.

The gas production and composition of the test run with the connected reactor R2 and R3 are shown in Figure 4. In this test run the output of the hydrogen step was used as carbon source of the methane step. Therefore both reactors were connected by a peristaltic pump. The temperature of both reactors was maintained at 35°C.

The gray line (on the left) in Figure 4 represents the hydraulic retention time, which was reduced at day 32 from 48 h to 30 h. Causes by this the gas production (dark blue line with squares) decreased from 6 NL/d down to 1 NL/d whereas the hydrogen concentration (blue line with X) increased up to nearly 50 % (v/v). After day 40 the gas production of the hydrogen step stopped.

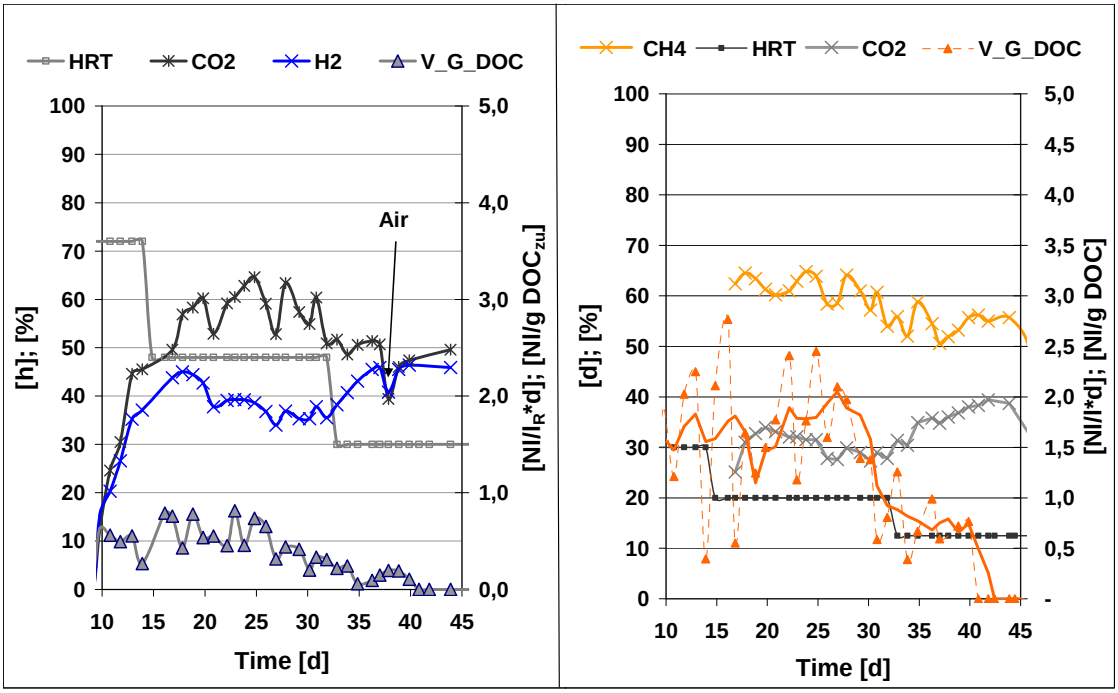

Figure 4: Gas production and –composition of the H2-reactor R2 (left) and CH4-reactor R3 (right).

The black lines with filled dots represents the hydraulic retention time (HRT), which was reduced at day 32 from 20 d to 12.5 h causes by reducing the HRT of the hydrogen step. This change influenced the methane concentration (orange line with X) slightly, but the gas production (orange line with filled triangles) was reduced by about a half. After day 40 the gas production of the methane step stopped like the gas production of the hydrogen step. This was caused by a leakiness of the tube which was connecting the both reactors. So both reactors were aerated.

4 Conclusions

The results show, that digested sludge pre-treated at 70°C for one hour include a stable mixture of bacteria, mainly of the family Clostridia, which are suitable for bio-hydrogen production by dark fermentation.

The results of R 1 exemplify, that a stabile hydrogen concentration in the range between 55 % and 60 % in the evolved gas at ambient temperature (23°C – 28°C) during continuous dark fermentation is possible. If the organic loading rate increases the hydrogen concentration in the gas increases too, but the gas production decreases. Furthermore a process break-down, caused by overloading the hydrogen reactor or flushing with air, could be repaired by turning the reactor temporally into batch process.

Results of experiments of a two stage test set up with bio-hydrogen production as first stage, followed by a “conventional” anaerobic digestion step with a tenfold volume show, that it is possible to combine these processes. By doing so, it is important to strictly divide both steps from each other because the methanisation stage can affect the hydrogen production negatively.

The combination of the two treatment steps bio-hydrogen production and “conventional” anaerobic digestion is a feasible option for example for the treatment of mono-charges, which is otherwise ensured by cost intensive enlargement of digester volume or massive reduction of organic load rate (OLR). However, further research is necessary to evaluate if the energy recovery with the combination hydrogen and methane with fuel cell is comparable to the conventional anaerobic digestion by using combined heat and power plants (CHP) to produce electricity.

References

[1] D. B. Levin, L. Pitt and M. Love. Bio-hydrogen production: prospects and limitations for practical application Int. J. Hydrogen Energy, Vol. 29 (2004) pp. 173 – 185

[2] Krupp M. Bio hydrogen production from organic waste and wastewater by dark fermentation - a promising module for renewable energy production. Schriftenreihe Forum Siedlungswasserwirtschaft und Abfallwirtschaft Universität Essen. Band 30, Shaker Verlag 2007. ISBN: 978-3-8222-6478-9

[3] Hawkes F. R., Dinsdale R., Hawkes D.L., Hussy I, (2002), Sustainable fermentative hydrogen production: challenges for process optimization, Int. J. Hydrogen Energy, Vol. 27, (2002) p. 1339 – 1347

[4] Hawkes F. R., Hussy I, Kyazze G., Dinsdale R., Hawkes D. L. (2007): Continuous dark fermentative production by mesophilic microflora: Principles and process, Int. J. Hydrogen Energy, Vol. 32, 2007, pp. 172 - 184

[5] P. C. Hallenbeck, and J. R. Benemann. Biological hydrogen production, fundamentals and limiting processes, Int. J. Hydrogen Energy, Vol. 27, (2002) p. 1185 – 1193

[6] H. G. Schlegel. Allgemeine Mikrobiologie. 7. Auflage, Thieme Verlag 1997, ISBN: 3-13-444607-3

[7] I. Hussy, F.R. Hawkes, R. Dinsdale, D.L. Hawkes. Continuous Fermentative Hydrogen Production from a Wheat Starch Co-Product by Mixed Microflora. Biotechology and Bioengineering Vol. 84, (2003) No. 6, pp. 619 – 626

[8] Rechtenbach D. Fermentative Erzeugung von Biowasserstoff aus biogenen Roh- und Reststoffen. Hamburger Berichte, Band 34, Verlag Abfall aktuell Stuttgart 2009, ISBN: 978-3-9812867-1-7

A Novel Biological Hydrogen Production System: Impact of Organic Loading

Hisham Hafez, **George Nakhla**, **Hesham El Naggar**, University of Western Ontario, Canada

Abstract

The patent-pending system comprises a novel biohydrogen reactor with a gravity settler for decoupling of SRT from HRT. Two biohydrogenators were operated for 220 days at 37 °C, hydraulic retention time 8 h and solids retention time ranged from 1.4 to 2 days under four different glucose concentrations of 2, 8, 16, 32, 48 and 64 g/L, corresponding to organic loading rates of 6.5-206 kg COD/m^3-d, and started up using anaerobically-digested sludge from the St. Marys wastewater treatment plant (St.Mary, Ontario, Canada) as the seed. The system steadily produced hydrogen with no methane. A maximum hydrogen yield of 3.1 mol H_2 /mol glucose was achieved in the system for all the organic loading rates with an average of 2.8mol H_2 /mol glucose. Acetate and butyrate were the main effluent liquid products at concentrations ranging from 640-7400 mg/L and 400-4600 mg/l, respectively, with no lactate detection. Microbial community analysis using denaturing gradient gel electrophoresis (DGGE) confirmed the absence of lactate producing bacteria *Lactobacillus fermentum* and other non-hydrogen producing species, and the predominance of various *Clostridium* species. Biomass concentrations in the biohydrogenators were steady, during the runs, varying form 1500 mg/L at the OLR of 6.5 kg COD/m^3-d to 14000 mg/L at the 104 kg COD/m^3-d, thus emphasizing the potential of this novel system for sustained stable hydrogen production and prevention of biomass washout.

1 Introduction

Hydrogen production from renewable substrates can reduce reliance on fossil fuels. It produces only water upon combustion, thus is considered as a clean energy source that can help mitigate pollution and global warming [1]. Biological hydrogen production is potentially regarded as one of the most promising alternatives for sustainable green energy production despite the feasibility of hydrogen production through water electrolysis and chemical cracking of hydrocarbons [2]. Among different biological processes for hydrogen production, dark fermentation is the most attractive one because of its potential of direct use of wastewater streams and organic wastes and its higher rate of hydrogen production in comparison with photo-fermentative processes [3].

Organic loading rate (OLR) is an important parameter in studying hydrogen bioreactors. In order to optimize a system for hydrogen production, it is essential to define either a range of the organic loading rates that the system can handle effectively, or an optimal organic loading rate for a maximum hydrogen yield. In the literature, there is no clear relationship between the hydrogen yield and the organic loading rate. In some cases higher OLRs decreased the hydrogen yield [4] whereas in some others higher OLRs increased the hydrogen yield [5]. For waste activated sludge as a seed material, it appears that increasing

the OLR within the 40-160 gCOD/L-d increased hydrogen yield to an optimum of 1.6 mol H_2/mol glucose at an OLR of 120 gCOD/L-d [6], whereas hydrogen yield decreased with increasing OLR for both anaerobically digested sludge [7] and soil microorganisms [4]. Although lower molar H_2 yields at higher OLRs have been attributed to the inhibitory effect of higher H_2 partial pressures in the growth medium [4, 8], variations in the composition of bacterial communities that become established at different OLRs [9] may be a major reason for lower yields. Hydrogen yield with digester sludge at an OLR of 45 gCOD/L-d was 1.3 mol H_2/mol glucose [7] as compared with 0.9 mol H_2/mol glucose with waste activated sludge [6]. Moreover, comparing the biomass concentration in two studies with continuously stirred tank reactors (CSTRs) utilizing agricultural soil as the seed and glucose as a substrate under approximately same OLRs, Van Ginkel and Logan [4] achieved much higher hydrogen yield (2.2 mol/mol) at a biomass concentration of 8 g/L compared to Zhang et al. [10] who reported 0.72 mol H_2 /mol hexose with 0.9 g/L biomass. Oh et al. [11] achieved a hydrogen yield of 0.4 mol/mol at a biomass concentration of 2.2 g/L in a CSTR and Wu et al. [6] using a CSTR seeded with silicone-immobilized sludge realized a hydrogen yield of 1.6 mol/mol at 3.5 g/L of biomass compared to a hydrogen yield of 2.1 mol/mol achieved by Zhang et al. [5] at a similar OLR with a higher biomass concentration (4.6 g/L). It is thus clear that the higher biomass concentration in the reactors improved the hydrogen yield, which in essence shows that one of the key factors affecting the stability of hydrogen producing systems is maintaining higher biomass concentrations in the system. In addition, the low hydrogen yield and system failure was attributed to low concentrations of biomass due to washout [4].

This main objectives of this paper focuses primarily on the investigation of the effect of organic loading rate on the performance of a novel integrated biohydrogen reactor clarifier system (IBRCS) [12] and to specify an optimal range for organic loading rate that maximizes hydrogen yield. The premise of the IBRCS is decoupling of hydraulic retention time (HRT) from solids retention time (SRT), which has been demonstrated in a previous work. [13]

2 Materials and Methods

Systems set up and operations

Two lab-scale systems were operated at 37 °C for 220 days (Figure 1), at six different organic loading rates ranging from 6.5 gCOD/L-d to 206 gCOD/L-d. Two integrated biohydrogen reactor clarifier systems (IBRCSs) comprised a continuously stirred reactor (CSTR) for biological hydrogen production (5 L working volume), followed by an uncovered gravity settler (volume 8 L) i.e. open to atmosphere for the decoupling of solids retention time (SRT) from the hydraulic retention time (HRT). Details of the operational conditions for the six runs are listed in Table 1. In order to enrich hydrogen producing bacteria, the sludges were heat treated at 70 °C for 30 minutes. Following the completion of each run and the attainment of steady-state conditions, the systems were cleaned and inoculated with pre-treated sludges. OLR-1 and 2 were run simultaneously, followed by OLR-3 and 4, and lastly OLR-5 and 6. The systems were monitored for total chemical oxygen demand (TCOD), soluble COD, volatile fatty acids (VFA), ethanol, lactate, glucose, volatile suspended solids (VSS), total suspended solids (TSS) and biogas composition including hydrogen, methane

and nitrogen. The quantity of produced biogas was recorded daily using a wet tip gas meter (Rebel wet-tip gas meter company, Nashville, TN, USA).

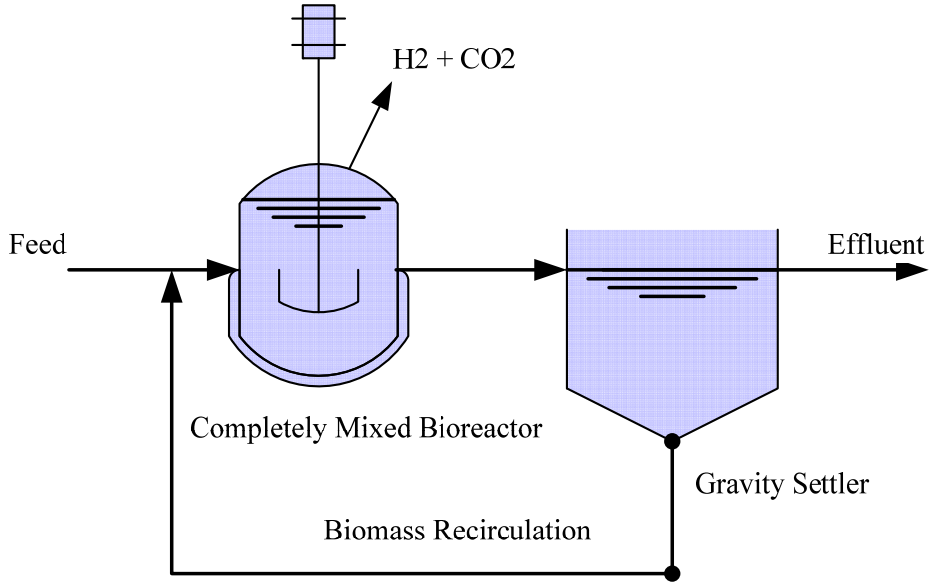

IBRCS

Figure 1: Experimental Setup for the integrated biohydrogen reactor clarifier system.

Inocula and media compositions

Anaerobically-digested sludge from the St.Marys wastewater treatment plant (St.Marys, Ontario, Canada) was used as the seed. The two systems operated in parallel at the same time under two different OLRs for a total of six OLRs (three consecutive runs). The systems were seeded with 5 liters of sludge and started up in a continuous mode with the feed containing glucose at different concentrations as highlighted in Table 1. The same startup technique was repeated for the three runs. It must be emphasized that there was no sludge wastage from the clarifier throughout the operation, and the values of SRTs presented in Table 1 represent the average ± standard deviation (SD) during steady state operation. It is noteworthy that the reactors operation was consistent over time and accordingly the average SRT with SD of less than 10% of the mean SRT is representative of the overall SRT during the run. As expected, the clarifier effluent VSS was substantially lower than the reactor VSS and remained unchanged during steady-state operation. The feed contained sufficient inorganics (mg/L): $NaHCO_3$, 2000-16000; $CaCl_2$, 140; $MgCl_2.6H_2O$, 160; NH_4HCO_3, 600; $MgSO_4.7H_2$ O, 160; urea, 500-2000; Na_2CO_3, 124-300; $KHCO_3$, 156; K_2HPO_4, 15-20; trace mineral solution, 500; H_3PO_4, 250-1500.

Table 1: Operational conditions.

	Glucose (g/L)	HRT (h)	SRT (h)	OLR (gCOD/L-d)
OLR -1	2	8	50 ± 5	6.5
OLR -2	8	8	45 ± 4	25.7
OLR -3	16	8	45 ± 6	51.4
OLR -4	32	8	42 ± 6	103
OLR -5	48	8	27 ± 3	154
OLR -6	64	8	26 ± 2	206

Note: Values represent average ± standard deviation

3 Analytical Methods

The biogas composition including hydrogen, methane, and nitrogen was determined by a gas chromatograph (Model 310, SRI Instruments, Torrance, CA) equipped with a thermal conductivity detector (TCD) and a molecular sieve column (Molesieve 5A, mesh 80/100, 6 ft X 1/8 in). Argon was used as carrier gas at a flow rate of 30 mL/min. The temperatures of the column and the TCD detector were 90 and 105 °C, respectively. The concentrations of volatile fatty acids (VFAs) were analyzed using a gas chromatograph (Varian 8500, Varian Inc., Toronto, Canada) with a flame ionization detector (FID) equipped with a fused silica column (30m × 0.32 mm). Helium was used as carrier gas at a flow rate of 5 mL/min. The temperatures of the column and detector were 110 and 250 °C, respectively. Lactic acid concentrations were measured using a high-performance liquid chromatography system (1200 series, Agilent Technologies) equipped with Aminex HPX-87H ion exclusion column (300 mm × 7.8 mm I.D.; BIO-RAD), and a UV-detector at 210 nm. The column temperature was adjusted to 30 °C. The same instrument with a refractive index detector (RID) was used to measure the concentrations of glucose. The temperature of the RID detector was set to 35 °C. The amount of volatile suspended solids (VSS) and chemical oxygen demand (COD) were measured according to standard methods [14]. Particle size distribution was determined by Malvern Mastersizer 2000 (version 5.22) laser beam diffraction granulometer.

4 Results and Discussion

Figures 2 (a and b) shows the diurnal variation of hydrogen production rate and yield (based on the amount of glucose converted). Although steady-state was observed in all runs after 3-7 days of startup, the systems were kept in operation at steady state for 55-75 days. The systems showed stable hydrogen production during the experimental period. The coefficient of variation (calculated as standard deviation divided by the average) for hydrogen production rate and yield in all runs was approximately less than 10%. The two integrated biohydrogen reactor clarifier system (IBRCS) were operated at OLRs of 6.5 gCOD/L-d and 25.7 gCOD/L-d for 55 days in steady state. The hydrogen production rate averaged 12 L/d and 48 L/d for OLR-1 and OLR-2, respectively. The two IBRCSs were then restarted and tested under OLRs of 51.4 gCOD/L-d and 103 gCOD/L-d. The operational period was

extended for a period of 75 days. The hydrogen production rate increased to 97 L/d and 179 L/d for OLR-3 and OLR-4, respectively. The glucose conversion in the system under the three OLRs was almost 100 % and decreased to approximately 95 % at OLR-4.

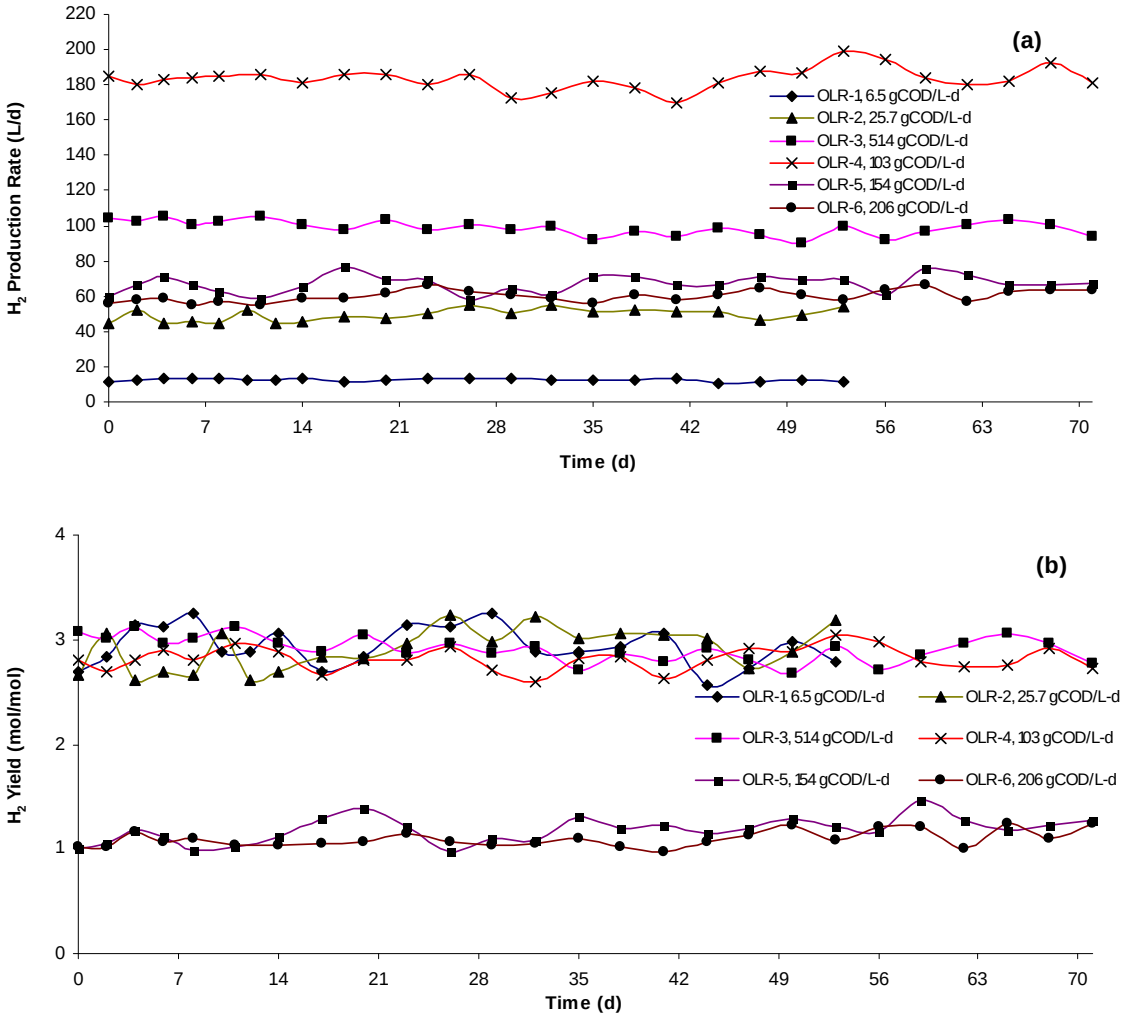

Figure 2: Diurnal variation for: a) hydrogen production rate, b) hydrogen yield

Figure 3 depicts the steady-state volumetric hydrogen production and molar yields, calculated based on the data of the last 55 days for OLR-1 and 2, and 75 days for OLR 3 to 6. As illustrated in Figure 3a linear increase in the hydrogen production rate with the increase of the OLR was observed up to 103 gCOD/L-d. On the other hand, the hydrogen yield of 2.8 mol H_2/ mol glucose was almost constant during the same range of OLRs. To determine the optimum OLR that maximizes hydrogen production, the systems were restarted under an OLRs of 154 gCOD/L-d and 206 gCOD/L-d. The average hydrogen yields after 75 days of steady state operation were 1.2 mol H_2/ mol glucose and 1.1 mol H_2/ mol glucose for OLR-5 and OLR-6, respectively. The increase in OLR not only decreased the hydrogen yield but also the hydrogen production rate dropped to approximately 65 L/d (13 L/L/d). The hydrogen content in the biogas was around 72 % in OLR-1 and 2, 66 % in OLR-3 and 4, and 42 % in

OLR-5 and 6 with the balance in all cases CO_2. It is apparent from Figure 3 that the maximum OLR at the system HRT of 8 h in terms of hydrogen production is 103 gCOD/L-d.

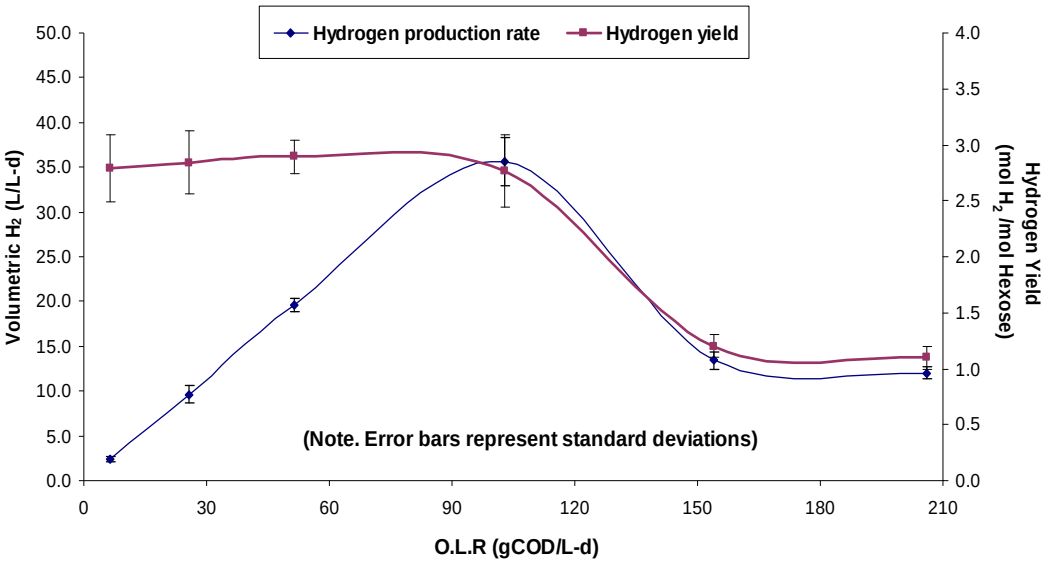

Figure 3: Relationship between hydrogen production rate and hydrogen yield versus OLR.

The biomass concentration in the reactor is an important operational parameter that affects both system stability and hydrogen yield. The average concentration of VSS in the biohydrogen reactor increased ten-fold from 1.5 g/L to 15.7 g/L with the increase in OLR from 6.5 gCOD/L-d to 103 gCOD/L-d. In OLR-5 and OLR-6 the concentrations of VSS were 18.4 g/L and 17 g/L, respectively. Using steady-state data for both VSS (g/L) and hydrogen production rate (L/d) at each OLR, the biomass specific hydrogen production rate was calculated. During the first four OLRs i.e. 6.5 to 103 gCOD/L-d, the average biomass hydrogen production rate was 2.1 ± 0.3 L H_2 / gVSS-d and the average food to microorganisms' ratio (F/M) was 5.7 ± 0.9 gCOD /gVSS-d. When the OLR was increased to 154 gCOD/L-d and 206 gCOD/L-d the biomass specific hydrogen production rate dropped to 0.7 L H_2 / gVSS-d with average F/M ratios of 8.5 and 12.1 gCOD /gVSS-d, respectively.

Microbial community analysis

The DGGE profiles of the 16S rDNA gene fragments at four organic loading rates are demonstrated in Table 2. Comparing the results from OLR-1 and OLR-2, revealed that the relatively higher OLR-2 (25.7 gCOD/L-d) resulted in a significant increase in microbial diversity. *Clostridium acetobutyricum* (band A), *Klebsiella pneumonia* (band B) and uncultured bacterium (DQ464539.1) (band F) were the only observed bands at OLR-1. *Clostridium acetobutyricum*, *Klebsiella pneumonia* are well known hydrogen producers that have been frequently used for hydrogen production [19,20] or detected as active microorganisms in mixed cultures of hydrogen producing bioreactors [21,22]. The uncultured bacterium DQ464539.1 (band F) had also been reported in an acidophilic ethanol-H_2-coproducing system. At OLR-2 another hydrogen producers including *Clostridium butyricum* (band C), a *Clostridium acetobutyricum* affiliated strain (band D) and *Clostridium*

pasteurianum (band E) were detected. High yields of hydrogen have been reported in the literature with *Clostridium butyricum* and *Clostridium pasteurianum* [23,24]. Band G which was available only at OLR-2 identified as an uncultured bacterium (DQ414811.1). This band was 97% similar to a strain which had been reported in a hydrogen production bioreactor by Koskinen et al. [25]. Increasing the OLR to OLR-5 and OLR-6 resulted in formation of different microbial community in the reactors. Although most of the hydrogen producers were also present at OLR-5 and OLR-6 some new bands also appeared with increasing the OLR. Two of these bands which were identified were *Lactococcus sp.* (band H) and *Pseudomonas sp.* (band I). *Clostridium acetobutyricum* (band A) was absent at both OLR-5 and OLR-6. It should be noted that some of the DGGE bands were not identified due to presence of a lot of bands in a small area could also be related to hydrogen producers. The increase in the microbial diversity with the increase in the OLR from 6.5 to 25.7 gCOD/L-d is in agreement with the findings of Luo et al. [9], while at the extremely high OLR-5 and OLR-6 clear microbial shifts *only* were identified.

Table 2: Affiliation of denaturing gradient gel electrophoresis (DGGE) fragments determined by their 16S rDNA sequence.

Affiliation (accession no.)	Bands	Similarity (%)	OLR-1	OLR-2	OLR-5	OLR-6
Clostridium acetobutyricum (FM994940.1)	A	99	×	×		×
Klebsiella pneumonia (GQ214541.1)	B	100	×	×		×
Clostridium butyricum (DQ831124.1)	C	99		×	×	×
Clostridium acetobutyricum (FM994940.1)	D	95		×	×	×
Clostridium pasteurianum (GQ214541.1)	E	99		×		
Uncultured bacterium (DQ464539.1)	F	96	×	×		×
Uncultured bacterium (DQ414811.1)	G	97		×		
Lactococcus sp. (YM05004.1)	H	95			×	×
Pseudomonas sp. (AJ846267.1)	I	96			×	×

Conclusions

Based on the findings of this study within the range of OLRs investigated (6.5 to 206 gCOD/L-d) and at HRT of 8 h and SRT of 1-2 d, the following conclusions can be drawn:

- The optimum volumetric hydrogen production rate occurred at an OLR of 103 gCOD/L-d
- Molar hydrogen yield remained relatively stable at 2.8 mol H_2/mol glucose at OLRs in the range of 6.5 to 103 gCOD/L-d, but declined rapidly thereafter to 1.1 mol H_2/mol glucose.
- Molar hydrogen yield correlated linearly with the acetate-to-butyrate molar ratios, and was mostly around 1 and 2.8 mol H_2/mol glucose at acetate-to-butyrate ratios ranging from 0.8 to 1.3 and 2 to 3, respectively.
- Glucose conversion decreased drastically from 99% at OLRs of 6.5 to 103 gCOD/L-d, to only 56% and 40% at OLRs of 154 and 206 gCOD/L-d, not due to acetate

inhibition, but primarily due to residual glucose concentrations of 21000 and 38000 mg/L.

- Microbial community analysis on OLR-1 and OLR-2 showed the predominance of hydrogen producers such as *Clostridium acetobutyricum, Klebsiella pneumonia, Clostridium butyricum, and Clostridium pasteurianum.* While at extremely high OLRs of 154 and 206 gCOD/L-d, a microbial shift was clearly evident due to the coexistence of the non hydrogen producers such as *Lactococcus sp.* and *Pseudomonas sp.*

References

[1] Billings RE. The H_2 world view. 1st ed. American Academy of Science; 1991.

[2] Levin DB, Pitt L, Love M. Biohydrogen production: Prospects and limitations to practical application. Int J Hydrogen Energy. 2004;29(2):173-85.

[3] Wang JL, Wan W. Factors influencing fermentative hydrogen production: A review. Int J Hydrogen Energy. 2009;34(2):799-811.

[4] Van Ginkel SW, Logan B. Increased biological hydrogen production with reduced organic loading. Water Res. 2005;39(16):3819-26.

[5] Zhang JJ, Li XY, Oh SE, Logan BE. Physical and hydrodynamic properties of flocs produced during biological hydrogen production. Biotechnol Bioeng. 2004;88(7):854-60.

[6] Wu SY, Hung CH, Lin CN, Chen HW, Lee AS, Chang JS. Fermentative hydrogen production and bacterial community structure in high-rate anaerobic bioreactors containing silicone-immobilized and self-flocculated sludge. Biotechnol Bioeng. 2006;93(5):934-46.

[7] Kyazze G, Martinez-Perez N, Dinsdale R, Premier GC, Hawkes FR, Guwy AJ, et al. Influence of substrate concentration on the stability and yield of continuous biohydrogen production. Biotechnol Bioeng. 2006;93(5):971-9.

[8] Ruzicka M. The effect of hydrogen on acidogenic glucose cleavage. Water Res 1996;30(10):2447–51.

[9] Luo Y., Zhang H., Salerno M., Logan B.E., Bruns M.A. Organic loading rates affect composition of soil-derived bacterial communities during continuous, fermentative biohydrogen production. Int J of Hydrogen Energy. 2008; 33 (22):6566-6576.

[10] Zhang JJ, Li XY, Oh SE, Logan BE. Physical and hydrodynamic properties of flocs produced during biological hydrogen production. Biotechnol Bioeng. 2004;88(7):854-60.

[11] Oh SE, Lyer P, Bruns MA, Logan BE. Biological hydrogen production using a membrane bioreactor. Biotechnol Bioeng. 2004;87(1):119-27.

[12] Hafez H, Nakhla G, El Naggar H. Integrated system for hydrogen and methane production during landfill leachate treatment. Pending patent, US Patent Application US 61/202,137, 2009.

[13] Hafez H, Nakhla G, El Naggar H. Biological Hydrogen Production from Corn-Syrup Waste Using a Novel System. Energies 2009, 2, 445-455.

[14] APHA, AWWA, WEF. Standard methods for examination of water and wastewater, 19th edition. ; 1995.

[15] Altschul SF, Gish W, Miller W, Myers EW, Lipman DJ. Basic local alignment search tool. J Mol Biol. 1990 OCT 5;215(3):403-10.

[16] O-Thong S, Prasertsan P, Birkeland N. Evaluation of methods for preparing hydrogen-producing seed inocula under thermophilic condition by process performance and microbial community analysis. Bioresour. Technol. 2009, 100, 909–918.

[17] Wang JL, Wan W. The effect of substrate concentration on biohydrogen production by using kinetic models. Sci China Ser B-Chem. 2008;51(11):1110-1117.

[18] Chen CC, Lin CY, Chang JS. Kinetics of hydrogen production with continuous anaerobic cultures utilizing sucrose as the limiting substrate. Appl Microbiol Biotechnol. 2001;57(1-2):56-64.

[18] Chin HL, Chen ZS, Chou CP. Fedbatch operation using *Clostridium acetobutylicum* suspension culture as biocatalyst for enhancing hydrogen production. Biotechnol Prog. 2003;19(2):383-8.

[19] Liu F, Fang B. Optimization of bio-hydrogen production from biodiesel wastes by *klebsiella pneumoniae*. Biotechnology Journal. 2007;2(3):374-80.

[20] Kim SH, Han SK, Shin HS. Effect of substrate concentration on hydrogen production and 16S rDNA-based analysis of the microbial community in a continuous fermenter. Process Biochemistry. 2006;41(1):199-207.

[21] Chen X, Sun YQ, Xiu ZL, Li XH, Zhang DJ. Stoichiometric analysis of biological hydrogen production by fermentative bacteria. Int J Hydrogen Energy. 2006;31(4):539-49.

[22] Kim DH, Han SK, Kim SH, Shin HS. Effect of gas sparging on continuous fermentative hydrogen production. Int J Hydrogen Energy. 2006;31(15):2158-69.

[23] Brosseau JD, Zajic JE. Hydrogen-gas production with citrobacter-intermedius and *Clostridium pasteurianum*. Journal of Chemical Technology and Biotechnology. 1982;32(3):496-502.

[24] Koskinen PE, Kaksonen AH, Puhakka JA. The relationship between instability of H2 production and compositions of bacterial communities within a dark fermentation. Biotechnol Bioeng. 2007;97(4): 742-58.

[25] Rodriguez J, Kleerebezem R, Lema JM, Van loosdrecht MC. Modeling product formation in anaerobic mixed culture fermentations. Biotechnol Bioeng. 2006;93(3): 592-606.

[26] Kim S-H, Han S-K, Shin H-S. Effect of substrate concentration on hydrogen production and 16S rDNA-based analysis of the microbial community in a continuous fermenter. Process Biochem. 2006;41(1):199-207.

[27] Hawkes FR, Hussy I, Kyazze G, Dinsdale R, Hawkes DL. Continuous dark fermentative hydrogen production by mesophilic microflora: Principles and progress. Int J Hydrogen Energy. 2007;32:172-184.

[28] Varma PBK, Kyazze GC, Premier R, Dinsdale R, Guwy AJ, Rodriguez J. Application of ADM1 with variable stoichiometry to simulate continuous bio-hydrogen production. 11th IWA World Congresss on Anaerobic Digestion. 2007, Brisbane, Australia.

[29] Hussy I, Hawkes FR, Dinsdale R, Hawkes DL. Continuous fermentative hydrogen production from wheat starch co-product by mixed microflora. Biotechnol Bioeng. 2003;84: 619-26.

[30] Hafez H, Baghchehsaraee B, Nakhla G, Karamanev D, Margaritis A, El Naggar M.H. Comparative Assessment of Decoupling of Biomass and Hydraulic Retention Times in Hydrogen Production Bioreactors. Int J Hydrogen Energy. 2009;34:7603-7611.

[31] Wu SY, Hung CH, Lin CY, Lin PJ, Lee KS, Lin CN, et al. HRT-dependent hydrogen production and bacterial community structure of mixed anaerobic microflora in suspended, granular and immobilized sludge systems using glucose as the carbon substrate. Int J Hydrogen Energy. 2008;33(5):1542-9.

[32] Youn JH, Shin HS. Comparative performance between temperature-phased and conventional mesophilic two-phased processes in terms of anaerobically produced bioenergy from food waste. Waste Manage Res. 2005;23(1):32-8.

[33] Lin CY, Jo CH. Hydrogen production from sucrose using an anaerobic sequencing batch reactor process. Journal of Chemical Technology and Biotechnology. 2003;78(6):678-84.

[34] Fang HHP, Liu H, Zhang T. Characterization of a hydrogen-producing granular sludge. Biotechnol Bioeng. 2002;78(1):44-52.

Operation of a Two-stage Continuous Fermentation Process Producing Hydrogen and Methane from Artificial Food Wastes

Kohki Nagai, **Shiho Mizuno**, **Yoshito Umeda**, Toho Gas Co., Ltd., Japan
Noriko Osaka, Tokyo Gas Co.,Ltd. Japan
Makiko Sakka, **Kazuo Sakka**, Mie University, Japan

Abstract

An anaerobic two-stage continuous fermentation process with combined thermophilic hydrogenogenic and methanogenic stages (two-stage fermentation process) was applied to artificial food wastes on a laboratory scale. In this report, organic loading rate (OLR) conditions for hydrogen fermentation were optimized before operating the two-stage fermentation process. The OLR was set at 11.2, 24.3, 35.2, 45.6, 56.1, and 67.3 g-COD_{cr} L^{-1} day^{-1} with a temperature of 60°C, pH5.5 and 5.0% total solids. As a result, approximately 1.8-2.0 mol–H_2 mol-hexose^{-1} was obtained at the OLR of 11.2-56.1 g-COD_{cr} L^{-1} day^{-1}. In contrast, it was inferred that the hydrogen yield at the OLR of 67.3 g-COD_{cr} L^{-1} day^{-1} decreased because of an increase in lactate concentration in the culture medium. The performance of the two-stage fermentation process was also evaluated over three months. The hydraulic retention time (HRT) of methane fermentation was able to be shortened 5.0 days (under OLR 12.4 g-COD_{cr} L^{-1} day^{-1} conditions) when the OLR of hydrogen fermentation was 44.0 g-COD_{cr} L^{-1} day^{-1}, and the average gasification efficiency of the two-stage fermentation process was 81% at the time.

1 Introduction

Global warming caused by increasing concentrations of carbon dioxide and other greenhouse gases has led to interest in renewable energy such as solar, wind, and biomass energy. Furthermore, although hydrogen is a secondary energy, it is well known as a clean energy which does not emit carbon dioxide itself. The future popularization of these energy sources is essential to preventing global climate change. For the exploitation of biomass energy, and especially for fermentation systems, it is desirable to downsize the fermentation reactor and improve the raw materials energy recovery efficiency. A two-stage continuous fermentation process composed of a hydrogenogenic stage in the hydrogen fermentation reactor followed by a methanogenic stage in the methane fermentation reactor (two-stage fermentation process) has been researched to solve these issues [1-3]. Theoretically, this process has the potential to improve the energy recovery efficiency up to approximately 9%, compared with a single-stage process, when glucose is used as the raw material [4]. Moreover, the methane production rate in the two-stage fermentation process is supposed to increase due to the production of volatile fatty acids (VFAs) such as acetate and butyrate in the hydrogen fermentation process. In this report, optimum organic loading rate (OLR) conditions for the hydrogenogenic process were evaluated using thermophilic microflora

mainly composed of *Clostridium* species screened through approximately 100 types of soil. Then, a two-stage fermentation process applying this hydrogen fermentation was conducted to evaluate the influence of the OLRs used in methane fermentation on methane production capacity.

2 Material and Methods

2.1 Feed material and seed organism

Artificial food wastes (AFW) composed of vegetables, chicken, fish and rice in wet-weight proportions of 87%, 3%, 3% and 7%, respectively, were prepared as a culture medium for hydrogen fermentation (H_2 fermentation). The AFW was then diluted with water to obtain a total solids concentration of 5%. The average amount of dichromate chemical oxygen demand (COD_{cr}) of the culture medium after water dilution was 62,350 mg L^{-1}. Thermophilic microflora mainly composed of *Clostridium* species, screened through approximately 100 types of soil were used for the hydrogenogenic process. An anaerobic digestion sludge obtained from a sewage treatment plant was used as the seed organism of the methane fermentation (CH_4 fermentation).

2.2 Experimental procedure

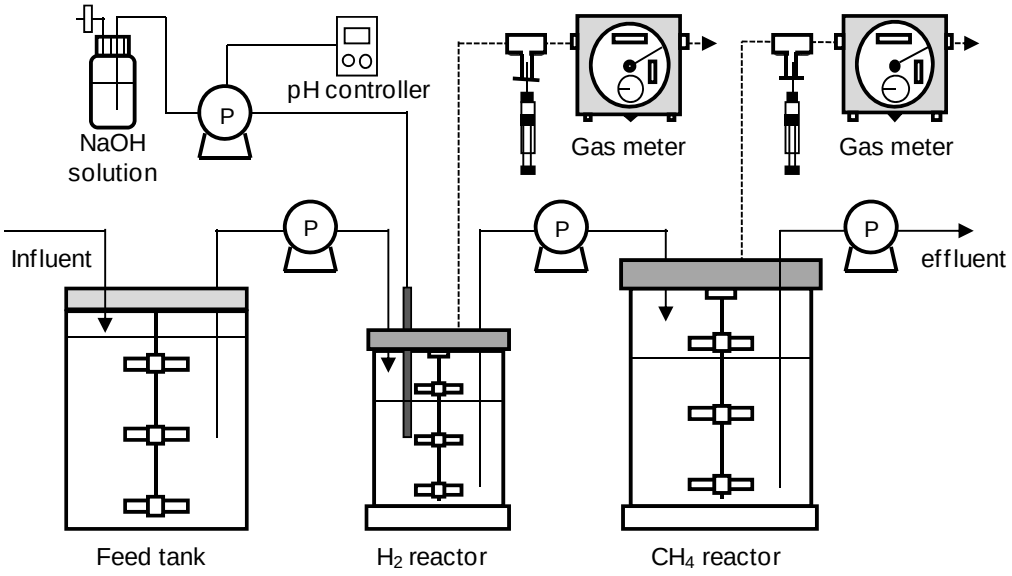

Figure 1: Schematic diagram of two-stage fermentation process (solid and dotted lines indicate the flow of raw material and product biogas, respectively).

A schematic diagram of the experimental apparatus for the two-stage fermentation process is shown in Figure 1. In the experiment, the food waste slurry was fed into a fermentation hydrogen reactor (H_2 reactor) with a 0.8 L effective volume (mini-jar fermentor TS-A1 (1L); Takasugi Corporation). The residue from the H_2 reactor was fed into a fermentation methane reactor (CH_4 reactor) with a 2.5 L effective volume (mini-jar fermentor TS-A3 (3L)). The effluent whose quantity was the same as the amount of residue supplied from the H_2 reactor was discharged from the CH_4 reactor. Although the pH of the culture medium in the H_2

reactor was regulated at 5.5 by automatic titration of a NaOH solution, the culture medium in the CH_4 reactor was not regulated. Electric heating apparatuses installed at the bottom of the reactor were automatically controlled to maintain the operational temperatures of the hydrogenogenic and methanogenic processes at 60°C and 55°C, respectively. All roller pumps, except for the pH regulation pump, were activated every four hours, and the working time of each pump was changed according to experimental conditions.

2.3 Methods of analysis

The amount of gas produced in the H_2 and CH_4 reactors was measured with a wet-gas meter (W-NK-0.5; Shinagawa Corporation). The proportions of hydrogen (H_2), methane (CH_4), nitrogen (N_2) and carbon dioxide (CO_2) in the biogas were measured with a micro-gas chromatograph (CP-4900; Varian Technologies Japan, Ltd.) equipped with a thermal conductivity detector and two columns. H_2 and CH_4 were analyzed using a 10-m stainless-steel column packed with Molsieve 5A. Injector, detector and column temperatures were kept at 170°C, 100°C and 100°C, respectively. CO_2 was analyzed using a 10-m stainless-steel column packed with PoraPLOT Q. Injector, detector and column temperatures were kept at 190°C, 80°C and 80°C, respectively.

The concentrations of lactate, acetate, propionate, n-butyrate and n-valeriate were determined with an ion chromatograph (ICS-1000; DIONEX Corporation) equipped with an Ion Pac ICE-AS1 analytical column, an AMMS-ICE-300 suppressor and an ICS-1000 conductivity detector. One mM octanesulfonate was used as the eluent (flow rate of 1.0 mL min^{-1}) and the detector temperature was set at 35°C.

The COD_{cr} was determined using a portable spectrophotometer (DR2800; HACH COMPANY) and HACH1076 as a reagent.

3 Results and Discussion

3.1 The performance of H_2 fermentation

The H_2 fermentation was optimized prior to carrying out the two-stage fermentation process experiment. Throughout the experiment, the composition of the product biogas was 50-52% H_2 and 48-50% CO_2, and no CH_4 was detected. Table 1 shows the results, which are calculated as average values, summarizing the effects of the OLR on H_2 production capacity and the concentration of VFAs in the hydrogenogenic process.

Table 1: Hydrogen production capacity and VFA concentration in the hydrogenogenic process.

OLR ($g\text{-}COD_{cr}\ L^{-1}day^{-1}$)	HRT (day)	H_2 yield		H_2 production rate	concentration of VFAs ($mg\ L^{-1}$)			
		($L\ kg_{AFW}^{-1}$)	($mol\text{-}H_2\ mol\text{-}hexose^{-1}$)	($L\ L^{-1}day^{-1}$)	lactate	acetate	propionate	n-butyrate
11.2	5.6	31.2	1.9	1.8	363	3049	37	10451
24.3	2.6	30.5	1.8	3.1	323	3956	45	9214
35.2	1.8	33.2	2.0	5.1	172	4648	54	10220
45.6	1.4	33.1	2.0	6.5	241	4863	47	11064
56.1	1.1	32.7	1.9	8.4	324	4881	28	9628
67.3	0.9	27.5	1.6	8.3	1748	4703	17	9973

The H_2 production rate increased along with the OLR up to 56.1 g-COD_{cr} L^{-1} day^{-1} with a hydraulic retention time (HRT) of 1.1 days. The H_2 yield was 1.8-2.0 mol-H_2 mol-hexose^{-1} under these conditions. However, the H_2 production rate decreased at the OLR of 67.3 g-COD_{cr} L^{-1} day^{-1} (HRT of 0.9 days), compared with the H_2 production rate at the OLR of 56.1 g-COD_{cr} L^{-1} day^{-1} (HRT of 1.1 days). An increase in the concentration of lactate was observed at the OLR of 67.3 g-COD_{cr} L^{-1} day^{-1}. It is known that, in anaerobic digestion, VFAs are produced as shown in Table 2. Since there is no H_2 production accompanying lactate production, it was inferred that the H_2 production capacity at the OLR of 67.3 g-COD_{cr} L^{-1} day^{-1} decreased because of an increase in lactate concentration in the H_2 fermentation culture medium. In addition, lactate bacteria have been reported to be inhibitory to H_2 fermentation [5].

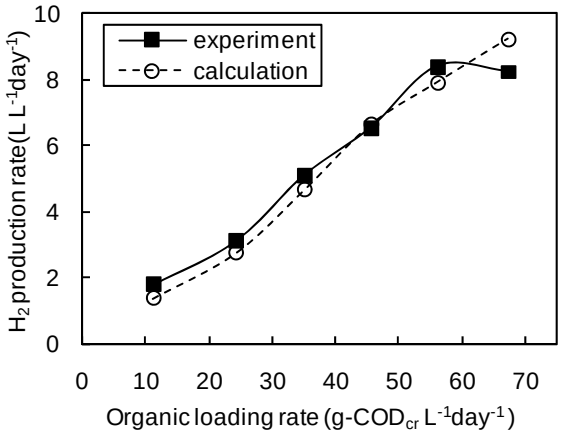

Figure 2: Comparison of experimental and theoretical value for H_2 production rate.

For further examination of the performance of H_2 fermentation, the H_2 production rate under each condition was compared with the theoretical H_2 production rate. The theoretical value was calculated from the concentration of VFAs in the H_2 reactor, assuming that the stoichiometry of H_2 production and consumption was as shown in Table 2 (a), (d) and (e) [6]. Figure 2 shows the comparison of experimental and theoretical values. The results show that the experimental values up to the OLR of 56.1 g-COD_{cr} L^{-1} day^{-1} are close to the theoretical values. H_2 can therefore be expected to be produced effectively under these conditions. At the OLR of 67.3 g-COD_{cr} L^{-1} day^{-1}, on the other hand, the experimental value is lower than the theoretical value. From this, it is inferred that, besides reaction (a), different reactions such as those in Table 2 (b) and (c) occurred to produce acetate, resulting in a decrease in the H_2 production rate. In addition, although the production of lactate is not a factor in the calculation, an increase in the lactic acid concentration is observed. This therefore suggests that the fermentation pattern is affected by an increase in the amount of lactate in the culture medium.

Table 2: VFA production with anaerobic digestion.

Products	Chemical reaction	
acetate	$C_6H_{12}O_6+2H_2O \rightarrow 2CH_3COOH+2CO_2+4H_2$	(a)
	$C_6H_{12}O_6 \rightarrow 3CH_3COOH$	(b)
	$4H_2+2CO_2 \rightarrow CH_3COOH$	(c)
n-butyrate	$C_6H_{12}O_6 \rightarrow CH_3CH_2CH_2COOH+2CO_2+2H_2$	(d)
propionate	$CH_3COCOOH+2H_2 \rightarrow CH_3CH_2COOH+H_2O$	(e)
lactate	$C_6H_{12}O_6 \rightarrow 2CH_3CH(OH)COOH$	(f)

3.2 Evaluation of performance of two-stage fermentation process with combined H_2 and CH_4 reactors

The two-stage fermentation process was evaluated over a period of more than three months. Figure 3 shows the time course for the H_2 and CH_4 production rates. Initial operation data are not shown because of unstable experimental conditions. The OLR used in the H_2 fermentation was set between 30.5-54 g-COD_{cr} L^{-1} day^{-1} in the experiment. On day 57, all the culture medium in the H_2 reactor was replaced with a new culture since a sufficient amount of H_2 could not be obtained due to feed putrefaction. After H_2 fermentation was restarted, H_2 production stabilized around 31.0 L kg_{AFW}^{-1}, which is equivalent to 1.8 mol-H_2 mol-hexose^{-1}. The composition of the biogas was 50-55 % H_2 and 45-50% CO_2, and no CH_4 was detected in the H_2 reactor.

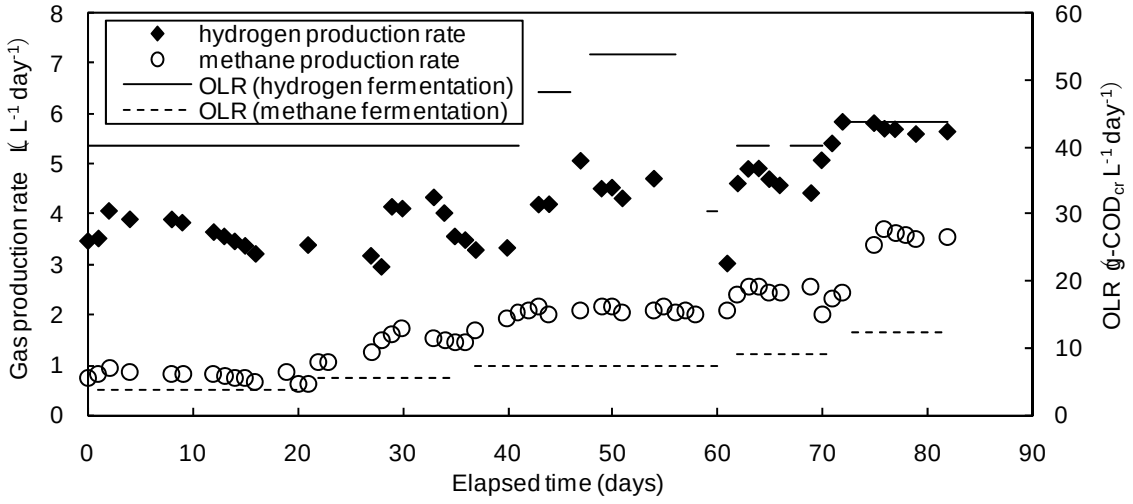

Figure 3: Time course of gas production in the two-stage continuous fermentation process.

In the methanogenic process, the initial OLR was set at 3.8 g-COD_{cr} L^{-1} (HRT of 16.3 days), and then gradually raised to 12.4 g-COD_{cr} L^{-1} day^{-1} (HRT of 5.0 days). The CH_4 production remained stable around 67-74 L kg_{AFW}^{-1} throughout the experiment. The proportions of CH_4

and CO_2 in the biogas were 68-71 % and 29-32 %, respectively. Table 3 shows the total COD_{cr} removal efficiency and the concentration of volatile fatty acids (VFAs) after the methanogenic process. Although there was no significant difference in the COD_{cr} before and after the hydrogenogenic process, the COD_{cr} removal efficiency reached approximately 80 % after the methanogenic process. Moreover, the concentration of VFAs such as acetate and n-butyrate was much lower after the methanogenic process than after the hydrogenogenic process. This indicates that the VFAs were efficiently converted into CH_4 in the methanogenic process.

The average gasification efficiency of the two-stage fermentation process when the OLRs of the H_2 and CH_4 fermentation were 44.0 and 12.4 g-COD_{cr} L^{-1} day^{-1}, respectively, was calculated using the calorific value of the AFW (4031 kJ kg^{-1}). The average gasification efficiency in the hydrogenogenic and methanogenic processes was calculated as 10 % and 71 %, respectively. Therefore, the total average gasification efficiency was 81 %.

Table 3: COD_{cr} removal efficiency and concentration of VFAs in the effluent from CH_4 reactor.

OLR	HRT	total COD_{cr}	concentration of VFAs (mg L^{-1})				
(g-COD_{cr} L^{-1} day^{-1})	(day)	removal (%)*	lactate	acetate	propionate	n-butyrate	n-valeriate
3.8	16.3	81.6	-	693	160	-	-
5.6	11.1	79.6	-	1039	633	-	47
7.3	8.5	79.6	-	776	503	-	-
9.0	6.9	81.3	-	733	377	-	-
12.4	5.0	76.9	-	351	658	-	-

*Total COD_{cr} removal (%) = $COD_{cr\ effluent\ from\ methane\ reactor}$ / $COD_{cr\ AFW\ after\ water\ dilution}$ x 100

These results show that the two-stage continuous fermentation process could be operated successfully under all experimental conditions. Further research needs to evaluate the possibility of operation with much higher OLRs in the methanogenic process.

4 Conclusions

The performance of a two-stage continuous fermentation process with combined H_2 and CH_4 reactors was evaluated on a laboratory scale. Artificial food wastes (AFW) were prepared as a culture medium for H_2 fermentation. In the experimental optimization of the H_2 fermentation, the H_2 production in the hydrogenogenic process was stable up to the OLR of 56.1 g-COD L^{-1} day^{-1}, and the amount produced was 1.8-2.0 mol-H_2 $mol\text{-}hexose^{-1}$. In contrast, the H_2 production capacity decreased at 67.3g-COD_{cr} L^{-1}a day^{-1}, suggesting that the fermentation pattern varied along with the increase in lactic acid in the culture medium. In the methanogenic process, the CH_4 production was approximately 67-74 L kg_{AFW}^{-1} without any accumulation of VFAs in the CH_4 fermentation culture medium throughout the experiment. The average gasification efficiency of the two-stage fermentation process was calculated as 81% when the OLRs of the H_2 and CH_4 fermentation were 44.0 and 12.4 g-COD_{cr} L^{-1} day^{-1}, respectively. These results indicate that the two-stage fermentation process could be operated successfully under these experimental conditions.

References

[1] Hawkes, F. R., Dinsdale, R., Hawkes, D. L., Hussy, I. Sustainable fermentative hydrogen production: challenges for process optimisation. *International Journal of Hydrogen Energy*, 2002, 27, 1339-1347

[2] Kraemer, J. T., Bagley, D. M. Continuous fermentative hydrogen production using a two-phase reactor system with recycle. *Environmental Science and Technology*, 2005, 39, 3819-3825.

[3] Kyazze, G., Dinsdale, R., Guwy, A. J., Hawkes, F. R., Premier, G. C., Hawkes, D. L. Performance characteristics of a two-stage dark fermentative system producing hydrogen and methane continuously. *Biotechnology and Bioengineering*, 2006, 97, 759-770.

[4] Kawano, T., Li, YY., Noike, T. Present status and prospective of the study on anaerobic bio-hydrogen (2). *Journal of Water and Waste*, 2005, 47 (11), 39-47.

[5] Takabatake, H., Kohno, Y., Tanno, Y., Noike, T. Influence of pH and metabolites on inhibition of anaerobic hydrogen fermentation by lactic acid bacteria, *Lactobacillus paracasei*. *Environmental Engineering Research.* 2006, 39, 55-65.

[6] Ueno, Y., Kawai, Y., Sato, S., Otsuka, S., Morimoto, M. Biological production of hydrogen from cellulose by natural anaerobic microflora. *Journal of Fermentation and Bioengineering*. 1995, 79, 395-397.

Investigating the Link between Fermentative Metabolism and Hydrogen Production in the Unicellular Green Alga *Chlamydomonas Reinhardtii*

S.J. Burgess, P.J. Nixon, Imperial College London, UK

Abstract

In the model green alga *Chlamydomonas reinhardtii*, the electrons required for hydrogen production can come from both the biophotolysis of water and from the fermentation of carbohydrate reserves. Anoxia leads to the activation of several fermentative pathways, which produce a number of end products including formic, malic and acetic acid along with ethanol, carbon dioxide and hydrogen. It has been proposed that by switching off competing fermentative pathways hydrogen production can be increased. Therefore the aim of this study was to devise an experimental strategy to down-regulate the expression of enzymes thought to control *C. reinhardtii's* fermentative metabolism. We demonstrate here that it is possible to use artificial microRNA (amiRNA) technology to generate knock-down mutants with reduced expression of pyruvate formate lyase (PFL1), a key fermentative enzyme in *C. reinhardtii*. This work opens up new possibilities to improve hydrogen yields through metabolic engineering.

1 Introduction

Certain types of green algae and cyanobacteria possess the ability to produce hydrogen, harnessing solar energy through photosynthesis to provide reductant to a [FeFe]- or [NiFe]-hydrogenase [1]. However, current maximum reported yields are low, at 5ml H_2 gas h^{-1} l^{-1} (>90% pure) [2, 3], and therefore must be improved if photobiological hydrogen production is to become an economically viable process [4, 5]. Many of the efforts to improve yields have focused on the unicellular (~10µm), freshwater micro-alga *Chlamydomonas reinhardtii*, due to good basal levels of H_2 production [6, 7], the availability of completely sequenced and transformable mitochondrial, chloroplast and nuclear genomes, detailed information of metabolic pathways and an extensive library of expressed sequence tags [8].

In order to overcome inhibition of the hydrogenase by oxygen evolved during photosynthesis, growth and H_2 production phases can be separated by sulphur depletion. During this process, the rate of oxygen evolution, catalysed by photosystem II (PSII), drops below respiration, driving sealed cultures into anoxia allowing sustained gas evolution over several days [7]. During sulphur depletion, electrons in the photosynthetic electron transport (PET) chain are passed via ferredoxin (Fd) to one of two 49-kDa [FeFe]-hydrogenases, HYDA1 or HYDA2 [9, 10], to produce hydrogen (Figure 1) [1]. Reductant is believed to come from a mixture of residual PSII activity and endogenous catabolism of starch and protein [11], which feeds electrons into the PET at the point of the plastoquinone pool, via a type II NADH dehydrogenase, or directly to ferredoxin by pyruvate ferredoxin oxidoreductase (PFOR) (Figure 1). The process is thought to be limited by supply of reductant [2] making it important

to maximize available sources of electrons and down regulate competing e- sinks to improve H_2 evolution.

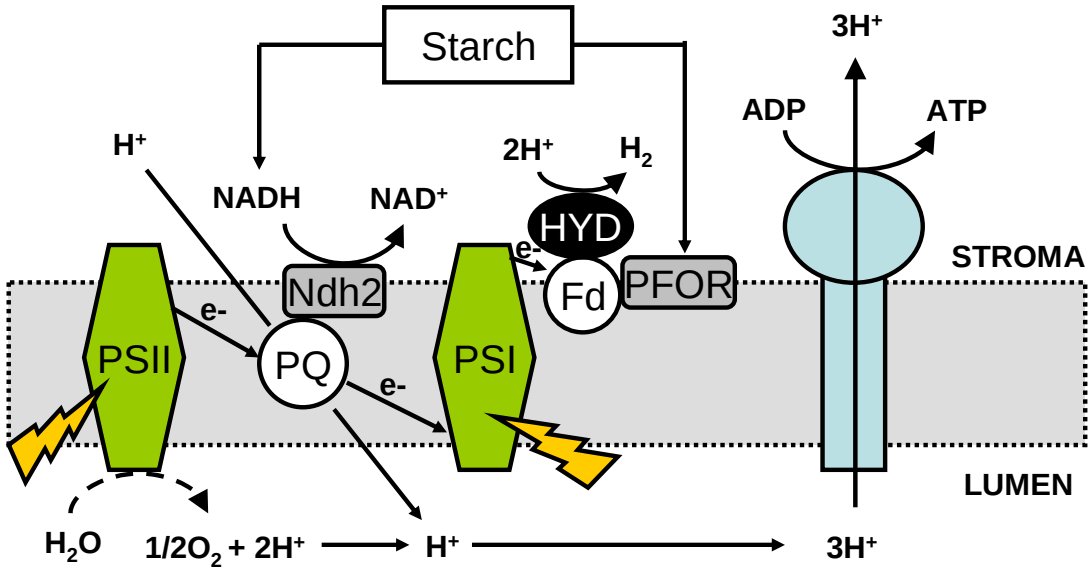

Figure 1: Diagram showing electron transfer in the photosynthetic electron transport chain (PET) during H_2 production: PSII, Photosystem II; PSI, Photosystem I; PQ, Plastoquinone; Fd, Ferredoxin; HYD, Fe-hydrogenase; Ndh2, type II NAD(P)H dehydrogenase; PFOR, Pyruvate:ferredoxin oxidoreductase.

Chlamydomonas is known to ferment starch under sulphur deprivation, creating a range of products that accumulate in direct competition with H_2 production [12]. Analysis of the *C. reinhardtii* genome sequence, the products of fermentation and inhibitor studies has suggested the presence of a three branched pathway (Figure 2) [13-15], in which pyruvate can be broken down to produce ethanol, formic acid or hydrogen along with acetic and malic acid further downstream [14, 16].

The predominant fermentative pathway is thought to involve the conversion of pyruvate to acetyl-CoA and formic acid by the enzyme pyruvate formate lyase (PFL1) (XM_001689667.1) [11] which has subsequently been identified as a good candidate for reverse genetic approaches to improve hydrogen production [12].

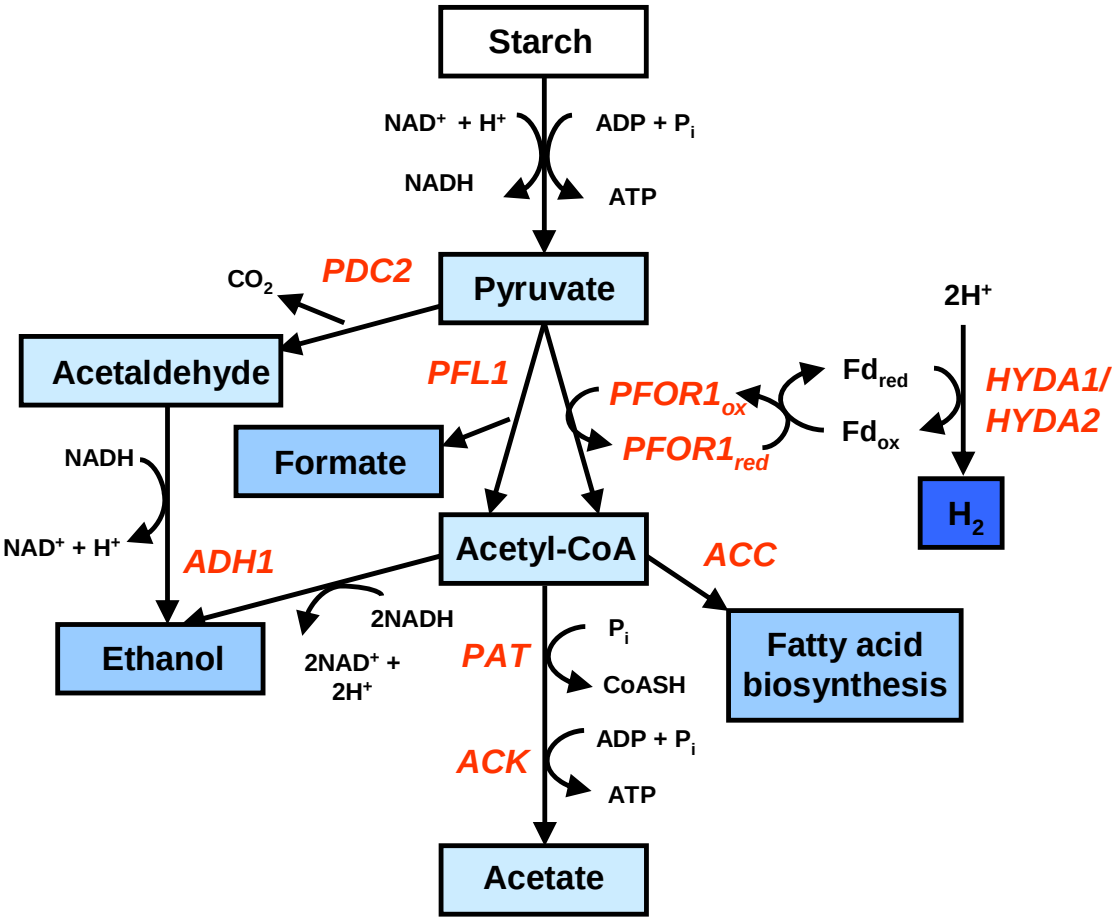

Figure 2: **Putative fermentative pathways *C. reinhardtii* (adapted from [14]). ACC, acetyl-CoA carboxylase; ACK, acetate kinase; ADH1, alcohol dehydrogenase; HYDA1/HYDA2, [FeFe]-hydrogenase 1 and 2; PDC2, Pyruvate decarboxylase; PFL1, Pyruvate formate lyase; PFOR, Pyruvate ferredoxin oxidoreductase; PAT, phosphate acetyltransferase.**

To date, problems transforming the *C. reinhardtii* nuclear genome by homologous recombination [17], and transcriptional silencing of conventional RNAi constructs, consisting of long dsRNAs [18], have hampered the ability to switch off or down regulate fermentative pathways. However, recent advances in artificial miRNA (amiRNA) technology have opened up the potential for stable metabolic engineering in *Chlamydomonas* [19, 20]. Here we describe the application of this technology to the generation of a strain with reduced levels of PFL1.

2 Experimental Procedures

Strains and culture conditions. Cell wall deficient *C. reinhardtii* strain CC406 (cw15) was grown in Tris acetate phosphate (TAP) media with $MgSO_4$ (or $MgCl_2$ in the case of sulphur-depletion experiments) at 25˚C under a constant illumination of 50µE$m^{-2}s^{-1}$.

Nuclear transformation of C. reinhardtii. Strains were transformed with ~2µg plasmid DNA by glass bead agitation and positive transformants selected on TAP plates containing paromomycin at 10µg/ml [21].

Construction of artificial microRNA (amiRNA) vectors. Oligonucleotides of 90 bases were designed using the online tool, WMD3, (http://wmd3.weigelworld.org/cgi-bin/webapp.cgi) and cloned into amiRNA vector pChlamRNAi3 as described [19].

Real time RT-PCR analysis. RNA was extracted using RNeasy Plant Mini kit (74903; QIAGEN, Germany) according to the manufacturer's protocol. cDNA synthesis was performed using High Capacity DNA Reverse Transcription Kit (4368814; Applied Biosystems, USA) and RT-PCR performed with 2x Taqman Fast Universal PCR Master Mix and analysed on 7500 Fast Real-Time PCR System (Applied Biosystems, USA)

3 Results

Reduction of PFL1 expression was performed by transforming a cell-wall deficient strain of *C. reinhardtii* (strain CC406) with a derivative of plasmid pChlamiRNA3 [19]. Nuclear transformants were selected on the basis of resistance to the antibiotic paromomycin (encoded by *aphVIII*) and the precursor artificial microRNA (amiRNA) was expressed from the *psaD* promoter (Figure 3A). The amiRNA was created by replacing a 90-nucleotide region of a WT pre-miRNA, which incorporates the targeting sequence and hairpin loop structure, by a synthetic construct designed using the online tool WMD3. The plasmid was used to transform the cell-wall deficient strain, CC406, by glass bead agitation. Screening of 30 paromomycin-resistant transformants by immunoblot identified two mutants, 4B23 and 4B24, with 70-80% reduction in PFL1 protein levels (Figure 3B). To check the phenotype was a result of decreased transcript accumulation, RNA was extracted from WT and 4B24 cultures, grown under sulphur depletion conditions, and analysed by real time RT-PCR. The results confirmed a significant knockdown of PFL1 mRNA (Figure 3C).

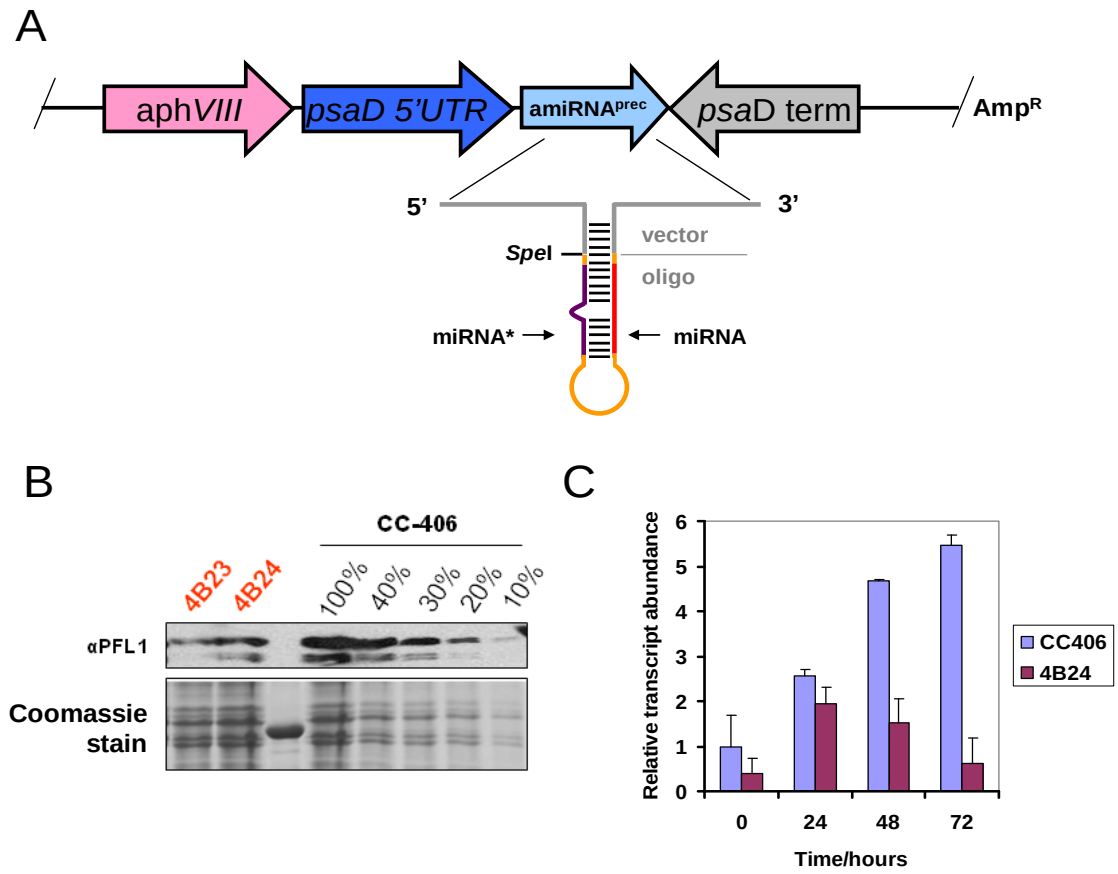

Figure 3: **(A) Map of amiRNAi vector pChlamiRNA3 used to transform *C. reinhardtii* strain CC-406. The *aph*VIII resistance cassette allows for selection on paromomycin and a *psaD* promoter was used to drive expression of amiRNAs (Adapted from [19]). (B) Immunoblot screening of transformants for knockdown of PFL1. Strains were grown under standard conditions and harvested at late log phase (OD_{750} 0.9-1). Loading is shown by Coomassie stained gel. (C) Real time reverse transcription-PCR analysis of PFL1 transcript levels, comparing parental strain CC406 to 4B24 at various times after sulphur deprivation. Values are given relative to CC406 t=0 and normalized to transcript levels of RPL10a which encodes the 60S ribosomal protein L10a, all measurements were done in triplicate.**

4 Summary

In conclusion, we report here the first successful knockdown of a key fermentative enzyme in *C. reinhardtii*. The application of amiRNA technology opens up exciting new possibilities for increasing hydrogen yields. Analysis of the impact of PFL1 knockdown on metabolite and H_2 yields is ongoing.

Acknowledgements

We would like to thank Dr. Attila Molnar (University of Cambridge), for supplying the amiRNA vector, pChlamiRNA3, and for his help in designing amiRNA oligo-nucleotides targeting PFL1.

References

[1] Ghirardi, M.L., Posewitz, M.C., Maness, P.C., Dubini, A., Yu, J., and Seibert, M. (2007). Annu Rev Plant Biol *58*, 71-91.

[2] Kruse, O., Rupprecht, J., Bader, K.P., Thomas-Hall, S., Schenk, P.M., Finazzi, G., and Hankamer, B. (2005). J Biol Chem *280*, 34170-34177.

[3] Doebbe, A., Rupprecht, J., Beckmann, J., Mussgnug, J.H., Hallmann, A., Hankamer, B., and Kruse, O. (2007). J Biotechnol *131*, 27-33.

[4] Kruse, O., Rupprecht, J., Mussgnug, J.H., Dismukes, G.C., and Hankamer, B. (2005). Photochem Photobiol Sci *4*, 957-970.

[5] Stephens, E., Ross, I.L., King, Z., Mussgnug, J.H., Kruse, O., Posten, C., Borowitzka, M.A., and Hankamer, B. Nat Biotech *28*, 126-128.

[6] Timmins, M., Thomas-Hall, S.R., Darling, A., Zhang, E., Hankamer, B., Marx, U.C., and Schenk, P.M. (2009). J. Exp. Bot. *60*, 1691-1702.

[7] Melis, A., Zhang, L., Forestier, M., Ghirardi, M.L., and Seibert, M. (2000). Plant Physiol *122*, 127-136.

[8] Merchant, S.S., Prochnik, S.E., Vallon, O., Harris, E.H., Karpowicz, S.J., Witman, G.B., Terry, A., Salamov, A., Fritz-Laylin, L.K., Marechal-Drouard, L., et al. (2007). Science *318*, 245-250.

[9] Happe, T., and Kaminski, A. (2002). Eur J Biochem *269*, 1022-1032.

[10] Forestier, M., King, P., Zhang, L., Posewitz, M., Schwarzer, S., Happe, T., Ghirardi, M.L., and Seibert, M. (2003). Eur J Biochem *270*, 2750-2758.

[11] Hemschemeier, A., Fouchard, S., Cournac, L., Peltier, G., and Happe, T. (2008). Planta *227*, 397-407.

[12] Matthew, T., Zhou, W., Rupprecht, J., Lim, L., Thomas-Hall, S.R., Doebbe, A., Kruse, O., Hankamer, B., Marx, U.C., Smith, S.M., et al. (2009). J Biol Chem *284*, 23415-23425.

[13] Hemschemeier, A., Jacobs, J., and Happe, T. (2008). Eukaryot Cell *7*, 518-526.

[14] Mus, F., Dubini, A., Seibert, M., Posewitz, M.C., and Grossman, A.R. (2007). J Biol Chem *282*, 25475-25486.

[15] Grossman, A.R., Croft, M., Gladyshev, V.N., Merchant, S.S., Posewitz, M.C., Prochnik, S., and Spalding, M.H. (2007). Curr Opin Plant Biol *10*, 190-198.

[16] Gfeller, R.P., and Gibbs, M. (1984). Plant Physiol *75*, 212-218.

[17] Zorin, B., Lu, Y., Sizova, I., and Hegemann, P. (2008). Gene *432*, 91-96

[18] Rohr, J., Sarkar, N., Balenger, S., Jeong, B.-r., and Cerutti, H. (2004). The Plant Journal *40*, 611-621.

[19] Molnar, A., Bassett, A., Thuenemann, E., Schwach, F., Karkare, S., Ossowski, S., Weigel, D., and Baulcombe, D. (2009). Plant J. *58*, 165-174

[20] Tao, Z., Wei, W., Xue, B., and Yijun, Q. (2009). The Plant Journal *58*, 157-164.

[21] Sizova, I., Fuhrmann, M., and Hegemann, P. (2001). Gene *277*, 221-229.

Biohydrogen Fermentation of Mixed Liquid of Kitchen Waste and Napier Grass with Anaerobic Fluidized Bed Process

Sheng-Shung Cheng, Department of Environmental Engineering, Sustainable Environment Research Center(SERC), National Cheng Kung University, No.1, University Rd., East District, Tainan City 701, Taiwan (R.O.C.)
Yu-Chieh Chao, **Yi-Chieh Chen**, **Yu-Min Tien**, Department of Environmental Engineering, National Cheng Kung University, No.1, University Rd., East District, Tainan City 701, Taiwan (R.O.C.)

1 Introduction

Hydrogen is an emerging energy carrier that produces only water after combustion. Biohydrogen technology can convert organic wastes into hydrogen and simple fatty acids. Among all of the organic wastes, carbohydrates were identified as the main electron donors, which contribute to the formation of hydrogen gas. Napiergrass (NG) can provide sufficient carbohydrates, be easily grown and produce a great yield in wild mountain area of Taiwan. The content of total carbohydrates (including soluble sugars, cellulose and hemicelluloses) was 51%, which made up of 57.6% in the organic part. Soluble sugar and cellulose made up 7.5% and 20 % respectively. The percentage of hemicellulose and other sugars is estimated to be 23%, with 8.5% protein content and 29 % lignin content. Nevertheless, Napier Grass could be a substrate for biohydrogenation, like other cellulosic materials, hydrolysis is the rate-limiting step in hydrogenation. As a result, in this study, an anaerobic fluidized bed reactor was adopted with a long solid retention time, which can provide complete reaction duration in hydrolyzing and producing hydrogen gas from cellulosic fermentation.

In Taiwan, the recycling amount of kitchen waste (KW) was collected locally up to 1,900 ton/day in average. Kitchen waste contains high organic substance, such as nitrogen and abundant nutrients which are necessary for microbial propagation. Ueno (Ueno et al., 2001 [1]) noticed that microbial diversity shifted when the nitrogen source was different. Kitchen waste is easy to obtain and can be collected for various objectives. Other than pig feeding and composting, anaerobic digestion is an efficient way to treat kitchen waste. The mixed liquid of kitchen waste is not suitable for pig feed and composting because of high water content. However, it contains ample nitrogen sources and other trace elements, which was lacking in the Napier Grass. Therefore, kitchen waste seived liquid (KWSL) was used as feeding substrate and mixed with Napier Grass for biohydrogenation in this study. The water content of KW was more than 75% and with abundant nutrient, KWSL is suited for biohydrogenation as well as mixed completely in anaerobic fluidized bed (AnFB) with less suspended solid.

2 Materials and Methods

The characteristic of KWSL are as follows: Total COD : 104,000 ± 16,000 mg/L (69% soluble) , Total Carbohydrate: 26,500 ± 6,300 mg/L (85% soluble) , Total Org-N: 2,560 ± 270 mg/L (70% soluble) , lipid: 8,300 ± 3900 mg/L , suspended solid: 26,000 ± 5,330 mg/L (91 % volatile SS) , and it contained acetate (2,500 ± 340 mg/L) and high concentration of lactate (10,700~14,500 mg/L) . Napier Grass (1.1 g-COD/g- Napier Grass dregs) is composed by about 20% cellulose and other lignin cellulose which are difficult to be decomposed. This study expected that adding the Napier Grass dregs with KWSL could co-metabolize the cellulose and serve as a kind of biofilm supporter in the AnFBR.

The advantage of operation in an AnFB is to maintain suspended solid (substrate and microbes) react for a longer contact time in reactor. Fluidized bed was most adopted on industrial wastewater treatment (Holst et al., 1997 [2]), but there was few study of fluidized bed performance with solid content substrates. This study would focus on the cellulose hydrolyzing and hydrogen production process of cellulosic feedstock. To promote the microorganism better hydrogen producing activity, high organic loading was necessary (Li et al., 2008 [3]; Wang et al., 2009 [4]), however, we would also experience some hardware operating problems. Recirculation pumps provide the driving power of fluidization. However, short fibers and lipid could easily clog centrifugal pumps and cause reactor shut down. Therefore, we selected an axis seal separation pump to improve the recirculation in the fluidized bed returning flow this year. Fig. 1 illustrates the flow chart of AnFB reactor.

There are three phases for this study and the operational parameters are showed in Table 1. The major substrates used in this study were KWSL and Napier Grass. The operational parameters of AnFB were shown as follows: with a hydraulic retention time (HRT) maintained about 7.3 days. pH was held at 6.0±0.1 and the temperature controlled at 55±0.5 ^{0}C. The AnFB was started-up in batch mode and KWSL was used as substrate. Seeding sludge was taken from the KW composting in Tainan city and was enhanced with vegetable kitchen waste (picking up the vegetables from kitchen waste as feeding substrate) in previous study (Li et al., 2008 [3]). After 37 days' operation, the influent of AnFB was changed to continuous-pulsed input for hydrogen fermentation. Continuous input for cultivating hydrogen-producing microorganisms is better than the batch culture (Herbert et al., 1956 [5]). It can also provide substrate continuously, dilute out the products from metabolism and reduce the product inhibition to the hydrogen-producing microorganisms. As a result, it can enable the hydrogen producing microorganisms to keep producing hydrogen stably.

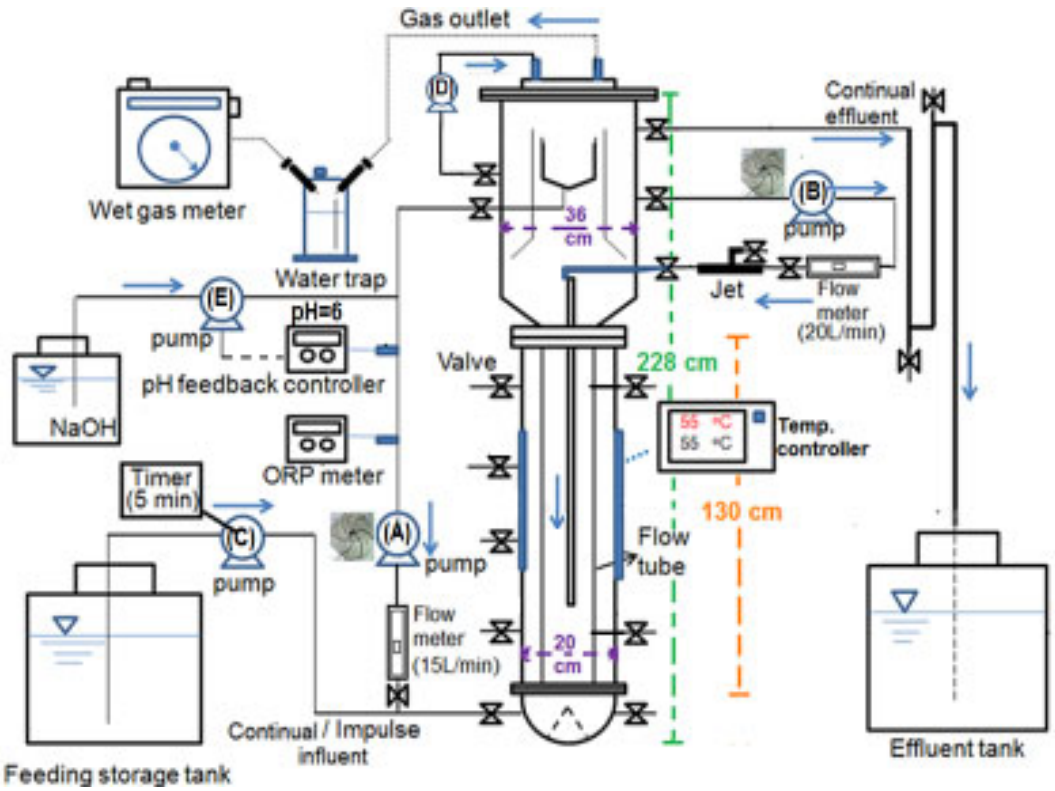

Figure 1: Schematic diagram of 110 L anaerobic fluidized bed (AnFB) hydrogen fermentor fed with Napier Grass and kitchen waste.

Table 1 illustrates the three runs conditions of AnFB process as follows.

(1) In Run 1: the input substrate was KWSL (operation days: 0~70).

In order to reduce the block-up problem of pump and tube we encountered in previous study (Li et al., 2008 [3]), and to cultivate the hydrogen-producing organisms, we controlled the concentration of the suspended solid in kitchen waste sieved liquid less than 26,000 mg/L.

(2) In Run 2: the major input substrate was KWSL and the minor substrate was 5,000 mg/L Napier Grass powder (operation days: 71~143).

In order to enhance the cultivation of cellulose-hydrolyzing and hydrogen-producing microorganisms, small amount of Napier Grass powder was added with 5 g/L in KWSL feeding, which could not only increase the organic loading rate but also served as a microbial carrier, resulting in a suitable circumstance for cellulose-degrading microorganisms.

(3) In Run 3: the major input substrate was KWSL and the minor substrate was 20 g/L Napier Grass powder to enhance the hydrogen production rate and the efficiency of AnFBR. (operation days: 144~193).

The biogas produced from the reactor was measured by a gas meter continuously; biogas was collected by water displacement method then analyzed by a gas chromatograph (Model China Chromatography, GC 8900T) equipped with a thermal conductivity detector (TCD). The concentration of sucrose was determined by phenol-sulfuric method(Herbert et al., 1971 [6]). Water quality analyses were conducted according to the procedures described in the Standard Method 19th edition (APHA, 1995 [7]).

Table 1: Operational parameters of AnFB for bio-hydrogenation fed with kitchen waste sieved liquid (KWSL) and Napier Grass (NG) from Run 1 to Run 3.

Parameters	Unit	Run 1	Run 2	Run 3
Period	Days	0~70 (70 days)	71~143 (74 days)	144~193 (50 days)
Feeding	-	KMSL	KMSL + 5 g-NG/L	KMSL + 20 g-NG/L
Feeding type	-	From Batch input to Impulse input	Impulse input (5 min a time)	Impulse input (5 min a time)
Feeding volume	L	15	15	15
HRT	Days	7.3	7.3	7.3
pH controlling	-	6.0	6.0	6.0
Recirculation liquid flow rate	L/min	35	35	35
Organic loading rate	g-COD/L/day	14.2±2.5	14.7±1.8	17.7±2.4

3 Results and Discussion

3.1 Experimental results of AnFB process performance

Three phases were conducted in the operation of AnFB. In the first phase, the KWSL was used as substrate. In the second phase, 5 g/L Napier Grass was added in the influent substrate of KWSL. In the third phase, the addition of Napier Grass was increased to 20 g/L with KWSL as substrates. The biogas variation and characterization of substrates and metabolites in these three phases were shown in Figure 2, Figure 3 and Table 3. The ORP varied between -300 to -500 mV and pH controlled in phase one is more stable. Under the organic loading rate of 14.2 g-COD/L/day and using only KWSL as substrate, AnFB can achieve a hydrogen performance up to 1.41 L H_2/L/day, which means KWSL can be converted into hydrogen stably.

5 g/L Napier Grass was added to KWSL in phase two, which contributed to a slight increase in total COD of the inflow. Therefore, the OLR was increased a little to 14.7 g-COD/L/day. The AnFB can convert 6.2 % of COD into hydrogen and the average hydrogen production rate was 1.41 L H_2/L/day. The hydrogen concentration was 40 % of total biogas production and the hydrogen yield was 3.84 mmol H_2/g-COD_{in}. The hydrogen performance was almost the same as in phase one. Because only a little amount of Napier Grass was added in the inflow, the increase of OLR was limited, resulting in no improvement to hydrogen production. Besides, cellulose and hemicellulose, which are both difficult to be utilized for microbes, contribute 43 % in COD basis in the Napier Grass and only 7.5 % of soluble sugars were contained. From the comparisons between inflow and effluent of the AnFB, the cellulose removal ratio was only 7.1 %, which indicated that cellulose was not converted by the microbes. The differences of cellulose concentration between inflow and effluent in the earlier stage of phase two was due to the entrapment of Napier Grass in AnFB reactor.

Table 2: Characteristics of Napier Grass from Livestock Research Institute.

Characteristics of Napier Grass dregs (w/w, %)			
Moisture	7.2	±	0.3
TVS	88.5	±	1.5
Total carbohydrate	51	±	4.0
Soluble carbohydrate	7.5	±	0.1
Cellulose	20	±	3.0
Protein	8.5	±	0.3
Inerts	4.5	±	0.3
COD	1.1 ± 0.05 g-COD/g-Napier Grass		

Accordingly, 20 g/L Napier Grass was added to KWSL during the third phase, attempting to cultivate cellulose degrading microbes and improve the hydrogen production rate. Because of the additional supplement of Napier Grass, the OLR in phase three was raised to 17.7 g-COD/L/day. However, only 6 % of electrons were transferred to hydrogen, and hydrogen yield was 3.74 mmol H_2/g-COD_{in}, which was slightly lower than phase two. In the later stage of phase three, the cellulose concentration in the effluent was almost the same as in the inflow. The cellulose removal ratio decreased to 1.5 %, which revealed that the microbes in the AnFB reactor still cannot utilize cellulose efficiently. The addition of 20 g/L Napier Grass only contributed to organic loading rate but little was converted into hydrogen. As a result, though the hydrogen production rate was the highest (up to 1.64 L H_2/L/day) among these three phases, the hydrogen yield was the lowest (only 3.74 mmol H_2/g-COD_{in}). From the aspect of the metabolites, the main volatile fatty acids (VFA) in the effluent were butyrate (13,000~17,000 mg/L) and acetate (2,300~33,00 mg/L) production. Remarkably, the high concentration lactate in KWSL was degraded remarkably (maximum removal efficiency was 98.3% in 2nd phase),and from the batch test of lactate degradation, it showed that lactate was degraded and hydrogen was produced, which the reaction was similar to "Lactate + 0.4 Acetate +0.7 H^+ → 0.7 Butyrate + 0.6 H_2 + CO_2 + 0.4 H_2O". Regarding the high lactate concentration in KWSL, it has great advantages for biohydrogenation in reducing the feed-back of alkali.

These could be the main pathways for biohydogenation in AnFB:

1. Lactate metabolism to produce hydrogen:

   Lactate + 0.4 HAc +0.7 H^+ → 0.7 HBu + 0.6 H_2 + CO_2 + 0.4 H_2O

2. Carbohydrate metabolism to produce hydrogen:

   $C_6H_{12}O_6 + 2H_2O \rightarrow 4H_2 + 2CO_2 + 2HAc$, $C_6H_{12}O_6 \rightarrow 2H_2 + 2CO_2 + HBu$

The existence of actate and butyrate could interact with the lactate metabolism and carbohydrate catabolism. If the butyrate produced from pathway (1) was excluded, which contributed to lactate metabolism, the ratio of HBu/HAc(mol:mol) was close to 1, infering that the stoichiometric equation of carbohydrate metabolism was close to : $3C_6H_{12}O_6 + 2H_2O \rightarrow 8H_2 + 6CO_2 + 2$ HAc + 2 HBu.

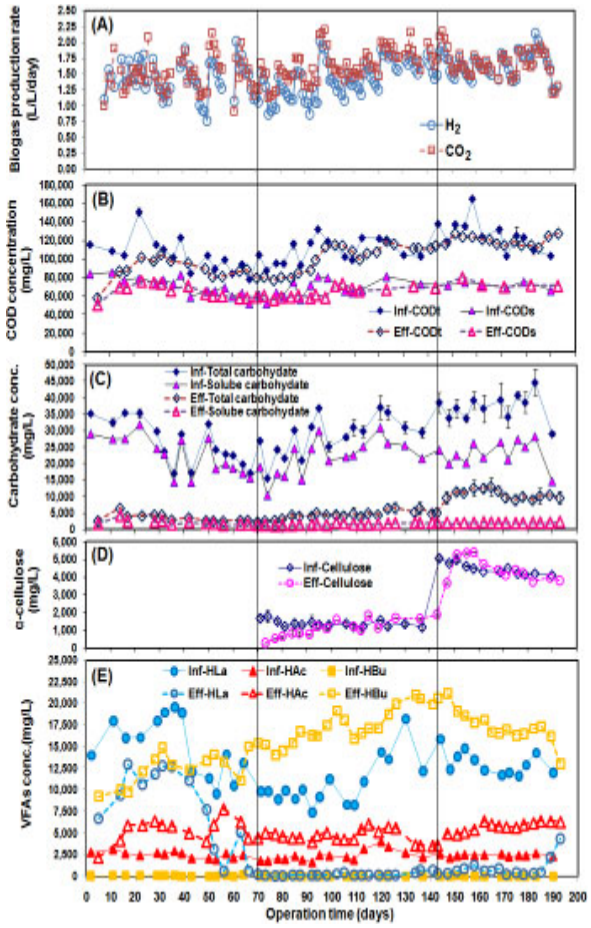

Figure 2: **Variation of (A) biogas production rate, (B) COD, (C) carbohydrate, (D) cellulose, and (E) volatile fatty acids in AnFB influent and effluent during operation time from run1 to run3.**

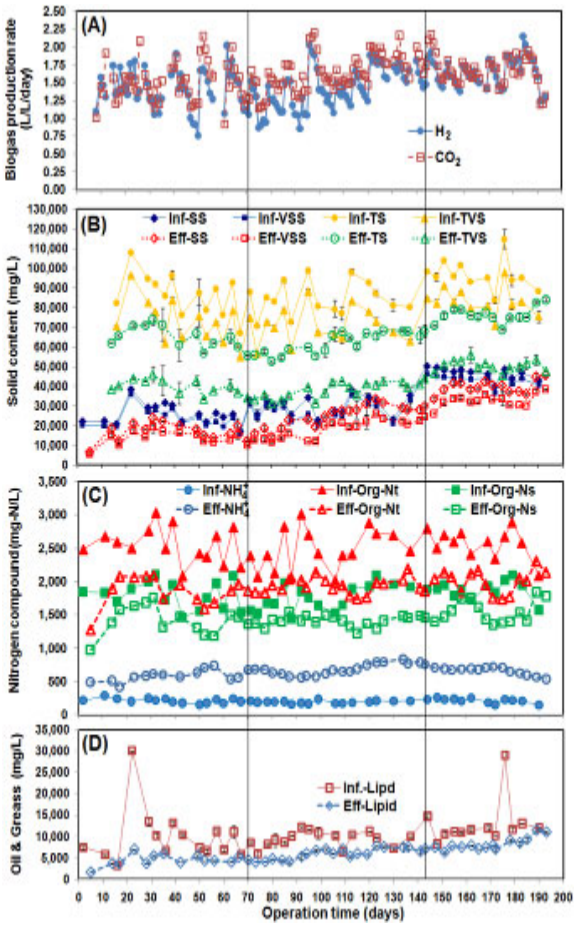

Figure 3: **Variation of (A) Biogas production rate, (B) solid contents, (C) nitrogen compounds, and (D) oil and grease in AnFB influent and effluent during operation time from run1 to run3.**

Table3: Characteristics of influent and effluent in Run 1 (n=15), Run 2 (n=16) and Run 3 (n=12).

Characteristic		Unit	Run 1 Influent	Run 1 Effluent	Run 2 Influent	Run 2 Effluent	Run 3 Influent	Run 3 Effluent
Solid content	TS	mg/L	86,800 ± 10,700	64,930 ± 8,160	84,670 ± 8,610	62,360 ± 5,390	96,760 ± 7,850	76,490 ± 4,000
	TVS	mg/L	72,900 ± 11,300	39,720 ± 6,600	70,880 ± 8,840	38,320 ± 4,050	83,220 ± 6,970	50,570 ± 2,860
	SS	mg/L	25,900 ± 5,330	17,860 ± 3,760	30,250 ± 4,770	25,250 ± 5,550	46,760 ± 2,970	39,770 ± 3,320
	VSS	mg/L	23,600 ± 5,050	14,390 ± 2,800	27,540 ± 4,520	18,660 ± 4,750	43,430 ± 2,640	32,830 ± 3,100
	VSS/SS	-	0.91 ± 0.05	0.81 ± 0.03	0.91 ± 0.05	0.78 ± 0.05	0.93 ± 0.01	0.83 ± 0.02
	TVS/TS	-	0.84 ± 0.04	0.61 ± 0.01	0.84 ± 0.03	0.61 ± 0.02	0.86 ± 0.01	0.66 ± 0.04
COD	CODt	mg/L	104,000 ± 18,000	90,400 ± 8,240	108,150 ± 13,100	101,700 ± 14,610	130,000 ± 17,270	119,710 ± 5,160
	CODs	mg/L	75,700 ± 8,240	69,000 ± 6,600	68,070 ± 9,210	64,018 ± 5,610	71,530 ± 3,620	73,020 ± 4,000
Carbohydrate	Total	mg-hexose/L	26,500 ± 6,340	3,240 ± 800	28,400 ± 5,900	4,880 ± 860	37,810 ± 3,300	10,705 ± 1,360
	Soluble	mg-hexose/L	23,500 ± 6,000	1,770 ± 470	21,900 ± 5,500	1,550 ± 340	23,860 ± 3,900	1,970 ± 110
	cellulose	mg-hexose/L	-	-	1,380 ± 180	1,280 ± 400	4,500 ± 330	4,420 ± 630
Protein	Org-N_{total}	mg-N/L	2,500 ± 270	1,890 ± 160	2,480 ± 310	1,940 ± 120	2,580 ± 220	2,010 ± 170
	Org-$N_{soluble}$	mg-N/L	1,800 ± 200	1,450 ± 180	1,760 ± 190	1,410 ± 80	1,880 ± 140	1,550 ± 170
	NH_4^+	mg/L	220 ± 40	590 ± 90	195 ± 20	690 ± 80	220 ± 40	665 ± 60
Lipid	Oil & Grease	mg/L	8,300 ± 3,060	4,710 ± 1,030	9,430 ± 1,810	6,440 ± 1,000	11,500 ± 1,630	8,300 ± 1,500
VFA	HLa	mg/L	14,500 ± 2,500	8,100 ± 4,550	10,700 ± 2,770	184 ± 190	13,100 ± 1,370	670 ± 550
	HAc	mg/L	2,500 ± 340	5,630 ± 1,070	2,360 ± 660	4,620 ± 750	2,420 ± 140	5,750 ± 540
	HPr	mg/L	205 ± 70	550 ± 170	100 ± 30	300 ± 70	100 ± 20	320 ± 40
	HBu	mg/L	54 ± 51	13,250 ± 1,230	N.D.	17,500 ± 2,110	N.D.	17,600 ± 1,400
Alcohols	EtOH	mg/L	3000 ± 800	3400 ± 720	3270 ± 1390	3450 ± 770	4120 ± 840	4220 ± 210

3.2 Microbial characterization with biomonitoring technology

A clone library was constructed to investigate the microbial diversity in AnFBR. There were three main groups of bacteria in this system. The most abundant microbe was similar to *Clostridium* sp. Strain Z6, which takes 37 % of total clone library. However, the similarity of the 16S rDNA fragment was only 93 %. It revealed that those bacteria enhanced by Napier Grass and KWSL were quite unique. About 18% of the clones were similar to *Thermoanaerobacterium thermosaccharolyticm* , which was reported as cellulose, starch, xylan, dextrin, xylose etc. degrading and hydrogen-producing bacteria (O-Thong et al., 2008 [8]). Finally, about 8 % of total clones were similar to *Lactobacillus plantarum* strain LMG 14188, and *Lactobacillus brevis* (2 % of total clone library). Those were isolated from Chinese sauerkraut fermentation broth and was related to lactate metabolism and cellulose hydrolysis. A diverse microbial community was revealled in this clone library, such as *Lactobacillus fermentum*, *Lactobacillus coryniformis*, *Lactobacillus crustorum*, *Lactobacillus curvatus*, *Lactobacillus sanfranciscensis*, *Lactobacillus vaccinostercus* and *Lactococcus lactis*. These diverse microbes were related to lactate metabolism and took up to 20 % of total clone library. This phenomenon in biohydrogen system is very unique; however, when kitchen waste was fed as substrate, this result was reasonable, because lactate accumulated very fast in kitchen waste. Lactate was reported to be utilized with acetate consumption by some species, such as *Clostridium beijerinckii*, *C. tyrobutyricum*, and *C. Acetobutylicum*. However, these Clostridia did not observed in this system. Accordingly, what/which microbes were responsible for lactate degrading is still unclear and further study is needed.

4 Conclusion

This study adopted an AnFB to conduct the hydrolysis of Napier Grass and co-digest with kitchen waste sieved liquid to produce hydrogen. KWSL could promote high loading to let microorganisms utilize the nutrients to produce hydrogen. In the first phase of the process, it was proved that KWSL as feeding substrate of AnFB could operate stably and was suitable for hydrogen production. In order to enhance the hydrolyzing ability of cellulosic materials, Napier Grass was added and increased to 20 g/L in the second and third phase.

During the operation period, a batch test was conducted to evaluate the cellulosic hydrolyzing potential. The result showed that microorganisms in an AnFB could not hydrolyze cellulose but could hydrolyze xylan. Lactate in the kitchen waste also contributed to the total hydrogen recovery and the stoichiometric equation of carbohydrate metabolism was close to: $3C_6H_{12}O_6 + 2H_2O \rightarrow 8H_2 + 6CO_2 + 2\ HAc + 2\ HBu$.

Three main groups of bacteria were identified by clone library construction of 16S rDNA, *Clostridium* sp., *Thermoanaerobacterium thermosaccharolyticm*, and a diverse *Lactobacillus* species.

Acknowledgements

The authors gratefully acknowledge financial support by Taiwan's National Science Council.

References

[1] Ueno, Y., Haruta, S., Ishii, M., Igarashi, Y., 2001. Microbial community in anaerobic hydrogen-producing microflora enriched from sludge compost. Applied Microbiology and Biotechnology 57, 555-562.

[2] Holst, T.C., Truc, A., Pujol, R., 1997. Anaerobic fluidized beds: ten years of industrial experience. Water Science and Technology 36, 415-422.

[3] Li, S.L., Kuo, S.C., Lin, J.S., Lee, Z.K., Wang, Y.H., Cheng, S.S., 2008. Process performance evaluation of intermittent-continuous stirred tank reactor for anaerobic hydrogen fermentation with kitchen waste. International Journal of Hydrogen Energy 33, 1522-1531.

[4] Wang, Y.H., Li, S.L., Chen, I.C., Cheng, S.S., 2009. Starch hydrolysis characteristics of hydrogen producing sludge in thermophilic hydrogen fermentor fed with kitchen waste. International Journal of Hydrogen Energy 34, 7435-7440.

[5] Herbert, D., Elsworth, R., Telling, R.C., 1956. The Continuous Culture of Bacteria; a Theoretical and Experimental Study. J Gen Microbiol 14, 601-622.

[6] Herbert, D., Philipps, P.J., Strange, R.E., 1971. Carbohydrate analysis. Methods Enzymol. 5B, 265-277.

[7] APHA, A.W., 1995. Standard Method for the Examination of Water and Wastewater, 19th edition ed, Washington, DC. USA.

[8] O-Thong, S., Prasertsan, P., Karakashev, D., Angelidaki, I., 2008. High-rate continuous hydrogen production by Thermoanaerobacterium thermosaccharolyticum PSU-2 immobilized on heat-pretreated methanogenic granules. International Journal of Hydrogen Energy 33, 6498-6508.

Hydrogen and Methane Production from Condensed Molasses Fermentation Soluble by a Two-stage Anaerobic Process

Chiu-Yue Lin, **You-Chyuan Liang**, **Chyi-How Lay**, Department of Environmental Engineering and Science, Feng Chia University, Taichung 40724, Taiwan
Chin-Chao Chen, Environmental Resources Laboratory, Department of Landscape Architecture, Chungchou Institute of Technology, Taiwan
Feng-Yuan Chang, Research Center for Energy and Resources, Feng Chia University, Taichung 40724, Taiwan

Abstract

The treatment of condensed molasses fermentation soluble (CMS) is a troublesome problem for glutamate manufacturing factory. However, CMS contains high carbohydrate and nutrient contents and is an attractive and commercially potential feedstock for bioenergy production. The aim of this paper is to produce hydrogen and methane by two-stage anaerobic fermentation process. The fermentative hydrogen production from CMS was conducted in a continuously-stirred tank bioreactor (working volume 4 L) which was operated at a hydraulic retention time (HRT) of 8 h, organic loading rate (OLR) of 120 kg COD/m^3-d, temperature of 35^{o}C, pH 5.5 and sewage sludge as seed. The anaerobic methane production was conducted in an up-flow bioreactor (working volume 11 L) which was operated at a HRT of 24 -60 hrs, OLR of 4.0-10 kg COD/m^3-d, temperature of 35^{o}C, pH 7.0 with using anaerobic granule sludge from fructose manufacturing factory as the seed and the effluent from hydrogen production process as the substrate. These two reactors have been operated successfully for more than 400 days. The steady-state hydrogen content, hydrogen production rate and hydrogen production yield in the hydrogen fermentation system were 37%, 169 mmol-H_2/L-d and 93 mmol-H_2/g carbohydrate$_{removed}$, respectively. In the methane fermentation system, the peak methane content and methane production rate were 66.5% and 86.8 mmol-CH_4/L-d with methane production yield of 189.3 mmol-CH_4/g $COD_{removed}$ at an OLR 10 kg/m^3-d. The energy production rate was used to elucidate the energy efficiency for this two-stage process. The total energy production rate of 133.3 kJ/L/d was obtained with 5.5 kJ/L/d from hydrogen fermentation and 127.8 kJ/L/d from methane fermentation.

1 Introduction

The treatment of condensed molasses fermentation soluble (CMS) is a troublesome problem for glutamate manufacturing factory. However, CMS contains high carbohydrate and nutrient contents and is an attractive and commercially potential feedstock for bioenergy production. Anaerobic fermentation is an effective and energy saving process to generate energy from organic wastes. There were many reports on hydrogen and methane production by two-stage anaerobic fermentation process (Ueno et al., 2007 [1]; Antonopoulou et al., 2008 [2];

Chu et al., 2008 [3]). The aim of this report is to produce hydrogen and methane by two-stage anaerobic fermentation process.

2 Materials and Methods

2.1 Feedstock and hydrogen fermentation system (HFS)

Feedsctock, CMS and hydrogenogenic microflora were prepared according to the previous report (Lay et al., 2010 [4]). Two liter of the heat-treated microflora was inoculated into 2 L of CMS with 40 g COD/L in a continuously-stirred tank bioreactor (working volume 4 L). The cultivation was carried out at a hydraulic retention time (HRT) of 8 h, organic loading rate (OLR) of 120 kg COD/m^3-d, temperature of 35°C and controlled pH 5.5 by automatic titration with 4 N NaOH. The effluent from hydrogen producing fermentor was collected into a gas and liquid separator. The amount of biogas produced was measured using a wet-gas meter (Ritter, Germany, TG 1/5).

2.2 Methane fermentation system (MFS)

The anaerobic methane production was conducted in an up-flow bioreactor (working volume 11 L). Anaerobic granular sludge was collected from a fructose manufacturing industry in central Taiwan. The pH, volatile suspended solids (VSS, to express the biomass concentrations) and (total chemical oxygen demand, T-COD) concentrations of the seed sludge were 8.0, 37.68 g/L and 70.24 g/L, respectively. Ten percent of working volume of the up-flow bioreactor was filled with the anaerobic granular sludge. The operation was conducted at a HRT of 24 -60 hrs, OLR of 4.0-10 kg COD/m^3-d, temperature of 35^{o}C and pH 7.0. The effluent from HFS was used as the substrate. The two-stage anaerobic fermentation process was shown in Figure 1.

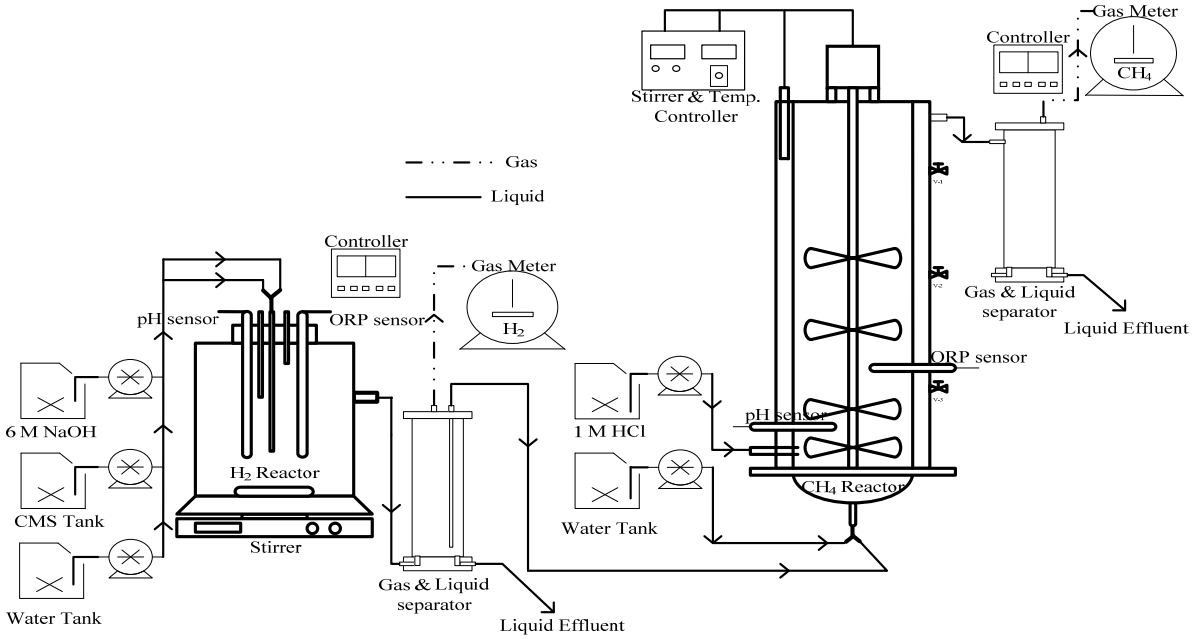

Figure 1: Schematic of the two-stage anaerobic biogas production fermentation system.

2.3 Analytical methods

The composition of product gas and the concentrations of ethanol and organic acids were measured as described previously (Lay et al., 2010 [4]). Analysis for the sampled broth for determination of residual sucrose concentration, pH, oxidation-reduction potential (ORP) and volatile suspended solid (VSS) concentration was carried out according to the previous report (Lin et al., 2010 [5]).

2.4 Monitoring

When a steady-state condition was reached, the hydrogen gas content and biogas production maintained stable, and the desired data obtained, the HRT was reduced. The monitoring parameters were pH, ORP (oxidation-reduction potential), alkalinity and gas production. The hydrogen production efficiency was evaluated using the hydrogen/methane productivity (the ability of converting carbohydrate and COD into hydrogen, respectively, HY and MY) and hydrogen/methane production rate (the rate of hydrogen/methane production from the reactor, HPR/MPR) and specific hydrogen/methane production rate (the rate of hydrogen/methane production from microflora, SHPR/SMPR). The total heating value could be calculated by Eq 1.

$$\text{Total energy (kJ)} = \sum V \times \frac{P}{R \times T} \times H_{H_2 \text{ or } CH_4} = V \times \frac{1}{0.082 \times 298} \times H_{H_2 \text{ or } CH_4} \qquad \text{Eq 1}$$

V is the H_2 or CH_4 production efficiency (L/L-reactor); P is the measurement pressure of the gas (1 atm); R is the gas constant (0.0821 L atm/mol K); T is the measurement temperature of the gas (273+25 K); H is heating value (kJ/mol). The heating values of hydrogen and methane are 285.8 and 896 kJ/mol, respectively.

3 Results

3.1 Performance of hydrogen fermentation system

Table 1 summarizes the experimental results obtained during the 491 days of fermentation. ORP value was about -420 mV which is close at the optimal value of -400 mV for HFS (Hippe et al., 1992 [6]; Kumar et al., 1995 [7]). The S-COD degradation was low (7.8%), because Organic material was converted into soluble metabolic products such as ethanol, acetate, propionate, butyrate. The carbohydrate was a good substrate for hydrogen producing bacteria (Koskinen et al., 2008 [8]). Therefore, the carbohydrate degradation was 65.9%. Figure 1 illustrates the daily variations at HRT of 8 h. The results shows the HPR, SHPR and HY were 162 mmol-H_2/L-d, 36 mmol-H_2/g VSS-d and 89.3 mmol-H_2/g Carbohydrate, respectively. The HPR value is similar with our previous study (Lay et al., 2010 [4]).

Table 1: The performance of hydrogen fermentation system at HRT 8 h.

OLR (kg COD /m^3-d)	ORP (-mV)	VSS (g/L)	S-COD (mg/L)			S-Carbohydrate (mg/L)		
			Influent (mg/L)	Effluent (mg/L)	Degradation (%)	Influent (mg/L)	Effluent (mg/L)	Degradation (%)
120±18.4	422±25	4.4±1.2	41,341±5,899	41,341±5,899	7.8	10,311±1,952	3,512±1,098	65.9

*OLR: organic loading rate

3.2 Performance of methane fermentation system

In our previous study (Lin, 2005 [9]), the optimal substrate concentration for methane fermentation of 10 g COD/L was obtained. However, the effluent concentration of the HFS was about 40 g COD/L. Therefore, the effluent of the HFS was diluted before seeded into the MFS. The MFS was started-up at HRT of 24 h with the fermentor performance enhanced successfully at HRT of 60 h. Table 2 shows the ORP was constant at -480 mV which is the optimal value for methane production (Dirasian et al., 1963 [10]). VSS was increased with increasing OLR. The S-COD and carbohydrate degradations were from 45.2 to 64.7% (Table 2).

Table 2: The performance of methane fermentation system at varied HRT.

HRT (h)	OLR* (kg COD /m^3-d)	ORP (-mV)	VSS (g/L)	S-COD (mg/L)			S-Carbohydrate (mg/L)		
				Influent (mg/L)	Effluent (mg/L)	Degradation (%)	Influent (mg/L)	Effluent (mg/L)	Degradation (%)
60	4±1.4	478±5	0.8±0.4	8,762±3,454	3,092±661	64.7	990±671	419±138	57.7
48	5±1.2	472±6	10.3±5.8	11,802±2,399	4,303±873	63.5	1,233±383	545±162	55.8
24	10±2.1	484±28	16.3±10	11,122±2,054	5,213±1,082	53.1	949±164	482±93	49.2
12	20±2.0	485±36	2.1±0.3	10,813±1,024	5,928±809	45.2	913±102	485±58	46.9

*OLR: organic loading rate

Figure 2 illustrates the daily variations in MPR, MY and SMPR at various HRTs. When the OLR was increased stepwise, the MPR increased along with the increasing OLR. The peak MPR of 151 mmol CH_4/L-d and MY of 313 mmol CH_4/g COD at 20 kg COD/m^3-d and HRT 12 h were 5 and 6-fold higher than 28 mmol CH_4/L-d and 51 mmol CH_4/g COD (at 4 kg COD/m^3-d and HRT 60 h). This value is 50% higher than HPR of 208 mmol H_2/L-d at HRT 4.4 h from molasses in CSTR (Liu et al., 2008 [11]).

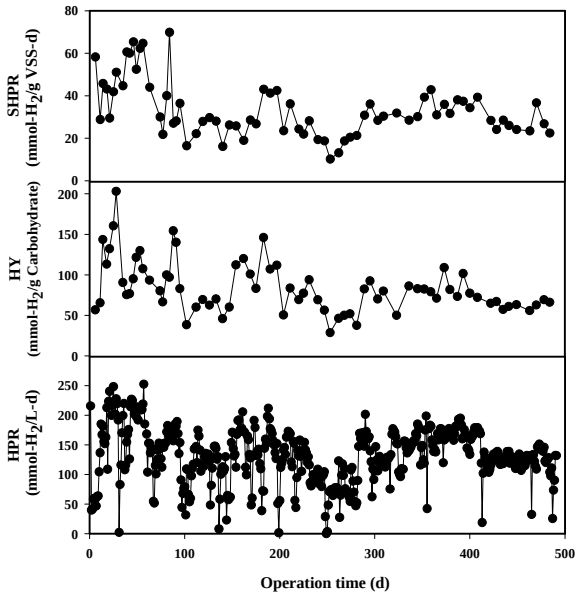

Figure 2: Hydrogen production rate, hydrogen yield and specific hydrogen production rate at HRT 8 h.

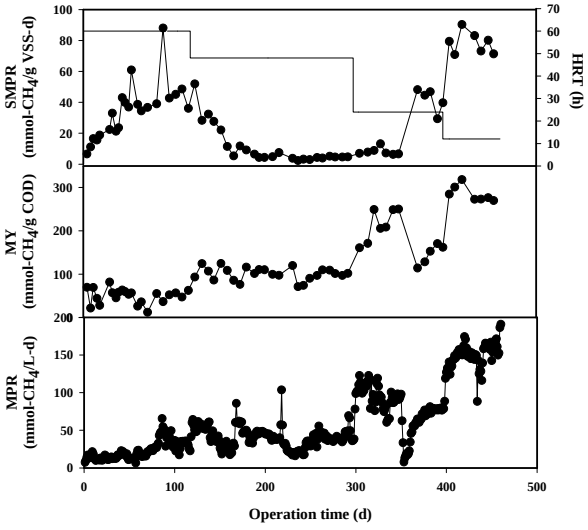

Figure 3: Daily evolution of methane production rate, methane yield and specific methane production rate.

3.3 Total energy production of two-stage anaerobic process

Table 3: Bioenergy production of two-phase bioenergy fermentation system.

Reactor	HRT (h)	HPR (mmol-H_2/L-d)	MPR (mmol-CH_4/L-d)	HY (mmol-H_2/g Carbohydrate)	MY (mmol-CH_4/g COD)	EPR (kJ/L-d)		EY (kJ/g Carbohydrate)	EY (kJ/g COD)
HFS	8	162	-	89.3	-	46.3	-	25.5	-
MFS	60	-	23.8	-	51.2	-	21.3	-	45.9
	48	-	46.9	-	120.2	-	42.0	-	107.7
	24	-	86.8	-	189.2	-	77.8	-	169.5
	12	-	151.1	-	312.8	-	135.4	-	280.3

Table 3 lists the total energy production calculated from hydrogen and methane production from the two-stage anaerobic process. The energy production rate (EPR) of 46.3 kJ/L-d and energy yield of 25.5 kJ/g carbohydrate were obtained from HPR of 162 mmol-H_2/L-d and HY of 89.3 mmol-H_2/g carbohydrate, respectively. The peak EPR in methane fermentation system was 135.4 kJ/L-d and the peak EY was 280.3 kJ/g COD at HRT 12 h. However, the total EPR of 181.7 kJ/L-d and EY of 305.8 kJ/g substrate for this two-stage anaerobic fermentation process were carried out at hydrogen fermentation system at HRT 8 h and methane fermentation system at HRT 12 h.

Acknowledgements

The authors gratefully acknowledge the financial support by Bureau of Energy, MOEA, Taiwan (Grant No. 98-D0137-2), National Science Council of Taiwan (96-2221-E-035-033-MY3) and Feng Chia University (FCU-08G27201).

References

[1] Ueno Y, Tatara M, Fukui H, Makiuchi T, Goto M, Sode K (2008) Production of hydrogen and methane from organic solid wastes by phase-separation of anaerobic process, Bioresource Technology 98: 1861–1865

[2] Antonopoulou G, Stamatelatou K, Venetsaneas N, Kornaros M, Lyberatos G (2008) Biohydrogen and Methane Production from Cheese Whey in a Two-Stage Anaerobic Process, Ind. Eng. Chem. Res. 47, 5227–5233.

[3] Chu CF, Li YY, Xu KQ, Ebie Y, Inamori Y, Kong HN (2007) A pH- and temperature-phased two-stage process for hydrogen and methane production from food waste, Int J Hydrogen Energy 33:4739–4746.

[4] Lay CH, Wu JH, Hsiao CL, Chang JJ, Chen CC, Lin CY (2010) Biohydrogen production from soluble condensed molasses fermentation using anaerobic fermentation, Int J Hydrogen Energy, doi:10.1016/j.ijhydene.2009.11.128.

[5] Lin CY, Wu SY, Lin PJ, Chang JS, Hung CH, Lee KS, Chang FY, Chu CY, Cheng CH, Lay CH, Chang AC (2010) Pilot-scale hydrogen fermentation system start-up performance, Int J Hydrogen Energy, doi:10.1016/j.ijhydene.2009.11.123.

[6] Hippe H, Andreesen JR, Gottschalk G. (1992) The Genus Clostridium-Nonmedical. 1800-1825, In :Balows H, Trüper HG, Dworkin M, Hareder W, Schleifer KH. The Prokaryotes, Vol 3, Springer-Verlag, New York.

[7] Kumar A, Jain SR, Sharma CB, Joshi AP, Kalia VC (1995) Increased H2 Production by Immobilized Microorganisms. World J Microbiol Biotechnol 11:156-159.

[8] Koskinen PEP, Lay CH, Puhakka JA, Lin PJ, Wu SY, O ¨ rlygsson J, Lin CY (2008) High-Efficiency Hydrogen production by an anaerobic, thermophilic enrichment culture from an Icelandic hot spring, Biotech. Bioeng. 101:665-678.

[9] Lin CI (2005) Bioenergy Production from Molasses Wastewater, Master degree thesis, Feng Chia University, Taichung, Taiwan.

[10] Dirasian HA, Molof AH, Borcharch JA (1963) Electrode Potential in Digestion. JWPCF 35: 424.

[11] Liu M, Chen Y, Ren NQ (2008) Energy recovery from molasses wastewater using two-phase. The 2008 Asian Bio-hydrogen Symposium.

Effect of Alkalinity and Organic Loading Rate in the Fermentative H_2 Production from an Anaerobic Fluidized Bed Reactor

E. L. C. Amorim, Department of Hydraulic and Sanitation, University of São Paulo, Av. Trabalhador Sãocarlense, 400 – Centro, CEP 13566-590 – São Carlos/SP, Brazil
A. R. Barros, E. L. Silva, Department of Chemical Engineering, Federal University of São Carlos, Rod. Washington Luis, km 235, CEP 13565-905 – São Carlos/SP, Brazil

1 Introduction

Currently, 90% of global energy is generated from fossil fuels. However, we now know that fossil fuel reserves are scarce, and their combustion generates various environmental problems. Replacing fossil fuels, which produce carbon dioxide as a combustion product, with hydrogen could be an alternative to ameliorate the greenhouse effect. Hydrogen is considered a clean fuel, generating water as a combustion product in electrolytic fuel cells, and it presents a high energy per unit mass (122 kJ g^{-1}), which is 2.75-fold greater than that of hydrocarbon fuels (Das and Verziroglu, 2001 [1]).

Several biological processes have shown potential for the sustainable production of hydrogen and require low energy inputs; thus, they are considered to be promising alternatives to conventional physical/chemical production of H_2. Hydrogen can be produced from biomass and/or a fraction of biodegradable waste, for use as a biofuel. Among the several alternatives of biological H_2 production, the use of an anaerobic fluidized-bed reactor (AFBR) has been shown to be efficient (Wu et al., 2006 [2]; Zhang et al., 2007 [3]). There are still several practical issues to be studied; among these are the conditions for optimized hydrogen production and limited growth of methanogens. These conditions include short hydraulic retention time (HRT), short cell retention time and low pH. Another method that can increase biological hydrogen production is thermal shock treatment of the inoculum, which removes spore-forming bacteria, some of which are consumers of hydrogen (Lay, 2001 [4], Van Ginkel et al., 2002 [5]). In previous studies (Van Ginkel et al., 2002 [5]), the heat treatment along with low pH were limiting factors for the growth of hydrogen-consuming microorganisms. Chen et al. (2005) [6] concluded that the optimum pH was 5.0 for hydrogen production. Fan and Chen (2004) [7] and Fang and Liu (2002) [8] obtained an optimum pH of 5.5. Khanal et al. (2004) [9] also obtained an optimum pH of 5.5 for hydrogen production; however, for volatile organic acid production (acetic and butyric acid), the optimum pH was between 3.0 and 4.0. However, Mu et al. (2006) [10] found the optimum pH for hydrogen production to be 4.2.

Due to this lack of consistent information on the optimum pH for hydrogen production, the stability of two identical anaerobic fluidized-bed reactors using expanded clay for microbial adhesion, R1, operated without pH control, and R2, operated with the addition of alkalinity to

control pH, were compared by varying the HRTs (organic loading rate) and evaluating their performances.

2 Material and Methods

2.1 Medium composition

The reactors were operated using a synthetic substrate containing glucose as the sole carbon source at a concentration of 2,000 mg L^{-1} plus the following nutrients (mg L^{-1}): CH_4N_2O, 125; $NiSO_4 \cdot 6H_2O$, 1; $FeSO_4 \cdot 7H_2O$, 5; $FeCl_3 \cdot 6H_2O$, 0,5; $CaCl_2 \cdot 6H_2O$, 47; $CoCl_2 \cdot 2H_2O$, 0.08; SeO_2, 0.07; KH_2PO_4, 85; $KHPO_4$, 21.7; and $Na_2HPO_4 \cdot 2H_2O$, 33.4. Reactor R1 was operated without pH control and R2 was operated with the addition of alkalinity (sodium bicarbonate 2,000 mg L^{-1}) as needed to maintain a pH of 5.0-5.5.

2.2 H_2-producing sludge and immobilization of H_2-producing

The inoculum used was sludge from an upflow anaerobic-sludge blanket (UASB) reactor treating effluent from swine-manure wastewater. The sludge was subjected to heat-treatment in accordance with the methodology described by Kim et al. (2006) [11]. This heat treatment allowed for the removal of vegetative cells of methanogenic and acidogenic bacteria not capable of forming endospores, which are structures resistant to adverse conditions. Acidogenic cells capable of spore formation remained as a viable culture. The selection was performed as described in Maintinguer et al. (2008) [12]. Particles of expanded clay (2.8–3.35 mm) were used as a support material for biomass immobilization.

2.3 Analytical methods

Hydrogen gas was identified with a gas chromatograph (GC-2010, Shimadzu, Tokyo, Japan) that was equipped with a thermal conductivity detector (TCD). The carrier gas was argon, and the column was packed with Supelco Carboxen 1010 Plot (30 m × 0.53 mm i.d.) (Maintinguer et al., 2008 [12]). The volatile fatty acid (VFA) and alcohol concentrations were measured using a gas chromatograph (GC-2010, Shimadzu, Tokyo, Japan) that was equipped with a flame-ionization detector (FID), a COMBI-PAL headspace autosampler (AOC model 5000) and an HP-INNOWAX column (30 m × 0.25 mm i.d. × 0.25 μm of film thickness) (Maintinguer et al., 2008 [12]). The pH and chemical oxygen demand (COD) were measured according to the procedures described in the Standard Methods (1998) [13]. The glucose concentrations of the reactor influent and effluent were determined by a method using an enzymatic reaction with glucose oxidase (Amorim et al., 2009 [14]).

2.4 Set-up and operation of AFBR for H_2 production

The experiments were carried out in two conventional anaerobic fluidized-bed reactors. The main body of the reactor was a vertical cylindrical column 5.3 cm in diameter and 190 cm in height. For the AFBR, the recycle rate was controlled at 128 L/min (bed expansion = 30%), which maintained good fluidization of the particles in the reactor. The bioreactor was initially operated in batch mode for 48 h to activate the H_2-producing sludge before it was switched

to a continuous mode at a designated hydraulic retention time (HRT = 8 h, 6 h, 4 h, 2 h or 1 h). The schematic diagram of the experimental system is shown in Figure 1.

After reaching steady-state operation (based on a constant volumetric H_2-production rate within a variation of 5-10% for 10-15 days), the HRT was decreased progressively from 8 h to 1 h. The compositions of the gaseous products (H_2 and CO_2) and soluble metabolites (volatile fatty acids and alcohol) produced during H_2 fermentation were monitored as functions of time. The reactor was operated at a temperature of 30°C. Reactor R1 was operated at an effluent pH within 3.68-4.05. Reactor R2 was operated at an effluent pH within 5.09-5.54. A gas meter (Type TG1; Ritter Inc., Germany) was used to measure the amount of gaseous products generated.

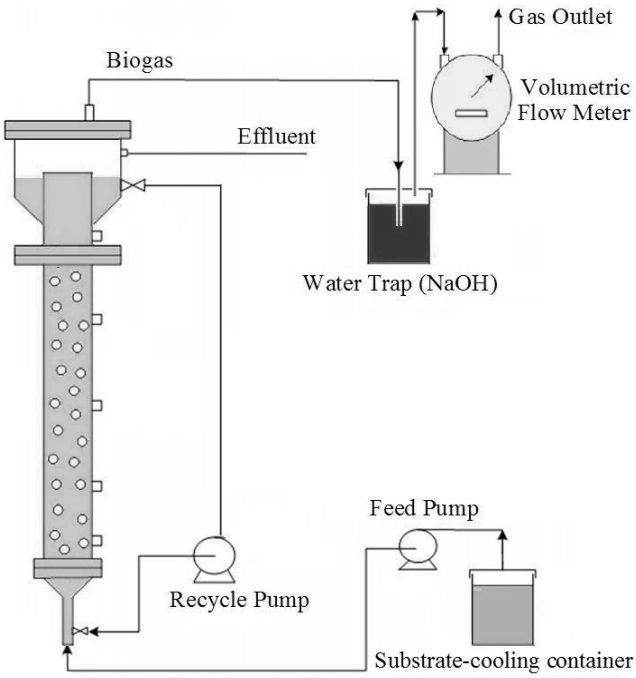

Figure 1: Diagram of the anaerobic fluidized-bed reactor (AFBR).

3 Results and Discussion

The effect of HRT on hydrogen production was evaluated as the reactors were operated without the addition of alkalinity (R1), with the addition of alkalinity (R2) and influent glucose concentration of 2,000 mg L^{-1}.

Figure 2 shows the pH behaviour resulting from the varying HRT applied to reactors. In the reactor without the addition of alkalinity (R1), the pH ranged from 3.68 to 4.05; for the reactor with the addition of alkalinity (R2), the pH ranged from 5.09 to 5.54.

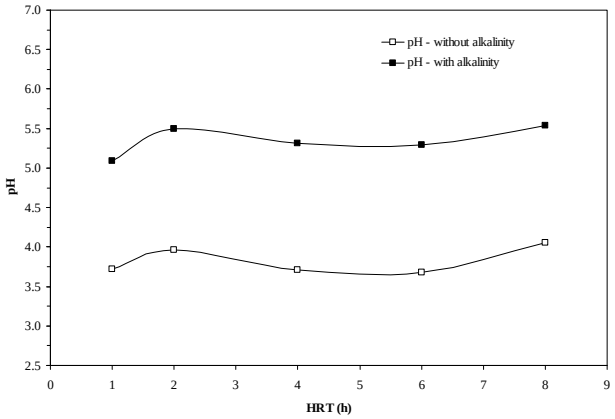

Figure 2: Performance of effluent pH in the reactors: R1 (□) (without added alkalinity) and R2 (■) (with added alkalinity).

As shown in Figure 3, the hydrogen-production rates (HPR) in reactors R1 and R2 increased from 0.08 to 0.97 L h^{-1} L^{-1} and from 0.12 to 0.76 L h^{-1} L^{-1}, respectively, by decreasing the HRT of 8 h to 1 h. For both reactors, the hydrogen-production rate increased slightly from an HRT of 8 h to 4 h but almost doubled at an HRT of 2 h compared to that at 4 h (Figure 3). A substantial increase was observed with an HRT of 1 h; this increase was related to the increased organic loading and growth of biomass. This finding indicates that the metabolic flux may have shifted during the transition of HRT from 8 h to 1 h, when most of the substrate was shifted to the reactions of end-products instead of bacterial growth and maintenance, resulting in increased hydrogen yield (Zhang et al., 2007 [3]). With a decrease of HRT from 8 h to 2 h, the hydrogen yield (HY) increased from 1.41 to 2.49 mol H_2/mol glucose in R1 and from 0.96 to 1.90 mol H_2/mol glucose in R2. However, when HRT was decreased to 1 h, the hydrogen yield in reactors R1 and R2 also decreased, to 2.41 and 1.24 mol H_2/mol glucose, respectively. This decrease in HY during the transition of the HRT from 2 h to 1 h may be attributed to kinetic limitations caused by the increase in the organic-loading rate in the reactor.

The glucose conversion in reactors R1 and R2 varied between 89.5-93.6% or 79.0-99.3%, respectively (Figure 4). The H_2 content of the biogas in reactors R1 and R2 increased from 8% to 35% and from 8% to 40%, respectively, with the decrease in the HRT from 8 h to 1 h (Figure 4). Also using AFBRs, Wu et al. (2003) [2] and Lin et al. (2006) [15] obtained substrate conversions above 90% and between 92% and 99%, respectively, for HRTs of 8 h and 1 h. However, Zhang et al. (2007) [3] found that the glucose conversion decreased from 99.47% to 71.44% when the HRT was decreased from 4 h to 0.5 h.

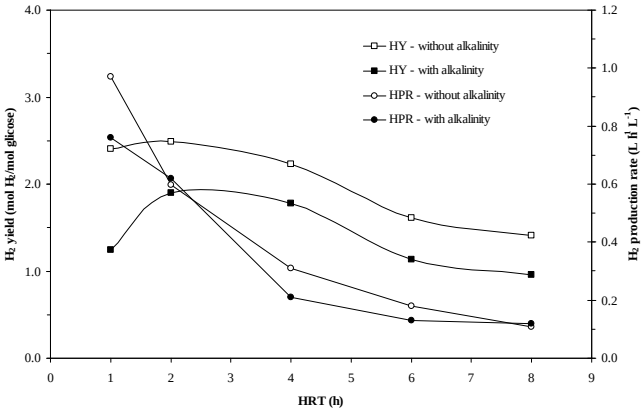

Figure 3: Effect of HRT on the AFBR performance: H_2 production rate and H_2 yield production. (□) R1-HY and (■) R2-HY; (○) R1-HPR and (●) R2-HPR. HY: H_2 yield ([mol of H_2 formed]/[mol of glucose consumed]); HPR: H_2-production rate.

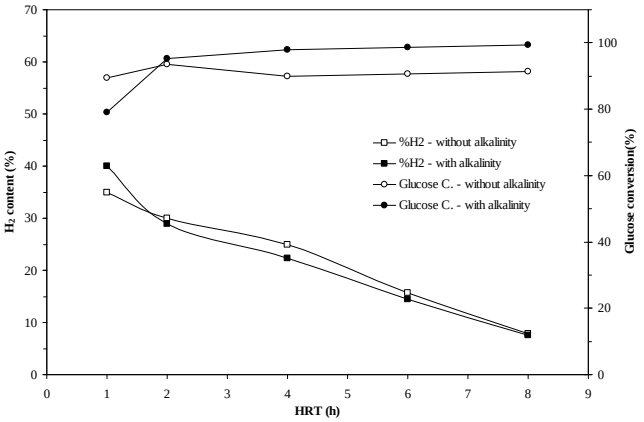

Figure 4: Effect of HRT on the performance of the reactors: H_2 content and glucose conversion. (□) R1 H_2 content and (■) R2 H_2 content; (●) R2 glucose conversion and (○) R1 glucose conversion. Glucose conversion: (mol of glucose utilized)/(mol of glucose fed into the reactor).

Table 1 shows the behaviour of the levels of the main metabolites produced in reactors R1 and R2 during operation under different HRTs.

Table 1: Composition of soluble metabolites under different HRTs in the AFBRs.

	Reactor R1 (without pH control)				Reactor R2 (with pH control)			
HRT (h)	HAc (%)	HBu (%)	HPr (%)	EtOH (%)	HAc (%)	HBu (%)	HPr (%)	EtOH (%)
8	36.28	44.66	0.00	19.06	31.58	11.84	8.53	48.05
6	36.12	44.87	0.00	19.01	39.94	12.93	14.57	32.56
4	48.85	37.73	0.00	13.42	46.47	12.67	10.55	30.31
2	53.32	39.65	0.00	7.03	52.51	13.77	7.37	26.34
1	50.55	41.60	0.00	7.85	36.12	26.04	16.89	20.95

HAc: acetate; HBu: butyrate; HPr: propionate; EtOH: ethanol.

In the reactor without added alkalinity (R1), the products, in ascending order, were ethanol (7.03%-19.06%), acetate (36.12%-53.32%) and butyrate (37.73%-44.87%). Propionate was not detected during the entire operation of reactor R1. This should enhance the increase in hydrogen production in these reactors, as the biosynthetic route for the production of propionate results in the consumption of two moles of H_2 for every two moles of propionic acid produced (Eq. 1), and may be related to inhibition likely caused by low pH and sensitivity to short HRT, as has been reported by other researchers (Zhang et al., 2007) [3].

$$C_6H_{12}O_6 + 2H_2 \rightarrow 2CH_3CH_2COOH + 2H_2O \quad (1)$$

In the reactor with alkalinity addition (R2), the products in ascending order were propionate (7.37%-16.89%), butyrate (11.84%-26.04%), ethanol (20.95%-48.05%) and acetate (31.58-52.51%).

4 Conclusion

The hydrogen production rate, hydrogen yield and H_2 content all increased with the reduction of HRT from 8 h to 1 h. The reactor without added alkalinity (R1) showed higher hydrogen production rates and hydrogen yields at all HRTs evaluated, although the H_2 content as a percentage of the biogas was similar in both reactors. The reactor R1 did not produce propionic acid, resulting in a higher hydrogen yield. These results indicate that both conditions (with or without the addition of alkalinity) are suitable for hydrogen production; however, the production in the reactor without added alkalinity was higher at all stages, and therefore that setup is the better option for hydrogen production in an anaerobic fluidized-bed reactor.

Acknowledgement

The authors gratefully acknowledge the financial support of CNPq and FAPESP.

References

[1] Das, D., Verziroglu, T. N. (2001). Hydrogen production by biological process: a survey of literature. **International Journal of Hydrogen Energy, 26**, No. 1: 13-28.

[2] Wu, S.Y., Lin, C.N., Chang, J.S., Lee, K.S., Lin, P.J. (2003). Hydrogen production with immobilized sewage sludge in three-phase fluidized-bed bioreactor. **Biotechnology Prog, 19**, No. 3: 828-832.

[3] Zhang, Z.P., Tay, J.H., Show, K.Y., Yan, R., Liang, D.T., Lee, D.J., Jiang, W.J. (2007). Biohydrogen production in a granular activated carbon anaerobic fluidized bed reactor. **International Journal of Hydrogen Energy, 32**, No. 2: 185-191.

[4] Lay J.J. (2001). Biohydrogen generation by mesophilic anaerobic fermentation of microcrystalline cellulose. **Biotechnology and Bioengineering, 74**, No. 4, 280-287.

[5] Van Ginkel, S., Sung, S.W., Lay, J.J. (2002). Biohydrogen production as a function of pH and substrate concentration. **Environmental Science and Technology, 32**, No. 24: 4726-4730.

[6] Chen, W.M., Tseng, Z.J., Lee, K.S., Chang, J.S. (2005). Fermentative hydrogen production with *Clostridium butyricum* CGS5 isolated from anaerobic sewage sludge. **International Journal of Hydrogen Energy, 30**, No. 10: 1063-1070.

[7] Fan, K.S., Chen, Y.Y. (2004). H_2 production through anaerobic mixed culture: effect of Batch S0/X0 and shock loading in CSTR. **Chemosphere, 57**, No. 9: 1059-1068.

[8] Fang, H.H.P., Liu, H. (2002). Effect of pH on hydrogen production from glucose from a mixed culture. **Bioresource Technology, 82**, No. 1: 87-93.

[9] Khanal, S.K., Chen, W.H., Li, L., Sung, S. (2004). Biological hydrogen production: effects of pH and intermediate products. **International Journal of Hydrogen Energy, 29**, No. 11: 1123-1131.

[10] Mu, Y., Yu, H.Q., Wang, Y. (2006). The role of pH in the fermentative H_2 production from an acidogenic granule-based reactor. **Chemosphere, 64**, No. 3: 350-358.

[11] Kim, S., Han, S., Shin, H. (2006). Effect of substrate concentration on hydrogen production and16s rDNA-based analysis of the microbial community in a continuous fermenter. **Process Biochemistry, 41**: 199-207.

[12] Maintinguer, S.I., Fernandes, B.S., Duarte, I.C.S., Saavedra, N.K., Adorno, M.A.T., Varesche, M.B. (2008). Fermentative hydrogen production by microbial consortium. **International Journal of Hydrogen Energy, 33**, No. 16: 4309-4317.

[13] APHA (1998). Standard methods for the examination of water and wastewater, 20th ed. American Public Health Association / American Water Works Association / Water Environment Federation, Washington, DC, USA.

[14] Amorim, E.L.C., Barros, A.R., Damianovic, M.H.R.Z., Silva, E.L. (2009). Anaerobic fluidized bed reactor with expanded clay as support for hydrogen production through dark fermentation of glucose. **International Journal of Hydrogen Energy, 34** , No. 2: 783-790.

[15] Lin, C.N., Wu ,S.Y., Chang, J.S. (2006). Fermentative hydrogen production with a draft tube fluidized bed reactor containing silicon-gel-immobilized anaerobic sludge. **International Journal of Hydrogen Energy, 31**, No. 15: 2200-2210.

[16] Leite, J.A.C., Fernandes, B.S., Pozzi, E., Barboza, M., Zaiat, M. (2008). Application of an anaerobic packed-bed bioreactor for the production of hydrogen and organic acids. **International Journal of Hydrogen Energy, 33**, No. 2: 579-586.

Biohydrogen Production from Combined Dark-photo Fermentation under a high Ammonia Content in the Dark Fermentation Effluent

Chun-Yen Chen[1,2], Yung-Chung Lo[1], Kuei-Ling Yeh[1], Jo-Shu Chang[1,2,3]
[1] Department of Chemical Engineering, National Cheng Kung University
[2] Sustainable Environment Research Center, National Cheng Kung University
[3] Microalgae Biotechnology and Bioengineering Laboratory, Center for Biotechnology and Biosciences, National Cheng Kung University, Tainan, Taiwan

Abstract

Integrated dark and photo (two-stage) fermentation was employed to enhance the performance of H_2 production. First, the continuous dark fermentation using indigenous *Clostridium butyricum* CGS5 was carried out at 12 h HRT and fed with sucrose at a concentration of 18750 mg/l. The overall H_2 production rate and H_2 yield were fairly stable with a mean value of 87.5 ml/l/h and 1.015 mol H_2/mol sucrose, respectively. In addition, a relatively high ammonia nitrogen content (574 mg/l) in the dark fermentation effluent was observed. The soluble metabolites from dark fermentation, consisting mainly of butyric, lactic and acetic acids, were directly used as the influent of continuous photo-H_2 production process inoculated with *Rhodopseudomonas palutris* WP 3-5 under the condition of 35^{o}C, 10000 lux irradiation, pH 7.0 and 48 h HRT. The maximum overall hydrogen production rate from photo fermentation was 16.4 ml H_2/l/h, and the utilization of the soluble metabolites could reach 90%. The maximum H_2 yield dramatically increased from 1.015 mol H_2/mol sucrose (in dark fermentation only) to 6.04 mol H_2/mol sucrose in the combined dark and photo fermentation. Surprisingly, the operation strategy applied in this work was able to attain an average NH_3-N removal efficiency of 92%, implying that our photo-H_2 production system has a higher NH_3-N tolerance, demonstrating its high applicability in an integrated dark-photo fermentation system.

1 Introduction

Hydrogen is a clean energy since combustion of H_2 produces only water without greenhouse gases. Hydrogen can also be directly utilized by hydrogen fuel cell to generate electricity at very high efficiency [1], thereby being considered a promising alternative energy carrier of the future [2,3]. To this end, developing hydrogen production technology leading to a sufficient and sustainable H_2 supply is highly demanded. Biological H_2 production considered as the most environmentally friendly route of producing H_2 [4], thereby fulfilling the goals of recycling of renewable resources and clean energy production [5]. Hydrogen can be produced biologically through dark fermentation and photo fermentation [6]. These routes all possess advantages and drawbacks, but they seem to interact complementarily. Thus, effective integration of the three pathways may lead to optimal performance of biohydrogen

production [7]. In this study, sucrose was used in a dark-fermentation batch bioreactor with *Clostridium butyricum* CGS5 to produce hydrogen and volatile fatty acids. The effluent from dark fermentation broth (containing mainly volatile fatty acids) was continuously introduced to photo fermentation culture inoculated by *Rhodopseudomonas palustris* WP3-5. The stability of continuous operation of the integrated dark/photo H_2 fermentation system was evaluated.

2 Materials and Methods

2.1 Bacterial strain and cultivation medium

The strain used for dark fermentation was *Clostridium butyricum* CGS5 isolated from municipal sewage sludge in central Taiwan [8]. The *Rhodopseudomonas palustris* WP3-5 isolated from a swine wastewater treatment plant located in central Taiwan [9] was used for phototrophic H_2 production. The culture medium was using 2000 mg/l sodium acetate as a sole carbon substrate. The cells were cultivated at 32^{o}C anaerobically for 48 h under a light intensity of approximately 50 W/m^2 (illuminated by tungsten filament lamp). The initial pH value of medium prior to incubation was adjusted to 7.0-7.1. Argon gas was used to create an anaerobic condition.

2.2 Setup of the bioreactor

The batch dark H_2 fermentation conducted by inoculating 3 ml of *C. butyricum* CGS5 into 200 ml flasks containing 150 ml of dark-fermentation medium, which was incubated at 37^{o}C and an initial pH of 7.5. A continuously stirred tank reactor (CSTR) was also conducted to produce H_2 from sucrose via dark fermentation using *C. butyricum* CGS5 as the H_2 producer. The continuous culture was operated at 37^{o}C, pH 6.5. The dark H_2 fermentation broth was centrifuged (9000 × g, 10 min) and the collected supernatant was diluted and then the pH was adjusted to 7.1. This pretreated supernatant was used as the substrate for phototrophic H_2 production with *R. palustris* WP3-5. The photobioreactor (PBR) was a 1-liter glass-made vessel equipped with external light sources (100 W tungsten filament lamps) adjusted to a light intensity of ca. 95 W/m^2.

3 Results and Discussion

3.1 Continuous dark-fermentation H_2 production using sucrose as substrate

In this work, a pure strain of *Clostridium pasteurianum* CGS5 was used to produce H_2 via continuous dark fermentation using sucrose as the carbon source. The soluble products generated from dark fermentation were then used for phototrophic H_2 production in the following stage. The dark fermentation operated at 32 ^{o}C, 12 h HRT and fed with a sucrose concentration of 18750 mg/l gave an H_2 yield of 1.105 mol H_2/mol sucrose, and overall H_2 production rate of 87.5 ml/l/h, respectively. Moreover, a relatively high ammonia nitrogen content of 574 mg/l was observed in the effluent of dark fermentation system. Meanwhile, the nearly 70-90% of soluble metabolites in the dark fermentation broth (mainly lactate, acetate, and butyrate) was produced to serve as substrates for photo fermentation, which

seems to be feasible substrates for H_2 production in the photo fermentation system as will be discussed next.

3.2 Continuous bioH_2 production with integrated photo fermentation processes

The dark fermentation metabolites mentioned above were further utilized as the influent of continuous photo-H_2 fermentation process inoculated with *R. palutris* WP3-5 under the condition of 32^{o}C, 100 W/m^2 irradiation, pH 7.0 and 96 h HRT. The overall H_2 production rate in photo fermentation was fairly stable with a mean value of 16.4±1.31 ml H_2/l/h. The cell concentration also reached a steady-state value of nearly 5.18±0.51 g/l over a 5-day operation. The H_2 content in biogas was essentially constant at 91.3±1.75% for 5-fold soluble metabolites. The total hydrogen yield calculated from integration of the yield from dark and photo fermentation reached a high value of 6.04 mol H_2/mol sucrose, which is nearly 5.95-fold of that obtained from using dark fermentation alone (1.015 mol H_2/mol sucrose). Nearly 92.0±1.5% for 5-fold soluble metabolites of the ammonia nitrogen entering the photo fermentation process was consumed, implying that our photo-H_2 production system has a higher NH_3-N tolerance, demonstrating its high applicability in an integrated dark-photo fermentation system. This suggests the feasibility and advantage of using the two-stage process combining dark and photo fermentation for high-yield bioH_2 production with an excellent stability.

References

[1] H. Su, J. Cheng, J. Zhou, W. Song, K. Cen, Improving hydrogen production from cassava starch by combination of dark and photo fermentation, Int. J. Hydrogen Energy, 34 (2009) 1780-1786.

[2] C.Y. Chen, J.S. Chang, Enhancing phototropic hydrogen production by solid-carrier assisted fermentation and internal optical-fiber illumination, Process Biochem, 41 (2006) 2041-2049.

[3] N.Q. Ren, B.F. Liu, J. Ding, G.J. Xie, Hydrogen production with *R. faecalis* RLD-53 isolated from freshwater pond sludge, Biores. Technol., 100 (2009) 484-487.

[4] S. Meher Kotay, D. Das, Biohydrogen as a renewable energy resource—Prospects and potentials, Int. J. Hydrogen Energy, 33 (2008) 258-263.

[5] V. Gadhamshetty, A. Sukumaran, N. Nirmalakhandan, M. Thein Myint, Photofermentation of malate for biohydrogen production-- A modeling approach, Int. J. Hydrogen Energy, 33 (2008) 2138-2146.

[6] P.C. Hallenbeck, J.R. Benemann, Biological hydrogen production: fundamentals and limiting processes, Int. J. Hydrogen Energy, 27 (2002) 1185-1193.

[7] J.S. Chang, Bioenergy engineering for clean and sustainable energy production, J. Biosci. Bioeng., 108 (2009) S41.

[8] S.D. Chen, K.S. Lee, Y.C. Lo, W.M. Chen, J.F. Wu, C.Y. Lin, J.S. Chang, Batch and continuous biohydrogen production from starch hydrolysate by Clostridium species, Int. J. Hydrogen Energy, 33 (2008) 1803-1812.

[9] C.Y. Chen, W.B. Lu, J.F. Wu, J.S. Chang, Enhancing phototrophic hydrogen production of *Rhodopseudomonas palustris* via statistical experimental design, Int J Hydrogen Energy, 32 (2007) 940-949.

A Pilot Study of Nitrogen Composition and Effect on Biohydrogen Production

Sheng-Shung Cheng, Energy and Environmental Laboratories, Industrial Technology Research Institute, 1955, sec 4, Chung Hsing Rd., Chungtung, Hsinchu, 31040, Taiwan (R.O.C.)
Ming-Der Bai, **Yu-Chieh Chao**, **Yun-Huin Lin**, Department of Environmental Engineering, National Cheng Kung University, No.1, University Rd., East District, Tainan City 701, Taiwan (R.O.C.)

1 Introduction

Biohydrogen is a potential technology that converts industrial wastes into hydrogen and simple fatty acids. However, there has been only little research working on continuous operation in large scale. Ren et al, [2006] [1] operated a 1.48 m^3 pilot-scale bioreactor using molasses as substrate. Hydrogen can be recovered and the maximum hydrogen production rate was 5.57 m^3-H_2/m^3-reactor/d. For the lack of performances data of biohydrogen system applying on industrial wastes, commercial popularization is very difficult. To improve this situation, a biohydrogen pilot plant with a 1,000 L working volume was built on an industrial site. This study was, therefore, carried out to collect operational parameters and performance indexes for scaling up.

It is universally known that carbohydrate was most suitable for hydrogen production, and most feedstock used in biohydrogen fermentation containing nitrogen source to enhance growth and activity of hydrogen-producing bacteria. However, few studies paid their attention to the important and effects of nitrogen on hydrogen fermentation. Yokoi [1995] [2] notice that polypepton could enrich hydrogen production, but it would react with glucose in high temperature to produce some chemical to inhibit hydrogen production. Ueno [2001] [3] commented the different bacteria community caused by different nitrogen source. Nitrogen source influents the cell growth and hydrogen production of hydrogen-fermenting bacteria.

2 Materials and Methods

A continuously flow biohydrogen reactor with a working volume of 1 m^3 was used in this study. Total volume of the reactor was 1.6 m^3 and sucrose and fodder wastes were used as substrates.

The feeding stuff was made of 1 portion of fodder waste and 4 portions of sucrose, and the organic concentration of the substrate was about 10 g-COD/L. Different hydraulic retention time (HRT) was controlled for different OLR operation.

The biogas produced from the reactor was measured by a gas meter continuously; biogas was collected by water displacement method then analyzed by a gas chromatograph (Model 6890N, HP) equipped with a thermal conductivity detector (TCD). The concentration of sucrose was determined by phenol-sulfuric method [Herbert et al., 1971 [4]]. Water quality

analyses were conducted according to the procedures described in the Standard Method 19th edition [APAH 1995 [5]].

3 Results and Discussion

A biohydrogen pilot plant was built in an industrial field, which was consisted of an acidogenesis tank for hydrogen production and a methanogenesis tank for methane production by using several industrial wastes or wastewater as raw materials. During the decomposing process of the raw materials, hydrogen and methane were produced. The units of the process were adjusted and the hardware facilities were improved during the operation time. In the start-up phase, sucrose and fodder waste were used as substrates for microbial propagation. The objective of this phase was to make hydrogen-producing bacteria active so as to endure higher volumetric organic loading in the next phase. In the second phase, volumetric organic loading rate was controlled at 3.3 kg-COD/m^3-day initially, then the loading was increased to 6.7 kg-COD/m^3-day. By applying the two-phase organic loading control, a high hydrogen yield of 120~133 L H_2/kg-COD was achieved. However, the fodder waste in the feedstock limited organic nitrogen, which cannot supply sufficient nitrogen for microbial growth.

In this case study, fodder wastes was the only nitrogen source in the substrate, which used only as assimilation for bacteria propagation. The nitrogen content in the fodder waste was around 3 to 4%. Therefore, the nitrogen supply in the total feedstock was about 1.2-1.6%. It was too little for the hydrogen production bacteria to grow under the OLR of 6.7 kgCOD/m^3/d. Besides, the amount of total Kjeldahl nitrogen in the reactor decreased gradually to 20 mg-N/L, which was only enough for composing a biomass amount about only 160 mg/L. Gradually, hydrogen yield was reduced in the condition of nitrogen lacking, and the profile of valitile fatty acids was shifted to a pathway which is unfavourable for hydrogen producing.

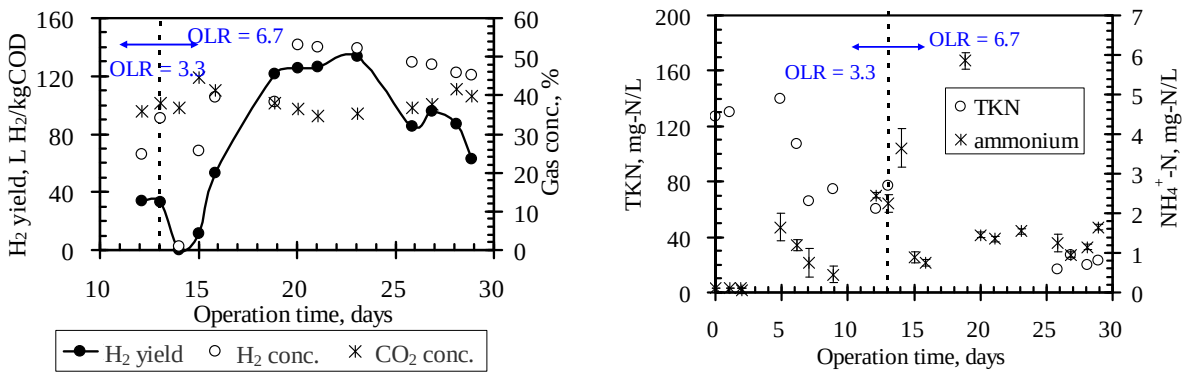

Figure 1: The hydrogen production (left) and nitrogen concentration (right) profile in the biohydrogen fermentor.

To resolve the problem, urea was added to make up the shortage of nitrogen content in the substrate. After urea was added, hydrogen yield was recovered to 100 L H_2/kg-COD and the fermentation pathway was shifted back to the desired butyrate/acetate-leading process. Although the hydrogen yield was recovered, the troublesome scum problem was caused by rapid hydrogen production rate. The foam can overflow the gas purifying tank, obstruct the

gas tube, and nullify the gas flow meter. Several low hydrogen production data obtained in the urea addition duration was caused by the troublesome scum problem. However, the substantially increase in the biohydrogen fermentation byproducts, acetate and butyrate indicated that the metabolism pathway in the fermentor had shifted to the hydrogen production metabolism.

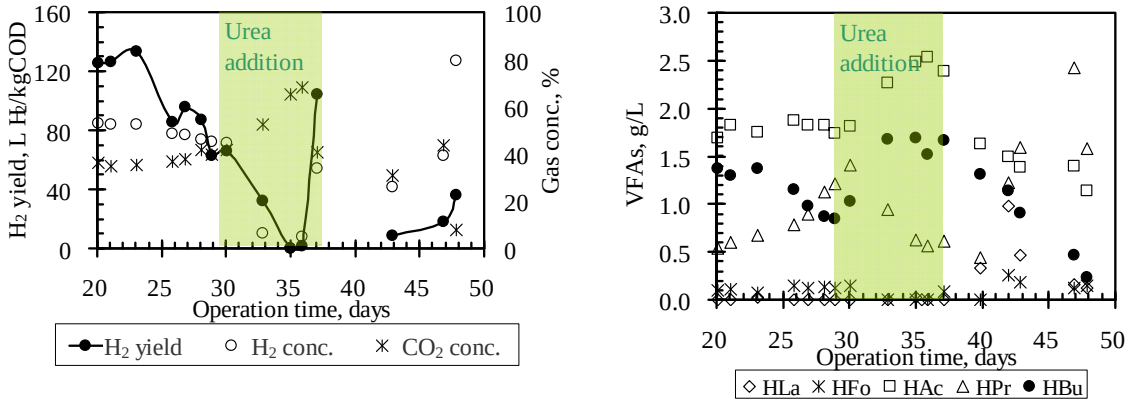

Figure 2: The hydrogen production (left) and fatty acid byproducts (right) profile in the biohydrogen fermentor operated with and without extra nitrogen addition.

Because of the hydrogen gas meter nullified and biomass washed out by the scum problem, the urea addition was broken off after 8 days, and the hydrogen, acetate and butyrate production decreased immediately. The metabolism pathway in the fermentor had shifted away from the hydrogen production metabolism.

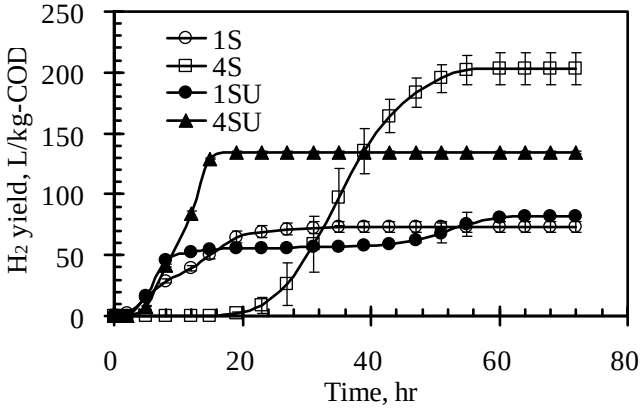

Figure 3: Hydrogen production profile in the batch hydrogen fermentation. (U: urea extra addition; 4S : 4 g/L sugar +1 g/L waste fodder; 1S : 1 g/L sugar +4 g/L waste fodder)

A batch test was conducted to investigate this nitrogen insufficient phenomenon. The results (Figure 3) showed that urea addition can greatly shorten the lag phase and increase the maximum hydrogen production rate. However, urea addition also limited the hydrogen recovery at high sucrose content. This may result from the energy consumption for bacteria

growth, and therefore shifted the electron flow from hydrogen to cell division. Under continuous operation, with limit organic nitrogen the growth rate of bacteria was low and can't be retained in the reactor resulting in a decline in hydrogen production.

4 Conclusion

Used as feedstock in hydrogen fermentation, waste fodder could not provide enough nitrogen for cell growth, which causes biomass concentration decreasing and shifting the metabolism pathway away from biohydrogen production. The best hydrogen production was caused in the exponation phase, the cell growth rapidily phase. However, the batch biohydrogen fermentation test results showed that urea addition also limited the hydrogen recovery that may result from the energy consumption for bacteria growth.

Acknowledgements

The authors gratefully acknowledge financial support by Taiwan's Bureau of Energy, Ministry of Economical Affairs.

References

[1] Ren N., J. Li, B. Li,Y. Wang, S. Liu. "Biohydrogen production from molasses by anaerobic fermentation with a pilot-scale bioreactor system", Int. J. of Hydrogen Energy, 31:2147 – 57. 2006.

[2] Yokoi, H., Ohkawara, T., Hirose, J., Hayashi, S. and Takasaki, Y. (1995) Characteristics of Hydrogen Production by Aciduric Enterobacter aerogenes Strain HO-39. Journal of Fermentation and Bioengineering, 80(6), 571-574

[3] Ueno, Y., Haruta, S., Ishii, M. and Igarashi, Y. (2001) Microbial community in anaerobic hydrogen-producing microflora enriched from sludge compost. Applied Microbiology and Biotechnology 57, 555-562.

[4] Herbert D., P. J. Philipps and R. E. Strange, "Carbohydrate analysis," Methods Enzymol., 5B, 265-277. 1971.

[5] Standard Method for the Examination of Water and Wastewater, 19 th ed. APAH, Washington, DC. 1995.

Biochemical Hydrogen Potential Assessment with Anaerobic Batch Biodegradation of Organic Leachate from Aerobic Bio-leaching Bed Feeding Kitchen Waste and Napier Grass

Sheng-Shung Cheng, **Son-Chi Wong**, **Keng-Hao Yang**, **Ya-Fei Yang**, Department of Environmental Engineering, National Cheng Kung University, No.1, University Rd., East District, Tainan City 701, Taiwan (R.O.C.)

1 Introduction

Napier Grass is an herbage which consists of abundant cellulose. Due to its advantages of easy planting, high-growing rate (it can be reaped every 8 or 10 weeks), high yield density per year (dry matter yield is about 60~80 ton/hectare/year), inexpensive and high electron density (COD/TOC = 3.02 gCOD/gTOC), we decided to choose Napier Grass as one of the substrates in this study. In Napier Grass, nevertheless, considering the abundant cellulose which can lead to the difficulties in hydrolysis, we added kitchen waste as another substrate in order to co-metabolize with Napier Grass. Kitchen waste is a mixture containing different kinds of organic compound such as starch, protein, cellulose, fat and so on. Therefore, we speculated that the cellulose-hydrolyzing microorganisms might exist in kitchen waste. In addition, kitchen waste contains not only high organic loading but also a great deal of nutrients and trace elements, so it can provide microorganisms with abundant nutrition. That is why we want to add kitchen waste to co-metabolize with Napier Grass in order to increase the efficiency of hydrolysis.

In the conventional anaerobic biohydrogen reactor, the efficiency of hydrolysis is limited by the anaerobic condition. In this study, therefore, the hydrolysis is conducted under aerobic condition. We divide the fermentative biohydrogen into two parts. The first part is to hydrolyze cellulose using aerobic leaching bed. The second part is to produce hydrogen with the leaching from the leaching bed. Because of the fine and long configuration of cellulose and its difficulty in hydrolysis, cellulose in high concentration can result in fouling easily on reactor such as fluidized bed, CSTR and so on. So this study exploited the aerobic leaching bed to solve the fouling problems. Dividing the fermentative biohydrogen into two parts, we can optimize the conditions of hydrolyzing cellulose and producing hydrogen respectively in order to increase the efficiency of hydrolysis and hydrogen production.

This study examined the feasibility of producing hydrogen by fermentation of the leaching from the ABB in batch culture. The seeding is from the anaerobic hydrogen fermentor fed with vegetable kitchen waste and we use the leaching as the substrate to carry out the biochemical Hydrogen Potential (BHP) test with different food to microorganism ratio (S0/X0). Discussing the pH variation, water quality variation, cumulative hydrogen yield, hydrogen production rate and so on, we hope to find out if the leaching is suitable for producing hydrogen or not and the optimistic condition for hydrogen production as well.

2 Materials and Methods

The biochemical hydrogen potential test was modified from biochemical methane potential test (Owen, Stuckey et al. 1979 [1]). The carbohydrate was determined by phenol-sulfuric method (Herbert, Philipps et al. 1971 [2]). Water quality analyses were conducted according to the procedures described in the Standard Method 19th edition (APHA 1995 [3]). Microbial diversity was monitored by Terminal-Restriction Fragment Length Ploymrphism (Duangmanee, Padmasiri et al. 2007 [4]) and primers used in this assay were EUB338-6FAM and 1392R-HEX and the restriction enzyme for digestion was MseI.

3 Results and Discuss

3.1 The water quality of the leaching

Table 2 shows that the leaching contains total COD (49 g/L), soluble COD (43 g/L) and the total COD contains up to 88% soluble COD. From this percentage, we can know that the solid content is not high and the predominant utilizable nitration is soluble. Soluble TOC is 17 g/L and soluble COD to soluble TOC ratio is 2.49 which is very close to the value of glucose which is 2.67. This ratio (2.49) revealed that reductive carbon in the leaching is very abundant and therefore it can provide sufficient electrons for the subsequent hydrogen production process. From the result of Figure 1, we can find that the majority is lactic acid containing about 49% of electron in the leaching. The secondary is organic nitrogen. The leaching contains 27% and 9% of electron as soluble and solid organic nitrogen respectively. The last one is carbohydrate. Therefore, we can know from the electron mass balance that there is plentiful nitrogen in the leaching and this is contributive to the growth of microorganisms in the subsequent BHP test. The extra 6% unknown can be ignored due to the operational errors.

Table 2: The water quality analyses of aerobic leaching fed with Napier Grass and kitchen waste mixture.

Characteristics		Unit	Mixed effluent of trickling bed
Solid	SS	g/L	4.71 ± 0.145
	VSS	g/L	4.34 ± 0.152
Carbo-hydrate	Total	g hexose/L	7.65 ± 0.351
	Soluble	g hexose/L	6.21 ± 0.491
	Reducing sugar	g hexose/L	1.06 ± 0.141
Protein	$Org\text{-}N_{total}$	g N/L	1.88 ± 0.012
	$Org\text{-}N_{soluble}$	g N/L	1.39 ± 0.12
	NH_4^+-N	g N/L	0.13 ± 0.007
COD	COD total	g/L	49.5 ± 0
	COD soluble	g/L	43.6 ± 0
VFA Conc.	Lactate	g/L	22.7 ± 0.82
	Acetate	g/L	1.7 ± 0.013
	Propionate	g/L	0.30 ± 0.003
Carbon	TOC solid	g C/g	0.20
	TOC liquid	g C/L	17.47
	TOC total	g C/g	0.11

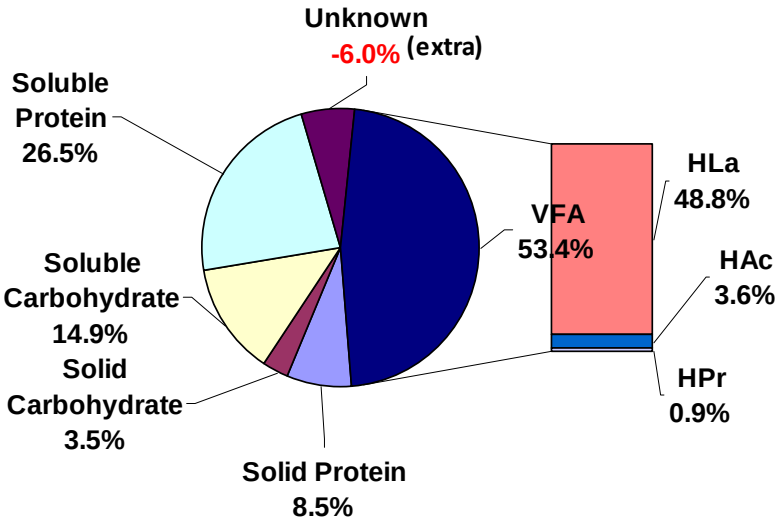

Figure 1: Electron distribution in the leaching from the leaching bed fed with kitchen waste and napiergrass.

3.2 The biochemical hydrogen potential tests (BHP)

The batch test was proceeded about 120 hours. The cumulative hydrogen and carbon dioxide production curve of different food to microorganism ratio (S_0/X_0) is showed in Figure 2. The feed blank (S_0/X_0=0 g COD/ g VSS) produced almost no hydrogen, so the high concentration of COD and carbohydrate would not disturb the experimental result.

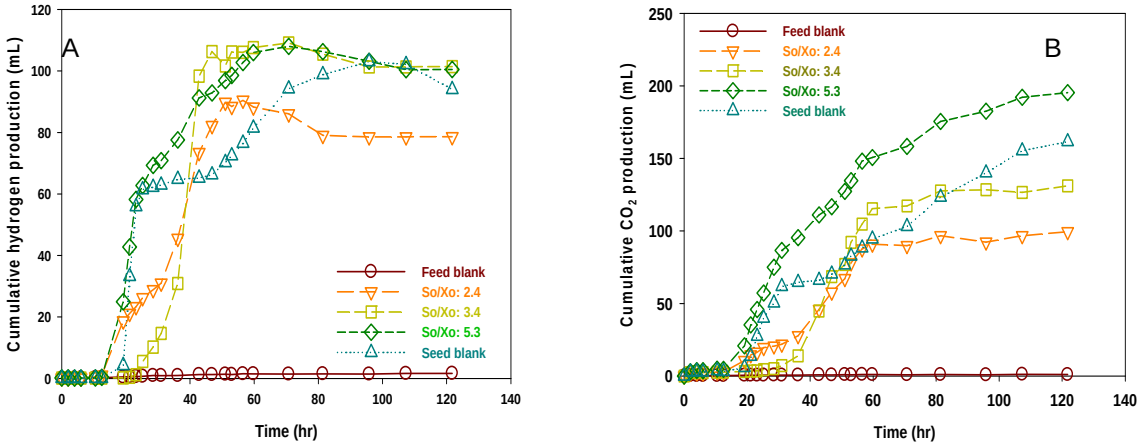

Figure 2: Cumulative (A) Hydrogen (B) Carbon dioxide production curve of different substrate concentrations degraded by hydrogen producing bacterium.

Except the feed blank, others produced hydrogen obviously. When the batch test is carried on about 60 hours, the hydrogen production rate became much lower except the seed blank which still had the tendency to produce hydrogen. The higher the S_0/X_0 was, the more hydrogen yield would be produced and also the shorter the lag phase was. It is worth paying attention that the seed blank had quite good hydrogen yield about 94 ml and its maximum hydrogen production rate 21.2 ml/hr was even higher than that of S_0/X_0=3.4g COD/ g VSS and S_0/X_0=5.3 g COD/ g VSS. The hydrogen concentration in each group was over 45%. The group which S_0/X_0 is 3.4 mg COD/mg VSS possessed the highest hydrogen concentration about 62%. The cumulative carbon dioxide production curve was similar to that of hydrogen. According to the increase of the S_0/X_0, the carbon dioxide yield increase. On the sixtieth hour, the production of carbon dioxide in each group slowed down except for the seed blank. We speculate that it is because of the two-stage hydrogen production in the seed bland. In other words, microorganisms degrade organic matter in two different time. The first and the second one were about the twenty-first and sixtieth hour respectively. As a result, microorganisms were still carrying the biochemical reaction out at the sixtieth hour and this led to the increasing production of carbon dioxide.

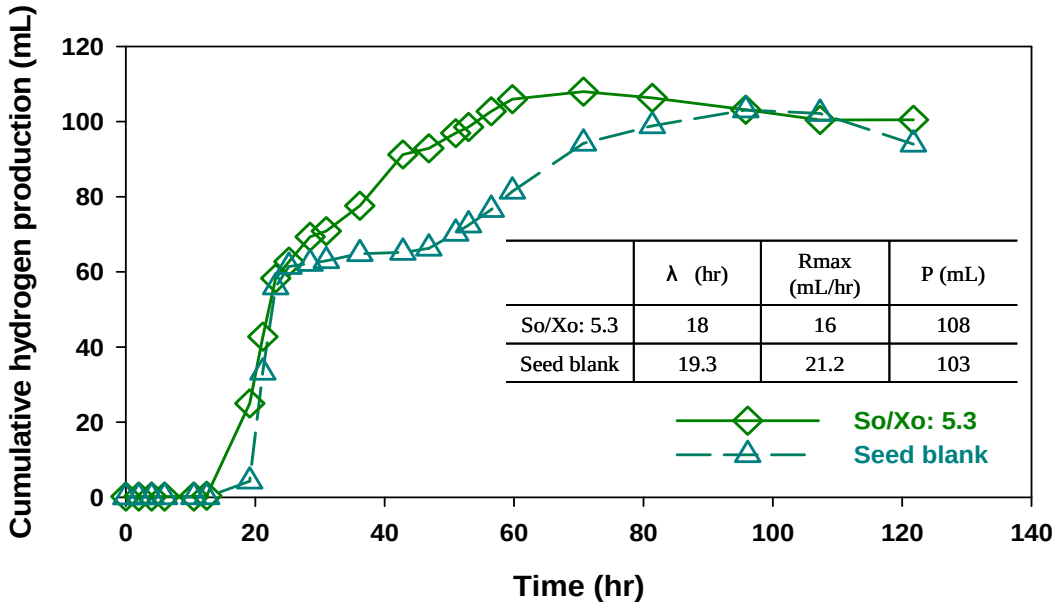

Figure 3: Cumulative hydrogen curve of So/Xo:5.3, Seed blank degraded by hydrogen producing bacterium

Due to the quite good hydrogen production of the seed blank, we compared it with the highest S_0/X_0 group (S_0/X_0=5.3 g COD/ g VSS) intentionally. According to the regression of the improved Conpertz equation (2), the lag phases of the seed blank and the highest S_0/X_0 group (S_0/X_0=5.3 g COD/ g VSS) were very similar and the values of them were 19.3 and 18 hr respectively (Fig3). The hydrogen yields of these two groups were similar also. However, the R_{max} of the seed blank was 21.2 ml/hr and it is higher than that of the highest S_0/X_0 group which was 16 ml/hr. According to this comparison, hence, we can speculate that there was abundant hydrogen-producing organisms in the leaching and they were possible to be the contributors in this biochemical hydrogen potential test (BHP test).

$$y = P\exp\left\{-\exp\left[\frac{R_m e}{P}(\lambda - t) + 1\right]\right\} \quad (2)$$

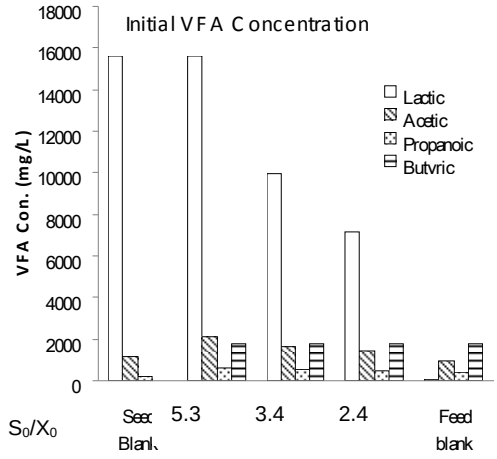

Figure 4: Initial VFA concentration at different conditions

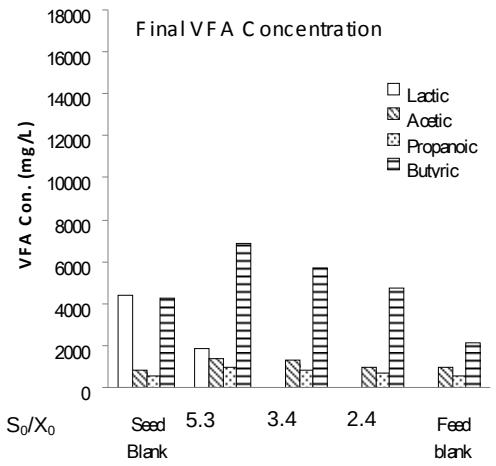

Figure 5: Final VFA concentration at different conditions

Figure 4 and Figure 5 show the volatile fatty acids (VFAs) concentration before and after experiment respectively. Degraded after 120 hours, lactic acid in each group has quite good degradation rate. In the groups which S_0/X_0 are 2.4 and 3.4, there are approximate 100% degradation rate. Moreover, the degradation rates of the group which S_0/X_0 is 5.3 mg COD/ mg VSS and the seed blank are 88% and 72% respectively. The degradation rate of acetic acid in each group is about 30% except the 3.4 mg COD/mg VSS group which degradation rate is 21%. On the other hand, propionic and butyric acids have obvious production. The concentration of propionic acid increase according to the increase of the S_0/X_0. The highest production, which is 376 mg/L, appears in the highest S_0/X_0 group (S_0/X_0=5.3 g COD/ g VSS). The secondary is the seed blank and its propionic acid production is 354 mg/L. Butyric acid has a like increasing tendency with propionic acid. Its concentration also increase with the increase of the S_0/X_0, but the increasing extent is much more than that of propionic acid. The increasing production in each group is over 3,000 mg/L. The highest S_0/X_0 group (S_0/X_0=5.3 g COD/ g VSS) has the highest production (5,097 mg/L). The secondary is also the seed blank which production is 4,261 mg/L.

3.3 The result of T-RFLP

In this study, we exploited the Terminal Restriction Fragment Length Ploymrphism (T-RFLP) to observe the variety of the microorganism relationships. The advantage of this technique is that it can examine the microorganism diversity quickly, so it is a beneficial tool to the mixed culture system. The results from this assay show that the microorganism relationships between the feed and the seed blank vary obviously (Fig. 6). In the feed blank, the fragments of 497 bp (forward) and 318 bp (reverse) are predominant. The microorganism matched with these fragments is similar to *Thermoanaerobacterium thermosaccharolyticum*. This microorganism can utilize starch, cellodextrin, sucrose, xylose and other small molecular saccharides to produce hydrogen, acetic and butyric acid [O-Thong et al., 2007]. In addition, the forward fragments of 227 bp and 255 bp are predominant in the seed blank. The microorganism matched with 255 bp (forward) and 314 bp (reverse) is also similar to

Thermoanaerobacterium thermosaccharolyticum, which is reported in (Wang, Li et al. 2009). Comparing the analytic results of S_0/X_0 5.3 group with that of the seed blank, we can find that the position of both fragments has some difference. It infers that while the microorganisms in the seed and the feed are competing with each other, the former will be disappeared and finally the microorganisms in the feed will be the dominant. This phenomenon, hence, can illustrate that the microorganisms in the feed can utilize the feed more efficient than in the seed. Moreover, comparing the results of S_0/X_0 5.3 group with the others, we can know that the microorganisms cultured in the serums finally were dominated by the microorganisms came from the feed. We can verify, therefore, that there is abundant hydrogen-producing microorganisms in the leaching. As a result, we can infer that anaerobic hydrogen-producing microorganisms can still exist in the system of aerobic leaching bed. Being the seed directly, therefore, the microorganisms in the leaching can be exploited in the subsequent fermentative biohydrogen reactor.

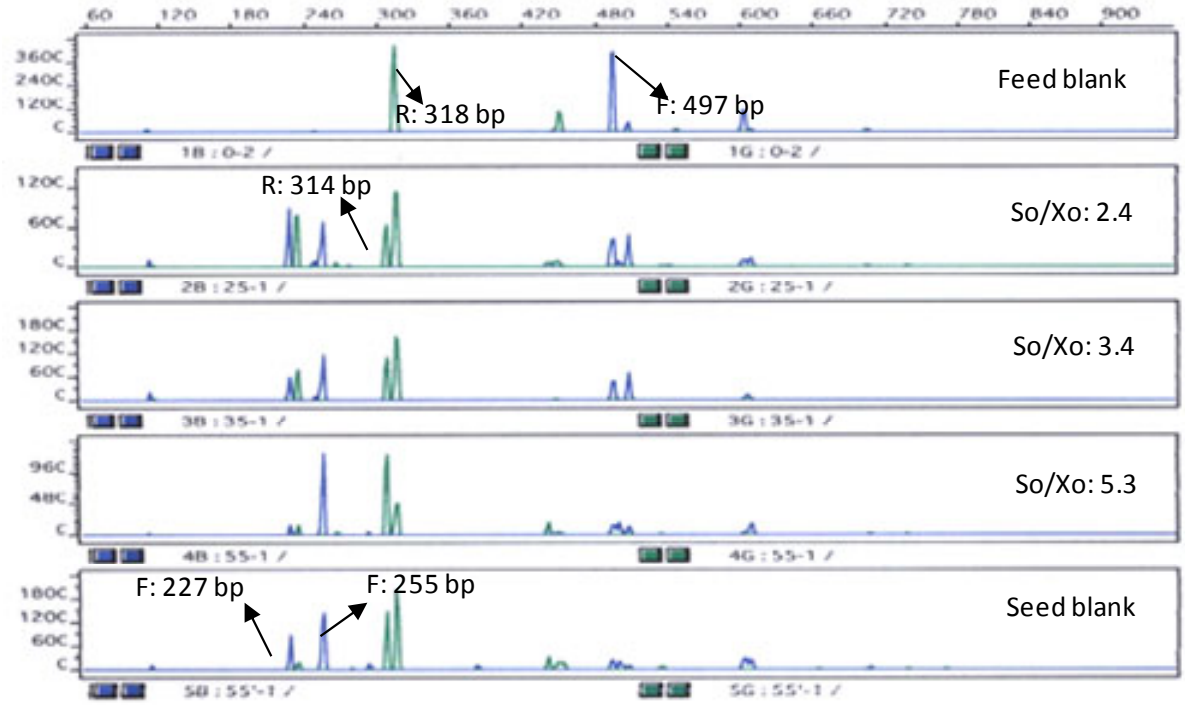

Figure 6: T-RFLP analysis with MseI digested 16S-rDNA fragment. The total DNA was extracted from final liquid of BHP test fed with trickling bed effluent. (F: forward, R: reverse)

4 Conclusions

1. In the leaching of aerobic leaching bed, the soluble COD, organic nitrogen and carbohydrate are 88%, 78% and 81% of the total respectively and this infers that the leaching bed has good hydrolyzing ability. Lactic acid (49% of the total COD) is maintained abundantly in the leaching and it can be utilized by the subsequent hydrogen-producing process.
2. Due to the similarity of hydrogen yield, hydrogen concentration, lag phase in the seed blank and the highest S_0/X_0 group (S_0/X_0=5.3 g COD/g VSS), and the higher hydrogen production rate (21.2 ml/hr) of the seed blank, we can infer that there are

abundant hydrogen-producing microorganisms in the feed and they are very possible to be the major contributors in this fermentative hydrogen experiment.

3. According to the results of T-RFLP, we can know that the leaching possesses abundant hydrogen-producing microorganisms which major species is Thermoanaerobacterium thermosaccharolyticum matched with the fragment length of 255 bp and this microorganism will grow better than those in the seed and ultimately become the predominant species.
4. In summary, we can utilize the microorganisms in the leaching as inoculums for the subsequent fermentative hydrogen production reactor.

Acknowledgements

The authors gratefully acknowledge financial support by Taiwan's National Science Council.

References

[1] Owen, W. F., D. C. Stuckey, et al. (1979). "Bioassay for Monitoring Biochemical Methane Potential and Anaerobic Toxicity." Water Research 13(6): 485-492.

[2] Herbert, D., P. J. Philipps, et al. (1971). "Carbohydrate analysis." Methods Enzymol. 5B: 265-277.

[3] APHA, A. W. (1995). Standard Method for the Examination of Water and Wastewater. Washington, DC. USA.

[4] Duangmanee, T., S. I. Padmasiri, et al. (2007). "Hydrogen production by anaerobic microbial communities exposed to repeated heat treatments." Water Environment Research 79(9): 975-983.

[5] Wang, Y. H., S. L. Li, et al. (2009). "Starch hydrolysis characteristics of hydrogen producing sludge in thermophilic hydrogen fermentor fed with kitchen waste." International Journal of Hydrogen Energy 34(17): 7435-7440.

Analysis of the Glycolytic Pathways of the Hydrogen Producing *Caldicellulosiruptor Saccharolyticus*

Servé Kengen, **Bram Bielen**, **Marcel Verhaart**, **Fons Stams**, Wageningen University, The Netherlands

Caldicellulosiruptor saccharolyticus is an extremely thermophilic, gram-positive anaerobe which ferments cellulose-, hemicellulose- and pectin-containing biomass to acetate, CO_2, and hydrogen. Its broad substrate range, high hydrogen-producing capacity, and ability to co-utilize glucose and xylose make this bacterium an attractive candidate for microbial bioenergy production. Despite these profitable features, still little is known about the different sugar uptake systems, the subsequent pathways and the regulatory aspects determining the final hydrogen yield. It is our goal therefore, to investigate the main sugar degradation pathways and their regulation by a systems biology approach.

1 Genomics

The genome of *Caldicellulosiruptor saccharolyticus* DSM 8903 consists of one circular chromosome of 2,970,275 base pairs (bp), which has a G+C-content of 35.3% [1]. The complete genome sequence confirms the phylogenetic position of *C. saccharolyticus* as member of the class Clostridia and reveals *Thermoanaerobacter tengcongensis* as closest relative. When compared to other thermophilic hydrogen producing bacteria and archaea, like *Clostridium thermocellum, T. tengcongensis*, *Thermotoga maritima* and *Pyrococcus furiosus,* the *C. saccharolyticus* genome harbors the largest number of carbohydrate transport and metabolism genes. In fact, the *C. saccharolyticus* genome contains at least 177 ABC-transporter genes, outnumbering the 165 identified in *T. maritima* [1, 2].

1.1 Polysaccharide degrading enzymes

The capacity of *C. saccharolyticus* to hydrolyze a broad range of polysaccharides prior to fermentation differentiates this bacterium from many thermophilic anaerobes. The carbohydrate-utilizing enzymes are often clustered on the chromosome and can be assigned to substrate specific catabolic pathways for cellulose, hemicellulose and, to a lesser extent, starch and pectin. The α-1,4-glucan polymers, for instance, can be transported into the cell using a maltodextrin ABC-transport system (Csac_0427-0428/0431). An intracellular α-amylase (Csac_0426) and a 1,4-α-glucan phosphorylase (Csac_0429) further degrade the intracellular maltodextrins, releasing glucose-1-phosphate. Several starch-degrading enzymes, such as an α-amylase precursor (Csac_0408), an oligo-1,6-glucosidase (Csac_2428), a pullulanase (Csac_0689), a 4-α-glucanotransferase (Csac_0203), and a putative glucan 1,4-α-glucosidase (Csac_0130) were identified. Besides this putative starch-degrading regulon, *C. saccharolyticus* has a glycogen metabolic cluster (Csac_0780-0784), a maltose ABC-transport system (Csac_2491-3), and a second pullulanase (Csac_0671). Taken together, *C. saccharolyticus* is well-equipped for starch utilization.

C. saccharolyticus does not metabolize cellulose by means of a cellulosome as the typical molecular components of a cellulosome, *i.e.*, dockerin domains and scaffolding proteins, were not identified in the genome. Nevertheless, a gene cluster (Csac_1076-1081) containing cellulase precursors is present. These highly modular cellulases are potentially capable of degrading this plant polysaccharide. Moreover, another gene cluster (Csac_1089-1091) and an extracellular cellulase (Csac_0678) may assist in completely hydrolyzing cellulose to glucose.

C. saccharolyticus has an enzyme system to cleave the glycoside bonds and hydrolyze ester bonds in hemicellulose (Csac_2404-2411). These mostly extracellular enzymes, which are variable in domain composition as well, might be co-expressed with a smaller putative xylan-utilizing cluster (Csac_0203-0205). Furthermore, putative genes that encode enzymes to degrade galactomannan (Csac_0663-0664), galactoarabinan (Csac_1560-1562) and laminarin (Csac_2548) were identified [1].

Various genes coding for the degradation of the main pectin component, D-galacturonate could be identified, except that a tagaturonate reductase and altronate dehydratase were not detected in the genome of *C. saccharolyticus*. In contrast, a gene cluster for the conversion of glucuronic acid to KDG (Csac_2686-2689) was identified, and includes fructuronate reductase, mannonate dehydratase, a putative β-galactosidase/β-glucuronidase, and an α-glucuronidase. Glucuronic acid is a common substituent of xylan. Enzymes for the subsequent conversion of KDG to pyruvate and GAP are present as well (Csac_0355 or Csac_2720, and Csac_0345). The encoding genes of these last two steps are clustered with genes (Csac_0356-0357 and Csac_2718-2719) that both metabolize 5-keto-4-deoxyuronate, an unsaturated cleavage product from pectate, to KDG. The enzymes that are able to hydrolyze the pectate backbone and the side chains, β-galactosidase and a glycoside hydrolase with unknown substrate specificity are in proximity to these KDG metabolic enzymes as well. However, neither a pectate lyase nor a methylesterase could be definitively identified in the genome [1].

C. saccharolyticus is also able to grow on L-rhamnose and on L-fucose, thereby producing 1,2-propanediol as end product. A putative rhamnose catabolic pathway can be assigned that generates dihydroxy-acetone phosphate and 1,2-propanediol. Fucose can be processed by a similar pathway.

1.2 Central carbon metabolism

The genome sequence reveals all the components of a complete Embden-Meyerhof (EM) pathway. In addition, a gene coding for an additional phosphofructokinase was identified (Csac_2366), which might be PPi-dependent instead of ATP-dependent (PPi-PFK; Csac_1830). Moreover, a PPi-dependent pyruvate phosphate dikinase (PPDK; Csac_1955) was present as well. However, the oxidative branch (ox) of the Pentose Phosphate Pathway (PPP) and the Entner-Doudoroff (ED) pathway were not detected, which is consistent with previous reports using ^{13}C-NMR [3]. Xylose, a major constituent of hemicellulose, is apparently funneled into the non-oxidative branch of the PPP. Galactose also enters the EM via the Leloir-pathway. Remarkably, none of the established types of fructose-bisphosphatase (Class I to IV) are evident in the *C. saccharolyticus* genome. Since fructose-bisphosphatase is an essential enzyme of the gluconeogenesis, *C. saccharolyticus*

presumably uses a novel phosphatase. Moreover, a gene for the gluconeogenic PEP synthetase is also missing. Alternatively, although the conversion of pyruvate to PEP could occur via the reversible PPDK or via oxaloacetate.

Pyruvate, the end product of the EM-pathway, is subsequently decarboxylated to acetyl-CoA by pyruvate:ferredoxin oxidoreductase (Csac_1458-1461). Acetyl-CoA is used to generate acetate and ATP (Csac_2040/2041), or it enters the tricarboxylic acid (TCA) cycle for biosynthetic purposes.

1.3 Fermentation products

Reducing equivalents are produced at the level of NAD and ferredoxin. Since *C. saccharolyticus* can produce almost 4 H_2 per mol of glucose, both NADH and reduced ferredoxin should ultimately be able to transfer their reducing equivalents to protons to form hydrogen. In the genome, two hydrogenase gene clusters could be identified, which are very similar to the two related clusters in *Thermoanaerobacter tengcongensis* [4]. The first cluster (Csac_1534-1539) encodes subunits of a Ni-Fe hydrogenase (EchA-F) and various genes required for maturation of the hydrogenase complex (HypA-F; Csac_1540-1545). For *T. tengcongensis,* this Ni-Fe hydrogenase is ferredoxin-dependent, membrane-bound, and may act as a proton pump to generate a proton motive force. The second cluster (Csac_1860-1864) codes for a Fe-only hydrogenase (HydA-D), which is NAD-dependent and located in the cytoplasm, similar to the case for *T. tengcongensis*. Altogether, information available suggests that *C. saccharolyticus* is able to produce hydrogen from ferredoxin, but can also do this directly from NADH. Production of hydrogen would seem to be preferable, because under these conditions all pyruvate is converted to acetate (and CO_2), which is coupled to the synthesis of ATP.

When the hydrogen partial pressure becomes too high, hydrogen formation from NADH is no longer thermodynamically favorable. In that case, NADH is oxidized through the formation of lactate or ethanol. A gene for a lactate dehydrogenase could be identified (Csac_1027), but genes for acetaldehyde dehydrogenase and alcohol dehydrogenase were not obvious.

2 Transcriptomics

One of the beneficial features of *C. saccharolyticus* for hydrogen production is its ability to degrade cellulosic substrates as well as hemicellulose. Moreover, mixtures of glucose and xylose can be fermented simultaneously suggesting that classical Carbon catabolite repression (CCR) by glucose does not occur. To elucidate the central carbon metabolic pathways and their regulation, transcriptome analysis was performed after growth on glucose, xylose and a 1:1 mixture of both substrates [1]. L-Rhamnose, which was likely to follow another pathway, was used as a reference substrate. The transcriptional data clearly show that glucose, xylose and the glucose:xylose mixture all trigger up-regulation of genes in the EM pathway, when compared to rhamnose. In particular, the fructose-bisphosphate aldolase, GAP dehydrogenase, PPDK and POR are significantly stimulated. The ultimate acetate-forming acetate kinase is also highly up-regulated. A catabolic role for PPDK is intriguing, since it normally is associated with gluconeogenesis, and PEP is usually converted by pyruvate kinase.

None of the identified putative CCR genes were differentially transcribed, confirming the fact that catabolite repression by glucose was not a factor [1, 2].

Transcriptional response to growth on monosaccharides enabled the identification of genes and groups of adjacent genes, that were specifically up-regulated in response to either glucose or xylose. On glucose, several genes coding for α-glucan hydrolases responded. On xylose, several gene clusters required for xylan or xylose conversion were up-regulated (Csac0692-0696; Csac0240-0242; Csac2416-2419). These clusters encode ABC transport systems, transcriptional regulators and endo-xylanases. In addition, genes, specifically required for growth on rhamnose, were highly up-regulated during growth on rhamnose, thus indicating the utilization pathway for this sugar.

3 Pyrophosphate as Alternative Energy Carrier

To manipulate the pathways leading to hydrogen it is important to know their exact composition and how the individual metabolic steps are regulated. Although the operation of the EM pathway has been confirmed for *C. saccharolyticus*, our genome and transcriptome data also suggested that PPi-dependent steps may be involved. Interestingly, recent studies on the acetate-lactate metabolic shift in *C. saccharolyticus* revealed that PPi is a strong modulator of the lactate dehydrogenase [4]. These observations motivated us to investigate the role of inorganic pyrophosphate in the energy metabolism of *C. saccharolyticus* [5].

The two genes that were annotated to code for a phosphofructokinase (Csac_1830 and Csac_2366) were analyzed more closely and it could be demonstrated that Csac_1830 contains the typical ATP-dependent PFK amino acid combination (G_{104} and G_{124}) and that Csac_2366 contains the typical PPi-dependent PFK amino acid residues (D_{104} and K_{124}). These results strongly suggest that Csac_1830 is an ATP-dependent PFK and that Csac_2366 is a PPi-dependent PFK. As mentioned previously, *C. saccharolyticus* also has the genes coding for two alternative enzymes for the conversion of PEP to pyruvate, viz. the more common pyruvate kinase (PK) and the PPi-dependent PPDK. In addition we also identified a gene coding for a membrane-bound proton-pumping pyrophosphatase (PPase), whereas a cytosolic PPase encoding gene was absent. To confirm the genome sequence based predictions, we performed enzyme assays on crude cell extracts. Activities of PK, PPDK, PPi-PFK, ATP-PFK and membrane-bound PPase could all be detected in cell extracts of *C. saccharolyticus*. Under the specified assay conditions the average PPDK activity (0.4 U/mg) was twice the PK activity. For the ATP- and PPi-dependent PFKs no significant difference was observed in the activity levels (~0.05 U/mg). The presence of PPi-dependent enzymes in the central metabolic pathway suggested the involvement of PPi as an energy carrier in the metabolism of *C. saccharolyticus*. Therefore, the levels of both ATP and PPi were determined during growth. PPi levels were relatively high (approx. 4±2 mM), while ATP levels were remarkably low (0.43±0.07 mM). Strikingly, PPi was recently shown to act as allosteric effector of the pyruvate kinase and the lactate dehydrogenase (LDH) of *C. saccharolyticus* [4, 5].

Altogether, the presented results indicate that PPi has a central role in the metabolism of the hydrogen-producing *C. saccharolyticus*. This type of metabolism agrees well with the observed physiology with respect to its sugar utilization [2]. The wide range of high-affinity

sugar uptake systems and the absence of carbon catabolite repression suggests that *C. saccharolyticus* is not fastidious, but rather has evolved to conserve energy in many different ways.

References

[1] van de Werken HJG, Verhaart MR, VanFossen AL et al. (2008) Hydrogenomics of the extremely thermophilic bacterium *Caldicellulosiruptor saccharolyticus*. Appl Environ Microb 74: 6720-6729.

[2] VanFossen AL, Verhaart MR, Kengen SWM & Kelly RM (2009) Carbohydrate utilization patterns for the extremely thermophilic bacterium *Caldicellulosiruptor saccharolyticus* reveal broad growth substrate preferences. Appl Environ Microb 75: 7718-7724.

[3] de Vrije T, Mars AE, Budde MAW, Lai MH, Dijkema C, de Waard P, Claassen PAM (2007) Glycolytic pathway and hydrogen yield studies of the extreme thermophile *Caldicellulosiruptor saccharolyticus*. Appl Microbiol Biot 74: 1358-1367.

[4] Soboh B, Linder D, Hedderich R (2004). A multisubunit membrane-bound [NiFe] hydrogenase and an NADH-dependent Fe-only hydrogenase in the fermenting bacterium *Thermoanaerobacter tengcongensis*. Microbiology 150:2451-63.

[4] Willquist K, van Niel EWJ (2010) Lactate formation in *Caldicellulosiruptor saccharolyticus* is regulated by the energy carriers pyrophosphate and ATP. Metab Eng doi: 10.1016/j.ymben.2010.01.001.

[5] Bielen AAM, Willquist K, Engman J, van der Oost J, van Niel EWJ, Kengen SWM (2010) Pyrophosphate as a central energy carrier in the hydrogen producing extremely thermophilic *Caldicellulosiruptor saccharolyticus*. FEMS Microbiol lett DOI: 10.1111/j.1574-6968.2010.01957.x

Using Biomass of Starch-rich Transgenic *Arabidopsis Vacuolar* as Feedstock for Fermentative Hydrogen Production

Yung-Chung Lo, **Chieh-Lun Cheng**, **Chun-Yen Chen**, Department of Chemical Engineering, National Cheng Kung University, Tainan, Taiwan
Li-Fen Huang, **Jo-Shu Chang**, Graduate School of Biotechnology and Bioengineering, Yuan Ze University, Tao-yuan, Taiwan

Abstract

Cellulose is the major constitute of plant biomass and highly available in agricultural wastes and industrial effluents, thereby being a cost-effective feedstock for bioenergy production. However, most hydrogen producing bacteria (HPB) could not directly convert cellulosic materials (such as rice husk and rice straw) into hydrogen whereas most HPB could utilize sugar and starch for hydrogen production. In this work, we used an indigenous bacterial isolate *Clostridium butyricum* CGS2 as HPB, which could directly convert soluble starch into H_2 with a maximum H_2 production rate and a H_2 yield of 205.07 ml H_2/h/l and 6.46 mmol H_2/g starch, respectively. However, *C. butyricum* CGS2 could not ferment pure cellulosic materials such as carboxymethyl cellulose and xylan. Moreover, we found that *C. butyricum* CGS2 could utilize rich husk to produce H_2 at a rate of 13.19 ml H_2/h/l due to the starch content in rice husk (H_2 yield = 1.49 mmol H_2/g rice husk). In contrast, since lacking starch content, rice straw cannot be converted to H_2 by *C. butyricum* CGS2. The foregoing results suggest that increasing the starch content in the natural agricultural wastes may make them better feedstock for fermentative H_2 production. Hence, a genetically modified plant (*Arabidopsis vacuolar*) was constructed to enhance its starch concentration. The starch concentration of mutant plant S1 increased to 10.67 mg/fresh weight, which is four times higher than that of wild type plant. Using mutant plant S1 as carbon source, *C. butyricum* CGS2 was able to give a high cumulative H_2 production and H_2 production rate of 285.4 ml H_2/l and 43.6 ml/h/l, respectively. The cumulative H_2 production and H_2 production rate both increased when the concentration of the transgenic plant was increased. Therefore, this study successful demonstrated the feasibility of expressing starch on genetically-modified plants to create a more effective feedstock for dark H_2 fermentation.

1 Introduction

The increasing demand of petroleum and the decreasing global petroleum reserve triggered the crude oil price rise from 30 to 54–70 US$ per barrel since 1990 (OPEC., 2007 [1]). Combustion of fossil fuels has also caused global warming due to excessive emission of greenhouse gases. As a result, developing a new and more environmentally compatible alternative energy has become a hot issue in recent years. Among the potential energy alternatives being developed, hydrogen is recognized as the most promising energy carrier since it is clean, pollution-free, sustainable, and efficient (Das and Veziroglu, 2001 [2]).

Lignocellulosic resources, such as agricultural residues, paper wastes, wood chips, etc., are the most abundant organic substance in nature and considered to be promising and economically feasible feedstock for producing the new generation of biofuels (Kim et al., 2004 [3]). However, cellulosic materials are usually not readily fermentable by microorganisms for the yield of energy products, such as ethanol and hydrogen, thereby pretreatment or hydrolysis steps are often required (Xia et al., 2004 [4]). However, most hydrogen producing bacteria (HPB) could not directly convert cellulosic materials (such as rice husk and rice straw) into hydrogen whereas most HPB could utilize sugar and starch for hydrogen production. Dark fermentative hydrogen production from direct starch utilization was achieved using starch-fermenting bacteria, such as *Clostridium butyricum* (Yokoi et al., 1998 [5], Yokoi et al., 2001 [6], Yokoi et al., 2002 [7]). By using a mixed culture of *C. butyricum* and *Enterobacter aerogenes*, Yokoi, et al. reported a H_2 yield of 2.0–2.7 molH_2/mol glucose from single-stage H_2 production with sweet potato starch (Yokoi et al., 1998 [5], Yokoi et al., 2001 [6], Yokoi et al., 2002 [7]). Our recent work has identified several powerful H_2-producing bacterial isolates (mainly *Clostridial* species) from municipal sewage capable of producing H_2 from sugar very efficiently (Lo et al., 2008 [8]).

2 Materials and Methods

2.1 Microorganism and medium

Hydrogen-producing bacterial strain *Clostridium butyricum* CGS2 was isolated from effluent sludge of a continuous dark fermentation bioreactor able to produce H_2 from synthetic wastewater containing sucrose (20 g COD l^{-1}) or xylose (20-40 g COD l^{-1}) as the sole carbon source (Lo et al. 2008). The detailed procedures for strain isolation and identification were described in our recent work (Lo et al., 2008). The 16S rRNA gene sequence of *C. butyricum* CGS2 used in this study has been deposited in the NCBI nucleotide sequence database with an accession number of AY540106. The pure strain was pre-cultured under anaerobic conditions (Lo et al., 2008) on the medium consisted of (g l^{-1}): sucrose, 17.8; NH_4HCO_3, 6.72; $NaHCO_3$, 5.24; K_2HPO_4, 0.125; $MgCl_2.6H_2O$, 0.1; $MnSO_4.6H_2O$, 0.015; $FeSO_4.7H_2O$, 0.025; $CuSO_4.5H_2O$, 0.005; $CoCl_2.5H_2O$, 1.25×10^{-4}.

2.2 Fermentation medium and condition for bioH2 production

The medium for dark H_2 fermentation with the pure cultures was (g/l): starch or *Arabidopsis vacuolar*, (adjustable); NH_4HCO_3, 6.72; $NaHCO_3$, 5.24; K_2HPO_4, 0.125; $MgCl_2.6H_2O$, 0.1; $MnSO_4.6H_2O$, 0.015; $FeSO_4.7H_2O$, 0.025; $CuSO_4.5H_2O$, 0.005; $CoCl_2.5H_2O$, 1.25×10^{-4}. The culture temperature and pH was 37 °C and 7.5, respectively. Batch fermentation was carried out by static incubation. During the course of fermentation, cell concentration, pH, residual carbon substrate concentration, and production of biogas and soluble metabolites were monitored with respect to culture time.

3 Results and Discussion

3.1 Effect of soluble starch, rice husk and rice straw on the H_2 production performance

Using soluble starch (include starch), rice husk (include lignocellulose and starch) and rice straw (include lignocellulose) as carbon source to investigate dark-H_2 production performance of *Clostridium butyricum* CGS2. Fig. 1 shows the dark-H_2 production performance of *C. butyricum* CGS2 from soluble starch, rice husk and rice straw. Soluble starch and rice husk could be convert into hydrogen, the maximum H_2 production rate was 205.07 ml/h/l and 13.19 ml/h/l, respectively. Rice straw was not utilize. Model simulation analysis by modified Gompertz equation (Eqn. 1) shows that using soluble starch as carbon source resulted in maximum H_2 production rate (R_{max}) of 30.8 ml/h (Table 1). The lag time was similar (λ=9.7 h) for all carbon sources examined (Table 1).

$$H = H_{\max} \exp\{-\exp[\frac{R_{\max,H_2} \times e}{H_{\max}}(\lambda - t) + 1]\} \quad (1)$$

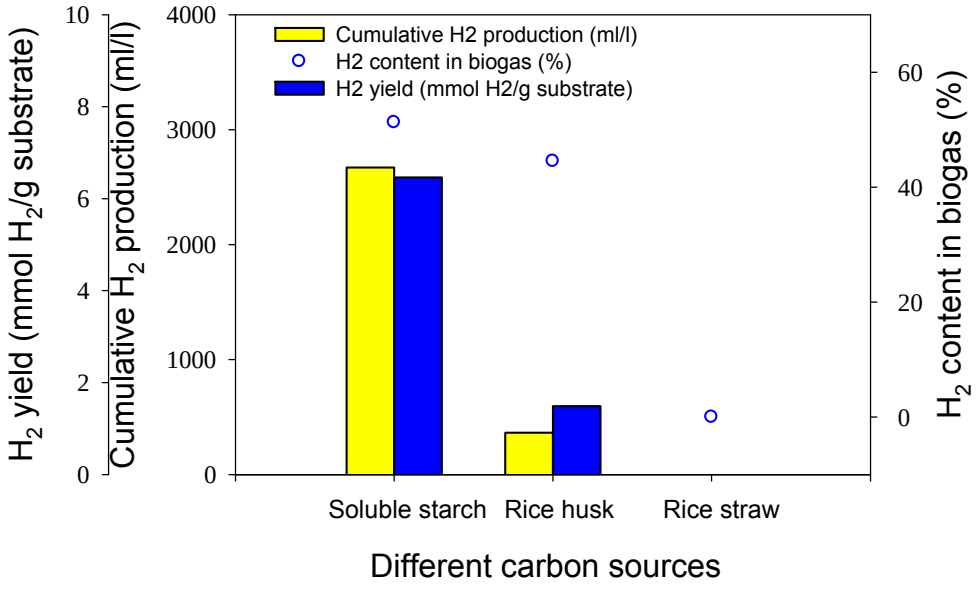

Figure 1: Dark-H_2 production performance of *C. butyricum* CGS2 at soluble starch, rice husk and rice straw.

3.2 Effect of *Arabidopsis vacuolar* on H_2 production performance

The foregoing results suggest that increasing the starch content in the natural agricultural wastes may make them better feedstock for fermentative H_2 production. Hence, a genetically modified plant (*Arabidopsis vacuolar*) was constructed to enhance its starch concentration. Figure 2 show the starch concentration was enhanced. The starch concentration of mutant

plant S1 increased to 10.67 mg/fresh weight, which is four times higher than that of wild type plant. Figure 3 show the H_2 performance of *C. butyricum* CGS2 from wild type plant and mutant S1 plant. Using mutant plant S1 as carbon source, *C. butyricum* CGS2 was able to give a high cumulative H_2 production and H_2 production rate of 285.4 ml H_2/l and 43.6 ml/h/l, respectively. The cumulative H_2 production and H_2 production rate both increased when the concentration of the transgenic plant was increased. Therefore, this study successful demonstrated the feasibility of expressing starch on genetically-modified plants to create a more effective feedstock for dark H_2 fermentation.

Table 1: Effect of soluble starch, rice husk and rice straw on H_2 production.

Carbon sources	H_2 content	Model simulation			
	(%)	Hmax(ml)	Rmax(ml/h)	λ(h)	R^2
Soluble starch	51	400.8	30.8	9.7	0.999
Rice husk	44	54.6	1.98	13	0.999
Rice straw	Cell non-growth				

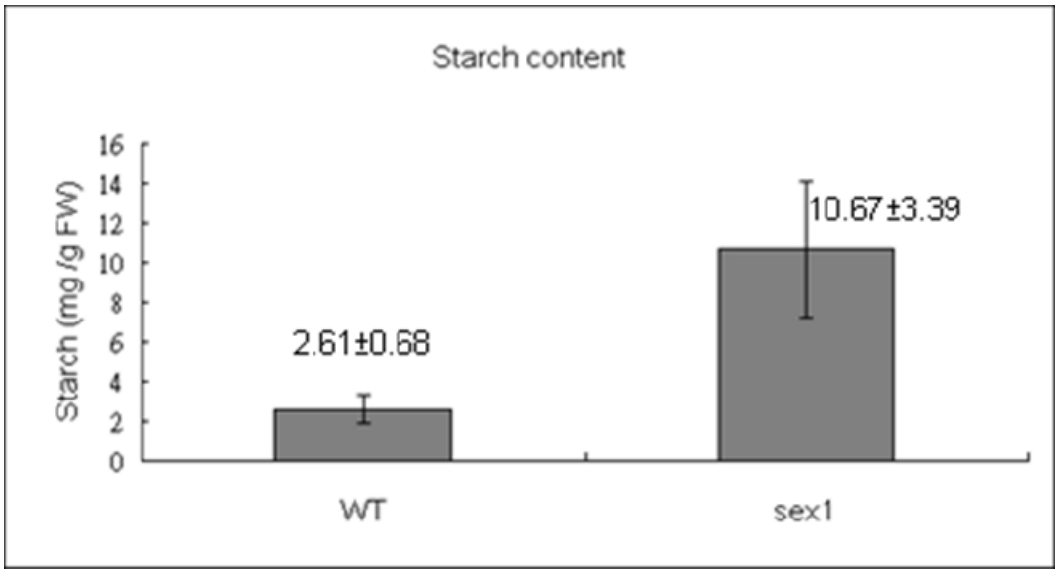

Figure 2: The starch concentration of wild-type plant and mutant plant S1.

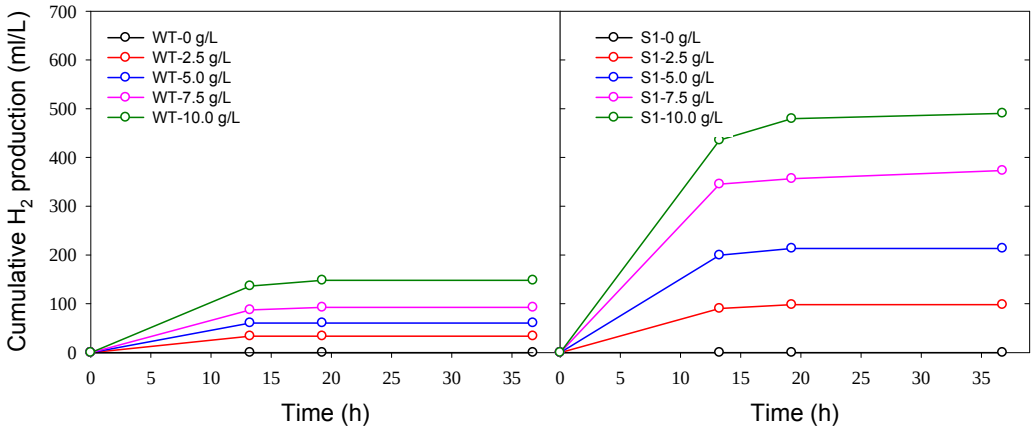

Figure 3: **H_2 performance of *C. butyricum* CGS2 from different wild type plant and mutant S1 plant concentration.**

References

[1] OPEC. Organization of the petroleum exporting countries,http://www.opec.orgi, 2007 [Retrieved March 22, 2007].

[2] Das D, Veziroglu TN. Hydrogen production by biological processes: a survey of literature. Int J Hydrogen Energy 2001;26(1):13–28.

[3] Kim, S., Dale, B.E., 2004. Global potential bioethanol production from wasted crops and crop residules. Biomass Bioenergy, 26, 361-375.

[4] Xia, L.M., Sheng, X.L., 2004. High-yield cellulase production by *Trichoderma reesei* ZU-02 on corncob residues. Bioresour. Technol., 91, 259-262.

[5] Yokoi H, Tokushige T, Hirose J, Hayashi S, Takasaki Y. H_2 production from starch by a mixed culture of *Clostridium butyricum* and *Enterobacter aerogenes*. Biotechnol Lett 1998;20(2):143–7.

[6] Yokoi H, Saitsu A, Uchida H, Hirose J, Hayashi S, Takasaki Y. Microbial hydrogen production from sweet potato starch residue. J Biosci Bioeng 2001;91(1):58–63.

[7] Yokoi H, Maki R, Hirose J, Hayashi S. Microbial production of hydrogen from starch manufacturing wastes. Biomass Bioenerg 2002;22:389–95.

[8] Lo, Y.C., Chen, W.M., Hung, C.H., Chen, S.D., Chang, J.S., 2008. Dark H_2 fermentation from sucrose and xylose using H_2-producing indigenous bacteria: Feasibility and kinetic studies. Water Res. 42, 827-842.

Optimizing Fermentation Conditions for bioH2 Production with Clostridium Butyricum CGS2 Using Statistical Experimental Design

Yung-Chung Lo, **Yung-Sheng**, **Chun-Yen Chen**, **Jo-Shu Chang**, Department of Chemical Engineering, National Cheng Kung University, Taiwan

Abstract

As the global temperature keeps rising, the demand for reliable and effective energy alternatives is increasingly urgent. Among the developing alternative energy resources, hydrogen is recognized as a clean and recyclable energy carrier and is considered one of the major energy sources in the future. Hydrogen fermentation is a non-pollutant way of producing H_2. Among fermentative H_2 production processes, the H_2 production rate by dark fermentation is higher than photo fermentation, thereby having higher viability for commercial applications. In this study, an indigenous isolate *Clostridium butyricum* CGS2 able to convert sugar (such as glucose, fructose, sucrose and xylose) into hydrogen was used the bacterial H_2 producer. Using sucrose as the carbon source in a batch process, *C. butyricum* CGS2 gave a maximum H_2 production rate (v_{H2}) and H_2 yield (Y_{H2}) of 262.2 ml/h/l and 2.26 mol H_2/mol sucrose, respectively. Response surface methodology (RSM) was employed to identify the optimal conditions for hydrogen production of *C. butyricum* CGS2 using sucrose concentration, temperature and pH as the primary operation parameters. With a performance index of Y_{H2}, the optimum condition predicted from RSM analysis was: pH, 5.2; temperature, 35.1 °C; sucrose concentration, 22.5 g COD/l. Under this condition, the hydrogen content in the biogas was 58.5%, □H_2 was 0.54 l/h/l, total hydrogen production was 7.2 l, and Y_{H2} was 2.91 mol H_2/mol sucrose. On the other hand, when □H_2 was used as the performance index, the optimum condition was: pH, 5.36; temperature, 35.1°C; sucrose concentration, 26.1 g COD/l. This condition gave a hydrogen content of 63.3%, a Y_{H2} of 3.26 mol H_2/mol sucrose, a total hydrogen production of 10.5 l, and a □H_2 of 0.50 l/h/l. The validity of RSM predictions was confirmed by additional experiments, suggesting that using RSM design could attain an optimal culture condition for *C. butyricum* CGS2 to enhance its hydrogen production performance.

1 Introduction

As biomass energy becomes one of the major global energy alternatives, many research efforts have been devoted to converting inexpensive waste biomass feedstock (e.g., agricultural wastes) into bioenergy, such as ethanol, biodiesel, and hydrogen (Tsai et al., 2007 [1]; Vrije et al., 2002 [2]). Although bioethanol and biodiesel are currently the major targets of biomass energy, hydrogen is still considered the ultimate solution of clean and recyclable energy carrier in a long term (Kapdan and Kargi, 2006 [3]). Biomass feedstock contains a large amount of cellulosic materials, such as cellulose, hemicellulose, and lignin

(Chandrakant and Bisaria, 1998 [4]). Among those three major components, cellulose and hemicellulose are much easier to degrade biologically, thereby being more economically viable for energy conversion (Chandrakant and Bisaria, 1998 [4]). Direct fermentation of raw cellulosic feedstock is usually inefficient because cellulose and hemicellulose are not readily assimilable to most energy-producing bacteria (for instance, yeast or H_2-producing acidogenic bacteria). Thus, it seems to be more feasible to use a two-stage biomass energy producing process, in which cellulosic materials are first hydrolyzed via physico-chemical or biological means, followed by a fermentative energy conversion step (Chandrakant and Bisaria, 1998 [4]).

In anaerobic digestion of organic substrates, the acidogenic process, producing hydrogen and volatile fatty acids as major products, is considered an efficient and promising way of producing clean H_2 energy (Levin et al. 2004 [5]). Most effective fermentative H_2 producers belong to anaerobic acid-forming bacteria (such as *Clostridium* sp.) (Levin et al., 2004 [5]). In our recent work, several highly efficient bioH2-producing processes were developed using mixed-cultures (Lee et al., 2003 [6]). Bacterial community structure analysis revealed that the sludge contained several *Clostridium* species (e.g., *C. butyricum* and *C. pasteurianum*) (Lo et al. 2008 [7]), which are known effective H_2 producers from organic substrates (esp. carbohydrates). It is thus of great value to isolate and characterize effective H_2-producing pure strains from the aforementioned sludge for the potential use in maintaining or improving H_2 production performance of mixed-culture systems via bioaugmentation strategies.

2 Materials and Methods

2.1 Microorganism and medium

Hydrogen-producing bacterial strain *Clostridium butyricum* CGS2 was isolated from effluent sludge of a continuous dark fermentation bioreactor able to produce H_2 from synthetic wastewater containing sucrose (20 g COD l^{-1}) or xylose (20-40 g COD l^{-1}) as the sole carbon source (Lo et al. 2008 [7]). The detailed procedures for strain isolation and identification were described in our recent work (Lo et al., 2008 [7]). The 16S rRNA gene sequence of *C. butyricum* CGS2 used in this study has been deposited in the NCBI nucleotide sequence database with an accession number of AY540106. The pure strain was pre-cultured under anaerobic conditions (Lo et al., 2008 [7]) on the medium consisted of (g l^{-1}): sucrose, 17.8; NH_4HCO_3, 6.72; $NaHCO_3$, 5.24; K_2HPO_4, 0.125; $MgCl_2.6H_2O$, 0.1; $MnSO_4.6H_2O$, 0.015; $FeSO_4.7H_2O$, 0.025; $CuSO_4.5H_2O$, 0.005; $CoCl_2.5H_2O$, 1.25×10^{-4}.

2.2 Fermentation medium and condition for bioH2 production

The medium for dark H_2 fermentation with the pure cultures was (g/l): sucrose, 17.8 (adjustable); NH_4HCO_3, 6.72; $NaHCO_3$, 5.24; K_2HPO_4, 0.125; $MgCl_2.6H_2O$, 0.1; $MnSO_4.6H_2O$, 0.015; $FeSO_4.7H_2O$, 0.025; $CuSO_4.5H_2O$, 0.005; $CoCl_2.5H_2O$, 1.25×10^{-4}. The culture temperature and pH was 37 °C and 7.5, respectively. Response surface methodology (RSM) was employed to identify the optimal conditions for hydrogen production of *C. butyricum* CGS2 using sucrose concentration, temperature and pH as the primary operation parameters. During the course of fermentation, cell concentration, pH, residual carbon

substrate concentration, and production of biogas and soluble metabolites were monitored with respect to culture time.

3 Results and Discussion

Table 1: Dark-H_2 production performance of *C. butyricum* CGS2 at different sucrose concentration.

Sucrose conc.	H_2 content	Conversion	Vmax,H_2	Model simulation			
(mg COD/l)	(%)	(%)	(ml)	Hmax(ml)	Rmax(ml/h)	λ(h)	R^2
5000	33	100	32	33.7	5.77	13.3	0.996
10000	44	97	51	53.5	5.97	18.3	0.999
20000	47	45	5	104.9	28.0	19.8	0.999
30000	48	41	82	83.3	20.1	22.9	0.999

Effect of sucrose concentration on the H_2 production performance

Using different sucrose concentration to investigate dark-H_2 production performance of *Clostridium butyricum* CGS2. Table 1 shows the performance of dark-H_2 production in temperature of 37°C and initial pH of 7.5. When sucrose concentration was increased, H_2 content was increased from 33% to 48%. Model simulation analysis by modified Gompertz equation (Eqn. 1) shows that using sucrose concentration of 20000 mg COD/l resulted in maximum H_2 production rate (R_{max}) of 28.0 ml/h (Table 1). The lag time was similar (λ=13-22 h) for all sucrose concentration examined (Table 1). Table 2 show the soluble metabolites production during fermentative H_2 production of *C. butyricum* CGS2. The main soluble metabolites were butyrate and acetate. When sucrose concentration was increased, the butyrate concentration, acetate concentration and total volatile fatty acids concentrations were increased. The results shows the high H_2 yield and high H_2 production was get, the butyrate concentration, acetate concentration and total volatile fatty acids concentrations were increased.

$$H = H_{\max} \exp\{-\exp[\frac{R_{\max,H_2} \times e}{H_{\max}}(\lambda - t) + 1]\} \quad (1)$$

Table 2: Production of soluble metabolites during fermentative H_2 production of *C. butyricum* CGS2

Carbon source		Soluble metabolite (mg COD/l)						
		EtOH	HAc	HPr	HBu	HVa	TVFA	SMP
Sucrose	5000	545	361	12	2586	16	2975	3520
	10000	624	790	79	5451	34	6354	6978
	20000	422	1441	92	6255	96	7884	8305
	30000	505	1442	151	6289	115	7997	8502

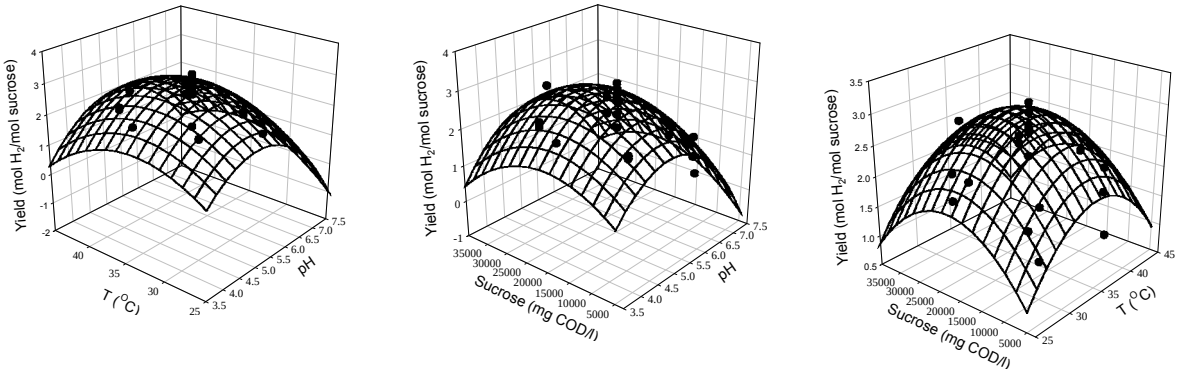

Figure 1: Response surface methodology (RSM) for optimal condition (sucrose concentration, temperature and pH).

Response surface methodology (RSM) was employed to identify the optimal conditions for hydrogen production of C. butyricum CGS2 using sucrose concentration, temperature and pH

Optimal condition (sucrose concentration, temperature and pH) was identified with response surface methodology (RSM). Figure 1 show the results of response surface methodology for optimal condition (sucrose concentration, temperature and pH). With a performance index of Y_{H2}, the optimum condition predicted from RSM analysis was: pH, 5.2; temperature, 35.1 °C; sucrose concentration, 22.5 g COD/l. Under this condition, the hydrogen content in the biogas was 58.5%, $\square H_2$ was 0.54 l/h/l, total hydrogen production was 7.2 l, and Y_{H2} was 2.91 mol H_2/mol sucrose. On the other hand, when $\square H_2$ was used as the performance index, the optimum condition was: pH, 5.36; temperature, 35.1°C; sucrose concentration, 26.1 g COD/l. This condition gave a hydrogen content of 63.3%, a Y_{H2} of 3.26 mol H_2/mol sucrose, a total hydrogen production of 10.5 l, and a $\square H_2$ of 0.50 l/h/l. The validity of RSM predictions was confirmed by additional experiments, suggesting that using RSM design could attain an optimal culture condition for *C. butyricum* CGS2 to enhance its hydrogen production performance.

References

[1] Tsai, W.T., Lin, C.C. and Yeh, C.W. (2007) An analysis of biodiesel fuel from waste edible oil in Taiwan. Renewable and Sustainable Energy Reviews **11**(5), 838-857.

[2] Vrije, T.d., Haas, G.G.d., Tan, G.B., Keijsers, E.R.P. and Claassen, P.A.M. (2002) Pretreatment of *Miscanthus* for hydrogen production by *Thermotoga elfii*. Int. J. Hydrogen Energy **27**(11-12), 1381-1390.

[3] Kapdan, I.K. and Kargi, F. (2006) Biohydrogen production from waste materials. Enzyme Microb. Technol. **38**(5), 569-582.

[4] Chandrakant, P. and Bisaria, V.S. (1998) Simultaneous bioconversion of cellulose and hemicellulose to ethanol. Crit. Rev. Biotechnol. **18**(4), 295-331.

[5] Levin, D.B., Pitt, L. and Love, M. (2004) Biohydrogen production: prospects and limitations to practical application. Int. J. Hydrog. Energy **29**(2), 173-185.

[6] Lee, K.S., Lo, Y.S., Lo, Y.C., Lin, P.J. and Chang, J.S. (2003) H_2 production with anaerobic sludge using activated-carbon supported packed-bed bioreactors. Biotechnology Letters **25**, 133-138.

[7] Lo, Y.C., Chen, W.M., Hung, C.H., Chen, S.D., Chang, J.S., 2008. Dark H_2 fermentation from sucrose and xylose using H_2-producing indigenous bacteria: Feasibility and kinetic studies. Water Res. 42, 827-842.

Sequential Evolution of Bio-hydrogen from Rubber Industrial Effluent and its Microbial Interaction to Fermentation Kinetics

A.G. Murugesan, **K. Bala Amutha**, Manonmaniam Sundaranar University, SPKCES, Alwarkurichi-627412, Tamil Nadu, India

Summary

Rubber industrial (RI) effluent was evaluated for the biological hydrogen (H_2) production in 1 litre capacity bio reactor employing the pretreated mixed micro flora at temperature (37°C) under neutral conditions (pH 7.0) for 20 days. The physicochemical characteristic of the RI effluent was analyzed. The cumulative hydrogen production reached the maximum values with 447.2 ml/l at the end of 20th day and the maximum hydrogen potential of 72ml/l was reached on 7th day. The hydrogen production rate of RI effluent was found to be 0.608ml/gVSS/h. At the end of the fermentation, n-butyrate was obtained as the end product. The dominant microorganisms in RI effluent were *Clostridium* sp., which is responsible for n-butyrate fermentation in hydrogen production. The maximum production rate of 5.934ml/gVSS/h was reached at the present study. The effect of cell biomass and hydrogen production was predicted using (R^2=0.9561) with the modified Luedeking-Piret model. The gas production was predicted using the model modified logistic and gompertz. Therefore the finding of this study can be applied in the design of high rate bio hydrogen in the bioreactor

1 Introduction

Hydrogen is considered as a viable alternative fuel and energy carrier of the future with wide range of applications. It is a clean fuel with no CO_2 emission and used in fuel cells for electricity generation. Bioconversion of biomass to hydrogen has been demonstrated using the anaerobic fermentation from wastewater [1], solid waste [2], glucose [3], crystalline cellulose [4], peptone [5]. Moreover organic wastes like sugary effluent and starch manufacturing effluent [6] has been reported as the substrates for hydrogen production with an advantage of cost reduction and waste disposal.

Rubber industrial effluent is an important renewable biomass energy source with high nutrient content makes an ideal consideration as fermentative substrate for biological hydrogen production. Fermentative hydrogen production was studied by using organic wastes such as high strength wastewater, lingo cellulosic waste [7], food manufacturing waste and waste activated sludge [8]. The cumulative hydrogen production in the batch experiment was analyzed by using the gompertz model [9] and by the modified logistic model [10]. The present study employs pretreated rubber industrial effluent as the primary substrate for the microbial hydrogen production. This endeavour would lead to a great extent to solve the problem of rubber industrial effluent disposal and concurrently attend several limitations of biological hydrogen production.

2 Experimental Work

Effluent sample was collected at the disposal point (Rubber factory, Nagarkoil, India) and the physico chemical and biological characteristics were analyzed [11]. The culture medium was supplemented with the ingredients (1g, K_2HPO_4; 0.05mg, $MgCl_2 \cdot 6H_2O$; 0.75g, KH_2PO_4; 5ml) and trace element solution (5mg, H_3BO_4; 0.5mg, $ZnCl_2$; 30 mg, $CuCl_2$; 500 mg, $MnSO_4 \cdot H_2O$, 50 mg; $(NH_4)6Mo7O_2$ $4 \cdot 4H_2O$, 50 mg; $AlCl_3$; 50 mg, $CoCl_2 \cdot 6H_2O$; 50 mg, $NiCl_2$; 1 ml, HCl (36 %) and 0.1% resazurin) was used for the present study. Batch fermentation was conducted at 37ºC with initial pH 7. The evolved gas was collected in a gas collection bag (Mylor bag). Gas composition was measured by GC and the samples from the supernatant were taken to analyze pH and organic concentrations. Various unstructured models were proved to be sufficient for characterizing the fermentation kinetics along with the growth kinetics [10]. The cumulative hydrogen production in batch experiment was analyzed using the gompertz model [9] and by the modified logistic model [10].

3 Results and Discussion

RI effluent contains rubber hydrocarbons, fresh latex, non rubber constituents such as resins, sugars, glycosides, tannins, alkaloids, mineral salts, waxes and crystals. Table 1 explained the result of physicochemical characterization of RI effluent taken for the hydrogen production. Total solids and dissolved solids were found to be 16000mg/l and 4800mg/l respectively. BOD and COD of the RI effluent were found to be 26100mg/l and 450mg/l respectively.

Table 1: Physico chemical characterization of the rubber industrial effluent.

Parameters	Unit	Mean ± SD
pH	-	7.09 ±0.2
Colour	-	Brown/Black
Total suspended solids	mg/l	11700± 2.9
Total dissolved solids	mg/l	4800 ± 2.3
Total solid	mg/l	16000 ± 0.22
Alkalinity	mg/l	4200 ± 0.42
Biochemical oxygen demand	mg/l	26100± 1.79
Dissolved oxygen demand	mg/l	4500± 5.68
Phosphate	mg/l	1.200±0.05

Total bacterial count from RI effluent was found to be 24 x 10^6 Cfu/ml whereas in heat treated industrial effluent (100ºC - 20 minutes), the total count was 5 x 10^6 x Cfu/ml, which indicated the presence of spore formers. Hydrogen production stops by the growth of methanogens in continuous flow systems and the coexistence of hydrogen consuming microorganisms [12]. Single batch experiment was conducted using the mixed culture without heat treatment to study the hydrogen fermentation [13]. So in this study, batch experiments were conducted using the heated RI effluent for the hydrogen production to reduce the process of methanogenesis.

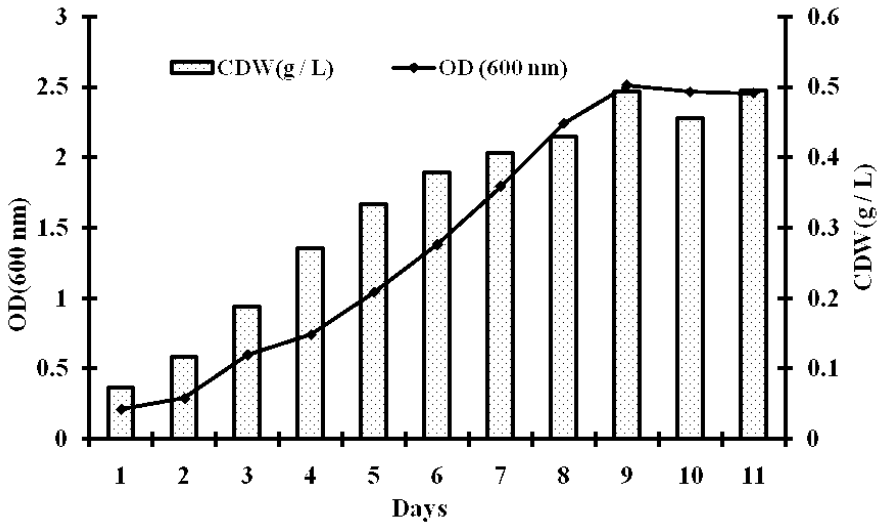

Figure 1: Growth profile of the hydrogen producing pretreated mixed micro flora: CDW (g/l) and OD (600nm).

Growth profile of the mixed micro flora taken from pretreated RI effluent was given in Figure 1. At the end of the study, the hydrogen production stopped which was due to the accumulation of the metabolites in the fermentor. The optimum growth range of methanogens was 30-37ºC [14]. In this batch experiment, the gas production showed remarkable increase on 7th day with 72 ml/day (Figure 2).

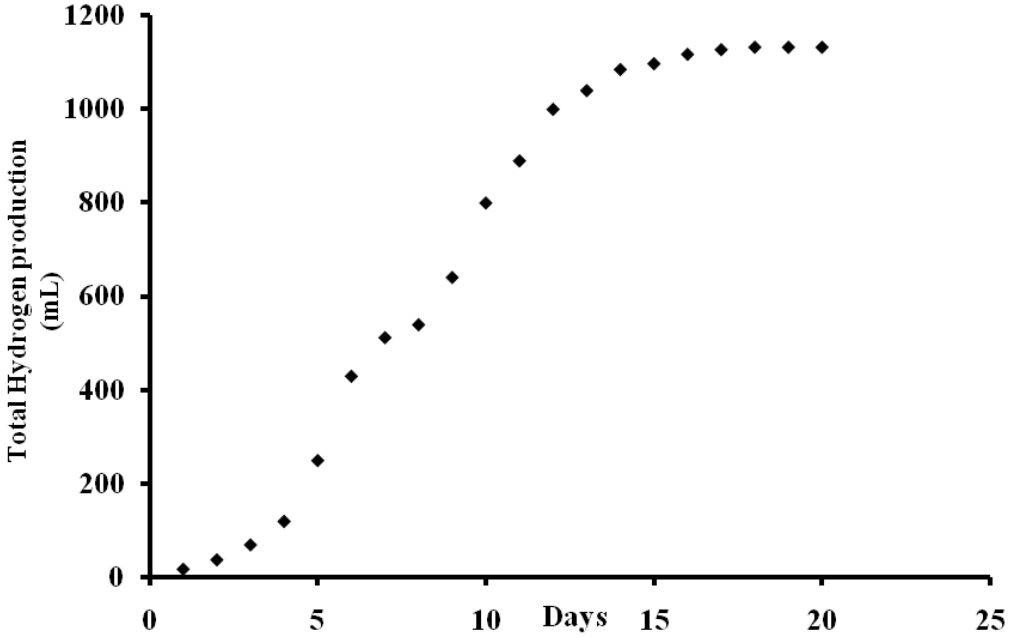

Figure 2: Total hydrogen production (ml/l) of the pretreated mixed micro flora from the rubber industrial effluent.

Total hydrogen production was found to be 447.2 ml/l at 20th day. The effect of pretreated mixed micro flora on hydrogen production profile (ml/h/day) was given in Figure 3.

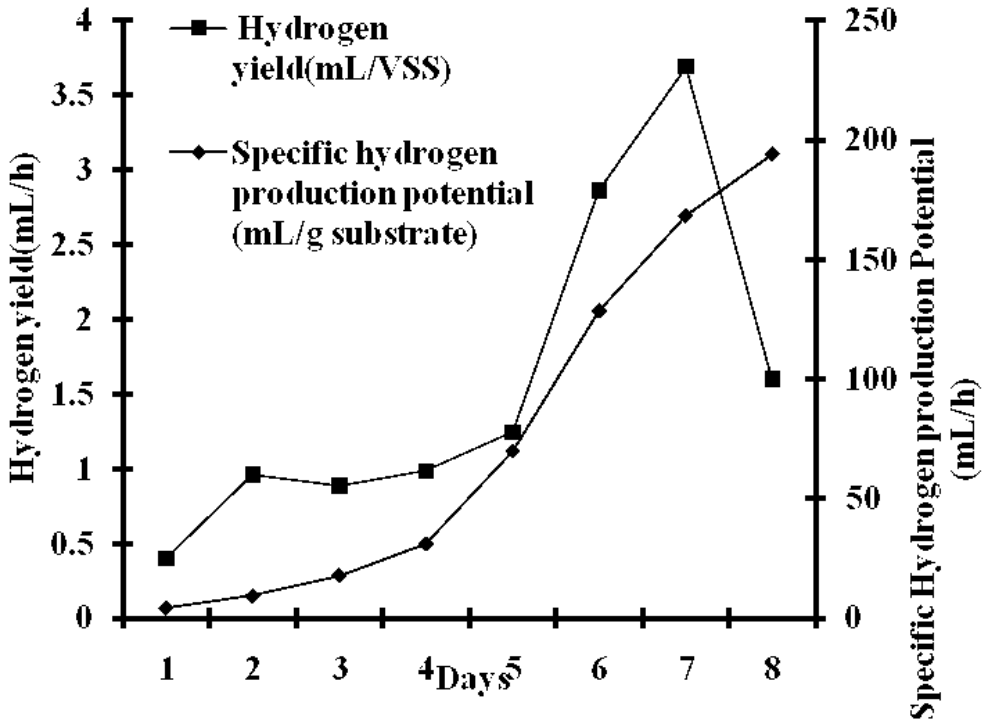

Figure 3: Effect of pretreated mixed micro floral concentration (OD 600nm) on hydrogen production (ml/day).

The modified logistic model predicted for the hydrogen production (ml/h/l) using the pretreated mixed micro flora (Figure 4) yields high (R^2=0.95). The total hydrogen yield (ml/l) was determined by Luedeking-Piret model and given in (Figure 5) with R^2, 0.94.The optimum temperature for hydrogen production was 50-60ºC [19]. CREST compost and sludge compost produce high amount of hydrogen at 60ºC with rate 0.07l/h and 0.125 l/h respectively [15]. The anaerobic spore forming bacteria forms an important part of the acidogenic population in hydrogen production [16]. The capability of the hydrogen producing mixed micro flora using the RI effluent was found to have maximum hydrogen production potential with 72ml/day on 7th day. Hydrogen production per unit biomass was constant [17]. Thus this study also confirmed the relation of the hydrogen productions and the cell concentration as growth associated.

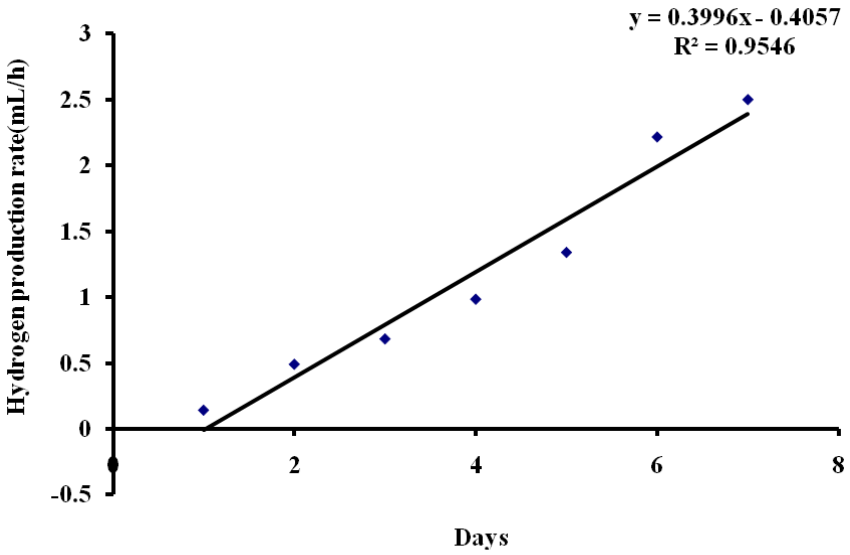

Figure 4: **Modified logistic model parameters for the hydrogen production (ml/h/l) using the pretreated mixed micro flora from the rubber industrial effluent.**

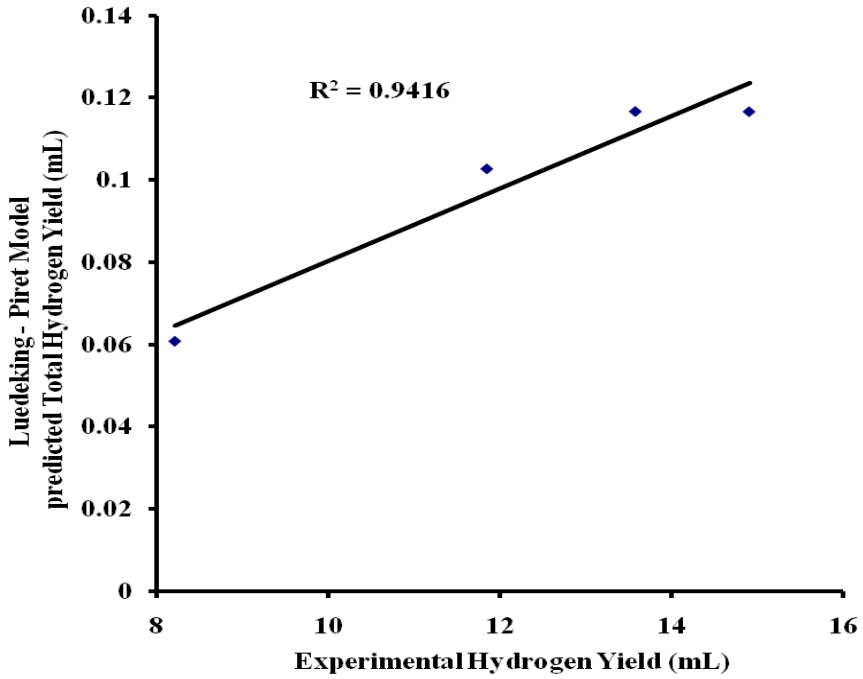

Figure 5: **Comparison of the observed and predicted values of the total hydrogen yield by Luedeking-Piret model.**

Table 2 shows the estimated parameters for both the modified gompertz model for cell growth and total hydrogen yield using the rubber industrial effluent. The values for the kinetic parameters, μ_o, α, β and Xo were found to be 2.476 (h), 0.0088 (ml/gcell biomass), 0.0078 (ml/gcell biomass/h) and 0.364g/l respectively. The modified gompertz model and modified

logistic model were widely used to describe the cumulative hydrogen production in batch experiment [18]. The fermentative kinetics for the anaerobic culture taken from CREST compost at 50ºC and 60ºC exhibited gradual hydrogen gas evolution after 10h with 27.7mmol/l and 53.4mmol/l [16]. Similar results were noticed in the study as earlier [19] conducted at 60ºC with hydrogen evolution after 48 h. In this study, the maximum hydrogen production potential of 447.2ml/l was obtained on 20th day with the estimated final glucose concentration of 0.06g/l at the end of fermentation. The other end products were the trace concentrations of acetate and propionate. In this study, hydrogen production occurred in higher amount than the other end products. Because it was suspected that the metabolisms of hydrogen producing acidogenes shifted to form hydrogen rather than other products. The present study also confirmed the hydrogen production with similar phenomenon which yielded higher amount of hydrogen. The hydrogen production was found to be around pH 6 at the end of the present study. The optimum pH for the hydrogen production was observed in the pH 5 – 6 [19]. The proposed model also interpreted the trends of experimental data. The maximum specific growth rate of the micro flora (μo), and its yield coefficient (Y*x/s*) were estimated with 0.44 (h), 0.100 ml/gVSS/h, and 0.99 respectively.

Table 2: Modified Gompertz parameters for the hydrogen production using the natural micro flora from the rubber industrial effluent.

Temperature	37ºC
λ h	48
R_m (ml / h)	7.5
P (ml)	180
Maximum specific production rate (ml/gVSS/h)	3.04
Specific Hydrogen production (ml/g VSS)	29.67
Hydrogen yield (ml/g substrate)	55.6
R^2	0.9711

The result from this present study concludes that the substrate utilization, growth rate of micro flora, glucose utilization and by product formation has the remarkable influence on increased hydrogen production. Therefore under appropriate conditions natural micro flora from RI effluent were considered as the best choice of hydrogen production at cheap cost. The results from the present study can be also applied in the design experiment of the hydrogen production.

4 Conclusion

In this study, RI effluent was used as the substrate for the hydrogen production. Bio hydrogen production from renewable substrates is a promising element in the sustainable hydrogen economy. The statistical design offers efficient methods to identify the significant variables and optimized factors for hydrogen yield from RI effluent. Maximum hydrogen production potential was found to be 447.2 ml/l at the end of fermentation. The modified Gompertz and modified logistic model for hydrogen production also depicted the hydrogen production profile using the RI effluent. There was no formation of methane and the evolved

gas was only hydrogen and carbon dioxide at 37ºC under pH 7. Very little work has been done on bio hydrogen production from renewable substrates using defined or complex microbial consortia. Therefore natural pretreated mixed micro flora from the RI effluent as the main substrate seems feasible way to produce hydrogen.

References

[1] Zhu, H., Suzuki, T., Tsygankov, A.A., Asada,Y., Miyake, J., 1999. “Hydrogen production from tofu wastewater by *Rhodobacter sphaerodies* immobilized in agar gels,” Int. J. Hydrogen Energy. 24, 305

[2] Mizuno, O.R., Dinsdale, F.R., Hawkes, D., Hawkes, L., Noike, T., 2000a. “Enhancement of hydrogen production from glucose by nitrogen gas sparging, Bioresource Technol. 5, 73 - 59.

[3] Lin, C.Y., Chang, R.C., 1999. Hydrogen production during the anaerobic *acidogenes c*onversion of glucose. J. Chem. Technol. Biotechnol. 47(6), 498 – 500.

[4] Cai, M.L., Liu, J.X., 2005. Factors effecting hydrogen production from anaerobic fermentation of excess sewage sludge. Env. Science. 26(2), 98-101. (P.R.China).

[5] Kim, S.H., Han, S. K., Shin, H. S., 2004. Feasibility of bio hydrogen production by anaerobic co digestion of food waste and sewage sludge. Int. J. Hydrogen Energy 29, 1607-1616.

[6] Lin, C. Y., Lay, C. H., 2004a. Carbon/nitrogen-ratio effect on fermentative hydrogen production by mixed micro flora. Int. J. Hydrogen Energy. 29(1), 41- 45.

[7] Sparling, R., Risbey, D., Poggi-Varaldo, H.M., 1997. “Hydrogen production from inhibited anaerobic composters,” Int. J. Hydrogen Energy, 22, 563.

[8] Wang, G.S., Hsieh, S.T., 2003a. Monitoring natural organic matter in water with scanning spectrophotometer. Environ. Int. 26, 205 – 212.

[9] Chen, W.M., Tseng, Z.J., Lee, K.S., Chang, J.S., 2005. Fermentative hydrogen production with Clostridium butyricum CGS5 isolated from anaerobic sewage sludge. Int. J. Hydrogen Energy. 30(10), 1063.

[10] Chen, C. C., Lin, C. Y., Chang J.S., 2001. Kinetics of hydrogen production with continuous anaerobic cultures utilizing sucrose as the limiting substrate. *Appl.* Microbiol. Biotech. 57(1-2), 56.

[11] Loewus, F. A., 1952. Improvement in the anthrone method for determination of carbohydrates. Anal Chem. 24, 219.

[12] Mulin, C., Junxin, L., Yuansong, W., 2004. Enhanced bio hydrogen production from sewage sludge with alkaline pretreatment. Environ. Sci. Technol. 38, 3195 - 3202.

[13] Lin, C. Y., Lay, C. H., 2005. A nutrient formulation for fermentative hydrogen roduction using anaerobic sewage sludge micro flora. Int. J. Hydrogen Energy. 30(3), 285 -292.

[14] Roychowdhury,, S., Cox, D., Levandowsky, M., 1988. Production of hydrogen by microbial fermentation. Int. J. Hydrogen Energy. 13, 407 - 410.

[15] Taguchi, F., Mizukami, N., Hasegawa, K., Taki, T.S., Morimoto, M., 1994. Effect of amylase accumulation on hydrogen production by *Clostridium beijerinckii* strain AM21B. Ferment. Bioeng. 77(5), 565 - 7.

[16] Morimoto, M., Atsuko, M., Atif, A.A.Y., Ngan, M.A., Fakhru'l-Razi, A., Iyuke, S.E., Bakir, A.M., 2004. Biological production of hydrogen from glucose by natural Anaerobic micro flora, Int. J. Hydrogen Energy, 29, 709 – 713.

[17] Mu, Y., Wang, G., Yu, H.Q., 2006. Kinetic modeling of batch hydrogen production process by mixed anaerobic cultures. Bioresource Technol. 97(11), 1302-1307.

[18] Lo, Y.C., Chen, W.M., Hung, C.H., Chen, S.D., Chang, J.S., 2008. Dark H_2 fermentation from sucrose and xylose using H_2 producing indigenous bacteria: Feasibility and kinetic studies. Water Research. 42(2), 827 - 842.

[19] Ueno, Y., Kawai, T., Sato, S., Otsuka, S., Morimoto, M., 1995. Biological production of hydrogen from cellulose natural anaerobic micro flora. Ferment. Bioeng. 79(4), 395 – 7.

Influence of the Carbon/Nitrogen Ratio on the Hydrogen Production in a Fixed-bed Anaerobic Reactor

Mélida del Pilar Anzola Rojas, **Marcelo Zaiat**, Escola de Engenharia de São Carlos, Universidade de São Paulo, Brazil
Wilton Lopes da Silva, Universidade Estadual de Paraiba, Brazil

This study evaluated the effect of the carbon/nitrogen (C/N) ratio on the hydrogen production from a sucrose-based synthetic wastewater. Up-flow fixed-bed anaerobic reactors with recycled low-density polyethylene for biomass attachment were operated at 25ºC and with a 2-h hydraulic detention time. Several C/N relationship were studied (40, 90, 140 and 190), using sucrose and urea as carbon and nitrogen sources, respectively. Average values of hydrogen yield of 0.6 mol-H_2.mol-sucrose^{-1}, 1.3 mol-H_2.mol-sucrose^{-1}, 2.7 mol-H_2.mol-sucrose^{-1} and 1.7 mol-H_2.mol-sucrose^{-1} were reached when the reactors were operated with C/N of 40, 90, 140 and 190, respectively. It was estimated an optimal value for C/N of 137, which would result in maximum hydrogen yield of 3.5 mol-H_2.mol-sucrose^{-1}. Biogas produced was composed of H_2 and CO_2, with average H_2 content of 53%, 49%, 61% and 52% for C/N of 40, 90, 140 and 190, respectively. The main intermediary fermentation products were similar for all the C/N ratios, being specially detected acetic acid, butyric acid and ethanol. Under excess of nitrogen, the biomass growth was higher with negative effects on hydrogen production while deficiency of nitrogen permitted the control of biomass growth and resulted in higher hydrogen yields.

1 Introduction

In the last decades high population growth has increased the demand of energy, leading to excessive use of fossil fuels. Due to this crescent demand and need of clean fuels, many studies focused on the hydrogen production as alternative energy source. Biological hydrogen production is interesting due to two main reasons: the use of a renewable energetic source and the easy operation of the productive plants at ambient temperature and pressure [1]. The use of cheaper sources, as wastewater with considerable amount of organic fraction, makes the hydrogen production a sustainable process, since the treatment of the wastewater is mandatory for pollution control and hydrogen is a by-product of this process [2]. Several factors affect the hydrogen production in anaerobic reactors as temperature, pH, type and operational condition of reactor, procedure of inoculation, source and processing of the inoculum, wastewater type, among others. The characteristic of the wastewater is extremely important since hydrogen production will depend on the organic contents, being the carbohydrates the main compounds of interest in the process, Moreover, the composition of macro (N, P, S) and micronutrients (K, Mg, Ca, Fe, Mn, Co, Cu, Mo, Zn) is essential for the metabolism and can affect hydrogen production. Among the macronutrients, nitrogen is the most requested for the microorganism and metabolism can be altered due to deficiency or excess this nutrient in the medium. Concerning hydrogen production, the

nitrogen availability can be a factor of great importance to increase hydrogen yield, as shown by Lin & Lay (2004) and Peixoto (2008) [3, 4].

This paper reports on the influence of the carbon/nitrogen (C/N) ratio on the hydrogen production in an up-flow fixed-bed anaerobic reactor.

2 Experimental Setup

The up-flow fixed-bed anaerobic reactor was comprised of acrylic tubes with 80 mm internal diameter, 88 mm external diameter and 750 mm long, with total volume of 3,77 L. Recycled low-density polyethylene was used as inert support for biomass attachment and the synthetic wastewater was composed by sucrose as carbon source, urea as nitrogen source and with micronutrient composition according to Leite *et al*. (2008) [5]. pH was maintained close to 6,5 with addition of $NaHCO_3$ (500 $mg.L^{-1}$) and HCl (0,45 $mL.L^{-1}$ – 10 $mol.L^{-1}$). The reactor was inoculated according to the procedures described by Leite *et al.* (2008) [5].

Four experiments were carried-out, each one with a different C/N ratio (40, 90, 140 and 190). In each stage, the reactor was operated for 60 days at 25ºC and with hydraulic detention time of 2 h.

In each experimental stage influent and effluent samples were collected for pH, temperature, chemical oxygen demand (COD) and volatile suspended solids (VSS) analyses according to Standard Methods [6]. Biogas composition, volatile acids, alcohols and acetone analyses were performed by gas chromatography (GC-2021 and GC-2010, Shimadzu, Tokyo, Japan). Sucrose was determined as proposed by Dubois *et al.* (1956) [7] and the volume of produced biogas was measured with a gas meter (Type TG1, Ritter Inc., Germany).

3 Results and Discussion

3.1 Hydrogen production

This research demonstrated clearly the influence of C/N ratio in the biogas production, indicating that the biogas production increased as the C/N ratio was increased from 40 to 140, thus decreasing for higher values of C/N ratio (Figure 1a). It is important to note that, although the C/N ratio has influenced biogas production in the reactors, the behaviour along the experimental time was the same for all C/N ratios. Biogas production increased up to 25th day of operation, with subsequent drop toward null values of biogas flow-rate around the 60th day of operation. Therefore, stabilization of the biogas production was not observed in any experiment. However, the analysis of the liquid phase indicated stabilization of the fermentative process after approximately 25 days of operation, as observed for sucrose conversion (Figure 1b).

Sucrose conversion efficiencies were similar in all C/N ratios, with values above 88%, similar to those observed by Fernandes (2008) [8]. The content of hydrogen in the biogas ranged from 49% for C/N ratio of 90 and 61% for C/N of 140. This hydrogen content was similar to that observed by O-Thong *et al*. (2008) in up-flow anaerobic sludge blanket (UASB) reactor fed with sucrose [9]. Carbon dioxide ranged from 28% for C/N ratio of 40 and 35% for C/N of 140. Methane was not detected in the biogas during the experiments, indicating absence of methanogenic activity in the reactors under all C/N ratios. Maximum values of hydrogen molar flow-rate (16.2 $mmol\text{-}H_2.h^{-1}$) and hydrogen yield (3.5 $mol\text{-}H_2.mol\text{-}sac^{-1}$) were obtained

when reactor operated with C/N ratio of 140. This yield value is 43.5% of the theoretical maximum value, established by the reaction stoichiometry and considering that sucrose would be converted only in acetic acid. Maximum value of hydrogen volumetric production was 162.5 mL-H_2.h^{-1}.L^{-1}, also achieved with C/N ratio of 140.

The same behaviour of biogas production, hydrogen molar flow-rate and hydrogen yield was observed for all C/N ratio assayed (Figure 1c). The decrease of the nitrogen concentration in the medium resulted in favourable conditions for hydrogen production with hydrogen yield 3.5 times higher when C/N ratio was increased from 40 to 140. It is worth mentioning that, in this range of C/N ratio, the increase in hydrogen yield was proportional to the decrease in the nitrogen concentration. This behaviour can be related to the metabolic pathway. Under excess of nitrogen (low C/N ratios), energy was mainly used to cell assimilation and growth, thus resulting in lower hydrogen production. However, as the C/N ratio was increased, nutritional deficiency probably prevents the use of energy for growth, with positive effect in hydrogen production. The drop in hydrogen production under the highest C/N ratio can indicate severe nutritional deficiency, thus suggesting an optimal C/N ratio for the process. These results are according with those described by Lin & Lay (2004), who suggested that less nitrogen contents can be insufficient for cell growth [3]. The hypothesis of cell growth favoured by low C/N ratio could be checked through biomass concentration (as total solid - TS) in the reactor. Biomass concentration decreased as C/N ratio increased, with stabilization for C/N ratio 140 and 190. The decrease in the biomass concentration indicates that specific organic load increased as the C/N ratio was increased, causing a positive effect in hydrogen production due to unbalance of the anaerobic process, essential for hydrogen production.

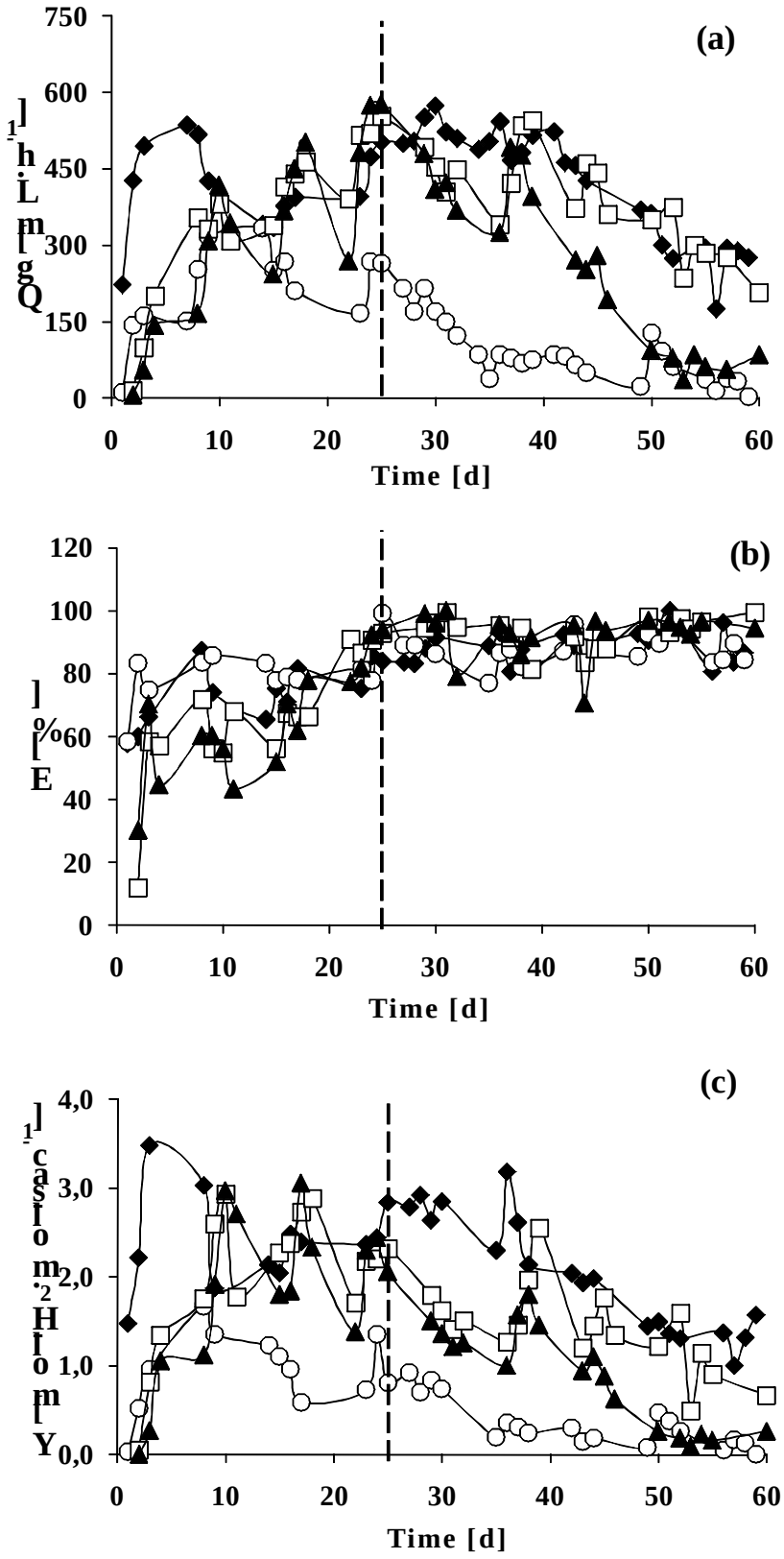

Figure 1: **Biological hydrogen production with C/N ratio of 40 (○), 90 (▲), 140 (◆) and 190 (□). (a) Biogas production (Qg). (b) Sucrose degradation (E). (c) Hydrogen yield (Y).**

3.2 Fermentation products in liquid medium

The composition of soluble products was similar in all experiments independent of the C/N ratio, being predominant acetic and butyric acids, related to maximum hydrogen production [10], besides the ethanol, undesirable when hydrogen is the desirable product. Other detected products were propionic acid, n-butanol, acetone, isobutyric acid, methanol, caproic, valeric and isovaleric acids.

4 Conclusions

The C/N ratio affected biological hydrogen production in anaerobic fixed-bed reactor. Maximum molar flow-rate, yield and volumetric production amount were 16.2 mmol-H_2.h^{-1}, 3.5 mol-H_2.mol-suc^{-1} e 162.5 mL-H_2.h^{-1}.L^{-1}, respectively, obtained under C/N ratio of 140. The biogas was composed mainly by H_2 and CO_2, with hydrogen average percentages of 53%, 49%, 61% and 52% with C/N ratio of 40, 90, 140 and 190 respectively. The main organic acids produced in the process were acetic and butyric, and the main solvent produced was the ethanol.

References

[1] Das, D. (2009) Advances in biohydrogen production processes: An approach towards commercialization. *International Journal of Hydrogen Energy,* 34**,** 7349-7357.

[2] Babu, V. L., S. V. Mohan & P. N. Sarma (2009) Influence of reactor configuration on fermentative hydrogen production during wastewater treatment. *International Journal of Hydrogen Energy,* 34**,** 3305-3312.

[3] Lin, C. Y. & C. H. Lay (2004) Carbon/nitrogen-ratio effect on fermentative hydrogen production by mixed microflora. *International Journal of Hydrogen Energy,* 29**,** 41-45.

[4] Peixoto, G. 2008. Produção de hidrogênio em reator anaeróbio de leito fixo e fluxo ascendente a partir de água residuária de indústria de refrigerantes. In *Escola de Engenharia de São Carlos, Departamento de Hidráulica e Saneamento*, 107. São Carlos: Universidade de São Paulo.

[5] Leite, J. A. C., B. S. Fernandes, E. Pozzi, M. Barboza & M. Zaiat (2008) Application of an anaerobic packed-bed bioreactor for the production of hydrogen and organic acids. *International Journal of Hydrogen Energy,* 33**,** 579-586.

[6] Standard Methods for the Examination of Water and Wastewater (1998) 20th ed. American Public Health Association (APHA)/ American Water Works Association / Water Environment Federation, Washington, DC, USA.

[7] Dubois, S.M.; Gilles, K.A.; Hamilton, J.L.; Rebers, P.A.; Smith, F. Colorimetric Methods for determination of sugar and related substance. *Analytical Chemistry*, v. 228, p. 13 – 21. 1956.

[8] Fernandes, B. S. 2008. Produção de hidrogênio em reator anaeróbio de leito fixo. In *Departamento de Hidráulica e Saneamento, Escola de Engenharia de São Carlos*, 100. São Carlos: Universidade de São Paulo.

[9] O-Thong, S., P. Prasertsan, N. Intrasungkha, S. Dhamwichukorn & N. K. Birkeland (2008) Optimization of simultaneous thermophilic fermentative hydrogen production

and COD reduction from palm oil mill effluent by Thermoanaerobacterium-rich sludge. *International Journal of Hydrogen Energy,* 33, 1221-1231.

[10] Levin, D.B.; Pitt, L.; Love, M. (2004) Biohydrogen production: prospect and limitation to practical application. *International Journal of Hydrogen Energy*, v. 29, p. 173-175.

Two-Phase Anaerobic Digestion of Mixed Waste Streams to Separate Generation of Bio-hydrogen and Bio-methane

Z. Siddiqui, N.J. Horam, School of Civil Engineering, University of Leeds, W. Yorkshire, UK

Abstract

The purpose of this study was to investigate the net energy potential of single stage mesophilic reactor and two phase mesophilic reactor (hydrogeniser followed by methaniser) using the mix of process industrial food waste (IFW) and sewage sludge (SS). Two-phase reactor efficiency was analysed based on individual optimum influent/environmental (C:N and pH) and reactor/engineering (HRT and OLR) conditions achieved using the batch and continuous reactor study for the hydrogen and methane. Optimum C:N 20 and pH 5.5±0.5 was observed using the Bio-H_2 potential (BHP) and C:N 15 and pH 6.5±0.3 for the biochemical methane potential (BMP) test. The maximum hydrogen content of 47% (v/v) was achieved using OLR 6 g VS/L/d and HRT of 5 days. Increase in hydrogen yield was noticed with consistent decrease in OLR. The volatile solids (VS) removal and hydrogen yield was observed in range 41.3 to 47% and 112.3 to 146.7 mL/ $gVS_{removed}$. The specific hydrogen production rate improved at low OLR, 0.2 to 0.4 L/(L.d) using OLR 7.1 and 6 g VS/L/d respectively was well corroborated comparable to previous reported results at OLR 6 gVS/L/d using the enriched carbohydrate waste stream in particular to food wastes. A significant increase in VFA concentrations were noticed shifting OLR higher from 6 g VS/L/d thereby unbalancing the reactor pH and the biogas yield respectively. In similar, maximum methane content of 70% (v/v) was achieved using OLR of 3.3 gVS/L/d and HRT of 10 days. Slight decrease in methane content was noticed thereby increasing HRT to 12 and 15 days respectively. The volatile solids (VS) removal and specific methane production rate was observed in range 57.6 to 68.7 and 0.22 to 1.19 L/(L.d). The specific methane production potential improved thereby reducing the HRT and optimium yield was recorded as 476.6 mL/$gVS_{removed}$ using OLR 3.3 gVS/L/d. The energy potential of optimum condition in single stage hydorgeniser is 2.27 MW/tonne VS_{fed}. Using the two phase and sub optimal conditions improves the energy potential to 8.27 MW/tonne VS_{fed} with VS(removal) efficiency as 80.7% in total 15 days of HRT. The net energy balance results indicated the co-digestion of IFW with waste products of SS treatment plant viz. primary sludge (PS) and waste activated sludge (WAS) are amenable substrates for the two-stage anaerobic bio-hydrogen and bio-methane digestion process.

1 Introduction

A conventional phase-separated two-stage approach was implemented for biomethane production by introducing the hydrolyser/acidogeniser reactor in front of the methaniser (Pohland and Ghosh, 1971 [3]). This improves the buffering capacity of methaniser to feed shock-loads and to inhibitors such as ammonium and organic acids. It also improves the digester performance as the first phase accepts a higher loading in terms of OLR. The

production of biohydrogen is an attractive one as hydrogen is clean energy and a renewable energy production option for the future. However methane production has historically become more popular due to a lack of information on the process and complications involved in its optimisation. The results achieved from the batch and continuous reactor studies of biohydrogen and biomethane (Siddiqui, 2010 [2]) production that an integrated phase-separated two-stage anaerobic hydrogeniser and methaniser might be an ideal option for an optimised blend of organic feed-stocks. Whereas it was observed that a C:N 15 demonstrated optimum methane production (Siddiqui et al. 2010 [2]), the effluent characteristics of the hydrogeniser produced a C:N of 18 which may the methaniser for optimum methane production. One approach would be to have an intermediate feed directly to the methaniser to correct the imbalance, but initially it was decided to operate the methaniser under sub-optimal conditions by feeding the effluent from the hydrogeniser without correcting the C:N ratio. The aim of this study to investigate the net energy potential of single stage mesophilic reactor and two-phase mesophilic reactor (hydrogeniser followed by methaniser) using the mix of process industrial food waste (IFW) and sewage sludge (SS).

2 Material and Methods

2.1 Feedstock and seed inoculum

Feedstocks and nutrient supplements were selected from the earlier study described in Siddiqui (2010 [2]) with an ideal blend of carb:pro 2.78 (C:N 20) and pH 5.5±0.3 selected and employed. The required feed with a blend of C:N 20 was achieved by mixing fractions of processed industrial food waste IFW, sewage sludge SS (primary sludge PS and waste activated sludge WAS). The second digester (methaniser) was fed by the residual effluent received from the hydrogeniser. The methaniser was operated by correcting to optimise conditions of pH to 6.5±0.3 and an HRT of 10 days and sub-optimal feed conditions of C:N 18 and OLR of 1.9 g VS/L/d. Acclimatised seed inoculum was developed in two lab-scale mesophilic CSTRs, one for hydrogen production and one for methane. The hydrogeniser was operated at a temperature of 37^{o}C±0.2 and an HRT of 5 days. A co-blended waste of IFW and SS with OLR of 6 g VS/L/d was continuously supplied to the reactor. The conditions were: pH, 5.5±0.3; alkalinity, 5,000 mg/l; VFA, 46,200 mg/L and hydrogen composition, 38.5%. The methaniser was operated at a temperature of 37^{o}C±0.2 and an HRT of 10 days and feed with a co-blended waste of IFW and SS with OLR of 3.4 g VS/L/.d. The conditions were: pH, 6.5±0.3; alkalinity, 5,000 mg/L; VFA, 31,200 mg/L and methane composition, 70.1%.

2.2 Experimental setup

A phase separated two-stage hydrogeniser followed by methaniser was operated in semi-continuous mode (feeding once a day). Both digesters were fabricated using 0.8cm thick perspex with a gas-tight, hermetically sealed, rubber sealing, the internal temperature (37±2^{o}C) of the contents was controlled by a thermostatically heat controlled jacket. The total volume of the hydrogen producing digester was 1.67 L with a working volume 1.5 L (Figure 1) and the total volume of the methaniser was 5.0 L with a working volume 4.0 L (Figure 1). Feeding of the hydrogeniser was carried out using the top feed inlet; the second

digester (methaniser) was fed by residual effluent received directly from the hydrogeniser effluent port, fixed at effective height. The gas was continuously collected from the gas ports and it was volumetrically measured at normalized pressure using a water displacement method; later the gas volume was then corrected to STP. Both digesters were mechanically mixed at 100 rpm witha paddle guided by an IKA overhead stirrer at 100 rpm and a cycle: reaction time of 20 minutes with mixing every hour, up to 16 hours followed by continuous mixing for 1 hour and settling of 6 hours. Manual correction of pH to a value of 5.5 for the hydrogeniser and 6.5 for the methaniser was undertaken using 6M NaOH and 1M HCl.

2.3 Analytical methods

The analytical parameters of total solids (TS), volatile solids (VS), total alkalinity (TA), ammoniacal nitrogen (NH_4-N) and total volatile fatty acids (TVFA) were carried out following the procedures outlined in APHA (1998 [1]). Samples for analysis of TA, NH_4-N, and TVFA were centrifuged at 60,000 rpm for 1 hour prior to analysis. The elemental composition of all feed-stocks was determined with vanadium pentoxide by flash combustion method using the CHNSO Analyser (Thermo Flash EA-1112 series, Italy). Gas composition was analysed using a gas chromatograph (Hewlett Packard HP 5890 Series II, USA) with a thermal conductivity detector TCD using a PLOT capillary molisieve column (30 m × 0.32 mm × 12 µm; Hewlett Packard HP, USA). The temperature of injector, detector and column were kept at 80, 90 and 40^{o}C respectively. To determine hydrogen and methane, nitrogen was used as carrier gas with a flow of 6 mL/min. VFA profile (organic acids) were quantified using the same GC and flame ionization detector FID using a wall cotted open tubular (WCOT) capillary fused silica column (25 m × 0.32 mm × 0.44 mm; Nordion, FI). Before analysing the acids and alcohols, samples were acidified with 10% and 3% formic acid. The temperature of injector, detector and column were kept at 200, 185 and 160^{o}C respectively. Helium was used a carrier gas with a flow of 60 mL/min.

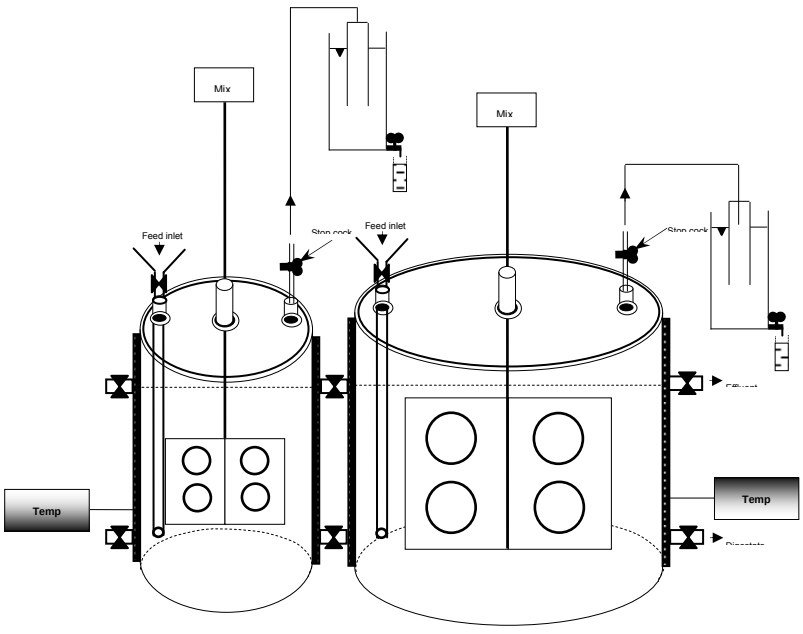

Figure 1: Laboratory scale two-stage phase-separated hydrogeniser followed by methaniser.

3 Results and Discussion

3.1 Recovery of hydrogen and methane using the two-stage phase-separated process

The specific hydrogen production (SHP) was observed in the range of 0.49 to 0.54 L with an average of 0.53 L (Table 1). The SMP of the methaniser of the second stage was observed in range of 2.2 to 3.7 L with an average of 3.2 L. An improvement in SHPR was observed and found in range of 0.3 to 0.4 L/(L.d) (rec vol) with an average of 0.4 L/(L.d). The SHPR confirmed the earlier SHPR from the single-stage CTSR (HRT of 5 days) (Siddiqui, 2010 [2]). A similar gradual improvement was observed in SMPR and varied over the range of 0.6 to 1 L with an average of 0.8 L/(L.d) (Table 1). A decrease of 0.4 L/(L.d) was noted compared to the average SMPR of CTSR (HRT of 10 days) (Siddiqui, 2010 [2]). It was thought that the reduction in SMPR was due to a decrease in the OLR from 3.3 g VS/L/d (Table 1) to 1.6 g VS/L/d (Table 1). Nevertheless the SMPR was twice the SHPR. This verified that the volumetric methane production is more than the volumetric hydrogen production. The concentration of hydrogen (38%) was comparable to the earlier study; in contrast a decrease in methane level was observed in the second stage.

The efficiency of anaerobic fermentation is determined mainly through production of intermediary metabolites and the biohydrogen yield from a given substrate. The major organic acids produced were acetic acid and butyric acid and the projection of higher organic acids (acetic acid and butyric) produced at shorter retention times showed that hydrolysis of substrate would give an indication of the maximum biohydrogen yield. The hydrogen yield varied in the range of 106.1 to 146.7 mL/g $VS_{removed}$ (Table 1) with average of 129.1 mL/g $VS_{removed}$ (Table 1). The hydrogen yield was very similar to earlier yields achieved during single stage CSTR of HRT of 5 days (Siddiqui, 2010 [2]). It was observed that the effluent from the hydrogeniser had a residual volatile solids and organics acids that was amenable for recovery of biomethane in the subsequent methaniser. Using the same residual effluent, the methane yield varied in range of 496 to 762.3 mL/g $VS_{removed}$ (Table 1) with average yield of 617.6 mL/g $VS_{removed}$ (Table 1). A significant improvement in methane yield was noted compared to the earlier, single-stage CTSR 476 mL/g $VS_{removed}$ (Siddiqui, 2010 [2]) and was 1.3 fold higher. This enabled the conclusion that installing a hydrogeniser, hydrolysed the organic acids and was ideal for increasing the methane yield. The methane yield achieved was greater than other authors observed, for sinnlge and two stage instance 0.133 to 0.638 m^3/kg VS.

Table 1: Performance of phase-separated two-stage reactors and effluent characteristics after hydrogen and methane recovery.

Properties	Unit	2 stage digester	
		Hydrogeniser	Methaniser
HRT	d	5	10
$VS_{removed}$ Max(Avg)	%	56.5(47)	72.7(80.7)
SHP or SMP Max(Avg)	L	0.57(0.53)	3.7(3.2)
H_2 or CH_4 yield Max(Avg)	mL/g $VS_{removed}$	146.7(129.1)	617.6(476)
H_2 or CH_4 Avg	%	38	70
SHPR or SMPR Max(Avg)	L/(L.d)	0.4(0.4)	0.93(0.8)
Effluent pH[a]	-	5.3	7.2
Effluent C:N	-	18	-
Effluent NH_4-N[a]	mg/L	33.2	42
Effluent TVFA[a]	mg/L	38,173	27,828
Effluent Magnesium[b]	mg/L	199.7	140
Effluent Phosphate[b]	mg/L	121.9	12.7
Effluent Alkalinity[a]	mg/L	4,750	5,833
Effluent Struvite[b]	mg/L	2,597	814

[a] based on average results of effluent of hydrogeniser and methaniser

[b] based on mixing the last three samples attained during the operation of the reactors

3.2 Effluent characteristics

The residual ammonium and alkalinity levels were low but pH was still noted above neutral range (Table 1). This might be due to the efficient operational control of the two-stage reactor that has separated the hydrolysis step (as hydrogenesis) and methanogenesis regardless of pH (4.6) of the ideal blend (Siddiqui, 2010 [2]). In order to take advantage of the effluent characteristics: neutral pH, low level of ammonium nitrogen and high levels of phosphate and magnesium (Table 1), a trial was run to monitor the theoretical potential of struvite (Mg NH_4 PO_4. $6H_2O$) recovery. This was established as 2,597 mg/L in the effluent from hydrogeniser and 814 mg/L in effluent from the methaniser. The theoretical struvite potential demonstrated the feasibility of nutrient precipitation by reducing the tertiary treatment process. The experimental efficiency of struvite recovery was 70%. In a similar way, the residual organic acid level became steady and major organic acid produced were acetic acid and ethanol. Initially a high level of acetic acid (55% v/v) was observed that reduced to (38% v/v). In contrast an increase in ethanol production from 30% to 53% (v/v) was observed during the two stage process.

3.3 Total efficiency of two-stage phase-separated reactor

The efficiency of the anaerobic digestion process was considered by analysing the amount of volatile solids destroyed and total energy produced. The independent VS destroyed efficiency of the hydrogeniser was recorded as 47% (Table 1) and this increased to (80.7%)

for two stage process (Table 1). The performance efficiency of the two-stage process was significantly higher comparing to single stage CSTR (HRT of 15 days) 66.4% (Siddiqui, 2010 [2]) and also the efficiency was higher compare to ealier work.

The total energy production of two-stage phase-separated hydrogen and methane production was high compare to single-stage methaniser only. The hydrogen and methane yield was noted as 129.1 and 476 mL/g $VS_{removed}$ (Table 1). Significant improvement in methane yield was noted compare to the earlier single-stage CTSR operated at HRT of 10 and 15 days. The energy potential of optimum condition in single stage hydorgeniser is 2.27 MW/tonne VS_{fed}. Using the two phase and sub optimal conditions improves the energy potential to 8.27 MW/tonne $VS_{fed.}$

4 Conclusions

- A two-phase reactor was operated with the first phase at pH 5.5 and OLR of 6 g VS/L/d. A hydrogen yield of 129.1 mL/g $VS_{removedwas}$ obtained with a VS destruction of 27%
- The digestate was close to optimal for the second phase which operated at a pH of 6.5 and an OLR of 1.6 g VS/L/d to give methane yield of 476 mL/g $VS_{removed}$
- The two-phase reactor had a combined energy yield of 8.27 MW/tonnes of VS_{fed} and a VS destruction of 80.7%
- The effluent characteristics showed a viability of struvite, acid and ethanol recovery. The theoretical residual concentration of struvite from the hydrogeniser and methaniser were 2,597 mg/L and 814 mg/L. The organic acid produced were acetic acid (38% vol basis) and ethanol (53% vol basis).

References

[1] American Public Health Asssociation. (1998). Standard methods for the examination of water and wastewater. 20th ed. Washington, DC, USA

[2] Siddiqui, Z. (2010). Optimisation of hydrogen and methane production from co-digested food waste and biosolids using phase-separated anaerobic digestion. PhD thesis, University of Leeds, UK

Hydrogen Generation from Waste Glycerol in Dark Fermentation Process

Ewelina Wicher, **Michał Thiel**, **Marek Laniecki**, A. Mickiewicz University, Poland

1 Introduction

Recently, the international activities in the area of sustained world concentrate basically on three topics, strictly related to the energetic problems: more efficient use of fossil fuels, increase if the renewable sources of energy and elimination of the harms caused by human activities in the field of energy. One of the proposals is based on an application of biofuels as energy carrier – generated in transesterification process of plant oils. The easy access, regenerativity, low concentration of sulfur compounds and high biodegradability favour this process. The main disadvantage can be related with high viscosity of the biodiesel, emission of nitrogen oxides and generation of tremendous amounts of contaminated glycerol as a by-product [1] during production. Glycerol contaminated with potassium, sodium hydroxides and methanol and not complexly transformed methanol, represents almost 25 vol.% of total amount of the produced fuel. Although there are many industries in which glycerol can be applied, the amount generated in transesterification is still extremely high and is a challenge both for academia and industry [2].

Among different alternative fuels which can be used in future, the biofuels and hydrogen are most frequently cited. High energetic value (33 Wh/g) of hydrogen is as twice as big as of this for methane (14.2 Wh/g) [3]. Moreover, burning of hydrogen both chemically or electrochemically always leads towards harmless water.

Hydrogen, often called the fuels of XXI century, becomes very attractive alternative to direct solar energy, wind and geothermal energy. Hydrogen can produced on different ways: microbiological belongs to one of the most promising methods. In fermentation process the anaerobic bacteria of e.g. *Clostridium, Enterobacter* or *Bacillus* transforms simple organic compounds into hydrogen, carbon dioxide and light volatile organic acids [4]. Organic wastes of different origin can be applied as the substrates for this reaction, including non-purified glycerol fraction [5,6]. The efficiency of hydrogen generation depends on different factors, among the most important are: pH [7], concentration of products [8], substrates [9] and participation of the municipal sludge. During dark fermentation hydrogen and CO_2 are the main gaseous products, whereas the main liquid metabolites are 1,3–propanediol, 2,3-butanediol, butyric acid and ethanol [10]. Isolated metabolites such as 1,3-propanediol can be applied in production of polyurethanes or polyesters [11], excellent solvents, plasticizers, artificial silk or fragrances and dyes [12].

The main goal of this paper was focused on the possibility of application of waste glycerol for hydrogen production in “dark” fermentation process,. It was established that waste glycerol is a good candidate for this purposes. Established optimization conditions: pH and the best glycerol concentration allows now for expanding this research in larger scale. It was also

established the liquid metabolites, especially 1,3 –propanediol can be isolated from studied bacterial systems.

2 Materials and Methods

2.1 Inoculum

Anaerobic digested sludge received from municipal purification facility was boiled for 15 minutes and kept frozen at -20°C. In all experiments the sludge was defrosted and kept at 20°C for 4 hours a day before inoculation.

2.2 Methods and procedures

All experiments were performed in continuous stirred tank reactor L-1523 from Bioengineering A.G. (max. capacity – 7 litres, 200 rpm) with continuously controlled temperature (37°C) and pH. The nutrient solution was composed of: $NaHCO_3$ (1g), NH_4Cl (0,5g), KH_2PO_4 (0,25g), K_2HPO_4 (0,25g), $MgSO_4 \cdot 7H_2O$ (0,32g), $FeCl_3$ (50mg), $NiSO_4$ (32mg), $CaCl_2$ (50mg), $Na_2B_4O_7 \cdot H_2O$ (7mg), $(NH_4)_6Mo_7O_{24} \cdot 4H_2O$ (14mg) $ZnCl_2$ (23mg), $CoCl_2 \cdot 6H_2O$ (21mg), $CuCl_2 \cdot 2H_2O$ (10mg), $MnCl_2 \cdot 4H_2O$ (10mg). All given amounts are expressed per litre [13]. Working capacity was three litres but volume of inoculum was in the range of 10%. Systems with constant pH – 4,5; 5,0; 5,5; 6,0; 6,5, were stabilized and this values were kept till the end of the process. Concentration of this waste glycerol in medium was 23, 47, or 70 g/l.

2.3 Analysis

The cumulated amount of generated biogas containing only CO_2 and H_2 was measured volumetrically under atmospheric pressure. The composition of evolved gases was measured by gas chromatography (GC 3800 from Varian equipped with TCD detector) applying capillary column Carboplot P7. Liquid metabolites: butyric acid (HBu), acetic acid (HAc) and 1,3-propanediol (1,3-PD) were extracted from medium applying ethyl ether and analyzed with gas chromatography (GC 3900 from Varian equipped with FID detector) applying capillary column WF-WAXms. Lactic acid content was determined with colorimetric method [14].

3 Results and Discussion

Literature data and our earlier research [15] indicated that pure glycerol can be used as the substrate in dark fermentation process. With inoculum (10 vol.%) and concentration of glycerol equal 30 g glycerol/l medium and pH= 5.5 the highest amount of fermentative hydrogen was observed (almost 2l H_2/l medium). This prompted us to study hydrogen generation from waste glycerol. In the experiments with waste glycerol, pH was 5.5 and inoculum close to 10 vol.%. The highest volume of generated hydrogen (5.7 l) was found in bioreactor (working volume 1.5 l) containing equivalent of 47 ml of pure glycerol per litre (see Figure 1). Under these conditions system indicated the shortest lag time. At higher concentration of glycerol (eg.70 ml/l) no increase of evolved hydrogen was observed. This was explained by so called substrate inhibition [16].

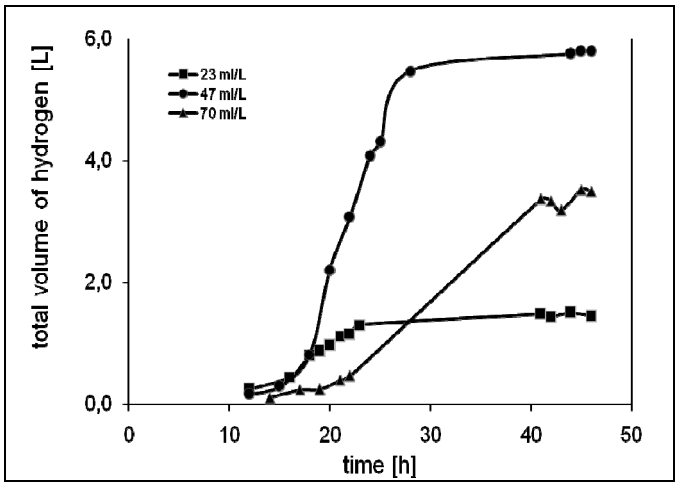

Figure 1: Hydrogen generation with medium containing different amounts of waste glycerol (pH=5.5, 10%vol. of inoculum).

The influence of initial pH (4.5-6.5) on the yield of hydrogen production was the next step of performed research. It was found the pH = 5.5 provide the best conditions for hydrogen biogeneration (see Figure 2). Our earlier studies with pure glycerol indicated that pH of 5.5 represents the best value for the fermentative generation of hydrogen [17].

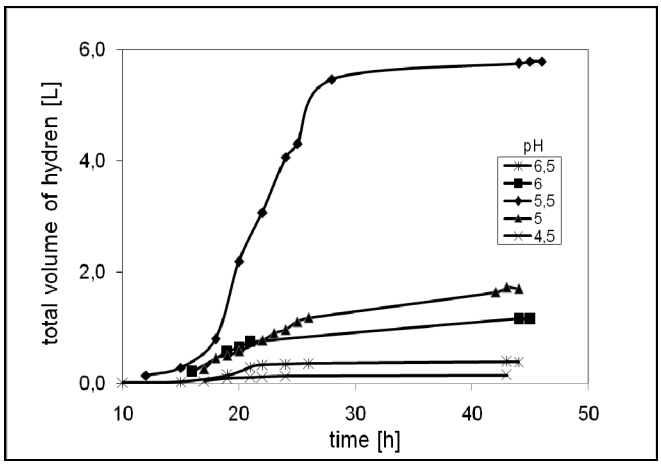

Figure 2: Hydrogen generation with medium containing waste glycerol (47ml/l, 10%vol. of inoculum) at different pH.

The qualitative and quantitative analysis of liquid metabolites showed that among liquid products of the reaction the highest concentration was reached for 1,3 – PD (Figure 3). This is the main metabolite in bacterial decomposition of glycerol. Other organic metabolites with certain practical use, when appropriately separated, are acetic acid (HAc), butyric acid (HBu) and lactic acid (HLac) [18]. The best concentration of 1,3 –PD (9.8 g/l) was found for the system producing the highest amount of generated hydrogen. Simultaneously, butyric acid produced in the same system reached the largest concentration (4.01 g/l). Both results are in agreement with glycerol biochemical pathway described by Papanikolau et al. [19].

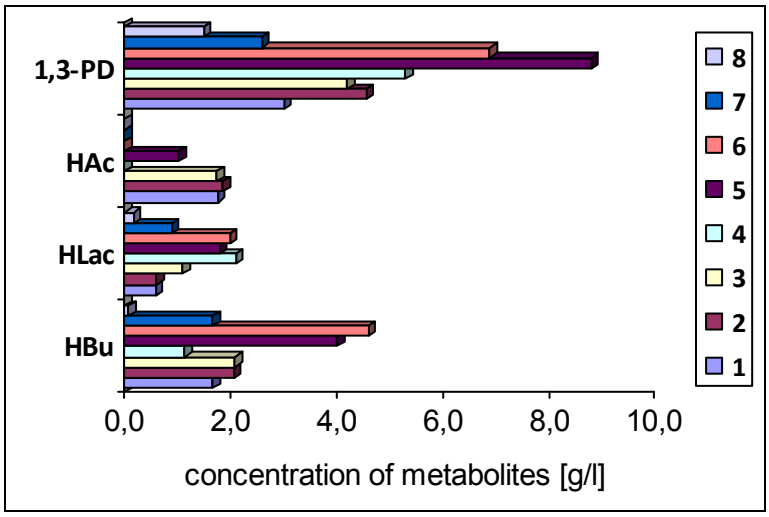

Figure 3: Concentration of 1,3-propanediol (1,3-PD), lactic(HLac), acetic (HAc) and butyric (HBu) acids in medium containing 10%vol. of inoculum, different pH and waste glycerol (1,2 - pH= 6.5; 3, - pH=6.0; 4,5,6 - pH=5.5; 7 - pH=5.0; 8 - pH=4.5; waste glycerol: 2,6 - 70ml/l; 1, 3, 5, 7,8 - 47ml/l; 4 - 23ml/l).

There are two ways of glycerol transformations: one in which mainly 1,3-PD is generated, and another one in which HBu and HAc are formed. Hydrogen generation accompanies both processes. Although both processes compete, the amount of generated hydrogen is independent from the chosen pathway. Theoretical speculations predict that large amount of HAc is strictly connected with large amount of hydrogen (1 mole of HAc is equivalent to 4 moles of H_2). Therefore, one could expect large amounts of acetic acid with high productivity of hydrogen. The lowered values for generated hydrogen show that metabolic pathway is directed to 1,3-PD rather than to HAc. The amounts of HLac are comparable with HAc.

Presented results show that waste glycerol can be used in fermentative hydrogen generation and to best conditions for large quantities of H_2 are obtained with systems operating at pH = 5.5 with 47 ml of glycerol per litre of medium. Moreover, fermentative glycerol decomposition is directed towards 1,3–PD formation. Appropriate separation technique can utilize the described processes towards microbiological production of 1,3–PD from wastewaters.

Acknowledgements

The financial support by the Ministry of Science and Higher Education (MNSiW – grant N204 031 32/0793) is gratefully acknowledged.

References

[1] A. Dembiras, *Importance of biodiesel as transportation fuel,* Energy Policy 35 (2007) 4661-4670.

[2] M..I. Galan, J. Bonet, R. Sire, J. M. Reneaume, *From residual to useful oil: Revalorization of glycerine from biodiesel synthesis,* Bioresource Technology 100 (2009) 3775-3778.

[3] P. Piela, P. Zelanay, *Researchers redefine the DMTC roadmap,* Fuel Cell Review 1 (2004) 17-23.

[4] M.-L. Chong, V. Sabaratnam, Y. Shirai, M. A. Hassan, *Biohydrogen production from biomass and industrial wastes by dark fermentation,* International Journal of Hydrogen Energy 34 (2009) 3277-3287.

[5] I. K. Kapdan, F. Kargi, *Biohydrogen production from waste materials,* Enzyme and Microbiology Technology 3 (2006) 569-582.

[6] T. Ito, Y. Nakashimada, K. Senba, T. Matsui, N. Nishio, *Hydrogen and ethanol production from glycerol -containing waste discharged after biodiesel manufacturing process,* Journal of Bioscience and Bioengineering, vol. 100. No. 3, (2005) 260-265.

[7] Y. J. Lee, K. Miyahara, T. Noike, *Effect of pH on microbial hydrogen fermentation*. Journal of Chemical Technology and Biotechnology 77 (2002) 694–8.

[8] S. K. Khanal, W.-H. Chen, L. Li, S. Sung, *Biological hydrogen production: effects of pH and intermediate products,* International Journal of Hydrogen Energy 29 (2004) 1123-1131.

[9] S.Van Ginkel, S. W. Sung, J. J. Lay, *Biohydrogen production as a function of pH and substrate concentration*. Environmental Science and Technology 35 (2001) 4726-4730.

[10] L.T. Angenent, K. Karim, M. Al-Duhhan B.A. Wrenn, R. Espinosa, *Production of bioenergy and biochemicals from industrial and agricultural wastewater,* TRENDS in Biotechnology, vol.22 No.9 (2004).

[11] S. Papanikolaou, P. Ruiz-Sanchez , B. Pariset, F. Blanchard, M. Fick, *High production of 1,3-propanediol from industrial glycerol by a newly isolated Clostridium butyricum strain,* Journal of Biotechnology 77 (2000) 191-208.

[12] G. P. da Silva, M. Mack, J. Contiero*, Glycerol: A promising and abundant carbon source for industrial microbiology,* Biotechnology Adnances 27 (2009) 30-39.

[13] Herbert H. P. Fang, Hong Liu., *Effect of pH hydrogen production from glucose by a mixed culture,* Bioresource Technology (2002) 87-93.

[14] J. Gołębiowska, H. Kaszubiak, Z. Pędziwilk, W. Kaczmarek, *Microbiology exercises,* Poznan, (2001).

[15] K. Seifert, M. Waligorska, M. Wojtowski, M. Laniecki, *Hydrogen generation from glycerol in batch fermentation process.* International Journal of Hydrogen Energy, 34 (2009) 3671-78.

[16] M-L. Chong, N'A. A. Rahman, P. L. Yee, S. A. Aziz, R. A. Rahim, Y. Shirai, M. Hassan, *Effect of pH, Glucose and iron sulfate concentration on the yield of biohydrogen by Clostrdium butyricum EB6,* International Journal of Hydrogen Energy 34 (2009) 8859-8865.

[17] E. Wicher, M. Łaniecki, *Microbial hydrogen generation from waste glycerol,* Proceedings HYdrogen POwer - THeoretical and Engineering Solutions - International Symposium HYPOTHESIS VIII; April, Lisbon, Portugal (2009), p 5.

[18] G. P. da Silva, M. Mack, J. Contiero, *A promising and abundant carbon source for industrial microbiology,* Biotechnology Advances 27 (2009) 30-39.

[19] S. Papanikolaou, S. Fakas, M. Fick, I. Chevalot, M. Galiotou-Panayotou, M. Komaitis, I. Marc, G. Aggelis, *Biotechnological valorization of raw glycerol discharged after bio-diesel (fatty acid methyl esters) manufacturing process: Production of 1,3-propanediol, citric acid and single cell oil,* Biomass and Bioenergy 32 (2008) 60-71.

Continuous Hydrogen Production from Starch by Fermentation

Keigo Yasuda, **Shigeharu Tanisho**, Yokohama National University, Japan

Abstract

This study was investigated the effect of hydraulic retention time (HRT) on hydrogen production rate, hydrogen yield and the production rate of volatile fatty acid. The experiment was performed in a continuous stirred tank reactor (CSTR) with a working volume of 1 L by using a *Clostridium* sp. The temperature of the CSTR was regulated 37 °C. The pH was controlled 6.0 by the addition of 3 M of NaOH solution. Starch was used as the carbon source with the concentration of 30 g L^{-1}. Hydrogen production rate increased from 0.9 L-H_2 L-culture^{-1} h^{-1} to 3.2 L-H_2 L-culture^{-1} h^{-1} along with the decrease of HRT from 9 h to 1.5 h. Hydrogen yield decreased at low HRT. The major volatile fatty acids are acetic acid, butyric acid and lactic acid. The production rates of acetic acid and butyric acid increased along with the decrease of HRT. On the other hand, the rate of lactic acid was low at high HRT while it increased at HRT 1.5 h. The increase of the production rate of lactic acid suggested one of the reasons that hydrogen yield decreased.

1 Introduction

Biological H_2 production has been studied widely. Fermentative H_2 production, one of the biological H_2 productions, is promising compared with another biological H_2 production by photosynthetic organisms because it is possible to produce H_2 all day long without light. Continuous H_2 production by fermentation has been studied. There are some problems for the commercialization. One of the problems is H_2 productivity such as production rate and yield of H_2. Wu *et al*. reported that H_2 production rate reached 15 L L-culture^{-1} h^{-1} by using silicone immobilized sludge with self-flocculated under the condition of sucrose concentration 40 g-COD L-culture^{-1} and HRT 0.5h [1]. H_2 fermentation utilizes various sources such as wastewater [2], molasses [3] and palm oil mill effluent [4]. *Thermotoga maritime* attained 4 mol-H_2 mol-hexose^{-1}, the theoretical maximum yield of H_2, at 80 °C by batch cultivation, while H_2 production rate was 10 mmol L-culturee^{-1} h^{-1} [5]. However, almost all the H_2 yield reported is lower than 4 mol-H_2 mol-hexose^{-1}.

In this study, continuous H_2 production from starch was examined to investigate the effect of HRT on H_2 production.

2 Materials and Methods

Clostridium sp HN001 was used in this study. This bacterium was found by screening and isolated [6].

The culture medium contained starch 30.0 g, casamino acids 10.0 g, yeast extract 10.0 g, L-cysteine hydrochloride 0.3 g, thioglycolic acid 0.3 g $FeCl_2$ 0.1 g per 1 L of ion exchanged water. The culture was sterilized at 121 °C, 15 minutes.

Figure 1 shows the outline of experimental apparatus. A 1.0 L continuous stirred tank reactor was used. The volume of culture liquid was 0.5 L. The temperature was maintained at 37 ℃. The pH was automatically regulated by the addition of 3 M of NaOH solutions. The culture was stirred by a magnetic stirrer. The liquid level was controlled by using micro tube pomp. Feeding the medium at HRT 9 h started after appropriate period of batch fermentation. HRT was decreased from 9 h to 1.5 h when a steady state reached.

Product gases were collected in a bottle filled with 1 M of NaOH solution. The NaOH solution was replaced in accordance with the volume of H_2 and the replaced volume was measured by an electric scale.

The gases were analyzed by a gas chromatograph (SHIMADZU).

VFA was analyzed by a high performance liquid chromatograph (HITACHI, Ltd 655A), equipped with refractive index detector. The assay was analyzed by a packed column for organic acid analysis (HITACHI Chemical Co., Ltd. GL-C610-S). The carrier liquid was 0.1 % phosphoric acid at flow rate of 0.5 ml/min.

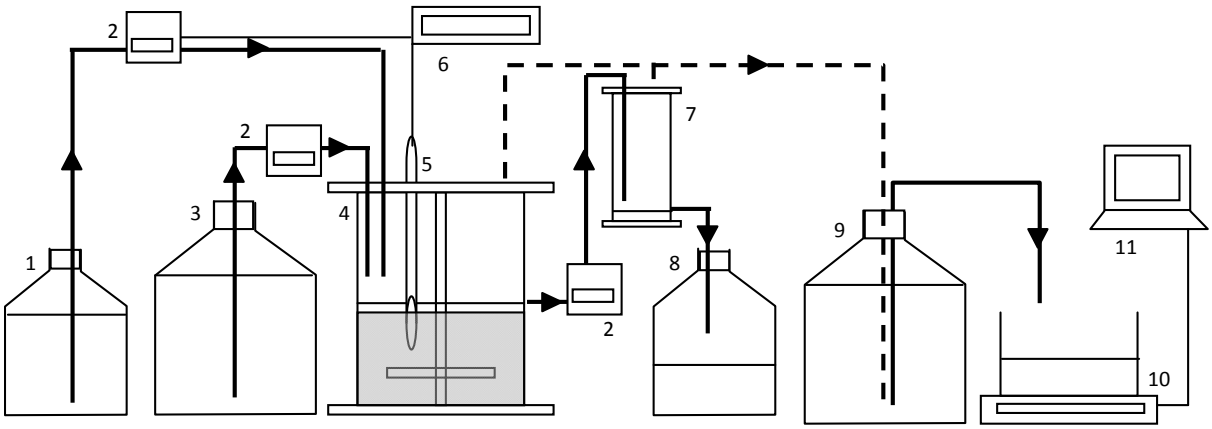

1. 1M NaOH tank 2. Peristric pump 3. Feed tank 4. Continuous stirred tank reactor 5. pH electric pole 6. pH controller 7. Gas liquid separator 8. Effluent tank 9. Gas tank 10. Electric scale 11. PC

Figure 1: The outline of experimental apparatus.

3 Results and Discussions

Figure 2 shows the effect of HRT on H_2 production rate and H_2 yield. H_2 production rate was 0.9, 1.2, 1.9 and 3.2 L L-culture^{-1} h^{-1} at HRT 9.0, 6.0, 3.0 and 1.5 h, respectively. H_2 yield was 2.0 mol mol-hexose^{-1} at HRT 9.0 and 6.0 h. However, it decreased to 1.5 and 1.3 mol mol-hexose^{-1} when HRT was shortened to 3.0 and 1.5 h, respectively.

Figure 3 shows the effect of HRT on butyrate, acetate and lactate production rate. Acetate production rate was 4.9, 7.3, 12.2 and 24.7 mmol L-culture^{-1} h^{-1} and butyrate production rate was 9.3, 13.4, 19.7, 46.1 mmol L-culture^{-1} h^{-1} when HRT was 9.0, 6.0, 3.0 and 1.5 h,

respectively. On the other hand, lactate production rate was relatively low when HRT was shortened from 9.0 to 3.0 h. However, it increased to 15.8 mmol L-culture^{-1} h^{-1} at HRT 1.5 h. The decrease of H_2 yield at short HRT has been reported [7, 8, 9]. As seen in the following equations from glucose by H_2 producing bacteria under anaerobic conditions, acetate and butyrate were produced with H_2 and lactate was produced without H_2.

$$C_6H_{12}O_6 + 2H_2O \rightarrow 2CH_3COOH + 2CO_2 + 4H_2$$
$$C_6H_{12}O_6 \rightarrow C_3H_7COOH + 2CO_2 + 2H_2$$
$$C_6H_{12}O_6 \rightarrow 2CH_3CHOHCOOH$$

One of the reasons that H_2 yield decreases seems lactate production. Wang *et al*. reported that H_2 yield decreases with the addition of acetate [10]. Zheng *et al*. also reported that H_2 yield decreases with the addition of butyrate [11]. The metabolic shifts cause the decrease of H_2 yield in this study. H_2 partial pressure inhibits H_2 productivity [12]. Mizuno *et al*. achieved a 68% increase of H_2 yield by N_2 sparging [13]. Kim *et al*. reported that H_2 yield was improved from 0.77 mol mol-hexose^{-1} to 1.68 mol mol-hexose^{-1} by gas sparging of N_2 and CO_2, respectively [14]. Therefore continuous H_2 production at short HRT with the decrease of H_2 partial pressure would be future work to improve H_2 productivity.

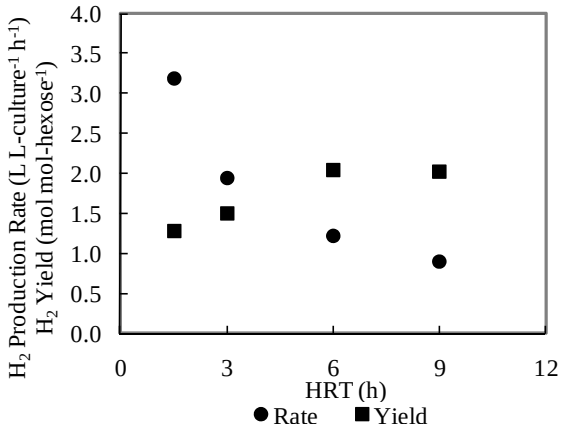

Figure 2: The effect of HRT on H_2 production rate and H_2 yield.

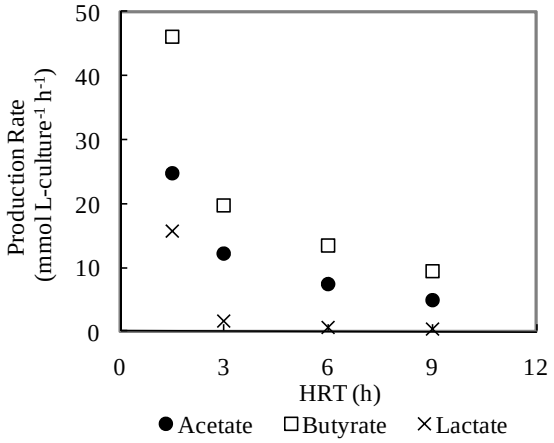

Figure 3: The effect of HRT on VFA production rate.

4 Conclusions

In this study, the following conclusions can be drawn:

- H_2 production rate increased from 0.9 to 3.2 L L-culture^{-1} h^{-1} when the HRT was shortened from 9.0 to 1.5 h.
- H_2 yield was 2.0 mol mol-hexose^{-1} at HRT 9.0 and 6.0 h and decreased to 1.3 mol mol-hexose^{-1} along with the decrease of HRT from 6.0 to 1.5 h. The reason was the shift of metabolites.

References

[1] Wo S-Y, Hung C-H, Lin C-N, Chen H-W, Lee A-S, Chang J-S. Fermentative hydrogen production and bacterial community structure in high-rate anaerobic bioreactors containing silicone-immobilized and self-flocculated sludge. *Biotechnol Bioeng* 2006; 93: 934-946

[2] Ginkel SWV, Oh S-E, Logan BE. Biohydrogen gas production from processing and domestic wastewaters. *Int J Hydrogen Energy* 2005; 30: 1535-1542

[3] Ishiwata Y, Tanisho S. Continuous hydrogen production from molasses by the bacterium *Enterobacter aerogenes. Int J Hydrogen Energy* 1994; 19: 807-812

[4] Atif AAY, Fakhru'l-Razi A, Ngan MA, Morimoto M, Iyuke SE, Veziroglu NT. Fed batch production of hydrogen from palm oil mill effluent using anaerobic microflora. *Int J Hydrogen energy* 2005; 29: 1393-1397

[5] Schroder C, Selig M, Schonheit P. Glucose fermentation to acetate, Co2 and H2 in the anaerobic hyperthermophilic eubacterium *Thermotoga maritima*: involvement of Embden-Meyerhof pathway. *Arch Microbiol* 1994; 161: 460-470

[6] Nishiyama H, Tanisho S. Fermentative hydrogen production by a newly isolated mesophilic bacterium HN001. Proceedings of 16th World Hydrogen Energy Conference in CD-ROM

[7] Yu H, Zhu Z, Hu W, Zhang H. Hydrogen production from rice winary wastewater in an upflow anaerobic reactor by using mixed anaerobic cultures. *Int J Hydrogen Energy* 2002; 27: 1359-1365

[8] Lee K-S, Lin P-J, Fangchaing K, Chang J-S. Continuous hydrogen production by anaerobic mixed microflora using a hollow-fiber microfiltaration membrane bioreactor. *Int J Hydrogen Energy* 2007; 32: 950-957

[9] Chang J-J, Wu J-H, Wen F-S, Hung K-Y, Chen Y-T, Hsiao C-L, Lin C-Y, Huang C-C. Molecular monitoring of microbes in a continuous hydrogen-producing systems with different hydraulic retention time. *Int J Hydrogen Energy* 2008; 33: 1579-1585

[10] Wang Y, Zhao Q-B, Mu Y, Yu H-Q, Harada H, Li Y-Y. Biohydrogen production with mixed anaerobic cultures in the presence of high-concentration of acetate. *Int J Hydrogen Energy* 2008; 33: 1164-1171

[11] Zheng X-J, Yu H-Q,. Inhibitory effects of butyrate on biological hydrogen production with mixed anaerobic cultures. *J Environ Manage* 2005; 74: 65-70

[12] Chung k-T. Inhibitory effects on H_2 on growth of *Clostridium cellobioparum. Appl Environ Microbiol* 1976; 31: 342-348

[13] Mizuno O, Dinsdale R, Hawks FR, Hawkes DL, Noike T. Enhancement of hydrogen production from glucose by nitrogen sparging. *Bioresource Technol*. 2000; 73: 59-65

[14] Kim D-H, Han S-K, Kim S-H, Shin H-S. Effect of gas sparging on continuous fermentative hydrogen production. *Int J Hhdrogen Energy* 2006; 31: 2158-2169

A High Yield, Hydrogen Producing, Bacterial Community Enriched from Anaerobic Digester Leachate

Hang Zheng, **Cathryn O'Sullivan**, **William Clarke**, Biomass BioEnergy Group, School of Civil Engineering, University of Queensland, Australia
Raymond Zeng, Advanced Water Management Centre, University of Queensland
Mikel Duke, Institute of Sustainability and Innovation, Victoria University, Australia

1 Introduction

Hydrogen is a carbon-free energy source with high energy density (based on per unit of mass) [1]. Beyond that, it produces only water when combusted. In light of this, hydrogen is regarded as a promising energy carrier for the future.

The most widely used method for hydrogen production is the steam reforming [2], which reforms natural gas into hydrogen and carbon dioxide. This process needs extensive energy supply (electricity) and fossil fuels (natural gas), which makes it an environmentally unfriendly method. In order to make hydrogen a truly sustainable and carbon-free energy source, its production has to avoid the usage of fossil fuel based feedstocks.

In light of the above, fermentative hydrogen production from organic waste is regarded as the most feasible method for hydrogen production [3]. The theoretical maximum hydrogen yield from the fermentation of glucose is 4 mole-H_2/mole-glucose with acetate as the end product [4]. However, this yield has only been reported in a study using pure culture [5], which is not possible when working with real waste streams. To date, the reported hydrogen yields usually vary from 0.5-2.2 mole-H_2/mole-hexose by using mixed cultures [6]. Fermentation of glucose to other end products results in a lower theoretical yield, with butyrate yielding only 2 mole-H_2/mole-glucose whilst fermentation to ethanol yields no hydrogen [7].

The hydrogen yield can be improved by increasing the operating temperature. Several studies have shown that operation in thermophilic temperature ranges improves hydrogen yields relative to mesophilic temperatures due to higher reaction rates and decreased problems with contamination by methanogens [8, 9].

Therefore, thermophilic temperatures (65°C) were applied in this study to improve the hydrogen yield in batch experiments.

2 Materials and Method

2.1 Inoculums and substrate

Biological hydrogen production was assessed in 120 mL serum bottles with a working volume of 50 mL. An inoculum of hydrogen producing organisms was obtained by enriching an original culture from the leachate phase of an anaerobic digester treating mixed organic waste at a temperature of 47^{o}C for biogas production. The culture was enriched through successive generations of batch cultures grown on glucose and media as described below.

Glucose (0.5 g/l) was used as substrate in all tests with nutrient solution containing minerals [10]. The solution was buffered with 4.1 g/l (20 mM) 3-Morpholinopropanesulfonic acid (MOPS) to pH 5.5.

2-Bromoethanosulfonate (BES, 20 mM) addition was used in the first 3 digestions (each time a reactor is started with fresh media and inoculated, it is considered a new digestion) in order to inhibit the growth of methanogens and associated CH_4 production. After the third transfer, BES addition was stopped completely. Erythromycin and Chloramphenicol (125 µg/ml for each) was used to inhibit the growth of bacterium.

2.2 Analysis

Hydrogen in the headspace of batch reactors was sampled by using a syringe with a pressure lock (SGE Analytical Science, Australia), and then analysed by gas chromatography (GC), which has been previously described elsewhere [11].

Liquid samples were taken after the gas sampling and filtrated with 0.22 µm filters (Milipore Corporation, USA). Glucose, formate, lactate and succinate were analyzed by using high performance liquid chromatography (HPLC). VFAs, and alcohols were analyzed by using GC, which has been previously described elsewhere [11].

3 Results and Discussion

An average yield of 2.49±0.09 mol-H_2/mol-glucose was obtained in the initial pH 5.5 batch experiments. The 3.12% error of the COD balance (Table 1) shows that the measurements were accurate.

Table 1: COD balance of initial pH 5.5 batch experiments. All units are in mg·COD except H_2 yield is in the unit of mol-H_2/mol-glucose. Carbon balances for all the batches were within 97% (data not shown). Lactate, formate, succinate, propionate and valerate were not detected in all the batches.

	Glucose Consumed	A.A.	B.A.	ETOH	BTOH	H_2	Biomass	Balance	H_2 yield
Average	-27.23	6.44	5.66	5.78	1.65	5.66	2.59	-1.04	2.49
Percentage (%)	-100	23.63	20.77	21.22	6.06	20.78	9.50	-3.84	
Stdev (n=5)	0	0.32	0.82	0.86	0.18	0.21	0.27	0.14	0.09

* Notations: A.A., acetic acid; B.A., butyric acid; ETOH, ethanol; BTOH, butanol

As shown in the Table 2, the measured hydrogen production was always higher than the yield associated with fermentation products by 30%. This suggested that the high hydrogen yields were associated with other path-ways which give a higher yield than the well known acetate fermentation path-way, or the continued oxidation of acetate to CO_2 and hydrogen in a process known as acetate oxidation.

Table 2: Summary of yield of acetate, butyrate, and hydrogen and in comparison with calculated hydrogen from experimental acetate and butyrate values.

	Measurements				Calculated H_2 from			
	Acetate (mmol)	**Butyrate (mmol)**	**H_2 (mmol)**		**Acetate (mmol)**	**Butyrate (mmol)**	**Sub-total (mmol)**	**Delta H_2 (Mea-Cal) (mmol)**
Average	0.10	0.04	0.35		0.20	0.07	0.27	0.08
stdev (n=5)	0.005	0.008	0.01		0.01	0.02	0.02	0.02

Since the inoculums were from a methane producing digester, it is possible that the methanogens are still there to oxidize VFAs, e.g. acetate and butyrate. In order to confirm if the missing acetate and butyrate were due to the methanogens, a mixture of two anti-biotics were added to achieve final concentrations of 125 µg/ml of Erythromycin and 125 µg/ml of Chloramphenicol in the media. This should kill all bacterium and get rid of the effects of bacterium in the culture (Figure 1, top). No hydrogen or methane was produced in those batches. Analysis show that glucose was not consumed at all (data not shown).

While this was an expected result, a surprising result was achieved when 2-Bromothanosulfonate (BES, 20mM) was applied to the serum bottles to inhibit possible methanogens that has survived through the enrichments. Tiny amount of hydrogen has been produced on the 1st day but no more hydrogen or methane was produced after the 1st day in those batches (Figure 1, bottom). Further analysis show that glucose was not consumed at all (data not shown).

After washing away the inhibitors, hydrogen yield was again retrieved (Figure 1). This result suggests that the enriched culture contains bacterium and possibly methanogens. This indicates that both bacterium and the archaea are needed to give a high hydrogen yield in the glucose fermentation. The presence of the two groups of microorganisms might improve the energy efficiency through the interspecies cooperation, which made the acetate oxidation possible. Further work is needed to explore the mechanisms.

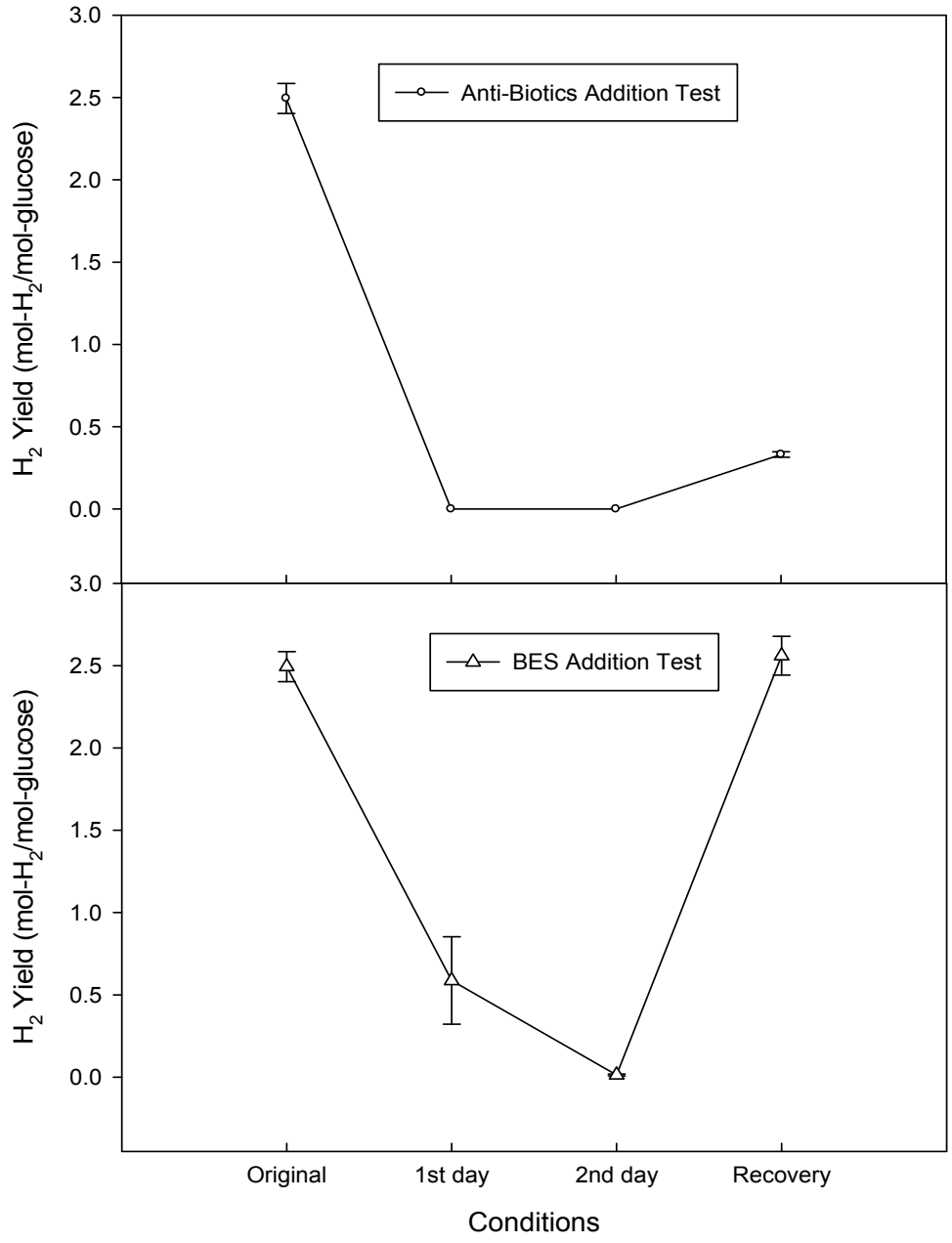

Figure 1: Hydrogen yields of batch experiments after application of antibiotics (top) and BES (bottom).

4 Conclusion

A culture has been enriched for fermentative hydrogen production. The hydrogen yield achieved was 2.49 mol-H_2/mol-glucose.

The applications of inhibitors for bacterium and methanogens showed that the enriched culture contains bacterium and methanogens and it needs the presence of both the two to give the high hydrogen yield from degradation of glucose.

In all, this study suggests that high hydrogen yields can be achieved if favourable conditions are provided.

References

[1] Midilli, A., M. Ay, I. Dincer, and M.A. Rosen, On hydrogen and hydrogen energy strategies I: current status and needs. Renewable & Sustainable Energy Reviews, 2005. 9(3): p. 255-271.

[2] Elam, C.C., C.E.G. Padro, G. Sandrock, A. Luzzi, P. Lindblad, and E.F. Hagen, Realizing the hydrogen future: the International Energy Agency's efforts to advance hydrogen energy technologies. International Journal of Hydrogen Energy, 2003. 28(6): p. 601-607.

[3] Benemann, J., Hydrogen biotechnology: Progress and prospects. Nature Biotechnology, 1996. 14(9): p. 1101-1103.

[4] Nandi, R. and S. Sengupta, Microbial production of hydrogen: An overview. Critical Reviews in Microbiology, 1998. 24(1): p. 61-84.

[5] Schroder, C., M. Selig, and P. Schonheit, Glucose Fermentation to Acetate, Co2 and H-2 in the Anaerobic Hyperthermophilic Eubacterium Thermotoga-Maritima - Involvement of the Embden-Meyerhof Pathway. Archives of Microbiology, 1994. 161(6): p. 460-470.

[6] Hawkes, F.R., I. Hussy, G. Kyazze, R. Dinsdale, and D.L. Hawkes, Continuous dark fermentative hydrogen production by mesophilic microflora: Principles and progress. International Journal of Hydrogen Energy, 2007. 32(2): p. 172-184.

[7] Hawkes, F.R., R. Dinsdale, D.L. Hawkes, and I. Hussy, Sustainable fermentative hydrogen production: challenges for process optimisation. International Journal of Hydrogen Energy, 2002. 27(11-12): p. PII S0360-3199(02)00090-3.

[8] Cheong, D.Y. and C.L. Hansen, Feasibility of hydrogen production in thermophilic mixed fermentation by natural anaerobes. Bioresource Technology, 2007. 98(11): p. 2229-2239.

[9] O-Thong, S., P. Prasertsan, N. Intrasungkha, S. Dhamwichukorn, and N.K. Birkeland, Optimization of simultaneous thermophilic fermentative hydrogen production and COD reduction from palm oil mill effluent by Thermoanaerobacterium-rich sludge. International Journal of Hydrogen Energy, 2008. 33(4): p. 1221-1231.

[10] Raghoebarsing, A.A., A. Pol, K.T. van de Pas-Schoonen, A.J.P. Smolders, K.F. Ettwig, W.I.C. Rijpstra, S. Schouten, J.S.S. Damste, H.J.M. Op den Camp, M.S.M. Jetten, and M. Strous, A microbial consortium couples anaerobic methane oxidation to denitrification. Nature, 2006. 440(7086): p. 918-921.

[11] Zheng, H., R.J. Zeng, C. O'Sullivan, and W.P. Clarke, Biohydrogen Production from Acetate Oxidation in association with Glucose Fermentation at Thermophilic Conditions (65°C) - A new concept for studying the mixed cultures hydrogen fermentation. Environmental Science & Technology, 2010(Submitted).

Non-Thermal Production of Pure Hydrogen from Biomass: HYVOLUTION

Pieternel A.M. Claassen, Truus de Vrije, Emmanuel G. Koukios, Ed W.J. van Niel, Ebru Özgür, İnci Eroğlu, Isabella Nowik, Michael Modigell, Walter Wukovits, Anton Friedl, Dominik Ochs, and Werner Ahrer

Abstract

HYVOLUTION is the acronym for the Integrated Project (IP) “Non-Thermal Production of Pure Hydrogen from Biomass,” which was defined in the 6th EU Framework Programme on Research, Technological Development and Demonstration, Priority 6.1 Sustainable Energy Systems. This IP started on 1 January 2006 and will end on 31 December 2010. Its aim, “Development of a blueprint for an industrial bioprocess for decentral hydrogen production from locally produced biomass,” adds to the number and diversity of hydrogen production routes giving greater security of supply at the local and regional level. Moreover, this IP contributes a complementary strategy to fulfill the increased demand for renewable hydrogen expected in the transition to the Hydrogen Economy. The novel approach adopted in the project is based on a combined bioprocess employing thermophilic and phototrophic bacteria, to provide the highest hydrogen production efficiency in small-scale, cost-effective industries. In HYVOLUTION, 10 EU countries, Turkey, Russia, and South Africa are represented to assemble the critical mass needed to make a breakthrough in cost-effectiveness.

How Environmental Parameters Controls Metabolic Pathways to Hydrogen

Karin Willquist, Ahmad Zeidan, **Ed van Niel**

1 Introduction

Anthropogenic CO_2 emissions to the atmosphere have generally been recognized as the major contribution to global warming and the associated climate changes. Therefore, several measures have been made to decrease the CO_2 emissions; e.g., the European Union strives at substituting 20% of the liquid fuel with biofuels by 2020. In recent years, much effort has been devoted to rendering biofuel production economically competitive with regard to fossil fuels. In this quest, the choice of the raw material is of central concern. First-generation biofuels are produced from sucrose and starch-rich material, which are also used for human consumption - a fact that drives up market prices. Based on this, more focus should be directed to second-generation biofuels produced from lignocellulosics materials as well as domestic and industrial wastes, which would significantly reduce the cost of the fuel, leading to it becoming competitive. Moreover, lignocellulosics constitute the most naturally abundant raw materials [1].

Biohydrogen is a typical example of an environmentally friendly, second-generation biofuel. It has a high molar energy content and it can be produced from both lignocellulosic and waste materials [2-5]. When sugar-based materials are used to produce H_2, the biohydrogen process is called dark fermentation. For a cost-effective dark fermentation process, high H_2 yields have to be obtained at relatively elevated partial H_2 pressures (P_{H2}) to eliminate the need for continuous stripping of the produced H_2 from the bioreactor and accordingly reduce the central cost of subsequent gas upgrading [6]. The current status for mesophilic co-cultures is an H_2 yield of ≤ 2 mol/mol hexose, and thus a substrate-conversion efficiency of merely 17%. In addition, these yields are usually obtained at low P_{H2} [7]. These low yields and the requirement for a low P_{H2} are major obstacles that need to be overcome before biohydrogen production as we know it today can be industrially feasible [7]. As for yields, a theoretical maximum of 4 mol H_2 per mol hexose can be obtained by using clostridia, thermophilic bacteria or Archaea.

The genus *Caldicellulosiruptor* consists of extreme thermophilic bacteria which have high potential for industrial biological hydrogen production due to their ability to: i) produce high yields of hydrogen (>3.6 moles of hydrogen per mole of C6 sugar), ii) metabolise a wide spectrum of carbohydrates including both pentose and hexose sugars, and iii) break down hemicelluloses and many other complex polysaccharides. The genome of the most studied member of this genus, *C. saccharolyticus*, has been recently sequenced enabling an increased insight into its metabolic network [8].

Interestingly, *C. saccharolyticus* can produce high H_2 yields [10] and are at the same time insensitive to relatively high P_{H2} (Willquist, K. Zeidan A., Pawar S. and. van Niel E.W.J, manuscript in preparation). However, its tolerance to different environmental parameters

needs to be further explored. This study is focusing on the physiology of *C. saccharolyticus* and the effect of enviromics on its growth and H_2 yields. It aims at unraveling several of the physiological characteristics which, in many perspectives, make *C. saccharolyticus* a superior H_2 cell factory.

2 Hydrogenomics

A major advantage of using *C. saccharolyticus* as a model H_2 cell factory is that its genome has been sequenced and protocols for genome-wide analysis of its transcriptome have been developed, thus facilitating the understanding of its physiology [8]. It has a relatively small genome with 2,970 kbp and 2,760 protein-coding open reading frames (ORF). From the genome-curation project, several new insights were obtained such as the fact that *C. saccharolyticus* possesses an unusually high number of transposons and transposable derivatives, as opposed to other organisms [8]. Since transposons increase the number of gene variations in the genome, a large amount can enhance the adaptive ability of this organism. Such an adaptation has obvious benefits process-wise, since it allows *C. saccharolyticus* to grow under a variety of environmental conditions. However, this may also have a negative impact on the stability of the process.

The bioinformatics study also shows that *C. saccharolyticus* possesses several polysaccharide-degrading enzymes, an unusually high number of ATP binding cassette (ABC) transporters [8] for the uptake of monomers and dimers and only one phosphotransferase (PTS) system, which is believed to be used for fructose transport [8, 9]. In addition, it possesses a complete gene setup for the Embden-Meyerhof-Parnas (EMP) pathway and the non-oxidative part of the pentose phosphate pathway (PPP; [8, 10]) to convert these sugars to building blocks and energy. No essential genes for the Entner Doudoroff pathway (EDP) have been found [8, 10], and this observation has been supported by ^{13}C-NMR analysis, demonstrating the EMP as the sole pathway for glucose oxidation in *C. saccharolyticus* [10]. Overall, the genome analysis revealed that *C. saccharolyticus* is well equipped for utilizing starch and lignocellulytic materials [8]. These indications are well in line with the growth analysis results which confirm the wide carbon utilization spectrum and its ability to grow and produce H_2 from complex lignocellulosic material (e.g. Miscanthus hydrolysate; [2]) and paper waste [11].

3 Effect of Dissolved H_2 Concentration on Hydrogen Yield and Productivity

For practical reasons the P_{H2} is generally used as a measure for H_2 tolerance. The currently quoted critical P_{H2}, defined as the partial H_2 pressure at which lactate formation is initiated, in *C. saccharolyticus* is 10-20 kPa [12]. This critical P_{H2} was determined in batch cultivations on sucrose with no gas sparging in a closed bioreactor. However, in similar experiments, using the same conditions but with xylose as the substrate, the P_{H2} in the headspace reached 60 kPa before the metabolism is partly shifted to lactate (Willquist K., Zeidan A., Pawar S. and van Niel E.W.J., manuscript in preparation). In addition, novel results have shown that during batch growth of *C. saccharolyticus* on glucose (5 g/L), lactate formation was triggered in the deceleration phase (the transition phase between logarithmic and stationary growth phases), which was independent of the P_{H2} (Willquist, Zeidan, Pawar and van Niel, manuscript in

preparation), i.e. during sparging with N_2, lactate formation was triggered at a P_{H2} of 6.3 kPa, whereas without sparging exponential growing cells initiated lactate formation at a P_{H2} of 30 kPa. Moreover, growth and H_2 production were still observed in continuous cultures at a low dilution rate ($0.05h^{-1}$) at a P_{H2} of 67 kPa. However, at this high P_{H2}, the metabolism had shifted predominantly (57%) to lactate, thereby decreasing the H_2 productivity and thus the dissolved H_2 concentration substantially (Ljunggren, Willquist, Zacchi and van Niel, submitted to Biotech. Biofuels).

In a comparative study on another *Caldicellulosiruptor* species, namely *C. owensensis,* we have also found a clear sugar-dependent H_2 tolerance pattern. In this organism, however, a dramatic increase in lactate production was observed when it was grown under elevated P_{H2} on xylose but not on glucose. As compared to acetate, the formation of one mole of lactate is accompanied by (i) the consumption of an extra mole of NADH, (ii) production of one mole less of both ATP and reduced ferredoxin and, most importantly, (iii) production of no H_2. Accordingly, the induction of lactate formation is most probably a regulatory response to changes in the energy and/or redox state of the cells at different growth phases and on different carbon sources.

Due to the lack of a clear pattern in the critical P_{H2} values found for each fermentation condition, one may wonder whether P_{H2}, a parameter for H_2 in the gas phase, is an appropriate measure of the critical H_2 concentration for growth and lactate formation. Since the cells are in the liquid phase, they are confronted with the dissolved H_2, which therefore should be a better choice as a parameter. In a recent work (Ljunggren, Willquist, Zacchi and van Niel, submitted to Biotech. Biofuels) we have demonstrated that the dissolved H_2 concentration is indeed a better parameter, being a function of H_2 productivity and the mass transfer rate, rather than the P_{H2}. The mass transfer rate is, in turn, a function of the gas sparging rate and the stirring rate. In addition, cultivations performed in closed systems without sparging have lower mass transfer rates. Thus, in that case the dissolved H_2 concentration and the P_{H2} are even further from equilibrium (Henry constant) than in a sparged and open system. This means that the critical P_{H2} determined in a closed system gives a more underestimated value than when determined in an open system. This corresponds well with the data acquired in our studies.

As a consequence of H_2 saturation in the liquid, the cells will decrease their H_2 productivity to avoid exceeding the critical dissolved H_2 concentration at which growth is inhibited, for instance by shifting the metabolism to lactate to re-oxidize NADH. Consequently, the NADH/NAD ratios remained low in continuous cultures even in the absence of sparging (Willquist K., Zeidan A., Pawar S. and van Niel E.W.J., manuscript in preparation).

4 Effect of CO_2 as a Sparging Gas on Growth and Hydrogen Production

As described above H_2 yields and productivities are influenced by the dissolved H_2 concentration. As a consequence, several studies have been carried out to remove H_2 from the liquid phase with an appropriate sparging gas [13]. Sparging increases the mass transfer of H_2 from the liquid to the gas phase (Ljunggren M., Willquist K., Zacchi G. and van Niel E.W.J., submitted to Biotech. Biofuels), which generally results in higher H_2 yields [14]. Although N_2 is commonly used as a sparging gas for lab-scale H_2 production, it is not a cost-

effective at an industrial scale since it is inert, thus difficult to remove from the effluent gas stream [6]. Instead, CO_2 might be an appropriate candidate since it can be more easily separated from H_2 and since it is already a product of the same fermentation process [6].

However, CO_2 is an inadequate choice of sparging gas for H_2 production by *C. saccharolyticus* as it negatively influences its growth rates and H_2 productivity [13]. Higher P_{CO2} values increase the concentration of dissolved CO_2, which hydrolyzes to bicarbonate and protons. This requires the addition of larger amounts of a caustic agent to maintain the fermentation pH, which in total contributes to an increased osmotic pressure and a higher environmental burden [13].

5 Effect of Osmotic Pressure on Growth and Metabolic Shift

As discussed above, *C. saccharolyticus* has several advantages as a H_2 cell factory such as its elevated H_2 yields, its relatively large tolerance to high P_{H2}, and the ability to grow on complex sugars. However, it also presents some major disadvantages which should be considered before it can be used industrially. Primarily, its sensitivity to osmotic pressures should be addressed. Growth of *C. saccharolyticus* is inhibited by osmolarities above 0.218 ± 0.005 osm/kg H_2O [13]. The critical molarity when growth is completely ceased is estimated to be 400-425 mM [12]. To avoid growth inhibition, sparging with CO_2 should be avoided and a maximum glucose concentration of 5 g/L should be used. The latter would obviously have a negative effect on the productivity. In addition, osmolaritiesabove 0.218 ± 0.005 osm/kg H_2O were found to induce cell lysis in *C. saccharolyticus* [13]. Increased protein and DNA concentrations in the culture supernatant were strong indications of lysis, but it remains to be investigated what can be the cause.

Interestingly, an increased osmolarity also triggers lactate formation in *C. saccharolyticus* (Ljunggren M., Willquist K., Zacchi G. and van Niel E.W.J., submitted to Biotech. Biofuels). The effect of osmotic pressure could be that elevated osmolarities inhibit growth in *C. saccharolyticus* [13]. This leads to a metabolic shift to lactate due to an induction of lactate dehydrogenase (LDH) activity, which will be explained below.

6 Regulation of Metabolic Shift to Lactate

During non-limited growth conditions, acetate and hydrogen are the soleproducts in *C. saccharolyticus* cultures, hence the superior H_2 yields. However, as described above, when the growth is inhibited and the cells enter a deceleration phase, the metabolism is partly directed to lactate [15]. To describe this observation a kinetic model of LDH activity was developed [15] and the influence of vital metabolites such as ATP, PPi, NADH and NAD were determined ([15]; Bielen A., Willquist K., Engman J., van der Oost J, van Niel E. W. J. and Kengen S.W.M., accepted for publication in FEMS Microb. Lett.).

Kinetic analysis of LDH activity revealed that the enzyme is regulated through i) competitive inhibition by pyrophosphate (PPi, ki=1.7mM) and NAD (ki=0.43mM) and ii) allosteric activation by FBP (300%), ATP (160%) and ADP (140%). In addition, metabolite analysis showed that the ATP/PPi decreased by an order of magnitude during the deceleration phase Bielen A., Willquist K., Engman J., van der Oost J, van Niel E. W. J and Kengen S.W.M., accepted for publication in FEMS Microb. Lett.) resulting in an induction of LDH activity [15].

Moreover, the decrease in growth resulted in a sudden increase in NADH/NAD ratio and subsequently decrease in the same as a result of an increased lactate flux [15]. The activation of LDH by ATP indicates that *C. saccharolyticus* uses LDH as a means to adjusts its flux of ATP and NADH production.

Other tools used in this study include metabolic flux analysis and pathway- as well as genome-wide mathematical modelling.

7 H_2 Production by Designed Co-cultures of Caldicellulosiruptor Species

Although using an undefined microbial consortium is a common practice during fermentative H_2 production, little attention has been given to using a mixture of known organisms in a defined co-culture. The usefulness of applying *C. saccharolyticus* in biological H_2 production was brought into a wider context through testing the performance of designed co-cultures of this bacterium with other members of the genus, including *C. owensensis* and *C. kristjanssonii*. The fermentations were carried out on a mixture of glucose and xylose, the major sugars in lignocellulosic hydrolysates. The H_2 yield obtained with *C. saccharolyticus*–*C. kristjanssonii* co-culture was approaching the maximum theoretical stoichiometry (3.8±0.2 mol H_2/ mol hexose equivalent), and was significantly higher than that of the pure culture of either organism. This suggests the existence of synergy between both organisms on hydrogen production. In addition, a number of other potential advantages should be expected by using a co-culture instead of a pure organism, including an increased probability of biofilm formation as well as extending the spectrum of substrate utilization. However, these experiments were carried out in batch mode and the stability of the co-culture in a continuous system remained questionable. Accordingly, we have developed a quantitative real-time PCR protocol for monitoring each species in the co-culture and it is currently being used to assess the possibility of their co-existence in a continuous system under carbon and non-carbon limitation. This is particularly important since in practical application chemostat conditions are more likely to be used for H_2 production.

References

[1] Claassen, P.A.M., et al., *Utilisation of biomass for the supply of energy carriers.* Appl. Microbiol. Biotechnol., 1999. **52**(6): p. 741-755.

[2] de Vrije, T., et al., *Efficient hydrogen production from the lignocellulosic energy crop Miscanthus by the extreme thermophilic bacteria Caldicellulosiruptor saccharolyticus and Thermotoga neapolitana.* Biotech. Biofuels., 2009. **2**(12): p. 12.

[3] Liu, D., R.J. Zeng, and I. Angelidaki, *Hydrogen and methane production from household solid waste in the two-stage fermentation process.* Water Res., 2006. **40**(11): p. 2230-6.

[4] Levin, D.B., et al., *Challenges for biohydrogen production via direct lignocellulose fermentation.* International Journal of Hydrogen Energy, 2009. **34**(17): p. 7390-7403.

[5] Ivanova, G., G. Rakhely, and K.L. Kovacs, *Hydrogen production from biopolymers by Caldicellulosiruptor saccharolyticus and stabilization of the system by immobilization.* International Journal of Hydrogen Energy, 2008. **33**(23): p. 6953-6961.

[6] van Groenestijn, J.W., et al., *Energy aspects of biological hydrogen production in high rate bioreactors operated in the thermophilic temperature range.* Int. J. Hydrogen Energy, 2002. **27**(11-12): p. 1141-1147.

[7] Hallenbeck, P.C. and D. Ghosh, *Advances in fermentative biohydrogen production: the way forward?* Trends Biotechnol., 2009. **27**(5): p. 287-97.

[8] van de Werken, H.J.G., et al., *Hydrogenomics of the extremely thermophilic bacterium Caldicellulosiruptor saccharolyticus.* Appl. Environ. Microbiol., 2008. **74**(21): p. 6720-6729.

[9] Van Fossen, A.L., et al., *Carbohydrate utilization patterns for the extremely thermophilic bacterium Caldicellulosiruptor saccharolyticus reveal broad growth substrate preferences.* Appl. Environ. Microbiol., 2009.

[10] de Vrije, T., et al., *Glycolytic pathway and hydrogen yield studies of the extreme thermophile Caldicellulosiruptor saccharolyticus.* Appl Microbiol Biotechnol, 2007. **74**(6): p. 1358-1367.

[11] Kadar, Z., et al., *Hydrogen production from paper sludge hydrolysate.* Appl. Biochem. Biotechnol., 2003. **105 -108**: p. 557-66.

[12] van Niel, E.W.J., P.A.M. Claassen, and A.M.J. Stams, *Substrate and product inhibition of hydrogen production by the extreme thermophile, Caldicellulosiruptor saccharolyticus.* Biotechnol. Bioeng., 2003. **81**(3): p. 255-62.

[13] Willquist, K., P.A.M. Claassen, and E.W.J. van Niel, *Evaluation of the influence of CO_2 on hydrogen production by Caldicellulosiruptor saccharolyticus.* Int. J. Hydrogen Energy, 2009. **34**(11): p. 4718-4726.

[14] Kraemer, J.T. and D.M. Bagley, *Improving the yield from fermentative hydrogen production.* Biotechnol. Lett., 2007. **29**(5): p. 685-695.

[15] Willquist, K. and E.W.J. van Niel, *Lactate formation in Caldicellulosiruptor saccharolyticus is regulated by the energy carriers pyrophosphate and ATP.* Metab. Eng., 2010.

Process Investigations for Development of an Advanced Bioreactor System for Thermophilic H_2 Fermentations

Wolfgang Schnitzhofer, Innovative Energy Systems, Steyr-Gleink, Austria
Walter Wukovits, **Anton Friedl**, University of Technology, Vienna, Austria
Werner Ahrer, **Christian Peintner**, Profactor GmbH, Steyr-Gleink, Austria

1 Introduction

Hydrogen production via extreme thermophilic fermentation (70°C) of biomass has several advantages above mesophilic fermentations. The outstanding characteristic is the high hydrogen yield, which can reach nearly the theoretical amount of 4 moles H_2 per mole of hexose. Another advantage is the repression of methanogenic microorganisms, which consume the produced hydrogen, and the elimination of pathogenic organisms. Nevertheless there are several problems, which have to be reconsidered in order to set up a successful industrial process, like the product inhibition by the generated hydrogen, the rather low cell densities and the sensitivity towards high substrate as well as metabolite concentrations. The hydrogen partial pressure is conventionally reduced by applying stripping with inert gas [1, 2], which is a non economical method for bigger scales. To overcome hydrogen inhibition, different methods as vigorous stirring or recirculation have been investigated before [3]. In this work the effect of underpressure in order to reduce hydrogen partial pressure as well as the insertion of porous solid particles was studied, which are supposed to enforce bubble initiation and to drive the release of hydrogen from the liquid. This work is part of [4], an Integrated Project supported by the European Commission under the 6th Framework Program.

2 Materials and Methods

2.1 Organism and medium

The strain Caldicellulosiruptor saccharolyticus (DSM 8903) was obtained from Deutsche Sammlung von Mikroorganismen und Zellkulturen (DSMZ, Braunschweig, Germany).

The medium used for the experiments contained (per L): 5 g glucose, 0.9 g NH_4Cl, 0.75 g KH_2PO_4, 1.49 g K_2HPO_4, 1 g yeast extract, 0.4 g $MgCl_2 \cdot 6H_2O$, 0.6 g L-cysteine, 2.5 mg $FeCl_3 \cdot 6H_2O$ and 1 ml trace element solution, containing per L: 13 ml HCl 6M, 1.5 g $FeCl_2 \cdot 4H_2O$, 70 mg $ZnCl_2$, 100 mg $MnCl_2 \cdot 4H_2O$, 6 mg H_3BO_3, 190 mg $CoCl_2 \cdot 6H_2O$, 2 mg $CuCl_2 \cdot 2H_2O$, 24 mg $NiCl_2 \cdot 6H_2O$, 36 mg $Na_2MoO_4 \cdot 2H_2O$, 15 mg $Na_2WO_4 \cdot 2H_2O$, 15 mg $Na_2SeO_4 \cdot 5H_2O$.

For sterilization the medium was autoclaved for 20 minutes at 121 °C.

2.2 Reactor set-up

For the fermentations a continuously stirred tank reactor (Biostat BPlus, Sartorius, Germany) with a working volume of 1.5 L was applied. The temperature of the fermentation broth was kept at 70°C, the pH value was maintained at 6.5 using NaOH (1 mol/L) and the stirring rate

was set to 250 rpm. For continuous culture a hydraulic retention time of 15 h was adjusted. The flow rate of nitrogen as stripping gas was adjusted by a Flow Controller Bronkhorst HiTec 1000 mL/min.

Gas production rate was measured continuously by a Ritter gas counter Typ MGC-1 1000 mL/h for the bubble induction fermentation and a Ritter gas counter Typ TG01/5 10 L/h for the underpressure fermentation. For the experiments the tank reactor was sterilized, filled with 1.3 L sterile medium and sparged for 0.5 h with 15 L/h nitrogen. The inoculation was carried out with 250 mL of a *Caldicellulosiruptor saccharolyticus* culture grown overnight at 65 °C.

2.3 Bubble induction experiment

During the continuous operation of the fermentation the inert gas stripping rate was varied, it was stepwise reduced from 5, 3, 1 to 0 L/(h·L). At the different levels stable operation was awaited (ca. 5 retention times). After 75 h and 797 h of continuous operation bubble inducing particles (zeolite, 1 – 2.5 mm, IPUS, Rottenmann, Austria) were added to the fermentation broth. Prior to addition the particles were washed, dried, autoclaved and flushed with nitrogen. In a first step an amount of 10 g/L was added to the fermentation broth, which was increased to a total of 18 g zeolite per liter suspension in a second step. The cysteine amount in the medium was reduced to 0.1 g/L (333 h) and after 510 h of continuous operation, cysteine was omitted completely from the medium.

2.4 Underpressure experiment

For the variation of the underpressure a vacuum diaphragm pump KNF-Vacobox Typ PJ 9988-740.3 was used. The vacuum pump was connected to the head of the fermentor. In a first period the fermentation was performed under normal pressure (1000 mbar) and nitrogen gas stripping of 5 L/(h·L). Subsequently an underpressure of 600 mbar was applied. The nitrogen sparging was abated to 3 L/(h·L). Thereafter nitrogen gas stripping was further reduced to 1 L/(h·L). The underpressure was changed to 400 mbar and afterwards the inert gas stripping omitted completely. The underpressure was finally reduced to 305 mbar before it was raised to 500 mbar. The fermentation was stopped after 20 days of operation.

2.5 Analytical methods

The hydrogen content was determined with a gas chromatograph (PerkinElmer Clarus 500) equipped with a TCD (thermal conductivity detector), a molecular sieve column (Restek RT-Msieve 5A) and a poropak column (Restek Q-Plot). Nitrogen was used as carrier gas with a flow rate of 6 mL/min. The contents of CH4, N2, O2 and CO2 were measured with a gas chromatograph (PerkinElmer Autosystem XL) equipped with a TCD, a molecular sieve column (Restek RT-Msieve 5A) and a poropak column (Restek Q-Plot). As carrier gas helium was used with a flow rate of 6 mL/min. H2S was determined occasionally with a gas chromatograph (PerkinElmer Autosystem XL) equipped with a Restek Rt-XL Sulfur column and a flame photometric detector.

Glucose, acetate and lactate were analysed by a high performance liquid chromatograph (Waters Acquity UPLC) with a refractive index detector and a 300 mm 7.8 mm Aminex HPX-87H column. The optical density of the fermentation broth was determined via absorption at

620 nm using a PerkinElmer Lambda 35 UV/VIS spectrometer. The relation between optical density and cell dry weight was calculated as follows: CDW [g/L] = (0.3796 · OD620nm + 0.0288) (R2 = 0.9984). The measurement of dry matter and organic dry matter was carried out following DIN 38409-H1.

3 Results

3.1 Bubble induction experiment

Figure 1 shows the results of the analysis of the produced gas during the fermentation with induced bubble formation.

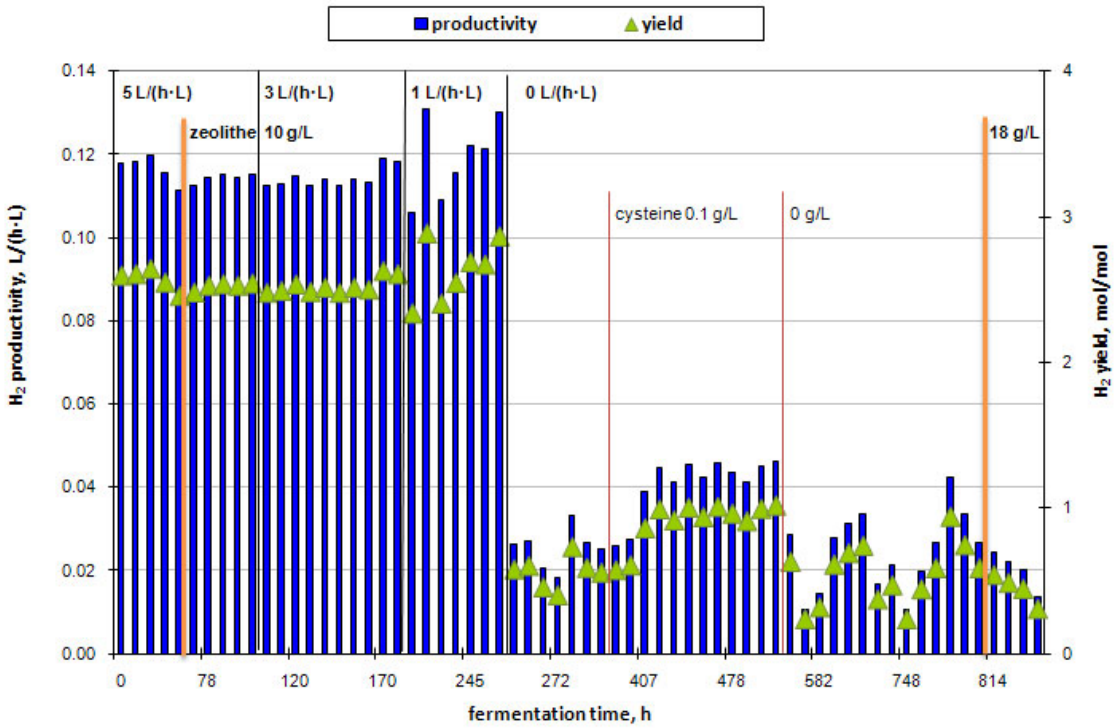

Figure 1: Hydrogen productivity and yield during the bubble induction experiment (*C. saccharolyticus* continuous culture, 15 h HRT).

The hydrogen productivity was constantly above 0.11 L/(h·L) during the first 200 h of the fermentation at a yield of 2.5 mol/mol glucose. The addition of the bubble inductor did not show discernible effects on the production of hydrogen. Similarly the reduction of inert gas stripping to 1 L/(h·l) did not influence the performance of the fermentation to a remarkable extent. Omitting stripping gas completely led to significant lower productivity and yield of 0.025 L/(h·L) and 0.56 mol/mol. The lower cysteine content (after 330 h) improved the production with a certain time delay. With no cysteine in the medium the mean values dropped and showed no continuity. After 800 h of continuous operation a steady decrease in hydrogen production occurred.

During fermentation hydrogen sulphide was found in the produced biogas. With the initial concentration of 0.6 g/L cysteine in the medium nearly 1500 ppm H_2S were detected. The reduced level of 0.1 g/L led to values of 600 ppm. With no cysteine in the medium no H_2S was produced at all.

A part of the inserted zeolite got clamped between the reactor wall and the baffle plate inside of the reactor. There the formation or rather the accumulation of gas bubbles was observed, even after stoppage of nitrogen gas stripping.

After 622 h of continuous operation a short-term switch to batch mode was necessary. The redox potential of the fermentation moved between -450 and -600 mV. The production rates of acids were situated between 2.3 and 14.8 mmol/h. During the experiment some technical problems concerning the pumps for the medium and the effluent occurred. Therefore, the pumps were adjusted manually.

The introduced glucose was totally consumed from the bacteria throughout the continuous operation (data not shown). The maximum concentration of acetic acid was found at the beginning of the fermentation with 2.5 g/L, thereafter the content decreased to 1 g/L. In contrast lactate increased after the strict reduction of gas stripping, after the omission of cysteine from the medium and after the second addition of zeolite. The optical density ranged from 0.45 to 1.05, corresponding to a dry cell weight of 200 to 430 mg/L. After addition of zeolite the optical density reached 1. The reduction of gas stripping to 1 L/(h·L) led to a drop in biomass formation. VFA analysis showed that the only organic acids produced were L-lactic acid and acetic acid.

3.2 Underpressure experiment

Figure 2 shows the results of the analysis of the produced gas during the fermentation with underpressure as method for hydrogen removal.

After the first period of the fermentation the hydrogen values dropped enormously. Changing the position of the vacuum controller led to an increase in hydrogen production. With each reduction of stripping gas the productivity as well as yield decreased. The best performance was achieved at the lowest pressure level of 305 mbar and no nitrogen stripping (0.104 L/(h·L), 2.31 mol/mol). Occasionally, analysis of the produced gas concerning N_2, O_2 and CO_2 concentrations were done. At ambient pressure and nitrogen stripping the gas produced was composed of 90% N_2, below 5% O_2 and CO_2 and about 2% H_2. At a pressure level of 400 mbar and omitted inertgas stripping the following composition was detected: 78% N_2, 20% O_2, 0.7% CO_2 and 1.5% H_2, indicating that the system was not completely tight and air was could enter the system.

The redox potential during fermentation fluctuated between -350 and -470 mV. The latter value was found at a pressure of 305 mbar without nitrogen stripping. The consumption rate of sodium hydroxide solution stayed constant throughout the fermentation. 3.6 mmol/h of organic acids were produced.

Glucose (data not shown) was entirely consumed by the bacteria until the end of the experiment, the concentration of unused sugar increased to more than 1 g/L. The acetate concentration fluctuated between 2 and 2.5 g/L. The metabolite lactate could not be detected throughout the fermentation. The lowest optical density was 0.7 which corresponded to a cell

dry weight of 300 mg/L. The highest biomass content was reached at a pressure of 305 mbar (OD 1.2, CDW 500 mg/L).

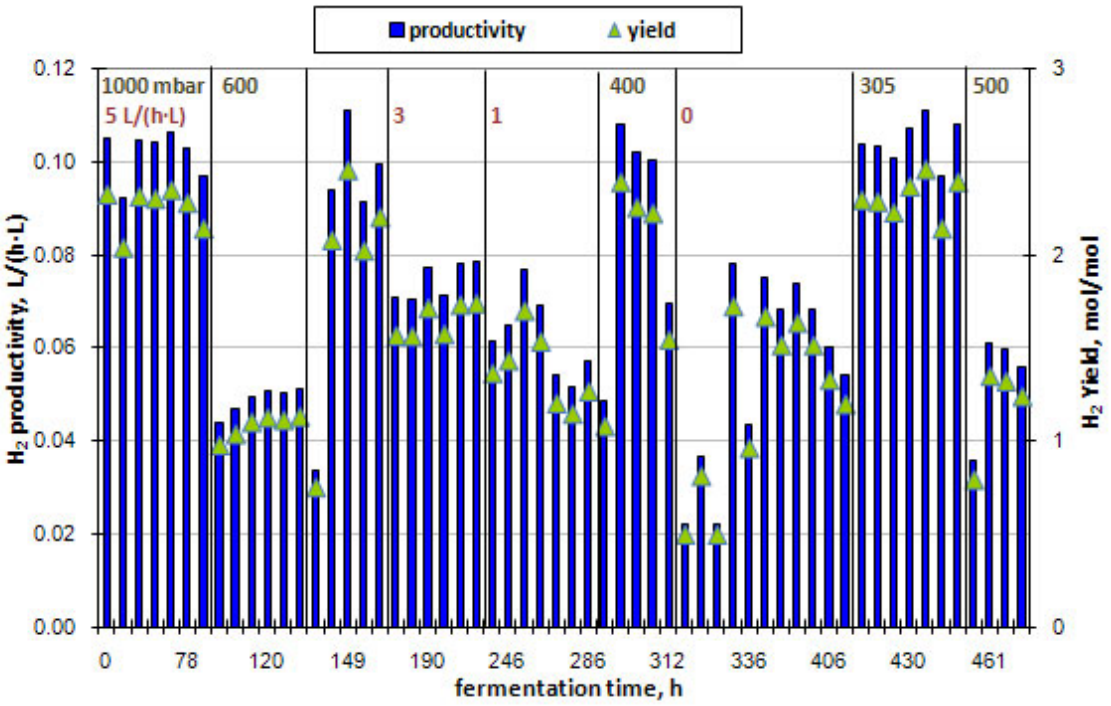

Figure 2: Hydrogen productivity and yield during the underpressure experiment (C. saccharolyticus continuous culture, 15 h HRT).

4 Discussion and Conclusion

The addition of a zeolite to induce bubble formation showed no direct effects on the fermentation. However a reduction of stripping gas to 1 L/(h·L) was possible without influencing the performance of hydrogen production. Hydrogen productivities of 0.115 L/(h·L) and yields of 2.5 mol/mol were achieved. In contrast to reference fermentations, inert gas stripping on a very low level was possible due to the bubble formation without reduced hydrogen productivity and yield. Omitting nitrogen sparging led to a radical decrease in hydrogen production, indicating that the produced hydrogen was not removed sufficiently from the liquid phase and led to an end product inhibition. By the use of zeolite the fermentation could be maintained without gas stripping but with far lower hydrogen yields and productivities. Therefore it is not profitable to ferment without nitrogen gas stripping to achieve adequate hydrogen values. Remarkably, no effect of the quantity of added zeolite could be detected, which one could expect. In contrast the bacterial growth was declining, when increasing the amount of zeolite. Anyway addition of zeolite caused an increase of the optical density, which could be due to the abrasion of the material. The gradual reduction of cysteine in the medium was necessary due to the high hydrogen sulphide content in order to avoid inhibition of the microorganisms and consumption of hydrogen for H_2S formation. The reduction of cysteine showed a positive effect on the fermentation. However, without cysteine

the fermentation became more unstable. The determination of VFAs showed that only lactic and acetic acid were produced. The carbon balance was considerably below 100 % indicating that other metabolites must have been produced. However, the results showed that the addition of bubble inducing materials was beneficial to a certain extent, but could not replace insertion of stripping gas to 100%. These findings could explain the better performance of fermentor systems using carrier materials due to enhanced bubble formation on the one hand and due to increased retention of biomass on the other [5, 6].

During each section of fermentation with underpressure the hydrogen productivities and yields remained almost constant. The appliance of underpressure led at first to a bisection of hydrogen production, which normalized after repositioning of the vacuum controller, avoiding high pressure surges and keeping up a stable vacuum. With each reduction of the stripping gas flow a decline of hydrogen values was observed, whereas each decrease of pressure led to an increased hydrogen production. The best data were obtained at a pressure level of 305 mbar without nitrogen sparging (0.100 L/(h·L) and 2.3 mol/mol hexose). Similar data were only achieved when applying high inert gas stripping rates (5 L/(h·L)) and pressures of 1000 or 600 mbar. Therefore underpressure is an applicable alternative to inert gas stripping for reduction of hydrogen partial pressure.

At the end of the fermentation around 20 % of the provided sugar was not consumed. This indicated, like the decrease in biomass, the death or rather the reduced metabolism of the bacteria. Therefore an applied underpressure of 500 mbar was not sufficient for stable operation of the fermentation. The progress of the experiment with successive increase of applied vacuum indicated that a further increase might lead to higher hydrogen productivities. This thesis was not tested because pressures lower than 300 mbar induced boiling of the fermentation broth at the used temperature of 70 °C.

Another approach for optimization is the reduction of the hydraulic retention time and hence higher organic loads. For further experiments it is certainly of great importance to get the whole system as vacuum-sealed as possible to maintain the underpressure in the tank reactor. Anyway the vacuum pump was not aligned to this small scale experiment and turned out to be too powerful. However, for the large-scale application vacuum-sealed systems are state of the art and are already in use for the production of bioethanol [7, 8, 9].

References

[1] Mizuno, O., R. Dinsdale, et al. (2000). "Enhancement of hydrogen production from glucose by nitrogen gas sparging." Bioresource Technology 73(1): 59-65.

[2] van Niel, E. W. J., P. A. M. Claassen, et al. (2003). "Substrate and product inhibition of hydrogen production by the extreme thermophile *Caldicellulosiruptor saccharolyticus*." Biotechnology and Bioengineering 81(3): 255-262.

[3] Schnitzhofer, W., Schuhmacher, M., et al. (2007). “Non-thermal production of hydrogen from biomass: Concept and bioprocess development.” Conference proceedings, 11th World Congress Anaerobic Digestion 2007, Brisbane, Australia.

[4] Claassen, P. A. M. and T. de Vrije (2006). "Non-thermal production of pure hydrogen from biomass: HYVOLUTION." International Journal of Hydrogen Energy 31: 1416-1423.

[5] Zhang, Z.-P., J.-H. Tay, et al. (2007). "Biohydrogen production in a granular activated carbon anaerobic fluidized bed reactor." International Journal of Hydrogen Energy 32: 185-191.

[6] Lee, K.-S., Lo, Y.-S. et al. (2004). "Operation strategies for biohydrogen production with a high-rate anaerobic granular sludge bed bioreactor." Enzyme and Microbial Technology 35(6-7): 605-612.

[7] Lee, J. H., Woodard, J. C. et al. (1981). “Vacuum fermentation for ethanol-production using strains of zymomonas mobilis.” Biotechnology Letters, 3: 177-182.

[8] Nguyen, V.D., H. Kosuge, et al. (2009). „Effect of Vacuum pressure on ethanol fermentation.” Journal of Applied Sciences, 9: 3020-3026.

[9] Cysewski, G. R., Wilke, C. R. (2004). “Rapid ethanol fermentations using vacuum and cell recycle.” Biotechnology and Bioengineering 19(8): 1125-1143.

Hydrogen Production by *Hup*- Mutant and Wild Type Strains of *Rhodobacter capsulatus* on Dark Fermenter Effluent of Sugar Beet Thick Juice in Batch and Continuous Photobioreactors

Ebru Özgür, Department of Chemical Engineering, Middle East Technical University, Ankara, Turkey
Basar Uyar, Department of Chemical Engineering, Kocaeli University, Kocaeli, Turkey
Muazzez Gürgan, **Meral Yücel**, Department of Biology, Middle East Technical University, Ankara, Turkey

Abstract

The HYVOLUTION project (EU 6th frame) is aimed to develop an integrated process in which biomass is fermented to acetate, lactate, CO_2 and hydrogen followed by photofermentation of acetate and lactate to hydrogen and CO_2 with photosynthetic purple nonsulfur bacteria (PNS bacteria). Growth and hydrogen production of *Rhodobacter capsulatus* was investigated on the dark fermenter effluent of thick juice (processed raw sugar beet juice) which contained acetate and NH_4Cl. In this effluent media, the hydrogen production of wild type bacterium and an uptake-hydrogenase deficient mutant (hup-) were compared in small scale (55 ml) batch and large scale (4 L) continuous photobioreactors in indoor conditions under constant illumination of 2000 lux. In continuous operation mode, the overall hydrogen production yields were 1.84 and 1.92 mol H_2/mol acetate, the maximum hydrogen productivities were 1.29 and 0.89 mmol H_2/L.h, for the wild type and mutant strains, respectively. On the other hand, in batch operation mode, the overall hydrogen production yields were 1.25 and 1.44 mol H_2/mol acetate, the maximum hydrogen productivities were 0.28 and 0.52 mmol H_2/L.h, for the wild type and mutant strains, respectively. The results show that *Rhodobacter capsulatus* is capable of using sugar beet thick juice effluent as substrate for hydrogen production; which makes it a suitable bacterium to be employed in integrated termophilic fermentation-photofermentation process.

1 Introduction

The HYVOLUTION project (EU 6th frame) is aimed to develop an integrated process in which biomass is converted to acetate, lactate, CO_2 and hydrogen by dark fermentation followed by photofermentation of acetate and lactate to hydrogen and CO_2 with photosynthetic purple nonsulfur bacteria (PNS bacteria). In order to combine thermophilic fermentation and photofermentation, it is mandatory to show the suitability of real dark fermentor effluents for the photofermentative hydrogen production by purple nonsulfur (PNS) bacteria.

Previously it was reported that *R. capsulatus* can grow and produce hydrogen successfully on synthetic substrates containing acetate/lactate mixtures [1] as well as dark fermentation

effluents of miscantus hydrolysate [2], potato steam peels hydrolysate [3] and molasses [4]. Those studies have been carried out at small scale, in batch mode.

In the present study, the effluent solution derived from the fermentation of thick juice (processed raw sugar beet juice) was used as a substrate for hydrogen production in photo-fermentation by wild type *Rhodobacter capsulatus* and its uptake-hydrogenase deficient (hup^-) mutant. The studies were carried out in small scale (50 ml) batch and large scale (4 L) continuous photobioreactors in indoor conditions under constant illumination of 2000 lux.

2 Material and Methods

2.1 Bacteria and culture

Photofermentative bacteria used in this study are wild type and an uptake-hydrogenase deficient mutant (hup^-) strain of *Rhodobacter capsulatus*.

Thick juice dark fermenter effluent (DFE) was obtained from PROFACTOR, Austria. It was centrifuged to obtain a visually clear liquid free from colloidal particles (i.e. bacteria) which may prevent light penetration. The DFE contained 94 mM acetate as the carbon source and 6 mM NH_4Cl as the nitrogen source. The concentration of acetate and NH_4Cl in the medium has a significant impact on the growth lag phase and hydrogen production of *R. capsulatus* [5]. Hence, the thick juice DFE was diluted in 1:2 ratio with distilled water and the acetate and NH_4Cl concentrations were decreased to 31 mM and 2 mM, respectively. In order to keep pH stable at the desired level (6.5-7.5), 20 mM of KH_2PO_4 was added into the diluted media as buffer and the initial pH was adjusted to 6.5. It was previously shown that Fe is an essential element for hydrogen production [6]. In order to enhance the hydrogen production, Fe (0.1 mM Fe-citrate) was added to the effluent solution. Finally, DFE solution was sterilized by autoclave before feeding into the photobioreactors.

2.2 Photobioreactors and operating conditions

In batch experiments, sealed glass bottles with 55 ml culture volume were used as photobioreactors. In continuous experiments, a photobioreactor made by acrylic sheet and PVC frame with 4L working volume was used. 10% (v/v) bacteria inoculation was made into the bioreactors. Argon gas was used to create anaerobic conditions. The bioreactors were connected to graded cylinders initially filled with water by capillary tubing made of steel. The produced gas amount was measured from the displaced water, escaping at the bottom of the gas collectors.

The photobioreactors were maintained at 30-33°C. The illumination was provided by 100 W incandescent lamps to attain a uniform light intensity of 2000 lux at the surface of photobioreactors. Initial pH in photobioreactors was 6.6-6.8.

During continuous runs, 400ml of media from bioreactor (10% of culture volume of 4L photobioreactor) was replaced by fresh media daily corresponding to the dilution rate of 0.1.

2.3 Analytical methods

Light intensity measurements were made by a luxmeter (Lutron). Evolved gas was analyzed by gas chromatography (Agilent Technologies 6890N) equipped with Supelco Carboxen 1010 column. The bacterial cell concentration was determined spectrophotometricaly at

660nm using Shimadzu UV-1201 Spectrophotometer. An optical density of 1.0 at 660nm corresponds to the biomass concentration of 0.54 gdcw/L_c for the wild type strain and 0.47 gdcw/L_c for the mutant strain. The consumptions of organic acids were followed by HPLC (Shimadzu, Alltech IOA-1000 Organic Acid Column).A pH-meter (Mettler-Toledo) was used to measure pH.

3 Results and Discussion

Hydrogen production on thick juice DFE was tested in batch and continuous modes. *Rhodobacter capsulatus* wild type and *Rhodobacter capsulatus hup-* mutant (YO3) were employed.

Batch mode study was carried out using 55ml bottle photobioreactors. Figure 1 shows the biomass growth and cumulative hydrogen production by wild type and mutant *R. capsulatus* (hup-) strains on thick juice DFE. Wild type cells reached to a higher maximum biomass concentration compared to the mutant cells. Hydrogen production started in the first day in both reactors. All the acetate was consumed in the first two days where logarithmic bacterial growth occurred.

Continuous hydrogen production on the DFE was tested using 4L panel photobioreactors. Daily feeding to the photobioreactors were provided at the 2nd day. Figure 2 illustrates the growth and hydrogen production of wild type and *hup-* mutant strains of *R. capsulatus*. Wild type bacteria grew successfully on DFE and reached to a maximum cell concentration of 1.8 gdcw/Lc. Maximum hydrogen productivity achieved was 1.29 mmol/L_c.h. After 9 days, hydrogen production stopped due to the biomass decrease. *R. capsulatus hup-* mutant cell density reached to a maximum of 1.3 gcdw/L_c. Hydrogen production started on the third day and it continued until the end of the experiment (for 23 more days). The productivity was at maximum in 3rd day (0.89 mmol/L_c.h), decreased afterwards but stabilized after 17th day between 0.28 – 0.37 mmol/L_c.h.

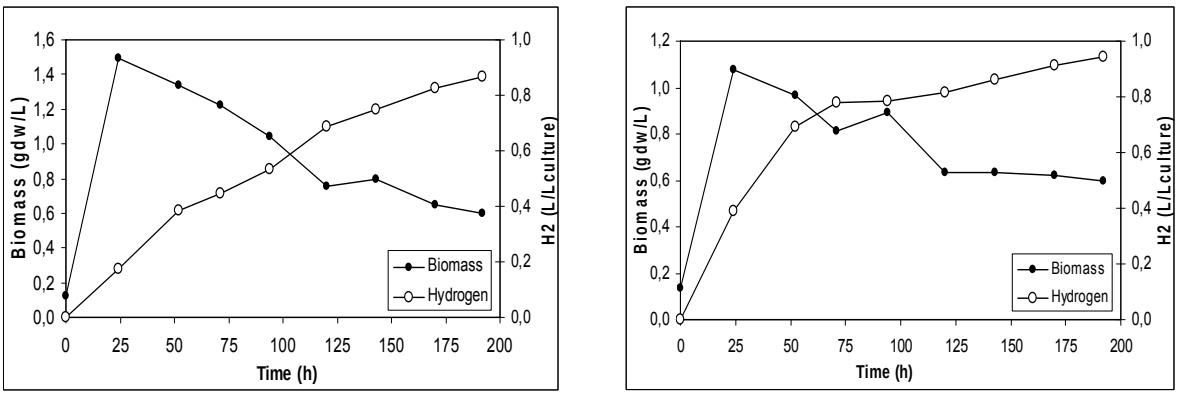

Figure 1: Growth and hydrogen production on DFE by (A) wild type *R. capsulatus* and (B) *R. capsulatus hup-* strain in 55mL batch photobioreactors.

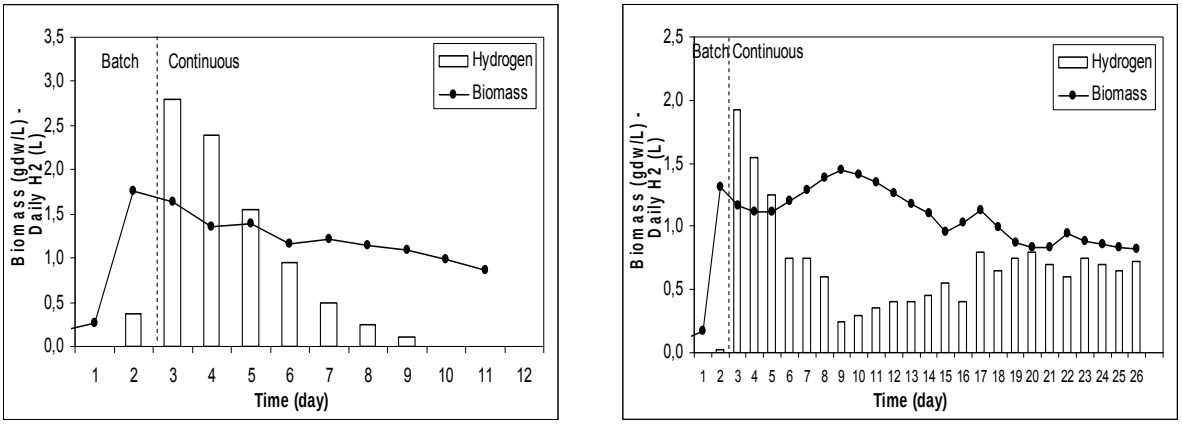

Figure 2: Growth and hydrogen production on DFE by (A) wild type *R. capsulatus* and (B) *R. capsulatus hup-* in 4L continuous panel photobioreactors.

Hydrogen production yields (as percent of theoretical maximum based on consumed substrate) and hydrogen productivities obtained by hup- mutant and wild type *Rhodobacter capsulatus* on the DFE in batch and continuous photobioreactors were compared in Table 1.

Table 1: Comparison of the yields and productivities obtained at different operations.

Operating mode	Strain	Duration (Days)	Max Biomass (gdw/L)	Yield (%)	Max Productivity (mmol/L_c.h)
Batch	WT	8	1.54	31	0.28
Batch	Hup^-	8	1.09	36	0.52
Continuous	WT	12	1.76	46	1.29
Continuous	Hup^-	26	1.44	48	0.89

Rhodobacter capsulatus hup- mutants strains reached to a lower maximum cell concentration but their yield and productivity were higher compared to the wild type cells in both batch and continuous operating modes. The maximum biomass concentration, yield and productivity of hydrogen were higher in continuous mode compared to the batch mode with both bacterial strains.

The presented results show that thick juice DFE is a suitable substrate for the photofermentative hydrogen production, provided that they are supplemented with buffer and nutrients, especially Fe, which is crucial for nitrogenase activity. The dilution of DFEs at the start-up is essential in adjusting the initial acetate concentration to 30 – 40 mM. Sterilization by autoclaving prevents contamination in long term operations. The recommended feeding rate is 10% by the volume of the reactor, daily. In order to control the pH, addition of 20 mM of potassium phosphate buffer to the DFEs was suggested.

Acknowledgement

This study was financially supported by the Commission of the European Communities, 6th Framework Programme, Priority 6, Sustainable Energy Systems (019825 HYVOLUTION).

References

[1] Özgür, E., Uyar, B., Öztürk, Y., Yücel, M., Gündüz, U., Eroglu, I. Biohydrogen production by *Rhodobacter capsulatus* on acetate at fluctuating temperatures. Resources, Conservation and Recycling 2010;54(5):310-314.

[2] Uyar, B., Schumacher, M., Gebicki, J., Modigell, M., Photoproduction of hydrogen by *Rhodobacter capsulatus* from thermophilic fermentation effluent. Bioprocess and Biosystems Engineering 2009;32:603–606.

[3] Afşar, N., Özgür, E., Gürgan, M., de Vrije, T., Yücel, M., Gündüz, U., Eroglu, I. Hydrogen production by *R. capsulatus* on dark fermenter effluent of potato steam peel hydrolysate, Chemical Engineering Transactions 2009;18:385-390.

[4] Özgür, E., Mars, A.E., Peksel, B., Louwerse, A., Yücel, M., Gündüz, U., Claassen, P.A.M., Eroglu, I. Biohydrogen production from beet molasses by sequential dark and photofermentation. International Journal of Hydrogen Energy 2010;35:511-517.

[5] Asada, Y., Ohsawa, M., Nagai, Y., Ishimi, K., Fukatsu, M., Hideno, A., Wakayama, T., Miyake, J., Re-evaluation of hydrogen productivity from acetate by some photosynthetic bacteria. International Journal of Hydrogen Energy 2008;33(19):5147-5150.

[6] Kars, G., Gündüz, U., Yücel, M., Türker, L., Eroglu, İ., Hydrogen production and transcriptional analysis of nifD, nifK and hupS genes in *Rhodobacter sphaeroides* O.U.001 grown in media with different concentrations of molybdenum and iron. International Journal of Hydrogen Energy 2006;31(11):1536-1544.

Removal of the Effect of Ammonium on the Regulation of Nitrogenase Enzyme in *Rhodobacter Capsulatus* DSM1710 for Improved Hydrogen Production

Gülsah Pekgöz, **Ufuk Gündüz**, Department of Biology, Middle East Technical University, Turkey
İnci Eroğlu, Department of Chemical Engineering, Middle East Technical University, Turkey
Gábor Rákhely, Department of Biotechnology, University of Szeged, Hungary

Abstract

Photofermentative biohydrogen production by purple non-sulfur (PNS) bacteria is a renewable and clean way of producing hydrogen. Hydrogen production by PNS bacteria, *Rhodobacter capsulatus*, is mediated mainly by nitrogenases, which primarily fix molecular nitrogen to ammonium and produce hydrogen as byproduct. The reaction catalyzed by nitrogenases requires a lot of energy. Hence, there is a complex regulation on nitrogenase enzyme complex, consequently, on hydrogen production. Whenever ammonium, which is the end product of nitrogen fixation reaction, is found in the environment, hydrogen production stops.

GlnB and GlnK proteins are the critical regulatory proteins in ammonium dependent regulation of the nitrogenase gene expression. In this study, the aim is to release the ammonium regulation on nitrogenase enzyme by inactivating *glnB* and *glnK* genes. For this purpose, relevant recombinant vectors were constructed; *R.capsulatus glnB*$^-$ strain was obtained. The double *R.capsulatus glnB*$^-$*glnK*$^-$ strain, able to produce hydrogen independent of ammonium concentration of the environment is to be obtained.

1 Introduction

Today, environmental pollution is one of the main problems of the world, mainly due to rapid industrialization and urbanization. Moreover, there is a high energy demand, whereas a limited amount of fossil fuels in the earth. Thus, increasing focus is being placed on clean and renewable energy. Hydrogen energy can be regarded as the fuel of future, since its commercial utilization is efficient and easy. Moreover, hydrogen can be completely recycled without CO_2 emission. Consequently, biohydrogen is a renewable and environmentally clean energy carrier [1].

The energy source of biohydrogen formation is the sun. Solar energy might be converted to hydrogen directly by some photosynthetic microorganisms or in two steps; first, the biomass is formed via photosynthetic organisms and second, the high energy compounds generated are converted to biohydrogen by fermentative organisms. In PNS bacteria, organic acids are utilized with light energy and nitrogenases in the photofermentation process. There are integrated biohydrogen production systems in which a dark fermentation process by fermentative bacteria is combined with a subsequent photofermentation process by PNS bacteria. Hence, the overall hydrogen yield can be enhanced to a great extent [1, 2]. One of

the projects which integrate dark fermentative and photofermentative hydrogen production is 'Hyvolution Project'. The effluent of the dark fermentation, which is rich in organic acids (i.e. acetate, lactate) and ammonium ions, is used in photofermentation. Biohydrogen is produced in both bioreactors.

Rhodobacter capsulatus is a PNS bacterium, which produces biohydrogen via photofermentation. It has two kinds of nitrogenase enzymes ([Fe-Mo] and [Fe-Fe]) that are responsible for hydrogen production. Nitrogenases normally reduce N_2 to ammonia, and also evolve hydrogen, particularly in the absence of N_2 gas. The overall reaction catalyzed by nitrogenase enzyme is [3]:

$$N_2 + 8H^+ + 8e^- + 16ATP \rightarrow 2NH_3 + H_2 + 16ADP + 16P_i$$

This process is energetically expensive for the cell; therefore hydrogen production is strictly controlled by NH_4^+ both at the expression level and the enzyme activity level [4, 5]. If enough NH_4^+ is present in the environment, nitrogen fixation and hydrogen production completely cease [6]. This phenomenon decreases the hydrogen production efficiency of the integrated systems. The effluent of dark fermentation (which is used in photofermentation) has high ammonium concentrations enough to inhibit photofermentative hydrogen production. In order to increase the overall efficiency, ammonium insensitive hydrogen evolving strains must be used. The aim of the present study is to inactivate GlnB and GlnK proteins which are the key elements in ammonium dependent regulation of the nitrogenase gene expression. *R.capsulatus glnB⁻glnK⁻* strain will be capable of producing hydrogen irrespective of the ammonium concentration present in the medium.

2 Materials and Methods

2.1 Bacterial strains, plasmids and growth conditions

E.coli XL1 Blue (Stratagene) and *E.coli* S17-1 (λpir) [7] are *E.coli* strains used in this study. *Rhodobacter capsulatus* DSM1710 is the wild type strain of *R.capsulatus*. The cloning vector pBluescript SK (+) [*Amp*^{r}] (Stratagene) and the suicide vector pK18*mobsacB [Km*^{r}*, sacB, RP4 oriT, ColE1 ori]* [8] are the plasmids used in this study. The plasmids pGBBU, pGBBD, pGKBU, pGKBD, pGBSD, pGKSD, pGBSUD and pGKSUD were obtained in the present study.

Rhodobacter capsulatus DSM1710 was grown under continuous illumination at 30ºC in Biebl and Pfennig (BP) minimal medium [9], in which malate (7.5 mM) and glutamate (10.0 mM) were used as carbon and nitrogen sources, respectively. The vitamin solution (thiamin, niacin and biotin), trace elements solution and ferric citrate solution were added. *E.coli* strains were grown in Luria Broth (LB) medium at 37ºC with antibiotics in the following concentrations (μg/mL): ampicillin 100; kanamycin 25; and tetracycline 10.

2.2 General recombinant DNA techniques

Polymerase chain reaction (PCR), genomic DNA isolation, plasmid DNA isolation, restriction enzyme digestion, sticky or blunt end ligation, dephosphorylation of linearized plasmids, kinase treatment of PCR products, transformation of *E.coli* and conjugation were performed

according to the protocols described previously (Ausubel et. al., 1996) [10] and the supplier's instructions. Generuler 50 bp and 1kb DNA ladders (Fermentas) were used in agarose gel electrophoresis as DNA marker.

2.3 Sequence and Primer Design

Since the genome of *R.capsulatus* DSM1710 is not sequenced yet, the genome sequence of another strain (SB1003) was used for sequence information. 10 kb sequences including *glnB* and *glnK* genes were annotated. After obtaining exact sequences of DSM1710 by sequencing the PCR products, primers were designed to amplify both upstream and downstream fragments of *glnB* and *glnK* genes. Site directed mutagenesis (by deleting the internal fragments of the genes) was preferred to insertional mutagenesis, because the possible transfer of the antibiotic cassette present in the mutant organism to wild type (WT) organisms possesses a potential biosafety risk. Moreover, in order to keep the genes active, which are in the same operon with the targeted genes, the reading frame was kept as original.

2.4 Preparation of constructs for inactivation *glnB* and *glnK*

After PCR amplification of the upstream and downstream of *glnB* and *glnK* genes, the fragments were individually cloned into pBtSK (+), giving rise to pGBBU, pGBBD, pGKBU and pGKBD plasmids. Then, downstream fragments of *glnB* and *glnK* were excised from the relevant plasmids and cloned into the suicide vector (pK18*mobsacB*), yielding the pGBSD and pGKSD plasmids. By ligating these plasmids with upstream fragments excised from pGBBU and pGKBU, the final constructs for inactivation of *glnB* and *glnK* were obtained: pGBSUD and pGKSUD. The clones were checked by colony PCR. The plasmids were analyzed by restriction enzyme digestion and sequencing.

2.5 Gene transfer into *R.capsulatus* - Diparental mating

E.coli S17-1 cells containing the constructs are able to conjugate with *R.capsulatus* cells. Through conjugation between donor (*E.coli* S17-1) and recipient (*R.capsulatus* cells), constructs were transferred into *R.capsulatus* cells. The targeted genes were inactivated by means of homologous recombination between the construct and the genomic DNA of the cell. After the exchange of the genes by a two step homologous recombination, the targeted genes were inactivated, since the *glnB* and *glnK* genes in the constructs were deleted, nonfunctional genes.

2.6 Selection of mutants

Following conjugation, the cell mixture was spread onto kanamycin containing plates. Single recombinants which integrate the entire plasmid into the genomic DNA were selected based on kanamycin resistance. In order to enable cells to perform the second recombination, cells were grown in nonselective BP medium for a few passages. In the second recombination event, the entire plasmid (except homologous regions) was excised from the genomic DNA. Double recombinants were selected by using pK18*mobsacB* suicide vector, in which there is a *sacB* gene whose product converts sucrose to a toxic compound. Spreading the cells onto sucrose containing plates eliminated single recombinants. Thus, only the double recombinants could form colonies on sucrose containing plates, which can be either WT or

the expected mutant strain. The mutant strains were further selected and confirmed by the length of the PCR amplicon and the sequence results of the deletion sites.

3 Results and Discussion

Upstream and downstream fragments of *glnB* and *glnK* genes were amplified by unique primers and cloned into the pBtSK (+) cloning vector. Downstream fragments (~1 kb) were individually excised and ligated into the pK18*mobsacB* suicide vector (~5700 bps); giving pGBSD and pGKSD (~6700 bps) (Figure 1a, 2a). The upstream fragment of *glnB* and *glnK* were ligated to pGBSD and pGKSD, respectively. The final constructs obtained for the inactivation of targeted genes were pGBSUD (~7700 bps) (Figure 1b) and pGKSUD (~7700 bps) (Figure 2b). The validity of the constructs was confirmed by double restriction enzyme digestion to excise 1 kb insert (Figure 1c, 2c), colony PCR and sequence analysis (data not shown).

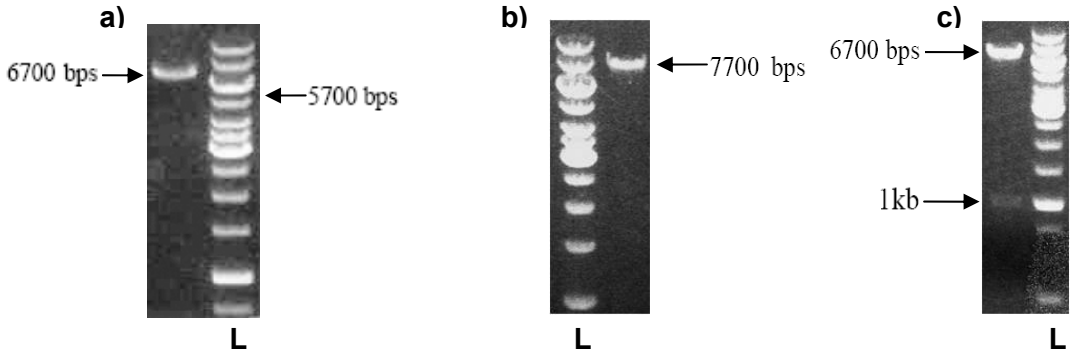

Figure 1: **a) Linearized pGBSD (~6700 bps) and the position of linearized pK18*mobsacB* in the ladder(~5700 bps), b) linearized pGBSUD (~7700 bps), c) double digestion of pGBSUD to excise the insert (~1 kb), L: 1 kb DNA ladder.**

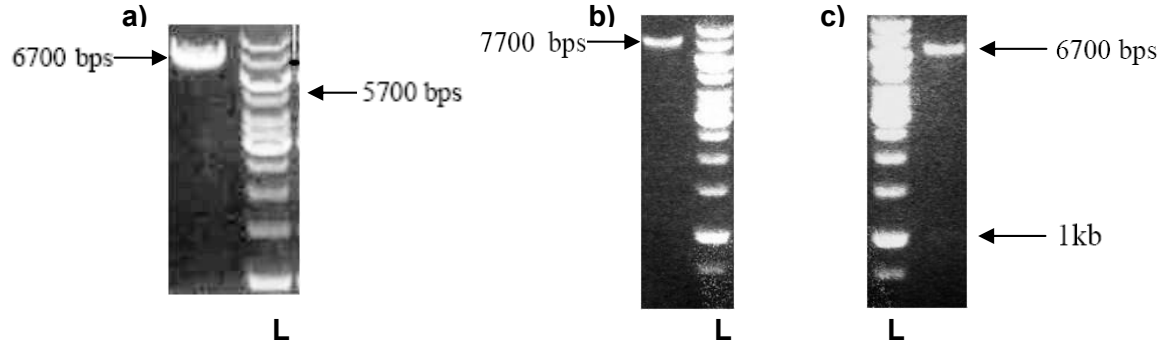

Figure 2: **a) Linearized pGKSD (~6700 bps) and correspondence of linearized pK18*mobsacB* (~5700 bps), b) linearized pGKSUD (~7700 bps), c) double digestion of pGKSUD to excise the insert (~1 kb), L: 1 kb DNA ladder.**

The constructs were transformed into *E.coli* S17-1 and conjugated with *R.capsulatus* DSM1710. Single recombinants were selected as colonies formed on BP plates containing 25 µg/mL kanamycin.

Double recombinants were obtained as described in Section 2.6. Colony PCR was performed for the colonies which grew on sucrose plates but not on kanamycin plates. The double recombinants lost their resistance to kanamycin after the second homologous recombination, since the entire plasmid was excised from genomic DNA of the mutants. The deletion mutation in the gene was confirmed by observation of the short amplicon (400 bps) obtained from colony PCR (Figure 3), as 626 bps long amplicon was routinely obtained from WT cells of the same PCR. The final confirmation step was the sequencing the genomic DNA of the mutant candidate, which also confirmed the deletion site in *glnB* gene.

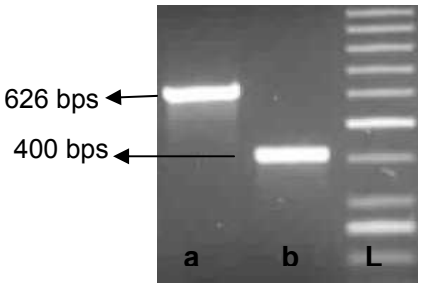

Figure 3: Colony PCR result for wild type *R.capsulatus* (a), *R.capsulatus glnB*⁻ mutant (b) and 50 bp DNA ladder (L).

The study to obtain the double mutant of *glnB* and *glnK* is currently continuing. After the double *glnB*⁻*glnK*⁻ mutant is obtained; the strain will be tested for hydrogen production using different ammonium containing media.

References

[1] Das D. and Veziroglu T. N. Hydrogen production by biological processes: a survey of literature. Int J Hydrogen Energy 26 (2001): 13–28.

[2] Basak N. and Das D. The prospect of purple non-sulfur (PNS) photosynthetic bacteria for hydrogen production: the present state of the art. World J Microbiol Biotechnol 23 (2007): 31–42

[3] Vignais P.M., Magnin J. P., Willison J. C. Increasing biohydrogen production by metabolic engineering. Int J Hydrogen Energy 31 (2006): 1478 – 1483

[4] Masepohl B., Drepper T., Paschen A., Groß S., Pawlowski A., Raabe K., Riedel K., Klipp W. Regulation of nitrogen fixation in the phototrophic purple bacterium Rhodobacter capsulatus. J Mol Microbiol Biotechnol 4 (2002): 243–248

[5] Drepper T., Groß S., Yakunin A. F., Hallenbeck P. C., Masepohl B., Klipp W. Role of GlnB and GlnK in ammonium control of both nitrogenase systems in the phototrophic bacterium Rhodobacter capsulatus. Microbiology 149 (2003): 2203–2212

[6] Akkose S., Gunduz U., Yucel M., Eroglu I. Effects of ammonium ion, acetate and aerobic conditions on hydrogen production and expression levels of nitrogenase genes in Rhodobacter sphaeroides O.U.001. Int J Hydrogen Energy 34 (2009): 8818 – 8827

[7] Herrero M. et al. Transposon vectors containing non-antibiotic resistance selection markers for cloning and stable chromosomal insertion of foreign genes in gram-negative bacteria. J Bacteriol 172 (1990): 6557 – 6567

[8] Schafer A., Tauch A., Jager W., Kalinowski J., Thierbach G., Pühler A. Small mobilizable multi-purpose cloning vectors derived from the Escherichia coli plasmids pK18 and pK19: selection of defined deletions in the chromosome of Corynebacterium glutamicium. Gene 145 (1994): 69-73

[9] Biebl H., Pfennig N. Isolation of member of the family Rhodosprillaceae. In: Starr MP, Stolp H., Trüper H. G., Balows A., Schlegel H. G., editors. The prokaryotes, vol. 1. New York: Springer; 1981. p. 267–73

[10] Ausubel F. M., Brent R., Kingston R. E., Moore D. D., Seidman J. G., Smith J. A. editors. Current protocols in molecular biology. Wiley, New York, N.Y. 1996

LCA of a Non-thermal Production of Pure Hydrogen from Biomass

Dominik Ochs, Werner Ahrer, **Wolfgang Schnitzhofer**, Profactor GmbH, Innovative Energy Systems, Steyr-Gleink, Austria

1 Introduction

The non-thermal decentralised small-scale production of hydrogen from biomass is currently under investigation within the EU FP6 project: HYVOLUTION. The HYVOLUTION process starts with the conversion of biomass to make a suitable feedstock for the following bioprocess, which consists of a thermophilic fermentation and a consecutive photo-heterotrophic fermentation. The selected biomasses are by-products from food industry, molasses and potato steam peels, and the specifically grown substrate Miscanthus. A dedicated gas upgrading is also developed [1].

The present paper aims an evaluation of the environmental impact of the non thermal hydrogen production of HYVOLUTION compared to the environmental impact of methane based hydrogen generation.

2 Methodology

The Life Cycle Assessment (LCA) methodology was chosen to evaluate the environmental impact of the biological hydrogen production. The environmental burdens and benefits of the entire production chain are discovered and quantified. The whole LCA was based on the ISO 14040 [2] and 14044 [3]. The analysis is conducted with the help of the SimaPro 7.1 software [4]. As an impact assessment methodology Eco-indicator 99 (H) V2.06/ Europe EI 99 H/A was used. The method uses an average weighting set to the three damage categories human health, ecosystem quality and resources. The functional unit set for the entire process is 1 kg H_2, due to its easy convertibility to other units and the fact that in the database data are available which are related to mass units.

2.1 Goal and scope

The final goal of HYVOLUTION is to establish a technology for decentralized production of hydrogen based on locally available biomass. The HYVOLUTION technology itself has the function to produce a manifold applicable energy carrier – H_2.

The LCA is deliberately carried out in parallel to the project development in order identify and foresee environmental high loaded in- and outputs. It can be regarded as a consulting tool for process development and optimization. As a consequence, the intended audience of this LCA is the partners of the project or generally scientists or engineers involved in the process development.

2.2 System boundary

The system boundaries (see Figure 1) include the entire process chain of the non thermal hydrogen production. It starts with the transport of the feedstock to the plant and ends with the upgraded hydrogen gas. The process steps in between are feedstock pre-treatment, thermophilic fermentation, photo fermentation and gas upgrading. The biological and chemical inputs (e.g. enzymes, phosphate and nutrients) as well as heat, electricity and water demand of the process steps are included in the system boundaries. The storage and transport of the produced hydrogen are out of the system boundaries and hence are not considered in the LCA.

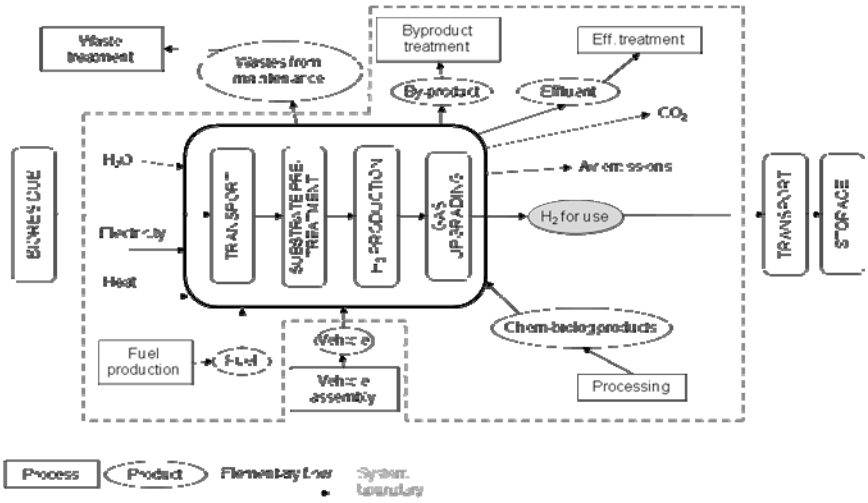

Figure 1: System boundaries of the HYVOLUTION process, including transport, pre-treatment, thermophilic and photo fermentation.

3 Life Cycle Inventory

The present analysis is based on potato steam peels (PSP) as a substrate for the HYVOLUTION process. According to the sensitivity analysis in the simulation activities in a work package of the project a number of data sets for the non-thermal hydrogen production using PSP as feedstock are available [5]. The base case data set only connects the different process steps without consideration of any process improvements due to process and heat integration. For this base case, the production of 1kg H_2 needs 249,3kg PSP and a total water amount of 2,390kg. The other data sets vary from the base case by the recirculation of sewage and the reduction of buffer concentration in the photo fermentation. Recirculation of sewage refers to the use of process effluents in the thermophilic and photo fermentation.

For the following three cases LCAs were conducted:

- HYVOLUTION – PSP 1(Base case): Simple balance, no recirculation, 20mM buffer
- HYVOLUTION – PSP 2: Simple balance, replacement of 90% of tap water by process effluents, 20mM buffer
- HYVOLUTION – PSP 3: Simple balance, no recirculation, 4mM buffer

Reference systems

The purpose of having a reference system is to compare the burden and benefit of the new developed process to a state-of-the-art technology of producing hydrogen. The hydrogen production by the HYVOLUTION process is compared to a fossil fuel based hydrogen generation and furthermore to a hydrogen production from biogas. Both reference systems are based on the steam methane reforming (SMR) which is a widely used, well discovered and is a documented process for centralized industrial plants.

4 Impact Assessment

4.1 Base case – HYVOLUTION – PSP 1

The total environmental impact of the case HYVOLUTION – PSP 1 (Base case) is 4.3 pts. The impact can be allocated to the four process steps: 0.5 pts from the pre-treatment, 0.8 pts from dark fermentation, 2.6 pts from the photo fermentation and 0.4 pts from the gas upgrading. The highest impact categories to the overall process are carcinogens (1.38 pts), fossil fuels (1.07 pts), respiratory inorganics (1.04 pts) and climate change (0.21 pts). Figure 2 shows further details to the described facts. The biggest impact on carcinogens and respiratory inorganics, is obviously caused by the use of phosphate in the photo fermentation. In the dark fermentation the highest impact is on fossil fuels, as well as in the pre-treatment, due to steam consumption. In case of gas upgrading it is not verified what impacts are caused, since detailed balance data for this process steps are not available yet from process simulation. The assumed loss of 10% of hydrogen would lead to environmental impact increase of 0.4 pts.

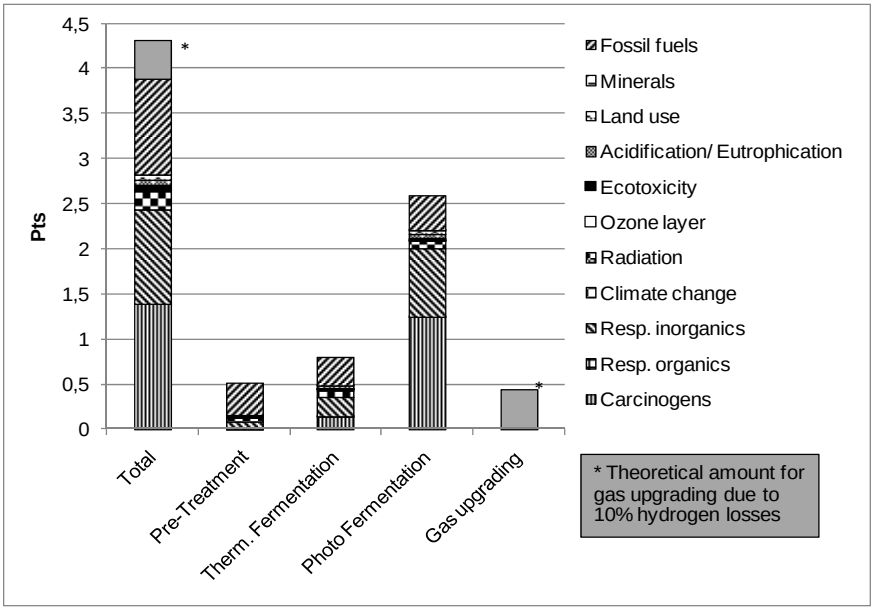

Figure 2: Environmental impact of HYVOLUTION - PSP 1 (Base case), displaying the total environmental impact allocated to the impact categories and the single process steps.

Allocating the impact to the inputs and outputs, three process ingredients are identified causing a high environmental load (see Figure 3). The highest environmental impact is caused by phosphate with 2.3 pts. It corresponds to 53.5% of the total environmental impact of the HYVOLUTION process. The phosphate is used in the photo fermentation as a buffer. It is furthermore used in the dark fermentation in a lower concentration, but also causes a nameable impact of 0.23 pts. The second highest impact of 0.47 pts is created by the use of a base in the dark fermentation. The use of steam for pre-treating the substrate causes the third highest impact of the total HYVOLUTION process. It can be seen that the inputs to the HYVOLUTION process are mainly responsible for its high environmental load. The outputs directly caused by the HYVOLUTION process are CO_2 and sewage. Its cumulative environmental load is only 0.07 pts, which corresponds to 1.7% of the total impact.

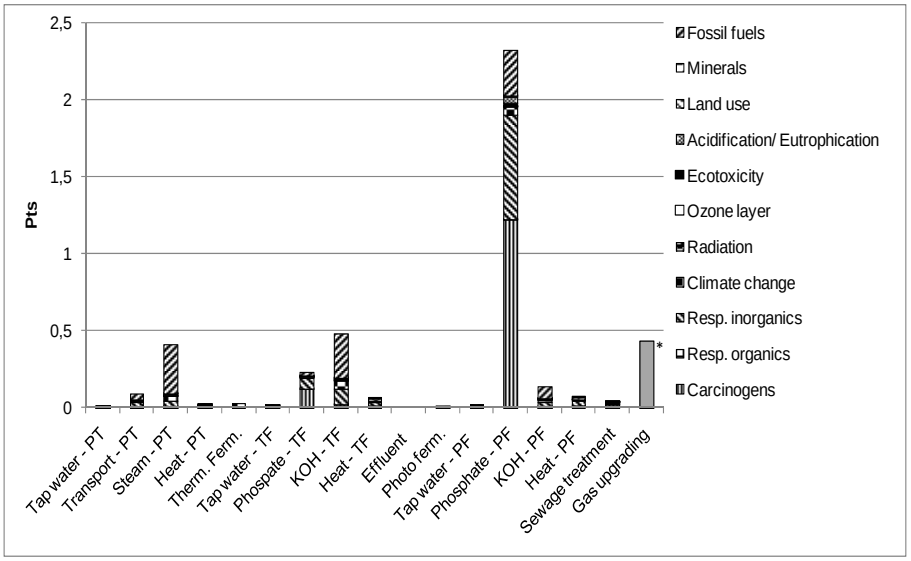

Figure 3: Allocation of the environmental impact to the inputs and outputs of the single process steps in HYVOLUTION – PSP 1 (Base case).

4.2 HYVOLUTION – PSP 2

In HYVOLUTION – PSP 2 it is foreseen to recirculate the major part (90%) of the sewage from the whole process to the dark and photo fermentation. As a positive consequence the fresh water and buffer demand would be reduced, leading to an environmental impact reduction of 65.8% to 1.47 pts. The process step giving the highest impact remains the photo fermentation, but its amount is reduced by 78.5% to 0.56 pts. The pre-treatment creates the second highest impact with 0.5 pts. The dark fermentation decreases its environmental impact by 67.5% to 0.26 pts. The highest impact categories in this process step are still fossil fuel (0.58 pts), respiratory inorganics (0.35 pts) and carcinogens (0.31 pts) with a change in order.

The impact allocation to the inputs and outputs of the HYVOLUTION process shows that the use of phosphate in the photo fermentation still has the highest environmental impact of 0.48 pts. In comparison to the total HYVOLUTION process it is 32.2%. The input with the second

highest impact is steam from the pre-treatment with 0.41 pts. The base used in the dark fermentation has the third highest impact with 0.19 pts. Further inputs getting more significant are transport of the substrate and the heat input necessary to run the bioprocesses and the pre-treatment. The impacts of the bioprocesses are also more visible in this evaluation. But in total the output of the HYVOLUTION process steps itself has an impact of only 0.07 pts which corresponds to 4.8% of the overall process including the input of feedstock, water heat and other chemicals.

4.3 HYVOLUTION – PSP 3

In HYVOLUTION – PSP 3 the buffer concentration used in the photo fermentation is reduced from 20mM to 4mM without any recirculation of sewage applied. The photo fermentation and the gas upgrading are the only process steps changing their environmental impact in comparison to HYVOLUTION – PSP 1. The total impact is reduced by 52.1% to 2.06 pts. The impact is allocated to the process steps as follows: 0.79 pts from dark fermentation, 0.5 pts from pre-treatment, 0.49 pts from photo fermentation and 0.26 pts from gas upgrading. The highest impact categories generally stay the same as in HYVOLUTION – PSP 1, but their order change: Fossil fuel (0.88 pts), Respiratory inorganics (0.49 pts) and Carcinogens (0.37 pts).

The impact allocation to the inputs and outputs of HYVOLUTION - PSP 3 shows a different result as the previous allocations. The input with the highest environmental load is the base used in the dark fermentation. Its impact is assessed with 0.47 pts follow by the steam production with 0.41 pts. The previously highly charged use of phosphate has now an environmental impact of only 0.28 pts which means a reduction by 87.8% compared to the base case. Further significant inputs are the phosphate to the dark fermentation (0.23 pts) and the transport of the substrate (0.09 pts). The outputs of the process have an impact of 0.07 pts which corresponds to 3.4% of the whole HYVOLUTION process.

4.4 Comparison

The reference systems generally show a lower environmental impact than the three HYVOLUTION – PSP cases (see Figure 4). The steam methane reforming of purified methane from biogas has the lowest impact of all the processes with 0.17 pts. The steam methane reforming has an environmental impact of 0.75 pts. Its main impact is caused by the extraction and use of natural gas.

A comparison of HYVOLUTION – PSP 1 (Base case) to the centralized steam methane reforming shows that the HYVOLUTION process in the current development stage has a 5.7 times higher impact. The recirculation of sewage, as done in HYVOLUTION – PSP 2, leads to a HYVOLUTION process with twice of the impact of the steam methane reforming. A comparison of the HYOLUTION processes to the steam methane reforming of a CO2 cleaned biogas shows a 252 time higher impact as HYVOLUTION – PSP 1 and a 86 times higher impact as HYVOLUITION – PSP 2.

5 Discussion and Conclusion

At the current state of development the non-thermal small-scale decentralized hydrogen production shows a 5.7 times higher environmental impact than the large scale centralized

SMR. A possible process improvement (recirculation of sewage) would lead to an environmental impact that is only twice high than the one of the SMR. In HYVOLUTION – PSP 1 (base case) 98.3% of the environmental impact is caused by the inputs; mainly phosphate, base and steam. The process emissions or solid outputs only cause 1.7% of the impact. This corresponds to 0.07pts of the LCA evaluation. The backpack the process ingredients are wearing is extremely high in the non-thermal hydrogen production and therefore their consumption needs to be degreased.

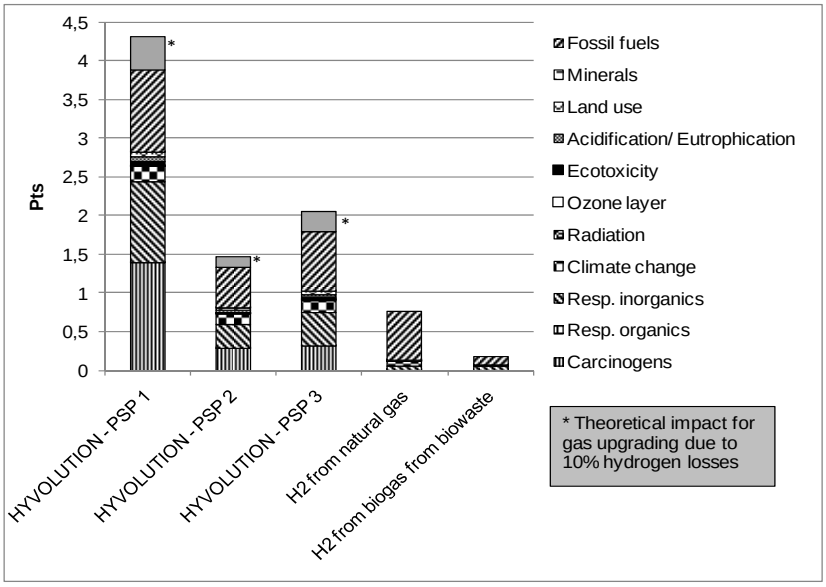

Figure 4: Comparison of HYVOLUTION - PSP 1, 2 and 3 to the reference systems, showing a generally higher environmental impact of the new developed HYVOLUTION technology in contrast to the state of the art technologies.

Compared to the SMR or the biogas technology the non thermal hydrogen production is a new development, which needs to be improved in future. During the HYVOLUTION project a lot of basic research was realized which established the process as a whole and needs to be adapted by engineering activities (heat integration). Furthermore a replacement of high loaded inputs (phosphate or potassium) with ecologically produced inputs needs to be realized, in order to lower the environmental impact.

References

[1] Claassen P.A.M., de Vrije T., 2006. Non-thermal production of pure hydrogen from biomass: HYVOLUTION. International Journal of Hydrogen Energy, Vol. 31, pp. 1416–1423.

[2] International Organization for Standardization, 1997. ISO 14040: Environmental management – Life cycle assessment – Principles and framework.

[3] International Organization for Standardization, 2006. ISO 14044: Environmental management – Life cycle assessment – Requirement and guidelines.

[4] PRé Consultants, 2006. Sima Pro 7.1 LCA software.

[5] Wukovits W., Friedl A., Schumacher M., Modigell M., Urbaniec K., Ljunggren M., Zacchi G., Claassen P.A.M., 2007. Identification of a suitable process route for the biological production of hydrogen. Proceedings of the 15th European Biomass Conference & Exhibition, pp. 1919–1923.

Optimization of a Two-stage Bio-hydrogen Fermentation Process

Walter Wukovits, **Domenico Foglia**, **Anton Friedl**, Vienna University of Technology, Austria
Mattias Ljunggren, Lund University, Sweden

1 Introduction

The transport sector accounts for 60% of the world's oil consumption. Substituting oil with a CO_2 free emission energy carrier would significantly slow down the increase in CO_2 concentration in the atmosphere and therefore solve most of the problems related to greenhouse gases [1].

Different processes are under investigation for the production of cheap sustainable hydrogen, including thermochemical conversion of biomass and waste, biological water splitting with algae and fermentative processes. Other processes under discussion involve electricity obtained from renewable resources to obtain hydrogen through electrolysis of water.

Compared to thermochemical conversion, advantages of fermentative hydrogen production are mainly connected to the possible integration of production facilities in the local agricultural context, due to the possible use of different types of wet feedstock and residues, the opportunity to produce hydrogen in small scale facilities, and the possible use of fermentation effluents as a fertilizer.

2 Process Description and Simulation Models

A 2-stage bioprocess investigated in the EU-project HYVOLUTION is a promising method for biological production of hydrogen from biomass [2]. The proposed process consists of a pretreatment step to make sugars contained in the feedstock available for the thermophilic bacteria, a thermophilic fermentation step (THF) to produce hydrogen, CO_2 and intermediates followed by a photo-heterotrophic fermentation step (PHF), in which these intermediates are converted to more hydrogen and CO_2. Produced raw gas from both fermentation steps is purified up to 97 % (v/v) hydrogen in a gas-upgrading step.

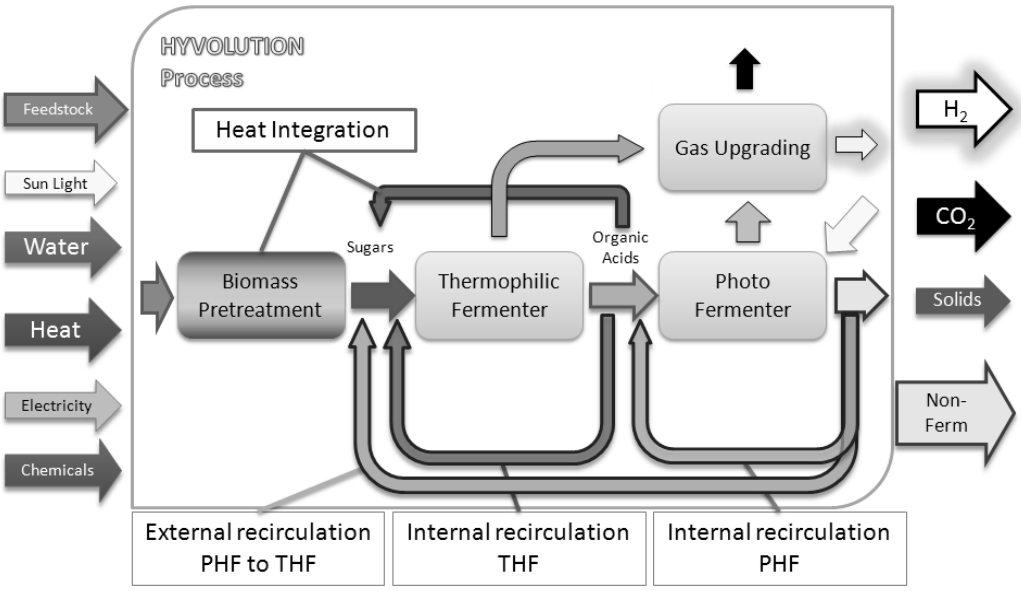

Figure 1: Scheme of HYVOLUTION process.

The different process steps has been implemented in the flow sheeting program Aspen Plus® (V7.1, Aspen Technology, Inc., Burlington, USA, 2008) which is used to solve mass and energy balances. The process has been scaled to obtain 60 kg/h of pure hydrogen 97 % (v/v), equivalent to 2 MW of thermal power, considering 10 % hydrogen losses during gas-upgrading.

Work presented here is based on feedstock molasses, a residue from processing of sugar beet. The investigated feedstock option does not require any pretreatment, since the sugars present in molasses can be directly fermented in the THF.

Table 1: Basic settings for HYVOLUTION process.

Plant capacity	60 kg/h Hydrogen (97 % v/v)
Feedstock	Molasses
Sugar conversion to H_2 in THF	80 % (wt)
Sugar conversion to cell mass in THF	15 % (wt)
Acetic acid conversion to H_2 in PHF	60 % (wt)
Acetic acid conversion to cell mass in PHF	15 % (wt)
Temperature THF	70 °C
pH THF	6.5
Substrate concentration THF	10 g/l Sugar
Temperature PHF	30 °C
pH PHF	7.3
Substrate concentration PHF	40 mM Acetic Acid
Hydrogen losses in Gas-Upgrading	10%

Feedstock has to be diluted before being introduced to the thermophilic fermentation to obtain a concentration of 10 g/l of sugars. The motivation of such a low concentration is that the selected bacteria are negatively affected by high osmotic pressure, which would reach harmful levels already at concentrations of 13 g/l sugars [3, 4].

The diluted liquid stream is heated to 70 °C and fed to the thermophilic or dark fermentor (THF). During THF, thermophilic bacteria convert the sugars into hydrogen and organic acids, preferably acetic acid. Part of the sugars is also used for cell growth. Process parameters and substrate conversion for the investigated case are presented in Table 1 and are based on feasible assumptions discussed with partners within the EU-project Hyvolution.

The liquid effluent from the THF is further diluted and fed to the photo-heterotrophic fermentation, where the organic acids are converted to more hydrogen and carbon dioxide. Photo-fermentation is a light driven process which requires sunlight and operates at a temperature of about 30°C.

3 Results and Discussion

To reduce heat and water demand, a previous study on wheat suggested the use of a combination of recirculation of process effluents of PHF to THF (external recirculation) and to PHF (internal recirculation PHF), together with heat integration by introducing a heat exchanger to the thermophilic fermentation step [3].

Recirculation has been defined as the percentage of reduction of dilution water, by substitution of fresh water with the PHF effluent. Four levels of recirculation have been selected for calculation: no reduction, 30%, 60% and 90% reduction of dilution water in the corresponding fermentation steps.

The influence of effluent recirculation on the mass and heat balance of the process based on feedstock molasses is presented below.

Figure 2 reports the simplified mass and energy balances of the heat integrated process option without effluent recirculation. At these conditions, Hyvolution process would require an high water demand of 198 t/h as well as thermal input of 2.6 MW, which is higher than the plant capacity corresponding to 2 MW thermal power.

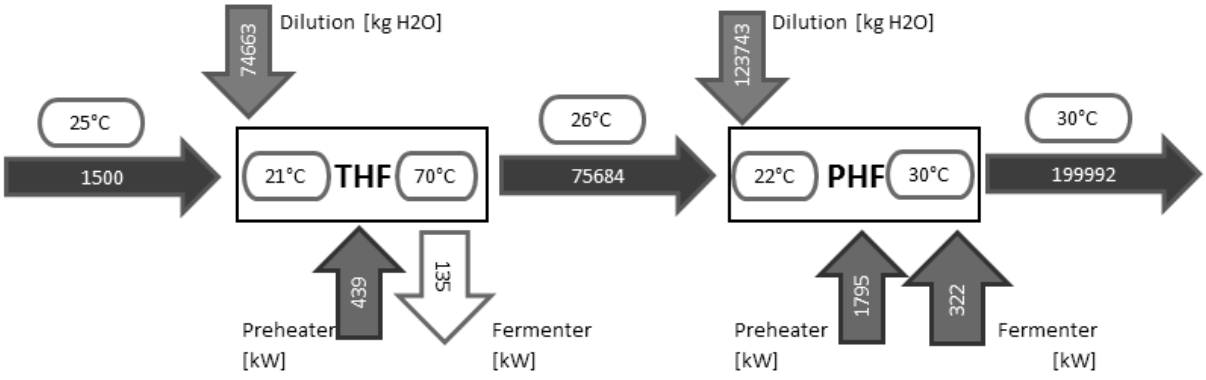

Figure 2: Basic mass and heat balance of heat integrated Hyvolution process based on Molasses (mass flow in kg/h).

Introduction of effluent recirculation in the process reduces heat and water demand of the process. Figure 3 illustrates the total heat and water demand for Hyvolution process based on molasses with increasing recirculation rate. The total heat demand is defined as the sum of all required heat inputs in the process steps. Replacing 90% of fresh water by effluent of PHF reduces the water and heat demand from 198 t/h to 21 t/h and 2570 kW to 760 kW, respectively.

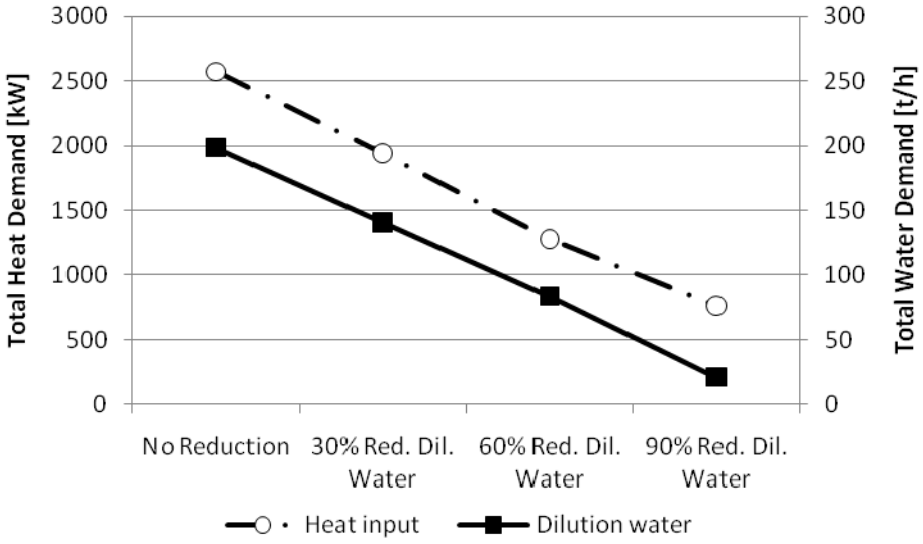

Figure 3: Comparison of overall heat (dashed/dotted line) and water (solid line) demand for different recirculation options.

An important point to take in consideration is the heat duty of PHF and the connected temperature levels (Figure 2). The photo-fermentor could be seen as a sun heater and would need rather cooling than heating. However, the simulation program calculates the heat or the cooling demand necessary to reach 30°C necessary for fermentation, by considering only the temperature of the photo fermentor inlet streams. Without recirculation the heat demand account for 80% of the heat demand of the entire process, but depending on outdoor conditions and season the heat demand of photo-fermentor might be covered completely by solar irradiation. As an alternative, low temperature heat could be applied by integration of hydrogen production with a sugar plant, as proposed by Markowski et al. (2009) [5], using the available off-heat from the sugar refining process at 60°C. In this way, the heat demand of the process (with/without recirculation) could be reduced to less than 500 kW.

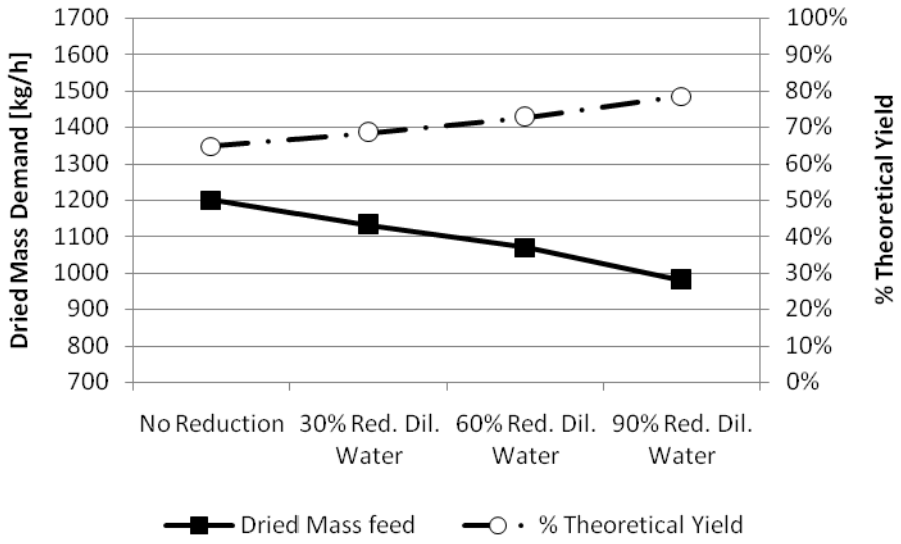

Figure 4: Comparison of dried mass feed (solid line) and overall conversion of sugars to hydrogen (dashed/dotted line) for different recirculation options.

Further analysis of the effects of recirculation, shows that with increasing recirculation rate, less feedstock is required to produce the same amount of hydrogen (Figure 4). This behaviour is caused by the not complete conversion of substrate in the PHF step: the recirculation of the not reacted organic acids allows a further reaction in PHF and thus the reduction of feedstock demand by 18%. The overall conversion of sugars to hydrogen in the process increases from 65% to 79% of the maximum theoretical value.

4 Conclusions

The work presents results of an integration study to reduce heat and water demand of the fermentative production of hydrogen from molasses. Recirculation of effluents from the photo-heterotrophic fermentor to the thermophilic and the photo-heterotrophic fermentor - referring to internal and external recirculation - together with a proper heat recovery seems to be practicable to obtain a reduction of heat and water demand up to 70% and 90%, respectively. Moreover the overall conversion of fermentable sugars into hydrogen would increase from 65% to 79% of the maximum theoretical value.

Implementation of improved process parameters extrapolated from experimental results will allow further insight to the feasibility of process and heat integration options and play an important role in the final selection of a promising process route for HYVOLUTION process.

Acknowledgments

The authors gratefully acknowledge the support of the project by the European Union's 6th Framework Program on Sustainable Energy Systems (Hyvolution, Contract-No 019825).

References

[1] L. Fulton. Reducing Oil Consumption in Transport: Combining Three Approaches, IEA/EET working paper, April 2004.

[2] P.A.M. Claassen; T. de Vrije. Non-thermal production of pure hydrogen from biomass: Hyvolution, Int. J. Hydrogen Energy, 31 (2006) 1416-1423.

[3] D. Foglia, W. Wukovits, A. Friedl, M. Ljunggren, G. Zacchi, K. Urbaniec, M. Markowski, M. Modigell. Integration study on a two-stage fermentation process for the production of biohydrogen, 2009, Chemical Engineering Transactions 18, pp. 345-350

[4] K. Willquist, P.A.M. Claassen, E.W.J. van Niel. Evaluation of the influence of CO_2 on hydrogen production by Caldicellulosiruptor saccharolyticus, Int. J. Hydrogen Energy, 34 (2009) 4718-4726.

[5] M. Markowski, K. Urbaniec ,A. Budek, M. Trafczynski , W. Wukovits ,A. Friedl, M. Ljunggren , G. Zacchi. Heat integration of a fermentation-based hydrogen plant connected with sugar factory, 2009, Chemical Engineering Transactions 18, pp. 351-356.

Thermochemical Cycles

Christian Sattler

Abstract

Thermochemical cycles promise to be one of the most efficient possibilities for large-scale hydrogen production. Therefore, nuclear and solar heated thermochemical cycles have been under development since the oil crises of the 1970s. During low oil prices in the 1980s and 1990s the interest on these technologies was low but since the ratification of the Kyoto Protocol thermochemical cycles are back in the focus. This chapter gives an overview on the different classes of thermochemical cycles and their state of development. It also describes where the limits of these technologies are and gives a view on possibilities for a future industrial application. Where possible it also discusses the economics of the processes.

Improving Sulphur Dioxide Yield in the Sulphuric Acid Thermal Decomposition Process through the Application of High Temperature Ceramic Membrane Separations

Rachael H. Elder, **Ian Atkin**, **Geof H. Priestman**, **Derek C. Sinclair**, **Ray W.K. Allen**, University of Sheffield, UK

1 Introduction

Sulphuric acid thermal decomposition is part of a number of promising thermochemical water splitting cycles, including the hybrid sulphur (HyS) [1, 2] and sulphur iodine (SI) [3] cycles. The decomposition reaction is endothermic and occurs in two stages, as seen in the reaction equation below [4]. Sulphur trioxide decomposition to sulphur dioxide exhibits a poor yield in the temperature range accessible by conventional heat sources. As such the reaction must be carried out at very high temperature (≥ 700°C) in order to achieve an appreciable yield of sulphur dioxide [5].

$$H_2SO_4 \leftrightarrow SO_3 + H_2O \leftrightarrow SO_2 + ½\ O_2 + H_2O$$

It is proposed that by preferentially removing oxygen from the equilibrium reaction products, the equilibrium will be in effect shifted, allowing super-equilibrium SO_2 yields at a given temperature. This would allow conventional heat sources such as current nuclear reactors to be used, as well as increasing the yield where a higher temperature heat source, e.g. solar energy, is used. This work investigates the feasibility of preferentially removing oxygen through the use of oxygen separation membranes.

2 Membrane Simulations

A membrane separation stage for the preferential removal of oxygen could take two forms:

- Standard catalytic reactor, with a membrane separator downstream and retentate recycling
- Use of a catalytic membrane reactor (CMR) in lieu of the standard catalytic reactor

A series of simulations were carried out in ProSimPlus to investigate both membrane reactor types, operating with both dense membranes and porous Knudsen regime membranes. These simulations showed that use of a selective separation process can increase yield at a given temperature. Figure 1 shows the ProSimPlus flowsheet for a downstream membrane separation as well as results for the same system. The ‘F’ values represent the selectivity of the dense membranes. Porous membranes which exhibit Knudsen separation produce a small yield improvement, however dense oxygen separation membranes produce significantly greater yield increases. The simulations also showed that CMRs produce greater SO_2 yield improvements than the downstream separation process. Given this evidence, use of a CMR may seem preferable to using downstream separation. However, a

CMR may be significantly more difficult to engineer in practice and hence the smaller SO_2 yield improvement offered by the downstream separation process may be more economic.

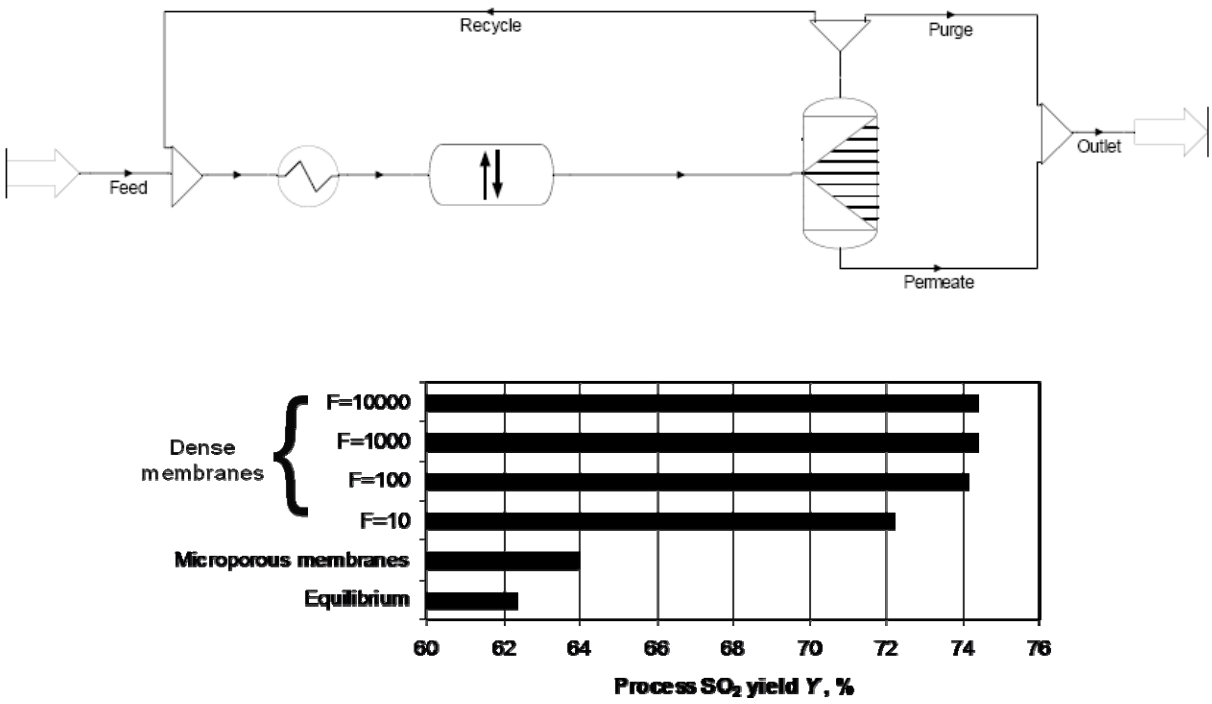

Figure 1: The ProSimPlus flowsheet and some results for the downstream membrane separation. F values indicate the selectivity of the membrane.

3 Membrane Material Selection

A review of electrically driven and mixed ion/electron conducting dense membranes was carried out and a number of candidate materials were identified. Calculations were performed in *HSC Chemistry* to evaluate the process stability of the candidate materials under the harsh process environment. Yttria and zirconia were both calculated to be stable in the temperature range of interest, except for zirconia at <750°C and 20 bara. Because of this, YSZ (yttria-stabilised zirconia) is considered to be a good candidate material and was selected for experimental testing. Based on the results of the equilibrium calculation, the majority of other metal oxides encountered/employed in ion conducting or MIEC membranes are not suitable for use with a sulphuric acid thermal decomposition process. The equilibrium data for silica strongly suggests it will be stable in the reaction environment, confirming the widespread use of quartz for high temperature apparatus.

YSZ belongs to a group of solid electrolytes that conduct oxygen ions at high temperatures, but which conduct electrons poorly. In order for the membrane to function, an external electron conduction path must be provided. Molecular oxygen from the process stream dissociates on contact with the porous cathodic membrane surface. The adsorbed atomic oxygen then moves across the electrode surface to the boundary with the electrolyte, at which point it is incorporated into the electrolytic membrane. Following transport through the

membrane, the ions recombine at the opposite porous anodic surface and pass into the product stream. A schematic of such a membrane is shown in Figure 2.

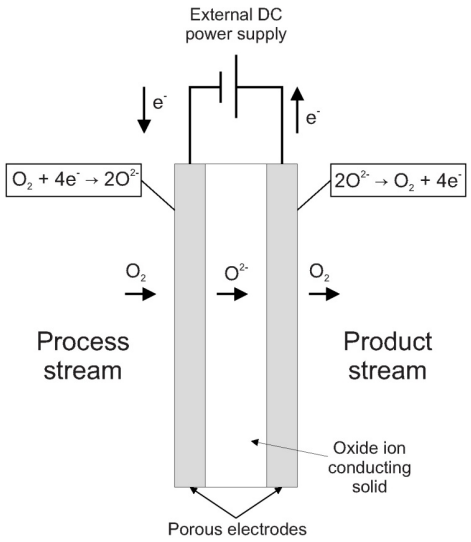

Figure 2: Schematic of an electrically driven dense oxygen separation membrane.

4 Experimental Work

The experimental rig process schematic is presented in Figure 3. The rig was designed to allow a measured mix of GC grade helium, high purity oxygen, and/or sulphur dioxide to be fed from high pressure cylinders to the feed side of the membrane.

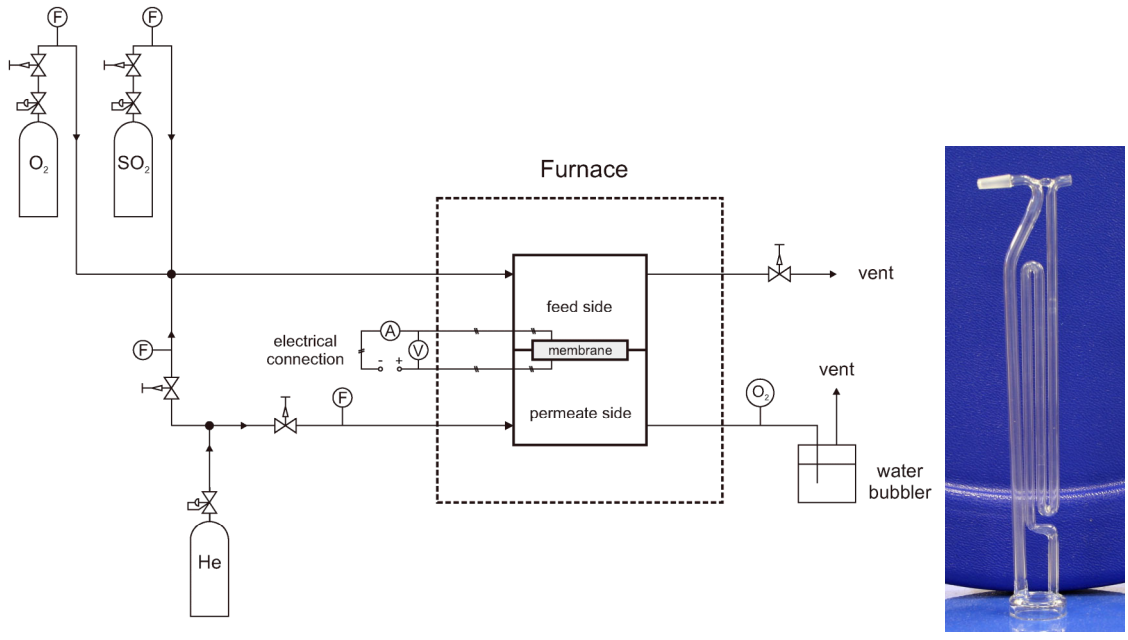

Figure 3: High temperature membrane separation rig schematic and Quartz membrane holder.

A measured supply of helium is fed to the permeate side to act as the sweep gas, maintaining zero oxygen partial pressure on the permeate side. A bespoke quartz membrane holder was designed, as seen in Figure 3, which is held inside a furnace whose temperature can be varied as required. A paramagnetic gas analyser in the permeate stream allows measurement of the oxygen concentration. Comissioning work verified the satisfactory operation of the rig and also showd gold foil to be a suitable sealing material.

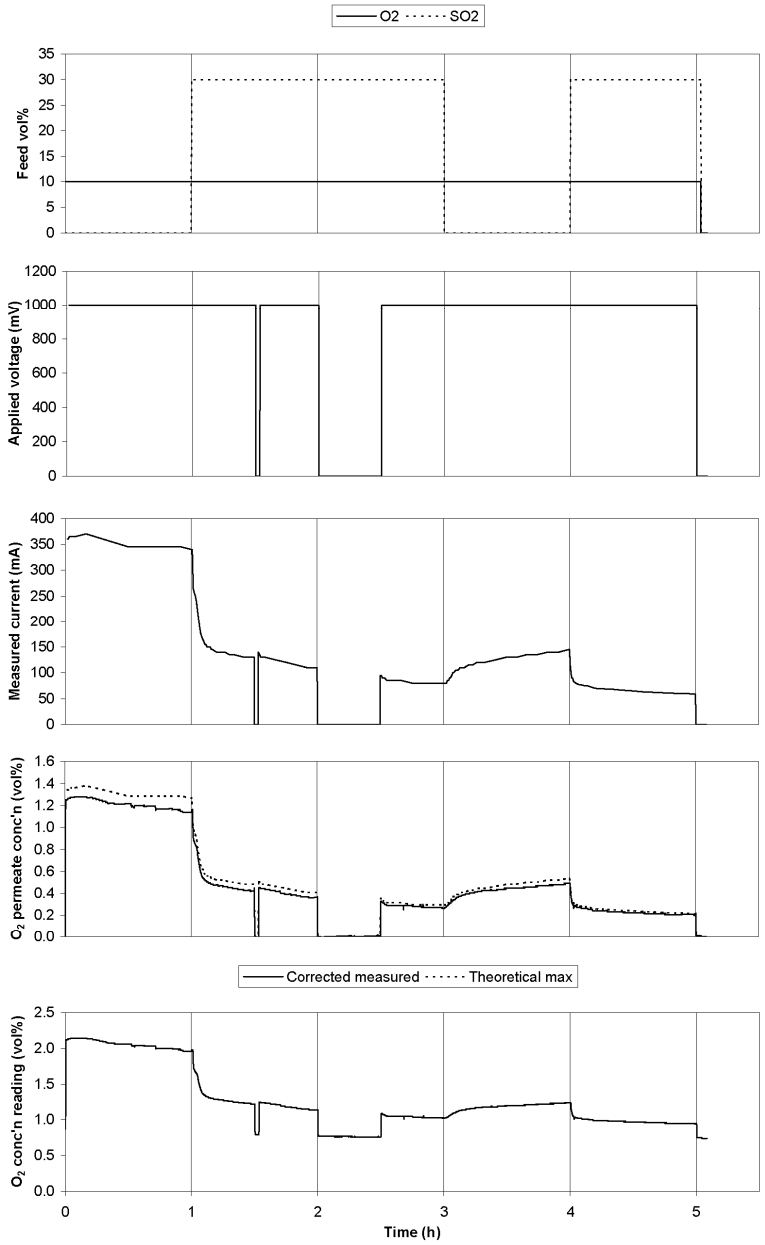

Figure 4: Experimental data for exposure of 8% YSZ/Pt pellet to SO_2 and O_2 at 800°C.

Experiments have been carried out at 800°C, 850°C and 900°C with an applied voltage of 1 V and a feedgas of 10% O_2 in helium for one hour, followed by 30% SO_2 and 10% O_2 in helium. Initial results at 800°C, seen in Figure 4, show that O_2 is conducted through the YSZ

membrane, however when SO_2 is introduced to the feed the permeate concentration decreases dramatically with an accompanying decrease in current. The IS (impedence spectroscopy) data showed no changes in the bulk or grain boundary electrical conductivity, but did indicate the presence of a surface layer on the YSZ/Pt pellet following SO_2 exposure.

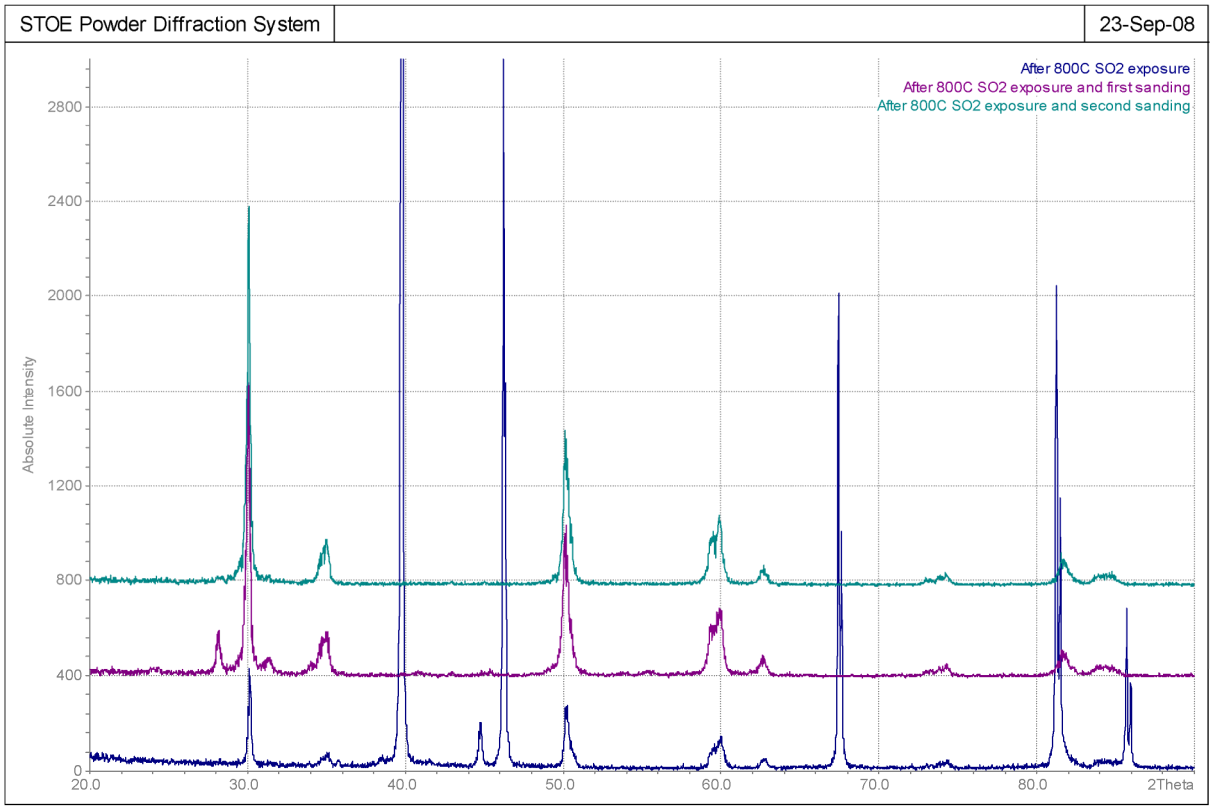

Figure 5: XRD data for YSZ/Pt membrane after initial 800°C SO_2 exposure and during post-exposure sanding.

Removal of the electrode and surface of the YSZ by sanding, followed by application of a new electrode and retesting, showed oxygen permeability comparable to that at the start of the test. The XRD (x-ray diffraction) data shows an extra peak after the first sanding, indicating a surface layer on the YSZ (Figure 5). Further experiments were carried out at 850^{o}C with a greater emphasis on surface analysis to investigate the cause of this surface layer. XPS (x-ray photoelectron spectroscopy) of an unused membrane disk showed the presence of bismuth as well as yttria, zirconia and platinum. This was determined to be from a bismuth based frit in the platinum ink used for the electrodes. Figure 6 shows the XPS data for a used membrane disk. The following observations can be made from these spectra:

- There is now sulphur present on the pellet surface;
- The proportion of oxygen on the surface has increased significantly;
- The ratio of yttria to zirconia has increased following the SO_2 exposure;
- None of the metal peaks have shifted significantly following exposure.

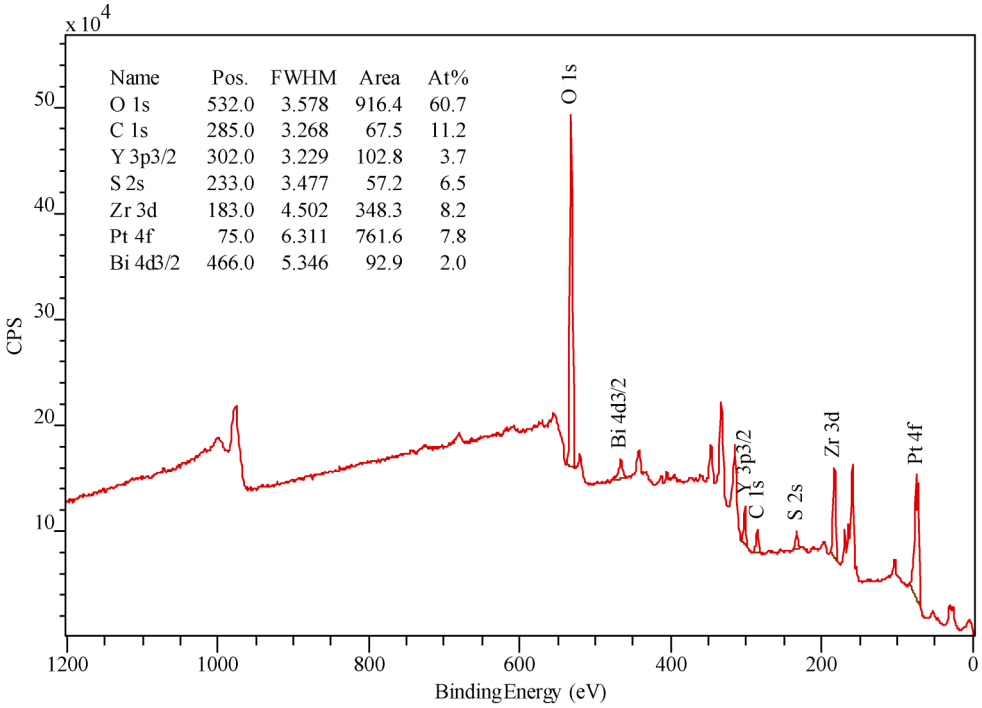

Figure 6: XPS wide scan of used 8YSZ/Pt pellet - thin electrode point.

The experiment at 850°C was repeated using a fuel cell grade platinum ink which does not contain a bismuth frit. This yielded similar IS and XRD results to those above, showing that the bismuth is not the cause of the surface layer. Figure 7 shows an SEM image of the electroded YSZ using the fuel cell grade platinum ink. No significant changes were seen in the SEM images after exposure to SO_2.

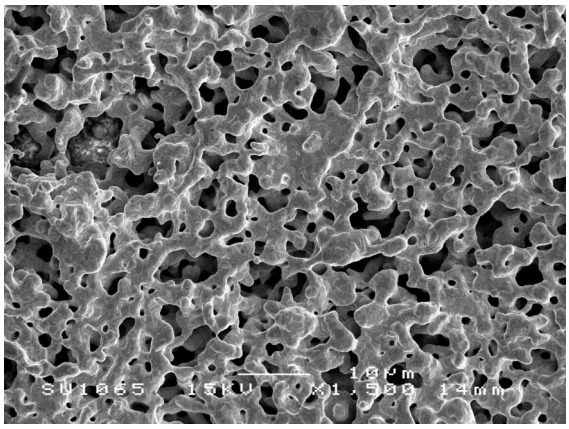

Figure 7: SEM image of electroded YSZ pellet (GEM ink), 1500x magnification, JEOL6400 SEM.

The results suggest that the drop in membrane performance is due to adsorbed sulphur species on the surface of the membrane. Work is ongoing to investigate ways to recover the membrane performance and thereby make it a viable option for increasing SO_2 yield in the sulphuric acid decomposition process.

5 Conclusions

Process Simulations showed that a selective membrane system could increase SO_2 yield in the sulphuric acid decomposition process at a given temperature. Experiments have shown that YSZ membranes are capable of separating oxygen from SO_2, although a rapid decrease in performance is seen compared to initial flux values. This decrease was found to be due to absorbed sulphur species on the surface of the membrane. Further testing is on going to investigate ways of recovering the initial performance.

References

[1] Brecher L, Spewock S, Warde C. The Westinghouse Sulphur Cycle for the thermochemical decomposition of water. Int J Hydrogen Energy 1977;2(1):7-15.

[2] Farbman GH. Hydrogen production by the Westinghouse sulfur cycle process: program status. Int J Hydrogen Energy 1979;4111-122.

[3] Norman JH, Besenbruch GE, Brown LC, O'Keefe DR, Allen CL. Thermochemical Water Splitting Cycle, Bench-Scale Investigations and Process Engineering. 1982, General Atomic Company. GA-A16713

[4] Barbarossa V, Brutti S, Diamanti M, Sau S, De Maria G. Catalytic thermal decomposition of sulphuric acid in sulphur-iodine cycle for hydrogen production. Int J Hydrogen Energy 2006;31(7):883-890.

[5] Atkin I. Improvement of Sulphur Dioxide Yield from the Sulphuric Acid Thermal Decomposition Process by Membrane Separation. PhD Thesis, Department of Chemical and Process Engineering, University of Sheffield. 2009

HycycleS – A Project on Solar and Nuclear Hydrogen Production by Sulphur-based Thermochemical Cycles

Martin Roeb, **D. Thomey**, **D. Graf**, **L. de Oliveira**, **C. Sattler**, Deutsches Zentrum für Luft- und Raumfahrt e.V. (DLR), Germany
S. Poitou, **F. Pra**, **P. Tochon**, **A. Brevet**, **G. Roux**, **N. Gruet**, **C. Mansilla**, **F. LeNaour**, CEA, France
R. Allen, **R. Elder**, **I. Atkin**, Univ. Sheffield, UK
G. Kargiannakis, **C. Agrafiotis**, **A. Zygogianni**, **C. Pagkoura**, **A.G. Konstandopoulos**, APTL, Greece
A. Giaconia, **S. Sau**, **P. Tarquini**, ENEA, Italy
T. Kosmidou, **P. Hähner**, JRC, Netherlands
S. Haussener, **A. Steinfeld**, ETH Zurich, Switzerland
I. Canadas, **A. Orden**, Empresarios Agrupados, Spain
M. Ferrato, Boostec, France

1 Introduction

HycycleS, a project funded under the 7th Framework Programme of the European Commission, is a cooperation of nine European partners and further non-European partners and aims at the qualification and enhancement of materials and components for key steps of solar and nuclear powered thermochemical cycles for hydrogen generation from water. The focus of HycycleS is the decomposition of sulphuric acid which is the central step of the sulphur-based family of those processes, especially the hybrid sulphur cycle [1] and the sulphur-iodine cycle [2] Emphasis is put on materials and components for sulphuric acid evaporation, decomposition, and sulphur dioxide separation. The suitability of materials and components is demonstrated by decomposing sulphuric acid and separating its decomposition products in scalable prototypes.

The key components, necessary for the high temperature part of the process, are a ceramic compact heat exchanger for solar or nuclear SO_3 decomposition, a receiver-reactor for solar H_2SO_4 evaporation and SO_3 decomposition and an oxygen separator that will on one hand separate the reaction products (i.e. SO_2 and O_2) and on the other hand will act as a promoter for SO_3 decomposition. One aspect essential for sufficient reaction rates is the development of dedicated catalyst systems, which is also part of HycycleS. The final aim is to bring thermochemical water splitting closer to realization by improving the efficiency, practicability and costs of the key components involved and by elaborating detailed engineering solutions.

2 Materials and Catalysts

Firstly, candidate materials for the construction of the targeted key components of sulphur-based thermochemical cycles as well as for possible and promising catalyst/substrate combinations for the catalytic high temperature reduction of SO_3 have been reviewed.

As a consequence of this review, HycycleS' main development route will be based on ceramic materials from the SiC family. Such materials seem to fulfil all necessary requirements for the solar absorbers of the planned receiver reactor,, the plates of the planned compact heat exchanger and for the catalyst support. As base material for the SO_2-O_2 separation membranes Yttria-Stabilised Zirconia (YSZ) has been identified and selected.

A first phase of the long-term exposure of samples concerning different corrosive environments has already been carried out and completed. One kind of treatment are corrosion tests of samples facing temperatures above 800 °C and a chemical environment typical for SO_3 reduction applying a gaseous feed. A second kind of treatment is applied to investigate the stability of samples facing boiling concentrated H_2SO_4. Several of the examined materials and samples, in particular the SiC based materials, withstand the conditions and keep their structural integrity over a substantial period of time (1000 hrs).

Promising catalyst "families" have been identified exhibiting high and stable catalytic activity. Catalysts based on mixed metal oxides with substantially higher activity than the reference oxide material (i.e. Fe_2O_3) have been identified. A number of mixed oxides were synthesized and tested in the decomposition of sulphuric acid for the production of SO_2 and O_2. Materials such as Fe-Cr, Cu-Al, Cu-Fe and Cu-Fe-Al mixed oxides showed initial activity comparable to that of Pt/Al_2O_3 [3], which is considered the most efficient material for this reaction so far. This indicates that such materials could provide promising alternatives to the precious-metal-based state-of-the-art catalysts. The reaction over these catalysts most likely proceeds via the formation of intermediate sulphate species and this requires that the temperature is sufficiently high in order to facilitate the rapid decomposition of these species.

An empirical kinetic law has been derived from experiments enabling the refinement of reactor design and prototype development. The first order kinetics probably indicates that the absorption of the reactant on the catalyst is the rate limiting step of the reaction mechanism.

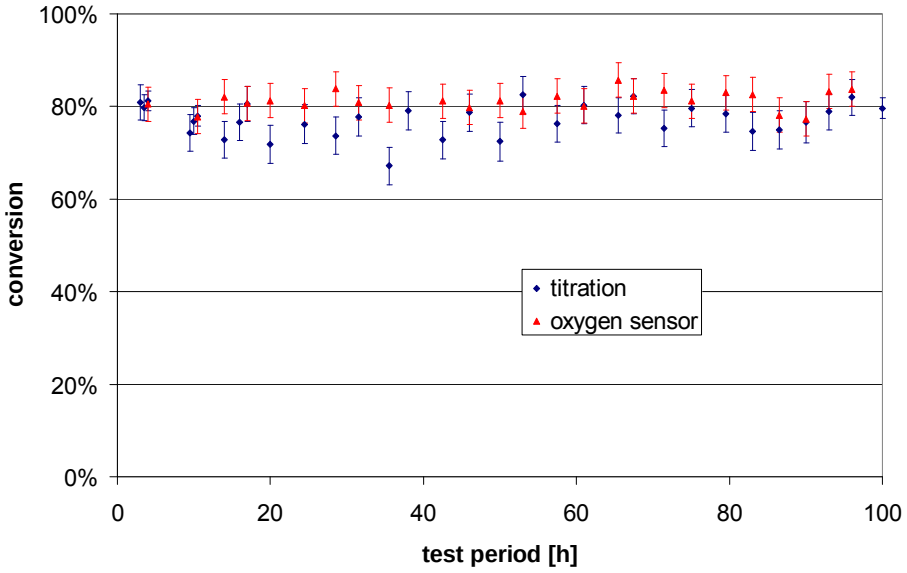

Figure 1: Conversion of H_2SO_4 with time on stream over a Fe_2O_3-coated SiSiC honeycomb (T = 850 °C, P=1bar).

Absorber monoliths coated with Fe_2O_3 and CuO catalyst were exposed to typical reaction environment for 100 hours without reduction of catalytic activity (Figure 1) and therefore qualified as the reference catalyst systems of choice for the first experimental campaigns with the solar receiver-reactor.

3 Heat Exchanger Reactor

The development and use of high temperature heat exchangers are essential for the accomplishment of hydrogen production by high temperature processes powered by concentrating solar systems or high temperature nuclear reactors.

Those heat exchangers have to withstand high temperature and, at the same time, have to operate as reactors. In the case of the present sulphur based thermochemical cycles they, therefore, have to resist in very corrosive environment. Only ceramics can match these specifications. A shell and tubes concept of SiC heat exchangers does not achieve the compactness required to reach the thermal efficiency aimed at. Therefore, a decision to develop a compact SiC plate heat exchanger was made.

The assembly of a plates stack is a key technological point for such a component. The heat exchanger will exhibit a large number of joints and some of them will have a large surface but at the same time all requirements related to tightness, corrosion and mechanical resistance must be satisfied. In terms of achieving an efficient assembly of the plates, brazing was regarded as the most promising solution.

The development and construction of a heat exchanger prototype has to take into consideration the possibilities and limitations of the specific fabrication process and therefore it was supported by modelling of different design options as well as by the fabrication and testing of manufacturability, tightness and structural integrity of smaller mock-ups representing crucial parts of the prototype.

The final aim of this development is the qualification of a pilot-scale heat exchanger as H_2SO_4 decomposition reactor. The main research challenge is to implement a large scale plate heat exchanger with a thermal efficiency of more than 85%.

From the beginning of the project, an optimized design has been proposed (about 800mm x 300mm x 200mm) taking into account kinetic and thermo-hydraulic correlations, chemical engineering approach for the modeling and possibility to braze the final prototype. For the hot source plates, wavy channels (so-called herringbone pattern, Figure 2 - left) were used to improve the local heat transfer coefficient and ensure turbulent flow regime compared to straight channels. For the reaction plates, large straight channels filled with catalyst and meandering inside plates are used to ensure satisfactory reaction efficiency with a sufficient residence time for the reactive fluid (Figure 2 - right). The main characteristic of this so-called “catalyst bed” exchanger-reactor design is that it consists of permanent thermal exchange and chemical reaction areas.

Figure 2: SiC channelled plates of the prototype: heat source plates (left) and a reaction plate with one large meandering channel (right).

The full-size prototype is currently being manufactured and is estimated to be ready for testing in June 2010.

4 Solar Receiver-reactor

As a concept for a direct coupling of concentrated solar radiation into the process, a multi-chamber reactor was chosen which allows adaptation of each part of the reactor to the requirements of both evaporation and decomposition reactions so that these two sub-processes are performed separately. In particular, such a concept is advantageous when considering a future up-scaling for a solar tower application. On the receiver of a solar tower, there are typically regions with high heat flux in the center while significantly less solar radiation reaches the outer part of the receiver. Consequently, a multi-chamber reactor with two different temperature levels can exploit the energy input on a solar tower more efficiently than a single-chamber requiring a more uniform heat flux distribution.

The reactions in the two chambers have different reaction enthalpies and require different operating temperatures:

Evaporation: $H_2SO_{4(aq)} \rightarrow H_2SO_{4(g)} \rightarrow SO_{3(g)} + H_2O_{(g)}$ T = 350-400 °C

SO_3 reduction: $SO_{3(g)} \rightarrow SO_{2(g)} + \frac{1}{2}O_{2(g)}$ T = 800-1000 °C

Consequently, the conditions needed for the evaporator and the decomposer differ considerably. Therefore, the reactor design for a prototype solar receiver-reactor includes two different chambers operating at different conditions: one for the evaporation of the acid, the second for the SO_3 reduction.

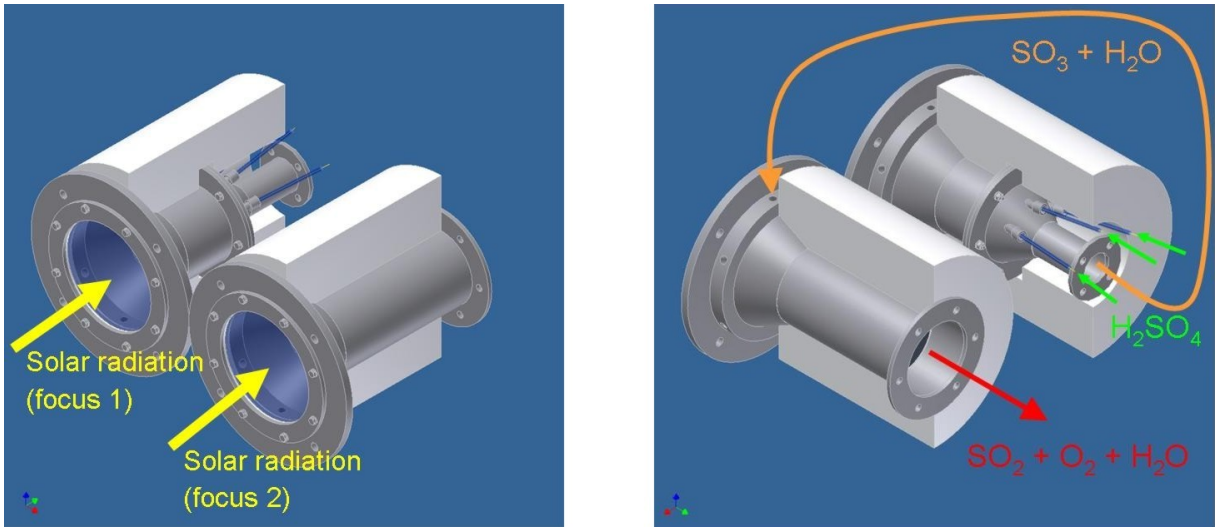

Figure 3: Front (left) and rear view (right) of the HycycleS multi-chamber solar reactor: focus 1 – evaporator; focus 2 – decomposer.

Evaporator

The solar radiation enters the reaction chamber through a quartz window held by a flange construction. The vaporization of the sulphuric acid is carried out in a cylindrical absorber made of SiSiC foam. The acid is fed to the interior of the foam by tubes. The product gases, primarily consisting of sulphur trioxide, water vapour and the carrier gas nitrogen, leave the reaction chamber through an exhaust pipe and are subsequently directed to the second chamber for the decomposition of SO_3.

Decomposer

The decomposer is powered by focus 2. The flange construction supporting the quartz window is the same as in the case of the evaporator. The inlet gas coming from the evaporator enters the decomposer through three inlets in the flange. The splitting of sulphur trioxide takes place on a SiSiC honeycomb structure coated by the catalyst material. Product gases of the decomposer are sulphur dioxide, unreacted sulphur trioxide, oxygen, water vapour and carrier gas. After leaving the second chamber, the gas is spectrometrically analyzed at the reactor outlet and subsequently neutralised in a gas washing unit.

The reactor has been constructed and installed at DLR's solar furnace in Cologne. Two test series have already been carried out. The tests proved the practicability and suitability of all reactor components. Moreover, sulphuric acid was successfully decomposed to provide the required SO_2 product with yields of up to 90 % of the respective thermodynamic value and with reactor efficiencies of up to 40 %.

Design activities and experimental series are accompanied and supported by different methods of reactor and process simulation, e.g. the SiC foam used for the evaporation chamber was analysed in depth. The accurate knowledge of its effective heat/mass transport properties is crucial for the optimal design and operation of the solar reactor. Structure and dimensions of the foam must allow for an efficient evaporation while avoiding reduced heat transfer at the Leidenfrost point.

The heat and mass transfer properties of the foam were determined. Computer tomography in conjunction with numerical techniques were used to determine the morphological characteristics and the effective transport properties of the foam, namely: extinction coefficient, scattering phase function, thermal conductivity, interfacial heat transfer coefficient, permeability, Dupuit-Forchheimer coefficient, tortuosity and residence time distributions as well as the dispersion tensor [4]. These effective transport properties are being incorporated in a continuum reactor model developed by spatial averaging the governing equation in the fluid and solid phases. This allows for treating the distinct phases as interpenetrating continuum, where the effective properties account for the complex pore-level structure.

5 SO_2-O_2 Separation

The decomposition of SO_3 to SO_2 is thermodynamically favourable at temperatures above 800°C in order to produce a sensible equilibrium conversion. Le Chatelier's principle suggests that oxygen removal will shift the equilibrium in favour of increased decomposition. Identifying suitable methods for carrying out this separation is complicated by the lack of membrane materials able to withstand the severe process conditions involved. Therefore dense oxygen transport membranes, made from novel and complex ceramics, are investigated to evaluate their stability and suitability to the H_2SO_4 decomposition section. This may enable a highly pure oxygen product stream to be produced without the need for a further oxygen separation step in the process. Alternatively, such a membrane could be used to reduce the maximum temperature required, enabling the use of a wider range of heat sources for the thermochemical cycle.

Calculations were performed to evaluate the process stability of candidate materials. As a result, YSZ is considered to be a good candidate material and is being investigated further. Experimental stability and permeation testing of the membranes is carried out using a high temperature membrane cell held within a furnace. It was found that at an operating temperature of 850°C, the oxygen flux through the membrane reaches a pseudo-steady state of approximately 20% of the original flux after eight hours of exposure to SO_2/O_2 mixtures. Work is currently concentrated on maximising the flux during that pseudo steady state.

In order to make commercial progress in the near future, it will be necessary to proceed with a detailed design of a conventional oxygen separator. The necessary materials information, in terms of reliable thermodynamic data on the equilibrium between oxygen and the solutions of SO_3 and SO_2 downstream of the decomposition reactor, do not exist in the literature and yet represent a major obstacle to the immediate design of an operating cycle. Thus, multi-component equilibrium data for SO_2, oxygen and water are being measured and models to allow prediction of the relevant properties are being developed. The data are being measured using a separate and independent apparatus which already exists in prototype form.

E.g. thermodynamic modelling of the binary SO_2-H_2O and multi-component SO_2-H_2O-O_2 systems has already been accomplished [5]. Equations to describe the vapour liquid equilibrium of sulphur dioxide in water have been developed. These equations were then solved and the results were compared with own experimental data and with data from the

literature. The resulting average error between the calculated and experimental solubility at the range of temperatures studied was in the region of ± 1.5 %.

An experimental apparatus was designed to provide data points to verify the thermodynamic models created. A photo of the apparatus, shown without insulation for illustration, is given in Figure 4a.

a) 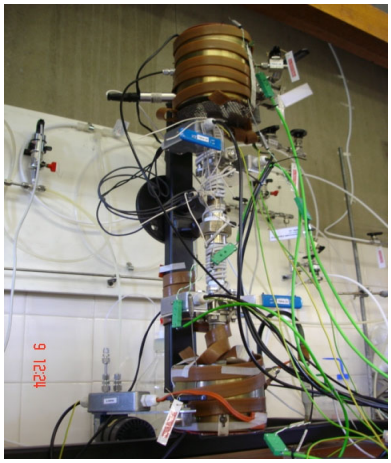

b) 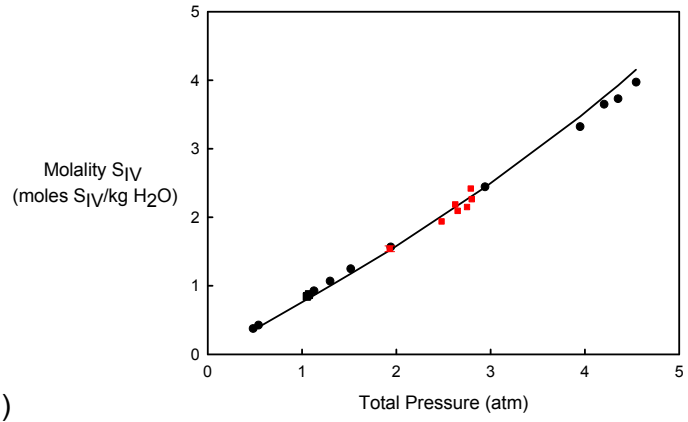

Figure 4: a) photo of the equilibrium still; b) Comparison of values for sulphur dioxide solubility at 40 °C.

Results obtained for the SO_2-H_2O system show very good agreement with both the model and the literature data, as shown in Figure 4b. The deviation is generally lower than 5%. This finding was taken as strong indication that equilibrium can be measured using the apparatus. Another test rig has been developed and is currently used to measure the oxygen solubility in multi-component mixtures.

6 Techno-economics

The main parameters that crucially influence the investment costs of a high temperature hydrogen production plant are the components costs mainly based on the obligatory choice of quite expensive materials. In the majority of cases, these are the only ones which are able to withstand the extreme conditions of the sulphur-based thermochemical cycles. HycycleS evaluates the impact of the key alternatives concerning the choice of materials, manufacturability, reliability etc. both on investment cost and on the production cost of hydrogen. An analysis is carried out in order to assess the critical aspects regarding component costs, reliability, maintenance that greatly influence the hydrogen production cost.

A general calculation method and a procedure of assessing the process have been developed. Currently, data from the experimental parts of the project including choice of materials, plant and components design, efficiencies and chemical yields are used to be fed into the model to calculate investment costs, operation and maintenance costs and consequently hydrogen production costs and to enable sensitivity studies.

7 Summary

The project HycycleS identified potential construction and catalyst materials for the targeted key components of solar and nuclear powered sulphur based thermo-chemical cycles and for the catalytic high temperature reduction of SO_3 as one of the crucial steps of those processes.

HycycleS' main development route is based on ceramic materials from the SiC family – to be used as construction materials for sulphuric acid decomposers of two different configurations: on the one hand a solar receiver reactor and on the other hand a compact heat exchanger. Base materials for separation membranes are YSZ.

Mock-ups of sub-units and prototypes of the mentioned decomposers have been developed and are currently being tested. Laboratory test rigs for different purposes such as corrosion tests, catalyst development, catalyst stability tests and selectivity of separation membranes - have been built and are being used to qualify materials and to prepare and accompany the prototypes' test operation.

The experimental data will be used to refine models of components, process units, and of the process as a whole to eventually enable the evaluation of plant and hydrogen production costs.

Acknowledgement

The authors thank the European Commission for co-funding the project HycycleS in the 7th Framework Program (contract no. 212470).

References

[1] Brecher L.E., Spewock S., Warde C.J., The Westinghouse sulfur cycle for the thermo-chemical decomposition of water, Proc. 1st World Hydrogen Energy Conference 1976.

[2] Schuster J.R., Status of thermochemical water-splitting development at General Atomics, GA-A14666, General Atomics 1977.

[3] Karagiannakis, G. P., Pagkoura, C., Zygogianni, A., Agrafiotis C., Konstandopoulos, A.G., Materials for Sulphuric Acid Decomposition in Solar Thermochemical Cycles for Hydrogen Production, SolarPaces2009, September 2009, Berlin.

[4] Haussener, S., Coray, P., Lipiński, W., Wyss, P., and Steinfeld, A., Tomography-based heat and mass transfer characterization of reticulate porous ceramics for high-temperature processing, ASME Journal of Heat Transfer - Transactions of the ASME, 132:023305, 2010.

[5] Atkin, I.; Priestman, G.H.; Sinclair, D.C.; Allen, R.W.K., Potential for Using High Temperature Membranes in the Sulphur Trioxide Decomposition Stage of a Thermochemical Cycle, 2008 AIChE Annual Meeting, Philadelphia, USA, 18th Nov. 2008.

The Effect of Anolyte Product Acid Concentration on Hybrid Sulfur Cycle Performance

Maximilian B. Gorensek, William A. Summers, Savannah River National Laboratory, Aiken, SC 29808, USA

1 Introduction

The Hybrid Sulfur (HyS) cycle (Fig. 1) is one of the simplest, all-fluids thermochemical cycles that has been devised for splitting water with a high-temperature nuclear or solar heat source. It was originally patented by Brecher and Wu in 1975 [1] and extensively developed by Westinghouse in the late 1970s and early 1980s. As its name suggests, the only element used besides hydrogen and oxygen is sulfur, which is cycled between the +4 and +6 oxidation states. HyS comprises two steps. One is the thermochemical (>800°C) decomposition of sulfuric acid (H_2SO_4) to sulfur dioxide (SO_2), oxygen (O_2), and water.

$H_2SO_4 = SO_2 + ½ O_2 + H_2O$.

The other is the SO_2-depolarized electrolysis of water to H_2SO_4 and hydrogen (H_2),

$SO_2 + 2 H_2O = H_2SO_4 + H_2$, $E°$ = -0.156 V [2],

explaining the "hybrid" designation. These two steps taken together split water into H_2 and O_2 using heat and electricity.

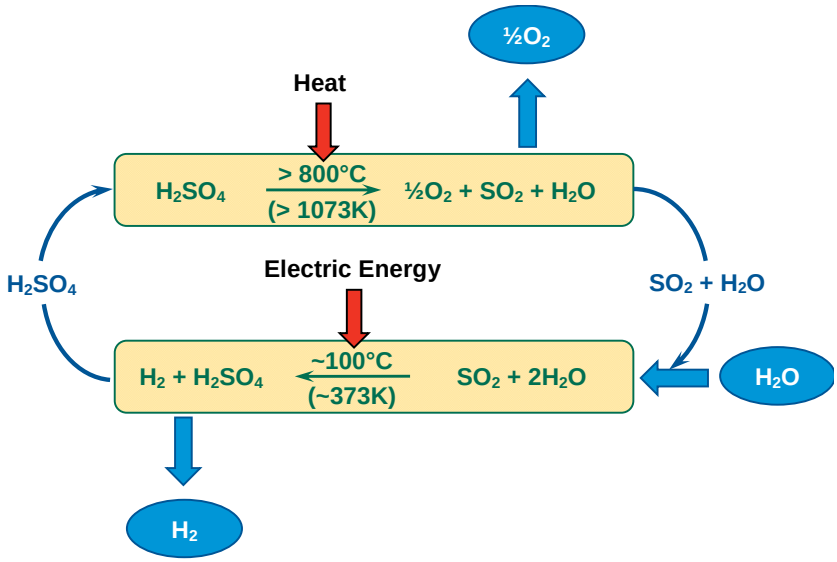

Figure 1: The Hybrid Sulfur cycle.

Researchers at the Savannah River National Laboratory (SRNL) and at the University of South Carolina (USC) have successfully demonstrated the use of proton exchange membrane (PEM) electrolyzers (Fig. 2) for the SO_2-depolarized electrolysis (sulfur oxidation) step [3-4], while Sandia National Laboratories (SNL) successfully demonstrated the high-

temperature sulfuric acid decomposition (sulfur reduction) step using a bayonet-type reactor (Fig. 3) [5]. This latter work was performed as part of the Sulfur-Iodine (SI) cycle Integrated Laboratory Scale demonstration at General Atomics (GA) [6]. The combination of these two operations results in a simple process that will be more efficient and cost-effective for the massive production of hydrogen than alkaline electrolysis. Recent developments suggest that the use of PEMs other than Nafion will allow sulfuric acid to be produced at higher concentrations (>60 wt%), offering the possibility of net thermal efficiencies around 50% (HHV basis). The effect of operation at higher anolyte concentrations on the flowsheet, and on the net thermal efficiency for a nuclear-heated HyS process, is examined and quantified.

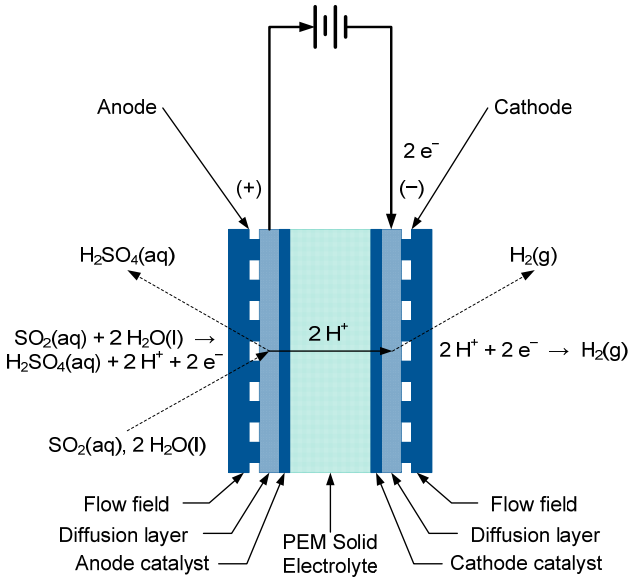

Figure 2: SRNL PEM SO_2-depolarized electrolyzer schematic.

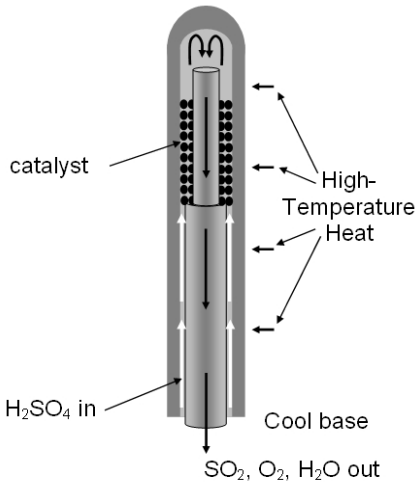

Figure 3: SNL high-temperature bayonet H_2SO_4 decomposer schematic.

2 Problem Statement

The combination of a PEM SO_2-depolarized electrolyzer (SDE) with a bayonet-type high-temperature sulfuric acid decomposition reactor has been described in detail elsewhere [7]. The simplicity of the two key components is an attractive feature and leads to a relatively simple flowsheet. However, there is more to the process than just these two operations, and their integration necessitates that some compromises be made.

The SDE cannot operate at high conversion because the cell potential depends on the concentration of SO_2 at the anode. Typically, the SDE is operated with about 40% SO_2 utilization, requiring a fairly large recycle stream and a significant SO_2 concentration in the anolyte effluent. That means unreacted SO_2 needs to be removed and recycled before the sulfuric acid product is fed to the decomposition reactor. More importantly, the concentration of sulfuric acid in the anolyte is limited by several factors. Higher H_2SO_4 concentration leads to lower SO_2 solubility and higher reversible potential [2]. It can also decrease the conductivity of the PEM separator, increasing the cell potential [8]. Since efficient operation of the SDE is favored by more dilute anolyte, the concentration of the sulfuric acid product also needs to be increased before it is fed to the decomposition reactor.

The decomposition of H_2SO_4 in the bayonet reactor is an equilibrium reaction that is limited by thermodynamics. That means not only does the SO_2 product have to be separated from the O_2 co-product before it can be fed to the SDE, but unreacted H_2SO_4 needs to be removed and recycled as well. The high-temperature heat requirement is governed by the opportunity for recuperation within the bayonet. It has been shown that the heat requirement is minimized by operating the bayonet at the highest possible temperature and pressure, and at a feed concentration of 80.1 wt% H_2SO_4 [9]. Lower concentrations result in more water being vaporized and condensed with incomplete recuperation, so more high-temperature heat is consumed. Feed concentrations below 65 wt% H_2SO_4 result in heating targets in excess of 400 kJ/mol H_2 which, when combined with the other process heat and power needs, affords a net thermal efficiency comparable to that of alkaline electrolysis. Given the greater complexity of the HyS cycle, it will not be more cost-effective than water electrolysis unless it has a significant efficiency advantage. An obvious way to maximize efficiency is to operate the SDE at the highest possible acid concentration without adversely affecting the cell potential.

3 Approach

As already noted, we have previously proposed a HyS flowsheet that combines a PEM SDE with a bayonet reactor [7]. The anolyte product acid concentration for this flowsheet was limited to 50 wt% H_2SO_4, based on the assumed use of Nafion® as the PEM separator material. Contact with concentrated sulfuric acid decreases the water content of Nafion® and increases its resistivity [8], which has been shown to reach impractical levels as concentrations exceed 50 wt% [10].

This limitation was removed by assuming the use of an alternative PEM material such as acid-doped poly[2,2'-(*m*-phenylene)-5,5'-bibenzimidazole] (PBI) instead of Nafion®. The resistivity of acid-doped PBI membranes, which can operate at much higher temperatures than Nafion®, actually decreases with acid concentration [11]. In fact, the results of

preliminary experiments at USC with PBI membranes show that significantly higher acid concentrations, in excess of 65% H2SO4 by weight may be feasible with acid-doped PBI PEM SDEs [12]. We assume, then, that the SDE uses a PEM capable of operation at anolyte H_2SO_4 concentrations of 65 wt% and temperatures of 120 to 140°C. (The reversible cell potential increases with acid concentration and temperature [2], so operation at temperatures or concentrations higher than this may be limited by thermodynamic considerations.)

The existing Aspen Plus flowsheet model of the SRNL HyS process [7, 13] (Fig. 4) was modified to simulate operation of the SDE at 120°C and 65 wt% H_2SO_4 anolyte product concentration. SO_2 conversion was also increased from 40% to 50%, and a cell potential of 0.6 V was imposed. (SDE operation at 0.6 V and 0.5 A/cm^2 is a development target that should be attainable with acid-doped PBI PEMs [12].) Water flux across the membrane was maintained at 1 mol H_2O / mol H_2 product despite the much lower water content of acid-doped PBI (compared to Nafion®). Since a significant water activity gradient will exist between the cathode and anode, it was assumed that the large driving force for water transport would compensate for the reduced water content of the membrane.

4 Results

By increasing the anolyte product acid concentration from 50 to 65 wt% H_2SO_4, the quantity of water that has to be removed in the concentration step (in order to increase the acid concentration of the bayonet reactor feed to 75 wt% H_2SO_4) is reduced by roughly two-thirds. This means less than half as much energy is needed to achieve the necessary concentration, so all of the heat input can be provided by recuperation from the SDE and the bayonet reactor. However, the water recovered in the acid concentration step is used to absorb SO_2 from the uncondensed product of the bayonet decomposition reactor. Since less water is available for the O_2/SO_2 separation, a single absorber is no longer sufficient; too much SO_2 would remain in the oxygen product.

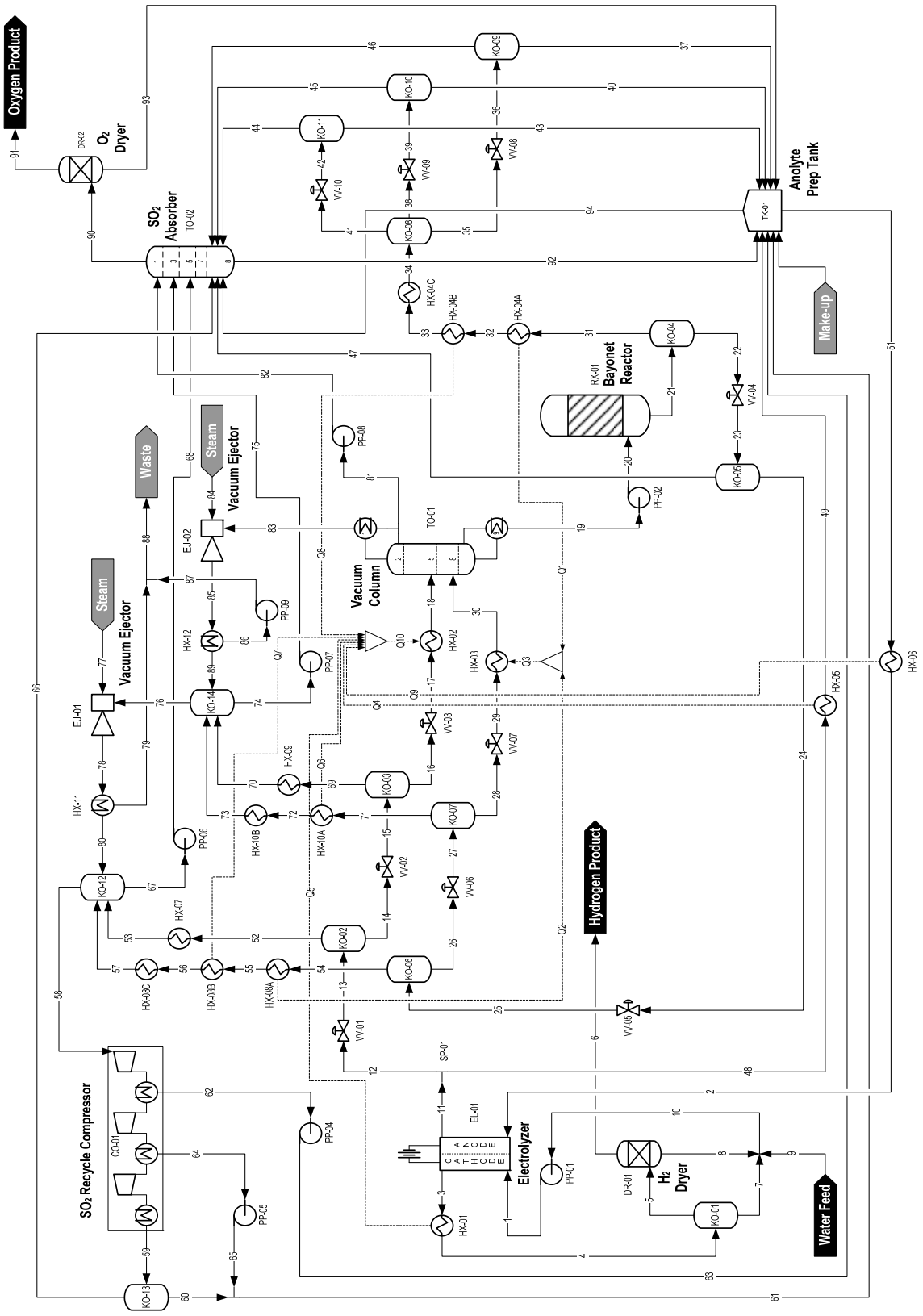

Figure 4: HyS flowsheet using a PEM SDE and a bayonet decomposition reactor [13].

We found that the addition of an absorber/stripper combination could reduce the SO_2 content of the oxygen co-product to ≤ 1 ppm using conventional process equipment and without introducing any new reagents. Water is the solvent; the absorber operates at the pressure of the SDE, while the stripper operates at atmospheric pressure, allowing low-pressure steam or recuperation to provide the necessary boil-up. An SO_2 compressor with atmospheric pressure feed is already being used to recycle unconverted SO_2 recovered from the anolyte product, so the overhead from the stripper can simply be added to the recycle compressor feed.

The resulting flowsheet requires two principal energy inputs: 340 kJ/mol H_2 product high-temperature heat for the bayonet reactor (assuming a peak decomposition temperature of 875°C, equivalent to a 950°C primary heat source temperature) and 116 kJ/mol H_2 product electric power for the SDE. Adding the shaft work needed for the recycle compressor and pumps brings the total power requirement to about 125 kJ/mol H_2 product. The atmospheric pressure stripper reboiler operates at around 100°C with a duty of approximately 40 kJ/mol H_2 product. If this heat input can also be provided by recuperation, then the net thermal efficiency of the process will be about 46% on a higher heating value (HHV) basis, assuming a 45% thermal-to-electric energy conversion efficiency. As an alternative, the heat could be supplied by low-pressure steam from the “bottom” of a coupled power conversion cycle.

This work is ongoing; more detailed and up-to-date results will be included in the presentation.

5 Conclusions

Replacing Nafion® in the SDE with a PEM material that does not rely on high water content for its conductivity (such as acid-doped PBI) will allow the anolyte acid product concentration to be increased beyond 50 wt% H_2SO_4. If the SDE is operated at 65 wt% H_2SO_4, Aspen Plus flowsheet simulation indicates that all of the heat needed to concentrate the bayonet reactor feed can be provided by recuperation from the SDE and from the bayonet product stream. However, the SO_2/O_2 separation can no longer be achieved by selective SO_2 absorption into the recycled water and acid using a single absorber column. The addition of an absorber/stripper combination provides the necessary separation with a minimal low-quality heat input. Net thermal efficiencies of 46% have been calculated to date.

Acknowledgments

This work was funded by the U. S. Department of Energy, Office of Nuclear Energy, NGNP Initiative. SRNL is operated by Savannah River Nuclear Solutions for the U. S. Department of Energy under Contract DE-AC09-08SR22470.

References

[1] Brecher, L. E.; Wu, C. K. Electrolytic decomposition of water. US Patent 3888750, June 10, 1975.

[2] Gorensek, M. B.; Staser, J. A.; Stanford, T. G.; Weidner, J. W., A thermodynamic analysis of the SO_2/H_2SO_4 system in SO_2-depolarized electrolysis. *International Journal of Hydrogen Energy* **2009,** *34*(15), 6089-6095.

[3] Elvington, M. C.; Colón-Mercado, H.; McCatty, S.; Stone, S. G.; Hobbs, D. T., Evaluation of proton-conducting membranes for use in a sulfur dioxide depolarized electrolyzer. *Journal of Power Sources* **2010,** *195*(9), 2823-2829.

[4] Sivasubramanian, P.; Ramasamy, R. P.; Freire, F. J.; Holland, C. E.; Weidner, J. W., Electrochemical hydrogen production from thermochemical cycles using a proton exchange membrane electrolyzer. *International Journal of Hydrogen Energy* **2007,** *32*(4), 463-468.

[5] Gelbard, F.; Moore, R.; Parma, E. *Status of Initial Testing of the H_2SO_4 Section of the ILS Experiment*; Sandia National Laboratories: Report No. SAND2007-7841; December 2007.

[6] Moore, R.; Naranjo, G.; Russ, B. E.; Sweet, W.; Hele, M.; Pons, N. *Nuclear Hydrogen Initiative, Results of the Phase II Testing of Sulfur-Iodine Integrated Lab Scale Experiments, Final Report*; General Atomics: Report No. GA-C26575; October 2009.

[7] Gorensek, M. B.; Summers, W. A., Hybrid sulfur flowsheets using PEM electrolysis and a bayonet decomposition reactor. *International Journal of Hydrogen Energy* **2009,** *34*(9), 4097-4114.

[8] Staser, J. A.; Gorensek, M. B.; Weidner, J. W., Quantifying Individual Potential Contributions of the Hybrid Sulfur Electrolyzer. *Journal of the Electrochemical Society* **2010,** *submitted for publication*.

[9] Gorensek, M. B.; Edwards, T. B., Energy Efficiency Limits for a Recuperative Bayonet Sulfuric Acid Decomposition Reactor for Sulfur Cycle Thermochemical Hydrogen Production. *Industrial & Engineering Chemistry Research* **2009,** *48*(15), 7232-7245.

[10] Junginger, R.; Struck, B. D., Separators for electrolytic cells of the sulfuric acid hybrid cycle. *International Journal of Hydrogen Energy* **1982,** *7*(4), 331-40.

[11] Wainright, J. S.; Wang, J. T.; Weng, D.; Savinell, R. F.; Litt, M., Acid-Doped Polybenzimidazoles: A New Polymer Electrolyte. *Journal of the Electrochemical Society* **1995,** *142*(7), L121-L123.

[12] Weidner, J. W., Personal Communication. Email dated June 17, 2009.

[13] Gorensek, M. B.; Summers, W. A.; Boltrunis, C. O.; Lahoda, E. J.; Allen, D. T.; Greyvenstein, R. *Hybrid Sulfur Process Reference Design and Cost Analysis*; Savannah River National Laboratory: Report No. SRNL-L1200-2008-00002; June 12, 2009.

In Situ Composition Measurements of Bunsen Reaction Solution by Radiation Probes

Shinji Kubo, Yasunobu Nagaya, Japan Atomic Energy Agency, Japan

Abstract

Measuring equipments are integral to chemical process controls. A stable hydrogen production by the Iodine-Sulfur thermochemical water-splitting process is relatively difficult because of lack of existing in situ composition measurement techniques for multiple components and corrosive solution. Composition regulations of Bunsen reaction solution is particularly important, since a closed cycle system provided with this process causes that the many streams with different composition return to this section. Accordingly Bunsen solution becomes changeable composition. Radiation probes have a potential for applications to determine this multiple component solution while the non-contact approach avoids the corrosive issues. Moreover the probes have features of the promptness, contact-less and sequential use. Laboratory scale experiments to evaluate these possibilities of the measurement were conducted with use of simulated Bunsen solution, HIx solution and H_2SO_4 solution, containing HI, I_2, H_2SO_4 and H_2O and sealed radiation sources. Radiations were counted, which were interacted with the solutions in various compositions around room temperature contained in vessels. For HIx solution, the obtained counting rates were correlated with hydrogen volume concentrations; moreover, the application of the Monte Carlo method suggests possibilities that the detector responses for HIx solution by the radiation probes are predictable. For H_2SO_4 solution, iodine atoms had significant influences on the relationship between output values of two gamma-ray density meters, cesium source as higher energy and barium source as lower energy. This results suggest that the neutron-ray probe, the gamma-ray probes of both lower energy and higher energy have possibilities to determine the composition of Bunsen solution of HIx and H_2SO_4 solutions.

1 Introduction

Measurement equipments are indispensable to chemical process controls. A stable hydrogen production by the iodine-sulfur thermochemical water-splitting process (IS process) is relatively difficult because of lack of existing in situ composition measurement techniques for multiple components and corrosive solution. Figure 1 shows a brief reaction scheme for IS process; Bunsen reaction produces two types of corrosive and multicomponent acids around 100 ^{o}C, a HI rich solution (HIx solution) and a H_2SO_4 rich solution (H_2SO_4 solution), which are separated by two-phase separation phenomenon. The HI rich solution is purified and concentrated, then decomposed. Products of I_2 should be recycled to Bunsen section. The H_2SO_4 rich solution is also processed in this manner. Looking at the return streams, closed cycle system causes that the streams concentrate on Bunsen section. Many streams with different composition return, so that Bunsen solution becomes changeable composition; accordingly, solution compositions which are consequent on Bunsen reaction, such as the HI and H_2SO_4 rich solutions, become also changeable.

Compositions of the HIx solution—this solution consists of, HI, I_2, H_2O, little amount of H_2SO_4—and the H_2SO_4 solution—this solution consists of, H_2SO_4, H_2O, little amount of HI and I_2—are important indices for stable process control, since throughputs of the HIx solution and the H_2SO_4 solution should be adjusted with the assistance of these composition values depending on the targeted hydrogen production rate. Methods by radiation probes [1] have a potential for applications to determine this multiple component solution while the non-contact approach avoids the corrosive issues. Moreover these probes have features of the promptness, contact-less, and continuous use. The purpose of this study is to evaluate applicability of the methods for measuring the composition of the HIx solution and the H_2SO_4 solution; we examined data which were obtained by a neutron moisture-meter and gamma-ray density- meters through laboratory-scale experiments with use of both simulated solutions.

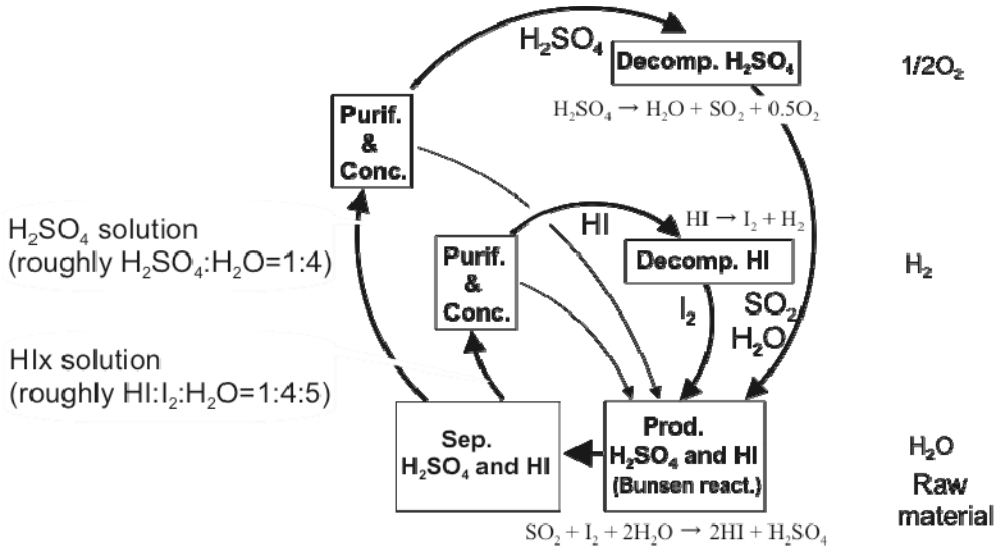

Figure 1: Reaction scheme of IS process. Solutions come out of Bunsen reaction are corrosive and multicomponent. Flow rate of HIx solution and H_2SO_4 solution must be adjusted with assistance of composition of both solutions, which must be obtained by measurement methods, for stable plant operation.

2 In Situ Composition Measurement by Radiation Probes

Figure 2 shows a concept scheme of an in situ composition measurement by radiation probes which are gamma probes and a neutron probe. Two different gamma-ray sources in energy levels are employed to measure transmittance through a solution and a fast-neutron source emitting fast neutrons is employed to measure thermal neutrons moderated by interactions with hydrogen atoms. Integrations of data from three different probes have possibilities that compositions of four component, at a maximum, solutions are determined. Two or three probes can be used properly depending on a type of a solution.

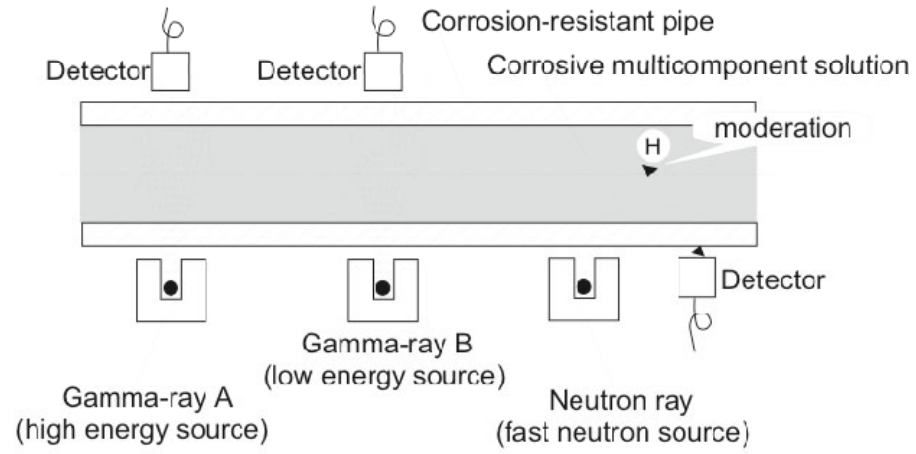

Figure 2: Conceptual scheme of in situ method in actual use to determine composition of corrosive and multicomponent solution. Non-contact approach avoids the corrosive issues. Two or three probes can be used properly depending on a type of a solution.

For the four-components solution of the HIx solution, the contained H_2SO_4 is minor component. To determine the composition of HIx solution requires the two radiation probes, since the solution is believed to be considered that this is consists of three components of HI, I_2, and H_2O. It has been generally recognized that the correspondences between the gamma-ray transmittance and solution densities are strong; moreover, there is a direct correlation between the densities of HIx solution and the iodine concentrations [2]. Accordingly, we focused on the hydrogen in HIx solution to explore residual or alternative information to complete the composition determination technique by the radiation probes. A system of neutron moisture meter employing the neutron ray provides advantages in quantification of the hydrogen.

For the four-components solution of the H_2SO_4 solution, the contained HI and I_2 are minor components; however, the heavy atom of the iodine, which has relatively high atomic number, affects a bulk density of this solution. Moreover the iodine atoms in both HI and I_2 supposedly have comparable effects. To determine the composition of H_2SO_4 solution requires the two radiation probes, since the solution is believed to be considered that this is consists of three components of H_2SO_4, H_2O, and the iodine. Accordingly, we chose two gamma-ray probes which are available with a cesium source and a barium source. A gamma-ray energy of the cesium source is higher than that of the barium source; a mass attenuation coefficient with the cesium source is nearly-constant with respect to object atoms ranging in broad atomic numbers, while a mass attenuation coefficient with the barium source is tending upward in accordance with a rise of the atomic numbers. The gamma-ray probe which has the higher energy determines the bulk density of the solution, besides the gamma-ray probe which has the lower energy probably determines the heaviest atom such as the iodine contained in the solution. A system of gamma-ray density meter employing the gamma-rays provides advantages in quantification of the bulk density and the heaviest atom concentration.

3 Experimental

A schematic of experimental apparatuses for HIx solution is shown in Figure 3. A container, which is open to the atmosphere, made of a plastic with diameter of 0.22 m was placed on a top board made of a stainless steel. A sensor assembly of a neutron moisture meter (NMA-2001, SHINKO EN&M) was put on to the underside of the top board; a fast-neutron source (californium, 2.5 MeV) and helium-3 proportional counters were built into this assembly, which were sealed by polyethylene walls. The thermal neutrons moderated by the interactions with the hydrogen atoms were counted by the counters housed in the assembly. Densities and compositions of the test solutions were determined by a oscillating density meter and a chemical titrator. Temperature of the solutions were obtained by a thermocouple. The test solutions were prepared by mixing regents of iodine powder and hydriodic acid. It is possible to take test solution in and out of the container by a tube pump. Levels of the solution in the container were calculated with weight changes of the tank, the densities of the test solutions, and the diameter of the container.

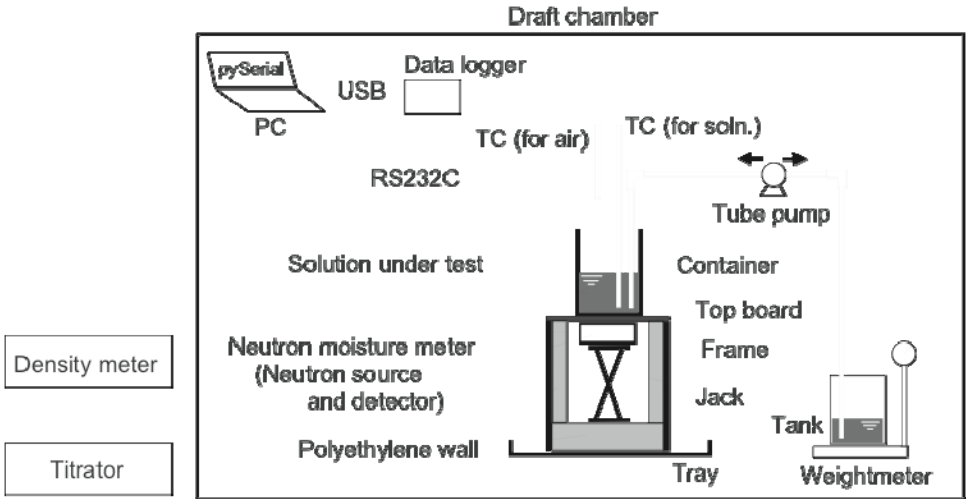

Figure 3: Experimental apparatus employing neutron moisture meter using fast neutron source to examine test solutions in container. Thermal neutrons moderated by interactions with hydrogen atoms were counted by detector. Densities and compositions of test solutions were determined by oscillating density meter and chemical titrator.

A schematic of experimental apparatuses for H_2SO_4 solution is shown in Figure 4. Graduated cylinders, which is open to the atmosphere, made of a glass with a inner diameter of 41.4 mm was placed on jacks. Two gamma-ray density meters (GD-4000, EARTHNIX) were placed for each cylinder; either of gamma-ray source (cesium, 0.6 MeV; barium, 0.3 MeV) and a scintillation detector made up the density meter. Intensities of the gamma-rays which passes through substances and decay by the interactions with atoms were counted by the detector at opposite side of the source. The tests were carried out at room temperature. In advance of the tests, the meters were calibrated using two solutions (water, 1.0 g/cm^3; sulfuric acid 98 wt%, 1.83 g/cm^3) of known densities. A integral time of 300 seconds to

measure was set though trial examinations. The test solutions were prepared by mixing reagents of sulfuric acid, water, hydriodic acid, and iodine powder. Compositions of the test solutions were determined by weights of the reagents of known concentration in preparation procedure. Sulfur formations could occur in the preparation, so that such solutions were withdrawn from test solution.

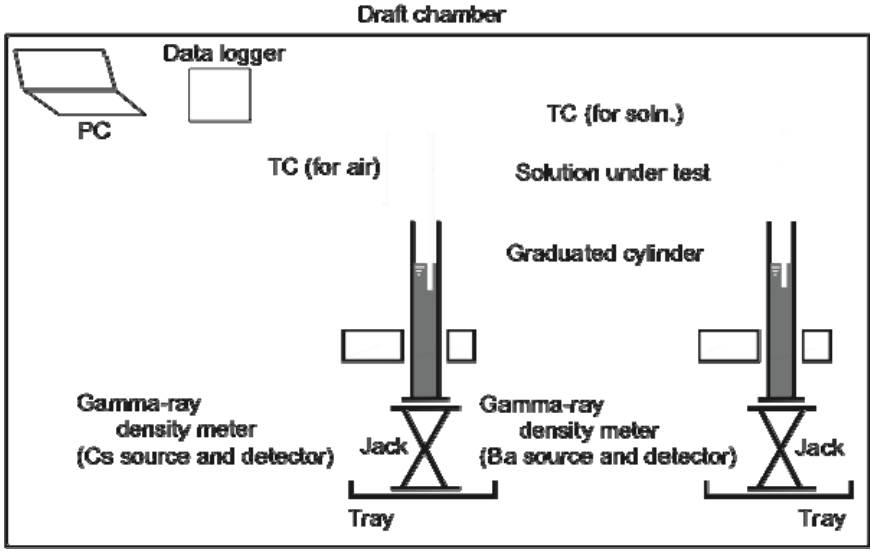

Figure 4: Experimental apparatus employing gamma-ray density meters using high-energy gamma-ray source and low-energy gamma-ray source to examine test solutions in graduated cylinders. Intensities of gamma-rays which passes through substances and decay by the interactions with atoms were counted by scintillation detector at opposite side of source.

4 Results and Discussion

For the HIx solution test, thought prior tests using water (23.5 ^{o}C, ρ=0.997 g/cm^{3}) to examine solution levels on the counting rates, the counting rate at that the solution level equivalent to zero displays a significant value, since the apparatus materials itself affect the measured values. An effect on the counting rates against the solution level disappears as certain value of the solution level is exceeded. Accordingly, influences on the counting rates by difference of the solutions might be compared through the use of a difference between two values which are the counting rate at solution level of zero and that in the flat region. A result for a HI solution (without iodine) and two HIx solutions appears in Figure 5. The volume concentration of hydrogen atom were calculated from measured densities and titrated composition. This figure illustrates the counting rates are correlated with the volume concentration; this fact suggests that the neutron probe has a possibility to determine the composition of HIx solution.

In order to develop a prediction method which enable to compute the counting rates for the measuring system, a Monte Carlo method was applied to this composition measuring system. For preliminary computation, a difference of the detector response between water and HIx solution was obtained, which suggests possibilities that the detector responses for HIx solution by the radiation probes are predictable.

For the H_2SO_4 solution test, sulfuric acids (H_2SO4-H_2O system) with various concentrations, sulfuric acid containing the hydriodic acid, and sulfuric acid containing the hydriodic acid and the iodine (below 1 mole%) were examined by two gamma-ray density meters. Figure 6 shows relationships between output values by the two density meters. Looking at the sulfuric acids which are free from the iodine atom, the densities with the cesium ray are proportionate to that of the barium ray. In cases of that the sulfuric acids contained HI or both HI and I_2, the iodine atoms had significant influences on the relationship. The densities as output values obtained by using the barium gamma-ray, which has relatively low energy, showed higher values than true values because the mass attenuation coefficient with the barium source is high regarding to the iodine which has large atomic number. Plots, which were affected by the iodine, of each sulfuric acid concentration, $C_{H2SO4}=x_{H2SO4}/(x_{H2SO4}+x_{H2O})$, were in lines, moreover the lines of each C_{H2SO4} and the lines of the solutions containing no iodine crossed at the intersections which shows the concentrations as H_2SO4-H_2O system. This result suggests that the gamma-ray probes of both lower energy and higher energy have a possibility to determine the composition of H_2SO_4 solution.

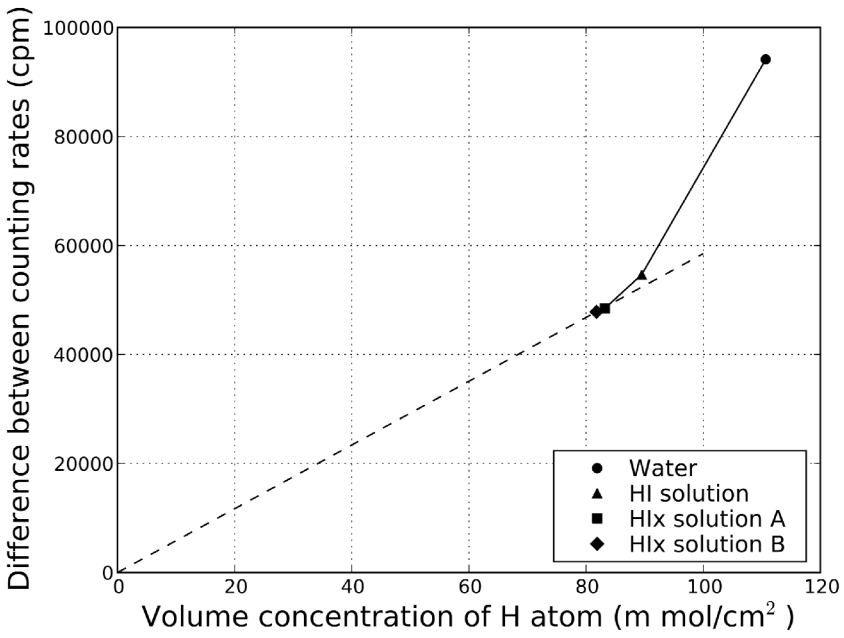

Figure 5: Counting rates of HI solution and HIx solution by neutron moisture meter (HI solution, 23.5 °C, ρ=1.691 g/cm^3, x_{HI}:x_{I2}:x_{H2O}=0.154:0:0.846; HIx solution A, 22.5 °C, ρ=1.861 g/cm^3, x_{HI}:x_{I2}:x_{H2O}=0.146:0.026:0.828; HIx solution B, 21.5 °C, ρ=1.881 g/cm^3, x_{HI}:x_{I2}:x_{H2O}=0.090:0.057:0.853). Values on vertical axis represent differences between counting rate at solution level of zero and that in region of sufficient solution levels.

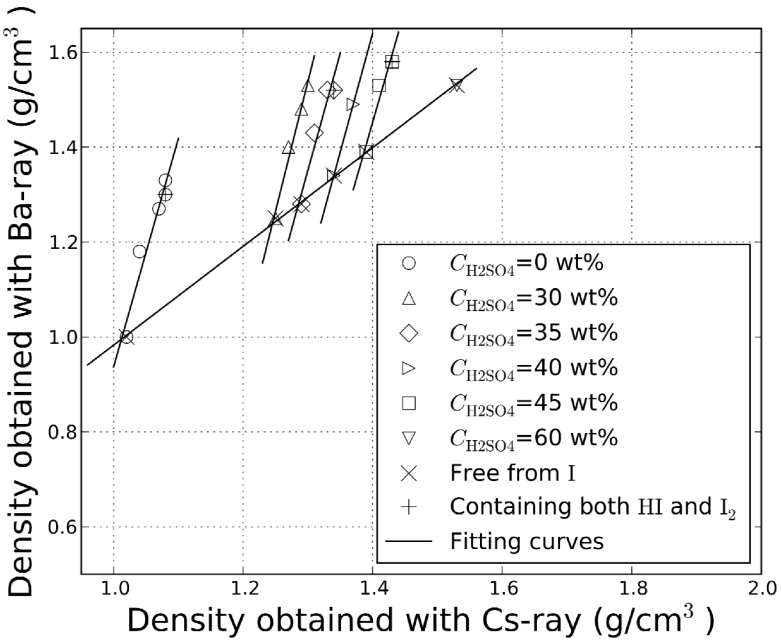

Figure 6: Relationships between output values by two gamma-ray density meters. Sulfuric acids without iodine atom, sulfuric acid containing hydriodic acid (below 1mole%), and sulfuric acid containing both hydriodic acid and iodine (below 1 mole%) were examined. $C_{H2SO4}=x_{H2SO4}/(x_{H2SO4}+x_{H2O})$ means concentration as H_2SO_4-H_2O system.

5 Summary

The Measurement equipments are indispensable to chemical process controls. A stable hydrogen production by the Iodine-Sulfur thermochemical water-splitting process is relatively difficult because of the lack of existing in situ composition measurement techniques for multiple components and corrosive solution. Methods by radiation probes have a potential to determine the composition of this multiple component solution while the non-contact approach avoids the corrosive issues. We focused on the neutron-ray for HIx solution to explore the technique to determine the composition for HIx solution. As for H_2SO_4 solution, we chose two gamma-ray which are available with the cesium source (higher energy) and the barium source (lower energy). Laboratory-scale experiments to examine its applicability were conducted with use of both simulated solutions by the neutron moisture meter with the sealed radiation source and by the gamma-ray density meters with the sealed radiations sources. For HIx solution, the obtained counting rates were correlated with hydrogen volume concentrations; this fact suggests that the neutron ray is a candidate probe to determine the composition of HIx solution. Moreover, the application of the Monte Carlo method suggests possibilities that the detector responses for HIx solution by the radiation probes are predictable. Also, for H_2SO_4 solution, densities as output values with the cesium ray of the sulfuric acids, which are free from the iodine atom, were proportionate to that of the barium ray. In cases of that the sulfuric acids contained HI or both HI and I_2, the iodine atoms had significant influences on the relationship. This result suggests that the gamma-ray probes of

both lower energy and higher energy have a possibility to determine the composition of H_2SO_4 solution.

Acknowledgement

This work was supported by KAKENHI (20560716).

References

[1] Hisao SUZUKI, Studies of Neutron Moisture Gauges, The Iron and Steel Institute of Japan, 57 (1971) 1, pp.175-181.

[2] Shinji Kubo, Hayato Nakajima, Yoshiyuki Imai, Seiji Kasahara and Kaoru Onuki, Control Techniques For Bunsen Reaction Solution To Regulate Process Condition, AIChE Annual Meeting, 357f, Nov. 2007, Salt Lake City, USA.

Relationship between Density and Composition of HI-I_2-H_2O in I-S Process

Songzhe Chen, **Hanfei Guo**, **Ping Zhang**, **Jingming Xu**, **Laijun Wang**, Institute of Nuclear Energy and New Energy Technology, Tsinghua University, China

1 Introduction

Iodine-Sulfur thermochemical cycle is one of the most promising massive hydrogen production methods. It consists of three main reactions (three sections) [1, 2], which are Bunsen reaction (Bunsen section), sulfuric acid decomposition (sulfuric acid section) and hydriodic acid decomposition (HIx section), as described by Eqs. (1)-(3):

$$I_2 + SO_2 + 2H_2O \rightarrow 2HI + H_2SO_4 \quad [393\ K] \tag{1}$$

$$2H_2SO_4 \rightarrow 2SO_2 + 2H_2O + O_2 \quad [1123\ K] \tag{2}$$

$$2HI \rightarrow H_2 + I_2 \quad [723\ K] \tag{3}$$

It is of great importance to determine the compositions of streams in the process, so as to monitor the performance of the iodine-Sulfur thermochemical cycle. Concerning the HI-I_2-H_2O mixture (HIx phase of IS process), it is time consuming to determine the concentrations of each species in the solution, especially for I_2. Hence, density which can be easily acquired is introduced to simplify concentration measurement [3].

According to Gibbs phase rule [4], the degree of freedom F of a system is

$$F = C - P + 2 \tag{4}$$

Where C is the number of components, P is the number of phases. Under the circumstance of given temperature and pressure, F equals to 2 for HI-I_2-H_2O ternary system. Thus, the composition of the solution can be determined once 2 independent variables of the system are known. As a result, if density and concentration of a certain component, e.g. HI, are measured, the composition of all the other substances is able to be calculated.

The relation between density and concentrations of each species can be formulated by Eq. (5).

$$\rho = M_{HI} \times C_{HI} + M_{I_2} \times C_{I_2} + M_{H_2O} \times C_{H_2O} \tag{5}$$

Where, ρ is density, M is molar mass of each substance, C is concentration, and the subscripts represent the components. It can be seen that, density is a linear combination of the concentrations of each component. In this research, HI-I_2-H_2O solutions of different compositions were prepared. Based on the density data and the concentration data of HI, I_2,

and H_2O, multiple linear regressions were carried out. Applying the resulted relational expression, the composition of the HI-I_2-H_2O could be secured once density and H^+ concentration of solution are measured.

2 Experimental

The experiments were carried out at fixed temperature 20°C and 1 atmospheric pressure. 50.0 ml hydriodic acid solution, i.e. HI-H_2O mixture, of certain concentration was first prepared in a glass vessel in a water bath of 20°C. Then pure solid iodine was added to the solution gradually until saturation. During the process, samples are taken every batch of 10.0 g iodine has been added into the solution. Densities of the sample were measured using an oscillating U-tube density meter (DMA 4100 M, Anton Paaran, Austria) at 20°C. The concentrations of HI and I_2 of sample are measured by the method of chemical titration.

The HI/H_2O molar ratio of initial hydriodic acid ranges from 1:9.46 to 1:5.43, which is very close to the composition of HI-H_2O azeotrope.

3 Result and Discussion

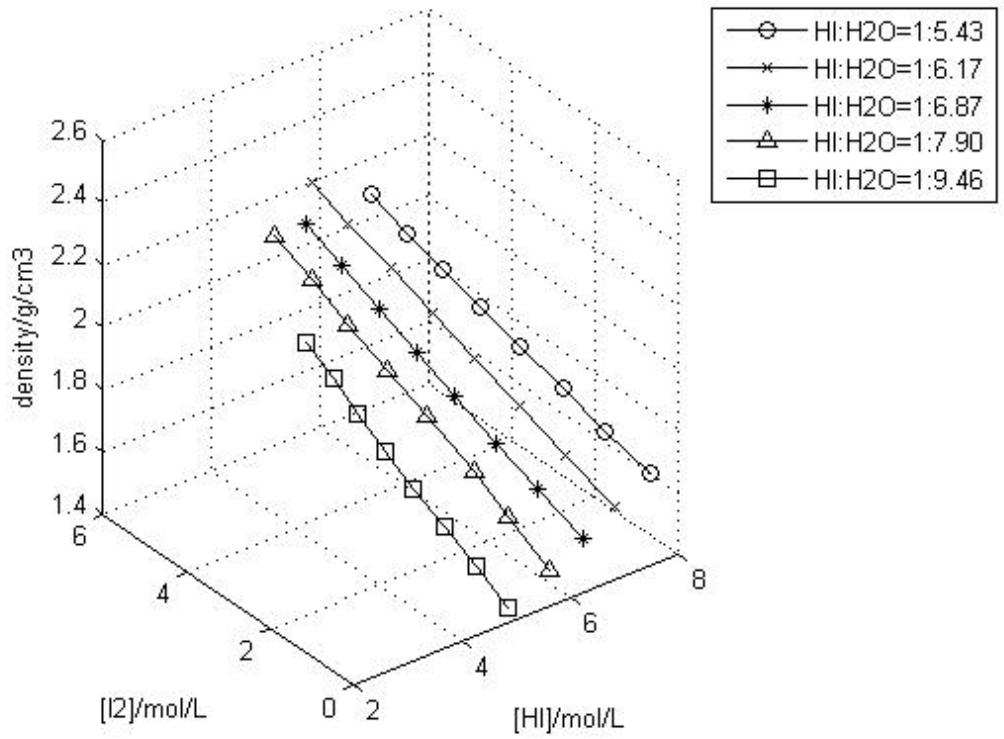

Figure 1: Relationship between density and concentrations of HI and I_2.

Fig. 1 illustrates the relationship between density and concentrations of HI and I_2. There is an obvious linear relation between them. In addition, such a linear relation covers a wide range from the molar ratio of HI:H_2O=1:5.43 to 1:9.46.

Based on experimental data, a multiple linear regression procedure was implemented so as to set up the math model [5]. As far as the experiment is concerned, the regression relationship is expressed by Eq. (6).

$$\rho = \alpha + \beta \times C_{HI} + \gamma \times C_{I_2} \quad (6)$$

Where ρ, C_{HI} and C_{I2} represent solution density, HI concentration and I_2 concentration, respectively, while *α*, *β* and *γ* are constants resulted from the regression. As shown in Fig.2, the relational expression Eq. (6) stands for a plane at the 3-dimensional space of ρ, C_{HI} and C_{I2}, and almost all the experimental points fall in this plane. Because density and HI concentration (i.e. H^+ concentration) could be measured rapidly, subsequently I_2 concentration are ready to be calculated applying Eq. 6, thus the composition of the whole HI-I_2-H_2O mixture could be determined within a time quite short.

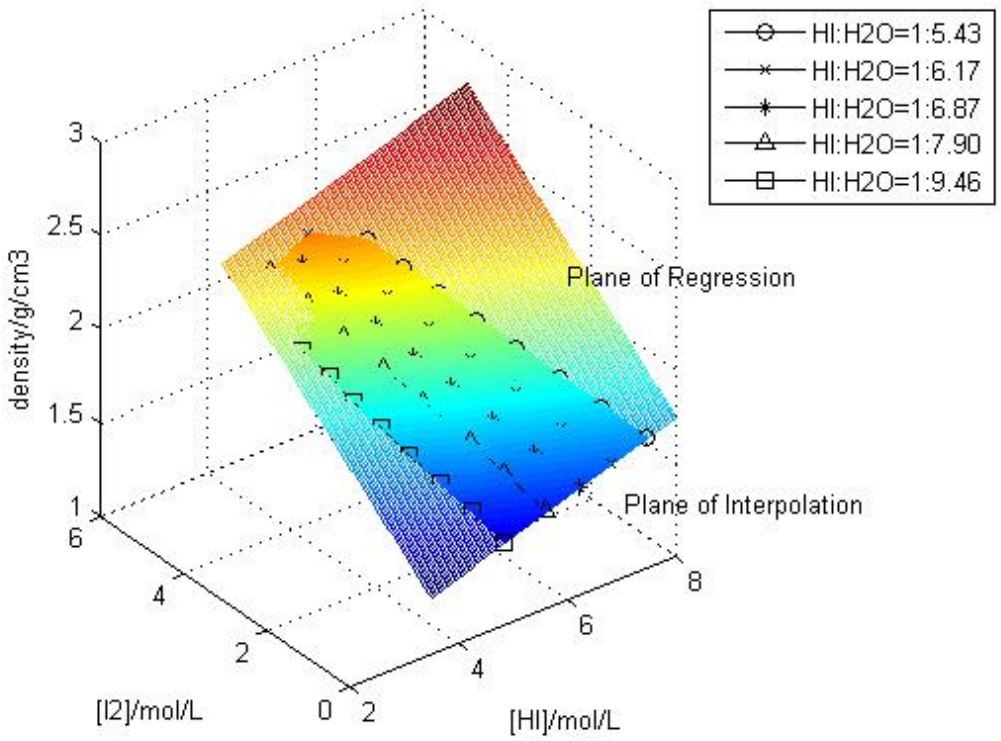

Figure 2: Plane of regression and plane of interpolation using experimental data.

In order to verify the performance of the regression result, values of the concentration calculated by Eq (6) were compared with those measured by chemical analysis. Six different samples were prepared for the verification, whose initial ratios of HI to H_2O are 1:5.77, 1:6.10, 1:6.35, 1:6.62, 1:7.60 and 1:8.50 respectively. Fig.3 indicates that the concentrations calculated using regression model agree with those obtained via chemical experiment very well. The average relative deviation of the calculated values against the experimental ones lays within 1.0%.

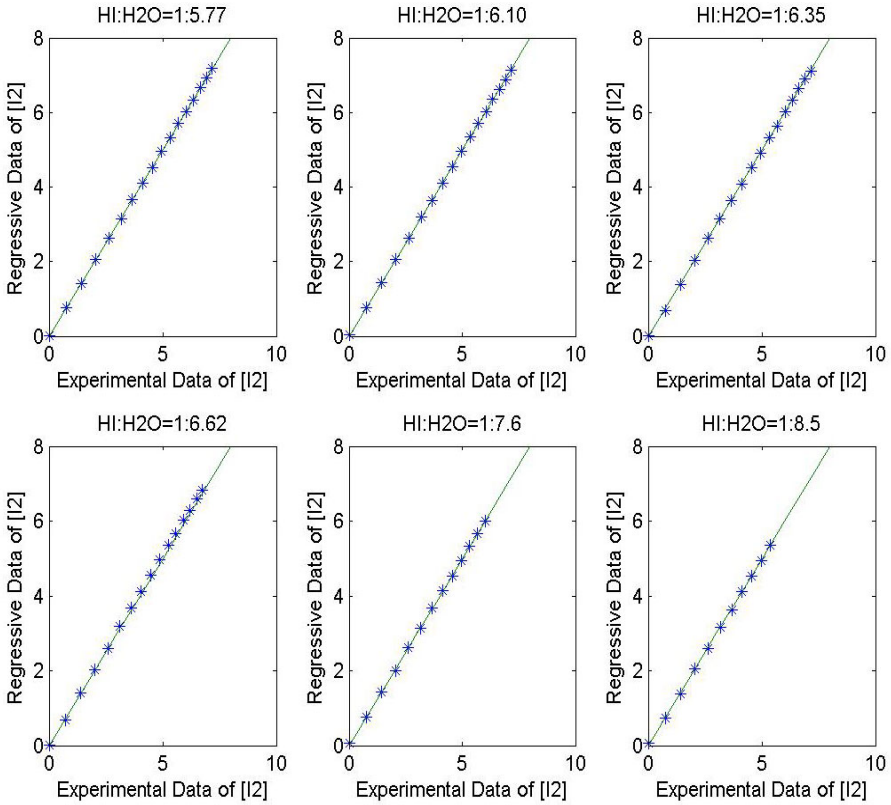

Figure 3: Comparison of calculated values and experimental data of I_2 concentration.

4 Conclusion

The relationship between solution density of HI-I_2-H_2O and composition was studied by multiple linear regressions. A relational expression describing above relationship was obtained, applying which the efficiency of composition analysis of HI-I_2-H_2O could be improved significantly.

References

[1] Norman J.H., Bensenbruch G.E., O'Keefe D.R. Thermochemical water-splitting cycle for hydrogen production. GRI-A 16713, 1981.

[2] Zhang P., Chen S.Z., Wang L.J., et al. Overview of nuclear hydrogen production research through iodine sulfur process at INET. International Journal of Hydrogen Energy, 2010, 35(7): 2883-2887

[3] Kubo S, Nakajima H, Imao Y, et al. An estimation technique for compositions of Bunsen reaction solutions on thermochemical water splitting IS process: 17th World Hydrogen Energy Conference. Brisbane, Australia, 2008.

[4] Mortimer R.G. Physical Chemistry, 3rd edition. San Diego, USA, Elsevier Academic Press, 2008. 199-205.

[5] Härdle W. Applied multivariate statistical analysis [M]. Berlin: Springer, 2003. 108-112.

Demonstration of Hydrogen Production by the Sulphur-Iodine Cycle: Realization of a 10 NL/h Plant

Raffaele Liberatore, **Giampaolo Caputo**, **Claudio Felici**, **Annarita Spadona**,
ENEA, CR Casaccia, via Anguillarese 301, 00123 Rome, Italy

In the hydrogen production framework, ENEA (Italian National Agency for New Technologies, Energy and Sustainable Economic Development) is involved in a study of the thermolysis through thermochemical cycles powered by solar energy. The TEPSI project, in this regard, has as it's main objective, the construction of a plant for the production of 10 NL/h of hydrogen by sulphur-iodine cycle, for the demonstration of scientific feasibility of the sulphur-iodine cycle and the collection of all data necessary to design a pilot plant.

TEPSI is a project funded by the Italian Ministry of Research and consists of 3 lines:

1. Hydrogen production from water by thermochemical cycles.
2. New materials for H_2 storage.
3. Hydrogen and electrical power production by hydro –gasification.

Line 1, in particular, has endeavoured to study and develop the sulphur-iodine and the mixed ferrites thermochemical cycles. It saw also the participation of several Italian Universities: Roma 1, Roma 3, Cagliari, Milan and Trento.

This paper deals with the realization of this laboratory plant for the sulphur-iodine cycle and concerns the experimental performances of all the equipments constituting the plant.

The tests of the equipment related to this cycle, executed in the ENEA laboratories, are described in order to analyze the reasons behind the choices of equipment, compositions, temperatures, pressures and devices, with particular emphasis on the ones concerning iodine purification. The equipment, indeed, consumes the most energy and, if not optimized, can invalidate the efficiency of all the cycles.

Since the objective of the laboratory plant is to verify the feasibility of the reactions and processes involved and to test their integrability and cyclicity, the heat source used, for simplicity, was provided by electrical devices. However, an evaluation concerning the realization of an industrial plant is possible starting from the acquired data.

Among all the thermochemical cycles proposed in literature over the last 30 years [1], the Sulphur–Iodine cycle [2] is widely considered one of the most promising, and it has been studied by several important research groups in the world [2–5]. The process, starting from water through a closed cycle of reactions that generate and consume iodine, hydriodic acid, sulphuric acid and sulphur dioxide, produces hydrogen and oxygen at a temperature compatible with current solar collectors technology.

The sulphur-iodine thermochemical cycle is based on three main reactions carried out at three different temperature levels (low, medium and high temperature):

- Reaction of acid production (called Bunsen, exothermic at 293 ÷ 393 K):
  $2H_2O + I_2 + SO_2 \rightarrow H_2SO_4 + 2HI$ (1)

- Decomposition of HI (endothermic at 573 ÷ 773 K):
  $2HI \rightarrow I_2 + H_2$ (2)
- Sulphuric acid decomposition (endothermic at 1073 K ÷ 1173 K):
  $H_2SO_4 \rightarrow H_2O + SO_2 + 1/2\ O_2$ (3)

In the section of Bunsen [6], water, iodine and SO_2 at a temperature between 293 K and 393 K, produce two immiscible liquid phases [7]: the upper one containing mainly a mixture of water and H_2SO_4 at 50% by weight, and the other containing HI, I_2 and water.

The sulphuric acid from the top section of the Bunsen reaction is concentrated up to (90 - 98)% by weight and then sent to the decomposition reactor where it produces water, oxygen and SO_2. The latter is re-sent in the Bunsen section.

The lower phase of the Bunsen reaction, however, is sent to the section of decomposition of HI, which is decomposed into hydrogen and iodine. The lower phase of the Bunsen reaction, however, consists of HI, water and H_2SO_4 residue and a high iodine content (~ 80-90% wt), since the reaction itself is conducted with an excess of iodine, to promote separation of the two phases.

The Iodidric phase is then subjected to a series of separation operations in order to obtain a binary azeotropic mixture HI-H_2O at 57 wt% of HI content in order to be sent to the decomposition reactor. This is one of more energy-cycle phases and requires considerable work on optimizing. To this end several techniques for purification-separation have been proposed. General Atomics has proposed the use of phosphoric acid (H_3PO_4) to obtain concentrated HI [8, 9] and the separation of iodine. Roth and Knoche [10] have proposed and studied the reactive distillation, which involves replacing the stills and decomposition in an integrated process. Further improvements in this technique were reported by Goldstein [11], Hong [12] and Kasahara [13] who studied an electro-electrodialysis as a method of concentration.

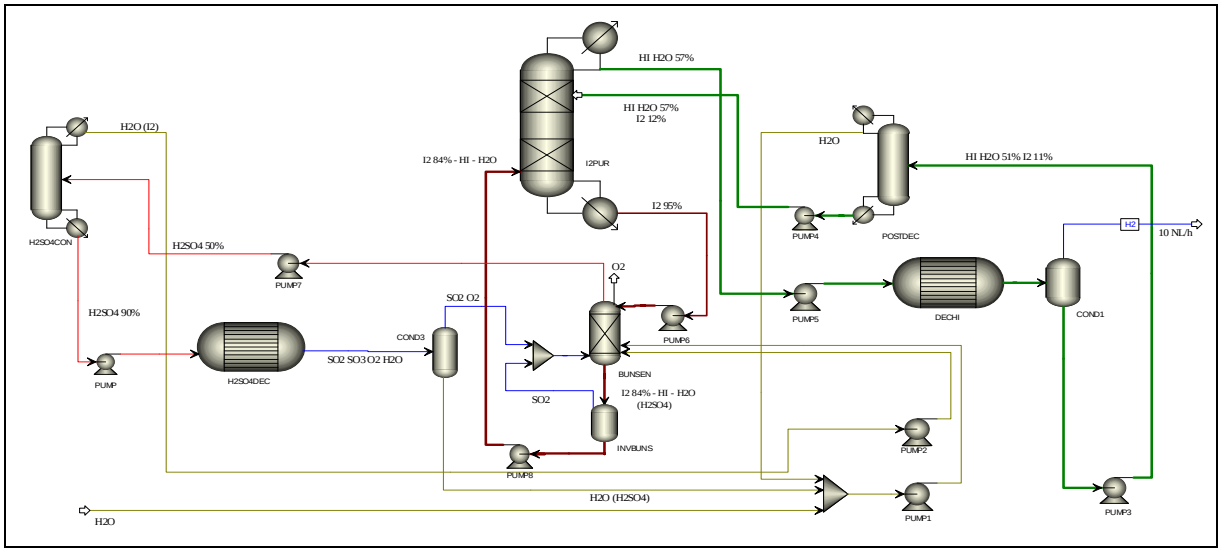

Figure 1: ENEA Laboratory Sulphur-Iodine plant schema, HI* =HI/(HI+H2O).

In order to achieve a sulphur-iodine system for small-scale hydrogen production (Figure 1), ENEA proposed the separation of iodine from HI-H_2O mixture in a distillation plant at atmospheric pressure after the reaction of Bunsen, in order to send to the HI decomposition reactor an HI-H_2O azeotropic mixture devoid of I2. This technique is a classic way to separate from I_2 in HI-HI-H_2O ternary mixture, considering the large difference in boiling point among the three components (at atmospheric pressure: 238 K for HI, 373 K for H_2O, 457 K for I_2). The distillate, however, is highly dependent on the composition of the [HI] / ([HI] + [H2O]). Depending on the concentration of the feed from the Bunsen reaction, two possible patterns of plant are possible. If the content of HI is greater than the pseudo-azeotrope (with pseudo-azeotrope [14], meaning the ternary mixtures HI-H_2O-I_2 with minimum vapour pressures in isothermal conditions, at varying concentrations of iodine), these mixtures have a ratio of concentration ([HI] / ([HI] + [H_2O])) close to 57% wt) and the distillate is enriched in HI, if the contents of HI is lower than the pseudo-azeotropic point, the distillate is instead enriched in water.

For this reason it was necessary to determine the most appropriate composition of the lower phase of the Bunsen reaction and the quantities of reagents to be introduced.

It is true that reaction (1) is entrusted with the production of acid phases: the hydriodic and the sulphuric one, but the two phases do not contain exclusively H_2SO_4 and HI, but also significant amounts of water, which has to be included in excess.

To obtain a good separation of phases and having no amount of H_2SO_4 in the hydriodic phase and / or sulphuric acid in the HI phase it is necessary to work with a large excess of iodine, which will go into the hydriodic phase.

In this way the Bunsen reaction appears to be:

$$(x+1)I_2 + SO_2 + (n+2)H_2O \rightarrow \left[H_2SO_4 + (n-m)H_2O\right]_{Sulf.-phase} + \left[2HI + xI_2 + mH_2O\right]_{HIx-phasae}$$

with n and m depending by temperature at constant pressure. We have seen, however, by the last experiments at ENEA Casaccia, that even if we operate at 353 K [11], a content of about 1%wt in H_2SO_4 is being and the iodine content is about 82%wt. Because of this, a purification of this phase is necessary: a way is the reversing of the Bunsen reaction at a temperature of about 403 K. This reaction, however, consumes 2 moles of HI for every mole of H_2SO_4 and forms 2 moles of H2O, further diluting the HI phase. Since this phase will be purified by iodine and sent to the decomposition reactor for the production of the H_2 at an appropriate concentration (at least 57% wt), we can understand that if this phase is more dilute more problems of distillation and recirculation will happen. Furthermore it was noted that high concentrations of iodine in the Bunsen reactor produce, in the HI phase, more content of HI against water, which further facilitates the distillation itself.

It could be preferred, at this point, to get even greater excesses of I_2 and higher temperatures (393 K) in the Bunsen reactor, but in this case, we would be forced to work with mixtures with high content of iodine, even 84 wt% leading to an over-sizing of certain equipment, particularly the Bunsen reactor. Furthermore we would have problems handling the mixture, which should always be kept warm (373-383 K) to avoid iodine precipitation. This would make it necessary to track and control the temperatures in the lines and the pumps. After careful experimentation, it was considered useful for this plant to operate under these conditions anyway.

Concerning the sulphuric acid decomposition, the temperature of reaction was 1123 K with an iron oxide based catalyst and with a feed mixture composed of H_2SO_4-H_2O with 90 %wt in H_2SO_4. This stream is the one leaving the Bunsen reactor after an appropriate distillation in H_2SO_4CONC.

Concerning the HI decomposition, it has been widely investigated in ENEA laboratories, usually feeding the reactor with HI-water azeotropic solution as starting reactant, since this is the expected composition coming from the other sections of the cycle; recently, some experimental test with pure gaseous HI has been executed too. Various catalysts have been investigated in order to enhance the kinetics of this reaction in the range of temperature 400-500°C, searching for efficiency (high conversions), time stability (no deactivation), low pressure drop and low cost. Ni-based catalysts using alumina as support, Pt-based catalysts supported over different carbon materials and carbon materials catalysts are used. The first ones provided starting conversion values at 500°C almost agree with the theoretical one (about 22%), but in any case a slow but gradual deactivation was evident. The second ones gave, in contrast, good results in terms of efficiency and stability, but we didn't consider them interesting for a large scale application because of their high cost. We focused therefore on carbon material ones, and they were used in the HI decomposition reactor of the lab plant. The temperature of reaction was fixed at 773 K and the obtained conversion was about 21.4 %.The stream leaving this reactor is essentially composed of H_2O, HI and the I_2 formed by the HI decomposition. It has to be purified from the iodine and reconcentrated to pseudo-azeotropic conditions, since the HI decomposition produced a more diluted mixture.

Consequently, this stream is sent to another distillation column (POSTDEC), that will produce H_2O as distillate and a pseudo azeotropic mixture as residue. The residue will be sent at the purification column (I_2PUR), another time, in order to eliminate the iodine.

Figure 2: ENEA Sulphur-Iodine laboratory plant picture.

As stated before, the goal is to construct a facility at ENEA Casaccia laboratories to experiment and develop a thermochemical cycle that, starting from water, produces hydrogen and oxygen continuously.

The plant, whose scheme is depicted in Figure 1, consists of equipment in Pyrex and quartz, PTFE tubing and it has an output of about 10 NL / h of H_2.

Before the plant realization (figure 2), all the equipment was tested.

As well as the authors of this paper, the ENEA equipment which realised this laboratory plant was constructed by Mauro Vignolini (Project Manager), Pietro Tarquini (Technical Manager), Antonio Ceroli, Paolo Favuzza, Alberto Giaconia, Michela Lanchi and Salvatore Sau.

References

[1] Russell Jr JL, McCorkle KH, Norman JH, Porter II JT, Roemer TS, Schuster JR, et al. Water splitting. A progress report. In: Proceedings of the first world hydrogen energy conference, Miami Beach, U.S.A., 1A105-1A124, 1–3 March, 1976.

[2] Brown LC, Besenbruch GE, Lentsch RD, Schultz KR, Funk JF, Pickard PS, et al. High efficiency generation of hydrogen fuels using nuclear power. GA-A24285 June 2003.

[3] Le Duigou Alain, Borgard Jean-Marc, Larousse Bruno, Doizi Denis, Allen Ray, Ewan Bruce C, et al. HYTHEC: an EC funded search for a long term massive hydrogen production route using solar and nuclear technologies. Int J HydrogenEnergy 2007;32:1516–29.

[4] Nakajima H, Ikenoya K, Onuki K, et al. Closed-cycle continuous hydrogen production test by thermochemical S–I process. Kagaku Kogaku Ronbunshu 1998;24:352.

[5] Fred Gelbard, James C Andazola, Gerald E Naranjo, Carlos E Velasquez, Andrew R Reay. High pressure sulphuric acid decomposition experiments for the Sulphur–Iodine thermochemical cycle. SAND2005-5598; 2005.

[6] Sakurai M, Nakajima H, Onuki K, Shimizu S. Investigation of two liquid phase separation characteristics on the Iodine–Sulphur thermochemical hydrogen production process. Int J Hydrogen Energy 2000;25:605–11.

[7] Giaconia A, Caputo G, Ceroli A, Diamanti M, Barbarossa V, Tarquini P, et al. Experimental study of two phase separation in the Bunsen section of the Sulphur–Iodine thermochemical cycle. Int J Hydrogen Energy 2007;32(5):531–6.

[8] O' Keefe, Allen C, Besenbruch B, Brown L, Norman J, Sharp R.Preliminary results from bench-scale testing of a Sulphur–Iodine thermochemical water-splitting cycle. Int J. Hydrogen Energy 1982;7(5):381–92.

[9] M. Lanchi, F. Laria, R. Liberatore, L. Marrelli, S. Sau, A. Spadoni, P. Tarquini. HI extraction by H3PO4 in the Sulphur–Iodine thermochemical water splitting cycle: Composition optimization of the HI/H2O/H3PO4/I2 biphasic quaternary system. International Journal of Hydrogen Energy, Volume 34, Issue 15, August 2009, Pages 6120-6128.

[10] Roth M, Knoche K. Thermochemical water splitting through direct HI-decomposition from H2O/HI/I2 solutions. Int J.Hydrogen Energy 1989;14(8):545–9.

[11] Goldstein Stephen, Borgard Jean-Marc, Vitart Xavier. Upper bound and best estimate of the efficiency of the iodine sulphur cycle. Int J. Hydrogen Energy 2005;30:619–26.

[12] Hong Seong-Dae, Kim Jeong-Keun, Kim Byeong-Kwon, Choi Sang-Il, Bae Ki-Kwang, Hwang Gab-Jin. Evaluation on the electro-electrodialysis to concentrate HI from HIx solution by using two types of the electrode. Int J Hydrogen Energy 2007;32:2005–9.

[13] Kasahara Seiji, Kubo Shinji, Onuki Kaoru, Nomura Mikihiro. Thermal effciency evaluation of HI synthesis/concentration procedures in the thermochemical water splitting IS process. Int J Hydrogen Energy 2004;29:579–87.

[14] R. Liberatore, A. Ceroli, M. Lanchi, A. Spadoni, P. Tarquini. Experimental vapour–liquid equilibrium data of HI–H2O–I2 mixtures for hydrogen production by Sulphur–Iodine thermochemical cycle.
International Journal of Hydrogen Energy, Volume 33, Issue 16, August 2008, Pages 4283-4290.

Development of Mixed Metal Oxides for Thermochemical Hydrogen Production from Solar Water-splitting

Alex Le Gal, Stéphane Abanades, Gilles Flamant, PROMES laboratory, CNRS, France

1 Introduction

Hydrogen is a promising energy carrier to replace fossil fuels that produce greenhouse gas and tend to decrease. However, it doesn't exist in the nature, thus it must be synthesized. Steam methane reforming along with electrolysis to a lower extent are currently the main used techniques to produce hydrogen but the former results in CO_2 emissions and the latter is limited by the energy efficiency. Thermochemical water splitting cycles are an alternative which use concentrated solar energy as the primary energy source. Direct water splitting needs a high temperature around 2500 K to allow dissociation and that's the reason why catalysts (reaction intermediates) are used. Mixed metal oxides are promising candidates for hydrogen production by solar thermochemical cycles. Such cycle consists of a two step process which implies a metallic oxide catalyst and water.

$$M_xO_y \rightarrow M_xO_{y-1} + ½\ O_2 \quad (1)$$

$$M_xO_{y-1} + H_2O \rightarrow M_xO_y + H_2 \quad (2)$$

During the first step, the oxide is thermally reduced by concentrated solar energy, which releases O_2 (1), then in the second step, the activated metallic oxide is hydrolyzed by steam, which produces H_2 (2).

There are many publications about such materials for this application. The cycle based on ZnO/Zn redox pair is investigated [1, 2] because it can theoretically produce a large amount of H_2/g (12,3mmol/g) during a single thermochemical cycle. But during the reduction step, the Zn produced is partially vaporized and partial recombination occurs during gas cooling, which requires a gas quench or a gas separation of Zn(g) and O_2 at high temperature to avoid recombination. The cycles with non volatile oxides thus appear as an attractive solution. Fe_3O_4/FeO cycle was first studied by Nakamura [3] and it presents a fairly good reactivity but the reduction temperature (1800K) is too high for current concentrated solar technologies and the reduced material is fused and sintered strongly, which decreases specific surface area and consequently material performance. To lower this activation temperature, the doping of magnetite with a metallic cation (Zn, Ni, Mn…) to form a ferrite is widely studied [4, 5, 6, 7, 8, 9]. Doped ferrites present a satisfactory theoretical production rate of H_2 (nearly 4.3 mmol/g depending on the metallic dopant) and a higher melting point than wustite induced by metal oxide properties. In this study, nickel ferrites were synthesized by different soft chemical routes such as coprecipitation of hydroxides, pechini process or hydrothermal treatment in view of enhanced thermal reduction yield. Then, the reactivity of the synthesized materials was investigated.

Abanades et al. [10] demonstrated that CeO_2/Ce_2O_3 cycle produces H_2 with a good reactivity of the Ce(III) species during hydrolysis (2,9 mmol/g), but the activation temperature is too high (2000°C) and there are mass losses induced by partial sublimation of ceria, which implies chemical efficiency decrease during cycling. Doping ceria with a metallic cation could reduce this activation temperature by inducing structural defects or oxygen vacancies [11, 12]. For the three-way catalysis application, Balducci et al. [13] showed that zirconium addition favors the reduction of ceria. Zirconium oxide can also contribute to avoid sintering thanks to the thermal properties of the oxide. In this study, the Zr-doped ceria was investigated targeting H_2 production. Ceria-based nano-materials are currently largely studied for their oxygen storage capacity or catalyst activity and thus, there are many researches about the synthesis of controllable morphology of this nanomaterial [14, 15, 16, 17]. Yuejuan [14] showed that using organic molecules as template agents for the preparation of high surface area and porous material improves catalytic activity. Yuan et al. [17] studied controlled synthesis to manipulate the shape, crystal plane and size of nano-materials in view of catalytic application and they demonstrated that better performing catalysts could be “designed” rather than prepared. In this paper, different synthesis methods of Zr-doped ceria were tested in view of enhanced reduction rate and hydrolysis reactivity. To conclude, the performances of nickel ferrite and Zr-doped ceria were compared in terms of H_2 production yield and cyclability.

2 Experimental

$NiFe_2O_4$ was synthesized by different wet chemical routes such as coprecipitation of hydroxides, pechini process, sol-gel or hydrothermal treatment to improve catalyst performance. These synthesis methods were initially chosen to obtain particular properties, typically powders with high surface area to favor kinetics and reduction rate during the first reduction step. Porous morphology with enhanced solid/gas interaction can also improve the hydrolysis yield. In a second part, zirconium-doped ceria ($Zr_xCe_{1-x}O_2$) was also synthesized by coprecipitation and the effect of a template agent (Cetyltrimethylammonium bromide) was studied targeting H_2 production improvement. X-ray diffraction analysis, SEM, BET and thermal gravimetric analysis were used to characterize the synthesized materials. Catalytic activity was investigated with a specific experimental device. The first step reduction was operated with a high temperature tubular furnace (1500°C max) which is equipped with an online O_2 trace analyzer (Zirconium oxide sensor). The powder was placed in an alumina crucible swept by an argon flow controlled with a mass flow-meter (200 $mL.min^{-1}$). The O_2 concentration was thus monitored continuously during the progress of the reduction reaction. The hydrolysis step was experimented in an other tubular furnace equipped with a catharometer for H_2 online measurement. A peristaltic pump was used to inject water which was vaporized inside the furnace and was transported by the carrier gas (argon).

3 Results

$NiFe_2O_4$ powders are well crystallized with cubic spinel structure and SEM images presented in figure 1 show three interesting morphologies. The powder synthesized by coprecipitation with surfactant PEG 400 (fig 1.a) is composed of spherical grains of 60 nm diameter and rods measuring some micrometers length and 200 nanometres width. The powder which was

synthesized by modified pechini process (fig 1.b) forms porous aggregates of about ten micrometers and non spherical grains appear relatively sintered. This porous morphology is explained by the fast degassing during the synthesis. The last image (fig 1.c) is representing $NiFe_2O_4$ synthesized by hydrothermal treatment; the material is composed of small spherical particles (60 nm diameter) without any sintering phenomenon. As it can be observed, the hydrothermal treatment avoids rod formation contrary to the synthesis without treatment. These three morphologies could enhance the reduction rate thanks to the porosity, the high surface area and good thermal properties.

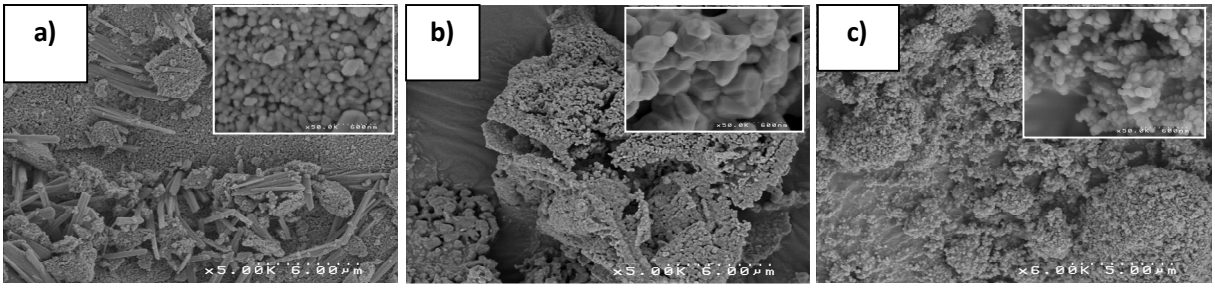

Figure 1: SEM images of $NiFe_2O_4$ synthesized by coprecipitation + PEG (a), modified pechini process (b) and with hydrothermal treatment (c).

The reduction step was investigated by thermal gravimetric analysis by heating a sample at 1400°C with a heating rate of 10°C/min and a dwell time of one hour. The mass loss associated to O_2 releasing begins at a temperature of about 1000°C for all the $NiFe_2O_4$ powders studied (fig. 2). The maximum reduction yield (Fe^{2+}/Fe^{3+}) of 19.2% is obtained for the powder synthesized by hydrothermal treatment but strong sintering of the powder decreases catalytic activity during the hydrolysis step. This reduction yield corresponds to 410 µmol of O_2 released per gram of material. The hydrolysis step was investigated using a tubular furnace and the H_2/O_2 ratio was calculated. Ideally, this ratio is equal to 2 but sintering phenomena reduce the hydrolysis yield, which implies reactivity losses during the cycle.

$Zr_xCe_{1-x}O_2$ was synthesized by coprecipitation of hydroxides with and without a template agent (CTABr). XRD patterns confirm that Zr-doped ceria samples are well crystallized with the CeO_2 cubic fluorite structure. FWHM of diffraction peaks of CTABr-synthesis are larger than for the powder synthesized without CTABr. The average crystallite sizes are calculated using the Scherrer's formula and are estimated around 7 nm and 17 nm, respectively. Surfactant effect thus allowed the synthesis of smaller particle size of doped-ceria. The reduction yield of CTABr-synthesized powder (Ce^{3+}/Ce^{4+}) measured by thermal gravimetric analysis is nearly three times higher than for the material synthesized by conventional coprecipitation (fig. 2). A reduction yield of 46% for CTABr-synthesized material corresponds to 565 µmol of O_2 released per gram.

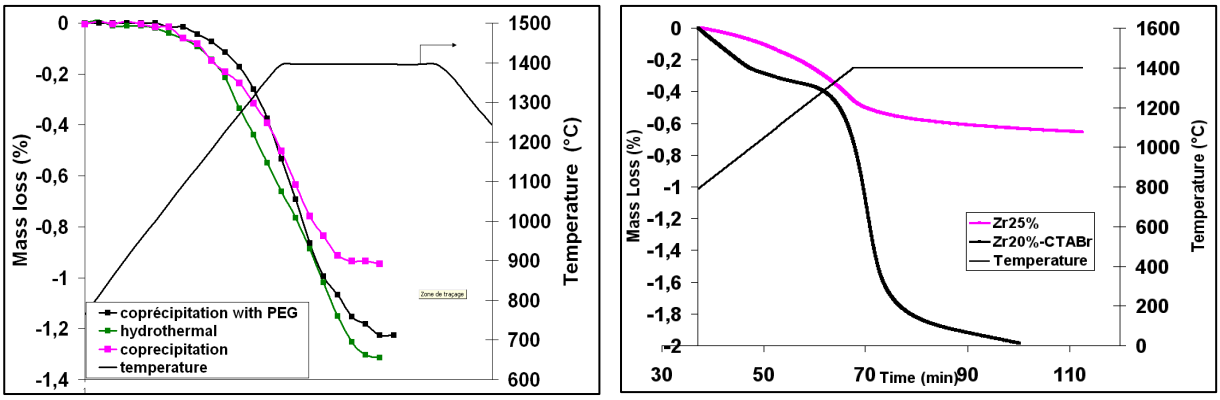

Figure 2: Thermal gravimetric analysis of $NiFe_2O_4$ (left) and Zr-doped ceria (right) synthesized by different methods.

After the reduction step, the CTABr-synthesized powder is strongly sintered, whereas the other material synthesized by coprecipitation still appears as a powder after the high temperature treatment. Consequently, the cycling was investigated with thermal gravimetric apparatus (fig. 3). First, the reduction step occurs by heating at 1400°C under argon flow, then the programmed temperature decreases to 1050°C and steam is introduced inside the furnace chamber with carrier gas (80%RH at 40°C) to react with the catalyst. This cycle was repeated twice to observe reactivity decrease. The Zr25% hydrolysis yield reached 83% and 89% during the first and the second hydrolysis reaction while it reached 18% and 22% for Zr20%-CTABr. The yield of the first hydrolysis reaction corresponds to 335 µmol of H_2 produced per gram of 25%Zr and 213 µmol of H_2 produced per gram of Zr20%-CTABr. The H_2/O_2 ratio, ideally equal to 2, which is a good indicator of materials cyclability is equal to 1.8 for Zr25%, which means that no significant reactivity losses happened during the cycle.

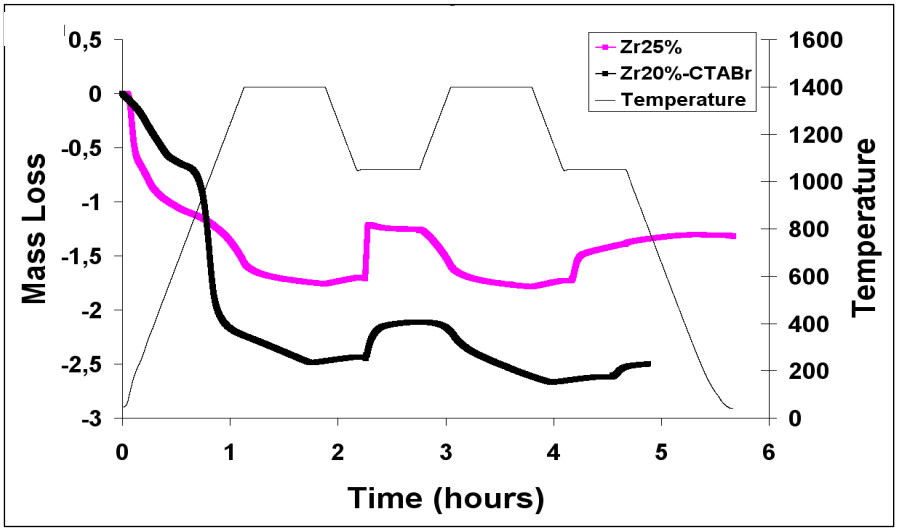

Figure 3: Thermal gravimetric analysis of water splitting cycle with $Zr0_{.25}Ce_{0.75}O_2$ synthesized by coprecipitation and $Zr_{0.2}Ce_{0.8}O_2$ synthesized with CTABr.

4 Conclusion

$NiFe_2O_4$ and Zr-doped ceria were synthesized by different soft chemical routes to improve thermal reduction rate. The highest reduction yield reached with a nickel ferrite was 19.2% (Fe^{2+}/Fe^{3+}) corresponding to 410 µmol O_2/g, while the highest yield with Zr-doped ceria was 46% corresponding to 565 µmol O_2/g. Both materials showed strong sintering after the reduction step, which implies reactivity losses during cycling. The synthesis methods did not avoid sintering for $NiFe_2O_4$ but concerning Zr-doped ceria, coprecipitation method without CTABr alleviated sintering and allowed the material cycling without reactivity loss. During cycling, the catalyst produced about 335 µmol of H_2 per gram with a H_2/O_2 ratio nearly approaching 2. This study demonstrated that Zr-doped ceria is a promising material because the reduction temperature is below 1500°C and no significant reactivity losses are observed during cycling.

References

[1] Steinfeld A. (2002) Solar hydrogen production via a two-step water-splitting thermochemical cycle based on Zn/ZnO redox reactions. Int J Hydrogen Energy [27] p 611-619

[2] Weidenkaff A., Reller A., Wokaun A., and Steinfeld A. (2000) Thermogravimetric analysis of the ZnO/Zn water splitting cycle, Thermochemical Acta [359] p 69-75

[3] Nakamura T. (1977) Hydrogen production from water utilizing solar heat at high temperature, Solar Energy, [19] p467-475

[4] Tamaura Y., Steinfeld A., Kuhn P., Seberger K. (1995) Production of solar hydrogen by a 2-step, water splitting thermochemical cycle, Energy [20] p325-330

[5] Tamaura Y., Kojima M., Sano T., Ueda Y., Hasegawa N., Tsuji M. (1998) Thermodynamic evaluation of water splitting by a cation excessive(Ni,Mn) ferrite, International Journal of Hydrogen Energy [23] p1185-1191

[6] Han S. B., Kang T. B., Joo O. S., Jung K. D. (2007) Water splitting for hydrogen production with ferrites, Solar Energy, [81] p 623-628

[7] Kaneko H., Yokoyama T., Fuse A., Ishihara N., Tamaura Y. (2006) Synthesis of new ferrite, Al-Cu ferrite, and its oxygen deficiency for solar H_2 generation from H_2O, International journal of hydrogen energy [31] p 2256-2265

[8] Kodama T., Gokon N., Yamamoto R., (2008) Thermochemical two-step water splitting by ZrO2-supported NixFe3-xO4 for solar hydrogen production, Solar Energy [82] p 73-79

[9] Gokon N., Muramyama H., Nagasaki A., Kodama T. (2009) Thermochemical two-step water splitting cycles by monoclinic ZrO2-supported $NiFe_2O_4$ and Fe_3O_4 powders and ceramic foam devices, Solar Energy [83] p 527-537

[10] Abanades S., Flamant G. (2006) Thermochemical hydrogen production from a two-step solar-driven water-splitting cycle based on cerium oxides, Solar Energy [80] p 1611-1623

[11] Kaneko H., Miura T., Ishihara H., Taku S., Yokoyama T., Nakajima H., Tamaura Y. (2007) Reactive ceramics of CeO_2-MO_x (M = Mn, Fe, Ni, Cu) for H_2 generation by two-step water splitting using concentrated solar thermal energy, Energy [32] p 656-663

[12] Kaneko H., Ishihara H., Taku S. (2008) Cerium ion redox system in CeO2-xFe2O3 solid solution at high temperature in the two-step water-splitting reaction for H2 generation, Journal of Materials Science [43] p 3153-3161

[13] Balducci G., Kašpar J., Fornasiero P., Graziani M., Islam M.S., Gale J.D. (1997) Computer simulation studies of bulk reduction and oxygen migration in CeO_2-ZrO_2 solid solutions. J Phys Chem B [101] p 1750-1753

[14] Yuejuan W., Jingmeng M., Mengfei L., Ping F., Mai H. (2007) Preparation of high surface area nano-CeO2 by template-assisted precipitation method, Journal of Rare Earth [25] p 58-62

[15] Feng R., Yang X., Ji W., Au C. T. (2008) Hydrothermal synthesis of stable mesoporous ZrO2-Y2O3 and CeO2-ZrO2-Y2O3 from simple organic salts and CTAB template in aqueous medium, Materials Chemistry and Physics [107] p 132-136

[16] Pan C., Zhang D., Shi L. (2008) CTAB assisted hydrothermal synthesis ,controlled conversion and CO oxidation properties of CeO2 nanoplates, nanotubes, and nanorods, Journal of solid state chemistry [181] p 1298-1306

[17] Yuan Q., Duan H., Li L., Sun L.D., Zhang Y., Yan C.H. (2009) Controlled synthesis and assembly of ceria-based nanomaterials, Journal of colloid and interface science [335] p 151-167

Demonstration of Solar Hydrogen Production from Water Splitting via Monolithic Honeycomb Reactors in a 100-kW-Scale Pilot Plant

C. Agrafiotis, **A.G. Konstandopoulos**, **S. Lorentzou**, **C. Pagkoura**, **A. Zygogianni**, Aerosol and Particle Technology Laboratory (APTL), Greece
M. Roeb, **J.-P. Säck**, **P. Rietbrock**, **C. Prahl**, **H. Schreiber**, **M. Neises**, **M. Ebert**, **W. Reinalter**, **M. Meyer-Grünefeld**, **C. Sattler**, DLR, Germany
A. Lopez, **A. Vidal**, CIEMAT, Spain
A. Elsberg, **P. Stobbe**, STC, Denmark
D. Jones, **A. Steele**, JM, U.K.

1 Introduction

The HYDROSOL research group has introduced the concept of monolithic honeycomb solar reactors for performing redox pair-based cycles for the production of hydrogen from water using solar energy [1] inspired from the well-known automobile catalytic converters. The basic idea proposed, developed and demonstrated within the HYDROSOL and HYDROSOL-II projects was to combine a monolithic honeycomb support structure capable of achieving high temperatures when heated by concentrated solar radiation [2], with a redox pair system [3,4] suitable for the performance of water dissociation and for regeneration at these temperatures. With this configuration, the complete operation of the whole process (water splitting and regeneration of the metal oxide) can be achieved by a single solar energy converter. In addition, by using a two-chamber reactor the two steps of the cycle can be performed in parallel and therefore a hydrogen production process in a quasi-continuous mode can be achieved [5] on a reactor configuration not involving either moving parts or moving solid particles. The present work describes the realisation and successful test operation and pilot plant demonstration of this technology in a 100 kW scale on a solar tower platform.

2 Reactor

The successful testing and the suitable behaviour of the laboratory-scale reactor in the earlier stages of the project [6] have provided a basis for the design of the pilot reactor. Whereas the general reactor concept was kept - i.e. a dual module solar hydrogen production reactor consisting of two adjacent reaction chambers that provides for quasi-continuous solar hydrogen production since one module splits water while the other is regenerating the redox material - the scale-up of the reactor from 10 kW_{th} to 100 kW_{th} was basically realised by increasing the absorber surface. Three times three (a total of 9) individual pieces of square-shaped monolithic honeycomb absorbers made of siliconized silicon carbide (siSiC) each with dimensions of 146x146 mm were assembled as one absorber module and mounted to form a square with slightly shaped concave surface (Fig. 1a).

(a) (b)

Figure 1: Pilot, 100 kW-scale HYDROSOL solar reactor: (a) front face of reactor's individual chamber consisting of nine SiC square-shaped blocks; (b) dual chamber reactor completely assembled and installed at the SSPS tower, ready for operation.

3 Operation and Control Concept

In a solar platform facility, the different heat demands of the two steps of the cycle are realized in the HYDROSOL process not by moving the reactors but by adjusting the flux density on each reactor module when the status of the cycle is switched from regeneration to splitting and vice versa by re-alignment of a part of the solar concentrators. Thus, for powering the two modules of the reactor with different solar flux, the heliostat field (Fig. 2a) is "partitioned" into different parts that are actuated separately [7]: a "fixed" part tracked as usually in solar fields covering the basic load for both receiver modules and a "flexible" part which is also tracked but additionally re-focused at regular intervals simultaneously to the switch over of modules from one process step to the other (Fig. 2b). During the splitting process, steam is fed in from a steam generator into the so-called "east" reactor chamber operating at e.g. 800°C. At the same time, nitrogen as flushing gas is fed into the "west" reactor chamber operating at e.g. 1200°C, in order to release the oxygen from the metal oxide redox system. After a half-cycle of 20-30 minutes, a part of the heliostats' focus is moved from the west to the east chamber to realise the necessary temperature increase up to 1200°C to perform the regeneration of the redox system in the east chamber, whereas the west chamber is cooled down to 800 °C to proceed with the splitting of water at that temperature.

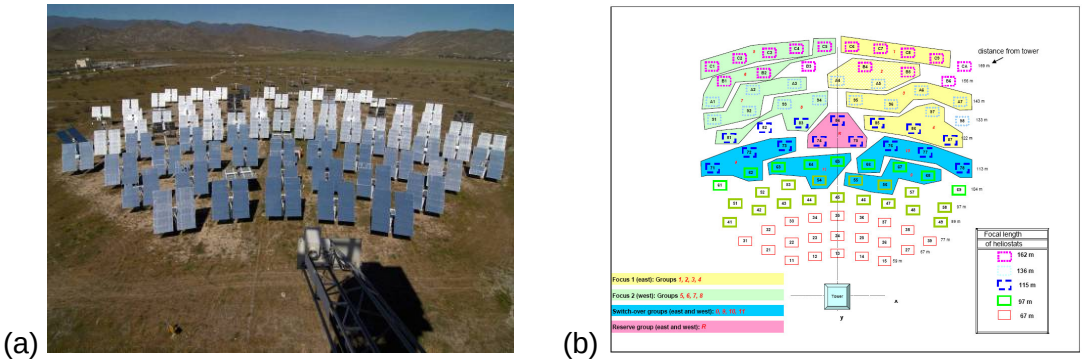

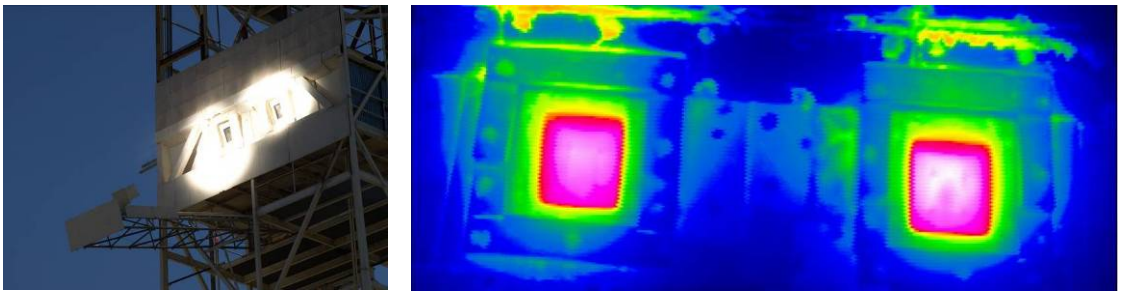

Figure 2: **(a) SSPS-CRS heliostat field view from the reactor's level; (b) implemented partitioning of heliostat field and selected partitioned groups for the operation of the reactor; (c) operation of the HYDROSOL reactor under irradiation; (d) dual focus produced by the solar field at the front face of the two reactor chambers; (e) temperature profiles at the front face of the two reactor chambers by thermal camera.**

4 Thermal Qualification

First, an exhaustive thermal qualification of the pilot plant has been carried out using uncoated ceramic honeycombs as absorbers i.e. without a redox system. All tests were carried out with air instead of nitrogen and without water vapour. Those tests helped to develop and validate the operational and measurement strategy. To control the temperature, the volume flow and pre-heater temperature for the working medium – air - as well as the

number of heliostats focused on the two modules of the receiver were systematically varied or used to compensate for the fluctuations of the receiver temperature caused by other (outer) parameters like Direct Normal Irradiance (DNI), ambient temperature, wind speed and direction. It was concluded that there is only little usefulness of employing feed gas preheating and mass flow of the feed gas as control parameters, whereas the preferred way of controlling the process temperature is by the heliostats themselves. Solar flux fluctuations are compensated by adding or removing individual heliostats to the two foci. A control strategy was set up by using high-flux mirrors for the “coarse” adjustment and low-flux heliostats for the “fine-tuning” of the temperature control. For both tested cycle temperatures, 800 °C and 1200 °C, the control by heliostats ensured sufficiently steady states.

5 Hydrogen Production Experiments

For the hydrogen production experiments, the “blank” siSiC monolithic absorber structures were replaced by a set of 18 monoliths coated with iron-zinc mixed oxide. The results of an experimental campaign on 23/04/2009 are shown in Fig. 3. Test conditions were as follows: 5 Nm/h of nitrogen, 2.5 kg/h of water steam, the temperature of the different gas preheaters was 200°C, a production temperature of 900°C and a regeneration temperature of 1200°C was applied (Fig. 3a). Though the pilot plant faced an operation break of several weeks before this campaign, the hydrogen production could be recovered with similar production rates as observed in the previous campaign. Obviously the system and in particular the metal oxide does not suffer significantly from longer operational breaks and from longer exposure to “outdoor” conditions. Beyond this only a slight decrease of hydrogen production rate and yield was observed (Fig. 3b).

Exemplarily the hydrogen production cycles of one test week in July 2009 are shown in Fig. 3c. The cycles involved faced different conditions, since the influence of process parameters was analysed. Parametric tests included the variation of the cycle length, the variation of mass flow of steam and the variation of the water splitting temperature. In this week more then thirty cycles were carried out with the same (fresh) coating. As a trend it can be stated that increased water splitting temperatures lead to higher hydrogen production rates. Higher water concentrations in the feed stream have only little influence since the there already is a surplus of steam in the reactor. The time needed to switch a module between water splitting and regeneration mode could be significantly reduced by defocusing all heliostats of the modules which has to be cooled down from regeneration temperature. The modified heliostat grouping turned out very helpful in term of process control, of a fast switch between operation modes, and of keeping conditions as constant and as reproducible as possible over a day.

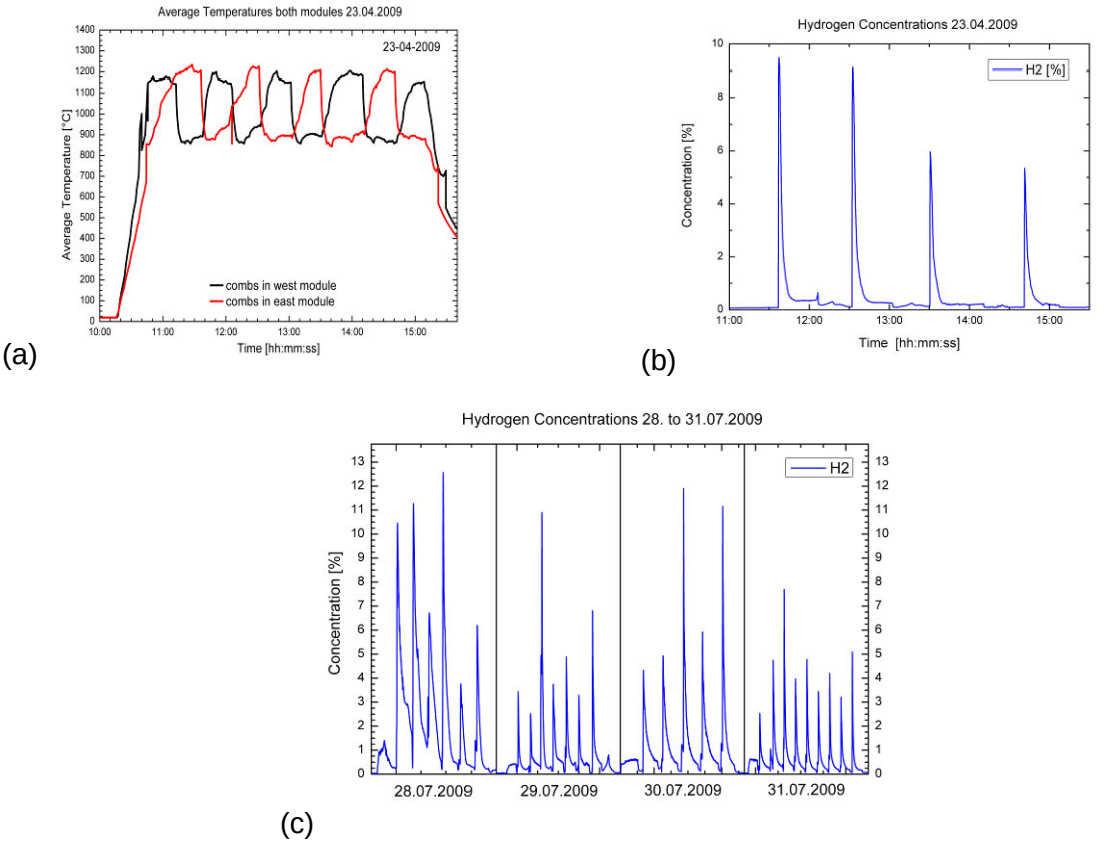

Figure 3: (a) Average temperatures of both modules and (b) Hydrogen concentrations, of experimental campaign of 23.04.2009; (c) Hydrogen concentrations (western module) of experimental campaign between 28-31.07.2009.

6 Summary

A 100 kW pilot plant for two-step solar thermo-chemical water splitting via monolithic honeycomb solar reactors based on the HYDROSOL two-chamber solar receiver-reactor technology has been developed, installed and test operated at the SSPS solar tower plant at PSA in Spain. At first, thermal qualification of the pilot plant has been carried out using uncoated ceramic honeycombs as absorbers, in order to develop and validate operational and measurement strategy as well as to create essential knowledge on the dynamics of the system during thermal cycling. Potential control parameters capable of ensuring sufficient constant temperature levels have been analyzed. It was concluded that the preferred way of controlling the process temperature is by the heliostats themselves which can be applied to ensure sufficiently steady states and compensation against solar flux fluctuations.

A number of hydrogen production cycles applying honeycombs coated with redox material in several experimental series have been successfully carried out demonstrating the feasibility of solar water splitting via the HYDROSOL technology in the 100 kW-scale pilot scale under real conditions. Significant concentrations of hydrogen were produced with a conversion of steam of up to 30 %. Pilot plant tests on optimizing the process conditions are being continued by using absorber monoliths with different coatings from on-going material

development studies, to demonstrate the high potential of the particular technology for further scale-up.

Acknowledgements

To the European Commission for co-funding of this work within the Project HYDROSOL-II "Solar Hydrogen via Water Splitting in Advanced Monolithic Reactors for Future Solar Power Plants" (SES6-CT-2005-020030), under the 6th Framework Programme of the European Union (2002-2006).

References

[1] Agrafiotis, C., Roeb, M., Konstandopoulos, A.G., Nalbandian, L., Zaspalis,V.T., Sattler, C., Stobbe P., Steele, A.M. (2005) *Solar water splitting for hydrogen production with monolithic reactors*, Solar Energy 79, 409–421.

[2] Agrafiotis C. C., Mavroidis I., Konstandopoulos A. G., Hoffschmidt B., Stobbe P., Romero M., Fernandez-Quero V. (2007) *Evaluation of Porous Silicon Carbide Monolithic Honeycombs as Volumetric Receivers/Collectors of Concentrated Solar Radiation*, Journal of Solar Energy Materials and Solar Cells, 91, 474-488.

[3] Steinfeld, A., Sanders, S., Palumbo, R. (1999) *Design aspects of solar thermochemical engineering - A case study: Two-step water-splitting cycle using the Fe_3O_4/FeO redox system,* Solar Energy, 65(1), 43 - 53.

[4] Kodama, T., Gokon, N. (2007) *Thermochemical Cycles for High-Temperature Solar Hydrogen Production,* Chemical Reviews, 107, 4048–4077.

[5] Roeb, M., Sattler, C., Klüser, R., Monnerie, N., deOliveira, L., Konstandopoulos, A.G., Agrafiotis, C., Zaspalis, V.T., Nalbandian, L., Stobbe, P., Steele, A., (2006), *Solar hydrogen production by a two-step cycle based on mixed iron oxides* Journal of Solar Energy Engineering - Transactions of the ASME, 128, 125-133.

[6] Roeb, M., Neises, M., Säck, J.-P., Rietbrock, P., Monnerie, N., Dersch, J., Schmitz, M., Sattler, C. (2009) *Operational strategy of a two-step thermochemical process for solar hydrogen production*, International Journal of Hydrogen Energy, 34(10), 4537-4545.

[7] Roeb, M., Säck, J.-P., Rietbrock, P., Neises, M., Ebert, M., Reinalter, W., Schmitz, M., Sattler, C., Lorentzou, S., Pagkoura, C., Zygogianni, A., Agrafiotis, C., Konstandopoulos, A.G., Stobbe, P., Jones, D., Steele, A., Lopez, A., Romero, M. (2008): *Development and verification of a two-step thermochemical process for solar hydrogen production from water*, In: Mancini, T. : 14th SolarPACES Biannual Symposium, Las Vegas, NV (USA), March 4-7.

Towards Industrial Solar Production of Zinc and Hydrogen – Modeling and Design of a 100 kW Solar Pilot Reactor for ZnO Dissociation

D. Gstoehl, T. Cooper, W. Villasmil, A. Meier, Paul Scherrer Institut, Solar Technology Laboratory, 5232 Villigen PSI, Switzerland

A two-step water-splitting thermochemical cycle based on the Zn/ZnO redox reactions is proposed for producing solar hydrogen; the two steps are (1) the endothermal dissociation of ZnO and (2) the exothermal reaction of H_2O with Zn to produce hydrogen. A preliminary engineering design of a 100 kW solar pilot reactor for the thermal dissociation of ZnO is presented. The reactor features a rotating cavity receiver lined with ZnO particles. With this arrangement, ZnO is directly exposed to concentrated solar radiation and serves simultaneously the functions of radiant absorber, chemical reactant, and thermal insulator. The functionality of the engineering design has earlier been demonstrated with a 10 kW reactor prototype at temperatures above 2000 K and peak solar concentration ratios exceeding 4000 suns. The solar chemical reactor, depicted in Fig. 1, is described in detail in a previous publication [1]. Here, we present a brief summary of the main features. The rotating cylindrical cavity is made of sintered Al_2O_3 tiles placed on top of a multi-layer Al_2O_3-SiO_2-Y_2O_3-based ceramics for thermal shock resistance, mechanical stability, gas diffusion barrier, and thermal insulation. Along the horizontal axis, a dynamic feeder extends and contracts within the rotating cylindrical cavity, forming a layer of ZnO particles along the cavity walls. The directly irradiated ZnO(s) is thermally decomposed, and the gaseous products Zn(g) and O_2 exit the cavity through a water-cooled annular gap between the outlet tube and the feeder. Inert Ar gas is injected for aerodynamic window protection and for minimizing recombination of product gases of Zn(g) and O_2 to ZnO(s) in the cavity.

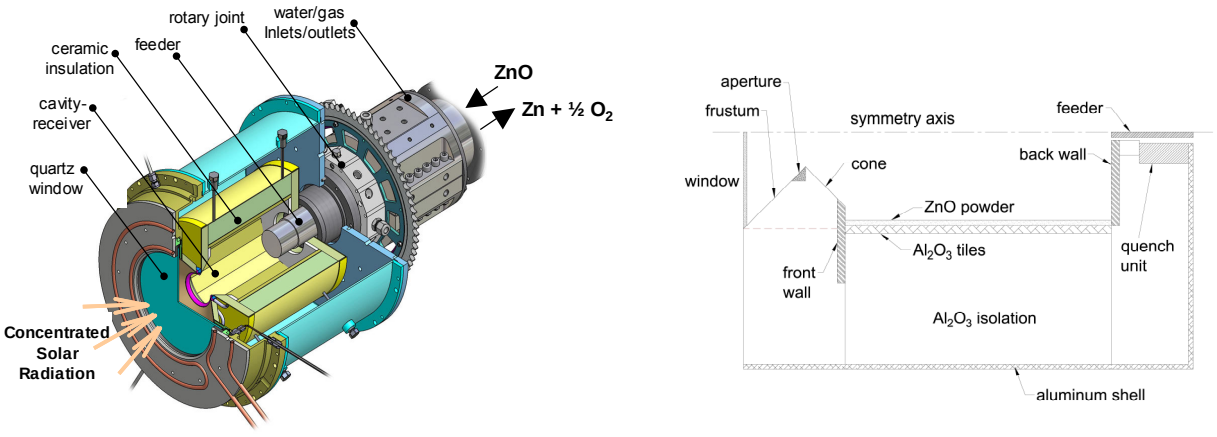

Figure 1: ***Left:*** **Schematic of the solar chemical reactor configuration. From [1].** ***Right:*** **Scheme of the reactor geometrical domain used for the numerical model.**

The planned test site for the 100 kW scale-up reactor is the Megawatt Solar Furnace (MWSF) at the Laboratoire PROcédés, Matériaux et Energie Solaire (PROMES) research facility in Odeillo, France [2].

The MWSF consists of a south-facing field of 63 flat heliostats (7.5 m x 6 m), a north-facing parabolic concentrator dish (height 40 m, width 54 m) , and a receiver tower (height 20 m) arranged as shown in Fig. 2. The heliostats are elevated on a series of eight stepped terraces such that the reflected beam from each heliostat is parallel to the axis of revolution of the parabolic dish. Each terrace contains two rows of heliostats such that, at moderate tilt angles, no horizontal gaps exist between heliostats as projected onto the parabolic dish. Additionally, the elevations of the terraces are arranged in a manner such that (again at moderate tilt angles) no vertical gaps exist between heliostats as projected onto the parabolic dish. Optical and geometric data of the site − receiver tower, heliostats and parabolic dish – were obtained from [2]. For the intended size of the scale-up reactor, the full capacity of the MWSF is not required. The 25 center heliostats will likely be sufficient to achieve the necessary power input of 100 kW. The subsequent analysis is therefore limited to these 25 heliostats of interest.

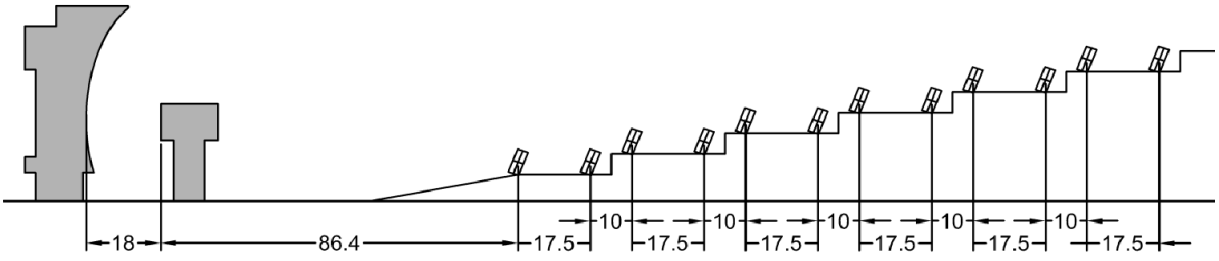

Figure 2: Side elevation of the MWSF showing distances in meters from the focal plane to the vertex of the parabolic dish and to each row of heliostats for the 25 heliostats of interest. Data provided by CNRS-PROMES.

An in-house Monte Carlo (MC) ray-tracing code VeGaS [3] has been adapted to the geometry of the MWSF with the goal of estimating the flux distribution within the scale-up reactor [4]. Parameter matching was performed to obtain close agreement between the MC ray-tracing results and the experimentally derived curve of incident solar flux for a flat target positioned at the focus [4]. Three parameters – the fraction of diffuse reflection, f_{diff}, and the angular dispersion error of the heliostats, $\phi_{err,helio}$, and parabolic dish, $\phi_{,err,PD}$ – were considered. The angular dispersion error includes the combined effect of macroscopic geometric imperfections and heliostat tracking errors. The fraction of diffuse reflection includes the combined effect of microscopic imperfections, such as surface roughness, and the degradation of surface reflectivity from dust and atmospheric exposure. The best fit parameter match yielded a total combined dispersion error of 6 mrad, split evenly between heliostats and parabolic dish ($\phi_{err,helio}$ = $\phi_{,err,PD}$ = 3 mrad) and a fraction of diffuse reflection of f_{diff} = 0.05 for the mirror surfaces. A comparison of the simulated and experimentally measured flux distribution on the flat target is given in Fig. 3.

A transient heat transfer model was adapted to simulate the thermal performance of the 100 kW pilot reactor for the solar-driven dissociation of ZnO at MWSF [5]. The model couples radiation, convection, and conduction heat transfer to the reaction kinetics for a shrinking domain and simulates a transient ablation regime with semi-batch feed cycles of ZnO particles. Experimental model validation was previously accomplished with a 10 kW reactor prototype in terms of temperatures and reaction extents [6].

Geometric dimensions used for the preliminary 100 kW reactor design are listed in Table 1 [6]. The porosity and the extinction coefficient of the ZnO layer have been taken as 0.5 and 7850 m^{-1}, respectively. In the proposed design, the cavity, as well as the back and front walls are assumed to be covered with a 40 mm thick sintered ZnO layer followed by 10 mm thick Al_2O_3 tiles. The function of the ZnO layer is to protect the Al_2O_3 tiles from the highly radiative environment. The power distribution obtained from the ray-tracing was scaled such that 100 kW input power is effectively absorbed within the reactor cavity.

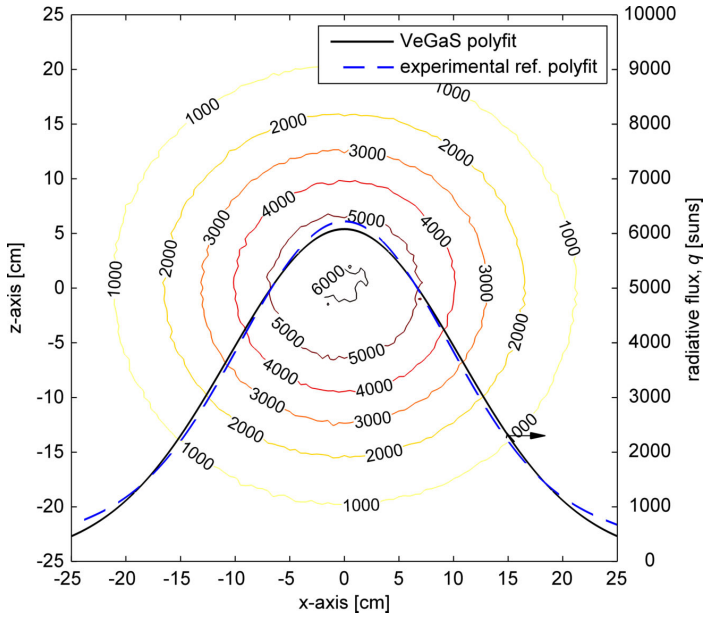

Figure 3: Contour map of incident radiative flux for a flat target at the focus of the parabolic dish comparing the parameter-matched VeGaS simulation ($\phi_{err,helio} = \phi_{,err,PD} = 3$ mrad; $f_{diff,helio} = f_{diff,PD} = 0.05$) to the experimentally measured distribution. Results are for a direct normal solar irradiance of 1 sun (1 sun = 1000 W/m^2) for a solar altitude angle of 45° at solar noon. Experimental data provided by CNRS-PROMES.

Table 1: Dimensions for the 100 kW pilot reactor as proposed by [6].

Cavity diameter	500	mm
Cavity length	750	mm
Sintered ZnO layer thickness	40	mm
Al_2O_3 tiles thickness	10	mm
Outer Al shell diameter	110	mm
Aperture diameter	190	mm
Window diameter	370	mm
Cavity outlet diameter	80	mm
Frustum angle	45	deg

The radiative flux distribution within the 100 kW reactor at the MWSF is illustrated in Fig. 4. Highest concentrations are obtained on the bottom part of the cavity cylinder and on the frustum. Nearly 90% of the radiative power that enters the aperture is absorbed on the cavity cylindrical wall, while the rest is mostly absorbed by the lateral back wall and the cone. Only 0.1% of the incoming solar radiation is lost through the back exit of the reactor by direct transmission or reflection. In the experimental runs, the rotary motion of the cavity effectively averages the radiative flux distribution along the circumference of the cylinder.

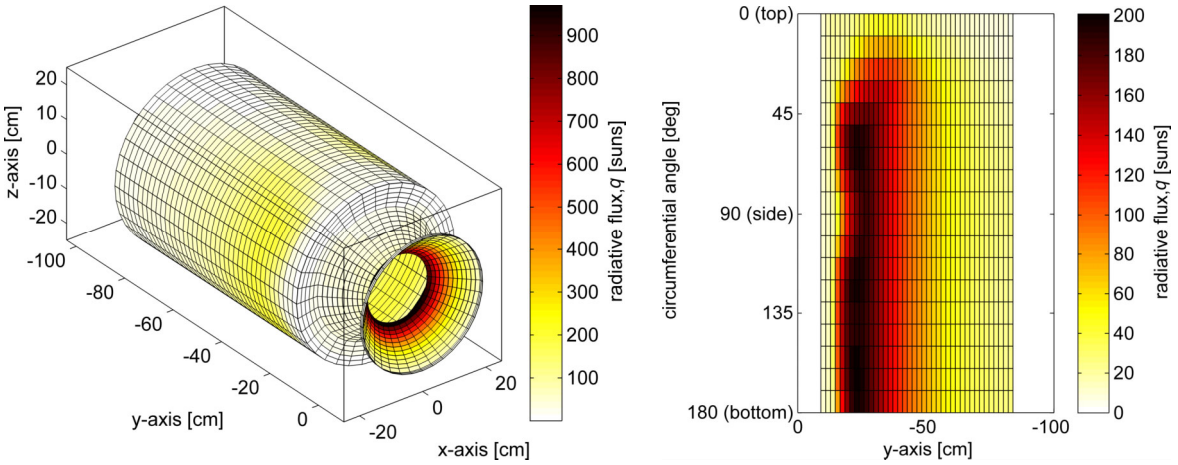

Figure 4: Radiative flux distribution on the reactor (*left*) and on the cylindrical cavity surface (*right*). Note that the radiative flux on the internal cavity walls is much less than on the frustum due to the distribution of the incident radiation over a much larger surface area within the cavity. 1 sun = 1000 W/m^2.

The 100 kW reactor was simulated for two consecutive days of operation. For the first day, the incoming radiative power is increased linearly from zero to the nominal power over a 1-hour time span to avoid overheating of the reactor components. The power is then held constant for 8 hours, followed by 15 hours of zero incident power, simulating the operation overnight when no solar radiation is available. The second day was modeled in a similar way, the only difference being that no time span was considered for heating up of the reactor as it would still preserve an important portion of the sensible heat accumulated during the previous day.

Figure 5 (left) shows the predicted temperatures at the sintered-ZnO surface and at the Al_2O_3-tile surface halfway along the cavity cylinder. The model results indicate that temperatures above 2000 K are likely to be reached at the sintered-ZnO surface. To avoid failure of the Al_2O_3 tiles at such high temperatures, a protecting layer of sintered ZnO is required on the cylindrical cavity walls as well as on the lateral front and back walls. With the proposed ZnO layer thickness of 40 mm, the maximum surface temperature of the Al_2O_3 tiles is not expected to exceed 1900 K.

The predicted reactor performance is illustrated graphically in Fig. 5 (right) and summarized in Table 2. The amount of ZnO dissociated is expected to be approximately 250 kg per day, corresponding to an average dissociation rate of about 8 g/s. The solar-to-chemical energy conversion efficiency, $\eta_{\text{solar-to-chemical}}$, is defined as

$$\eta_{solar \rightarrow chemical} = \frac{r\left(\Delta H_r(T) + \int_{T_0}^{T} c_{p,ZnO}\, dt\right)}{Q_{solar}}$$

where ΔH_r is the reaction enthalpy, c_p is the specific heat capacity, and Q_{solar} is the solar power absorbed by the cavity (100 kW). In contrast, the reactor efficiency, $\eta_{reactor}$, and the shares of the radiation, conduction, and convection losses presented in Table 2, have been calculated based on the total incident radiative power on the reactor window (190 kW). 10% of the incoming solar radiation is expected to be lost at the window due to reflections at its outer surface. The simulation anticipates the reradiation losses to account for approximately 40% of the total incident power on the window. The water-cooled components − namely, the quench unit, the reactor front shield and the aperture ring − were modeled at 298 K. As approximately 7% of the total incident radiative power is absorbed by the aperture ring, the heat loss associated to this component represents by far the highest share of the conduction losses.

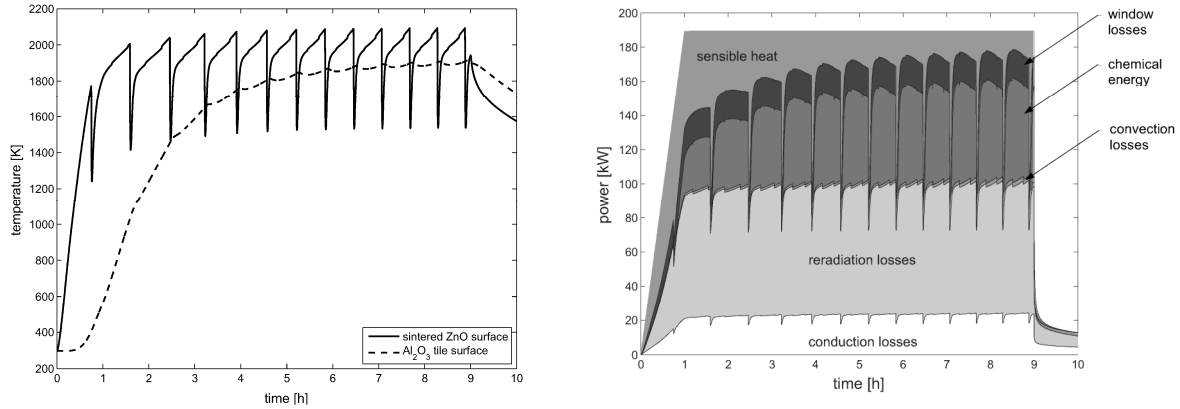

Figure 5: ***Left:*** **Predicted temperatures halfway along the cavity of the 100 kW ZnO dissociation reactor, both at the sintered-ZnO surface and at the Al_2O_3-tile surface.** ***Right:*** **Instant energy balance of the 100 kW ZnO dissociation reactor as it would operate at the Odeillo solar furnace. The concentrating solar system configuration is such that 100 kW input power is effectively absorbed within the reactor cavity.**

Since for the second day of operation less energy is required to heat up the reactor components, the average bulk reactor temperature is predicted to be higher for the second day, resulting in a higher dissociation rate and higher efficiencies. Scaling up the reactor to 100 kW solar thermal power input has thus the potential of reaching solar-to-chemical energy conversion efficiencies approaching 50%.

Table 2: Predicted energy balance for the 100 kW pilot reactor.

	Day 1	Day 2	
Reaction rate	26	30	kg/h
$\eta_{solar\text{-}to\text{-}chemical}$	42.4	46.2	%
$\eta_{reactor}$	22.3	24.2	%
Reradiation losses	40.6	40.9	%
Conduction losses	14.6	14.8	%
Convection losses	2.4	3.1	%
Sensible heat of the reactor	10.1	7.0	%
Window losses	10.0	10.0	%

Acknowledgments

Financial support by the Swiss Federal Office of Energy (SFOE) is gratefully acknowledged. We thank CNRS-PROMES for the collaboration, especially E. Guillot and J.-L. Sans for providing information concerning the MWSF. We are grateful to M. Hänchen and P. Coray for fruitful discussions and computational support.

References

[1] L.O. Schunk, P. Haeberling, S. Wepf, D. Wuillemin, A. Meier, A. Steinfeld: ***A receiver-reactor for the solar thermal dissociation of zinc oxide****, J. Solar Energy Eng.* 130 (2), 021009, 2008.

[2] CNRS-PROMES: "CNRS 1000 kW solar furnace," Centre National de la Recherche Scientifique (CNRS), 2010, http://www.promes.cnrs.fr/TOUT-PUBLIC/Les-fours/eng-lesfours1.htm

[3] J. Petrasch: ***Thermal modeling of solar chemical reactors: transient behavior, radiative transfer***, MS Thesis, ETH Zürich, 2002.

[4] T. Cooper: ***Ray-tracing analysis of a concentrating solar facility for the optical design of solar cavity receivers***, MS Thesis, ETH Zürich, 2010.

[5] W. Villasmil: ***Design of a 100-kW reactor for the solar thermal dissociation of zinc oxide***, MS Thesis, ETH Zürich, 2010.

[6] L.O. Schunk, W. Lipiński, A. Steinfeld: ***Heat transfer analysis of a solar receiver-reactor for the thermal dissociation of ZnO – Experimental validation at 10 kW and scale-up to 1 MW****, Chem. Eng. J.* 150, pp. 502-508, 2009.

“Steam-Iron” Process for Hydrogen Production: Recent Advances

J.A. Peña, E. Lorente, J. Herguido, Catalysis, Molecular Separations and Reactor Engineering Group (CREG), Aragón Institute of Engineering Research (i3A), Universidad de Zaragoza, Spain

The “Steam-Iron” process is one of the oldest commercial methods for the production of hydrogen. The process was practised from the early 1900s well into 1930s for supplying small quantities of pure hydrogen to some industries (e.g., aerial navigation). Later, the technology was supplanted by the more efficient and economical natural gas reforming process [1]. However, the interest in the “Steam-Iron” process has grown in recent times, due to its simplicity, the high purity of hydrogen obtained, which is especially important for the use of hydrogen in fuel cells, the feedstock flexibility and the possibility to use renewable energy sources in this process.

The “Steam-Iron” process produces high-purity hydrogen by separating the hydrogen production and feedstock oxidation steps using iron oxides subjected to redox cycles. Simplistically, the chemistry of the “Steam-Iron” process involves two subsequent reactions, as shown schematically in Figure 1.

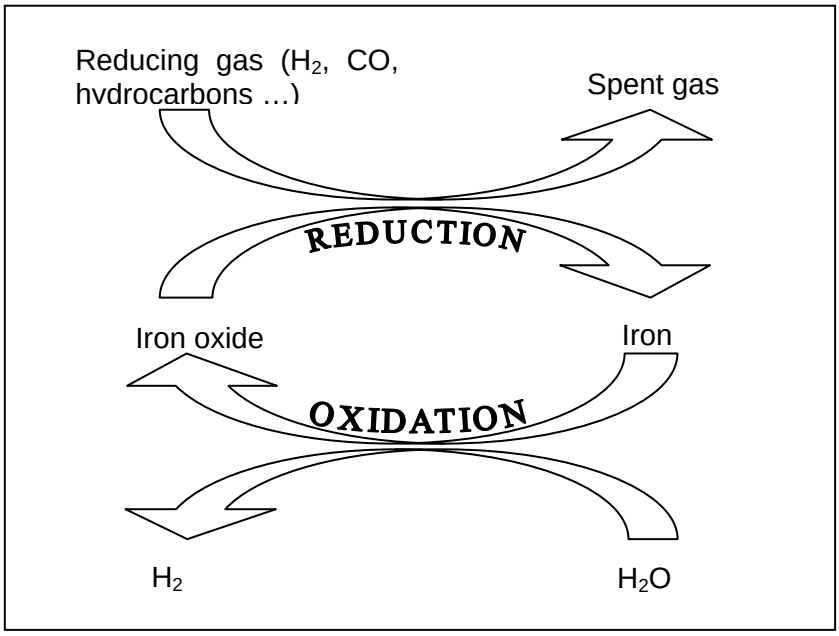

Figure 1: Principle of the “Steam-Iron” process.

In the reduction step, the iron oxide is treated with a reducing feedstock (such as hydrogen, mixtures of hydrogen and CO, and various other fuels), and as a result of the reaction, the metal (iron) or a partially reduced oxide is obtained. The second step consists in the oxidation of the reduced material by means of steam, which decomposes, resulting in a pure

hydrogen stream (without carbon oxides), while the metal oxide is partially regenerated and therefore it can be recycled to the reduction step.

In practice, the process is much more complex due to the presence of various reduced forms of iron oxides and the simultaneous ocurrence of a number of feedstock decompositon/oxidation reactions. A few studies have been devoted to the solid-state kinetics of the process [2-4]. Models based on nucleation and growth mechanisms have been proven to describe both the reduction and oxidation reactions. Furthermore, the decrease in reactivity of the oxide caused by cyclic operation of the alternative reduction and oxidation stages, has been investigated and mathematically modelled [5].

On the other hand, in order to improve the long-term stability of the oxide as well as enhance the rate of reactions, the use of foreign metals (acting as promoters) has been proposed. Several research groups have been exploring the influence of different metal additives on the redox properties of iron oxides [6-8]. The use of additives such as Al, Cr or Ce has shown to prevent the deactivation of the oxide associated with the repetition of reduction and oxidation cycles. Other metals (such as Rh) improve the oxidation rates at low temperatures. It has been also considered the combination of two/three promoters with different properties, in the search for a synergistic effect.

Alternatively, the use of fumed-Fe-dust [9] and mill-scale waste [10] from the steel industry has been suggested as inexpensive base materials rather than synthesized iron oxides.

One of the advantages of the “Steam-Iron” process relates to high feedstock feasibility. Table 1 shows a relation of several reducing gas stream for the “Steam-Iron” process that have been proposed and studied by different authors. The use of gas obtained from gasification or reforming in the reduction step, offers an interesting opportunity for developing and optimizing the “Steam-Iron” process in combination with a gasifier or a reformer unit. The advantage of this integrated process concept is the possibility of enhancing the overall efficiency of the system, by means of energy recovery and recycling of product streams.

Table 1: Reducing agents used in the “Steam-Iron” process.

Reducing agent	**Authors (reference No.)**
Gas resulting from coal gasification	Gupta et al., 2007 [11]
Gas resulting from biomass gasification	Hacker et al., 1998;2000 [12,1] Sime et al., 2003 [13]
Gas resulting from pyrolysis oil gasification	Bleeker et al., 2007 [14]
Gas resulting from light hydrocarbons reforming	Hacker, 2003 [15] Galvita et al., 2008 [16]
Methane	Takenaka et al., 2003; 2004 [17,18] Galvita and Sundmacher, 2005 [19]
Mixtures CH_4/H_2	Otsuka et al., 2001 [20] Peña et al., 2006 [2]

The “Steam-Iron” process can be performed in continuous as well as discontinuous manner. The main application of the continuous operation alternative is the selective separation of

hydrogen from other gases, such as hydrogen-containing natural gas, biomass or coal pyrolisis and/or gasification, or the stream resulting from thermal decomposition of natural gas. For this option, the simultaneity of the reduction and oxidation steps can be achieved by using either fixed bed reactors in parallel with alternate flows or fluidized bed reactors with circulation of solids between separated reaction zones. The application of a simulated moving bed-type reactor has been also proposed to achieve the advantages of the moving bed reactor by moving not the solid materials but the fluid stream [21].

When the "Steam-Iron" process is operated in the discontinuous manner, it can be considered as a method of hydrogen storage. The theoretical maximum amount of hydrogen capable to be stored and transported as the reduced oxide is 4.8 wt%, according to the mass ratio of H_2 to Fe in the hydrogen release reaction ($3Fe + 4H_2O \rightarrow Fe_3O_4 + 4H_2$). This corresponds to 537 L of hydrogen gas (STP) that can be stored per kg of iron, and it is comparable to the hydrogen storage density of conventional metal hydrides.

While reactor design and modelling are matters that have been anlaysed by several research groups [21-24], these topics still require more attention and investigation in order to increase the feasibility of hydrogen production by the "Steam-Iron" process in comparison with other technologies.

References

[1] Hacker V, Frankhauser R, Faleschini G, Fuchs H, Friedrich K, Muhr M, Kordesch K. *J. Power Sources* 86(1-2) (2000) 531-535.

[2] Peña JA, Lorente E, Romero E, Herguido J. *Catal. Today* 116(3) (2006) 439-444.

[3] Hacker V, Vallant R, Thaler M. *Ind. Eng. Chem. Res.* 46(26) (2007) 8993-8999.

[4] Go KS, Son SR, Kim SD. *Int. J. Hydrogen Energy* 33(21) (2008) 5986-5995.

[5] Lorente E, Peña JA, Herguido J. *Int. J. Hydrogen Energy* 33(2) (2008) 615-626.

[6] Otsuka K, Kaburagi T, Yamada C, Takenaka S. *J. Power Sources* 122(2) (2003) 111-121.

[7] Urasaki K, Tanimoto N, Hayashi T, Sekine Y, Kikuchi E, Matsukata M. *Appl. Catal. A* 288(1-2) (2005) 143-148.

[8] Lorente E, Peña JA, Herguido J. *J. Power Sources* 192(1) (2009) 224-229.

[9] Hui W, Takenaka S, Otsuka K. *Int. J. Hydrogen Energy* 31(12) (2006) 1732-1746.

[10] Kesavan SK, Azad AM. *Int. J. Hydrogen Energy* 33(4) (2008) 1232-1242.

[11] Gupta P, Velazquez-Vargas LP, Fan LS. *Energy Fuels* 21(5) (2007) 2900-2908.

[12] Hacker V, Faleschini G, Fuchs H, Fankhauser R, Simader G, Ghaemi M, Spreitz B, Friedrich K. *J. Power Sources* 71(1-2) (1998) 226-230.

[13] Sime R, Kuehni J, D'Souza L, Elizondo E, Biollaz S. *Int. J. Hydrogen Energy* 28(5) (2003) 491-498.

[14] Bleeker MF, Kersten SRA, Veringa HJ. *Catal. Today* 127(1-4) (2007) 278-290.

[15] Hacker V. *J. Power Sources* 118(1-2) (2003) 311-314.

[16] Galvita V, Schröder T, Munder B, Sundmacher K. *Int. J. Hydrogen Energy*, 33(4) (2008) 1354-1360.

[17] Takenaka S, Son VTD, Yamada C, Otsuka K. *Chem. Lett.* 32(11) (2003) 1022-1023.

[18] Takenaka S, Son VTD, Otsuka K. *Energy Fuels* 18(3) (2004) 820-829.

[19] Galvita V, Sundmacher K. *Appl. Catal. A* 289(2) (2005) 121-127.

[20] Otsuka K, Mito A, Takenaka S, Yamanaka I. *Int. J. Hydrogen Energy* 26(3) (2001) 191-194.

[21] Imanishi H, Maeda A, Maegawa T, Matsuno S, Aida T. *Int. J. Chem. Reactor Eng.* 5 (2007) A107.

[22] Seiler H, Emig G. Chem. Eng. Technol. 22(6) (1999) 479-484.

[23] Heidebrecht P, Hertel C, Sundmacher K. *Int. J. Chem. Reactor Eng.* 6 (2008) A19.

[24] Lorente E, Cai Q, Peña JA, Herguido J, Brandon NP. *Int. J. Hydrogen Energy* 34(13) (2009) 5554-5562.

Analysis of Reaction Kinetics for a Two-step Hydrogen Production Process Utilizing Porous Iron Powder

Fotouh Al-Raqom, Benjamin Greek, James F. Klasuner and S.A. Sherif , CEM, University of Florida, USA

Thermochemical water splitting is a hydrogen production process that has garnered significant attention in recent years. Unlike direct water splitting, which requires very high temperatures (2500 K), the dissociation of water into H_2 and O_2 via thermochemical water splitting uses reactive metals in a multi-step metal reduction-oxidation (redox) reaction. Many redox reactions have been proposed for hydrogen production, and this work considers the kinetics of thermochemical water splitting utilizing a porous iron powder in a fluidized bed reactor. Porous iron powder with particle diameters ranging from 45 to 150 μm is fluidized and heated within a furnace. The powder is classified as Geldart group B, and when fluidized, it exhibits good mixing, heat transfer and reactivity. A bench scale experimental facility was fabricated to carry out the investigations of hydrogen production via water splitting. The current analysis is limited to the water splitting (oxidation) step at different reactor temperatures. The temperature states for the fluidized bed under investigation are 450, 650 and 850 °C. The approximate reactive surface area of the iron powder is 60 cm^2/g, and thus the surface area of the 25 g sample in the fluidized bed is 0.158 m^2. For the duration of the experiments,18 to 26 minutes, the hydrogen yield is 0.37, 4.5 and 10.45 L for the 450, 650 and 850 °C, reactor temperatures respectively. The rate of hydrogen production decays exponentially with time.

Keywords: Hydrogen, thermochemical water splitting, fluidization, redox reactions, iron oxides.

1 Introduction

The abundance of hydrogen on earth, and its high energy per unit mass makes it attractive as an energy carrier. However, it is uncommon in its elemental form, due to its reactivity, and it is generally found combined with other elements, such as in water or hydrocarbons. In order to retrieve the hydrogen in elemental form, innovative separation methods are required. Currently available methods include electrochemical, biological, and thermal approaches. One promising technology for hydrogen production is thermochemical water splitting (TCWS). TCWS cycles have the potential to deliver overall system efficiencies in excess of 40% [7]. Direct water splitting requires very high temperatures (2500 K) to dissociate water into H_2 and O_2 [6], while thermochemical water splitting uses reactive metals to lower the reaction temperature [4] by splitting water through a series of two or more chemical reactions [2]. In addition, TCWS cycles release oxygen and hydrogen in two separate steps, hence avoiding any recombination which will eliminate any separation steps [2].

In a two-step reaction, the metal oxide is reduced as shown in reaction (1). In the water splitting (WS) step or oxidation step, reaction (2), the activated material is oxidized by the

water, releasing hydrogen. For reactions (1) and (2) M denotes the metal, which follows the convention utilized by Steinfeld [5].

$$MO_{oxidised} \rightarrow MO_{reduced} + O_2 \qquad \text{reduction step} \qquad (1)$$

$$MO_{reduced} + H_2O \rightarrow MO_{oxidised} + H_2 \qquad \text{oxidation step} \qquad (2)$$

Significant research activity with thermochemical water-splitting cycles began 40 years ago. Many Investigations were initiated in the 1970's as a result of the Energy Depot project that was carried out in 1960 [3]. The project aimed at investigating the opportunities to produce fuel from renewable sources. These investigations considered direct hydrogen production using a nuclear heat source. Currently over 350 thermochemical cycles have been identified [1]. Presently, there are two potential high temperature heat sources being considered for thermochemical hydrogen production, namely, concentrated solar energy or nuclear reactors. Several cycles were thermodynamically examined and tested in solar reactors, including zinc oxides and iron oxides. Other investigations have included titanium, cobalt, and manganese oxides, but the yield of hydrogen production is too low to be of any practical interest [5].

2 Experimental Facility

The water splitting step for the current investigation involves the conversion of iron (Fe) to magnetite (Fe_3O_4) and follows the reaction,

$$3Fe + 4H_2O \rightarrow Fe_3O_4 + 4\ H_2 \qquad (3)$$

A bench scale hydrogen production process that utilizes a fluidized bed reactor was fabricated and tested at temperatures of 450, 650, and 850 °C as shown in Figure 1. The reaction utilizes porous iron powder with a mean particle diameter of 91 μm. The reaction chamber includes a 0.6 m long fused quartz tube, capable of operating up to temperatures of 1200 °C. The tube has an inside diameter of 21 mm and a wall thickness of 2 mm. A porous quartz frit, with pore sizes ranging from 40-90 μm, is inserted at the top of the tube to minimize particle carry-over. The powder is placed on a distributer made of a ceramic thermal insulation material with a service temperature up to 1650 °C. The tube is sealed with stainless steel fittings utilizing high temperature silicon O-rings that can withstand temperatures up to 300 °C. The quartz fluidization chamber extends through an electric furnace with a range of 100 to 1200 °C.

To prevent condensation in the system, a low flow (2.5 LPM) of high purity nitrogen gas is used to preheat the reactor. A gas heating section is constructed using nickel-chromium wire, grounded to the system at one end and electrically insulated with ceramic beads. The heat input is controlled with a DC power source. All fittings and tubing, including the quartz tube, are preheated to at least 300 °C prior to introducing steam through the system. During the preheat cycle, the nitrogen gas is vented to atmosphere. An estimation of the nitrogen gas remaining in the system after the preheat cycle is used to compensate for its contribution to the hydrogen production.

A steam generator, consisting of four 200W (maximum) cartridge heaters inside an aluminum chamber, is used in a boiling mode. The rate of steam generation is controlled with a pulse-width modulated signal and solid-state relay at a frequency of two Hertz. An AC power source provides power to the boiling chamber. Using a three-way valve, the steam is either directed to a condenser, which empties into a graduated cylinder, or the steam is directed to the fluidized bed reactor. When steam is directed to the condenser, the rate of condensate is measured to determine the mass flow rate of steam production, which is controlled by the heat input to the boiler. The mass flow rate of steam to the reactor is 0.075 g/s for all experiments considered.

The outlet gas from the reactor is directed through a condenser in which any excess steam is removed from the hydrogen gas flow. The condenser empties into a sealed cylinder, and the weight of the condensate is measured. From the cylinder, the hydrogen gas is directed into inverted water-filled graduated cylinders, and the volume of hydrogen accumulation is determined.

Stainless-steel sheathed E-type and J-type thermocouples are used to monitor and record the gas temperatures entering and exiting the quartz reactor chamber as well as the temperatures of the fittings. The electric furnace is also equipped with a K-type thermocouple that allowes estimation of the bed temperature.

The sequence of operating the experiment is as follows. The system is preheated to approximately about 300 °C with nitrogen. During this time, the boiler is heated, and the constant-power steam flow rate is determined. The nitrogen is then shut off, and the steam is directed into the gas heater section and reactor. Hydrogen production is determined by visual observation of accumulation in the graduated cylinders. A data acquisition board, in conjunction with a LabView virtual instrument panel, is used to monitor and log the temperatures at the inlet and outlet of the reactor, as well as the temperatures of the quartz tube fittings, boiler vapor temperature and pressure.

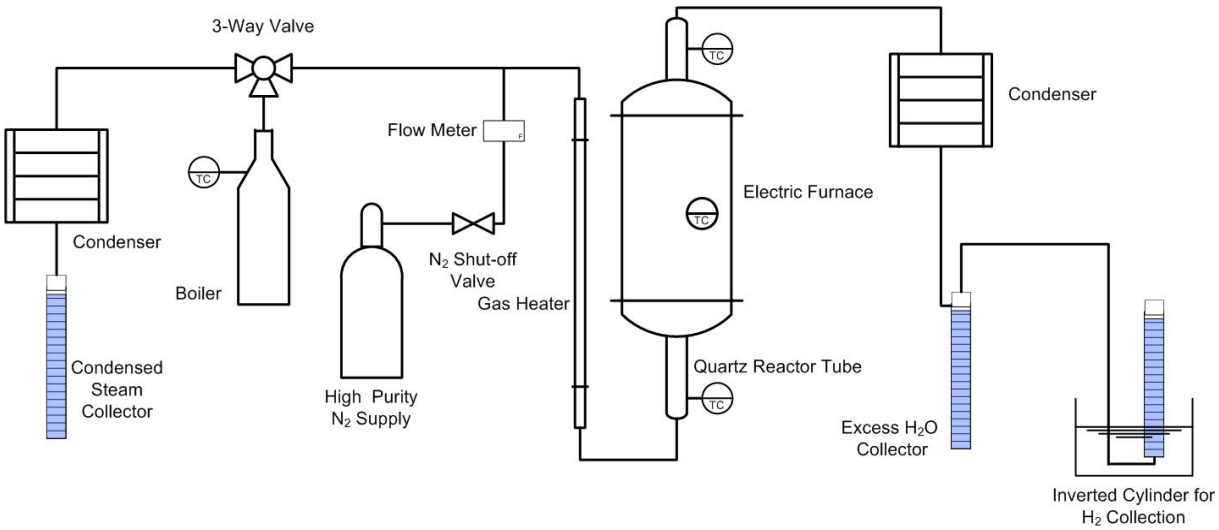

Figure 1: Experimental fluidized bed hydrogen production facility.

Iron Powder Characterization

For the current reactor configuration, steam is introduced to a fluidized bed of iron powder. The powder has a particle density of 7800 kg/m^3 and an estimated surface area of 60 cm^2/g. This powder is classified as Geldart B. The powder particles, shown in Figure 2, are porous, and the mass fraction weighted average particle diameter is 91 µm.

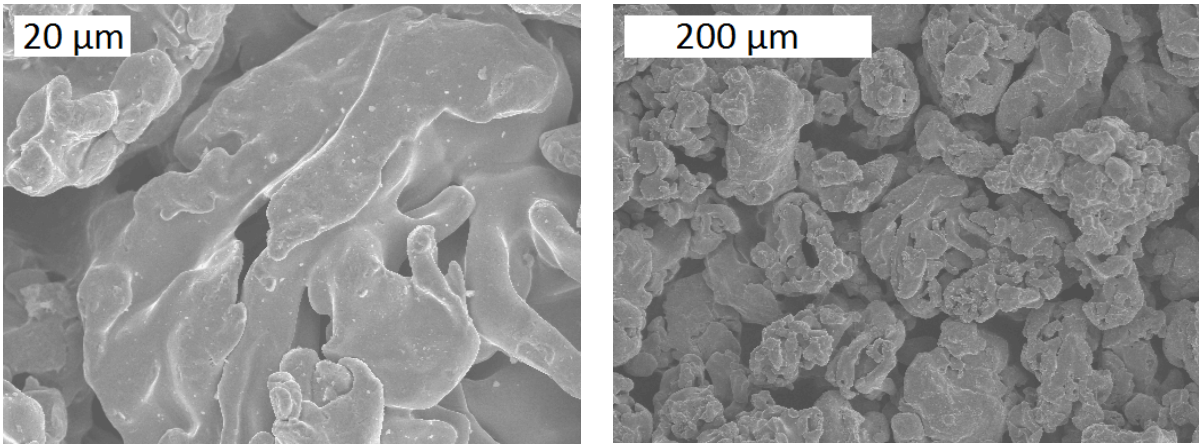

(a) (b)

Figure 2: SEM image of the iron powder at (a) 500X and (b) 110X magnification.

3 Hydrogen Production

Hydrogen production rates have been experimentally assessed for the oxidation (water splitting) reaction at various bed temperatures. The various reaction temperatures are measured at the particle bed and controlled by the electric furnace. The total volume of hydrogen collected for the duration of each experiment is limited by the amount of excess steam. Since the excess steam is collected in a container to be condensed and weighed, as illustrated in Figure 1, the volume limitation of the duration time is governed by the volume of the container.

The measured hydrogen volume for each reaction temperature is shown in Figure 3. As the temperature of the reactor increases, the amount of hydrogen produced increases. The total volume of hydrogen produced for 25g of iron is 0.35, 4.5 and 10.5 L for 450, 650 and 850 °C respectively. All volumes are measured at atmospheric conditions. The trend of increasing hydrogen production with increasing temperature is expected since the reaction rate increases exponentially with temperature, according to the Arrhenius equation.

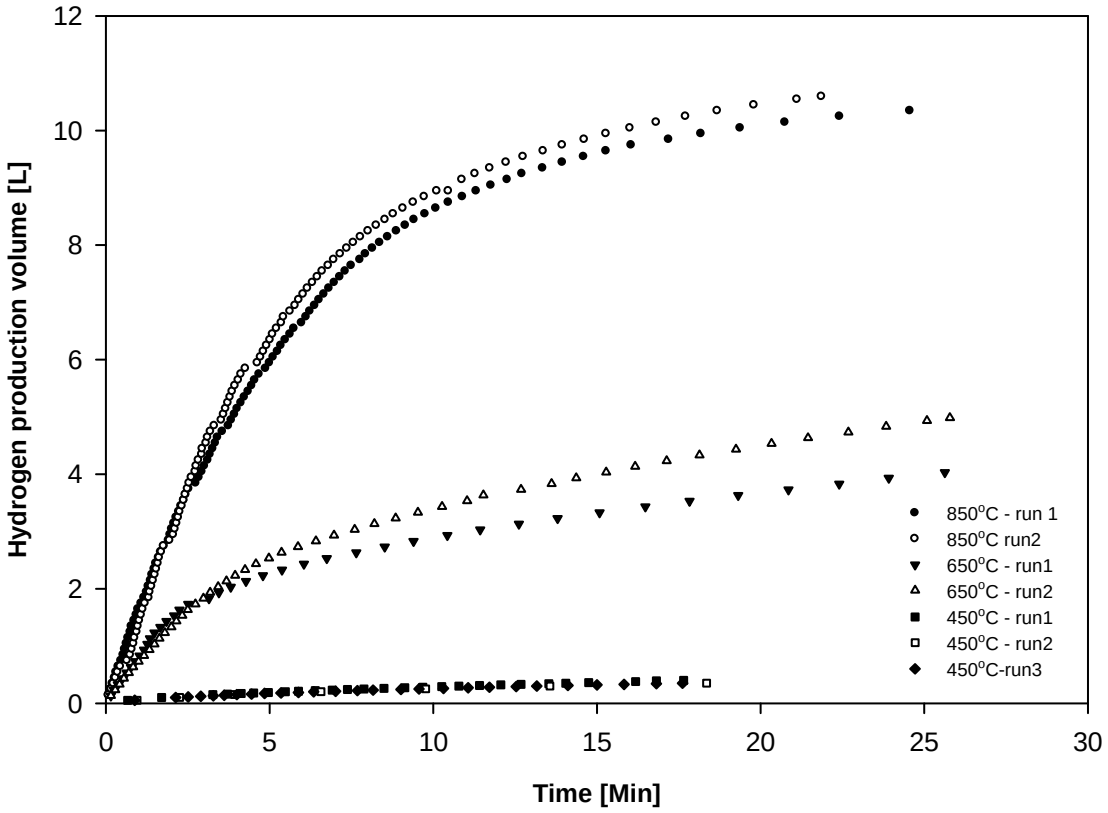

Figure 3: Hydrogen production at various bed temperatures.

The rate of hydrogen production is determined by differentiating the hydrogen production curves. The time varying hydrogen production rates at different bed temperatures are shown in Figure 4. The rate exponentially decays and is highest at the start of the reaction. As the temperature of the bed increases, the rate of hydrogen production increases substantially. The initial rates of hydrogen production are on average 0.035, 0.75 and 1.9 LPM, for 450, 650 and 850 °C bed temperatures, respectively. The exponentially decaying reaction rate is a result of the decrease of the available particle surface area as the iron particles are coated with an oxide layer. This reduction in surface area is highly transient, and thus a transient conservation of species analysis is required to extract the intrinsic reaction rate constants from the measured hydrogen production. This remains for further investigation.

In all experiments, 25 grams of iron are used to react with water vapor. According to Eq. (3), the reaction of 25g Fe will result in the production of 1.2 g H_2 at equilibrium. The percent conversion of H_2 on a mass basis in shown in Table 2. At the highest temperature the percent conversion of hydrogen is about 72% of the theoretical maximum.

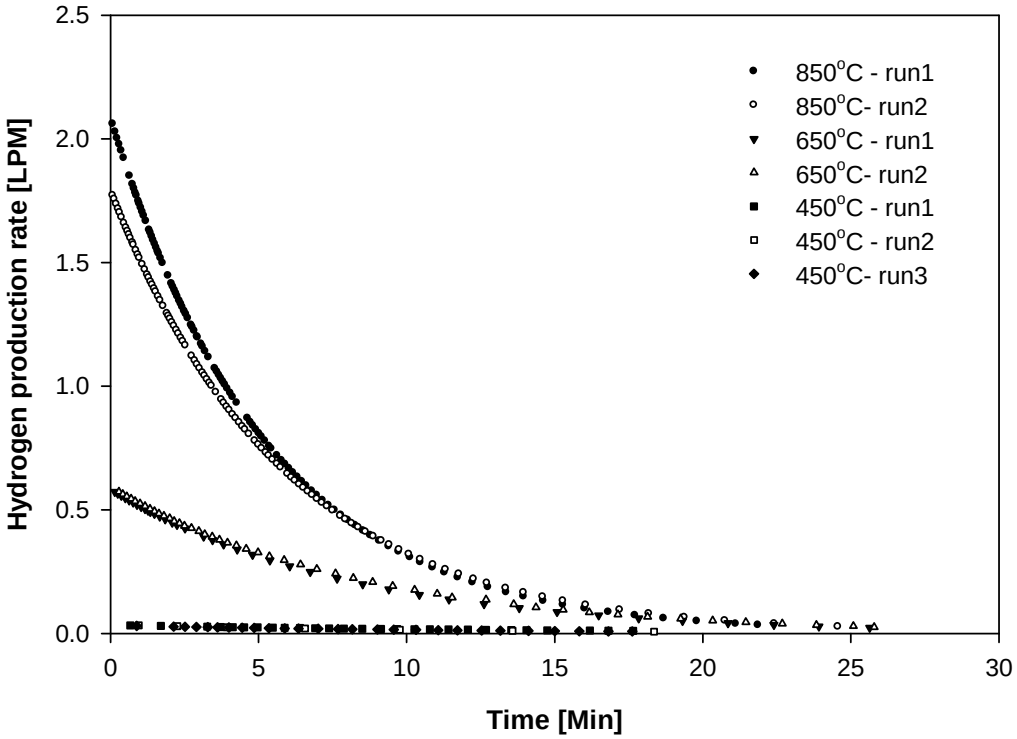

Figure 4: Hydrogen production rates at various temperature settings.

Table 2: Comparison of actual and theoretical equilibrium hydrogen production.

T [°C]	H_2 Produced [g]	$\%H_2$ conversion
450	0.030	2.5
650	0.368	30.9
850	0.856	71.7
Equilibrium	1.194	

4 Conclusions

An experimental evaluation of the water splitting (oxidation) step in a two-step thermochemical cycle was conducted utilizing a fluidized iron powder. 25 g iron powder samples with 60 cm^2/g surface area were used for the fluidized bed experiments. Three temperatures for the iron particle bed were investigated: 450, 650 and 850 °C. It is found that the reaction rate increases substantially with increasing temperature, as expected. The hydrogen production rate reaches a maximum of 2 LPM at 850 °C. Further transient analysis is required to evaluate the intrinsic reaction rate constants for the current hydrogen production data.

References

[1] Perret R., Weimer A. , Besenbruch G., Diver R., LewisM., and Chen Y., 2007. Department of Energy (DOE). FY 2007 annual progress report. Section II.F.1 Solar Hi-Temp Thermochemical Water Splitting DOE Hydrogen Program.

[2] Weimer A., Francis T., Carney C., Wyss J., Martinek J., and Kerins K., 2009. Department of Energy (DOE). FY 2009 annual progress report. Section II.F.3 Solar-Thermal Hydrogen Production Using a Metal-Oxide Based Thermochemical Water Splitting Cycle.

[3] Funk J. E., 2001. Thermochemical hydrogen production: past and present. International Journal of Hydrogen Energy. Volume 26, pp 185-190.

[4] Neises M., Roeb M., Schmücker M., Sattler C., and Pitz-Paal R., 2008. Kinetic Investigations of Two-Step Thermochemical Water Splitting Cycle using Mixed Iron Oxides Fixed on Ceramic Substrates. Proceedings of ES2008 Energy Sustainability 2008 August 10-14, 2008, Jacksonville, Florida USA.

[5] Steinfeld A., 2002. Solar Hydrogen Production via a Two-Step Water Splitting Thermochemical Cycle Based on Zn/Zno Redox Reaction. International Journal of Hydrogen Energy, vol. 27, pp 611-619.

[6] Steifeld A., 2005. Solar thermochemical production of hydrogen – a review. Solar Energy. Vol. 78, pp 603-615.

[7] T-Raissi, A., 2003. Analysis of Solar Thermochemical Water Splitting Cycles for Hydrogen Production. FY 2003 Progress report. University of Central Florida-Florida solar energy Center (FSEC).

Thermodynamic Performance Comparison of some Renewable and Non-Renewable Hydrogen Production Processes

M. Tolga Balta, Arif Hepbasli, Department of Mechanical Engineering, Faculty of Engineering, Ege University, 35100 Bornova, Izmir, Turkey
Ibrahim Dincer, Faculty of Engineering and Applied Science, University of Ontario Institute of Technology (UOIT), Oshawa, Canada

Abstract
This paper compares thermodynamic performance, through energy and exergy efficiencies, of the some renewable-based (e.g. geothermal) and non-renewable-based hydrogen production processes, namely: (1) steam methane reforming (SMR), (2) hybrid copper–chlorine (Cu–Cl) supplied by geothermal heat and electricity from a geothermal power plant, (3) high temperature steam electrolysis (HTSE) supplied by geothermal heat and electricity from a geothermal power plant. These processes are essentially driven by two different sources such as fossil fuel and geothermal. The results show that energy and exergy efficiencies during hydrogen production range from 65-89% and 63-80% for the SMR. The efficiencies of geothermal-based hydrogen production processes seem to be a bit lower than that of SMR. However, these processes can drastically reduce the GHG emissions compared to non-renewable energy based ones, e.g., SMR process.

Keywords: SMR, Thermochemical, Hybrid, Electrolysis, Energy, Exergy, Efficiency.

1 Introduction

Currently more than 80% of the world's energy supply comes from fossil fuels. As everyone knows, fossil fuel reserves are diminishing rapidly across the world. Beside of this, utilization of fossil fuels emits greenhouse gases, like carbon dioxide, which cause global warming to the environment and hence it is crucial to find alternative, emerging energy solutions that can help reduce greenhouse gas (GHG) emissions as soon as possible. Hydrogen is widely believed to be world's next-generation fuel, because of its reduced environmental impact, more significantly reduced greenhouse gas emissions. In this regard, hydrogen is seen as a sustainable energy carrier which can serve as a potential solution to the current environmental problems since it is a clean energy carrier that is environmentally-benign and sustainable, compared to fossil fuels [1-3].

Hydrogen, which does not exist alone in nature, can be produced from a variety of feedstocks; from fossil resources such as natural gas and coal and from renewable resources. It is always found in the form of compounds and high value energy needs to be consumed for its production. All hydrogen production processes are based on the separation of hydrogen from hydrogen containing compounds from either fossil fuels or water. Recently, further studies have been conducted to develop techniques/technologies for global-scale hydrogen production, in the short-term production of hydrogen from fossil fuels (mainly

natural gas), and in the long-term, hydrogen will be produced from renewable energy. Fig. 1 is a pie chart, showing that 96% hydrogen is currently produced directly from fossil fuels, while about 4% is produced indirectly by electricity utilization.

Although, some of hydrogen production methods, such as steam methane reforming (SMR), are well developed and established for commercial use, it has some disadvantages, such as using extensive amount of electricity and releasing high levels of CO_2. On the other hand, fossil fuel prices are anticipated to increase. Clearly, there is a strong and urgent need to find alternative, environmentally benign ways for hydrogen production. There are limited options for affordable environment friendly hydrogen production. Many researches conduct extensive research on "new technologies for producing hydrogen" that are more cost effective, without greenhouse gas emissions. Alternative clean and efficient pathways for the production of pure hydrogen are water electrolysis and thermochemical water-splitting cycles with renewable energy sources, e.g., solar energy, wind energy, hydropower, biomass and geothermal. These methods are considered the most promising processes for hydrogen production in the future hydrogen economy. Reducing the cost and environmental impact of hydrogen production is a key challenge facing the future transition to a hydrogen economy [5].

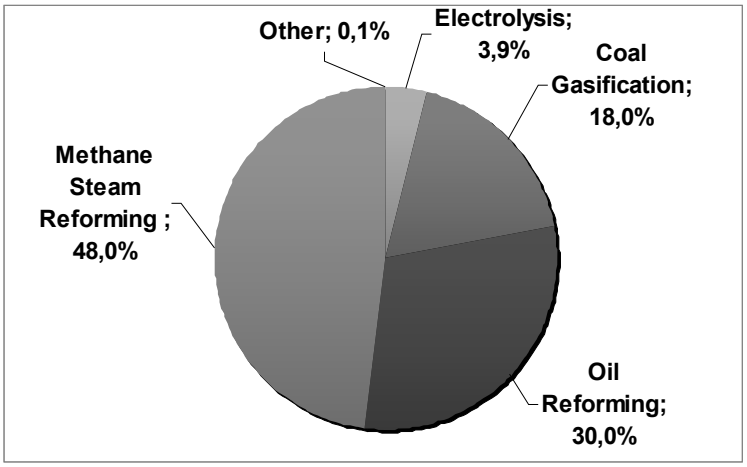

Figure 1: Feedstock used in the present global hydrogen production (data taken from Ref. [4]).

When considering the use of renewable energy for hydrogen production, geothermal resources seem to be an important and attractive option. In countries with abundant amounts of geothermal energy, certainly geothermal-based hydrogen production will become a major player in hydrogen economy. This can be done in two ways: namely i) by using both geothermal heat and electricity for high temperature steam electrolysis and/or hybrid processes, ii) by using the heat available from geothermal resource in thermochemical processes, of which has been identified in more detail [6-8]. These production methods are still in the developmental stage for commercial applications and require further research and development.

Although numerous studies have been conducted on non-renewable-based hydrogen production processes in the open literature [e.g., 9-15], very few papers and reports are available on hydrogen production from geothermal resources [e.g., 6-8, 16-18]. To the best knowledge of the authors, no studies have been undertaken to compare the performances of some renewable-based (e.g. geothermal) and non-renewable-based (e.g., SMR) hydrogen production processes through exergy analysis. In this study, a geothermal-based (and non-renewable-based hydrogen production processes, namely: (1) steam methane reforming (SMR), (2) hybrid copper–chlorine (Cu–Cl) supplied by geothermal heat and electricity from a geothermal power plant, (3) high temperature steam electrolysis (HTSE) supplied by geothermal heat and electricity from a geothermal power plant compared thermodynamically through energy and exergy efficiencies. Moreover, sustainability index and environmental impact ratios of the considered processes are compared each other.

2 Description of Processes

Here, energy and exergy efficiencies of some renewable-based (e.g. geothermal) and non-renewable-based hydrogen production processes are compared for: (1) steam methane reforming (SMR), (2) hybrid copper–chlorine (Cu–Cl) driven by geothermal heat and electricity from a geothermal power plant, (3) high temperature steam electrolysis (HTSE) driven by geothermal heat and electricity from a geothermal power plant.

Steam methane reforming (SMR): This is the most common method of producing hydrogen. Fig. 2 shows a simplified schematic diagram of a SMR system. Here, the required heat is obtained from an external energy source. Also, it can be provided through combustion of additional methane and/or from using the available energy in the separated exhaust stream through combustion or simple heat exchange [15].

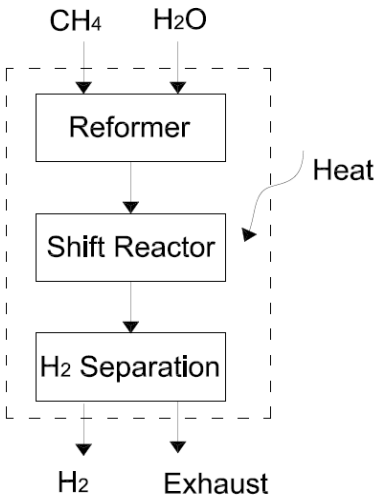

Figure 2: Simplified schematic diagram of an SMR process. (adopted from Ref. [15])

In this process, methane and steam react over a high-temperature catalyst.

$$CH_4 + H_2O\ (g) \rightarrow CO + 3H_2 \quad (1)$$

The reaction is endothermic. And then syngas exiting the reformer is passed through a reactor that converts the CO in the syngas to CO_2 and H_2 using the available H_2O in the syngas or additional H_2O to system.

$$CO + H_2O\ (g) \rightarrow CO_2 + H_2 \quad (2)$$

which is exothermic, but the overall reactions in Eqs. (1) and (2) are endothermic. The last step of the SMR process is the separation of the hydrogen from the syngas exiting the reactor, which is mostly H_2, H_2O, and CO_2 [15].

Simpson et al. [15] evaluated the performance of hydrogen production via steam methane reforming (SMR) process using exergy analysis to study both energy and exergy efficiencies. This comparison is given in Table 1. As can be seen in this table, the efficiencies during hydrogen production range between 65-89% for energy efficiency and 62-80% for exergy efficiency.

Table 1: Comparison of SMR energy and exergy efficiencies. (Adopted from Ref. [15])

References	η (%)	ψ (%)	Notes
Rosen [9]	86	78.5	Detailed system analysis with heat-integration. Uses global reformation model with PSA CO_2 separation and methanation.
Lambert et al. [10]	-	76.62[a]	Purpose of paper was to analyze SMR with oxygen enriched combustion. Uses equilibrium reformer model. Separation method is not described.
Sorin et al. [11]	-	79.88	Only analyzes natural gas reformation to syngas. Reformation heat is provided by combustion of extra fuel.
Simbeck [12]	65.3 , 76.2	-	Purpose of paper was to determine hydrogen production costs. Details of SMR were not described.
Lutz et al. [13]	89[b], 81[c]	-	First law based analysis. Analyzes both a global and equilibrium reformer. Reformer heat is provided by combustion of retentate stream exiting membrane. Does not use detailed heat-integration.
Bargigli et al. [14]	77[d]	71[d]	Purpose of paper was to use a multi-criteria approach to compare hydrogen production pathways through energy, exergy, and emergy analysis.
Simpson et al. [15]	66.7	62.7	Purpose of paper is to apply exergy analysis to the production of hydrogen via natural gas SMR. In this study, the reformer operates at 6.8 bar.

a Uses slightly different exergy efficiency definition.
b Maximum energy efficiency using global reaction model going to equilibrium.
c Maximum energy efficiency using equilibrium reformer model.
d Values taken from National Renewable Laboratory report.

Hybrid copper–chlorine (Cu–Cl) cycle: This cycle was originally proposed in the 1970s and has recently been proven at laboratory level. It is a hybrid cycle using mainly heat and some electricity to disassociate water into hydrogen and oxygen at a maximum process

temperature of 550°C. In the literature, numerous studies on hydrogen production using Cu-Cl cycles have recently been carried out by many researchers. For example, the steps of the Cu–Cl cycle for nuclear-based hydrogen production have been examined in detail by Orhan et al. [19–23] using exergy analysis approach. Naterer et al. [24] have analyzed the heat requirements for the steps and studied the ways to recover heat in order to minimize the net heat supply for the overall cycle which will improve its overall efficiency. Lewis et al. [25, 26] have studied the Cu-Cl cycle's performance and extended the study for hydrogen production costs. A simple conceptual layout of the Cu-Cl cycle is shown in Fig. 3. It basically consists of five main steps:

(i) $HCl_{(g)}$ production step,
(ii) O_2 production step,
(iii) Cu production step,
(iv) drying step, and
(iv) hydrogen production step.

A chemical reaction takes place in each step, except the drying step. These chemical reactions form a closed internal loop that recycles all of the copper–chlorine compounds on a continuous basis, without emitting any greenhouse gases externally to the atmosphere [27].

Balta et al. [8] analyzed the performance of low temperature thermochemical cycles through energy and exergy efficiencies. The energy and exergy efficiencies of the Cu-Cl cycle were calculated as 51% and 65%, respectively, based upon the complete reactions. This cycle was identified as a highly promising cycle for geothermal-hydrogen production.

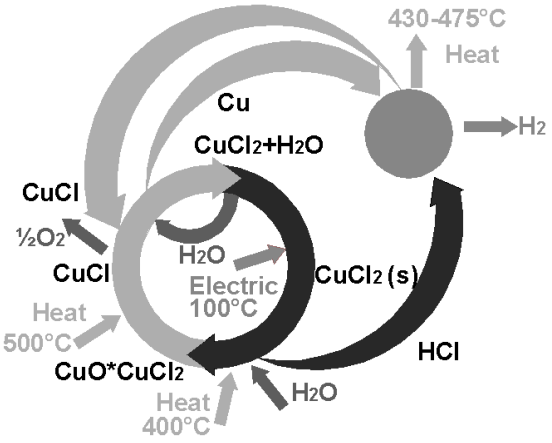

Figure 3: Simplified schematic diagram of Cu-Cl cycle.

High temperature steam electrolysis (HTSE): In this process, hydrogen production through direct thermal decomposition of water can be done only if the temperature of primary heat source is more than 2500 K. This is not feasible at an industrial level with the present technology. From a thermodynamic viewpoint of water decomposition, it is more advantageous to produce hydrogen if the energy is supplied in mixed form of electricity and heat. Geothermal heat and electricity can be used in HTSE. Balta et al. [6, 7] investigated the thermodynamic performance, through energy and exergy efficiencies, of the HTSE process

coupled with and powered by a geothermal source. The energy and exergy efficiencies at a temperature range of 473 K to 1173 K were found to be from 80% to 87% and from 79% to 86%, respectively.

3 Analysis

In the analysis, the following parameters are studied and the compared with each other.

Exergy efficiency and sustainability index

Sustainable development requires not only that the sustainable supply of clean and affordable energy resources be used, but also the resources should be used efficiently. Exergy methods are very useful tools for improving efficiency, which maximize the benefits and usage of resources and also minimize the undesired effects (such as environmental damage). Exergy analysis can be used to improve the efficiency and sustainability [24].

The relationship between exergy efficiency (ψ) and the sustainability index (SI), as given in [7], is modified here for this application:

$$\psi = 1 - \frac{1}{SI} \tag{3}$$

where

$$SI = \frac{1}{D_P} \tag{4}$$

Here, D_P is the depletion factor defined by Connelly and Koshland [28] as the ratio of exergy destruction rate to the input exergy rate to the system and can be given as,

$$D_P = \frac{\dot{E}x_D}{\dot{E}x_{in}} \tag{5}$$

Exergy and Environmental Impact Factor

Many researchers have suggested that the most proper method to reduce the environmental impact is through exergy because it is a measure of the departure of the state of a system from that of the environment [29-32]. Thus, exergy has an important role to play in providing better environment. Environmental impact can be reduced by the increasing the energy and exergy efficiency. Increased efficiency also reduces the exergy losses.

Environmental Impact Ratio

The concentrations of most of greenhouse gases have increased drastically since the industrial revolution. One of the most important greenhouse gases is CO_2. The emissions of CO_2 play a crucial role in climate change. Greenhouse effect increases with the increase of the amounts of CO_2 in the atmosphere. Actually, all resource use leads to some degree of environmental impact. In this context, environmental impact ratio can be given as

$$EIR = \frac{CO_{2_{es}}\,(g/kWh)}{CO_{2_{coal}}\,(g/kWh)} \tag{6}$$

which is defined as ratio of CO_2 emission by a particular renewable/non-renewable technology to CO_2 emission by coal based technology. In other words, the environmental impact ratio is a fraction of CO_2 emitted by a renewable/non-renewable technology as compared to coal based technology.

4 Results and Discussion

The exergy efficiencies of various processes are shown in Fig. 4, as studied earlier by Refs. [6, 8, 9-11, 14, 15]. The overall exergy efficiency of the HTSE becomes 79% [6], and for Cu-Cl cycle it becomes 65% [8], and for SMR process it varies from 63% to 80% [9-11, 14,15]. As can be seen in this figure, the exergy efficiency of the HTSE system is nearly same as SMR process. Note that the overall electrolyser system efficiency is always less as compared to the electrolysis process efficiency due to some various irreversibilities and losses taking place in various components, including coupling pumps, turbines etc. Since some energy losses may occur if such devices are used. In this regard HTSE exergy efficiency may lower than 79%.

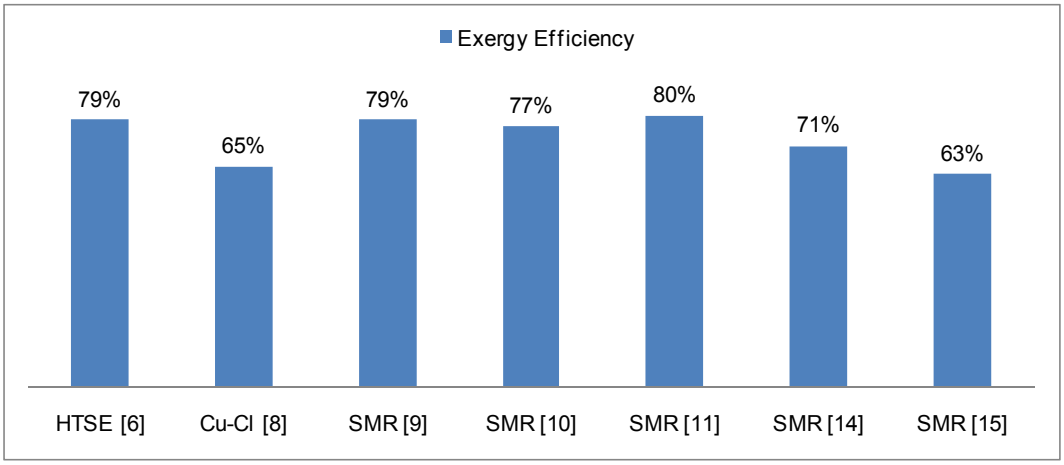

Figure 4: Exergy efficiencies of various hydrogen production processes.

Figure 5 shows the corresponding sustainability index for the processes considered for hydrogen production respectively. The sustainability index for the HTSE process of Balta et al. [6] is 4.76 and for the Cu-Cl cycle of Balta et al. [8] is 2.86 and for SMR process [9-11, 14,15] it varies from 2.70 to 5.00. A higher sustainability index shows better sustainability of the process.

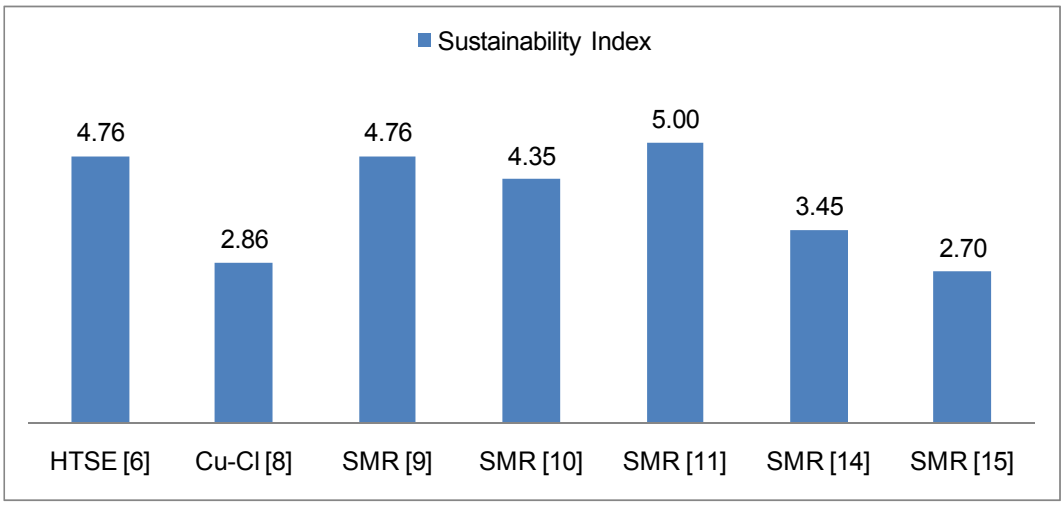

Figure 5: Sustainability Index values of various hydrogen production processes.

Increasing greenhouse gas emissions, particularly CO_2 is a potential environmental impact and affects sustainability of energy usage, generation and transportation. Here, we calculate the environmental impact ratio of some energy technologies based on CO_2 emissions. In this regard, Fig. 6, shows the environmental impact ratio of coal, natural gas and geothermal options for hydrogen production (using the data taken from Refs. [33,34]). Geothermal plants emit typically only 25-30% of the total CO_2 emitted by a coal or natural gas plant, per kWh. Geothermal based emissions vary significantly depending on the technology chosen [35] and may vary from one region to another.

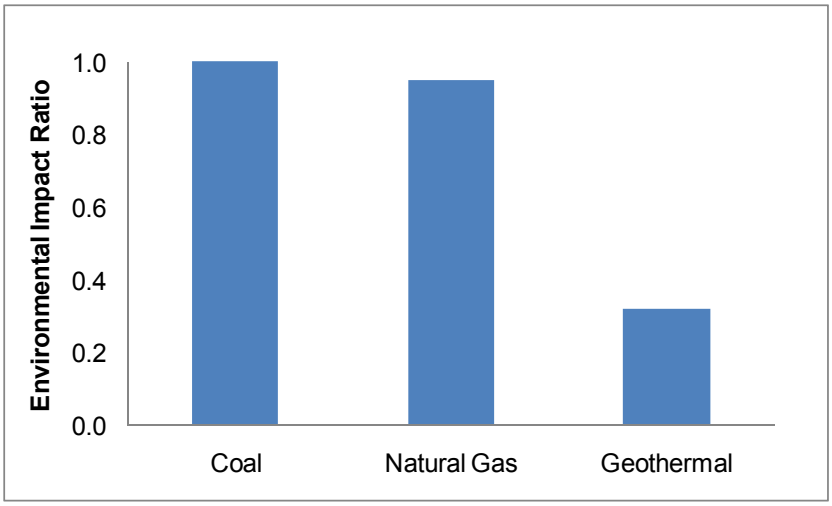

Figure 6: Environmental impact ratios of various energy options.

5 Conclusions

In this paper, we have studied and compared various hydrogen production methods, namely: (1) steam methane reforming (SMR), (2) hybrid copper–chlorine (Cu–Cl) driven by

geothermal heat and electricity from a geothermal power plant, (3) high temperature steam electrolysis (HTSE) driven by geothermal heat and electricity from a geothermal power plant thermodynamically through energy and exergy efficiencies. Moreover, sustainability index and environmental impact ratios of these processes are studied and compared to each other. Since geothermal based hydrogen production processes are essentially at developmental stage, there is a need for further research and development for better design, analysis and performance assessment. The following main conclusions are drawn from the main results of the present study:

The exergy efficiencies of the SMR processes vary from 63% to 80% while it is 79% for the HTSE and 65% for a Cu-Cl cycle.

The sustainability index for the SMR process varies from 2.70 to 5.00 while it is 4.76 for the HTSE and 2.86 for a Cu-Cl cycle.

Using geothermal-based hydrogen production via either HTSE or Cu-Cl cycle reduces the CO_2 emissions by about 70%-75% compared to other options.

Geothermal-based hydrogen production methods, particularly by the thermo-chemical cycles, offer opportunities for better environment and sustainability.

Acknowledgements

The authors gratefully acknowledge the support provided by Ege University, Aksaray University, University of Ontario Institute of Technology (UOIT), and in particular the Natural Sciences and Engineering Research Council of Canada.

References

[1] Veziroglu TN, Sahin S. 21st century's energy: Hydrogen energy system, Energy Conversion and Management 2008; 49(7):1820-1831.

[2] Dincer I. Environmental and sustainability aspects of hydrogen and fuel cell systems, International Journal of Energy Research 2007;31:29–55.

[3] Orhan MF, Dincer I, Rosen MA. Exergoeconomic analysis of a thermochemical copper–chlorine cycle for hydrogen production using specific exergy cost method, Thermochimica Acta, 2008; doi:10.1016/j.tca.2009.08.008.

[4] Kothari R, Buddhi D, Sawhney RL. Comparison of environmental and economic aspects of various hydrogen production methods Renewable and Sustainable Energy Reviews; 2008; 12:553–563.

[5] Orhan MF, Dincer I, Rosen MA. Cost and efficiency analysis of nuclear-based hydrogen production through a copper-chlorine thermochemical cycle, Global Conference on Global Warming 2009, pp 683-693. July 5-9, 2009, Istanbul,Turkey.

[6] Balta MT, Dincer I, Hepbasli A. Thermodynamic assessment of geothermal energy use in hydrogen production. International Journal of Hydrogen Energy, 2009,34(7):2925-2939.

[7] Balta MT, Dincer I, Hepbasli A. Potential methods for geothermal-based hydrogen production, Proceedings of the International Conference on Hydrogen Production, Paper No: ICH2P-88, pp:225-242, May 03-06, 2009, Oshawa, Canada.

[8] Balta MT, Dincer I, Hepbasli A. Geothermal-based hydrogen production using thermochemical and hybrid cycles: A review and analysis, International Journal of Energy Research, 2009, DOI: 10.1002/er.1589.

[9] Rosen MA. Thermodynamic investigation of hydrogen production by steam-methane reformation. Int J Hydrogen Energy 1991;16(3): 207–17.

[10] Lambert J, Sorin M, Paris J. Analysis of oxygen-enriched combustion for steam methane reforming SMR. Energy 1997;22(8):817–25.

[11] Sorin M, Lambert J, Paris J. Exergy flows analysis in chemical reactors.Trans IChemE 1998;76(A).

[12] Simbeck DR. Hydrogen costs with CO2 capture. Presented at the 7th international conference on greenhouse gas control technologies (GHGT- 7), Vancouver, British Columbia, Canada, September 6–10; 2004.

[13] Lutz A, Bradshaw R, Keller J, Witmer D. Thermodynamic analysis of hydrogen production by steam reforming. Int J Hydrogen Energy 2003;28:159–67.

[14] Bargigli S, Raugei M, Ulgiati S. Comparison of thermodynamic and environmental indexes of natural gas, syngas and hydrogen production processes. Energy 2004;29:2145–59.

[15] Simpson AP, Lutz AE. Exergy analysis of hydrogen production via steam methane reforming, International Journal of Hydrogen Energy 32 (2007) 4811 – 4820

[16] Mansilla C, Sigurvinsson J, Bontemps A, Maréchal A, Werkoff F. 2007. Heat management for hydrogen production by high temperature steam electrolysis, Energy, 32:423–430.

[17] Sigurvinsson J, Mansilla C, Arnason B. Bontemps A, Maréchal A, Sigfusson TI, Werkoff F. 2006. Heat transfer problems for the production of hydrogen from geothermal energy, Energy Conversion and Management, 47: 3543–3551.

[18] Sigurvinsson J, Mansilla C, Lovera P, Werkoff F. 2007. Can high temperature steam electrolysis function with geothermal heat? International Journal of Hydrogen Energy, 32: 1174 – 1182.

[19] Orhan MF, Dincer I, Rosen MA. The oxygen production step of a copper–chlorine thermochemicalwater decomposition cycle for hydrogen production: energy and exergy analyses, Chemical Engineering Science 2009;64:860–869.

[20] Orhan MF, Dincer I, Rosen MA. Energy and exergy analyses of the fluidized bed of a copper–chlorine cycle for nuclear-based hydrogen production via thermochemical water decomposition, Chemical Engineering Research and Design 87 (2009) 684–694.

[21] Orhan MF, Dincer I, Rosen MA. Thermodynamic analysis of the copper production step in a copper–chlorine cycle for hydrogen production, Thermochimica Acta 480 (2008) 22–29.

[22] Orhan MF, Dincer I, Rosen MA. Energy and exergy assessments of the hydrogen production step of a copper–chlorine thermochemical water splitting cycle driven by nuclear-based heat, International Journal of Hydrogen Energy 2008; 33: 6456–6466.

[23] Orhan MF, Dincer I, Rosen MA. Energy and exergy analyses of the drying step of a copper–chlorine thermochemical cycle for hydrogen production, International Journal of Exergy, in press (2009).

[24] Naterer GF, Gabriel K, Wang ZL, Daggupati VL, Gravelsins R. Thermochemical hydrogen production with a copper–chlorine cycle. I. Oxygen release from copper oxychloride decomposition, International Journal of Hydrogen Energy 2008; 33: 5439–5450.

[25] Lewis MA, Masin JG, O'Hare PA. Evaluation of alternative thermochemical cycles-Part I. The methodology, International Journal of Hydrogen Energy 2009;34(9):4115–4124.

[26] Lewis MA, Ferrandon MS, Tatterson DF, Mathias P. Evaluation of alternative thermochemical cycles – Part III further development of the Cu–Cl cycle, International Journal of Hydrogen Energy 2009;34(9):4136–4145.

[27] Naterer GF. Economics of a thermochemical pilot plant for nuclear-produced hydrogen in Ontario, Technical Report. Oshawa, Ontario, Canada,: University of Ontario Institute of Technology; 2007.

[28] Connelly L, Koshland CP. Two aspects of consumption: using an exergy-based measure of degradation to advance the theory and implementation of industrial ecology. Resources, Conservation and Recycling,1997, 19: 199–217.

[29] Rosen MA. 1986. The development and application of a process analysis methodology and code based on exergy, cost, energy and mass, Ph.D. Thesis, University of Toronto, Toronto.

[30] Rosen MA, Dincer I. 1997. On exergy and environmental impact, International Journal of Energy Research, 21;643-654.

[31] Rosen MA, Dincer I. 1999. Exergy analysis of waste emissions, International Journal of Energy Research, 23;1153-1163.

[32] Cornelissen RL. 1997. Thermodynamics and sustainable development. Ph.D. Thesis, University of Twente, The Netherlands.

[33] Armannsson H, Fridriksson T, Kristjansson BR. CO2 emissions from geothermal power plants and natural geothermal activity in Iceland, Geothermics,2005, 34:286–296.

[34] IAEA. Sustainable development and nuclear power, International Atomic energy Agency, Vienna, Austria, 1997.

[35] DiPippo R. 1991. Electricity generation and environmental impact, Renewables series - geothermal energy; Energy Policy, 798-807.

Two-step Water Splitting by Cerium Oxide-Based Redox Pairs

Heike Burghardt, Martin Schmücker, Institute of Material Research, German Aerospace Center DLR, Germany
Björn Hansen, Martina Neises, Martin Roeb, Institute of Technical Thermodynamics, Solar Research, German Aerospace Center DLR, Germany

1 Introduction

The utilization of hydrogen as clean energy becomes important for solving global environmental problems and securing future energy supply. A possible method for producing hydrogen is a two-step water splitting reaction in a thermochemical cycle. In the first step metal oxides being in a low oxidation state (oxygen deficit phases) are used for water splitting. By that the water splitting material transforms in a higher oxidation state. In a second step the metal oxide is regenerated by heating using concentrated solar energy. In recent years various redox systems have been studied e.g. Zn/ZnO and Ferrites [1,2]. Especially CeO_2-based solid solutions are considered to be promising redox materials for water-splitting purposes. Ceria in general is beneficial since its fluorite structure allows a wide range of Ce oxidation states (Ce^{4+} - $Ce^{3.x+}$) charged balanced by oxygen vacancies. However, for the reduction of pure cerium oxide, temperatures higher than 1500°C are required. The redox process can be shifted towards lower temperatures by doping ceria with another transition metal oxide. It was found out doping ceria with up to 20% iron oxide allows the regeneration step at 1400°C and the hydrogen production step at 1000°C [3-6]. On the other hand, additional structural vacancies are formed by the Ce^{4+}/Fe^{3+} substitution which typically results in higher atomic mobility, thus leading to increased sinterability and grain growth. This lowers the surface activity of the metal oxide and degrades the efficiency of the water splitting process. A long lifetime of the functional oxide with a constant productivity is the precondition for any industrial application.

For a constant high water splitting activity two main conditions must be fulfilled by the material. On the one hand, transition between metal's oxidation states should take place easily without nucleation barrier. On the other hand the high porosity and surface activity must be retained throughout many cycles. In the present study we report about a novel approach to increase the microstructure stability of $(Ce,Fe)O_x$ solid solutions: The functional compound is applied as a coating on 0.5 mm zirconia spherules. By using a counteracting substrate sintering shrinkage should be reduced in two dimensions. Additionally a higher secondary surface area can be realized and highly effective turbulent fluidized bed technologies can be applied for the water splitting process. Moreover, submicron oxide particles bound on an inert substrate allow toxicological harmless handling which is an important advantage in industrial-scale application.

2 Syntheses

Fe-modificated CeO_2 coatings on ZrO_2-beadlets were produced by a single-step precipitation process using a nitrate route. $Ce(NO_3)_4 \cdot 6H_2O$ and $Fe(NO_3)_3 \cdot 6H_2O$ were mixed in an atomic ratio of Ce/Fe 80:20 and solved in distilled water and glycerin (10 weight % of water) at 40°C. The whitish ZrO_2 particles were wet by the aqueous nitrate-glycerin solution. The admixture was heated up to 150°C on air to vaporize the water and dried at 500°C for two more hours. The dried material contains coated spherules and surplus $(Ce,Fe)O_x$ oxide, the latter was removed by sieving. Visual inspection after drying suggested that $(Ce,Fe)O_x$ coated ZrO_2 spherules were obtained as evidenced by their orange coloration (Figure 1). At this point the functional oxide exists in its highest oxidation state. To use the functional coating for water splitting purposes the cations must be transferred in reduced oxidation states (Fe^{2+} , potentially $Ce^{(4-x)+}$). For this purpose the coated spherules were mixed with a defined amount of graphite and heated up to 1100°C for one hour. The reaction took place in a tubular furnace in inert gas atmosphere using nitrogen (purity 5.0) with a flow rate of 300ml/hour. Subsequent rapid cool down of the sample is important to freeze the reduced oxidation state. This was performed by removing the sample as fast as possible (< 1sec) from the hot zone of the furnace, still under inert atmosphere.

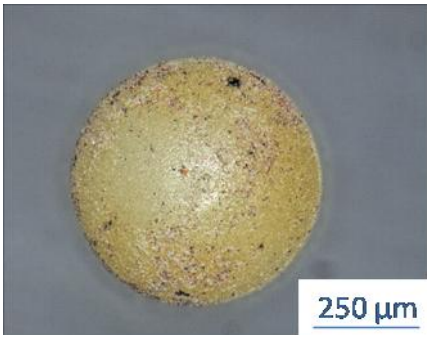

Figure1: $(Ce,Fe)O_x$ coated ZrO_2 beadlets.

As reference material and for easier microstructural analyses of $(Ce,Fe)O_x$ precipitates powder samples without ZrO_2 substrate were synthesized. $Ce(NO_3)_4 \cdot 6H_2O$ and $Fe(NO_3)_3 \cdot 6H_2O$ in atomic ratio 80:20 were mixed with water and glycerin and heated up to 200°C until water was removed. The powder was milled and heated up to 500°C for two hours.

3 Results and Discussion

The powder is orange and nano-crystalline as evidenced by TEM analyses (Figure 2). To analyze chemical compositions and especially the elemental distribution of the coating transmission electron microscopy (TEM) analysis with corresponding microanalyses were carried out. For this powdered coating material was spread on a holy carbon film supported by a copper grid. This method enables a combination of quantitative chemical analysis with high local resolution. The TEM analysis showed an Fe content of 5-10 at% in the $(Ce,Fe)O_x$ phase. Residual iron could be localized in a second iron oxide phase.

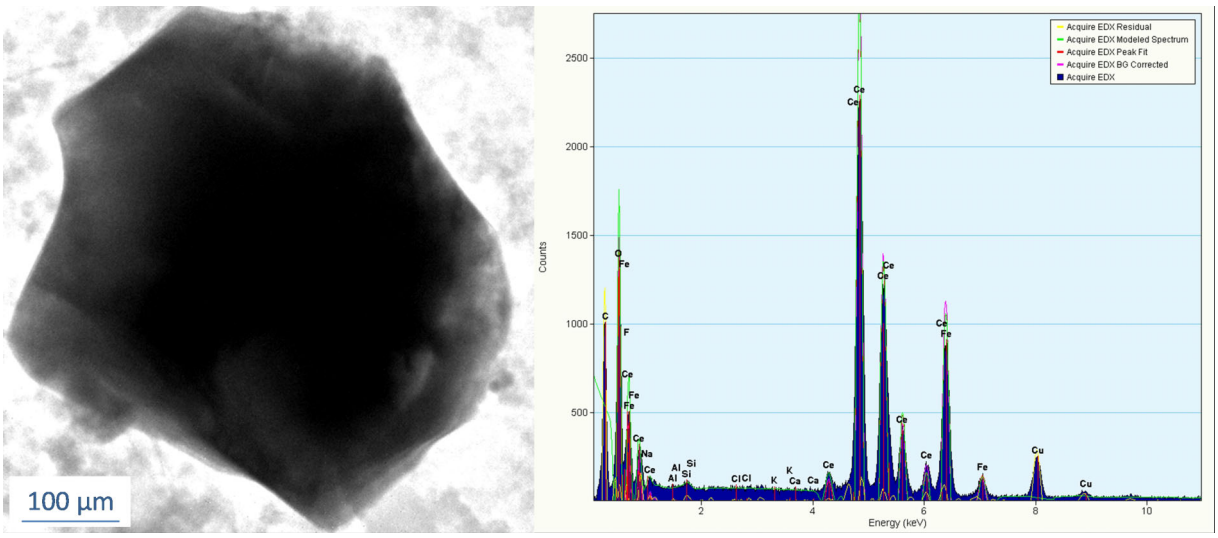

Figure 2: TEM image of $(Ce,Fe)O_x$ coating material with corresponding EDX spectrum.

$(Ce,Fe)O_x$ coatings on ZrO_2-beadlets were characterized by electron microscopy and corresponding microanalysis. After sintering for one hour at 1100°C a disrupted and highly porous coating occurs on the ZrO_2 substrate. The coating has an average thickness of about one micrometer. Figure 3 shows an overview and a detail image of the coating. The degree of coating, i.e. the spherule surface, which is covered by $(Ce,Fe)O_x$ assuming a layer thickness of 1µm is measured by weighing. To do so the average weight of untreated and coated ZrO_2 beadlets was determined thus leading to an average covering degree of ≈12%.

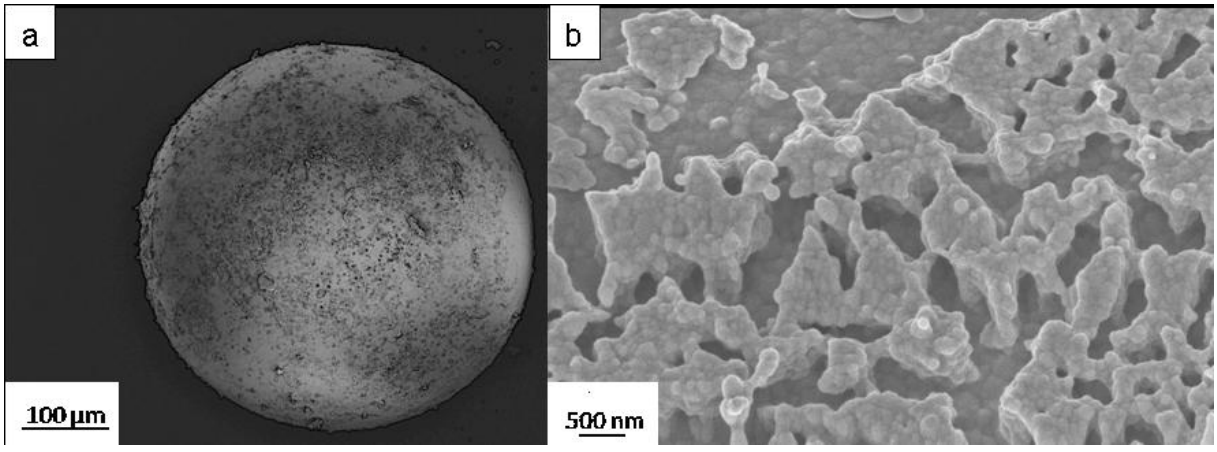

Figure 3: $(Ce,Fe)O_x$ coatings on ZrO_2-beadlets; a) overview image of coating beadlets, b) detail image of disrupted, porous layer.

Thermally induced sintering and coarsening of $(Ce,Fe)O_x$ coatings on ZrO_2-spherules was investigated by heating the material for 100 hours at 1100°C in air atmosphere. After the thermal treatment the disrupted layer was still about 1µm thick and porous. The grain size

ranged between 150 and 350 nm and the appearance of the coating on the substrate surface was virtually unchanged. Obviously, the disrupted and porous coating was highly stable against sintering processes and grain coarsening. The interface region of coating and substrate was studied by REM using a cross section specimen. Elemental maps of Zirconium and Cerium show virtually no interdiffusion between coating oxides and ZrO_2 substrate.

To simulate the water splitting reaction in a solar furnace, a test set-up consisting of a water evaporation system, an electrical tubular furnace and a mass spectrometer was employed. For testing a sample is placed in an alumina crucible inside a reaction tube and flushed by nitrogen (purity of 2.8, 500sccm) which is mixed with water vapor during the water splitting step. The amount of water is controlled by a peristaltic pump. The regeneration step is carried out in pure nitrogen at 1200°C for 60 min. The product gas is cooled by a gas cooler (ABB) and analyzed by a calibrated mass spectrometer (Pfeiffer Vacuum). At this point of investigations it is difficult to define the reacting oxide mass and so the produced mass of hydrogen per mass oxide could only be estimated. During the first water splitting step of 10 min ≈2.5mmol H_2 per gram oxide coating were produced. The H_2 formation rate is shown in Figure 4. There is a high peak of hydrogen production at the very beginning of the water splitting step but the production rate rapidly drops down.

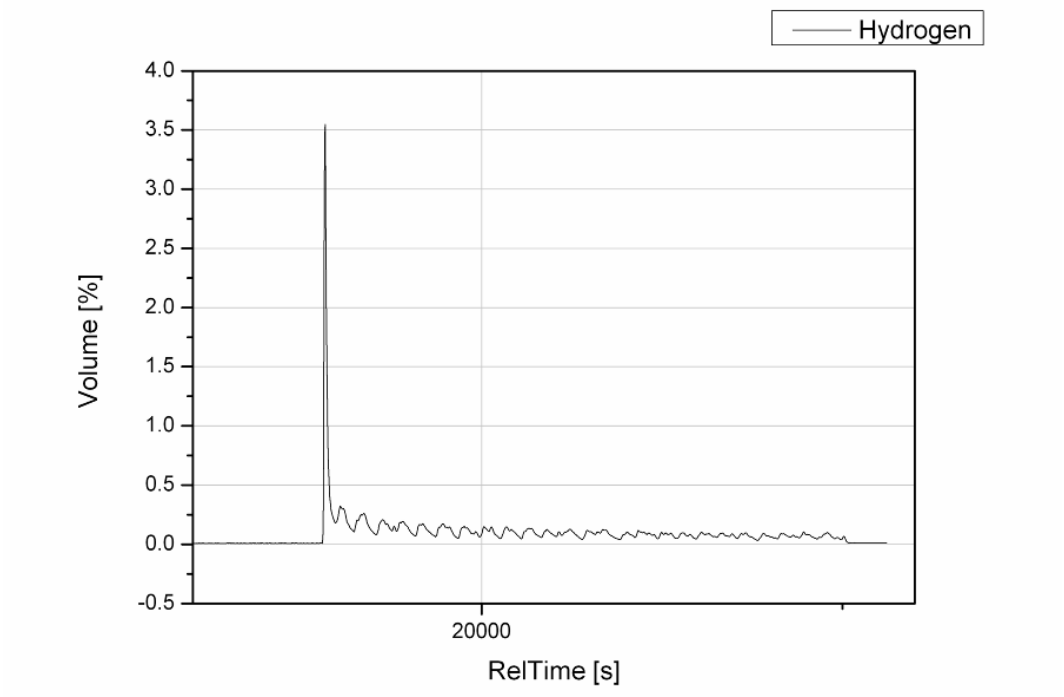

Figure 4: Hydrogen production rate vs. time.

After two cycles, which implicates two water splitting reactions at 830°C and two regeneration steps at 1200°C, $(Ce,Fe)O_x$ coatings exhibit some grain growth with grain size up to 1µm. Microstructural evidence suggests only little reduction in surface area. The general appearance of the insular coating remains virtually unchanged.

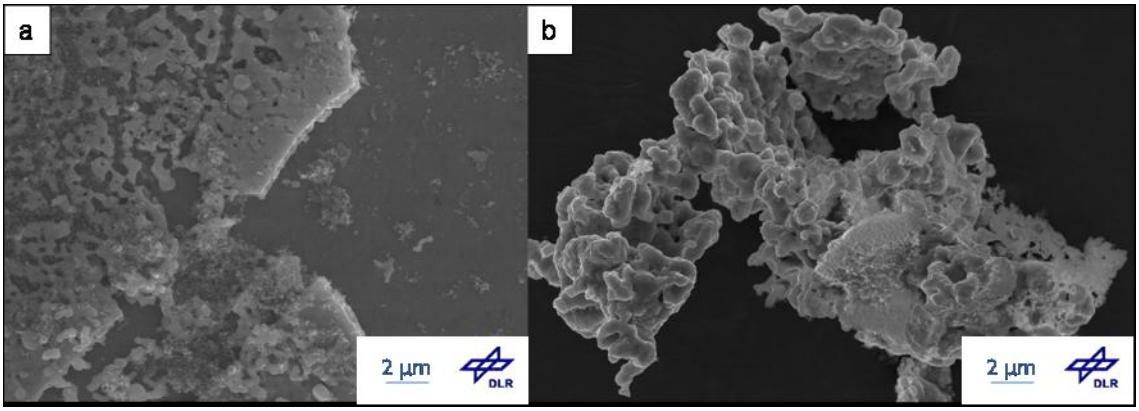

Figure 5: a) $(Ce,Fe)O_x$ coatings on ZrO_2; b) reference $(Ce,Fe)O_x$ powder without substrate, both after 2 water splitting cycles.

Obviously, the rigid substrate counteracts volume shrinkage in two dimensions. In contrast, a corresponding substrate-free reference powder which was treated in the same way shows significant densification and hence already after two cycles the surface activity is reduced (Figure 5b). This study shows that coating of inert ceramic spherules with functional oxides is a suitable way to retain relatively high surface areas. This is particularly important because presence of water vapor generally accelerates diffusion-controlled processes (grain coarsening, sintering) in oxide phases. In subsequent investigations the size effect of the substrate beadlets will be studied in more detail.

References

[1] T. Kodama, N. Gokon, Chem Rev (2007), 107, 4048-4077.

[2] S. Abanades, P. Charvin, G. Flamant, P. Neveu, Energy (2006), 31, 2805-2822.

[3] H. Kaneko, H. Ishihara, S. Taku, Y. Naganuma, N. Hasegawa, Y. Tamaura, J Mater Sci (2008), 43, 3153-3161.

[4] K. Z. Li, H. Wang, Y. G. Wie, D. X. Yan, J Phys Chem C (2009), 113, 15288-15297.

[5] T. Zhang, P. Hing, H. Huang, J. Kilner, J Eur Ceram Soc (2001), 21, 2221-2228.

[6] H. Kaneko, H. Ishihara, S. Taku, T. Yokoyama, H. Nakajima, Y. Tamaura, Energy (2007), 32, 656-663.

Low Temperature Separations in the Sulphuric Acid Decomposition Stage of the Sulphur Iodine and Hybrid Sulphur Thermochemical Water Splitting Cycles

Rachael H. Elder, **Andrew Shaw**, **Moises Romero**, **Najwa Elbakhbakhi**, **Geof H. Priestman**, **Ray W. K. Allen**, University of Sheffield, UK

The Sulphur Iodine and Hybrid Sulphur thermochemical cycles are promising routes for large scale production of hydrogen from water [1-3]. The thermal decomposition of aqueous sulphuric acid to form SO_2, O_2 and H_2O is common to both cycles and involves high temperatures and difficult separations. The energy requirement is large due to the excess of water present. This work investigates the separations involved with a view to improving efficiency.

1 SO_2-O_2-H_2O VLE

Oxygen is a by-product of the decomposition process and must be separated from the reaction products. This could be achieved via conventional low temperature processes, such as absorption. Before design of such a system can be carried out, thermodynamic data and reliable models are required for the multicomponent phase equilibrium relationships between SO_2, O_2 and H_2O.

The binary mixture of sulphur dioxide and water has been modelled using the methodology derived by Zemaitis [5]. These initial simulations were extended, on the same mixture, using a similar methodology, but adding oxygen into the multicomponent VLE equations. The model of the mixture including Oxygen, was analysed extensively and compared with predictions from the salting out equation derived by Setschénow [4]. By observing and comparing the results with the existing literature, the mathematical simulation results were shown to lay a solid foundation for describing the PVT behaviour of both mixtures. The multicomponent equilibria calculations, rather than the salting out equation, were found to be more reliable when trying to estimate dissolved concentrations of oxygen in aqueous sulphur dioxide solutions. Although the methods used to predict solubility parameters are consistent with the literature, measurements are required to prove the actual behaviour of these species at operating conditions more relevant to the design process that is to follow. In order to verify the calculations, accurate and updated VLE data for the ternary system is required.

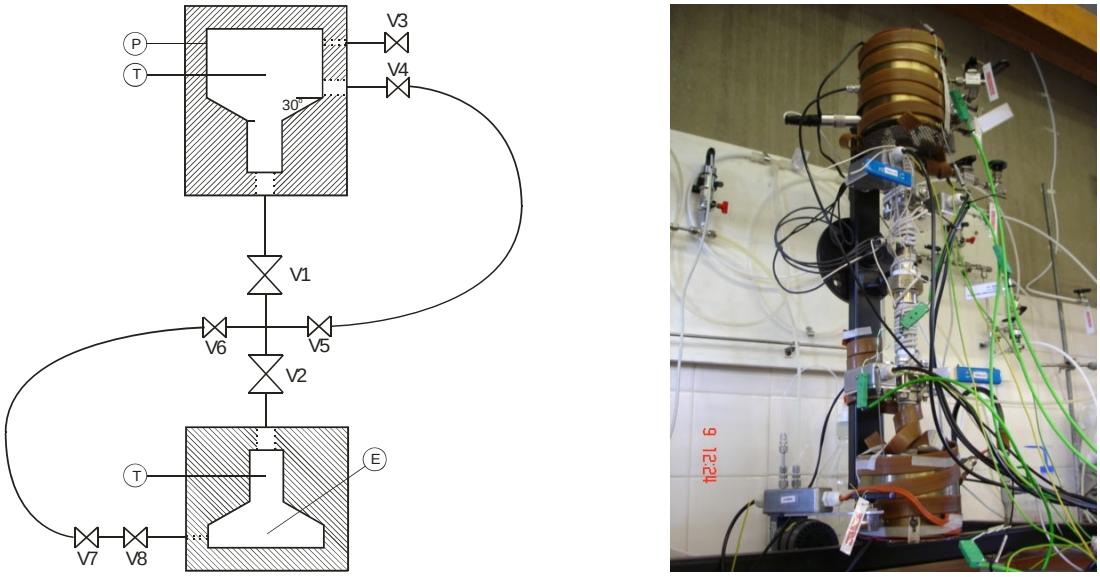

Figure 1: Schematic and Photo of the Equilibrium Still (insulation removed for clarity).

A novel experimental apparatus has been designed, constructed and commissioned as seen in Figure 1. Known amounts of each species are brought in contact in a vessel of known volume providing large interfacial areas for mass transfer and having a controllable uniform temperature distribution in the range of 20 to 120 °C. The pressure range is between atmospheric and 30 bara. The main apparatus consists of two chambers connected by a pipe through two valves, V1 and V2. Once equilibrium is established, the chambers are isolated and representative samples of the gas and liquid phases are removed for analysis without disturbing the equilibrium. The whole apparatus is PTFE lined as contact with metal ions can disrupt the equilibrium.

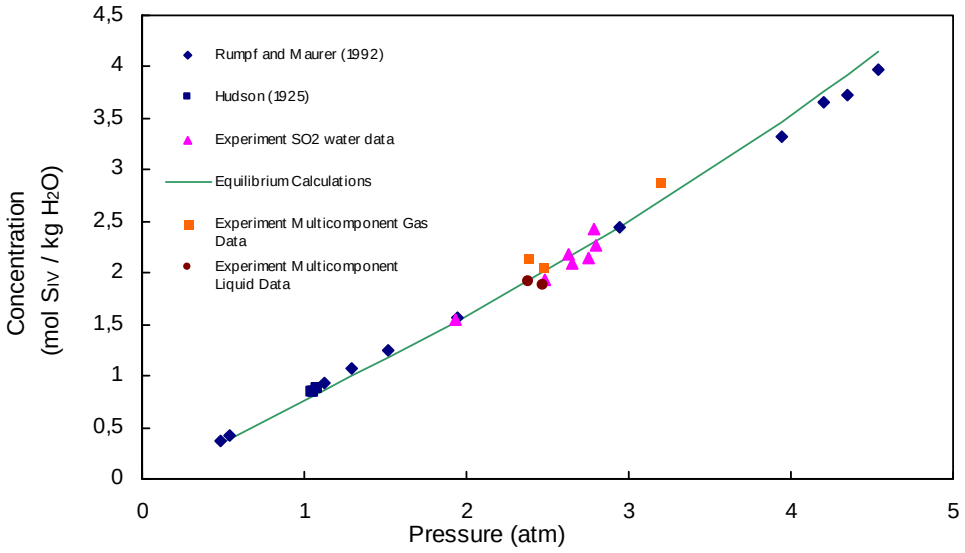

Figure 2: Comparison of experimental SO2 solubility in water at 40 ºC with calculations.

Data points have been collected for a number of binary and ternary solutions and further data collection is currently underway. These experimental results have been used to validate the calculations of the multi-component equilibria, as shown in Figure 2.

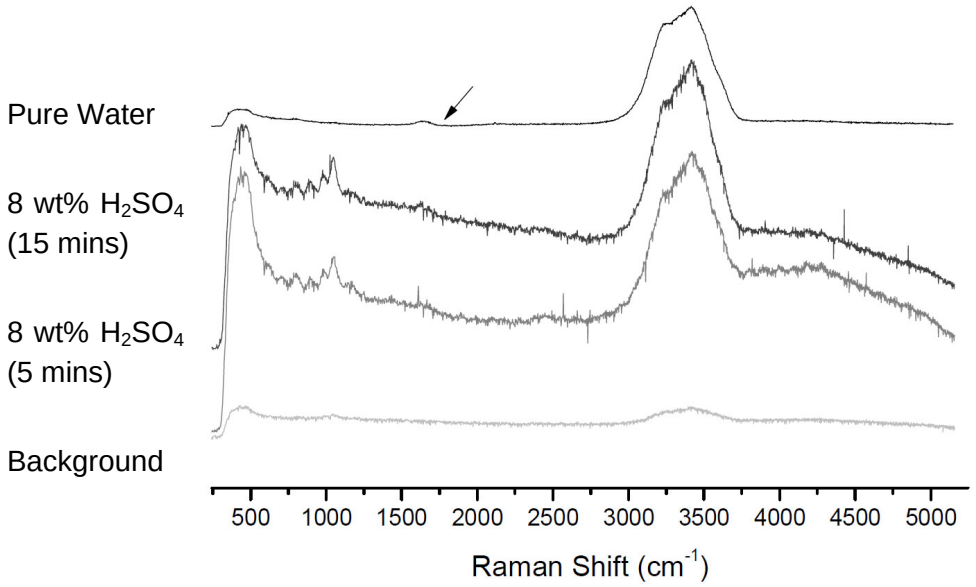

Figure 3: Raman Spectra of Aqueous Sulphur Species. The arrow shows an OH^- stretching, particular from water.

Improvements to the experimental rig to allow online analysis are being investigated. Raman spectroscopy has been identified as a suitable analysis technique. Figure 3 shows an exploratory Raman spectra for a sample of 8 wt% H_2SO_4 aqueous solution. The graph shows the different acquisition times for different samples, water being the darker spectrum on the top with parametric smoothing and the lightest the dark-room spectrum that was subtracted from the two samples in the middle.

2 Low Temperature Membrane Separations

The aqueous sulphuric acid stream entering the decomposition section is currently concentrated by a series of evaporators and distillation columns; however this is complex and energy intensive. Membrane separations are under investigation as a low energy alternative. Dewatering by pervaporation is investigated experimentally to find the fluxes and selectivities achievable through different membranes. Nafion membranes of varying thicknesses have been tested in the setup shown in Figure 4 and a sample of the results are shown in Figure 5. The permeate is almost pure water with only trace amounts of sulphuric acid which are below detection limits.

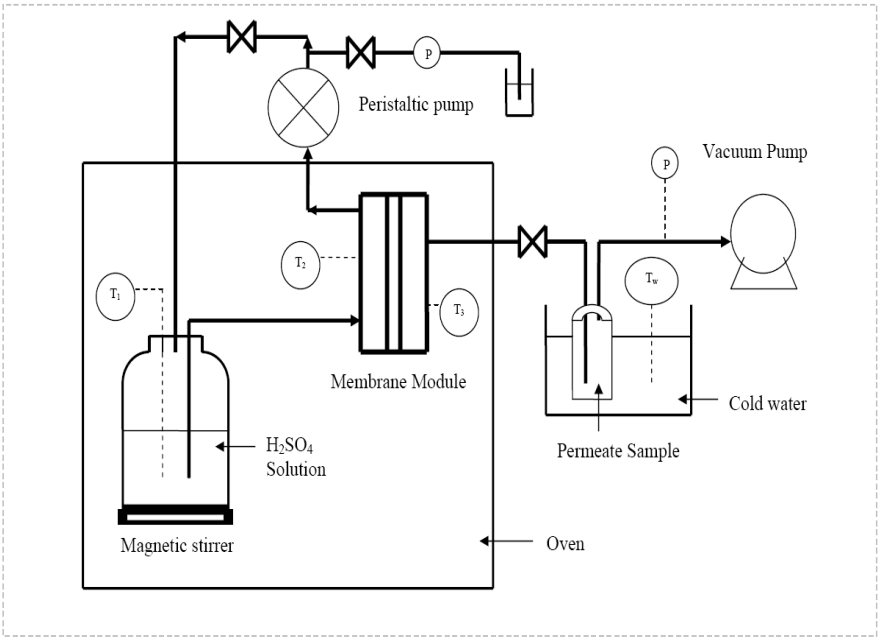

Figure 4: Experimental setup for membrane flow testing.

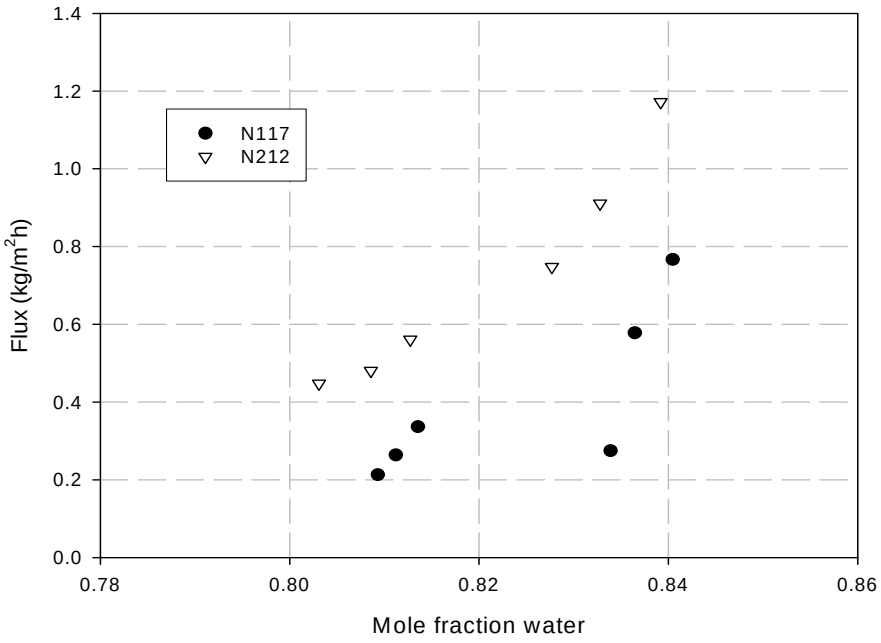

Figure 5: Flux through Nafion membranes for aqueous H_2SO_4 solutions.

An investigation into boundary layer formation has also been undertaken, using a different, semi-batch membrane testing apparatus shown in Figure 6. The aim of this series of

experiments is to find out what causes the flux decrease seen as each experiment progresses. An example results graph is shown in Figure 7.

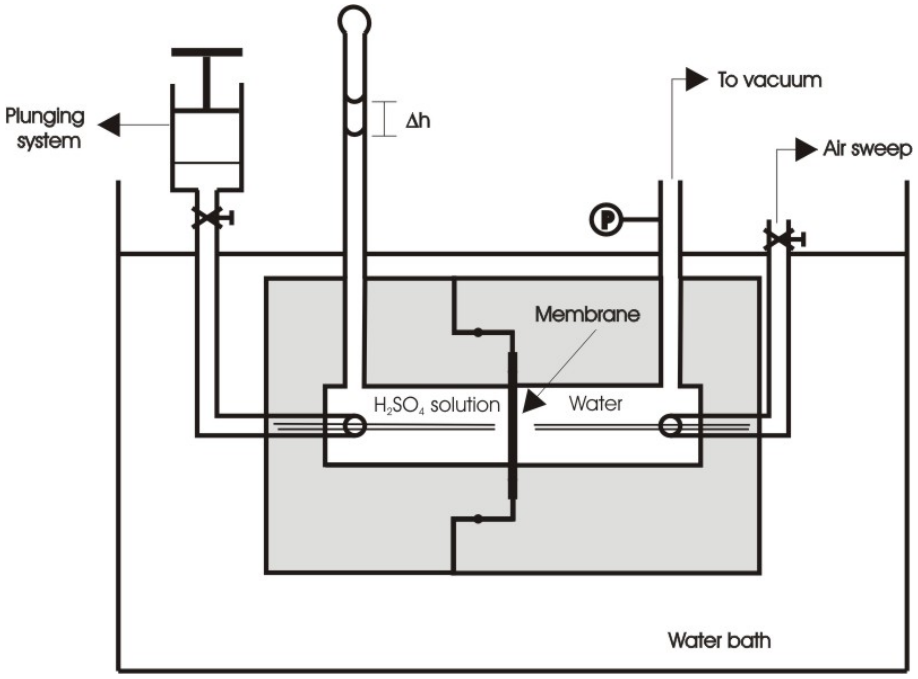

Figure 6: Experimental setup for membrane semi-batch testing.

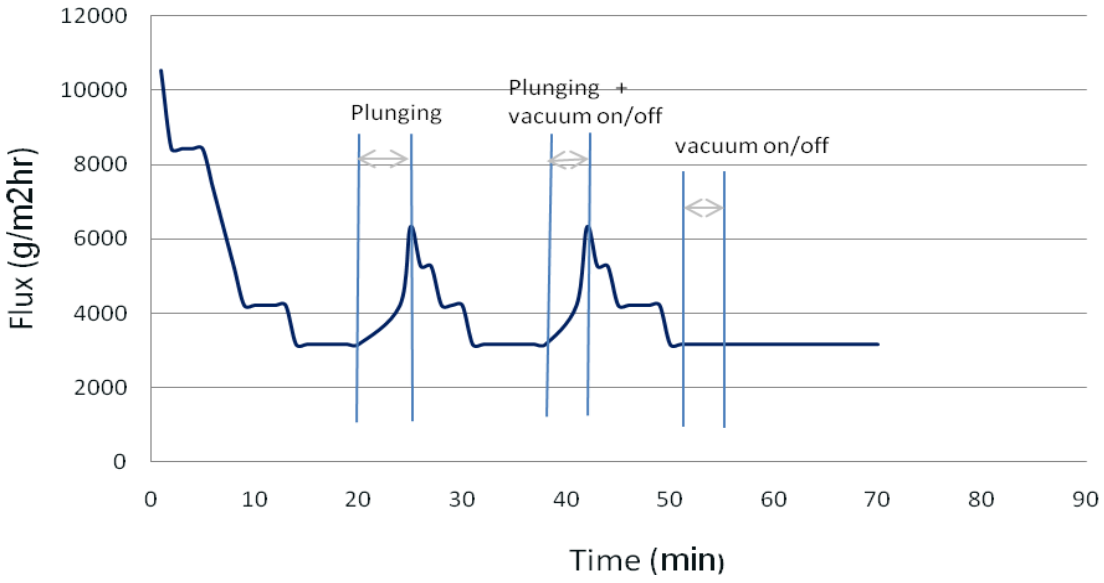

Figure 7: Example results graph for boundary layer formation investigations.

Plunging of the system, causing an abrupt change in the feed side flow rate and hence mixing, leads to an increase in flux. This suggests that a boundary layer is indeed the cause of the flux decrease. Further work will identify appropriate mixing techniques to allow the maintenance of high flux levels.

References

[1] Brecher, L., Spewock, S. & Warde, C. (1977) The Westinghouse Sulphur Cycle for the thermochemical decomposition of water. *International Journal of Hydrogen Energy,* **2,** 7-15.

[2] Le Duigou, A., Borgard, J. M., Larousse, B., et al. (2007) HYTHEC: An EC funded search for a long term massive hydrogen production route using solar and nuclear technologies. *International Journal of Hydrogen Energy,* **32,** 1516-1529.

[3] Norman, J. H., Besenbruch, G. E., Brown, L. C., et al. (1982) *Thermochemical Water Splitting Cycle, Bench-Scale Investigations and Process Engineering*. General Atomics, GA-A16713

[4] Setschénow, J. Z. (1889) Uber Die Konstitution Der Salzlosungenauf Grund Ihres Verhaltens Zu Kohlensaure. *Zeitschrift für Physikalische Chemie,* **4,** 117–125.

[5] Zemaitis, J. F., Scrivner, N. C., Clark, D. M., et al. (1986) *Handbook of aqueous electrolyte thermodynamics theory and application*, WILEY.

Analysis and Development of the Bunsen Section in the Sulphur-Iodine Process

Alberto Giaconia, **Salvatore Sau**, **Giampaolo Caputo**, Italian National Agency for New Technologies, Energy and Sustainable Economic Development (ENEA), Italy
Mariapaola Parisi, Dept. Chemical Engineering, University "La Sapienza", Rome, Italy

1 Introduction

Thermochemical water-splitting cycles (TWSCs) are a promising carbon-free route for nuclear or solar hydrogen production. Among the hundred cycles proposed yet, the Sulphur-Iodine (S-I) process is one of the most deeply studied: differently from other TWSCs, it basically does not involve either solid management, electrolysis, or membrane exploitation, but it consists of more "conventional" chemical engineering large-scale operations (heat exchange, fixed-bed tubular reactors, distillation column, etc.). The S-I cycle involves the following three reactions [1]:

$$2H_2O + I_2 + SO_2 \rightarrow H_2SO_4 + 2HI \quad (1)$$
$$2HI \rightarrow I_2 + H_2 \quad (2)$$
$$H_2SO_4 \rightarrow H_2O + SO_2 + ½\ O_2 \quad (3)$$

Reaction (1) between SO_2 with I_2 and water to produce H_2SO_4 and HI, called Bunsen reaction, is a fundamental process step. Differently from the acid decomposition sections, this stage proceeds under "mild" temperatures (< 150°C) and requires rather low heat duty (the reaction is slightly exothermic). However, this section must be carefully designed to obtain two concentrated and unpolluted acid streams. This optimization involves some issues like determination of best working conditions, Bunsen reactor design and the separation and purification of the two product streams.

Basic experimental studies have firstly been carried out to characterize the Bunsen reaction, using a jacketed mixed glass reactor at 30-120°C, under different initial compositions. Removal of H_2SO_4 and residual SO_2 from the hydriodic acid phase is also studied, monitoring the possible sulphur or H_2S formation. Also separation of the iodine from the sulphuric acid stream is studied.

A lab-scale continuous apparatus to carry out the Bunsen reaction, together with subsequent purification/concentration of the produced acids, has been tested.

Some experimental results are here presented and discussed. Moreover, the possible application of the Bunsen reactor and separation units to an "open S-I cycle" for sulphur recovery is discussed.

2 Experimental Studies with Batch and Semi-batch Apparatus

A preliminary analysis was carried out to identify the most convenient operation conditions to produce H_2SO_4 and HI as pure and concentrated as possible, in order to enhance downstream operations and maximize the overall S-I cycle efficiency. Thus, several reaction options were initially considered and investigated with batch laboratory experimental tests [2-4]: electrochemical Bunsen reaction, the Bunsen reaction in an organic solvent or liquid (pressurized) SO_2, or the Bunsen reaction with precipitation of insoluble solid salts. Each of these routes proved potential but also showed some important technical/energetic drawbacks. For this reason, subsequent research was mainly focused on the Bunsen reaction in water media, with a large excess of iodine in order to prevent side reactions and allow segregation of the two acids (H_2SO_4 and HI) within two respective immiscible liquid phases, namely the "H_2SO_4 phase" and the "HI_x phase":

$$(x+1)I_2 + SO_2 + (n+2)H_2O \rightarrow [H_2SO_4 + (n-m)H_2O] + [2HI + xI_2 + mH_2O] \quad (1bis)$$

According with reaction (1bis) stoichiometry, iodine excess (x) is almost quantitatively dissolved in the HI_x phase, while water excess (n) splits between the two phases. In this preliminary study this LLE behaviour was characterized too [2], measuring iodine and sulphur impurities and in the H_2SO_4 and HI_x phases, respectively.

The influence of the iodine concentration and the operating temperature on the Bunsen reaction was investigated with a semi-batch procedure in a 500 mL temperature-controlled jacketed stirred reactor (Figure 1). Since the iodine solubility depends on temperature, these two operative parameters are not independent (maximum iodine concentration increases with temperature).

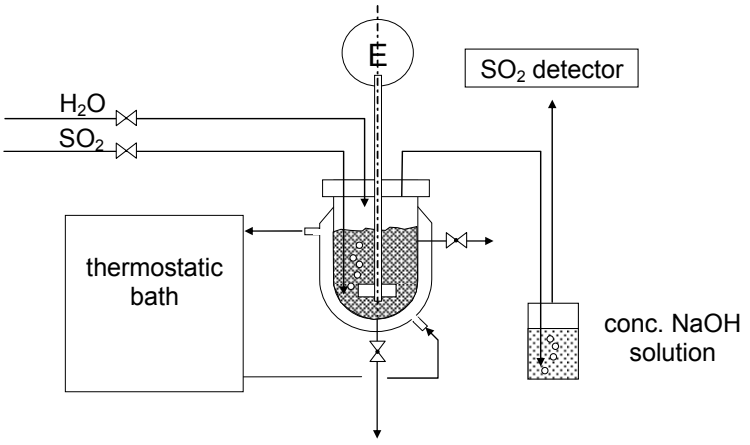

Figure 1: The mixed semi-batch Bunsen reactor.

The reactor was initially filled with iodine and a liquid azeotropic HI/water mixture (57 %wt. HI), and the thermostatic bath and the stirrer were switched on. Once the desired temperature was attained and after complete iodine dissolution, gaseous SO_2 was fed at a rate of 83 NmL/min, until the SO_2 sensor detected the saturation of both the reactor and the alkaline (NaOH) trap. The upper H_2SO_4 phase was produced only in very small quantity, but always visually detected. Then the stirrer was stopped and the mixture was kept motionless for 30 minutes to allow the stratification of the H_2SO_4 and HI_x phases: afterwards the two

phases were separated, and the HI_x phase sampled and analysed. The NaOH trap was weighted before and after the experiment to exactly determine the quantity of SO_2 absorbed in the reactor. For each run, the temperature was controlled at a constant value within the range of 30-120°C.

We observed that the amount of SO_2 absorbed and reacted in the Bunsen reactor decreases by increasing the temperature due to the exothermicity of Bunsen reaction (equilibrium shifts towards SO_2 by increasing the temperature) and to the lower SO_2 solubility in the liquid.

A representative sample of HI_x phase was bubbled at constant temperature (the same previously adopted for the reaction) with a continuous N_2 flow at (40 NmL/min) for 30 minutes in order to strip the SO_2. After stripping, the residual sulphate content was measured: the stripping should remove all the sulphuric compounds (SO_2 and H_2SO_4) from the HI_x phase by reversing the Bunsen reaction, leading to a dilution of the lower phase:

$$H_2SO_4 + 2HI \rightarrow I_2 + 2H_2O + SO_2\uparrow \qquad (1rev)$$

The sulphates content in the HI_x phase before and after the stripping is reported in Figure 2. The measured sulphates contents before stripping are in good agreement with the ones previously measured in the LLE measurement [2]. Clearly, the stripping operation significantly lowered the sulphates content in the produced HI_x phase, but sulphates were completely removed only at the highest temperature of 120°C (Figure 2). On the other hand, when the temperature is increased with an iodine molar fraction not high enough (i.e. < 0.35) secondary reactions took place, as solid sulphur formation was observed in the stripping device. In other words, insufficient iodine excess in the Bunsen reactor results into the formation of solid sulphur (and eventually H_2S) in the required HI_x phase purification stripper to remove sulphates prior HI decomposition.

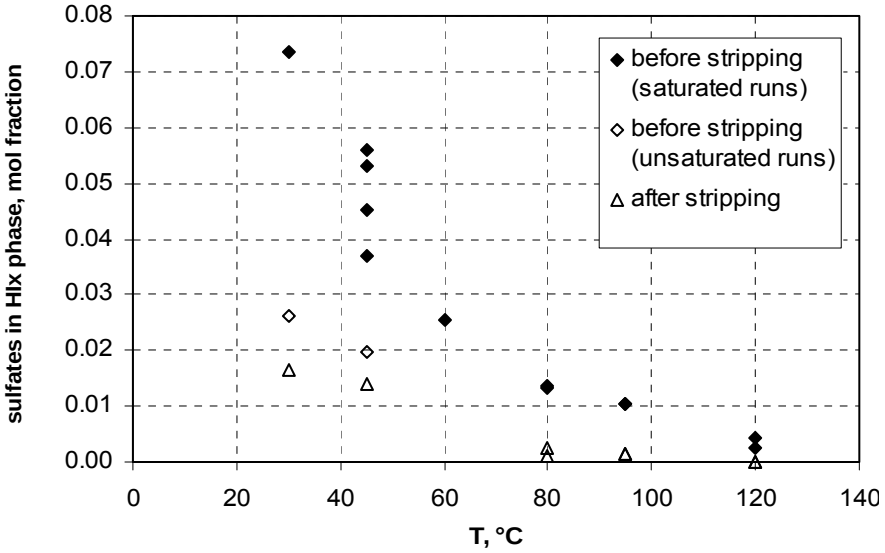

Figure 2: Sulphates content in the HI_x phase before and after stripping at different temperatures [5].

3 Continuous Flow Operation of a Counter-current Reactor

Next step of our research program was the set up of a continuous Bunsen reactor to be integrated within a closed S-I bench loop demonstrator. A packed counter-current column was considered, represented in Figure 3, where the selected flow rates of gaseous SO_2 and liquid water are fed from the bottom, and iodine is introduced from the top. Packing made of glass rings is set in the lower region, and tantalum rings in the upper section (to avoid glass rings floating on the heavier phase). Solid iodine pellets are also used as reactive packing in the upper section. Since it was difficult to find a metering pump suitable for liquid iodine, molecular iodine was fed step-by-step as solid powder from the top of the column and the packed bed with iodine pellets continuously restored above the inert glass-tantalum packing; hence a I_2-saturated HI_x phase was ensured throughout the experiment in the upper section of the reactor.

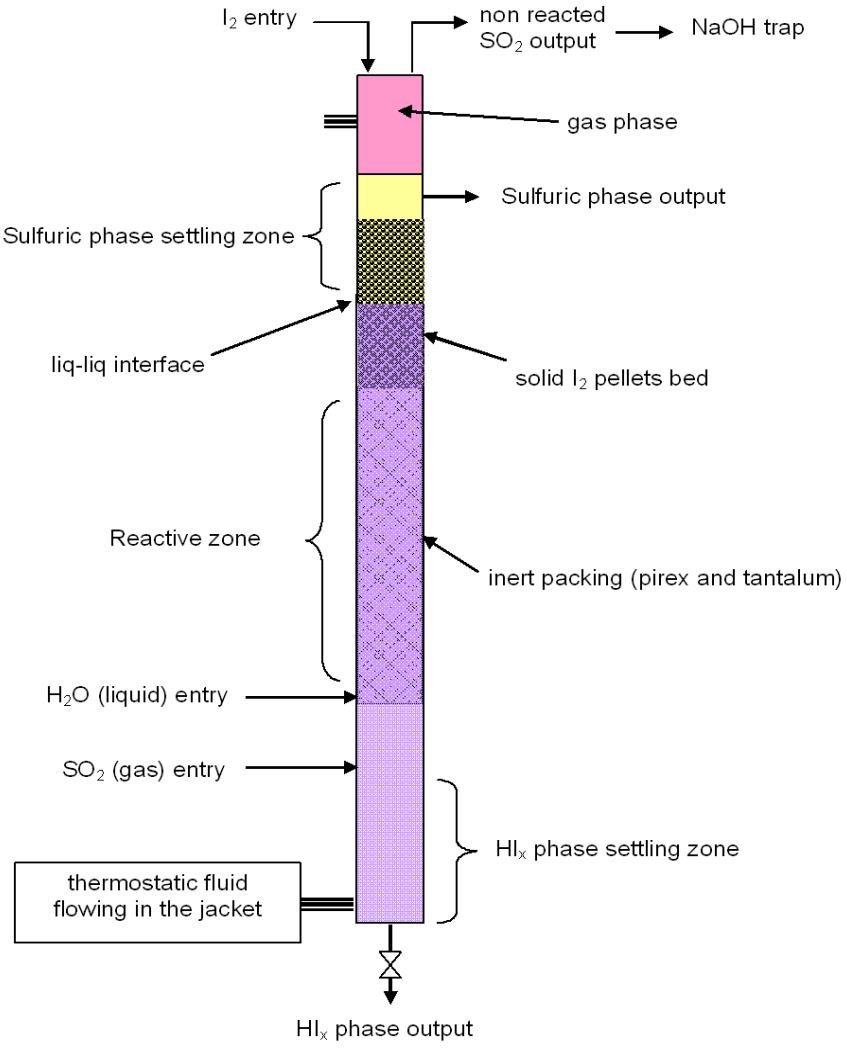

Figure 3: Counter-current Bunsen reactor scheme.

In the fixed packed bed of reactive zone (Figure 3) the rising SO_2 bubbles are adsorbed in the liquid phase. After adsorption, SO_2 reacts with the dissolved iodine and water according

to the Bunsen reaction stoichiometry (1bis). Hence, droplets of lighter sulphuric phase will nucleate, grow and rise to be collected near the top of the column; simultaneously, the denser HI_x phase will settle near the bottom. In Figure 3 is shown the location of the liq-liq interface between the HI_x phase and the settling sulphuric phase, within the "iodine-packed section".

According with this scheme the sulphuric phase can be continuously drained from the top, while the HI_x phase from the bottom, to be analysed and collected for further treatments like purification and distillation. The experimental reactor is glass made and its temperature controlled by thermostatic liquid (water or ethylene glycol) circulation in the jacket. This apparatus can process about 5-10 Nl/h of SO_2.

This reactor was integrated in a continuous system were the drained HI_x phase was sent into a temperature controlled flash drum at 130°C to eliminate dissolved SO_2 and achieve reverse Bunsen reaction (1rev) without the use of a stripping gas. Moreover, the collected H_2SO_4 phase was separately distilled in a batch apparatus to eliminate I_2/HI impurities. Finally, the collected purified HI_x phase was distilled too in a batch apparatus to remove the I_2 and obtain a HI/H_2O mixture suitable for decomposition. Hence, all units operations involved in a complete Bunsen section were studied, as represented in Figure 4. Each unit is connected with gas traps (NaOH or H_2O_2 solutions) to prevent overpressure and trap non-reacted SO_2.

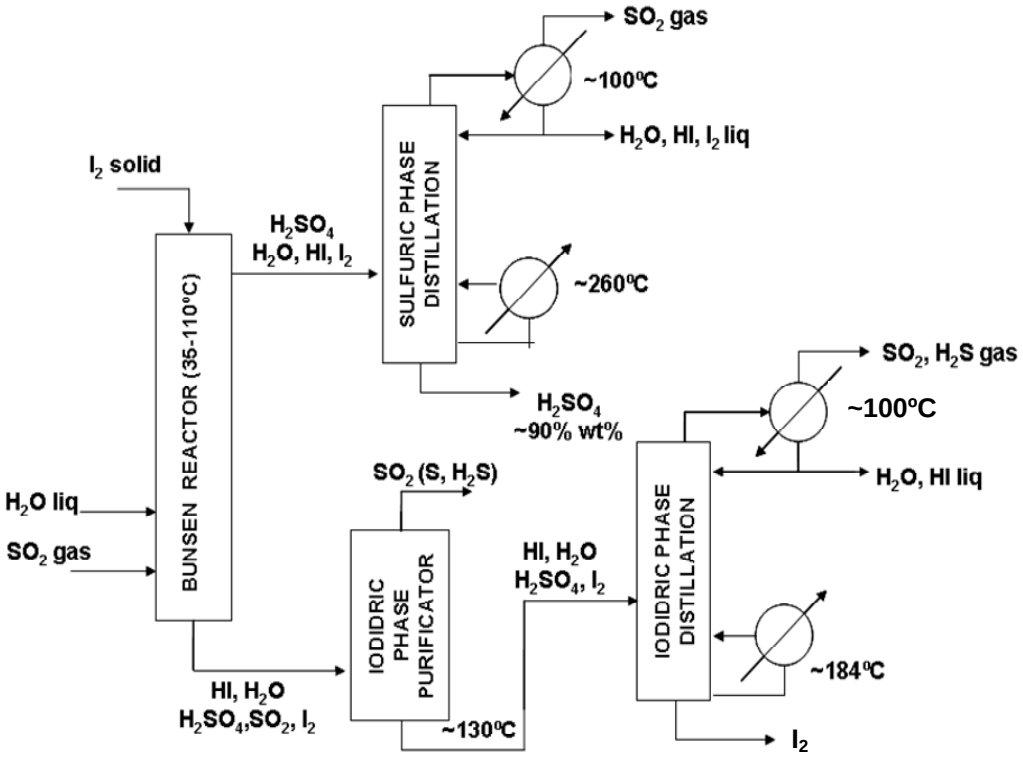

Figure 4: Schematic representation of the Bunsen section, with purification and distillation parts, as in the experimental apparatus. In brackets are species expected to be present in traces or present only under certain experimental conditions.

Bunsen reactor was operated in continuous for 4-6 hours, at constant temperatures in the 35-110°C range, with H_2O-to-SO_2 feed ratio of 12.5-13.7 mol/mol and I_2-to-SO_2 feed ratio of 3.0-8.2 mol/mol (depending on temperature). Recovered phases had similar composition as that one obtained in previous LLE measurements [2]. It was possible to quantitatively purify the H_2SO_4 phase to a iodide content < 10^{-3} %wt. by heating to 270°C, corresponding to simultaneous water vaporization to a final H2SO4 concentration of about 89 %wt. As far as the HI_x phase purification is regarded, the presence of sulphur in the top of the flash drum was observed at the lowest Bunsen reactor temperatures (< 85°C), corresponding to the lowest iodine concentration in the outlet HI_x phase; moreover, substantial reduction of sulphates was achieved when the reactor was operated at the highest temperatures (> 85°C). These results are in agreement with those discussed in the previous section.

4 Application to Industrial Sulphur Recovery

It is noteworthy that integrated process scheme shown in Figure 4, coupled with a HI decomposition reactor for H_2 production, represents a “open S-I cycle”, i.e. a process to convert SO_2 and water to hydrogen and sulphuric acid. This process basically requires heat at temperatures lower than 300°C; the additional low thermal duty at 450-650°C for HI decomposition can be recovered from sulphur or H_2S combustion to SO_2, that is a common industrial process in H_2SO_4 plants. The overall thermal burden of the process can be evaluated to be about 3500 kJ/mol$_{H2}$ at 184°C, that corresponds to a thermal efficiency of about 8 %. This value seems rather low, if compared with the thermal efficiency values reported for many thermochemical water-splitting cycles. On the other hand, it must be recognized that this is obtained with “low-grade” heat, i.e. heat input at < 200°C, while most thermochemical cycles require high-temperature heat (> 800°C). However, other flowsheets for the S-I cycle have been proposed, especially regarding the HIx section, leading to much lower heat consumption (< 600 kJ/mol$_{H2}$).

5 Summary

The breakthrough of the S-I process still goes by the overcome of some technical issues dealing with the increase of efficiency and management of the HI_x process section, i.e. the treatment of the iodine-rich solution produced in the Bunsen reactor until hydrogen production. These operations have been studied at the ENEA in the framework of a National program on “New Energy Systems”, in cooperation with other Italian Academic partners.

Most convenient operative conditions for the Bunsen section operations have been determined and discussed.

Moreover, a possible short-term exploitation of the developed technology in the sulphur recovery field was proposed for industrial sulphuric acid production from sulphur wastes (e.g. sulphur from Clauss plants) with co-production of hydrogen using low-grade heat (< 300°C).

Acknowledgements

This work was carried out within the framework of the Italian National Program TEPSI (New Systems for Energy Production and Management – Hydrogen), financially supported by the Special Supplementary Fund for Research (FIRS DM 1757/Ric.28/07/2005).

Besides the authors, the following scientists, laboratory assistants and students have appreciably contributed to this work: Pietro Tarquini, Annarita Spadoni, Claudio Felici, Vanessa Arnàs Simancas, Paolo Favuzza.

References

[1] Brown L.C., Besenbruch G.E., Lentsch R.D., Schultz K.R., Funk J.F., Pickard P.S., et al. High efficiency generation of hydrogen fuels using nuclear power. General atomics project 30047, June 2003.

[2] Giaconia A., Caputo G., Ceroli A., Diamanti M., Barbarossa V., Tarquini P., Sau S.: “Experimental study of two phase separation in the Bunsen section of the sulfur-iodine thermochemical cycle”; Int. J. Hydrogen Energy, 2007, vol.32, p.531-536.

[3] Sau S., Giaconia A., Caputo G., Prosini P.P.: “Decrease the rate of recycling agents in the sulfur-iodine cycle by solid phase separation”; Int. J. Hydrogen Energy, 2008, vol.33, p.6439-6444.

[4] Giaconia A., Caputo G., Sau S., Prosini P.P., Pozio A., De Francesco M., Tarquini P., Nardi L.: “Survey of Bunsen reaction routes to improve the sulfur-iodine thermochemical water-splitting cycle”; Int. J. Hydrogen Energy, 2009, vol.34, p. 4041-4048.

[5] Parisi M., Giaconia A., Sau S., Spadoni A., Caputo G., Tarquini P.: "Experimental Studies of the Bunsen Reaction in the Sulfur-Iodine Process"; Proc. AIChE Annual Meeting 2009, Nashville (TN), November 2009.

Chemical Characterization of Sulphur-Iodine Thermochemical Cycle Flowstreams by Raman Spectroscopy

Raffaele Liberatore, Mauro Falconieri, Michela Lanchi, Annarita Spadoni, ENEA CR Casaccia, Italy

Abstract

The Sulphur–Iodine (S-I) thermochemical cycle for hydrogen production from water is one of the widest investigated cycles in the world. Considered the complexity of the S-I process scheme, the focus on chemical characterization of the flowstreams in the loop plant is crucial in order to fully understand chemical equilibriums involved at varying hydriodic acid: ($HI:I_2$) ratio in the mixtures and to determine HI and I_2 contents as well. Raman spectroscopy has been widely used to investigate iodine solutions, however few works deals with I_2 in HI aqueous mixtures. The aim of the present study is to use Raman spectroscopy for a rapid qualitative and quantitative characterization of the $HI–H_2O–I_2$ mixtures involved in the S-I process. At this purpose, Raman spectra of solutions with known HI and I_2 concentration have been recorded at varying I_2 and HI compositions. It has been found that the chemistry of these solutions is highly dependant on $HI:I_2$ molar ratio. For ratio up to 1:1, the dominant iodine compounds are I_3^- and its corresponding ion pair HI_3. At higher values, close to those of the hydriodic phase HIx of the Bunsen reaction, there is experimental evidence of the formation of higher polyiodine and polyiodides compounds.

1 Introduction

The Sulphur–Iodine (S-I) thermochemical cycle for hydrogen production from water is one of the widest investigated cycles in the world [1]. As it is known, the S-I cycle is based on three main sections: the Bunsen reaction, the hydriodic acid decomposition and the sulphuric acid decomposition. A very crucial step in this process concerns the optimization of the phases separation occurring in the Bunsen section and the consequent hydriodic phase HIx purification. Up until now, the improvement of operative parameters in those steps have been attained mainly by experimental tests, but the relationship between the chemico-physical behaviour of these solutions and the chemical structures of the iodine compounds involved are not yet fully understood.

The literature have earned a wide attention [2] over iodine chemistry. Despite this, few works were dedicated to the experimental determination of the chemical species contained in aqueous solutions of iodine I_2 and hydriodic acid HI. Improving this understanding is the basis for the present experimental investigations and Raman scattering is a proper probe of structure over aqueous solutions because it is sensitive to both local and long-range chemical order, so it is an effective diagnostic mean for short and long iodine compounds. One of the major controversy regarding $HI-I_2$ aqueous solutions is about the existence or not of I5- or heavier polyiodide and the presence of polyiodine forms. Calabrese [3] suggested

the formation of triiodide ions I_3^- and other polyiodine species, designated as I2x, where x=2,3 etc, stabilized by H^+ ions in the solution and does not support the formation of polyiodide ions such as I_5^- and I_7^-. Milne [4] findings were consistent with Calabrese. Raman spectroscopy was used to identify the various iodine species present in aqueous solutions of I_2 in HI (1:1 mole ratio). It has been shown that the changing of Raman spectra with changing concentration is a result of ion-pairing $H^+I_3^-$ caused by interaction between H^+ and I_3^- and not from vibrational modes of I_2 or I_5^-. However, Ramos-Sànchez [5] was in contrast and suggested that the major iodine containing species were the triiodide anion I_3^-, and two other compounds such as I-(I_2), and I-(I_2)$_2$.

The aim of the present work is to understand chemical equilibriums existing in HI-I_2 aqueous solutions and whether I_3^- or higher polyiodide and polyiodine species are present. At this purpose, Raman spectra of HI-I_2-H_2O solutions with known HI and I_2 concentration were recorded over a range of HI concentrations c(HI) from 1 to 7.6 M varying I_2 content c(I2) from 0.2 to 15 M. Since, in this case, the peak intensity ratio is proportional to the concentration of the species that originates the peak, the course of the peak intensity ratio obtained experimentally was compared to the calculated concentration ratio of polyiodides and polyiodines species hypothesised. This comparison has furnished the evidence of the existing species in solution.

2 Experimental

HI aqueous solutions and I_2 in pellets were purchased from Sigma–Aldrich. Ultra pure water (oxygen free) were used. Standardized sodium thiosulfate ($Na_2S_2O_3$) solution and standardized sodium hydroxide (NaOH) solution were supplied by Carlo Erba Reagents Company in order to determine by titration I_2 and HI content respectively. Raman measurements were carried out using an He-Ne: 633 nm laser radiation (incident laser power at the sample ~5 mW) which was directed onto the samples through an optical microscope objective and collected along the same optical pathway in a backscattering mode. Raman spectra were obtained using a Notch holographic filter to attenuate the laser Raylight scattering. The remaining light was focused through the entrance slit of a 500 mm single monochromator and the spectrum was measured by a charge-coupled device (CCD) detector. Overlapping peaks has been deconvoluted assuming Gaussian line shapes.

3 Results and Discussion

Peak assignment for aqueous solutions containing iodine compounds is still not completely understood. This is mostly due to the fact that Raman vibrational modes of possible iodine species are quite close and tend to overlap: each band can't be assigned univocally to each compound. In general, for a linear I_3^- ion the bands obtained in a Raman spectrum derive from the v1 (symmetric stretching), v2 (deformation) and v3 (asymmetric stretching) modes and can be expected at approximately 110, 50-70 and 130-140 cm-1 respectively [2]. Theoretically, v2 and v3 are formally forbidden Raman modes and arise from selection rules departures according to symmetry lowering. In table 1 are summarized the Raman vibrational frequencies observed experimentally with the relatives peak assignments for I_3^- and I_5^- in various solutions at varying concentrations[6-9].

Table 1: Raman vibrational frequencies observed experimentally for I_3^- and I_5^-.

compound	wavenumber (cm-1)	mode designation	remarks
	70-80	v2, bending deformed linear I3-	various solutions
	103-114	v1, symmetric stretching linear I3-	various solutions
I3-	125 145 143-152 150	v3, asymmetric stretching linear I3- v3, asymmetric stretching linear I3- v3, asymmetric stretching linear I3- 2v2, Fermi Resonance	(dbcr)I3 in the solid state1 (R3S)I3 solid2 various solutions HI-I2 solutions (1:1) in water
	170-172	v I-I stretching ion-pair HI3	HI-I2 solutions (1:1) in water
	164	v1, linear I5-	
I5-	140 155	v2, bent I5- v1, linear I5-	Polyvinylalcool thin film (iodine doped PVA)
	170	I2 v1 mode I-.2I2 or I3- I2	(R3S)I3 liquid2
	168	I2 v1 mode L-shaped I5-	(dbcr)I51

1,(dbcr)= dibenzo-18-crown-6
2,(R3S)I3= alkylsulfur triiodide

Extra spectral features in the Raman spectra were found at 150 and 172 cm-1 by Milne [4] investigations over HI/I_2 solutions (1:1 mole ratio) ranged from 0.1 M up to 3,3 M. The 150 cm-1 band was assigned to Fermi resonance between v1 and 2v2, while the 172 cm-1 band was attributed to the I-I stretch of the ion-pair $H^+I_3^-$, designated as HI_3. Milne envisioned the change in I-I bonding in triiodide in terms of strengthening of one of I-I bonds (D1) lying at 172 cm-1 and weakening of the other (D2) which would be shifted to 84 cm-1, according to the scheme 1.

Scheme 1: ion pair formation I-I-I + H+ → I-I------I- H+ , where I-I =D1; I------I- =D2

The Raman spectra of $HI-I_2-H_2O$ solutions were measured over a range of HI concentrations c(HI) from 1 to 7.6 M (1-2.3-3.6-4.9-6.2-7.5 M) at I_2 fixed concentration of 0.2 M and varying I_2 content c(I_2) from 0.2 to 15 M (0.2-1.68-4.47-6.7-8.3-10-11.5-13-15.8-30 M) at HI fixed concentration of 7.6 M.

The spectra of the $HI-H_2O$ solutions for HI concentrations c(HI) from 1 to 7.5 M, shown in figure 1A, are representative of the spectra as observed. These solutions contain a very small concentration of I_2, determined by titration, arising from the photocatalysed oxidation of HI solutions: $2HI+1/2O_2=I_2+H_2O$. The spectra consist of a strong peak at 114 cm-1, a shoulder at 140 cm-1, a peak at 162 cm-1 and a weak line at 220 cm-1. In figure 1B are reported the normalized intensities on the basis of the peak at 114 cm-1: it can be noted that as the concentration c(HI) increases, the peak intensity at 162 cm-1 grows into the spectrum. According to previous findings, it can be seen that the peak at ca. 114 cm-1 is attributable to triiodide I_3^- symmetric v1 stretch. The peak at 140 cm-1 has been variously attributed to linear I3- asymmetric stretching, v3 or to Fermi resonance between v1 and 2v2; but in any

case this peak is not diagnostic to discriminate between I_5^- and I_3^-. The peak at 162 cm-1 could be assigned to the νI_2 mode in a I_5^- configuration or to the νI_2 mode in a triiodide ion-paired HI_3, as it is shown in scheme 1.

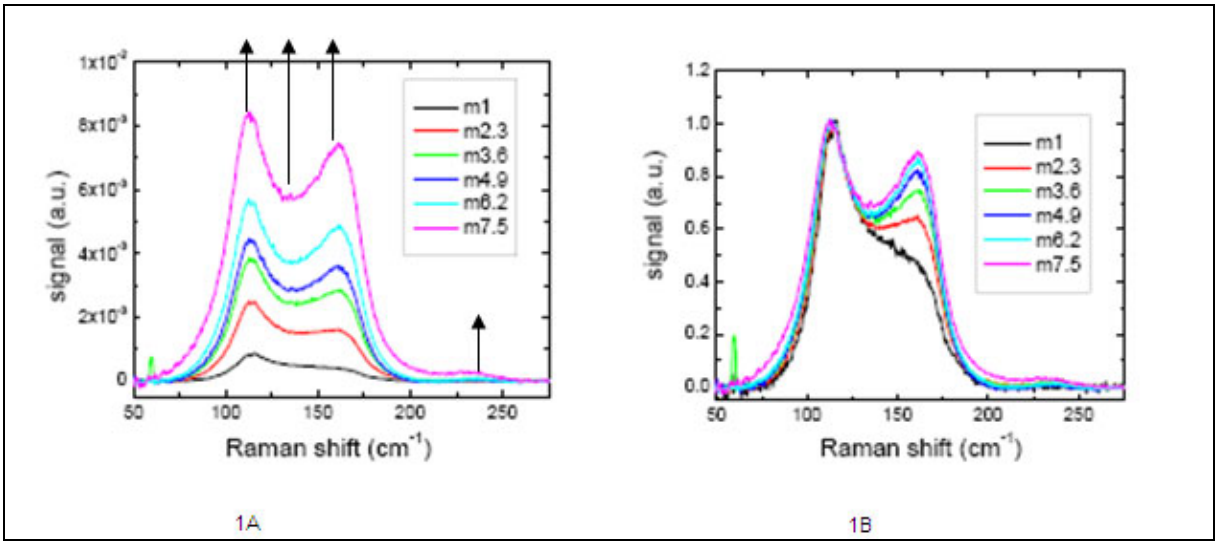

Figure 1: Raman spectra of HI-H_2O solutions at varying HI concentrations and fixed I_2 content of 0.2 M.

As it is known the area of a band is correlated to the concentration of the species that generates the peak. In this case, the concentration of the chemical species in the solution has been related to the intensity of the peaks, because it has been seen by the deconvolution of the bands obtained that the forbidden mode at 140 cm-1 is not very intense and does not interfere significantly with the area of the peaks at 114 cm-1 and 162 cm-1. For the calculation of the concentration of the existing species in solution, the following equilibrium existing in the solutions have been considered [10,11]

Polyiodide In- formation reactions:	$I^- + I_2 \rightarrow I_3^-$	(1)
	$I_3^- + I_2 \rightarrow I_5^-$	(2)
	$2I_3^- \rightarrow I^- + I_5^-$	(3)
Ion pair HIn dissociation:	$HI \rightarrow H^+ + I^-$	(4)
	$HI_3 \rightarrow H^+ + I_3^-$	(5)
	$HI_5 \rightarrow H^+ + I_5$-	(6)
Polyiodine I2x formation:	$2I_3^- \rightarrow I_6^-$	(7)
	I2x +H+→ I2xH+ x=2,3	(8)
Charge transfer complex:	$I_2 + H_2O \rightarrow I2\ldots H_2O$	(9)
HI dissociation:	$5H_2O + HI \rightarrow (5H_2O, H+) + I$-	(10)

An estimate of the concentration of major species arising from the above equilibriums has been made using the charge and mass balance equations according to Milne's assumptions [4]. Species such as I-, I_3^-, I_5^- and their respective $H+In^-$ ion pairs, designated as HIn and I_{2x}

species have been taken into account. The ratio of the concentrations of these compounds has been compared to the change in I162/I114 ratio observed in Raman Spectra.

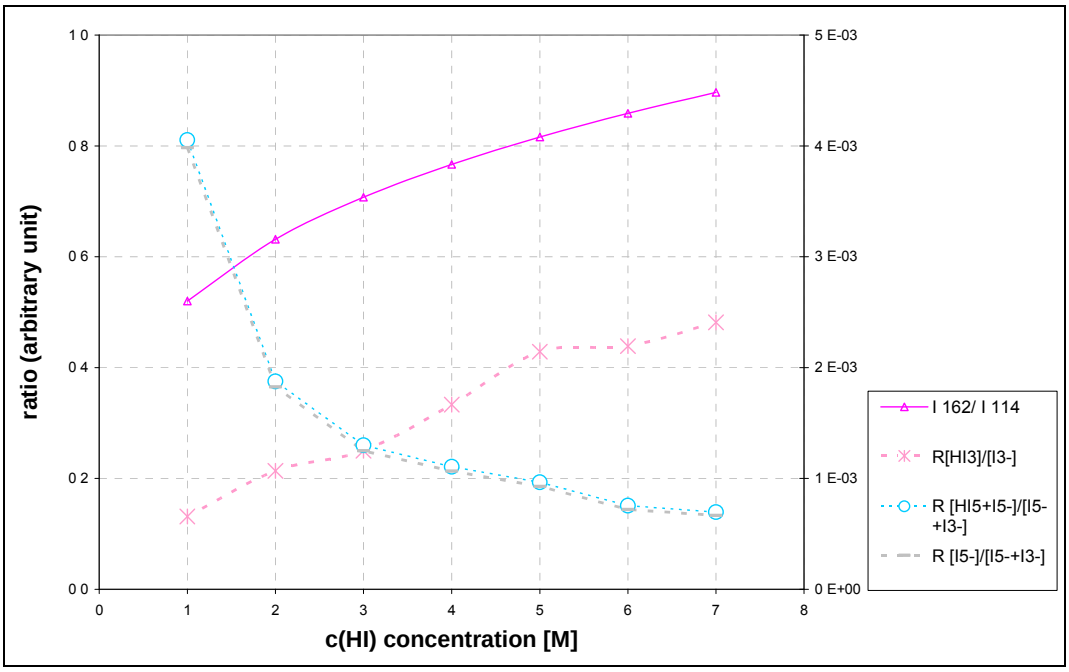

Figure 2: Experimental I162/I114 ratio and calculated iodine species concentrations ratio against cHI concentration.

In figure 2 are shown the trends of "I_5" and "I_3" species, designated as R[HI5]+[I5]/[I5-]+[I3-] and the ratio of [HI3] to [I3-], R[HI3]/[I3-] as a function of c(HI) concentration. It could be noted that its trend reflects the change of R[HI3]/[I3-] with c(HI) concentration: the increase of I162/I114 ratio suggests that the intensity of the bands attributed to I_3- (114 cm-1) decrease at the expense of that assigned to the νI_2 mode from triiodide ion-paired HI_3. It could be concluded that at low iodine concentration the peak at 162 cm-1 stems for triiodide ion-paired HI_3. Further evidence for these conclusions comes from ion to ion interaction's considerations: the more c(HI) is high, the less the I^- and I_3^- are rounded by H_2O molecules for solvatation and the more triiodides in solution tends to form the corresponding ion-pair. The weak broad peak at 220 cm-1 is ascribed to 2v1 Fermi Resonance [2].

The spectra of the HI-H_2O-I_2 solutions for I_2 concentrations c(I2) ranging from 0 to 10M with I_2:HI ratio corresponding to 0:1, 0.2:1, 0.6:1, 1:1, 1.3:1 to 15 M at HI fixed concentration c(HI) of 7,5 M, are shown in figure 3. If I2:HI molar ratio is lower than 1:1, the spectra obtained are similar to those obtained for HI-H_2O solutions, showed in figure 1. In figure 4 the course of I162/I114 ratio is shown against I2:HI ratio: it could be noted that the line that best reflects this behaviour is the one corresponding to the ratio R[HI3]/[I3]. It can be concluded that in the range of HI:I_2 concentration up to 1:1 no polyiodine higher than I_3^- and HI_3 are formed. These findings were consistent with Calabrese to the extent that species such as I_5^- or I_7^- are not formed in this range of iodine concentration. Additionally, these results agree with Milne's observation which showed that the existing iodine species in aqueous solutions of I_2 in HI

(1:1 mole ratio) are mainly I_3^- and the HI_3 ion pair neglecting higher polyiodides such as I_5^- or polyiodines such as I_6^-.

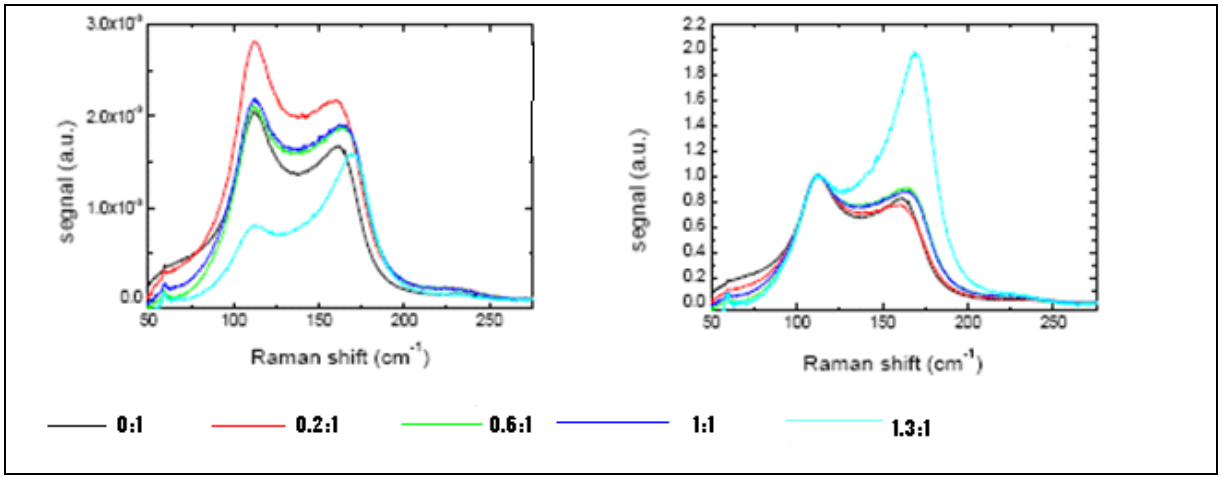

Figure 3: Raman spectra of HI-I_2-H_2O solutions at varying I_2 concentrations and fixed HI content of 7,6 M.

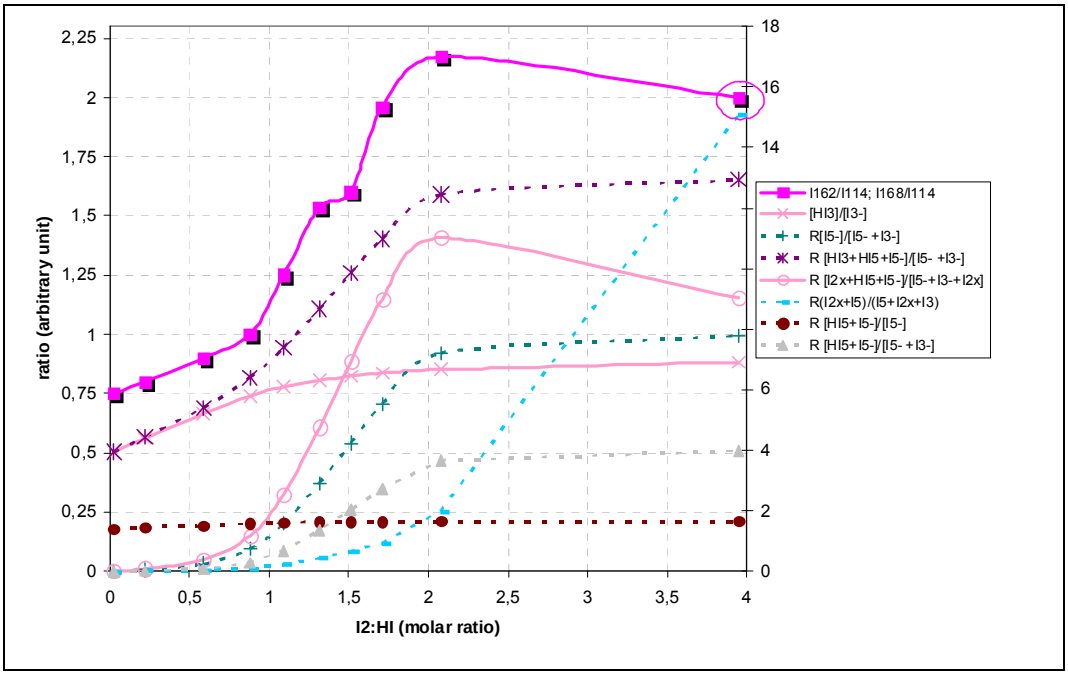

Figure 4: Experimental I162/I114 ratio and calculated iodine species concentrations ratio against I_2:HI molar ratio.

However, for I_2:HI ratios higher than 1:1, it can be observed (figure 3) that the band at 162 cm-1 is shifted to higher wavelength at 168 cm-1 and peak registered at 220 cm-1 becomes weaker/disappear. In figure 3 are reported the normalized intensities on the basis of the peak at 114 cm-1: as the concentration c(I2) increases, the peak intensity at 162 and 168 cm-1 grows into the spectrum. In figure 4 have been reported I168/I114 ratios as a function of I_2:HI

ratios. The value corresponding to the I_2:HI ratio of 4:1 has been obtained from Sanchez determinations [5]. It could be seen that the course of R [HI3]/[I3-] no longer matches the experimental I168/I114 trend as it happened for lower I_2:HI ratios: other chemical species than I_3^- and HI_3 must be taken into account. The peak assignment has been attempted from the comparison of experimental I168/I114 ratio with the ratio of the concentrations of chemical species deriving from equilibriums 1 to 5 , designed as “I5”, “I3” and “I2x” species. Several hypothesis have been proposed, as depicted in figure 4. It could be noted from figure 4 that the line that best reflects the experimental behaviour of I168/I114 ratio is the one corresponding to the ratio R[I2x+HI5+I5]/[I5-+I3-+I2x] for which I2x, I_5^- and HI_5 species must be considered.

4 Conclusions

It has been found that the chemistry of these solutions is highly dependant on I_2:HI molar ratio. For ratio up to 1:1, the dominant iodine compounds are I_3^- and its corresponding ion pair HI_3. However, in the range of I_2:HI concentrations higher than 1:1, polyiodine and polyiodide species must be taken into account: I_5^- and the corresponding HI_5 ion pair are formed while the HI_3 ion pair could be neglected. Additionally, the formation of polyiodine species such as I2x has been evidenced: at higher iodine concentration the cluster formation among the I_2 molecules becomes more favoured. Furthermore, since a correlation between I_2:HI ratio content and intensity peak ratio has been found, it is theoretically possible to determine HI concentration by comparing the experimental peak area value with the value in a matrix of data based over standardized solution with known concentration. This will be the object of further investigations.

References

[1] A. Le Duigou et al. An EC funded search for a long term massive hydrogen production route using solar and nuclear technologies. Int J Hydrogen Energy 2007;32:1516–29.

[2] Per H.Svensson et al. Synthesis, Structure, and Bonding in Polyiodide and Metal Iodine-Iodine Systems, Chemical Reviews, 2003, Vol. 103, No. 5

[3] V. T. Calabrese and A. Khan, Polyiodine and Polyiodide Species in an Aqueous Solution of Iodine +KI: Theoretical and Experimental Studies, 2000, J.Phys. Chem. A, Vol. 104 No.6, pp1287-1292

[4] J.Milne, A Raman spectroscopic study of the effect of ion pairing on the structure of the triiodide and tribromide ions, Spectrochimica Acta, 1992, Vol. 48A, No. 4, pp 533-542

[5] Ramos-Sanchez et al. Chemistry of the Bunsen section of the sulphur-iodine thermochemical cycle: in situ Raman characterization of the HIx and H2SO4 phases. 17 th WHEC 2008, Brisbane

[6] H.Sato, F.Hirata, A.B.Myers, Theoretical study of the solvent effect on triiodide ion in solutions, J.Phys.Chem.A, 1998,102,2065-2071

[7] J.H Z. dos Santos et al. High Pressure Fourier Transform micro-Raman Spectroscopic investigation of diiodine-heterocyclic thioamide adducts Spectrochimica Acta Part A, 58 (2002) 2725-2735

[8] F.W. Parret and N.J Taylor , J.Inorg.Nucl.Chem 32 2458 (1970)

[9] W. Kaya, N.Mikami, Y.Udagawa, M.Ito, Resonance Raman effect of I3- ion by ultraviolet laser excitation, Chem Phys Letters 16,151,(1972)

[10] R. Liberatore, A. Ceroli, M. Lanchi, A. Spadoni, P. Tarquini, Experimental vapour–liquid equilibrium data of HI–H2O–I2 mixtures for hydrogen production by Sulphur–Iodine thermochemical cycle, Int. J of Hydrogen Energy, 2008, 33: 4283 – 4290

[11] M. Lanchi, A. Ceroli, R. Liberatore, L. Marrelli, M. Maschietti, A. Spadoni, P. Tarquini, S–I thermochemical cycle: A thermodynamic analysis of the HI–H2O–I2 system and design of the HIx decomposition section , Int. J of Hydrogen Energy, 2009, 34: 2121–2132.

Thermoeconomic Analysis of a Copper-Chlorine Thermochemical Cycle for Nuclear-Based Hydrogen Production

Mehmet F. Orhan, Ibrahim Dincer, Marc A. Rosen, Faculty of Engineering and Applied Science, University of Ontario Institute of Technology, Canada

Abstract

Thermochemical water splitting with a copper–chlorine (Cu-Cl) cycle is a promising process that could be linked with nuclear reactors to decompose water into its constituents, oxygen and hydrogen, through intermediate copper and chlorine compounds. In this paper, a comprehensive exergoeconomic analysis of the Cu-Cl cycle is reported to evaluate the production costs as a function of the amount and quality of the energy used for hydrogen production, as well as the costs of the exergy losses and the exergoeconomic improvement potential of the equipment used in the process. An additional objective is to determine changes in the design parameters of the Cu-Cl cycle that improve the cost effectiveness of the overall system.

Keywords: Hydrogen, thermochemical water decomposition, nuclear, economic analysis, cost, thermoeconomic analysis, copper-chlorine cycle

1 Introduction

Energy consumption growth is closely related to population growth, although changes in life styles and efficiency improvement have a substantial influence on the per capita annual consumption. As a result of the worldwide increasing energy consumption due to increasing population and rising living standards, the world faces problems with depleting energy resources and the impairing impact of present energy consumption patterns on the global climate and consequently on humanity and the environment. The concerns regarding global climate change are significant and have resulted in extensive R&D on alternative, clean energy sources.

There are various alternative energy options to fossil fuels, including solar, geothermal, hydropower, wind and nuclear energy. While many of the available natural energy resources are limited due to their reliability, quality, quantity and density, nuclear energy has the potential to contribute a significant share of energy supply without contributing to climate change. Nuclear energy has in the past been used almost exclusively for electric power generation, but the direct utilization of nuclear thermal energy for other purposes has the potential to increase efficiency and thereby facilitate energy savings. Hydrogen production via thermochemical water decomposition is a potentially important process for direct utilization of nuclear thermal energy.

Thermochemical water splitting with a copper–chlorine (Cu-Cl) cycle is a promising process that could be linked with nuclear reactors to decompose water into its constituents, oxygen and hydrogen, through intermediate copper and chlorine compounds. The cycle consists of

five reaction main steps. Heat is transferred between various endothermic and exothermic reactions in the Cu-Cl cycle, through heat exchangers that supply or recover heat from individual processes.

Studies on the Cu-Cl cycle and its analyses have increased recently. Several studies of the Cu-Cl cycle have been carried out that aim to improve its overall efficiency. For example, the main steps of the Cu-Cl cycle have been assessed thermodynamically by Orhan et al. [1-5], using energy and exergy methods and considering relevant chemical reactions. Energy and exergy efficiencies of the steps in the cycle have been evaluated and parametric studies have been carried out on energetic and exergetic aspects considering variable reaction and reference-environment temperatures [1-5].

Heat is transferred between various endothermic and exothermic reactors in the Cu–Cl cycle, through heat exchangers that supply or recover heat from individual processes. Naterer et al. [6] have examined the heat requirements of these steps, in efforts to recover heat and minimize the net heat supply to the cycle, thereby improving its overall efficiency [6].

Naterer et al. [7] have examined the evaporative drying of aqueous cupric chloride ($CuCl_2$) droplets in the copper-chlorine (Cu-Cl) thermochemical cycle of hydrogen production. Analytical solutions have been developed for the cupric chloride spraying and drying processes, including empirical correlations for heat and mass transfer, based on a single droplet of aqueous $CuCl_2$ solution [7]. Selected design issues associated with reactor scale-up in the thermochemical copper–chlorine (Cu–Cl) cycle for hydrogen production have been studied by Wang et al. [8], focusing on the hydrogen, oxygen and hydrolysis reactors [8].

Orhan et al. [9] have performed an economic analysis of a Cu–Cl pilot plant with an associated parametric study. The analysis takes into account the different types of costs such as energy, operation and maintenance costs, fixed charges on capital investment, etc. The costs with their percentage ranges and factors that affect accuracy and scaling have been examined. Through this scaling method, the total capital investment and total cost of a Cu–Cl pilot plant have been estimated by scaling against the corresponding costs of a sulphur-iodine (S-I) thermochemical water decomposition plant for hydrogen production. The sensitivity studies show that costs vary significantly with the pilot plant capacity, breakdowns of cost components and the capacity factor. Parametric studies with variable plant capacities, approximations and capacity factors have been performed [9].

Although technical studies of the Cu-Cl cycle have been reported, there is a need to understand the potential economics of the cycle, to facilitate eventual commercialisation. Such economic assessments are lacking, especially utilizing advanced tools linked to thermodynamics. Thermoeconomics combines energy (and/or exergy) analysis and economic principles to provide the system designer or operator with information not available through conventional energy analysis and economic evaluations, but useful to the design and operation of a cost-effective system.

In this paper, principles of thermoeconomics are used to evaluate the production costs as a function of the amount and quality of the energy used for hydrogen production, as well as the costs of the exergy losses and the exergoeconomic improvement potential of the equipment used in the process. An additional objective is to determine changes in the design parameters of the Cu-Cl cycle that improve the cost effectiveness of the overall system. The

methodology used provides a plausible exploratory approach for improving the cost effectiveness of the Cu-Cl cycle.

2 System Description

Most thermochemical cycles require process heat at high temperatures, exceeding 850°C-900°C. However, existing nuclear power plants typically operate at 250°C-500°C. Recently, Atomic Energy of Canada Limited and Argonne National Laboratory in the U.S. have been developing low-temperature thermochemical cycles designed to accommodate heat sources around 500°C-550°C. Such cycles can be more readily integrated with nuclear reactors. For this temperature range, the copper-chlorine (Cu-Cl) cycle is one of the most promising. Several Cu-Cl cycles have been examined in the laboratory and various alternative configurations identified. Proof-of-principle experiments that demonstrate the feasibility of the processes have been undertaken and a preliminary assessment of the cycle efficiency has demonstrated its potential.

The Cu-Cl cycle consists of a set of reactions to achieve the overall splitting of water into its constituents, hydrogen and oxygen. The overall net reaction is $H_2O\,(g) \rightarrow H_2\,(g) + 1/2O_2\,(g)$. The Cu-Cl cycle uses a series of intermediate copper and chloride compounds. These chemical reactions form a closed internal loop that recycles all chemicals on a continuous basis, without emitting any greenhouse gases.

The Cu-Cl cycle has been shown [1-9] to be a potentially attractive option for generating hydrogen from nuclear energy. Compared with other hydrogen production options, the thermochemical Cu-Cl cycle is expected to have a higher efficiency, to produce hydrogen at a lower cost, and to have a smaller impact on the environment by reducing airborne emissions, solid wastes and energy requirements.

It can be observed in Fig. 1 that only water and nuclear-derived heat enter the Cu-Cl cycle and only H_2 and O_2 are produced, while greenhouse gas emissions are avoided. In the first step of the cycle (S1), steam at 400°C and solid copper chloride ($CuCl_2$) at 400°C from the dryer enter the fluidized bed, where an endothermic chemical reaction occurs that yields hydrochloric gas (HCl) and Cu_2OCl_2. The hydrochloric gas is compressed and the Cu_2OCl_2 is transferred to another process step after its temperature is increased to the oxygen production reaction temperature of 500°C. In the second (oxygen production) step (S2) an endothermic chemical reaction takes place in which Cu_2OCl_2 is heated and O_2 and copper monochloride (CuCl) are produced. Liquid copper monochloride is solidified by cooling it to 20°C, after which it enters the third (copper production) step (S3) together with the solid copper monochloride from the fifth step (S5). In the third step, solid copper monochloride and water interact endothermically at 20°C. The water acts as a catalyst in this reaction, and does not react with the other elements or compounds. The third reaction involves an electrolysis step, which makes it the most expensive step depending on the price of electricity. In this reaction, solid copper and a copper chloride-water solution are produced. A mixture of copper chloride and water is transferred to the dryer (S4), and solid copper enters the fifth step after its temperature is increased to that step's operating temperature. In the fifth (hydrogen production) step, hydrochloric gas and copper enter and are converted to hydrogen gas (H_2) and solid copper monochloride (CuCl) in a steady-state reaction at 450°C.

Three different variations of the Cu-Cl cycle are currently under investigation: 3-step, 4-step and 5-step cycles.

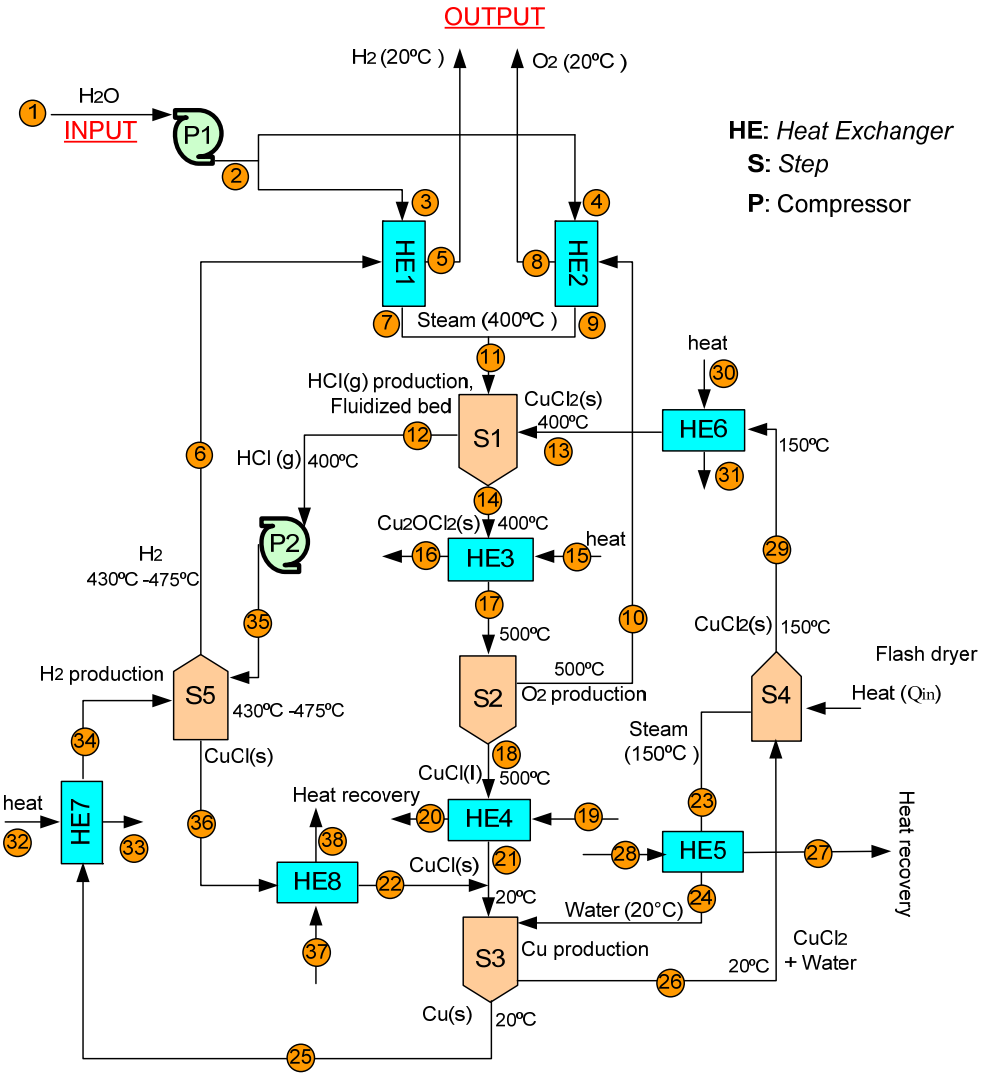

Figure 1: Conceptual layout of a thermochemical Cu-Cl hydrogen production cycle.

3 Analysis

The overall energy efficiency of the Cu-Cl cycle, η_e, can be expressed as the ratio of energy content of hydrogen based on lower heating value (*LHV*) to energy supplied. That is,

$$\eta_e = \frac{\dot{LHV}_{H_2}}{\dot{E}_{in}} \tag{1}$$

An exergy balance can be used in formulating an exergy efficiency for the reacting system; at steady state, the rate at which exergy enters the reacting system equals the rate at which

exergy exits plus the rate at which exergy is destroyed within the system. The overall exergy efficiency can be written as

$$\eta_{ex} = \frac{\dot{E}x_p}{\dot{E}x_{in}} = \frac{\dot{E}x_{H_2}}{\dot{E}x_{in}} \tag{2}$$

where $\dot{E}x_{in}$ and $\dot{E}x_p$ are the exergy content of entering and exiting (with products) flows, respectively. Using the exergy balance for the reacting system, the exergy efficiency expression can be written alternatively as

$$\eta_{ex} = 1 - \frac{\dot{E}x_{loss}}{\dot{E}x_{in}} \tag{3}$$

The total cost to produce the exiting streams (hydrogen) equals the total cost of the entering streams plus the cost of owning and operating the cycle. This is expressed by the following cost rate balance for the cycle:

$$\dot{C}_{H_2} = \dot{C}_{in} + \dot{Z} \tag{4}$$

where $\dot{C}$ is the cost rate of the respective stream and $\dot{Z}$, accounts for the cost rate associated with owning and operating the cycle (each in $ per hour, for example). This equation simply states that the total cost of the exiting exergy streams equals the total expenditure to obtain them: the cost of the entering exergy streams plus the capital and other costs. Although the cost rates denoted by in Eq. (4) are evaluated by various means in practice, the present discussion features the use of exergy for this purpose. Since exergy measures the true thermodynamic values of the work, heat, and other interactions between a system and its surroundings as well as the effect of irreversibilities within the system, exergy is a rational basis for assigning costs. With exergy costing, each of the cost rates is evaluated in terms of the associated rate of exergy transfer and a unit cost. Thus, for an entering or exiting stream, we write

$$\dot{C} = c\dot{E}x \tag{5}$$

where *c* denotes the cost per unit of exergy (in cents per kWh, for example) and $\dot{E}x$ is the associated exergy transfer rate. In exergy costing, a cost is associated with each exergy stream. Rewriting Eq. (4),

$$c_{H_2} = \frac{c_{in}}{\eta_{ex}} + \frac{\dot{Z}}{\dot{E}x_{H_2}} \tag{6}$$

4 Results and Discussion

Energy and exergy efficiencies of the Cu-Cl cycle are shown in Fig. 2. The energy efficiency is 0.43 while exergy efficiency is 0.13. The variation of the cost of hydrogen produced with respect to the efficiencies of the Cu-Cl cycle is shown in Fig. 3. This graph is obtained using Eq. (6). The cost of hydrogen decreases by improving the energy or exergy efficiency of the cycle. This is because as efficiencies increase, the destruction cost, which represents the cost that been lost by exergy destruction, decreases.

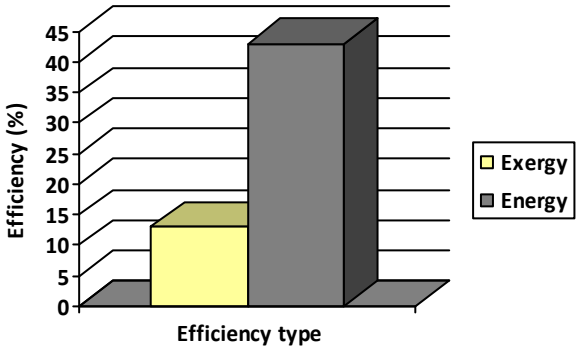

Figure 2: Energy and exergy efficiencies of the Cu-Cl thermochemical cycle.

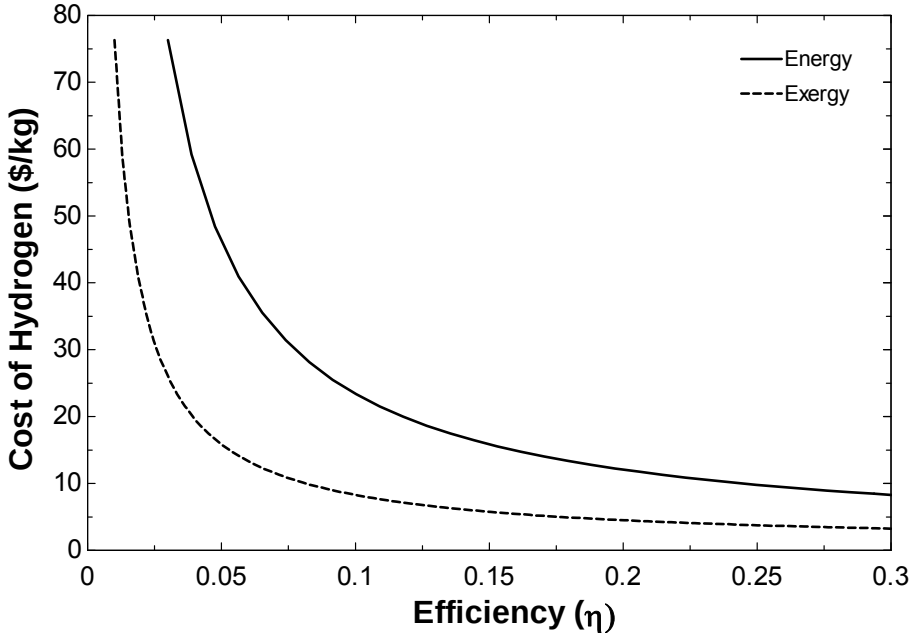

Figure 3: Variation of the cost of hydrogen produced with the efficiencies of the Cu-Cl cycle.

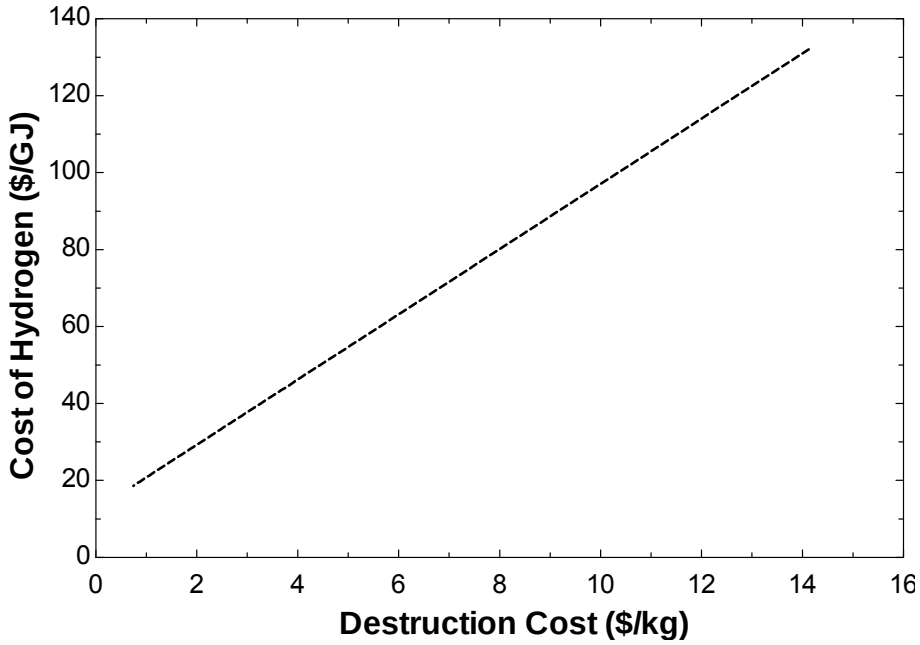

Figure 4: Variation of the cost of hydrogen produced with the cost of destruction in the Cu-Cl cycle.

The effect of the cost of destruction on the unit cost of hydrogen can be seen more clearly in Fig. 4. The cost rate of exergy destruction varies between $1 and $15 per kilogram of hydrogen while the cost of hydrogen rises from $20 to $140 per GJ of hydrogen energy. In Fig. 3, the cost of hydrogen is seen to be highest when the exergy efficiency approaches zero and it decreases as the exergy efficiency increases. The effect of exergy efficiency on the cost of hydrogen is very high in the efficiency range of 5 to 15% and very low in the efficiency range of 15 to 30%. The hydrogen cost approaches its lowest value and becomes roughly constant above an exergy efficiency of 30%. Clearly, an efficiency improvement measure should be evaluated carefully to determine whether it is economically worthwhile.

5 Conclusions

The Cu-Cl cycle has been shown to be a potentially attractive option for generating hydrogen from nuclear energy. Compared with other hydrogen production options, the thermochemical Cu-Cl cycle is expected to have a higher efficiency, to produce hydrogen at a lower cost, and to have a smaller impact on the environment by reducing airborne emissions, solid wastes and energy requirements.

This paper shows how exergy-related variables can be used to minimize the cost of a thermal system. The exergoeconomic analyses of the process reported in this paper for a Cu-Cl thermochemical water decomposition cycle for hydrogen production has allowed several findings. It identifies and evaluates the real energy waste and the real cost sources in the Cu-Cl cycle. The variations of hydrogen cost with parameters like energy and exergy efficiencies, exergy destruction and energy losses have been quantified and characterized. In particular, a parametric study is reported of how the unit costs of hydrogen and the cost rate of exergy destruction of the Cu-Cl cycle vary with the efficiency. This information should

assist efforts to understand the thermodynamic losses in the cycle, and to improve its efficiency and cost effectiveness.

References

[1] Orhan M. F., Dincer I., Rosen M. A., “The oxygen production step of a copper–chlorine thermochemical water decomposition cycle for hydrogen production: Energy and exergy analyses”, Chemical Engineering Science, Vol. 64, pp. 860-869, 2009.

[2] Orhan M. F., Dincer I., Rosen M. A., “Energy and exergy analyses of the fluidized bed of a copper-chlorine cycle for nuclear-based hydrogen production via thermochemical water decomposition”, Chemical Engineering Research and Design, Vol. 87, pp. 684-694, 2009.

[3] Orhan M. F., Dincer I., Rosen M. A., “Thermodynamic analysis of the copper production step in a copper–chlorine cycle for hydrogen production”, Thermochimica Acta, Vol. 480, pp. 22-29, 2008.

[4] Orhan M. F., Dincer I., Rosen M. A., “Energy and exergy assessments of the hydrogen production step of a copper–chlorine thermochemical water splitting cycle driven by nuclear-based heat”, International Journal of Hydrogen Energy, Vol. 33, pp. 6456-6466, 2008.

[5] Orhan M. F., Dincer I., Rosen M. A., “Energy and exergy analyses of the drying step of a copper-chlorine thermochemical cycle for hydrogen production”, International Journal of Exergy, Vol. 6, pp.793-808, 2009.

[6] Naterer G. F., Gabriel K., Wang Z. L., Daggupati V. N., Gravelsins R., “Thermochemical hydrogen production with a copper-chlorine cycle. I: oxygen release from copper oxychloride decomposition”, International Journal of Hydrogen Energy, Vol. 33, pp. 5439-5450, 2008.

[7] Naterer G. F., Daggupati V. N., Marin G., Gabriel K. S., Wang Z. L., “Thermochemical hydrogen production with a copper-chlorine cycle, II: Flashing and drying of aqueous cupric chloride”, International Journal of Hydrogen Energy, Vol. 33, pp. 5451-5459, 2008.

[8] Wang Z., Naterer G. F., Gabriel K., “Multiphase reactor scale-up for Cu-Cl thermochemical hydrogen production”, International Journal of Hydrogen Energy, Vol. 33, pp. 6934-6946, 2008.

[9] Orhan M. F., Dincer I., Naterer G. F., “Cost analysis of a thermochemical Cu-Cl pilot plant for nuclear-based hydrogen production”, International Journal of Hydrogen Energy, Vol. 33, pp. 6006-6020, 2008.

Effect of Impurities of the Solid on the Subsequent Hydrogen Release in Steam-Iron Process

J.A. Peña, A. Palacios, L. Martínez, E. Romero, P. Durán, J. Herguido, Aragon Institute of Engineering Research (I3A), Universidad de Zaragoza, Spain

1 Introduction

The greenhouse effect and the progressive fossil fuels depletion are the main motivations for searching new energy sources, which could replace the actual dependency to carbon based fuels. These sources must be green and renewable in a long term. Until this moment arrives, other substitutive must be found to lead the transient.

The hydrogen economy concept so explains that a large part of the generated energy must be obtained using hydrogen previously produced without greenhouse gas emissions [1]. The long-term objective of this study is the implantation of an alternative system to obtain, separate and storage, hydrogen without CO_2 added production, using for instance, streams from renewable sources like biogas, bio-oils or biomass pyrolysis gases.

The use of fuel cells is being proposed as an important possibility for automotive, where a high purity hydrogen feed is needed, since minimum gas impurities (e.g. CO) results in poisoning on the cell anode.

The “Steam-iron” process has been claimed as an interesting way to achieve this purity, and also to store hydrogen much safer than others storage methods. The process consists of a first step where a solid oxide is reduced by a H_2-rich stream. The reduced solid can then be stored for some time at open air and room conditions. When hydrogen is required, feeding steam to the solid containment can release hydrogen regenerating the former oxide.

The global reactions for this process will be:

$$3\ Fe_2O_3 + H_2 \leftrightarrow 2\ Fe_3O_4 + H_2O\ (g) \quad \text{Hematite to Magnetite} \quad \text{(r. 1)}$$

$$Fe_3O_4 + 4\ H_2 \leftrightarrow 3\ Fe + 4\ H_2O\ (g) \quad \text{Magnetite to Iron} \quad \text{(r. 2)}$$

Among the best suitable solids, iron oxides are proposed for this process, due to their high redox capacity, availability, and in addition their economic feasibility [2]. They have also a relatively low molecular weight, and the high oxidation state of the metal allows an interesting hydrogen storage density.

After proving the viability for this process [3], a strong decay in red-ox capacity has been evidenced when using pure hematite along the redox cycles [4]. Although some additives were considered [5], a ternary sample containing small amounts of alumina and ceria with Fe_2O_3 was prepared. Due to its low cost an iron oxide ore was also considered.

This work deals with the experimental study of steam-iron viability for these solids. Also in order to gain know about the process, kinetics of reduction and oxidation reactions were calculated from experimental data. These were better fit to an Avrami-based model.

2 Experimental

The ternary oxide (98 mol% Fe_2O_3–1.5 % Al_2O_3–0.5 % CeO_2) was prepared in laboratory using the citrate method [6]. The ore contains ~80 wt% Fe_2O_3, and SiO_2, Al_2O_3 and CaO as main impurities.

The experiments have been carried out in a thermogravimetric system (C.I. Electronics, MK2). The solid samples and flow conditions were chosen to ensure no external diffusional limitations. Reaction extent was measured as weight loss during reduction and gain at oxidation.

For studying the whole process, up to 7 red-ox cycles were carried out. Mixtures of hydrogen and nitrogen at 1 bar with different hydrogen partial pressures (0.1 to 0.9 bar) simulating the ones coming from a pyrolysis gas were checked, at 450 ºC and with a total flow rate of 750 Nml/min and P_{H2O}=0.05 bar in oxidations. Methane was checked out to exhibit an inert behavior in these experimental conditions. Also, with P_{H2}=0.5 bar different experiments were carried out at temperatures 400, 425, 450, 475 and 500 ºC. Oxidation reaction was studied conducting 7 red-ox cycles with P_{H2}=0,5 bar (in reduction steps) at 450 ºC for several steam partial pressures (0.01, 0.02, 0.05, 0.1 and 0.15 bar).

Weight loss or gain were fit to the Johnsson-Mehl-Avrami-Kolmogorov (JMAK) model [4]

$$X=1-\exp(-k*t^N) \qquad \text{(eq. 1)}$$

to obtain the characteristic parameters of the kinetics of reduction and oxidation. It were allowed to depend on temperature and reactant partial pressures. X is the solid conversion, k is the kinetic constant, t is the time, and N is the Avrami exponent (related to the nucleation grade and the characteristic dimension of morphologic growing). The constant k is expressed as:

$$k=k_0*\exp(-E_a/RT)*P_{gas}^n \qquad \text{(eq. 2)}$$

where P_{gas} is the partial pressure of reactant gas and n is the partial reaction exponent. The fittings were set for the second reduction (r.2, magnetite to iron) since r.1 (hematite to magnetite) is inhibited after the first reduction because of thermodynamic limitations at the used conditions of temperature and pressure.

3 Results

For the 7 red-ox cycles runs performed, the lab-made ternary solid exhibited a great stability, improving substantially the behavior of a pure hematite sample which lost its red-ox capacity quickly [4].

Weight losses and gains showed a strong effect of temperature and hydrogen partial pressure in reductions (Figure 1) in both solids. However, the stability of ternary solid was well maintained in the whole range of studied conditions, proving the good behavior of additives.

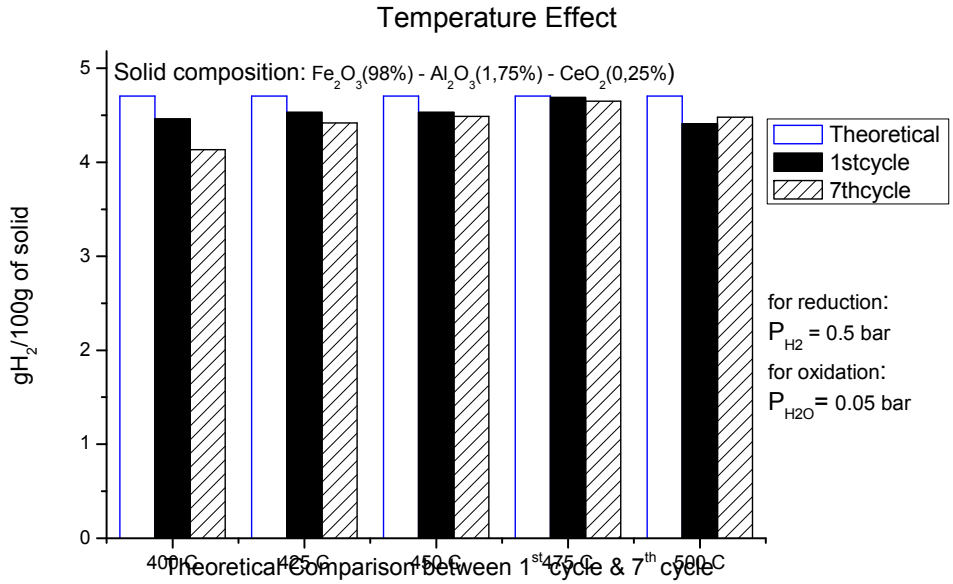

Figure 1: Hydrogen yield at different red-ox cycles vs. temperature in ternary oxide.

With the ternary oxide, nearly constant k values for each cycle were found in the same experiment (Table 1), which is in accordance to the solid red-ox stability. Reduction data showed an increase in k values at higher temperature and higher H_2 partial pressures, as expected. On the contrary, an increase in k values after each cycle at the same experiment is observed for the ore solid data fit (not shown here). This is due to the decay in red-ox capabilities with cycles (the maximum is reached at lower times, with apparent higher kinetics).

Data fit at different steam partial pressures showed similar behavior, increasing k values at higher partial pressures. However, oxidation results were fitted with decreasing k values at higher temperatures. This could be due to internal diffusion limits for water molecule (greater than hydrogen one) inside the particles.

Table 1: Parameters obtained from data fitting of the experimental red-ox cycles at different temperatures.

Reduction	k	Error	N	R^2
T = 400 ºC				
2	0.04436	±1,127E-4	1.396	0.99829
8	0.05567	±2,160E-4		0.99688
T = 425 ºC				
2	0.06802	±2,764E-4	1.440	0.99721
8	0.06999	±3,178E-4		0.99678
T = 450 ºC				
2	0.08467	±3,967E-4	1.463	0.99676
8	0.0872	±4,556E-4		0.99604
T = 475 ºC				
2	0.13073	±6,722E-4	1.517	0.99717
8	0.12792	±8,083E-4		0.9958
T = 500 ºC				
2	0.30821	±0,0018	1.517	0.99742
8	0.31512	±0,0023		0.99705

4 Conclusions

Ternary iron oxide-based solid showed a great stability after 7 red-ox cycles, strongly enhancing the pure iron oxide behavior. The ore also improved the pure iron oxide but some deactivation was not avoided.

Kinetics obtained for the ternary solid and the natural solid allow validate the proposed kinetic model in order to further simulation of same solids-based reactors.

References

[1] Lattin W.C., Utgikar V.P., Int. J. Hydrogen Energy 32 (2007) 3230 – 3237.

[2] Otsuka K., Yamada C., Kaburagi T., Takenaka S. Int. J. Hydrogen Energy 28 (2003) 335 – 342.

[3] Peña J.A., Lorente E., Romero E., Herguido J., Catal. Today 116 (2006) 439 – 444.

[4] Lorente, E., Peña, J.A., Herguido, J., Int. J. Hydrogen Energy, 33 (2008) 615-626.

[5] Lorente, E., Peña, J.A., Herguido, J., J. Power Sources, 192 (2009) 224-229.

[6] Ciambelli P, Cimino S, Lasorella G, Lisi L, De Rossi S, Faticanti M, Minelli G, Porta P. Appl. Catal. B: Environ. 37 (2002) 231-241.

Methanol from CO_2 and Solar Energy – A Literature Review

Mark Schmitz, **Sven Kluczka**, **Christiane Vaeßen**, Solar-Institut Jülich, Germany

1 Background and Motivation

In the future generation of methanol, hydrogen produced by solar energy will be one major source of primary energy. Different technologies are currently under investigation. Among these, high-temperature thermochemical cycles are considered very promising. Prerequisite for converting water with one or more chemical steps into hydrogen and oxygen is the concentration of solar energy to high flux levels.

At the solar tower facility at Jülich, a heliostat field of about 18000 m² focuses the sunlight onto an absorber surface of just 22 m² - a concentration high enough to reach temperatures beyond 1000°C, which is necessary to drive the endothermic steps of many thermochemical cycles.

The Solar-Institute Jülich, with its partners Ferrostaal and DLR, is now investigating in the project SolMethCO_2 the use of solar hydrogen for the reduction of CO_2 to methanol, addressing the issues of transportability of hydrogen and the exploitation of fossil resources for the methanol production.

The impending changes in the world climate are related to an accumulation of CO_2 in the atmosphere. One approach to counteract is by binding CO_2 in different chemical form like methanol. Concerning the high amount of energy, which is necessary for this process and generally derived from fossil energy sources, the implementation of solar technologies could be a key solution for delivering clean, carbon-free energy. The chemical and physical ways from solar energy and CO_2 to methanol are manifold and hard to compare with respect to their economical and ecological potentials due to different degrees of maturity of sub-processes. To make a comparison of the sub-processes possible, all established procedures have to be recorded and analysed systematically. Based on the results of literature research, practical experiences, experimental results and simulations, the aim of this project will be a final assessment of all CO_2-to-methanol processes.

2 Methods of Methanol Synthesis

Besides its technical use as a chemical feedstock, as e.g. for the production of acetic acid, formaldehyde or MTBE, methanol is a high potential energy carrier. Due to this, it is either used as a basis for the transformation into other fuels like dimethylether (DME), or it can be used pure or as a mixture with petrol or diesel fuels directly in combustion engines. Direct methanol fuel cells (DMFCs) directly convert the liquid fuel methanol into CO_2 while producing electric energy. This seems to be an attractive alternative to fuel cell systems operation with hydrogen, because of the higher volume-specific energy density of methanol.

Nowadays methanol is mainly produced by natural gas, which provides on the one hand carbon and hydrogen and on the other hand thermal energy during combustion.

The classical approach for the synthesis of methanol is via the transformation of synthesis gas, which is generally produced by the reformation or gasification of fossil energy carriers, as for example methane, at high temperatures (700-1100°C):

$$CH_4 + H_2O \rightarrow CO + 3\ H_2$$

In the next step, the synthesis gas reacts catalytically at 250°C and 50 to 100 bars to methanol:

$$CO + 2H_2 \rightarrow CH_3OH$$

Other carbon sources for the gasification process are coal or biomass.

Another promising approach for methanol synthesis is the direct or indirect use of carbon dioxide with hydrogen:

$$CO_2 + 3\ H_2 \rightarrow CH_3OH + H_2O$$
$$CO_2 \rightarrow CO + ½\ O_2$$
$$CO + 2H_2 \rightarrow CH_3OH$$

Besides methanol production from CO_2 and hydrogen it is also possible to generate methanol biotechnologically from biomass reformation or microbiological fermentation.

2.1 CO_2-capturing

In general there are three possible sources for the accumulation of CO_2: from the air, from sea- or other surface-waters and from industrial point sources.

On the one hand the adsorption of CO_2 from natural sources, especially from the atmosphere, depicts a promising method for lowering the concentrations of the harmful greenhouse gas but on the other hand, the comparatively low CO_2 content (currently ca. 380 ppm in atmospheric air as annual mean) makes an effective adsorption very difficult. [1] A higher CO_2-output can be reached with the more established methods of CO_2-capturing from industrial sources. These methods are restricted to a local application at fossil fuel combustion plants, however, most of which are far from places with optimal solar irradiation. All processes have in common that high energy amounts are necessary for the concentration of CO_2. **Fehler! Verweisquelle konnte nicht gefunden werden.** gives an overview of the most common techniques for CO_2 capturing, including artificial trees and carbon capture and storage (CCS) techniques.

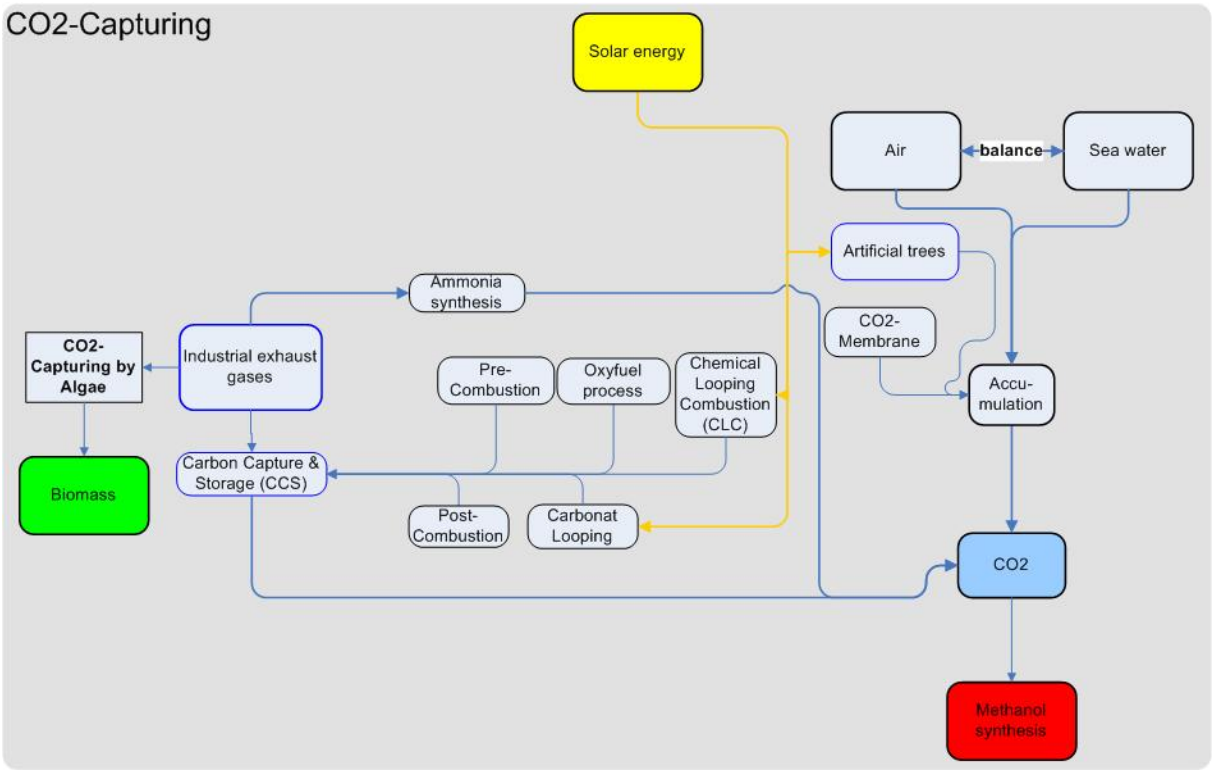

Figure 1: CO_2-Capturing.

2.2 H_2 / synthesis gas

In most processes for the conversion of CO_2 to methanol that are currently under investigation, hydrogen is used as a reactant. To provide hydrogen, according to the projects agenda, by use of solar energy, in principle three possible reaction pathways exist in which water is dissociated into oxygen and hydrogen: solar thermolysis, solar electrolysis and thermochemical cycles, using metal oxides or sulfuric acid. [2]

It is also possible to convert and energetically upgrade carbonaceous fossil fuels by means of solar energy to hydrogen or synthesis gas, accordingly. This can be achieved for example by reformation of methane, which is actually an intermediate step for the production of products like methanol or ammonia. [3] In solar reformation we distinguish between steam reformation and dry reformation, using CO_2 as reactant. Other “fossil” techniques for hydrogen/syngas production are solarthermal cracking of methane or solar degasification of solid fossil sources, like e.g. biomass or charcoal. [4]

2.3 Biotechnological techniques for methanol synthesis

As already mentioned in Chapter 2.2, an alternative route on the way solar methanol synthesis is using solid carbonaceous sources like biomass. The most classical approaches would be the processes of syngas production (gasification, pyrolysis) mentioned above.

Furthermore, biomass, in particular algae, can also be used for CO_2-capturing. In a newly developed technique, industrial exhaust gas is fed into large biomass production tanks, filled

with a microalgae-suspension, where the CO_2 is utilized by the algae as carbon source. The so produced biomass can be further processed for the production of biofuels. [5], [6]

By the use of special microorganisms it is also possible to generate methanol directly from biomass. Classical fermentation of biomass or the newly developed Helioculture process appear to be promising alternatives, but still demand further research. [7]

An overview of the biotechnological processes is given in Figure 2.

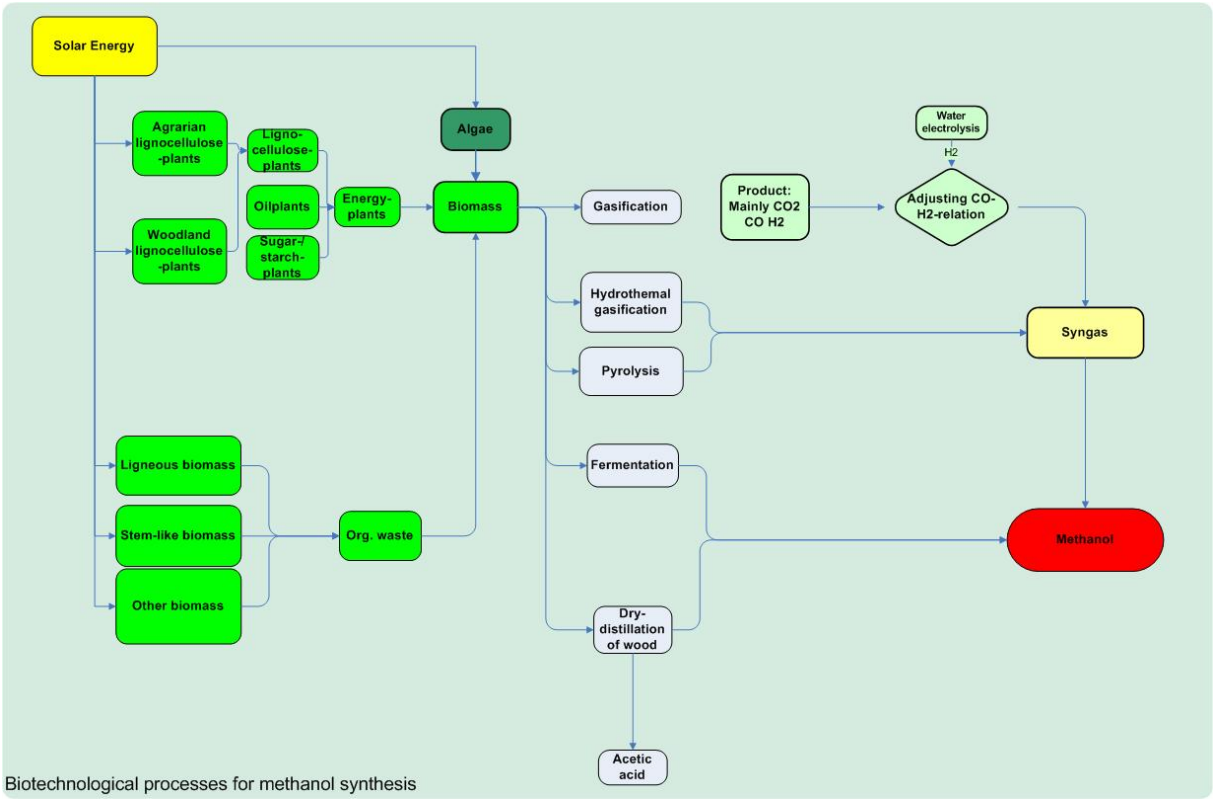

Figure 2: Biotechnological processes for methanol synthesis.

2.4 Integration of solar energy

Many of the processes presented in the previous chapters allow for the integration of solar energy. For example, in CO_2-capturing, the endothermic regeneration of absorption solution from artificial trees could be performed by solar technology. Most of the processes for hydrogen synthesis are already designed for solar operation. During the last years, many solar reactors for hydrogen and syngas production, using direct or indirect concentrated solar irradiation, have been developed, like e.g. vortex reactors, volumetric reactors or tubular reactors.

A completely different approach of solar methanol synthesis that is also accounted in our project is the use of special spectra of the visible sunlight in low-temperature processes like photochemical catalysis.

3 Further Steps

The first part of our project was a general literature research about all possible processes and sub-process involved in solar methanol synthesis from CO_2.

The upcoming steps include detailed analysis about the possibilities of solarisation of different process steps, the conduction of small and technical scale experiments for the analysis of photochemical and thermochemical reaction pathways, as well as the modelling of economic scenarios for a feasible solar methanol production based on information about possible location sites, meteorological influences and capital and operating costs. A list of several criteria will be generated to compare and evaluate different processes. Such criteria are capital and operational costs, cost effectiveness, resource productivity, technical maturity and scalability.

Acknowledgement

SolMethCO2 is a Ziel-2 project of the EU co-funded by the Ministry of Innovation of Northrhine Westphalia.

References

[1] Ausfelder, F.; Bazzanella, A. (2009): VCI-DECHEMA-Position Paper "CO_2-Nutzung". Published by VCI und DECHEMA. Available at http://www.dechema.de/dechema_media/Positionspapier_CO2.pdf

[2] Steinfeld, A. (2005): Solar thermochemical production of hydrogen--a review. Solar Energy 78(5):603–615

[3] Moller, S.; Kaucic, D.; Sattler, C. (2006) Hydrogen Production by Solar Reforming of Natural Gas: A Comparison Study of Two Possible Process Configurations. Journal of Solar Energy Engineering 128(1):16-23

[4] Melchior, T.; Perkins, C.; Lichty, P.; Weimer, A. W.; Steinfeld, A. (2009): Solar-driven biochar gasification in a particle-flow reactor. Chemical Engineering and Processing: Process Intensification 48(8):1279–1287

[5] Schmid-Staiger, U.; Preisner, R.; Trösch, W.; Marek, P. (2009) Kultivierung von Mikroalgen im Photobioreaktor zur stofflichen und energetischen Nutzung. Chemie Ingenieur Technik 81(11):1783-1789

[6] Winkler, M.; Kuhlgert, S.; Hippler, M.; Happe, T. (2009): Characterization of the Key Step for Light-driven Hydrogen Evolution in Green Algae. The Journal of Biological Chemistry, 284:36620-36627

[7] Borrell, B. (2009) Joule Biotechnologies announces new biofuel jargon, scant details. Scientific American. Available under https://www.scientificamerican.com/blog/post.cfm?id=joule-biotechnologies-announce-new-2009-07-27

1. **Einsatz von multispektralen Satellitenbilddaten in der Wasserhaushalts- und Stoffstrommodellierung – dargestellt am Beispiel des Rureinzugsgebietes**
von C. Montzka (2008), XX, 238 Seiten
ISBN: 978-3-89336-508-1

2. **Ozone Production in the Atmosphere Simulation Chamber SAPHIR**
by C. A. Richter (2008), XIV, 147 pages
ISBN: 978-3-89336-513-5

3. **Entwicklung neuer Schutz- und Kontaktierungsschichten für Hochtemperatur-Brennstoffzellen**
von T. Kiefer (2008), 138 Seiten
ISBN: 978-3-89336-514-2

4. **Optimierung der Reflektivität keramischer Wärmedämmschichten aus Yttrium-teilstabilisiertem Zirkoniumdioxid für den Einsatz auf metallischen Komponenten in Gasturbinen**
von A. Stuke (2008), X, 201 Seiten
ISBN: 978-3-89336-515-9

5. **Lichtstreuende Oberflächen, Schichten und Schichtsysteme zur Verbesserung der Lichteinkopplung in Silizium-Dünnschichtsolarzellen**
von M. Berginski (2008), XV, 171 Seiten
ISBN: 978-3-89336-516-6

6. **Politikszenarien für den Klimaschutz IV – Szenarien bis 2030**
hrsg.von P. Markewitz, F. Chr. Matthes (2008), 376 Seiten
ISBN 978-3-89336-518-0

7. **Untersuchungen zum Verschmutzungsverhalten rheinischer Braunkohlen in Kohledampferzeugern**
von A. Schlüter (2008), 164 Seiten
ISBN 978-3-89336-524-1

8. **Inorganic Microporous Membranes for Gas Separation in Fossil Fuel Power Plants**
by G. van der Donk (2008), VI, 120 pages
ISBN: 978-3-89336-525-8

9. **Sinterung von Zirkoniumdioxid-Elektrolyten im Mehrlagenverbund der oxidkeramischen Brennstoffzelle (SOFC)**
von R. Mücke (2008), VI, 165 Seiten
ISBN: 978-3-89336-529-6

10. **Safety Considerations on Liquid Hydrogen**
by K. Verfondern (2008), VIII, 167 pages
ISBN: 978-3-89336-530-2

11. **Kerosinreformierung für Luftfahrtanwendungen**
    von R. C. Samsun (2008), VII, 218 Seiten
    ISBN: 978-3-89336-531-9

12. **Der 4. Deutsche Wasserstoff Congress 2008 – Tagungsband**
    hrsg. von D. Stolten, B. Emonts, Th. Grube (2008), 269 Seiten
    ISBN: 978-3-89336-533-3

13. **Organic matter in Late Devonian sediments as an indicator for environmental changes**
    by M. Kloppisch (2008), XII, 188 pages
    ISBN: 978-3-89336-534-0

14. **Entschwefelung von Mitteldestillaten für die Anwendung in mobilen Brennstoffzellen-Systemen**
    von J. Latz (2008), XII, 215 Seiten
    ISBN: 978-3-89336-535-7

15. **RED-IMPACT**
    Impact of Partitioning, Transmutation and Waste Reduction Technologies on the Final Nuclear Waste Disposal
    SYNTHESIS REPORT
    ed. by W. von Lensa, R. Nabbi, M. Rossbach (2008), 178 pages
    ISBN 978-3-89336-538-8

16. **Ferritic Steel Interconnectors and their Interactions with Ni Base Anodes in Solid Oxide Fuel Cells (SOFC)**
    by J. H. Froitzheim (2008), 169 pages
    ISBN: 978-3-89336-540-1

17. **Integrated Modelling of Nutrients in Selected River Basins of Turkey**
    Results of a bilateral German-Turkish Research Project
    project coord. M. Karpuzcu, F. Wendland (2008), XVI, 183 pages
    ISBN: 978-3-89336-541-8

18. **Isotopengeochemische Studien zur klimatischen Ausprägung der Jüngeren Dryas in terrestrischen Archiven Eurasiens**
    von J. Parplies (2008), XI, 155 Seiten, Anh.
    ISBN: 978-3-89336-542-5

19. **Untersuchungen zur Klimavariabilität auf dem Tibetischen Plateau - Ein Beitrag auf der Basis stabiler Kohlenstoff- und Sauerstoffisotope in Jahrringen von Bäumen waldgrenznaher Standorte**
    von J. Griessinger (2008), XIII, 172 Seiten
    ISBN: 978-3-89336-544-9

20. **Neutron-Irradiation + Helium Hardening & Embrittlement Modeling of 9%Cr-Steels in an Engineering Perspective (HELENA)**
by R. Chaouadi (2008), VIII, 139 pages
ISBN: 978-3-89336-545-6

21. **in Bearbeitung**

22. **Verbundvorhaben APAWAGS (AOEV und Wassergenerierung) – Teilprojekt: Brennstoffreformierung – Schlussbericht**
von R. Peters, R. C. Samsun, J. Pasel, Z. Porš, D. Stolten (2008), VI, 106 Seiten
ISBN: 978-3-89336-547-0

23. **FREEVAL**
Evaluation of a Fire Radiative Power Product derived from Meteosat 8/9 and Identification of Operational User Needs
Final Report
project coord. M. Schultz, M. Wooster (2008), 139 pages
ISBN: 978-3-89336-549-4

24. **Untersuchungen zum Alkaliverhalten unter Oxycoal-Bedingungen**
von C. Weber (2008), VII, 143, XII Seiten
ISBN: 978-3-89336-551-7

25. **Grundlegende Untersuchungen zur Freisetzung von Spurstoffen, Heißgaschemie, Korrosionsbeständigkeit keramischer Werkstoffe und Alkalirückhaltung in der Druckkohlenstaubfeuerung**
von M. Müller (2008), 207 Seiten
ISBN: 978-3-89336-552-4

26. **Analytik von ozoninduzierten phenolischen Sekundärmetaboliten in *Nicotiana tabacum* L. cv Bel W3 mittels LC-MS**
von I. Koch (2008), III, V, 153 Seiten
ISBN 978-3-89336-553-1

27. **IEF-3 Report 2009. Grundlagenforschung für die Anwendung**
(2009), ca. 230 Seiten
ISBN: 978-3-89336-554-8

28. **Influence of Composition and Processing in the Oxidation Behavior of MCrAlY-Coatings for TBC Applications**
by J. Toscano (2009), 168 pages
ISBN: 978-3-89336-556-2

29. **Modellgestützte Analyse signifikanter Phosphorbelastungen in hessischen Oberflächengewässern aus diffusen und punktuellen Quellen**
von B. Tetzlaff (2009), 149 Seiten
ISBN: 978-3-89336-557-9

30. **Nickelreaktivlot / Oxidkeramik – Fügungen als elektrisch isolierende Dichtungskonzepte für Hochtemperatur-Brennstoffzellen-Stacks**
von S. Zügner (2009), 136 Seiten
ISBN: 978-3-89336-558-6

31. **Langzeitbeobachtung der Dosisbelastung der Bevölkerung in radioaktiv kontaminierten Gebieten Weißrusslands – Korma-Studie**
von H. Dederichs, J. Pillath, B. Heuel-Fabianek, P. Hill, R. Lennartz (2009), Getr. Pag.
ISBN: 978-3-89336-532-3

32. **Herstellung von Hochtemperatur-Brennstoffzellen über physikalische Gasphasenabscheidung**
von N. Jordán Escalona (2009), 148 Seiten
ISBN: 978-3-89336-532-3

33. **Real-time Digital Control of Plasma Position and Shape on the TEXTOR Tokamak**
by M. Mitri (2009), IV, 128 pages
ISBN: 978-3-89336-567-8

34. **Freisetzung und Einbindung von Alkalimetallverbindungen in kohlebefeuerten Kombikraftwerken**
von M. Müller (2009), 155 Seiten
ISBN: 978-3-89336-568-5

35. **Kosten von Brennstoffzellensystemen auf Massenbasis in Abhängigkeit von der Absatzmenge**
von J. Werhahn (2009), 242 Seiten
ISBN: 978-3-89336-569-2

36. **Einfluss von Reoxidationszyklen auf die Betriebsfestigkeit von anodengestützten Festoxid-Brennstoffzellen**
von M. Ettler (2009), 138 Seiten
ISBN: 978-3-89336-570-8

37. **Großflächige Plasmaabscheidung von mikrokristallinem Silizium für mikromorphe Dünnschichtsolarmodule**
von T. Kilper (2009), XVII, 154 Seiten
ISBN: 978-3-89336-572-2

38. **Generalized detailed balance theory of solar cells**
by T. Kirchartz (2009), IV, 198 pages
ISBN: 978-3-89336-573-9

39. **The Influence of the Dynamic Ergodic Divertor on the Radial Electric Field at the Tokamak TEXTOR**
von J. W. Coenen (2009), xii, 122, XXVI pages
ISBN: 978-3-89336-574-6

40. **Sicherheitstechnik im Wandel Nuklearer Systeme**
von K. Nünighoff (2009), viii, 215 Seiten
ISBN: 978-3-89336-578-4

41. **Pulvermetallurgie hochporöser NiTi-Legierungen für Implanat- und Dämpfungsanwendungen**
von M. Köhl (2009), XVII, 199 Seiten
ISBN: 978-3-89336-580-7

42. **Einfluss der Bondcoatzusammensetzung und Herstellungsparameter auf die Lebensdauer von Wärmedämmschichten bei zyklischer Temperaturbelastung**
von M. Subanovic (2009), 188, VI Seiten
ISBN: 978-3-89336-582-1

43. **Oxygen Permeation and Thermo-Chemical Stability of Oxygen Permeation Membrane Materials for the Oxyfuel Process**
by A. J. Ellett (2009), 176 pages
ISBN: 978-3-89336-581-4

44. **Korrosion von polykristallinem Aluminiumoxid (PCA) durch Metalljodidschmelzen sowie deren Benetzungseigenschaften**
von S. C. Fischer (2009), 148 Seiten
ISBN: 978-3-89336-584-5

45. **IEF-3 Report 2009. Basic Research for Applications**
(2009), 217 Seiten
ISBN: 978-3-89336-585-2

46. **Verbundvorhaben ELBASYS (Elektrische Basissysteme in einem CFK-Rumpf) - Teilprojekt: Brennstoffzellenabgase zur Tankinertisierung - Schlussbericht**
von R. Peters, J. Latz, J. Pasel, R. C. Samsun, D. Stolten
(2009), xi, 202 Seiten
ISBN: 978-3-89336-587-6

47. **Aging of ^{14}C-labeled Atrazine Residues in Soil: Location, Characterization and Biological Accessibility**
by N. D. Jablonowski (2009), IX, 104 pages
ISBN: 978-3-89336-588-3

48. **Entwicklung eines energetischen Sanierungsmodells für den europäischen Wohngebäudesektor unter dem Aspekt der Erstellung von Szenarien für Energie- und CO_2 - Einsparpotenziale bis 2030**
von P. Hansen (2009), XXII, 281 Seiten
ISBN: 978-3-89336-590-6

49. **Reduktion der Chromfreisetzung aus metallischen Interkonnektoren für Hochtemperaturbrennstofzellen durch Schutzschichtsysteme**
von R. Trebbels (2009), iii, 135 Seiten
ISBN: 978-3-89336-591-3

50. **Bruchmechanische Untersuchung von Metall / Keramik-Verbundsystemen für die Anwendung in der Hochtemperaturbrennstoffzelle**
von B. Kuhn (2009), 118 Seiten
ISBN: 978-3-89336-592-0

51. **Wasserstoff-Emissionen und ihre Auswirkungen auf den arktischen Ozonverlust**
Risikoanalyse einer globalen Wasserstoffwirtschaft
von T. Feck (2009), 180 Seiten
ISBN: 978-3-89336-593-7

52. **Development of a new Online Method for Compound Specific Measurements of Organic Aerosols**
by T. Hohaus (2009), 156 pages
ISBN: 978-3-89336-596-8

53. **Entwicklung einer FPGA basierten Ansteuerungselektronik für Justageeinheiten im Michelson Interferometer**
von H. Nöldgen (2009), 121 Seiten
ISBN: 978-3-89336-599-9

54. **Observation – and model – based study of the extratropical UT/LS**
by A. Kunz (2010), xii, 120, xii pages
ISBN: 978-3-89336-603-3

55. **Herstellung polykristalliner Szintillatoren für die Positronen-Emissions-Tomographie (PET)**
von S. K. Karim (2010), VIII, 154 Seiten
ISBN: 978-3-89336-610-1

56. **Kombination eines Gebäudekondensators mit H2-Rekombinatorelementen in Leichwasserreaktoren**
von S. Kelm (2010), vii, 119 Seiten
ISBN: 978-3-89336-611-8

57. **Plant Leaf Motion Estimation Using A 5D Affine Optical Flow Model**
by T. Schuchert (2010), X, 143 pages
ISBN: 978-3-89336-613-2

58. **Tracer-tracer relations as a tool for research on polar ozone loss**
by R. Müller (2010), 116 pages
ISBN: 978-3-89336-614-9

59. **Sorption of polycyclic aromatic hydrocarbon (PAH) to Yangtze River sediments and their components**
by J. Zhang (2010), X, 109 pages
ISBN: 978-3-89336-616-3

60. **Weltweite Innovationen bei der Entwicklung von CCS-Technologien und Möglichkeiten der Nutzung und des Recyclings von CO_2**
Studie im Auftrag des BMWi
von W. Kuckshinrichs et al. (2010), X, 139 Seiten
ISBN: 978-3-89336-617-0

61. **Herstellung und Charakterisierung von sauerstoffionenleitenden Dünnschichtmembranstrukturen**
von M. Betz (2010), XII, 112 Seiten
ISBN: 978-3-89336-618-7

62. **Politikszenarien für den Klimaschutz V – auf dem Weg zum Strukturwandel, Treibhausgas-Emissionsszenarien bis zum Jahr 2030**
hrsg. von P. Hansen, F. Chr. Matthes (2010), 276 Seiten
ISBN: 978-3-89336-619-4

63. **Charakterisierung Biogener Sekundärer Organischer Aerosole mit Statistischen Methoden**
von C. Spindler (2010), iv, 163 Seiten
ISBN: 978-3-89336-622-4

64. **Stabile Algorithmen für die Magnetotomographie an Brennstoffzellen**
von M. Wannert (2010), ix, 119 Seiten
ISBN: 978-3-89336-623-1

65. **Sauerstofftransport und Degradationsverhalten von Hochtemperatur-membranen für CO2-freie Kraftwerke**
von D. Schlehuber (2010), VII, 139 Seiten
ISBN: 978-3-89336-630-9

66. **Entwicklung und Herstellung von foliengegossenen, anodengestützten Festoxidbrennstoffzellen**
von W. Schafbauer (2010), VI, 164 Seiten
ISBN: 978-3-89336-631-6

67. **Disposal strategy of proton irradiated mercury from high power spallation sources**
by S. Chiriki (2010), xiv, 124 pages
ISBN: 978-3-89336-632-3

68. **Oxides with polyatomic anions considered as new electrolyte materials for solid oxide fuel cells (SOFCs)**
by O. H. Bin Hassan (2010), vii, 121 pages
ISBN: 978-3-89336-633-0

69. **Von der Komponente zum Stack: Entwicklung und Auslegung von HT-PEFC-Stacks der 5 kW-Klasse**
von A. Bendzulla (2010), IX, 203 Seiten
ISBN: 978-3-89336-634-7

70. **Satellitengestützte Schwerewellenmessungen in der Atmosphäre und Perspektiven einer zukünftigen ESA Mission (PREMIER)**
von S. Höfer (2010), 81 Seiten
ISBN: 978-3-89336-637-8

71. **Untersuchungen der Verhältnisse stabiler Kohlenstoffisotope in atmosphärisch relevanten VOC in Simulations- und Feldexperimenten**
von H. Spahn (2010), IV, 210 Seiten
ISBN: 978-3-89336-638-5

72. **Entwicklung und Charakterisierung eines metallischen Substrats für nanostrukturierte keramische Gastrennmembranen**
von K. Brands (2010), vii, 137 Seiten
ISBN: 978-3-89336-640-8

73. **Hybridisierung und Regelung eines mobilen Direktmethanol-Brennstoff-zellen-Systems**
von J. Chr. Wilhelm (2010), 220 Seiten
ISBN: 978-3-89336-642-2

74. **Charakterisierung perowskitischer Hochtemperaturmembranen zur Sauerstoffbereitstellung für fossil gefeuerte Kraftwerksprozesse**
von S.A. Möbius (2010) III, 208 Seiten
ISBN: 978-3-89336-643-9

75. **Characterization of natural porous media by NMR and MRI techniques: High and low magnetic field studies for estimation of hydraulic properties**
by L.-R. Stingaciu (2010), 96 pages
ISBN: 978-3-89336-645-3

76. **Hydrological Characterization of a Forest Soil Using Electrical Resistivity Tomography**
by Chr. Oberdörster (2010), XXI, 151 pages
ISBN: 978-3-89336-647-7

77. **Ableitung von atomarem Sauerstoff und Wasserstoff aus Satellitendaten und deren Abhängigkeit vom solaren Zyklus**
von C. Lehmann (2010), 127 Seiten
ISBN: 978-3-89336-649-1

78. **18th World Hydrogen Energy Conference 2010 – WHEC2010 Proceedings**
Speeches and Plenary Talks
ed. by D. Stolten, B. Emonts (2010)
ISBN: 978-3-89336-658-3

78-1. **18th World Hydrogen Energy Conference 2010 – WHEC2010 Proceedings**
Parallel Sessions Book 1:
Fuel Cell Basics / Fuel Infrastructures
ed. by D. Stolten, T. Grube (2010), ca. 460 pages
ISBN: 978-3-89336-651-4

78-2. **18th World Hydrogen Energy Conference 2010 – WHEC2010 Proceedings**
Parallel Sessions Book 2:
Hydrogen Production Technologies – Part 1
ed. by D. Stolten, T. Grube (2010), ca. 400 pages
ISBN: 978-3-89336-652-1

78-3. **18th World Hydrogen Energy Conference 2010 – WHEC2010 Proceedings**
Parallel Sessions Book 3:
Hydrogen Production Technologies – Part 2
ed. by D. Stolten, T. Grube (2010), ca. 640 pages
ISBN: 978-3-89336-653-8

78-4. **18th World Hydrogen Energy Conference 2010 – WHEC2010 Proceedings**
Parallel Sessions Book 4:
Storage Systems / Policy Perspectives, Initiatives and Cooperations
ed. by D. Stolten, T. Grube (2010), ca. 500 pages
ISBN: 978-3-89336-654-5

78-5. **18th World Hydrogen Energy Conference 2010 – WHEC2010 Proceedings**
Parallel Sessions Book 5:
Stategic Analysis / Safety Issues / Existing and Emerging Markets
ed. by D. Stolten, T. Grube (2010), ca. 530 pages
ISBN: 978-3-89336-655-2

78-6. **18th World Hydrogen Energy Conference 2010 – WHEC2010 Proceedings**
Parallel Sessions Book 6:
Stationary Applications / Transportation Applications
ed. by D. Stolten, T. Grube (2010), ca. 330 pages
ISBN: 978-3-89336-656-9

Schriften des Forschungszentrums Jülich
Reihe Energie & Umwelt / Energy & Environment

78 Set (7 Bände)

18th World Hydrogen Energy Conference 2010 – WHEC2010 Proceedings
eb. by D. Stolten, T. Grube, B. Emonts (2010)
ISBN: 978-3-89336-657-6